

Wear and Boundary Lubrication in Modular Total Knee Replacements

by

Jan-Mels Brandt

**A thesis
presented to the University of Waterloo
in fulfillment of the
thesis requirement for the degree of
Doctor of Philosophy
in
Mechanical Engineering**

Waterloo, Ontario, Canada, 2008

© Jan-Mels Brandt 2008

Author's declaration

I hereby declare that I am the sole author of this thesis. This is a true copy of the thesis, including any required final revisions, as accepted by my examiners.

I understand that my thesis may be made electronically available to the public.

Abstract

Wear of the polyethylene (PE) bearing surface and wear particle-induced osteolysis (bone resorption) can lead to failure of modular total knee replacements and make expensive revision surgery necessary. Gamma-in-air sterilization of the PE insert and having a modular tibial component are both risk factors for excessive backside wear that contribute to osteolysis and implant failure. The overall wear (backside and topside) of modular total knee replacements has been subjected to considerable research in order to avoid such implant failure. The investigations reported in the present thesis evaluated both the clinical and *in vitro* wear performance of modular total knee replacements.

The clinical investigations included damage assessment of retrieved PE inserts. A semi-quantitative grading method was developed and used to assess backside surface damage on 52 PE inserts retrieved from contemporary total knee replacement surgeries. Statistical analyses, such as univariate and multiple linear regression analysis, were performed to identify factors that influence backside damage including implant design features and patient characteristics. The damage features on the retrieved tibial PE inserts were also assessed with surface characterization techniques, such as scanning electron microscopy, energy dispersive X-ray analysis, and surface profilometry. To reduce surface damage and thus wear, PE inserts should be either gas-plasma or ethylene-oxide sterilized, used with polished tibial trays and held in place with a partial-peripheral locking mechanism.

Synovial fluid samples were aspirated from a total of twenty patients and some basic biochemical analyses were performed. The total protein concentration, protein constituent fractions, the level of osmolality, and trace element concentrations were measured and compared with the same characteristics of four serum lubricants that were frequently used in simulator wear testing to mimic synovial fluid.

In vitro investigations were conducted to explore the effects of some major constituents of the serum lubricants on the wear rate using a knee

simulator apparatus. Increased protein constituent degradation led to increased wear. Such findings suggested that a protein layer acted as a boundary lubricant to protect the PE surfaces of knee implants. The protein constituent fractions of alpha calf serum (ACS) were similar to those measured for synovial fluid. These ACS lubricants were used in further wear studies in which hyaluronic acid (HA) and phosphate buffer solution (PBS) were successively added. The PBS was used in place of the distilled water to generate a serum lubricant with a clinically relevant level of osmolality. The thermal stability of the ACS lubricants and synovial fluid were measured. The thermal stability of the ACS lubricant that contained HA and PBS was about the same as that of human synovial fluid. The simulator wear rate of PE was significantly influenced by both HA and PBS.

In further investigations, sodium azide, which has been used to inhibit microbial growth in simulator wear testing, was shown to be highly ineffective. Microbial contamination was recognized and the organism responsible was identified using standard microbiological methods. The use of an antibiotic-antimycotic mixture as the microbial inhibitor in the ACS + PBS + HA lubricant created a sterile environment and thus very clinically relevant environment for wear testing.

The content of this thesis represents a comprehensive data collection on retrieval analysis and lubricant-specific knee simulator wear testing of modular total knee replacements. A more clinically relevant lubricant composition for simulator wear testing was proposed (U.S. patent Serial number 60/899,894; pending since February 9th, 2007) that improved upon the current guideline from the *International Standards Organization* for knee simulator wear testing. The present thesis should serve as a guide for the surgeon, researcher and the implant manufacturer to evaluate retrieved implant components and to select lubricant additives for wear testing that closely mimics the *in vivo* wear conditions.

Acknowledgements

Firstly, I would like to thank my supervisor Prof. John B. Medley for his support and excellent guidance during my doctoral studies. His knowledge in tribology is truly outstanding and I am very grateful for his mentorship. I am looking forward to our discussions on our next road trip.

Secondly, I would like to thank Drs. Steven J. MacDonald and Richard W. McCalden at the Division of Orthopaedic Surgery, London Health Sciences Centre who acted as my co-supervisors and answered many orthopaedic questions without hesitation. I also would like to thank Drs. Robert B. Bourne, James McAuley, Douglas Naudie, Cecil H. Rorabeck, and James A. Johnson for accommodating me at London Health Sciences Centre and the University of Western Ontario in a superb manner. Their support aided much to the successful establishment of the Tribology Laboratory at London Health Sciences Centre. Dr. Daniel D. Auger, Donald McNulty, Todd Render, and Steve Swope from DePuy Orthopaedics Inc., Warsaw, IN, are also acknowledged for their frequent discussions on knee implant wear testing and for the donation of implant components.

Although the main research in this thesis was focused in Tribology and Orthopaedics, I was given the opportunity to extend my research into the areas of Biochemistry and Microbiology. Thus, I am very much in debt to Dr. Lin Zhao for introducing me to the field of Biochemistry and to Prof. Fred Possmeyer for allowing me to work in his laboratory; Dr. Susan Koval and Khaled K. K.E. Mahmoud for introducing me into Microbiology and for giving me some insight on the amazing abilities of *Bdellovibrio*. I would also like to thank Janice Restorick from the Immunology Laboratory at the London Health Sciences Centre; Lee-Ann Brière from the Department of Biochemistry, University of Western Ontario; Mike Meinert from the National Research Council, London; Dr. Heng-Yong Nie and Ross Davidson from Surface Science Western, and the lads from the Engineering group at the London Health Sciences Centre and Engineering workshop at the University of Western Ontario for their contribution to this thesis.

Thanks also to the staff at the Division of Orthopaedic Surgery, research nurses Julie Marr, and Abigail Thompson, and Administrative assistants Katharine Culbert, Linda McManus, Kathy Steed, Barb Keim, Penny Campbell, Joyce Belanger, and Karen Bosma. I will miss being fed those ever-delicious sweets and having those great Christmas potlucks. I would like to extend my acknowledgments to the many visiting orthopaedic fellows throughout the years for our discussions and projects involving knee implant wear.

I am very much in debt to Kory Charron, Jeff Guerin, and Sean Volkaert who made my time in London and my time as a *Coureur des bois* unforgettable. Christopher Haydon has to be also acknowledged for his assistance during the retrieval analysis of this thesis and of course, for many great times in London and elsewhere; Veronika Koleganova, Flavia “Chocolate” Vianna, and my hiking buddies Roland Broda and Dr. Ramin Mehin for their friendship. I would also like to acknowledge the members of the London Magpies, Australian Rules Football Club, for being great team mates.

I would also like to thank the Biegerl family and the Bücherl family for being such loyal and supporting friends over the past years. Above all, I have to thank my parents for their endless support and motivation that kept me pursuing my PhD.

...good times...good times...!

To my parents, Wiebke and Mels

In memory of
Miroslav Rendulič
** 20.12.1975*
† 13.08.1997

Table of Contents

List of Tables	xiv
List of Figures.....	xvi
Chapter 1: Introduction	1
1.1 Total Knee Replacements and Implant Wear	1
1.2 The Significance of Retrieval Analysis and Wear Testing.....	8
1.3 Thesis Objectives and Outline	10
Chapter 2: Literature Review.....	12
2.1 Introductory Remarks	12
2.2 Tribology.....	13
2.2.1 Theory.....	13
2.2.2 Wear and Wear Mechanisms	15
2.2.3 Wear of Polyethylene	19
2.2.4 Boundary Lubrication.....	21
2.3 Lubrication and Wear of Natural Synovial Joints and Knee Implant.....	26
2.3.1 Synovial Fluid Constituents and Characteristics	26
2.3.2 Lubrication of the Natural and Artificial Joint	32
2.3.3 Joint Simulator Wear Testing	35
2.4 Bearing Surface.....	40
2.4.1 Manufacturing Process	40
2.4.2 Properties	41
2.4.3 Sterilization Techniques and Oxidative Degradation.....	43
2.4.4 Microstructural Effects	45
2.4.5 Alternative Tibial Bearing Materials	46
2.5 Clinical Wear and Osteolysis.....	50
2.5.1 The Source of Biologically Active Wear Particles.....	50
2.5.2 Mechanisms of Bone Loss.....	54
2.5.3 Clinical Wear Assessment	58
2.6 Factors Influencing the Clinical Wear Performance.....	61
2.6.1 Implant Design.....	61

2.6.2 Femoral Component	63
2.6.3 Patient Characteristics	65
2.6.4 Surgical Factor	66
2.7 Concluding Remarks.....	67
Chapter 3: Materials and Methods	69
3.1 Introductory Remarks	69
3.2 Implant Retrieval Analysis	70
3.2.1 Implant Characteristics	70
3.2.2 Patient Characteristics	74
3.2.3 Damage Features	77
3.2.4 Damage Assessment Protocol.....	80
3.2.5 Melt Annealing.....	85
3.3 Lubricants	86
3.3.1 Collection of Synovial Fluid.....	86
3.3.2 Calf Sera	87
3.3.3 Lubricant Mixtures	88
3.4 Knee Simulator Wear Testing.....	90
3.4.1 Test Apparatus	90
3.4.2 Calibration	94
3.4.3 Imposed Loads and Displacements	96
3.4.4 Implants	98
3.4.5 Implant Mounting.....	99
3.5 Biochemical Analyses.....	100
3.5.1 Protein Concentration and Degradation.....	100
3.5.2 Electrophoresis	103
3.5.3 Peptide Concentration.....	106
3.5.4 Osmolality.....	108
3.5.5 Differential Scanning Calorimetry	108
3.5.6 Trace Elements	112
3.5.7 pH	112
3.6 Microbiological Analysis.....	113

3.6.1 Microbial Identification	113
3.6.2 Microbial Growth	114
3.6.3 Antimicrobial Susceptibility Test.....	116
3.6.4 β -lactamase Test	118
3.7 Analytical Techniques and Methods.....	119
3.7.1 Cleaning and Desiccation	119
3.7.2 Weighing and Precision.....	120
3.7.3 Interval Wear Volume and Wear Rate.....	122
3.7.4 Surface Characterization.....	122
3.8 Statistical Analysis.....	123
3.8.1 Univariate Analysis	123
3.8.2 Multiple Linear Regression Analysis	125
Chapter 4: Clinical Investigations: Results, Analysis and Discussion	127
4.1 Introductory Remarks	127
4.2 Retrieval Analysis: Part 1, A Comparison Between Grading Methods.....	128
4.2.1 Introductory Remarks	128
4.2.2 Preliminary Data Exploration	129
4.2.3 Multiple Linear Regression Analysis	134
4.2.4 Discussion.....	137
4.2.5 Concluding Remarks	139
4.3 Retrieval Analysis: Part 2, Factors Influencing BDS	140
4.3.1 Introductory Remarks	140
4.3.2 Preliminary Data Exploration	140
4.3.3 Multiple Linear Regression Analysis	144
4.3.4 Univariate Analysis	148
4.3.5 Surface Characterization.....	149
4.3.6 Melt-Annealing.....	158
4.3.7 Discussion on Retrieval Analysis	163
4.3.8 Discussion on Implant Design Issues	163
4.3.9 Discussion on Surface Characterization	168
4.3.10 Discussion on Melt-Annealing	169

4.3.11 Concluding Remarks	169
4.4 Lubricant Composition	170
4.4.1 Introductory Remarks	170
4.4.2 Protein Concentration	170
4.4.3 Electrophoresis	171
4.4.4 Osmolality.....	175
4.4.5 Trace Elements	177
4.4.6 Discussion.....	178
4.4.7 Concluding Remarks	180
Chapter 5: <i>In vitro</i> Investigations: Results, Analysis and Discussion	181
5.1 Introductory Remarks	181
5.2 Simulator Commissioning Tests	182
5.2.1 Introductory Remarks	182
5.2.2 Soak Testing	183
5.2.3 Discussion of Soak Testing	187
5.2.4 Concluding Remarks for Soak Testing.....	189
5.2.5 Wear Testing.....	190
5.2.6 Discussion of Wear Testing.....	194
5.2.7 Concluding Remarks on Wear Testing.....	198
5.2.8 Biochemical Testing of the Lubricating Fluid.....	199
5.2.9 Discussion of Biochemical Testing	204
5.2.10 Concluding Remarks for Biochemical Testing.....	209
5.3 The Effects of Calf Sera on Wear, Protein Degradation, and Bacterial Growth	211
5.3.1 Introductory Remarks	211
5.3.2 Wear.....	211
5.3.3 Protein Degradation	216
5.3.4 Protein Degradation versus Time	218
5.3.5 Electrophoresis	220
5.3.6 Peptide Concentration.....	223
5.3.7 pH	224

5.3.8 Bacterial Growth and Peptide Concentration	225
5.3.9 Discussion of Wear	231
5.3.10 Discussion of Protein Degradation and Electrophoresis	234
5.3.11 Discussion of Boundary Lubrication	236
5.3.12 Discussion of Bacterial Growth and Inhibition	242
5.3.13 Concluding Remarks	244
5.4 Effects of HA Additions and Osmolality Levels on PE Wear	245
5.4.1 Introductory Remarks	245
5.4.2 Wear	245
5.4.3 Protein Concentration and Electrophoresis	250
5.4.4 Peptide Concentration	255
5.4.5 Microbial Resistance	257
5.4.6 Differential Scanning Calorimetry	260
5.4.7 Scanning Electron Microscopy	265
5.4.8 Femoral Surface Roughness Measurements	268
5.4.9 Surface Profiles	270
5.4.10 Discussion of the Mass Gain Period	273
5.4.11 Discussion on the Effects of HA on PE Wear	273
5.4.12 Discussion on the Effects of Osmolality on PE Wear	280
5.4.13 Discussion on Clinical Relevance of the PE Wear Rates	282
5.4.14 Discussion on Microbial Resistance and Countermeasures	284
5.4.15 Concluding Remarks	289
Chapter 6: Conclusions and Future Work	291
6.1 Clinical Investigations	291
6.2 <i>In vitro</i> Investigations	292
References	299
Appendices	344
Appendix A: BDS following the Hood-method	344
Observer 1	344
Observer 2	346

Appendix B: BDS following the Modified-method.....	348
Observer 1.....	348
Observer 2.....	350
Appendix C: Statistical Analyses.....	352
Tests for Normality.....	352
Correlation Analysis.....	352
Regression Analysis.....	352
Paired Samples Analysis.....	353
Independent Samples Analysis.....	353
Analysis of Variance.....	354
Nomenclature	355

List of Tables

Table 2.1: The main constituents of synovial fluid (SF) for the healthy patient and for the OA patient ^{31,102}	27
Table 2.2: Properties of three main grades of PE resin used for orthopaedic devices (data adapted from ^{208,210}). For the GUR resins, the first digit “1” stands for polyethylene, the second digit for the presence (“1”) or absence (“0”) of calcium stearate that was used for corrosion resistance, as a whitening agent and as a lubricant to facilitate the extrusion process. The third digit indicates the average molecular weight (“2” for 3.5×10^6 g/mol; “5” for $5.5\text{-}6 \times 10^6$ g/mol). The GUR stands for Granular UHMWPE Ruhrchemie (where Ruhrchemie AG (changed to Hoechst AG and is now known as Celanese AG) was a company in Oberhausen, Germany).	42
Table 3.1: Implant design characteristics and the resultant classification.	70
Table 3.2: Implant characteristics for individual cases (Implant type: P = primary, R = revision; Insert type: CR = posterior cruciate retaining, PS = posterior cruciate substituting).....	72
Table 3.3: Patient features for individual cases (M = male, F = female, IP = implantation period).....	75
Table 3.4: Scoring procedure used with the Hood-method (see Fig. 3.5).	84
Table 3.5: Scoring procedure used with the Modified-method (see Fig. 3.5). ...	84
Table 3.6: Nomenclature and patient characteristics of SF samples.....	87
Table 3.7: Characteristics of four calf sera. Note the difference in constituents.	88
Table 3.8: Lubricants used in the simulator wear tests.	90
Table 3.9: Properties of the antibiotic discs.....	117
Table 3.10: Repeated measurements of the 20 g and 100 g reference weights to establish the precision of the balance.	121
Table 4.1: Comparison of the backside damage score (BDS) values obtained by the two observers.	129
Table 4.2: The BDS values (mean and the SD) for individual damage features found on the surfaces of model A, B and C implants.	133
Table 4.3: MLRA of the BDS from the Hood-method and from the Modified-method.	135

Table 4.4: MLRA of the BDS from the Hood-method.....	135
Table 4.5: MLRA of the BDS from the Modified-method.....	136
Table 4.6: Estimation of the BDS-gradient (and intercept) by linear regressions between BDS and IP for various independent categorical variables (BDS (IP) = BDS gradient (IP) + Intercept).....	143
Table 4.7: Multiple linear regression analysis (MLRA); see the legend at the bottom of the table for an explanation of the various terms.	146
Table 4.8: R_a roughness measured on a new, never implanted model A type PE inserts during the compression test.	162
Table 4.9: Calf sera diluted with either DW or PBS to different amounts to obtain a protein concentration of 17 g/l according to ISO-14243-3 ⁴¹	176
Table 5.1: Illustration of 11 soak tests performed on three AMK [®] inserts each (n = 3)*.....	183
Table 5.2: Illustration of the commissioning protocol (CP) used in the knee wear simulator testing from 0 - 3 Mc.	191
Table 5.3: Test protocol used in additional tests to find causes of peptide generation besides the tribology of the implant contact (BCS lubricant used in all tests).	207
Table 5.4: Test protocol from 0 - 6 Mc.....	212
Table 5.5: Test protocol showing the lubricant compositions and their corresponding osmolality levels.	246
Table 5.6: The zone of inhibition (ZOI) for several antibiotic disks (penicillin (P-10); streptomycin (S-10); carbenicillin (CB-100); tetracycline (CB-30), chloramphenicol (C-30)) incubated on E. cloacae JK-1 collected in Section 5.3 (no exposure to AA) and E. cloacae JK-2 collected in Section 5.4 after being exposed to AA for 5.5 Mc.	259
Table 5.7: Transition midpoint temperatures, T_m , of the DW lubricant, PBS lubricant, HA lubricant, SF 7, SF 8, and SF 18 (n = 3).	264
Table 5.8: Surface roughness measurements (R_a , R_q) for the AMK [®] femoral components.	268
Table 5.9: The lubricant composition used in the present study compared with the composition utilized by DesJardins et al. ¹⁰²	274

List of Figures

- Figure 1.1:** Anatomy of the human knee joint: ligaments, and bearing surfaces. The patella (not shown) articulates in the trochlear groove (from Clarke et al. ⁷).3
- Figure 1.2:** Intraoperative view of a right human knee joint during joint replacement surgery of a 62-year old female patient: a) showing severe cartilage wear on the medial condyle and b) showing the replaced knee joint. The femoral articulation, tibial articulation and the patella were replaced. The patient received a fixed, modular TKR system with PE insert of posterior ligament substituting (PS) design (Genesis II, Smith & Nephew, Memphis, TN). All components were implanted by cemented fixation.....4
- Figure 1.3:** Anterior radiograph of the left knee of a patient following cemented modular TKA (AMK[®], DePuy Orthopaedics Inc., Warsaw, IN). The circled, dark area in a) shows an example of osteolysis on a radiograph; b) intraoperative view the knee joint during revision surgery.....6
- Figure 1.4:** Schematic drawing of two surfaces in relative motion to each other. Some asperity contact may occur and lead to material removal due to adhesion or abrasion, for example.7
- Figure 1.5:** A failed modular TKR system (AMK[®], DePuy Orthopaedics Inc., Warsaw, IN) retrieved from the left knee of a 70-year old male patient (mass of 95 kg) after 5 years of implantation. The implant was initially implanted by cemented fixation and was revised for both severe PE wear and osteolysis.8
- Figure 2.1:** Schematic showing the dependence of the friction coefficient (μ_k) on the lubrication regime (boundary lubrication, mixed lubrication, and fluid film lubrication).14
- Figure 2.2:** Schematic illustration of the polymer chains adsorbed to both substrate surfaces under (a) pristine and (b) after being displaced by a distance δx (from Klein et al. ⁸⁵).22
- Figure 2.3:** (a) Kinetics of thinning of the polymer brush bilayer following the jump into adhesive contact, fitted by exponential decay (solid line). The drawings indicate the proposed configuration of the polymer brush bilayer shortly after the jump-in (left drawing) and at the end of the measurements (right drawing; also note the increase in mean brush-anchor spacing). (b) The lateral motion applied to the upper surface and the transmitted shear force at the lower surface at the points of the time/thickness indicated by corresponding letters in (a): (A) Motion between opposing polymer brushes following the jump-in proceeds with low shear force (from Tsarkova et al. ⁸⁹).24
- Figure 2.4:** Schematic drawing of the human serum albumin structure showing the primary, secondary and tertiary structure (from Sugio et al. ¹⁰³).28

Figure 2.5: Chemical structure of HA. Note that the “disaccharide” chain of HA consists of a glucuronic acid compound and an N-acetyl glucosamine compound.....	30
Figure 2.6: The proposed microstructure of synovial fluid: globular proteins (light grey) aggregate to form a tenuous polymeric network and the long HA chains (dark grey) entangle with this network (from Oates et al. ¹²³).....	30
Figure 2.7: Schematic showing how the wear process may affect the native, folded protein structure. Wear may lead to protein damage and cause protein unfolding, protein precipitation and protein shear.....	34
Figure 2.8: Microstructure of PE: transmission electron microscopy (a) and schematic (b) (from Kurtz et al. ²¹⁰).....	42
Figure 2.9: A failed AMK [®] (DePuy Orthopaedics Inc., Warsaw, IN) in a) intraoperative view during revision surgery and b) the retrieved PE insert. The PE insert was GA sterilized prior to implantation and showed severe delamination wear after its retrieval.....	44
Figure 2.10: Image showing (a) the distal (backside) surface of the PE insert and (b) the proximal surface of the Ti alloy tibial tray of a retrieved TKR system (AMK [®] , DePuy Orthopaedics Inc., Warsaw, IN). Note the wear pattern on the PE insert as well as on the tibial tray possibly caused by insert micromotion and presence of third-body wear particles. Such damage feature was referred to as stippling by Engh et al. ²⁹⁹ and associated with osteolysis.....	53
Figure 2.11: Display of the pathway of direct and indirect osteolysis mediated by wear particles and fluid pressure.....	56
Figure 2.12: Intraoperative view of the discoloured synovium due to excessive wear of the Ti alloy femoral component against PE.....	64
Figure 3.1: Typical backside surfaces of retrieved polyethylene (PE) inserts and their corresponding tibial trays for cases 12, 13 and 51 (see Table 3.1 for specific details). Model A is the AMK [®] , model B is Genesis I and model C is Genesis II [®] . The six regions for damage analysis are shown on the PE insert of the model C implant.....	71
Figure 3.2: Macrograph of a worn PE backside surface showing damage features such as burnishing, grooving, indentations, deformation, and pitting relative to the unworn, pristine machining marks.....	78
Figure 3.3: SEM image of an <i>elongated</i> surface crater possibly due to third-body abrasion. Such elongated craters were characterized as “grooving”.	79
Figure 3.4: SEM image of a <i>round</i> surface crater possibly due to surface fatigue. Such craters were characterized as “pitting”.	79

Figure 3.5: Schematic showing the illustration of 12 cases with 2 different areas of surface damage caused by one damage feature for the backside PE surface. Each of the large circles represents the total surface area. The increased darkness of the grey scales represented increasing damage and thus damage severity factors (DSF). The areas of damage and their severity were included in determining the total BDS for each case (Tables 3.4 and 3.5) ($r_i \equiv$ radius of the inner circle; $r_o \equiv$ radius of the outer circle).....81

Figure 3.6: The damage score for the cases 1 - 12 obtained with the Hood-method and the Modified-method. Note the similarities between the damage score obtained with either method for mode 9 - 11 (small surface damage) and higher damage score for Modified-method.....85

Figure 3.7: The left (L) bank of the AMTI knee simulator (AMTI, Waltham, MA). The stations L1, L2, and L3 are the wear stations (dynamic) while L4 and L5 are the load-soak (LS) stations (only vertical loading, no motion).....91

Figure 3.8: Image showing station L2 of the AMTI knee simulator (AMTI, Waltham, MA) with the following components: (1) an intravenous (IV) bag that contains the lubricant; (2) an externally located and heated fluid container; (3) a peristaltic recirculation pump; (4) a data transfer ribbon cable; (5) a PE hose that is connected to the IV bag and used to supply pressurized air to inflate the bag; (6) a thermo couple connected to the wear station to measure the lubricant temperature.93

Figure 3.9: Schematic of the control function for the vertical load implemented in the knee simulator.....95

Figure 3.10: Vertical loading for level walking according to ISO 14243-3. Note the loading pattern during the stance phase and the constant low loading during the swing phase.....96

Figure 3.11: The anterior/posterior (AP) linear displacement according to ISO 14243-3.97

Figure 3.12: The flexion/extension (FE) and internal/external (IE) angular displacements according to ISO 14243-3.97

Figure 3.13: The AMK[®] total knee system (DePuy Orthopaedics Inc., Warsaw, IN). The patella was not used in the wear tests.....99

Figure 3.14: Schematic of lubricant protein precipitation and centrifuging. The fresh unworn lubricant is referred to as the starting material (SM). After the wear test the worn lubricant contains suspended protein precipitates. Centrifuging the worn lubricant separates the protein precipitates from the remaining lubricant (supernatant; SUP) in from of a compacted pellet.....101

Figure 3.15: Procedure summary of running a BCA protein assay.103

Figure 3.16: Sieving of proteins by a porous polyacrylamide gel (reproduced from ³⁹⁸).	104
Figure 3.17: Image showing the characteristic migration pattern of a SF sample for the Hydragel 30-β1-β2 gel ³⁹⁹ .	105
Figure 3.18: The effect of shear and enzymatic digestion on the protein structure. The native proteins (polypeptides) change from a globular conformation into small protein chunks, referred to as peptides.	106
Figure 3.19: Peptide concentration of worn BCS determined in five separate VIVASPIN tubes to determine the accuracy and precision of the measurements (MWCO = 2,000 Da).	107
Figure 3.20: Schematic showing the principle of an irreversible unfolding process of a globular protein. Exposure to a heat source causes the protein to unfold from and to take on a random coil like structure.	109
Figure 3.21: Schematic representation of a thermogram.	110
Figure 3.22: The microbial growth behaviour versus incubation period shown for an example bacterium. Note the four characteristic phases of bacterial growth: lag, exponential, stationary and death.	115
Figure 3.23: Schematic diagram showing the antimicrobial susceptibility test. Disk A and disk B represent antimicrobial disks; the zone of inhibition (ZOI) is larger for A than for B; agent in disk A more effective than B in inhibiting bacterial growth.	118
Figure 3.24: Image showing the β-lactam antibiotic structure for penicillin. The arrow indicates the site where the antibiotic can be neutralized by β-lactamase, generated by the microbe (from ¹⁹⁵).	119
Figure 4.1: Backside damage score (BDS) obtained from the Hood-method and the Modified-method correlated with the implantation period (IP).	130
Figure 4.2: Backside damage score (BDS) for the three implant models analyzed with both damage assessment methods. Level of significance for each interaction term $p = 0.05/3 = 0.016$ following the Bonferroni-correction for multiple pair wise comparisons	131
Figure 4.3: Backside damage score (BDS) for the interaction between sterilization and gender (Sterilization*Gender) which resulted in four interactions terms such as GA*M, GA*F, NGA*M, and NGA*F. Level of significance for each interaction term $p = 0.05/4 = 0.012$ (Bonferroni-correction).	132

Figure 4.4: Standardised residuals obtained for the MLRA using the BDS from the Hood-method and from the Modified-method.....	136
Figure 4.5: Linear correlations of BDS versus IP for implant models A, B, and C.....	141
Figure 4.6: BDS grouped by implant model and gender.....	142
Figure 4.7: BDS grouped by sterilization techniques and gender.....	142
Figure 4.8: The backside damage scores of individual damage features grouped by implant model A, B and C.....	148
Figure 4.9: SEM image in SE mode of the backside of a PE insert from a model A implant (case 2; see Section 3.2 and for specific details) that had a polished tibial tray. Note the presence of ripples (aligned rows of nodules), dispersed smeared nodules and submicron pulled-out fibrils. This appearance was characteristic for the burnishing damage feature, most abundant on PE inserts from polished tibial trays.....	149
Figure 4.10: SEM image in SE mode of the backside of a PE insert from a model B implant (case 27): (a) at the circumference (anterior direction \equiv top of page).....	150
Figure 4.11: SEM image in SE mode of an individual stippling mark on the tray surface of a model B implant (case 27).	152
Figure 4.12: SEM image: (a) a retrieved model B tray (case 26) with the dark area rich in carbon and (b) a model B new, never implanted tibial tray (done in the BSE mode) with the dark area rich in silicon and oxygen (anterior direction \equiv top of page).	153
Figure 4.13: EDX spectra at 15 keV of (a) the carbon rich area on a retrieved model B tray (case 26), (b) the silicon and oxygen rich area on an as-manufactured model B tibial tray.	154
Figure 4.14: EDX mapping on a specific area conducted on the as-manufactured tibial tray: (a) the surface image taken in the BSE mode and specifically running the EDX mapping for (b) silicon.....	156
Figure 4.15: Surface profile of the retrieved model A implant PE inserts before melt-annealing: (a) retrieved and (b) the magnified area.....	159
Figure 4.16: Surface profile of the retrieved model A implant PE inserts after melt-annealing: (a) retrieved and (b) the magnified area.....	160

Figure 4.17: Linear surface scans taken on the backside surface of a new, never implanted model A insert: (i) before the compression tests (72 h pre-conditioned in PBS at 37 °C), (ii) after the compression test (48 h “relaxed” in PBS at 37 °C), and (iii) after melt annealing. During the compression test, a static vertical load of $F_n = 4000$ N was applied to the PE insert for 336 h.	162
Figure 4.18: Protein concentration of the SF samples collected from patients 1 - 20.	171
Figure 4.19: Electrophoretic profiles of six SF samples (patient SF 20) and six hyaluronidase samples. Note the migration of hyaluronidase towards albumin in the gel.....	172
Figure 4.20: The <i>measured</i> fractions and the <i>corrected</i> fractions of albumin, α -1-globulin, α -2-globulin, β -globulin, and γ -globulin.	173
Figure 4.21: The corrected fraction of albumin, α -1-globulin, α -2-globulin, β -globulin, and γ -globulin for the male patients (n = 10) and the female patients (n = 10).....	174
Figure 4.22: The fraction of albumin, α -1-globulin, α -2-globulin, β -globulin, and γ -globulin for the corrected SF (n = 20) and the calf sera such as BCS, NCS, ACS, and ACS-I according to the manufacturer (HyClone, Logan, UT).....	174
Figure 4.23: Osmolality of the SF samples collected from patient 1 - 20.	175
Figure 4.24: The osmolality for all SF samples, the undiluted calf sera (100 % BCS, 100 % NCS, 100 % ACS, 100 % ACS-I), and calf sera diluted with DW (BCS + DW, NCS + DW, ACS + DW, ACS-I + DW) and PBS (BCS + PBS, NCS + PBS, ACS + PBS, ACS-I + PBS) to a protein concentration of 17 g/l.	176
Figure 4.25: The trace element concentration of Ca, Mg, inorganic P, and Fe for SF, 100 % BCS, 100 % NCS, 100 % ACS, and 100 % ACS-I.....	177
Figure 5.1: The fluid uptake of PE inserts soaking in DW at RT. Note the increased fluid uptake for the disturbed inserts over the undisturbed inserts and GA inserts over GP inserts.....	184
Figure 5.2: The mass gain of PE inserts submersed in DW at RT. The RT dropped from 25 °C to 21 °C three times during the 46 days and this drop was associated with some temporary mass loss. The changes in RT occurred during power surges in the laboratory.....	185
Figure 5.3: The mass gain of PE inserts submersed in DW and in the BCS lubricant at RT and 37 ± 2 °C of GP, 14 mm insert. The inserts were either left undisturbed or were repeatedly disturbed for 46 days. Note the increased mass gain for PE inserts subjected to the BCS lubricant, increased temperature and repeated disturbances.....	186

Figure 5.4: The total mass gain (fluid uptake) of GA inserts soaked in DW or PBS at 37 °C undisturbed for 46 days. There was no significantly different between groups despite the higher osmolality of PBS (286 ± 0.57 mmol/kg) compared with DW (46 ± 2.08 mmol/kg).....189

Figure 5.5: The wear of (a) the L implants (L1, L2, and L3) and b) the R implants (R1, R2, and R3) during the commissioning protocol (CP) wear tests. The least squares linear-regression lines were fit through the wear data from 0.5 - 3 Mc. The interval from 0 - 0.5 Mc was regarded as the “run-in” phase.192

Figure 5.6: Interval wear volume of the L implants and the R implants during the 6 test intervals from 0 - 3 Mc. Note that the interval wear volumes of the L implants and R implants were significantly different between 1.5 - 2 Mc and 2 - 3 Mc ($p \leq 0.036$, ANOVA and Fisher’s).193

Figure 5.7: The average fluid uptake behaviour of the L4 and L5 implants and the R4 and R5 implants located in the LS stations (4 and 5; 9 and 10) from 0 - 3 Mc.193

Figure 5.8: Illustration of wear rates obtained with the commissioning protocol (CP) and the wear rate found by DePuy in a 3 - 5 Mc interval for AMK[®] implants (GP, 10mm, GUR 1050). There was no significant difference between the wear rate of the R implants from 2 - 3 Mc and the DePuy wear rate ($p = 0.053$, ANOVA and Fisher’s).....195

Figure 5.9: The AP force for (a) the L implants and (b) the R implants at test intervals of 1 Mc, 2 Mc, and 3 Mc.....197

Figure 5.10: The vertical load FB of the L bank and the R bank at 3 Mc in reference to the vertical load waveform recommended by ISO. Note the distinct differences in vertical load between banks at approximately 8 % of the gait cycle.198

Figure 5.11: The protein degradation determined for each implant (L1, L2, L3, R1, R2, and R3) after the test interval of 2.5 - 3 Mc.200

Figure 5.12: The peptide concentration of the starting material (SM) and implant-specific supernatant (SUP) for the BCS lubricant after a test interval of 2.5 - 3 Mc.....202

Figure 5.13: Schematic showing the settling out of protein precipitates in the BCS lubricant after 0.5 Mc compared with the BCS lubricant at 0 Mc. Such settling out of precipitated proteins led to obvious deposits in the each external fluid container after each test interval of 0.5 Mc. Note that the nozzle connected to the pump did not reach completely to the bottom of the fluid container.....202

Figure 5.14: The protein precipitate concentration of the BCS lubricant samples obtained from the wear stations and the external fluid containers for the L implants and the R implants.....	203
Figure 5.15: Micrograph showing the isolated bacterium <i>Enterobacter Cloacae</i> JK-1 (<i>E. cloacae</i> JK-1) present in the BCS lubricant after the test interval of 2.5 - 3 Mc.....	204
Figure 5.16: The peptide concentration of the BCS lubricant samples used in the additional tests described in Table 5.3. These tests were conducted to isolate sources that increased the peptide concentration besides the tribology of the implant contact.....	208
Figure 5.17: Schematic of the BCS lubricant at (a) 0 Mc and (b) after a test interval of 0.5 Mc. Note the presence of proteins, peptides and perhaps enzymes suspended in the fluid at 0 Mc. The characteristics of the BCS lubricant at 0.5 Mc were vastly different, showing precipitates (degraded, clustered proteins), more peptides (suspended protein chunks) and bacterial contamination (<i>E. cloacae</i> JK-1).....	210
Figure 5.18: The wear behaviour of the (a) L implants (L1, L2, L3) and (b) R implants (R1, R2, R3) during 0.5 - 6 Mc.....	213
Figure 5.19: The wear rates of (a) the L implants and (b) the R implants obtained after the wear tests during 0.5 - 6 Mc.	214
Figure 5.20: The correlation of wear rates with initial combined albumin + α -globulin fraction for the lubricants. Each data point represents the value obtained from a single wear test.	215
Figure 5.21: The protein degradation of (a) the L implants and (b) the R implants.....	217
Figure 5.22: The correlation of protein degradation during the wear tests with initial combined β -globulin + γ -globulin fraction. Four protein degradation values were determined for each wear station and so each data value above represents a single value.	218
Figure 5.23: Protein degradation measured every 0.1 Mc during a test interval of 0.5 Mc for the BCS lubricant, NCS lubricant, and ACS lubricant. The data points represent the mean value accompanied with their standard deviation....	219
Figure 5.24: Electrophoresis results for the starting material (SM) at the beginning of the test interval (0 Mc) and for the supernatants (SUPs) at the end of a test interval (after 0.5 Mc) for the BCS lubricant, NCS lubricant, and ACS lubricant.	221

Figure 5.25: The protein constituent fractions for the starting material (SM) at 0 Mc and the supernatant (SUP) after 0.5 Mc for each implant: (a) the BCS lubricant and (b) the NCS lubricant.....	222
Figure 5.26: The peptide concentration of the starting material (SM) and implant specific SUP (SUP1, SUP2, and SUP3) for all serum lubricants.....	224
Figure 5.27: The pH for the serum lubricants at the start (0 Mc) and at the end of a test interval (0.5 Mc).....	225
Figure 5.28: Images showing the L implants located at the L bank of the knee simulator for the serum lubricants with SA.....	226
Figure 5.29: The colony-forming units per ml serum (CFU/ml) for the BCS, NCS and ACS lubricants though a test interval from 0 - 0.5 Mc. Note that there was no bacterial growth at test initiation test but this could not be plotted above because the vertical axis had a log scale.....	227
Figure 5.30: Images showing the incubated LB agar dishes after they were plated with serum sample from (a) the BCS lubricant and (b) the NCS lubricant obtained after 0.5 Mc. Serum samples were diluted with LB buffer to allow the count of colony forming units.....	228
Figure 5.31: The protein degradation for BCS + DW, NCS + DW, and ACS + DW when either SA or AA was used as the microbial inhibitor. Note that the protein degradation was not different for NCS + DW and ACS + DW.....	230
Figure 5.32: The peptide concentration of the serum lubricants after 0.5 Mc when SA was replaced with AA as the microbial inhibitor.....	230
Figure 5.33: The protein concentrations of the starting material (SM) for the serum lubricants that were measured prior to the various test intervals.....	233
Figure 5.34: Graph showing the mass gain of the LS stations for the L implants (L4, L5) and the R implants (R4, R5). Note the mass loss during the interval from 3 - 3.5 Mc and from 4.5 - 5 Mc when the lubricant was changed between wear tests.....	234
Figure 5.35: The correlation between the protein degradation and the wear rates. Each data point represented a single protein degradation measurement taken from one station.....	235
Figure 5.36: A summary of the protein constituent degradation for the serum lubricants.....	236

Figure 5.37: Schematic of the protein constituents at the CoCr-PE interface: a) heterogeneous distribution of proteins when the normal force (F_n) is zero and some protein constituents are absorbed on the CoCr and PE surface; b) the protein constituents are compacted when the surfaces approach each other when F_n increases. This speculative model was based on the model by Georges et al. ⁹² for a thin colloid layer. The arrows indicate the direction of surface motion....	238
Figure 5.38: Magnified view of the compacted protein layer proposed in Fig 5.37.b. Protein adsorption may have led to protein-substrate bonds. Increased F_n may have been associated with interpenetration of protein constituents which may have led to entangled protein chains. The arrows indicate the direction of surface motion.....	239
Figure 5.39: The AP force for the serum lubricants.	241
Figure 5.40: The relationship between the initial β - γ -globulin concentrations and the colony forming units (CFU/ml) for three types of calf sera.....	243
Figure 5.41: The wear behaviour for (a) the L implants (L1, L2, and L3) and (b) R implants (R1, R2, and R3) from 0 - 2 Mc. Note the negative wear volume due to PE mass gain during the initial 1 Mc.	247
Figure 5.42: The wear behaviour of the (a) L implants (L1, L2, and L3) and (b) R implants (R1, R2, and R3) from 1 - 5.5 Mc.	248
Figure 5.43: The lubricant temperature in the wear stations of the L implants (L1, L2, and L3) and R implants (R1, R2, and R3) at 3.5 Mc and at 5 Mc.	249
Figure 5.44: The AP force for the L implants and the R implants tested with the PBS lubricants after 3.5 Mc.	250
Figure 5.45: The protein concentrations for (a) the L implants and (b) the R implants.....	252
Figure 5.46: The protein constituent fractions for the L implants after a test interval of 0.5 Mc: (a) the PBS lubricant and (b) the HA lubricant.....	253
Figure 5.47: The protein constituent fractions for the R implants after a test interval of 0.5 Mc: (a) the PBS lubricant and (b) the DW lubricant.....	254
Figure 5.48: The protein constituent degradation for the serum lubricants.....	255
Figure 5.49: The peptide concentration of the SM and the SUPs.....	256
Figure 5.50: The wear rate plotted versus the relative change in peptide concentration (peptide conc. "SUP" minus peptide conc. "SM").....	257

Figure 5.51: The MH-plates incubated with a) *E. cloacae* JK-1 collected in Section 5.3 (no exposure to AA). Note that *E. cloacae* JK-1 was resistant towards penicillin (P-10) and carbenicillin (CB-100).258

Figure 5.52: Thermogram of (a) the DW lubricant and (b) the PBS lubricant. Note the differences between the shapes of the curves of the DW lubricant and the PBS lubricant.261

Figure 5.53: Thermogram of (a) the HA lubricant and (b) SF 7. Note the differences between the shapes of the curves of the HA lubricant and SF 7.....262

Figure 5.54: Thermogram of SF 8 and SF 18. Note the similarity between the shapes of the curves of SF 8 and SF 18.263

Figure 5.55: The change in enthalpy, ΔH , for the DW lubricant, the PBS lubricant, the HA lubricant and SF (SF 7, SF 8, SF 18). Note the similarity in magnitude between the HA lubricant and SF.264

Figure 5.56: The change in entropy, ΔS , for the DW lubricant, the PBS lubricant, the HA lubricant, and SF (SF 7, SF 8, SF 18). Note the similarity between the HA lubricant and SF.265

Figure 5.57: SEM micrographs showing typical surface features on a) an as-received cast femoral component and b) a retrieved cast femoral component (IP = 102.05 months). Note the voids on the as-received femoral components and the pits on the retrieved femoral component (anterior direction \equiv top of page).266

Figure 5.58: SEM micrographs showing typical surface features on (a) a cast femoral component of the L implants (L2; worn with ACS-I + PBS + AA and ACS-I + PBS + AA + HA) and (b) a cast femoral component of the R implants (R2; worn with ACS-I + PBS + AA and ACS-I + DW + AA) after 5.5 Mc. Note the pitting in both micrographs (anterior direction \equiv top of page).267

Figure 5.59: Surface roughness for several femoral components.....269

Figure 5.60: Surface profile obtained with the WYCO profilometer (anterior direction \equiv top of page).....271

Figure 5.61: Surface profiles obtained with the WYCO profilometer after 5.5 Mc. Note the scaling difference between the surface profiles of (a) and (b), confirming the rougher surface for the R implants (anterior direction \equiv top of page).....272

Figure 5.62: Schematic showing the possible protein interactions in the protein layer at the CoCr-PE interface for ACS-I + PBS + AA and ACS-I + PBE + AA + HA during the wear test. Adding HA to ACS-I + PBS + AA increased the thermal stability of the lubricant. It was speculated that ACS-I + PBS + AA + HA was less ductile under load and motion than ACS-I + PBS + AA due to the protein-HA network. The limited ability of ACS-I + PBS + AA + HA to dissipate plastic deformation possibly led to higher temperature and higher shear inside the protein layer and increased the protein degradation and the peptide concentration despite its higher thermal stability compared with ACS-I + PBS + AA. It was speculated that such a conditions were comparable to the *kneading effect*, which is known to occur in ductile metals under high shear forces⁴⁵¹ and in polymer processing equipment⁴⁵² and was deemed responsible for the higher PE wear rate for ACS-I + PBS + AA + HA compared with ACS-I + PBS + AA. The arrows indicate the direction of surface motion.277

Figure 5.63: The AP force for the L implants tested with ACS-I + PBS + AA after 3.5 Mc and tested with ACS-I + PBS + AA + HA after 5 Mc. Note the higher AP force for the L implants at approximately 20 % gait cycle and 45 % gait cycle which may have been responsible for the higher wear rate for the L implants.279

Figure 5.64: The protein constituent fractions for the SF_{mix} starting material (SM; protein concentration = 30.90 ± 1.24 g/l) and the SF_{mix} supernatant (SUP; 25.98 ± 1.31 g/l) after a test interval 5,000 cycles. Note that all protein sub-constituents wear affected by the wear process.279

Figure 5.65: Schematic showing the possible protein interactions in the protein layer at the CoCr-PE interface for ACS-I + PBS + AA and ACS-I + DW + AA during the wear test. The higher protein constituent degradation and peptide concentration for the latter lubricant may have been initiated by diluting the ACS-I + AA with DW. The proteins in DW had a lower T_m, ΔH, and ΔS than the proteins in PBS and thus were deemed to have a lower conformational stability. Such lower conformational stability possibly caused more entanglements between protein chains which may explain the higher peptide concentration ACS-I + DW+ AA compared with ACS-I + PBS + AA after wear testing. Such circumstances may explain the higher PE wear rate obtained with ACS-I + DW + AA compared with ACS-I + PBS + AA used as the lubricant. The arrows indicate the direction of surface motion.281

Figure 5.66: The AP force for the R implants tested with ACS-I + PBS + AA after 3.5 Mc and tested with ACS-I + DW + AA after 5 Mc. Note the higher AP force for the R implants at 30 % gait cycle to 45 % gait cycle.282

Figure 5.67: Image showing the positive response (pink color) of the Cefinase[®] disk placed on *E. cloacae* JK-2 grown on LB agar. Cefinase[®] disk was placed on incubated *E. coli* ML35 as a control and showed no discoloration of the Cefinase[®] disk (negative response; not shown).284

Figure 5.68: Schematic of a microbe showing the chromosome, plasmid and flagellum.	285
Figure 5.69: Schematic of the two-phase life cycle of <i>Bdellovibrio</i> , which consists of a free-swimming phase in a solvent and a growth phase inside its Gram-negative prey bacterium ¹⁹³ (Max Planck Institute for Developmental Biology, Tübingen, Germany).	287
Figure 5.70: Turbidity measurements of HM-buffer with both <i>E. cloacae</i> JK-2 with AA and <i>E. cloacae</i> JK-2 + <i>Bdellovibrio</i> . The turbidity in Klett units is an indicator of the number <i>E. cloacae</i> JK-2 in the HM buffer. Note the decrease in turbidity for when <i>E. cloacae</i> JK-2 was doped with <i>Bdellovibrio</i> (1 Klett unit $\approx 5 \times 10^6$ CFU/ml). Such decrease in turbidity indicated that <i>Bdellovibrio</i> was able to prey on <i>E. cloacae</i> JK-2.	288
Figure 6.1: Wear rates for serum lubricants that did not have HA or PBS in them.	293
Figure 6.2: Wear rates for serum lubricants that included PBS with or without HA.	294
Figure 6.3: Wear rates for serum lubricants diluted with PBS or DW.	294
Figure 6.4: The peptide concentration for various ACS lubricants.	296
Figure 6.5: Wear rates for ACS with either SA or AA.	296
Figure 6.6: Schematic showing a CoCr-PE asperity in contact.	298

Chapter 1: Introduction

1.1 Total Knee Replacements and Implant Wear

The healthy human knee is a synovial joint consisting of articular surfaces that are covered with cartilage. The adjacent ligaments and muscles ensure the stability of the joint and the collagen-rich menisci dissipate the load (Fig. 1.1). The articulating cartilage surfaces are lubricated by synovial fluid (SF) in a sterile environment. SF is a protein-rich fluid that contains a variety of dissolved chemical substances, such as NaCl and hyaluronic acid (HA), which are responsible for the level of osmolality and the viscosity of SF, respectively. The integrity of cartilage lubrication may be compromised by trauma or various forms of arthritis such as osteoarthritis (OA) and/or rheumatoid arthritis (RA), leading to damage of the cartilage bearing surface. Such damage is often followed by structural degradation and wearing away of the cartilage so that direct bone-on-bone contact can occur (Fig 1.2). Cartilage degradation may be facilitated by increased patient age, mass and level of activity. Severe degradation is frequently referred to as end-stage arthritis and is associated with severe pain and reduced joint function for the patient. Immobility can cause an increase in patient weight leading to obesity and consequently lead to coronary heart disease that advocates morbidity ¹.

In order to eliminate pain and restore joint function, the worn bearing surfaces of the knee can be replaced with artificial bearing materials such as a total knee replacement (TKR) ^{2,3}. Depending on the age of the patient, end-stage arthritis location and severity, partial surface replacements such as uni-condylar knee replacements or patella-femoral (trochlear) replacements may alternatively be chosen. In 2005, approximately 450,000 TKRs were implanted in the US alone ⁴ and approximately 60,000 in Canada ². It was estimated that the number of patients undergoing TKR surgery (referred to as total knee arthroplasty; TKA) will increase by 673 % to 3.48 million procedures by 2030 ⁴.

At present, the majority of TKR systems are implanted by cemented fixation which has been shown to extend the durability ^{2,3}. Replacing the

natural, somewhat shock-absorbing knee joint with an artificial, stiffer bearing material reduces the effective contact area, depending on the TKR system ⁵. Today's TKR systems are categorized into either *fixed* or *mobile* bearings both of which consist in most cases of a cast cobalt-chrome alloy (CoCr alloy) femoral component. Fixed bearings are either classified into modular or non-modular systems. In modular systems, the ultra-high molecular weight polyethylene (PE) tibial component is locked onto a cast titanium alloy (Ti alloy) or a cast cobalt-chromium alloy (CoCr alloy) tibial tray at time of implantation and can be removed and replaced during surgery. In non-modular systems, the PE insert may consist of a mono-block component or a one-piece, metal-backed PE insert both of which are fixed by cement directly onto the tibia. In contrast, mobile bearings are characterized by a PE insert that is not solidly fixed onto the tibial tray but is able to translate or rotate. Such implants may have highly conforming articulations which reduce the contact pressure on the tibial PE inserts and wear ⁶. According to the Swedish Arthroplasty Registry ³, modular TKR systems represented the majority of implants used to treat end-stage arthritis in 2006. The patella can either be replaced or left non-resurfaced, independent of the TKR system.

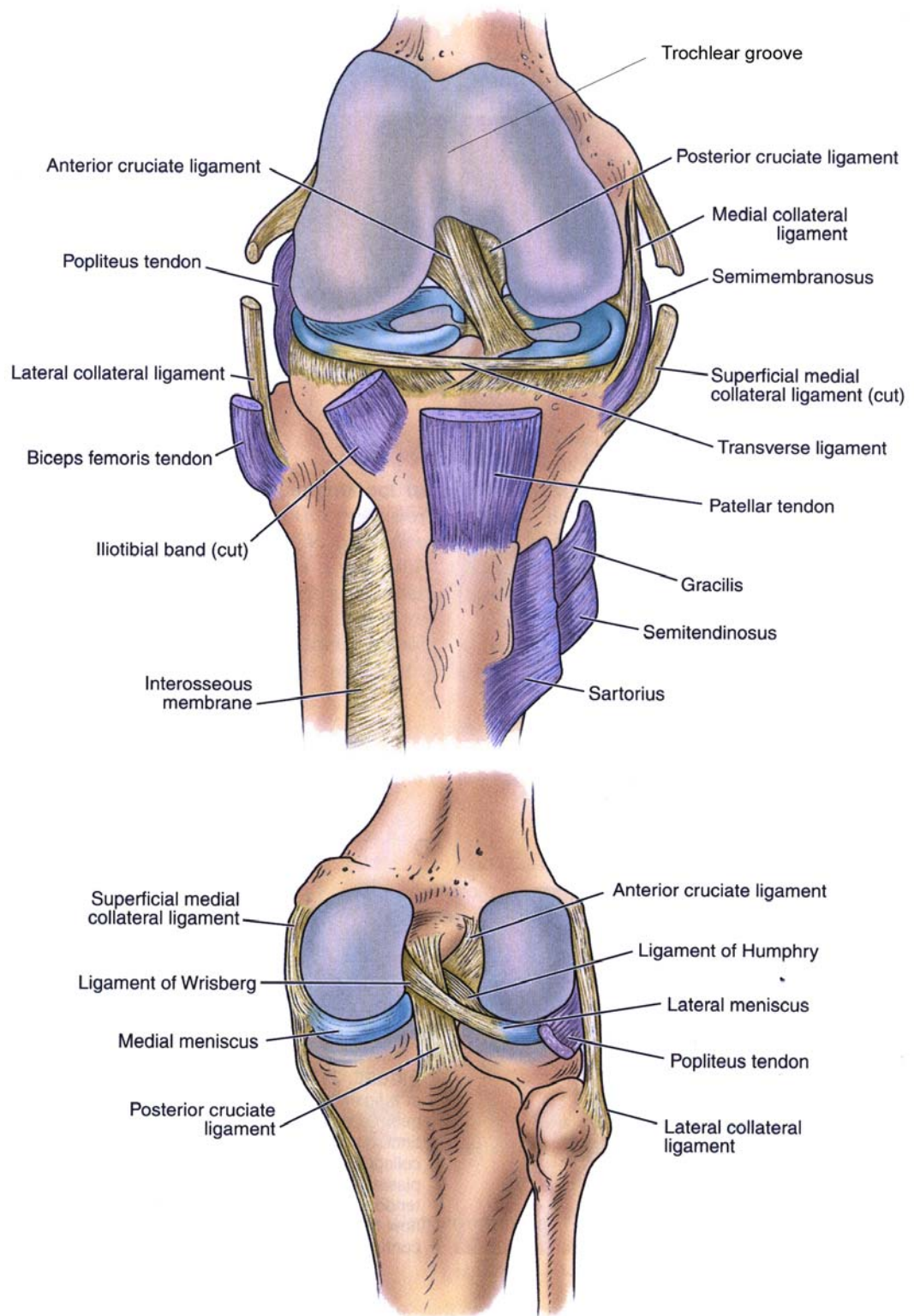
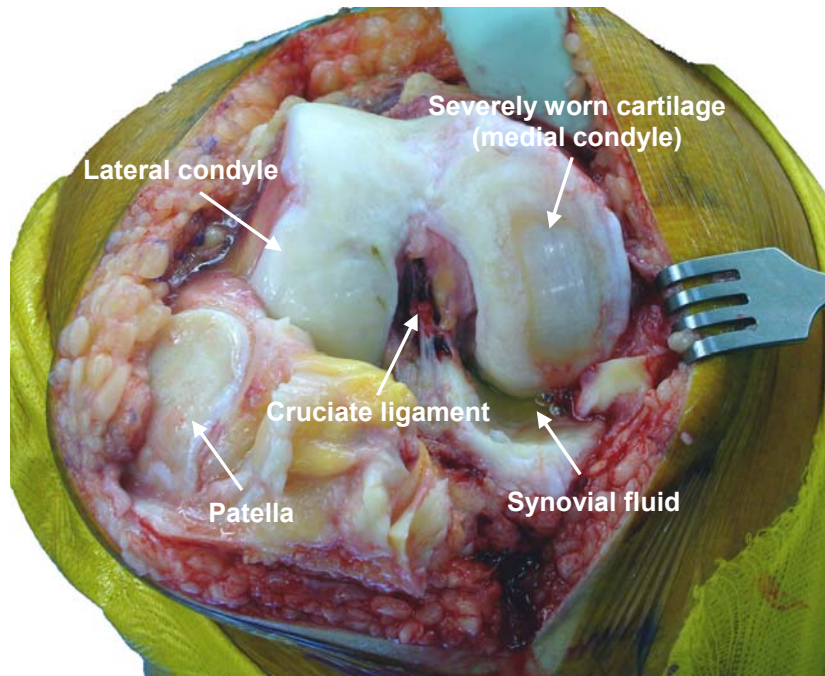
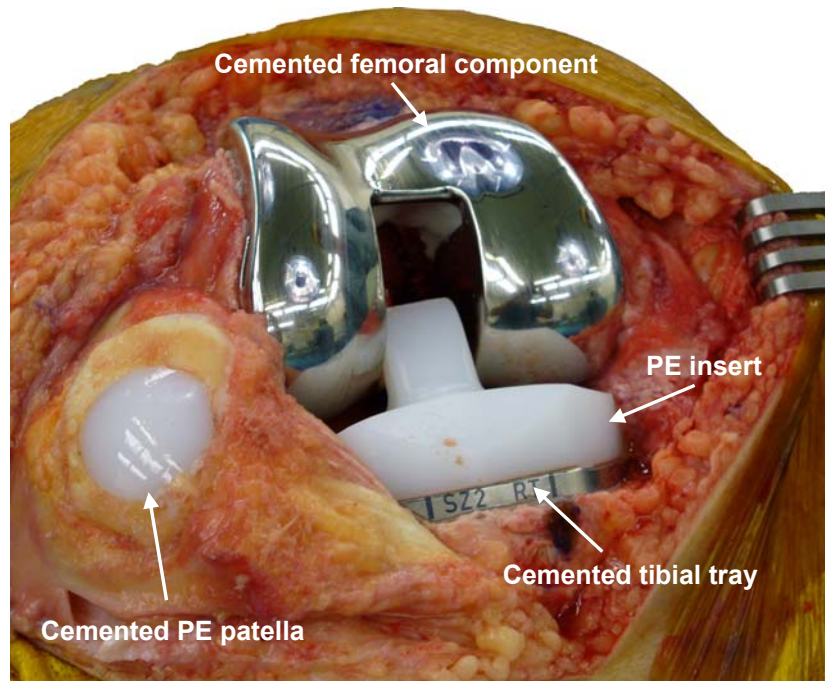


Figure 1.1: Anatomy of the human knee joint: ligaments, and bearing surfaces. The patella (not shown) articulates in the trochlear groove (from Clarke et al. ⁷).



(a)

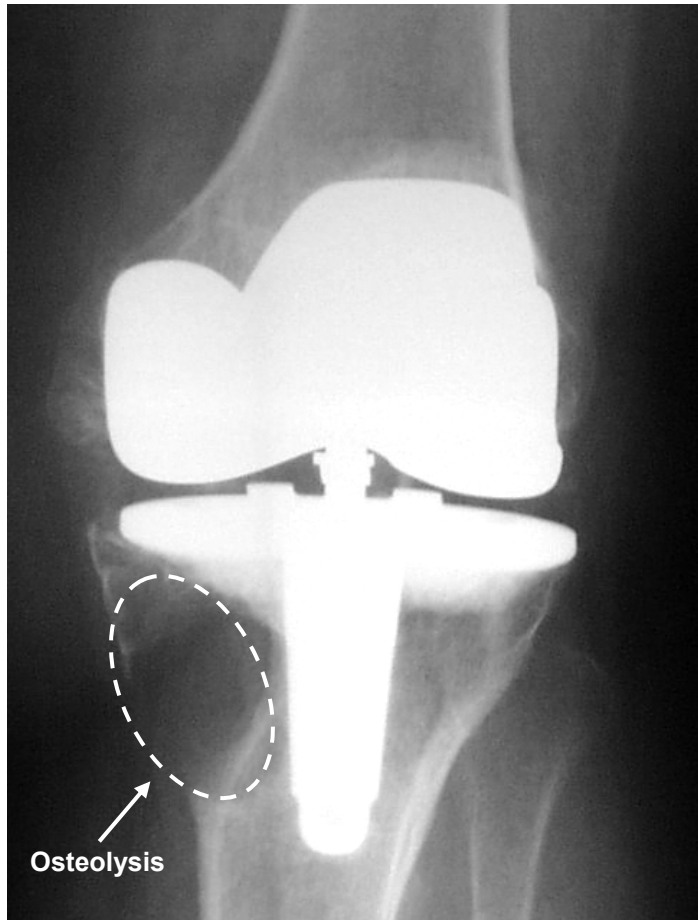


(b)

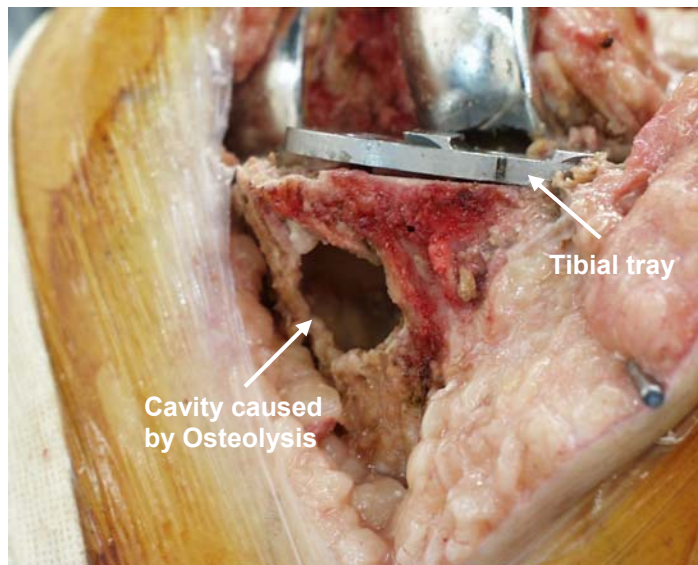
Figure 1.2: Intraoperative view of a right human knee joint during joint replacement surgery of a 62-year old female patient: a) showing severe cartilage wear on the medial condyle and b) showing the replaced knee joint. The femoral articulation, tibial articulation and the patella were replaced. The patient received a fixed, modular TKR system with PE insert of posterior ligament substituting (PS) design (Genesis II, Smith & Nephew, Memphis, TN). All components were implanted by cemented fixation.

Ninety percent of the patients that received a TKR performed well after ten years^{4,8}. However, there is a remaining group of 10 % for which the TKA is not successful and require revision surgery (Fig. 1.3)⁹. A number of different circumstances can lead to revision surgery and may be characterized into early failure and late failure^{8,9}. Early failure (~ 2 years after implantation) includes mainly infection, ligament imbalance, and insufficient knee flexion. Late failure (~ 7 years) includes severe fatigue wear of the PE insert due to gamma-in-air (GA) sterilization, implant loosening, and instability. Implant loosening is dominantly caused by wear particle-induced bone resorption (osteolysis) around the implant fixation. Osteolysis is governed by both an immunological reaction of the body to insidious wear particles and elevated fluid-pressure due to implant micro-motion¹⁰⁻¹². Such a reaction obliterates the bone adjacent to the implant, leading to compromised fixation and even further accelerated osteolysis. However, osteolysis is often detected around apparently well-fixed implants and thus implant wear is probably the most dominant root cause. In many cases, multiple mechanisms of implant failure may occur simultaneously and thus, the *dominant* reason of failure is difficult to establish. Severe PE wear may lead to both osteolysis-mediated implant loosening and instability. Osteolytic regions have a lower density than the adjacent bone and thus appear darker on radiographs (Fig. 1.3). Intraoperatively, such regions emerge as substantial cavities and are located around the implant.

Osteolysis is a major clinical concern in modular TKA¹³ and was deemed as the failure mechanism most relevant to this thesis. The interface between the tibial tray and the PE insert, so called *backside wear*, is regarded as the main source of wear particles with osteolytic potential. This may be supported by the fact that non-modular components have not been associated with osteolysis^{14,15}. Consequently, the initial idea for this thesis was to combine retrieval analysis and simulator wear tests with a concise focus on backside wear to propose recommendations of certain tibial tray design modification to reduce the amount of insidious wear particles.



(a)



b)

Figure 1.3: Anterior radiograph of the left knee of a patient following cemented modular TKA (AMK[®], DePuy Orthopaedics Inc., Warsaw, IN). The circled, dark area in a) shows an example of osteolysis on a radiograph; b) intraoperative view the knee joint during revision surgery.

Wear of materials, such as PE, is part of the discipline of tribology (derived from the Greek word *tribos* meaning “rubbing”). Tribology is the science and technology of interacting surfaces in relative motion and includes the study of friction, lubrication, and wear (Fig. 1.4). The mechanical performance of machinery with surfaces in relative motion depends to a large extent on tribology because excessive friction and/or wear can impair the motion and prevent the machine from performing efficiently. Zum Gahr¹⁶ noted that the cost of poor tribology can reach an estimated 4.5 % of a country’s gross national product. A report by the National Research Council of Canada¹⁷ estimated that in the 1980’s, poor tribological practice cost the Canadian economy an estimated 5 billion 1982\$ per year and the potential savings, using technology available in 1986, was estimated at 1.3 billion 1982\$ per year. Many of these savings can be made by relatively minor changes such as reducing the friction by adding a lubricant or by modifying the interface using solid lubricants or surface coatings. Orthopaedic tribology is a specific area of research with a focus on the friction and the wear of joint replacements and involves multiple disciplines such as Medicine, Mechanical Engineering, Materials Science, Biochemistry, and also Microbiology to some extent.

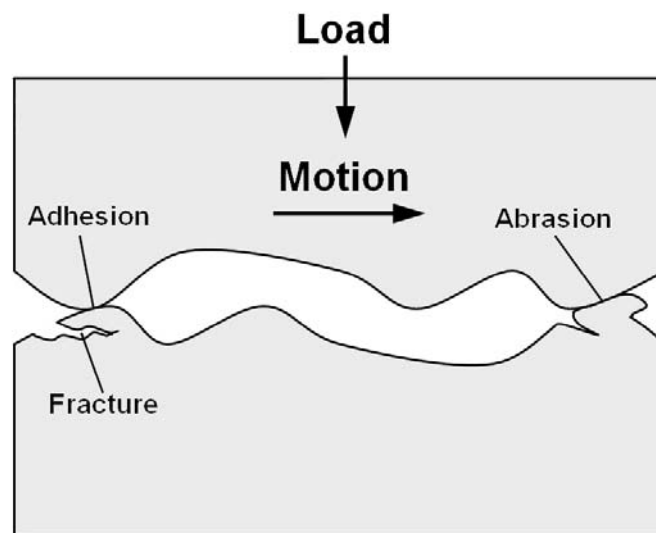


Figure 1.4: Schematic drawing of two surfaces in relative motion to each other. Some asperity contact may occur and lead to material removal due to adhesion or abrasion, for example.

1.2 The Significance of Retrieval Analysis and Wear Testing

Failure of the TKAs result in the need for expensive, time-intensive revision surgery^{18,19}. This is associated with a higher risk of morbidity for the patient than the primary surgery and causes the patient to suffer more pain and loss of both time and often income. In the United States alone, approximately 38,000 revision TKA were undertaken in 2005 with a total cost of approximately US \$ 11 billion^{4,20}. According to the report by Canadian Joint Registry², PE wear, late instability, and osteolysis accounted for the majority of revision surgeries performed in 2006. An example of a failed modular TKR system due to both severe PE wear and osteolysis is shown in Figure 1.5.

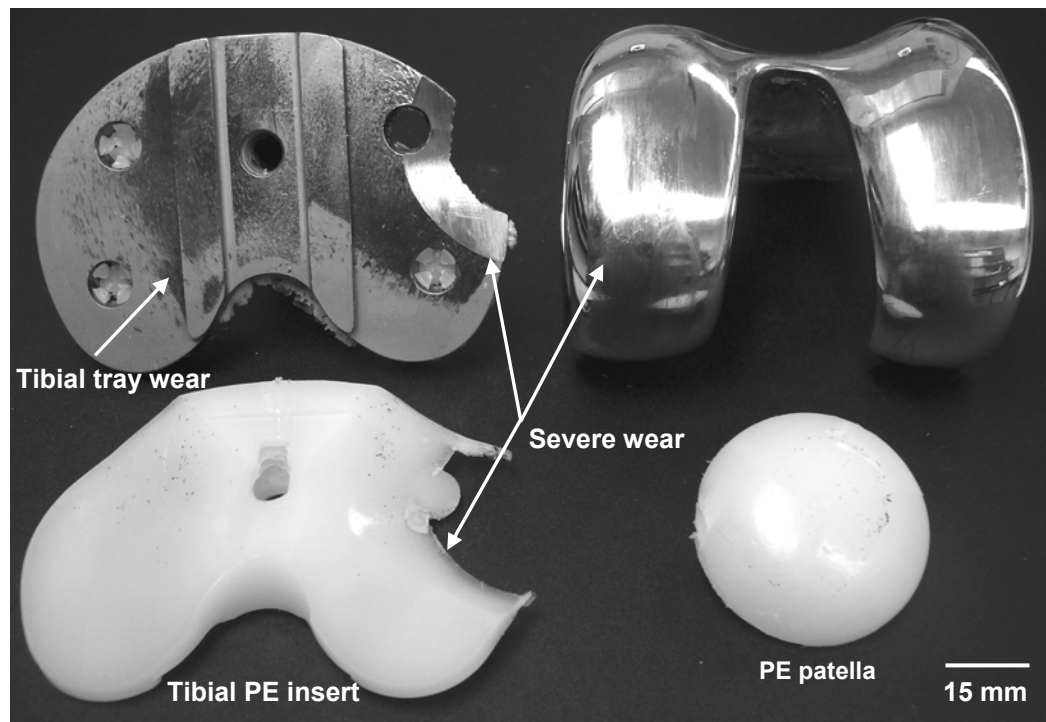


Figure 1.5: A failed modular TKR system (AMK[®], DePuy Orthopaedics Inc., Warsaw, IN) retrieved from the left knee of a 70-year old male patient (mass of 95 kg) after 5 years of implantation. The implant was initially implanted by cemented fixation and was revised for both severe PE wear and osteolysis.

Both the need for and the extended operating time of revision surgery makes fewer resources available for patients needing primary TKA and thus cause the waiting lists to increase which can have significant socioeconomic implications²¹⁻²⁵. Patients with arthritis may be unable to work, may become isolated, suffer from depression and have increased obesity. Such reduced quality of life is likely to lead to long-term medical treatments and additional costs. Reducing the timely wait lists for replacement surgery will increase the quality of life of the patient and reduce the care costs, particularly in societies with public funded health systems such as in Canada. Thus, using TKRs with improved wear characteristics may lead to increased implant durability consequently reducing revision surgery rates and waiting lists.

The research and development of new TKR systems with improved wear behavior is largely governed by the clinical wear performance of contemporary implanted TKRs as well as by the results from wear simulator testing. One way to quantify clinical performance of TKR systems is semi-quantitative damage assessment of retrieved components using grading systems, because the *in vivo* PE wear rate is unknown. Damage assessment of retrieved implants supplies direct evidence of *in vivo* failure mechanisms which is particularly useful for the surgeon and implant designer. Also, such damage assessment can be performed on implants undergoing simulator wear testing and the comparison of damage features to retrievals may permit test protocols to be adjusted for improved and more clinically relevant simulation. For example, both the retrieval assessment and simulator wear testing of gamma-in-air (GA) sterilized PE inserts showed severe fatigue wear on the PE component which caused catastrophic failure *in vivo*²⁶⁻²⁹.

Knee wear simulators are used for pre-clinical investigation of the *in vivo* wear behavior and wear particle characteristics, both of which are highly sensitive to the lubricant composition that mimics SF³⁰. Recent findings by Mazzucco et al.³¹⁻³⁴ suggested that none of the SF constituents affected the joint tribology based on friction experiments while others³⁵⁻³⁹ suggested quite the opposite based on hip simulator wear tests.

The effects of SF constituents on PE wear have not received significant attention in knee simulator wear testing. It was deemed possible that the lubricant composition, which varied significantly between wear testing laboratories³⁷, may affect the PE wear rate in TKA. The guidelines for TKR wear testing supplied by the International Standards Organization (ISO)^{40,41} do not give recommendations on the protein constituent fractions, level of osmolality, or suggest the use of HA. Although the use of microbial growth inhibitors are necessary to maintain sterile environment for wear testing, their efficacy remained uncertain³⁰. All major implant manufacturers now use knee wear simulators for their pre-clinical screening which is commendable. However, the implemented test conditions⁴⁰⁻⁴² still remain under scrutiny and vary significantly between implant manufacturers. The uncertainty regarding appropriate test conditions may ultimately result in wear related implant failure even for new designs and make revision surgery necessary and result in increased patient care costs and waiting lists.

1.3 Thesis Objectives and Outline

The main goal of this thesis was to develop strategies that significantly improve the current methods used for wear evaluation of TKR systems. Such improved methods may result in improved clinical performance of TKR systems and thus, provide benefit to the patient, surgeon and researcher. It was deemed necessary to review both the clinical performance of TKR systems and *in vitro* wear testing protocols as shown in Chapter 2. The Materials and Methods relevant for this thesis are shown in Chapter 3. Results, analyses and discussions were conducted in two consecutive Chapters; clinical investigations shown in Chapter 4 and included the retrieval analysis of PE inserts with a focus on backside wear. Chapter 4 was complimented by some biochemical analysis of SF sampled from a number of patients with OA. *In vitro* investigations shown in Chapter 5 contained substantial knee simulator wear tests with the focal point on SF lubricant constituents and their effects on PE wear. Creating a

sterile environment for implant wear testing was deemed particularly important and received further attention. The findings of both Chapter 4 and Chapter 5 were summarized in Chapter 6.

Some unanticipated circumstances, such as the delayed installation of the knee simulator and funding politics, influenced the strategy of the present thesis. Although the simulator was delivered in early 2003, restructuring of the laboratory space in the University Hospital at the London Health Sciences Centre (LHSC) delayed the initiation of the wear tests until late 2005. Extensive retrieval analyses with the focus on backside wear were initiated in 2002^{43,44} to overcome the delay, as shown in Section 4.2 and Section 4.3. Significant funding was eventually obtained from the Canadian Arthritis Network in 2005 to specifically focus on backside wear in knee wear simulator wear testing. Meanwhile, backside wear had received considerable attention from the fast-evolving, product-driven orthopaedic research community. Several knee wear simulator investigations on backside wear were completed by McNulty et al.⁴⁵⁻⁴⁷ (DePuy Orthopaedics Inc., Warsaw, IN) in 2005 and, rather than repeat them, the present author decided to focus his wear simulator studies on the lubricant used to mimic SF. Such facts motivated the author to initiate a SF analysis on patients with OA undergoing primary TKA (Section 4.4) and to further investigate the effects of protein constituent fractions, level of osmolality, HA, and microbial inhibitor on PE wear (Chapter 5). Such investigations were considered a logical approach to significantly improve the current wear evaluation of TKR systems.

Chapter 2: Literature Review

2.1 Introductory Remarks

The present thesis involved interdisciplinary research into the wear performance of TKR systems and thus, required a review of diverse subject areas such as Tribology, Orthopaedics, Biochemistry, and Microbiology. Background information on Tribology included explanations of lubrication regimes, friction, and wear mechanisms. The lubrication concepts proposed for natural joints and joint replacements were reviewed and summarized. The literature was reviewed on the composition of SF surrounding the natural synovial joint, OA joint and the composition of the lubricant used in the simulator wear tests of artificial joint replacement. The literature was also reviewed on the properties and characteristics of the PE bearing surface from the tribological and clinical perspective. Additional information was obtained on general polymer wear, specific PE wear and thin film boundary lubrication. The recent strategies for simulator wear testing were reviewed with a specific focus on the management of microbial contamination in the lubricant and the effects of simulator hardware on PE wear. Information was found on the clinical performance of TKRs to identify the predominant source of wear particles that causes osteolysis and implant failure in TKR systems. This included the review of implant survivorship to identify possible implant design features that may be considered as precursors for osteolysis. The techniques used to quantify clinical wear were investigated, particularly the damage assessment of retrieved implants.

2.2 Tribology

2.2.1 Theory

Tribology has been studied by many famous engineers and scientists such as Leonardo da Vinci, Amontons, and Colomb. They started with attempts to mathematically describe friction forces that opposed sliding motion⁴⁸. The friction force (F_f) that acted in the tangential direction and opposed sliding motion was found, in many cases, to be proportional to the normal load (F_n), independent of the area of apparent contact (A_a) and the sliding velocity. This resulted in the definition of the coefficient of friction ($\mu = F_f/F_n$) that was often called as Amontons' Law. However, the coefficient of friction at the initiation of sliding motion (μ_s) was often higher than its value during sliding (μ_k) and so a distinction between the two was made⁴⁹.

In journal bearings of large width, Stribeck⁵⁰ found that μ_k could be significantly reduced if a fluid lubricant was present and if a continuous fluid film of lubricant separated the surfaces. This phenomenon depended on the Sommerfeld number that was the product of lubricant viscosity and sliding velocity divided by the normal load per unit width. The value of μ_k increased slowly with increasing Sommerfeld number when fluid film lubrication separated the surfaces (Fig. 2.1) and depended on the viscous resistance of the lubricant film, but increased rapidly when the Sommerfeld number fell below the value needed to maintain a continuous fluid film. Bowden and Tabor⁴⁹ investigated the relationship between μ_k and the lubricant film thickness. They reported that the rapidly increasing μ_k values were a result of increasing asperity contact and consequently increasing adhesive forces. With further decreases in the Sommerfeld number, there was a complete breakdown of the fluid film leaving only a less reliable surface protection afforded by boundary lubrication that depended on elements of the lubricant which chemically adhered to the surfaces. Thus, when a fluid lubricant was present, μ_k and thus the friction forces associated with the interaction of the surface asperities depended on three "classical" lubrication regimes. These lubrication regimes were boundary

lubrication (asperities in contact), mixed lubrication (asperity tip contact), or fluid film lubrication (asperities separated).

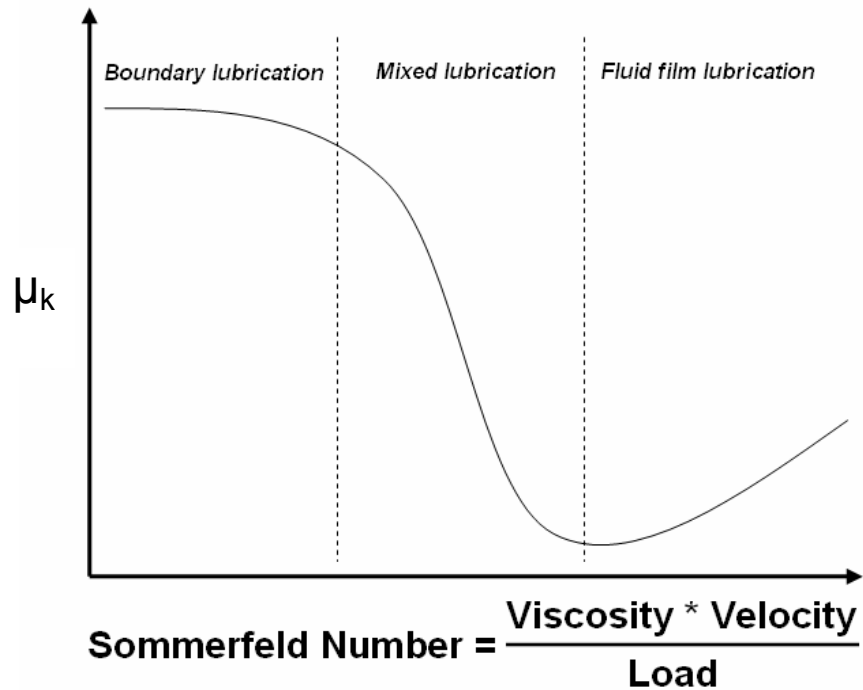


Figure 2.1: Schematic showing the dependence of the friction coefficient (μ_k) on the lubrication regime (boundary lubrication, mixed lubrication, and fluid film lubrication).

In boundary lubrication, the protective molecules might only form a several nanometers thick layer and might be removed by the friction forces and thus, providing only limited surface protection^{16,51}. This layer may consist of molecules that are able to adsorb to the surface where the polarity of the adsorbent is essential. Fatty acids, for example, may consist of a hydrophobic (-CH₃) and a hydrophilic part (-COOH). The hydrophilic part is then attracted by the hydrophilic part of the surface and may create a dense formed layer. The opposing hydrophilic layers may then provide a low interfacial shear stress. Stachowiak and Batchelor⁵¹ noted that the adsorption of molecules could occur by physisorption (van der Waal's, low-energy bonding mechanisms) at ambient temperatures or by chemisorption (chemical bonding) at elevated temperatures

that could develop from frictional heating. The wettability of the lubricant on a surface could be used as an indicator on how well the molecules comprising the fluid will “stick” to the surface and promote boundary lubrication⁵². In the boundary lubrication regime, the material properties are considered the main precursor of the wear process and the viscosity of the lubricant may only play a minor role^{16,51}. In mixed lubrication, the surfaces are partially separated by a lubrication film and thus some asperity contact may still occur^{16,51}. However, these contacting asperities may still be very well boundary lubricated. In fluid film lubrication, the fluid pressure may be high enough to cause a bulk deformation of the interacting surfaces thus creating a larger interacting zone in which a lower fluid pressure can act to separate the surfaces; this phenomenon is referred to as elastohydrodynamic lubrication (EHL). The ratio between the calculated EHL film thickness and the combined root mean square surface roughness (defined as $R_q = (R_{q1}^2 + R_{q2}^2)^{0.5}$) is referred to as lambda-ratio and used as an indicator of asperity contact and wear⁵³. An increasing lambda ratio indicates a lower incidence of asperity contact and, for almost complete separation; Chan et al.² suggest that it must be greater than about 3. As the Sommerfeld number increases, the film pressure moves forward from the point of load application and the bearing surfaces are completely separated by a thick fluid film giving full hydrodynamic lubrication^{16,51}. In hydrodynamic lubrication, the fluid is entrained into the gap by the relative motion of the surfaces and carries the applied load (normal load).

2.2.2 Wear and Wear Mechanisms

Surface damage and wear can occur for any surfaces in relative motion whether or not they are in direct contact. The surface asperities are always subjected to changing load levels (from normal or tangential friction forces) and can fail in fatigue. However, in most cases, significant wear involves direct and continuous asperity contact^{16,51}. In these cases, wear can occur due to material removal from one or both surfaces. This wear can either be on the large scale or

on the molecular level. The material removal from two materials in contact under relative motion may follow Archard's law^{16,51}. Essentially, Archard's law suggests that wear volume is proportional to the product of the real area of contact (A_r) which is the sum of all the small contact areas associated with each surface asperity contact) and the sliding distance (d). A proportionality factor (k) is included with the product of A_r and d because not every asperity interaction results in wear. In its classic form, the asperity contacts are assumed to be purely plastic and thus the real area of contact can be equated to the normal load divided by the hardness of the softer surface (H). Thus, Archard's law gives the following expression for the volumetric wear:

$$W = k \frac{F_n d}{H} \quad (2.1)$$

The k value basically represents the proportion of asperity contacts that cause wear. A high k value indicates that wear is caused by the majority of asperity contacts⁵¹. The total sliding distance traveled requires adjustment if k is compared between unidirectional and multidirectional tests. Archard's law is a useful approach to relate wear to asperity contact and also to the input parameters (F_n and d) whose product is proportional to the work done on the interface by the sliding action if the μ_k remains constant. Since many polymeric materials do not have a distinct hardness value, a wear factor (K) is often defined and used to replace k/H in Archard's law.

However, the problem arises that the k and H values often change during the wear process as new wear mechanisms act or as existing ones change in severity. Mathematical models implementing some mechanical and physical properties have been developed based on the microstructural and environmental conditions of the tribosystem¹⁶. However, these models remain remarkably inept at predicting wear performance of a given contact. Another approach is to classify the wear process as some combination of four fundamental wear mechanisms (adhesive, abrasive, tribochemical, and fatigue) and then look for

mechanism specific material response at the interface using surface analysis techniques. This approach yields an understanding of the wear occurring and some approximate idea of the expected wear performance over the lifetime of the contact.

Adhesive wear is caused by direct asperity contact that is accompanied by bonded junctions that can be caused by some combination of three mechanisms. These mechanisms are diffusion, electronic, and adsorption. The diffusion mechanism is caused by atoms or molecules diffusing between the surfaces at the interface and requires that the molecules are sufficiently mobile and mutually soluble^{16,51}. The electronic mechanism suggests that electrons are transferred between the interfaces that possess different electron band structures. This may cause the donor surface to expel electrons during contact and it may remain positively charged after separation. The adsorption mechanism relies on ionic, covalent, metallic, hydrogen and/or van der Waal's bonds that form between the surfaces. In polymeric-metal contacts, a polymer transfer layer can be generated on a metallic surface and this is often used as a dramatic illustration of the adhesive wear mechanisms¹⁶.

Abrasive wear is caused by a "ploughing" action of surface asperities or detached particles. It can be classified into grooving and rolling abrasion^{16,54,55}. In the grooving abrasion mode, a surface asperity of the harder surface or a trapped wear particle (often called a "third-body" because it is not attached to either of the two contacting "bodies") can penetrate into the softer surface and cause material removal during sliding. In the rolling abrasion mode, a wear (or third-body) particle rolls between the surfaces and causes repeated indentations in the opposing softer interface. The material removal in grooving abrasion mode is generally much higher than in rolling abrasion mode⁵⁵. In any case, the material removal in abrasion depends on the applied load, shape of the of particle (i.e. the angle of attack) and number of particles in the contact which can cause cutting, ploughing, fatigue and cracking^{54,55}.

Tribochemical wear is characterized by chemical reactions at the interface. Adhesive asperity contact may be accompanied by significant heat

generation^{49,56,57} that causes a chemical interaction of the surfaces and lubricant to generate a new material at the surface of one or both of the original contacting materials. The new material often involves various oxides and may enhance or reduce wear^{16,51,58-60}. Tribochemical wear depends on the reactivity of the surrounding medium/lubricant and on the ability of the interface to generate and maintain such oxide layer. If the new material forms into a layer and reaches a certain thickness, it may crack, become detached from the surface and promote abrasive wear. If the corrosion process is rapid, the layer may be quickly generated and may also be quickly removed by abrasive action. Tribochemical wear processes are often part of boundary lubrication in which the formation of a wear reducing, newly formed material is facilitated by specific chemical compounds (or additives) in the lubricant.

Fatigue wear can occur after cyclic loading (sliding/rolling) which can be associated with crack formation due to high shear and normal stresses in the contact^{16,51}. A fatigue-like process also occurs in the other basic wear mechanisms because not every asperity contact in adhesive, abrasive or tribochemical wear produces a wear particle. However, the classification of fatigue wear is reserved for larger scale material removal that depends mostly on the normal stress to initiate and propagate cracks. These cracks can either propagate from the surface or originate from the sub-surface and can lead to flaking of the material (small-scale pit formation) or to delamination wear (large-scale material removal). Repeated cyclic loading during sliding wear of ductile surfaces can initiate work-hardening at the interface due to dislocation movement^{16,51}. This can produce a thin work-hardened layer that is eventually detached after sub-surface crack propagation. These thin detached layers can then be extruded from the contact to form filmy wear particles; such a process is referred to as plastic ratchetting. For polymeric surfaces, fatigue wear depends on the molecular structure in that surface cracking is observed on amorphous polymers while stretching and reorientation of the molecular structure is observed on semi-crystalline polymers^{16,51}.

It is important to note that each wear mechanism can occur simultaneously or consecutively and cause a different material response. Thus, it is essential to observe the worn surface with surface analysis techniques at *early stages* of the wear process to determine the acting wear mechanism with the goal to implement possible countermeasures to reduce wear. For example, adhesive wear at early stages of wear may be associated with material transfer from one interface to the other. The microstructure of the transferred material may be affected by work-hardening with progressive wear and may eventually detach from the surface, act as a third-body wear particle and cause abrasive wear. Observing the damage features after advanced wear may suggest that increased hardness would be beneficial to counteract abrasive wear. Increasing hardness, however, may have limited success since it does not inhibit the initially acting adhesive wear mechanism. In this particular case, adhesion may be reduced by adding a lubricant and then abrasive wear could be reduced by increasing the surface hardness.

2.2.3 Wear of Polyethylene

Since it is relevant to this thesis, a short review on the wear behaviour of semi-crystalline polymers, i.e. polymers with an amorphous and crystalline structure⁶¹, such as PE will briefly be given. In contrast to the elastomers and duroplastics, the polymeric chains of the thermoplastics such as PE are not directly bonded. However, as discussed subsequently in the present thesis, it is possible to cut the polymeric chains and, if oxidization is avoided, the chains can reform with numerous cross-links thus becoming somewhat similar to elastomers and duroplastics.

Transfer films have been reported for PE on several counterfaces and it appears that the test temperature, lubrication, and sliding velocity may be precursors of this phenomenon⁶² and may also occur in the water lubricated CoCr-PE interface⁶³ or alumina-PE interface⁶⁴. Surprisingly, a transfer film has not been reported for PE when the lubricant contained proteins^{63,64}. Adding

proteins to the lubricant increased its wettability which was suggested to reduce the μ_k and may inhibit adhesion⁶⁵. Thus, increasing the hydrophilic nature of the PE surface was shown to promote adsorption of protein to the surface and to reduce μ_k ⁶⁴. Linear sliding under lubricated conditions with protein-rich fluid may allow the molecular chains of PE to become oriented at the interface referred to as *orientation softening*, which leads to low μ_k and low wear⁶⁶. Multidirectional motion has shown to disrupt these anisotropic films which even further increased the PE wear rate^{67,68}. PE wear has also been found to be sensitive to the magnitude of multidirectional shear and the ratio of rolling/sliding contact kinematics in combination with the applied load⁶⁹⁻⁷¹. Muratoglu et al.⁷² showed that gamma-irradiation of PE with subsequent melt-annealing in an inert environment led to cross-linking of the PE chains in the amorphous region. Such cross-linking counteracted the anisotropic surface change and led to reduced wear. It was also noted that fluid was mainly absorbed by the amorphous regions of the bulk of the PE which caused a decrease in mechanical properties such as hardness, modulus of elasticity and shear strength⁶². Such an effect was reduced after cross-linking⁷³.

Both conventional non-cross linked PE and cross-linked PE (XPE) are visco-elastic materials that exhibit both viscous and elastic characteristics under deformation (strain). Such a characteristic gives PE a time dependent strain rate⁶¹. A visco-elastic material loses energy during a loading cycle which is referred to as hysteretic loss. Such visco-elasticity is associated with rearrangements of polymer chains. Consequently, strain applied to the PE will result in some PE chains altering their position. Such polymer chain movement is referred to as creep and describes the ability of the material to deform permanently to mitigate stress (relaxation)⁶¹. In general, the creep behavior is characterized by three stages. The initial, primary stage of creep is associated with a high strain rate at a constant load. The strain rate declines and becomes steady-state which is referred to secondary stage of creep. Tertiary creep is associated with an exponential increase in strain rate at increased strain. The

creep of PE may be recoverable when the unloaded samples are heated to ~ 130 °C in an inert environment for ~ 20 min (melt-annealing) ⁷⁴.

Another characteristic feature of polymers is that their modulus of elasticity is temperature dependent ⁷⁵. Increased temperature may reduce the modulus of elasticity and may cause the PE to be extruded in the CoCr-PE interface. This may be promoted by low thermal conductivity of the PE (~ 0.42 Wm⁻¹k⁻¹) compared with the CoCr alloy (~ 16 Wm⁻¹k⁻¹). Low thermal conductivity of the PE may promote heat accumulation at the CoCr-PE interface and affect the wear behaviour.

2.2.4 Boundary Lubrication

In the present thesis, a very general and broad-based treatment of the various topics is given to provide a background on boundary lubrication that may be of relevance for the specific behaviour of implants. Recently conducted friction experiments and wear tests on the CoCr-PE interface suggested that the artificial joints may be boundary lubricated ^{45,63,76-78}. Thus, it was deemed important to review the literature on boundary lubrication.

Some interactions between adsorbed molecules/layers in the boundary lubrication regime were presented by Bowden and Tabor ⁴⁹ and further investigated on a more fundamental molecular level by Israelachvili and co-workers ⁷⁹⁻⁸¹ who proposed a concept on the liquid dynamics of molecular films based on some experimental results and computer simulations. The viscosity of the confined molecular layer was found to be no longer comparable to the bulk fluid viscosity. The effective viscosity of confined molecular layer, as thick as 10 molecular diameters, can be 10^5 -times and relaxation times 10^{10} -times slower than the bulk fluid viscosity. At high shear rates, the confined film was suggested to take on non-Newton like behaviour, i.e. the film experienced severe shear-thickening with increased shear rates ⁸⁰. It was suggested that shear-thickening occurs when the shear rate exceeds the molecular relaxation

time and may be associated with *entanglements* between the adsorbed molecules on the surface.

Klein and co-workers⁸²⁻⁸⁵ considered the fact that many boundary lubricants that were adsorbed to the interface consist of *polymer chains*. It was suggested that the adsorbed polymer chains became entangled and experienced a resistance towards motion (increase in μ_k) as each of the substrate surfaces' slide past each other under strong compressive load. A large enough normal load consequently causes an increase in effective viscosity and thus, the drag between the entangled polymer brushes may be large enough so that the film rips at the polymer-substrate interface, with bonds anchoring the brush chains to the substrate breaking and reforming (Fig. 2.2). Kong et al.⁸⁶ conducted molecular dynamic simulations of the boundary film and proposed that μ_k decreased with increasing normal load, decreased with increased density of adsorbed polymer chains, and increased with increasing shear velocity. Under shear, this film was suggested to dissipate frictional energy and may reduce wear and be beneficial for biological applications⁸⁷.

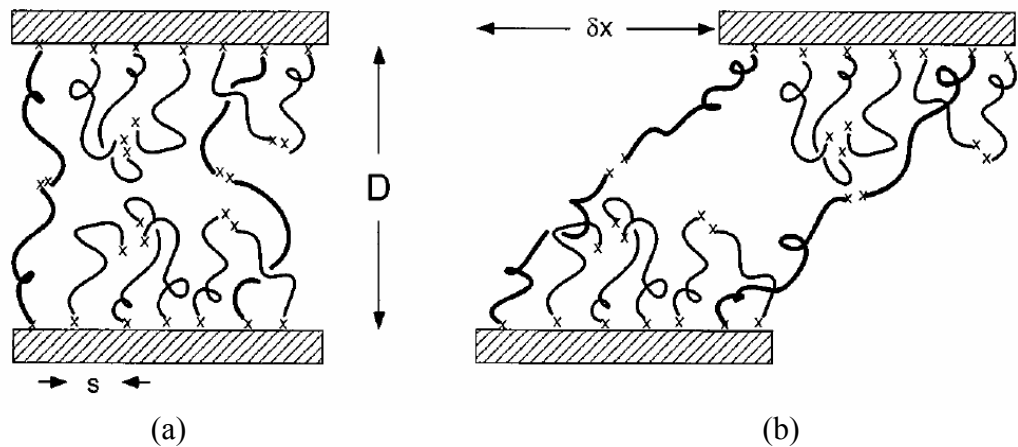
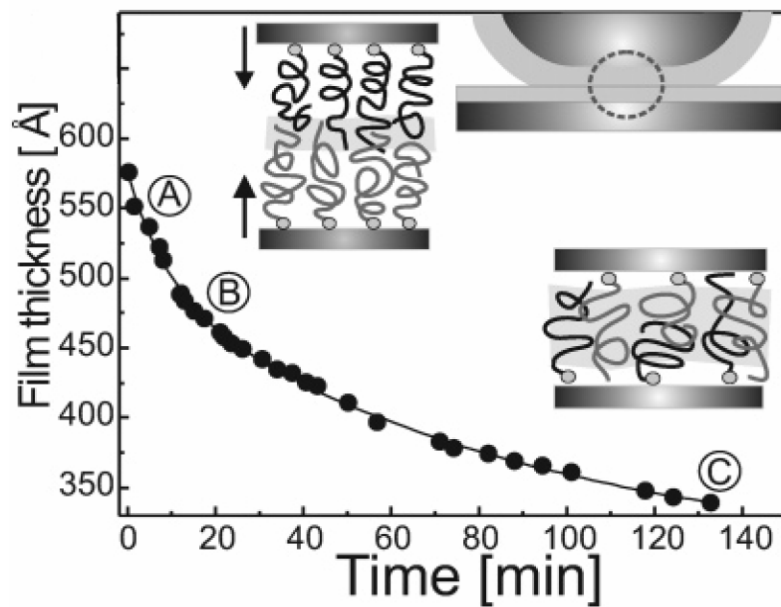


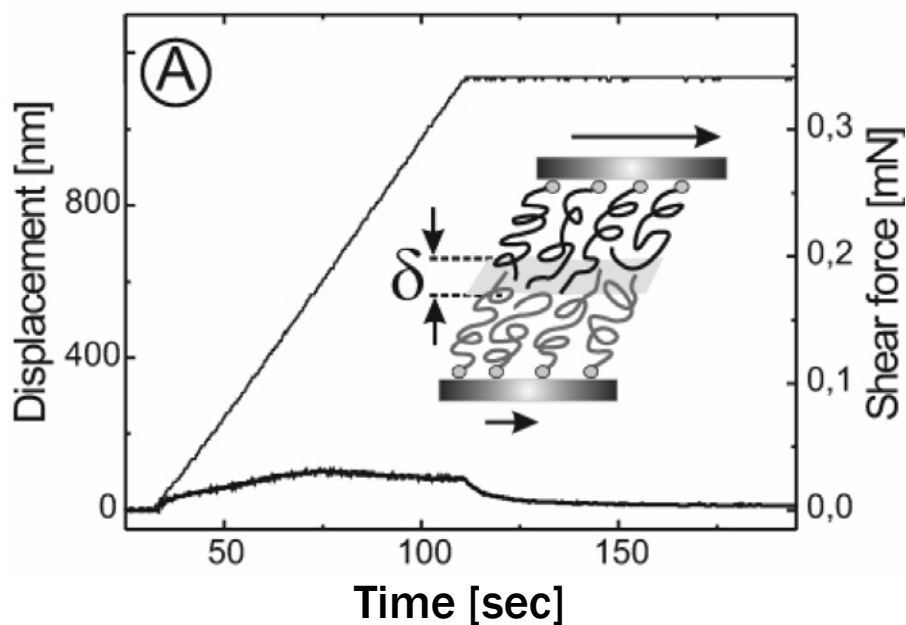
Figure 2.2: Schematic illustration of the polymer chains adsorbed to both substrate surfaces under (a) pristine and (b) after being displaced by a distance δx (from Klein et al.⁸⁵).

Most recently, Tsarkova et al.^{88,89} showed that the polymer brushes adsorbed to each surface were highly interactive and interpenetrated (Fig. 2.3). The head groups of the polymers were entangled with each other. On sliding, these entangled polymers stretched to provide shear force and increased the μ_k . Increased sliding may cause the *polymer-substrate bonds* to break and to reform. The polymer brushes adsorbed on each surface were shown to interpenetrate at a constant load and resulted in a reduction of film thickness from $\sim 575 \text{ \AA}$ to $\sim 350 \text{ \AA}$. This was accompanied with an increased spacing between polymer brushes. The shear rate (displacement/time) and following cessation of the displacement clearly affected the resulting shear force behaviour of this consolidated film. At a low shear rate, the polymer brushes were given time to relax and only slightly increased the shear force upon cessation. At a high shear rate, the polymer brushes did not relax and the film remained in its solid-like state and significantly increased the shear force. Depending on the test conditions and environment it may be possible that adsorbed protein chains may slip on both the polymer-substrate interface and inside the solid-lubricant interface⁹⁰.

Confined films in boundary lubrication were also suggested to be mediated by colloidal suspensions with particles that exceed the molecular size ($\sim 10 \text{ \AA}$)⁹¹. Colloidal suspensions are defined as homogenous mixture consisting of two phases; one phase consists of dispersed, small sizes particles/macromolecules while the other consists of a continuous solvent. Georges et al.⁹² conducted friction tests with colloids suspension with an average particle size of $\sim 50 - 100 \text{ \AA}$. They also found that the interfacial film consolidated upon increased compressive load. The colloidal film does not flow in the contact of two approaching surfaces at a pressure of 10^6 Pa which allowed the film to form a compacted contact zone⁹¹. The mechanical properties and the dynamic behaviour of these colloidal films were then assessed in more detail elsewhere⁹³⁻⁹⁶. In any case, the films in boundary lubrication comprised of compacted molecules or colloids may fail and allow direct asperity contact.

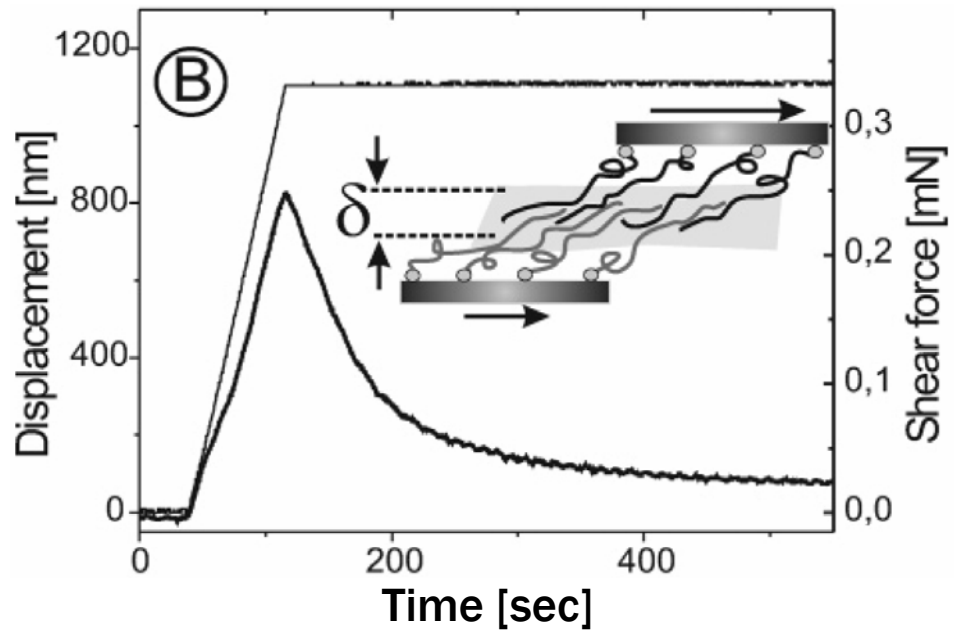


(a)

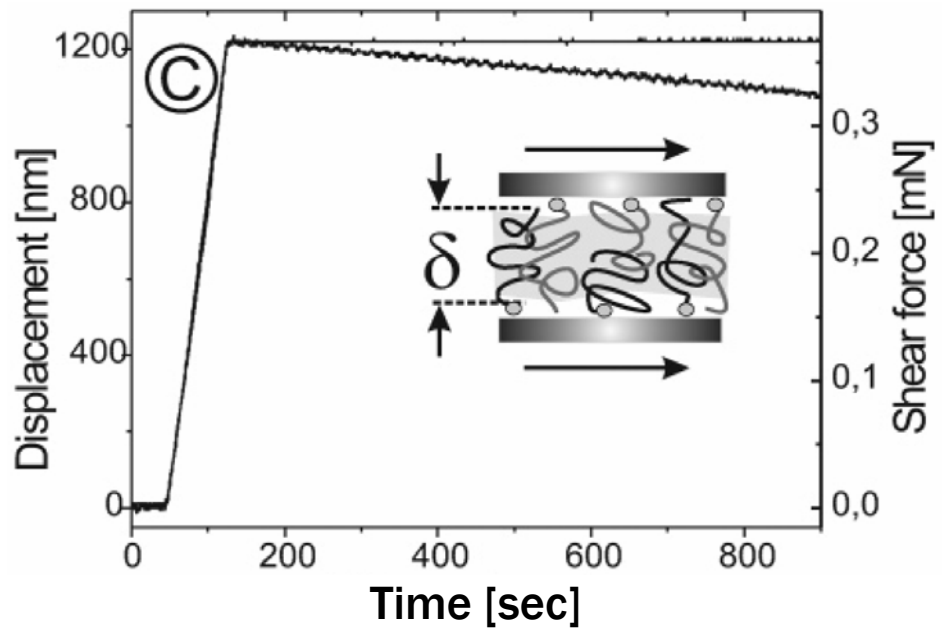


(b)

Figure 2.3: (a) Kinetics of thinning of the polymer brush bilayer following the jump into adhesive contact, fitted by exponential decay (solid line). The drawings indicate the proposed configuration of the polymer brush bilayer shortly after the jump-in (left drawing) and at the end of the measurements (right drawing; also note the increase in mean brush-anchor spacing). (b) The lateral motion applied to the upper surface and the transmitted shear force at the lower surface at the points of the time/thickness indicated by corresponding letters in (a): (A) Motion between opposing polymer brushes following the jump-in proceeds with low shear force (from Tsarkova et al. ⁸⁹).



(c)



(d)

Figure 2.3 (continued): (c) and (d): The lateral motion applied to the upper surface and the transmitted shear force at the lower surface at the points of the time/thickness indicated by corresponding letters in (a): The shear force across the bilayer increases with decreasing layer thickness B (shown in (c)) until a quasi-solid-like behavior is reached C (shown in (d)) (from Tsarkova et al.⁸⁹).

Persson et al.^{97,98} suggested that the yield of the boundary layer may be reached when the boundary layer is squeezed out of the confined zone at high enough normal load which may result in asperity contact and increase μ_k and possibly wear. The squeeze-out of the confined film may be initiated by a thermal nucleation process in which the density fluctuation forms a small “hole” of approximately $\sim 10 - 15 \text{ \AA}$. After a hole of a critical size has been generated, it was likely to spread across the entire contact area. The squeeze-out rate (and thus, the nucleation rate) was suggested to be amplified by lateral sliding, permitting the confined layer to take on a fluidized or disordered state and facilitate the ejection of the layer.

As a final comment, it needs to be noted that the above mentioned occurrences were only observed in friction tests and it remains uncertain how the inherent properties of a boundary layer may play a role in knee simulator wear testing. It may be beneficial to investigate the interactions between macromolecules, such as proteins, comprising the possible boundary layer; estimating the amount of sheared polymer chains by ultrafiltration⁹⁹ and linked to wear may indirectly confirm the involvement of the boundary lubricant in the lubrication process.

2.3 Lubrication and Wear of Natural Synovial Joints and Knee Implant

2.3.1 Synovial Fluid Constituents and Characteristics

The natural knee joint is a freely moving synovial joint that is encapsulated by fibrous tissue (synovium) and contains 0.2 - 10 ml of SF⁷⁷. The synovium provides the SF with nutrition for the chondrocytes of the articular cartilage. SF is a complex fluid which consists of many different solutes, including proteins, HA, and phospholipids (Table 2.1) that may aid in lubrication¹⁰⁰. It is important to note that the synovium is nowadays generally retained after total knee replacements, enabling the capsule to recover and to maintain its SF generating ability. Therefore, it is very likely that the SF

composition in the replaced joint is comparable to the SF of the diseased (usually OA) joint³³. The role of the synovium is to transport nutrients, to remove biological waste from the joint, to provide a lubricant and to add to joint stability¹⁰⁰. The synovium is composed of a relatively avascular structure with two distinct layers. The layer in contact with the joint cavity is referred to as the synovial lining (intima) and is responsible for the synthesis of glycosaminoglycans such as HA which is responsible for the high viscosity of SF. The intima consists of two types of cells, called type A and type B cells¹⁰¹. The type A cells are macrophages which are derived from the bone marrow which have migrated to the synovium via blood vessels. The type B cells are fibroblasts which serve as the dominant secretion of enzymes that are necessary in the synthesis of HA. The second layer is referred to as the subintima and is composed of fatty and fibrous forms of connective tissue. Every solute entering the synovial cavity from the lymphatic system must cross the intima and subintima.

Table 2.1: The main constituents of synovial fluid (SF) for the healthy patient and for the OA patient^{31,102}.

Main constituents	Patients	
	Healthy	OA
Protein [g/l]	10 - 30	24 - 44
HA concentration [g/l]	1 - 4	~ 1.5
HA molecular weight [MDa]	6 - 7	1.8
Phospholipid concentration [g/l]	~ 0.1	0.52

Proteins consist of multiple amino acids (peptides) that are linked together by peptide bonds and referred to as polymeric peptides or simply polypeptides¹⁰³ (Fig. 2.4). Proteins are also considered to be polyelectrolytes, which are substances whose repeating units bear an electrolyte group (amino acid group). Once the protein is placed into an aqueous environment, the amino acid groups dissociate and make the proteins “charged” which may affect the coil-like protein structure.

The thermal stability of proteins depends on the ionic strength¹⁰⁴ which can be determined by measuring the osmolality of a solution. The osmolality of a solution is the concentration of osmotically active particles (for example NaCl ions) in solution¹⁰⁵. An osmotically active particle is one that contributes to its osmotic pressure. Osmosis is the passage of water through a semi-permeable membrane from a region of low concentration of active particles to one of higher concentration. Apparently, osmosis occurs because osmotically active particles have charges that make them repel each other and thus encourage water to move between them. This is a more powerful effect in the solution with the higher concentration and thus water is drawn through the membrane from the lower concentration solution¹⁰⁵. Osmotic pressure is the pressure required to prevent the passage of water through a semi-permeable membrane from a region of low concentration of solutes to one of higher concentration. The osmolality of SF depends on the activity of the patient¹⁰⁶. In SI units, patients at rest have an osmolality of 404 ± 57 mmol/kg while patients after exercise had an osmolality of 303.3 ± 1.5 mmol/kg.

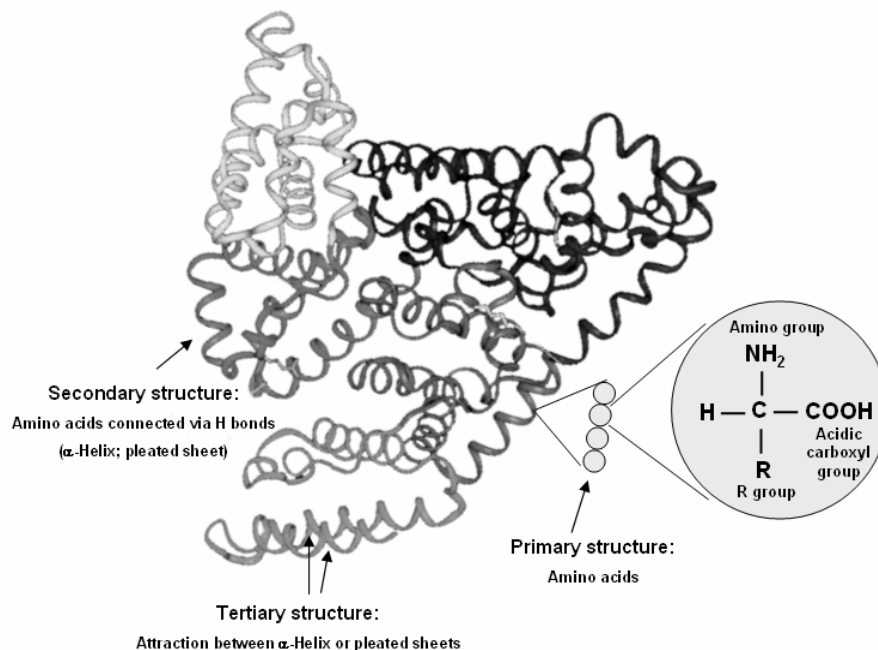


Figure 2.4: Schematic drawing of the human serum albumin structure showing the primary, secondary and tertiary structure (from Sugio et al.¹⁰³).

The main protein constituents of SF are human serum albumin (referred to as albumin), α -1-globulin, α -2-globulin, β -globulin, and γ -globulin and their fractions have been estimated for patients with rheumatoid arthritis¹⁰⁷. Yao et al.¹⁰⁸ showed that albumin accounted for almost 70 % of the total protein concentration in SF drawn from OA patients (n = 5). The total protein concentration of SF was \sim 30 g/l, and was not different between patients undergoing primary or revision surgery³³. Albumin has an average molecular weight 67 kDa and is produced by the liver. It has an ability to bind certain antibiotics onto its molecular structure¹⁰⁹⁻¹¹¹ and this allows it to be used for drug delivery. The acting forces (attraction and repulsion) between proteins in solution have been reported to be similar to those of colloids¹¹²⁻¹¹⁴, which may suggest that the tribological behaviour of proteins can be approached from a colloidal perspective⁹²⁻⁹⁶.

HA consists of long unbranched polysaccharide chains that are composed of repeated disaccharide chains (Fig. 2.5)¹¹⁵. It has been shown^{31,116} that HA is a main constituent of SF, is responsible for its viscosity and has the ability to bind a number of proteins. Healthy patients carry approximately 1 - 4 g/l HA in their SF while patients with OA only contain approximately 1.5 g/l HA in their SF (Table 2.1)³¹. The concentration of HA increases with increasing age of the patient while its molecular weight decreases¹¹⁷. Injecting a solution rich in high-molecular weight HA has become a pharmacologic alternative for patients who are functionally limited due to OA knee pain, especially patients who wish to postpone surgical intervention or for whom surgery is inappropriate¹¹⁸⁻¹²⁰. It is also important to note that HA retains water molecules and this characteristic has been used for cosmetic applications¹²¹. SF is a non-Newtonian fluid because its viscosity decreases with increased shear rate¹⁰². The type of bond (covalent, van der Waal's) between the HA chains and albumin was suggested to depend on the pH¹²²; low pH showed to promote covalent bonds while higher pH enabled only van der Waal's bonds. Recently, Oates et al.¹²³ suggested that HA in the presence of albumin builds a strong protein-HA network with rheopectic behaviour at low shear rates (Fig. 2.6).

Such rheopectic behaviour suggested that the viscosity of SF may increase with increased duration of shear.

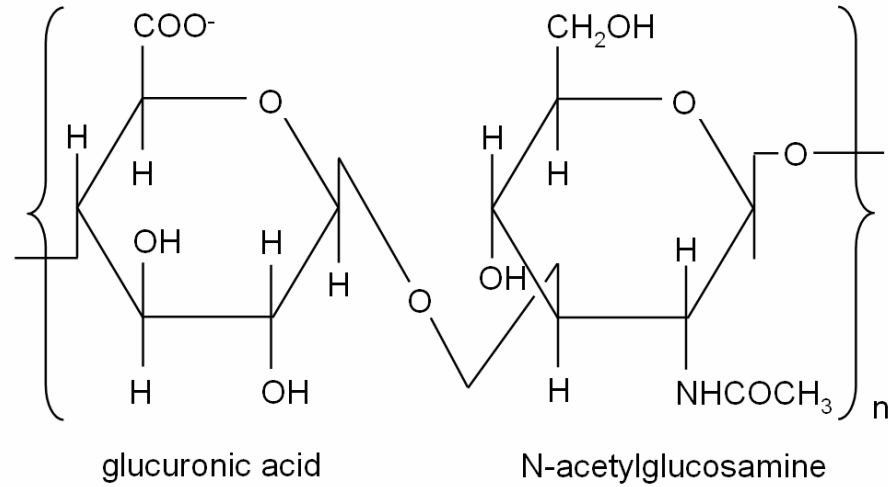


Figure 2.5: Chemical structure of HA. Note that the “disaccharide” chain of HA consists of a glucuronic acid compound and an N-acetyl glucosamine compound.

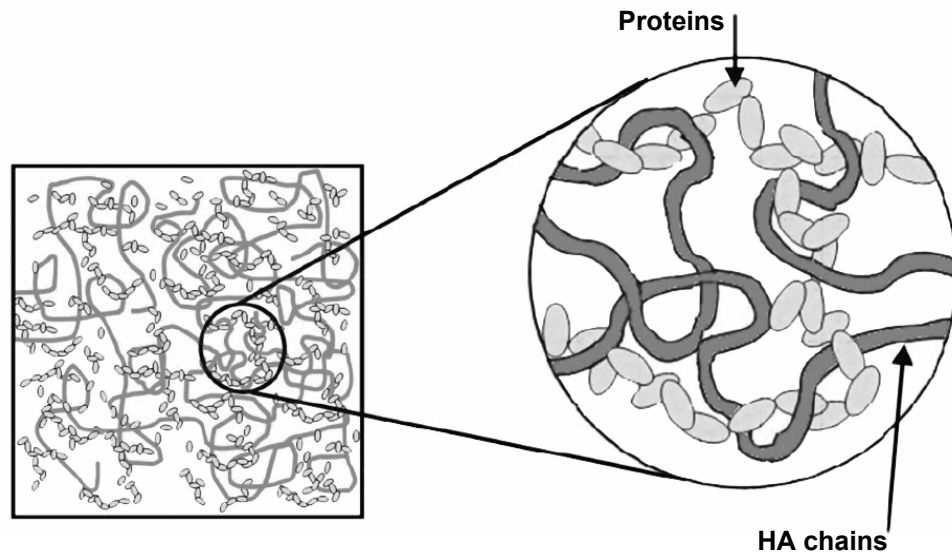


Figure 2.6: The proposed microstructure of synovial fluid: globular proteins (light grey) aggregate to form a tenuous polymeric network and the long HA chains (dark grey) entangle with this network (from Oates et al. ¹²³).

At higher shear rates, Mazzucco et al.³² suggested the SF to have thixotropic characteristics, i.e. the viscosity decreases with increased shear rate (shear thinning). In any case, rheological measurements only give the behaviour of viscosity and may not relate directly to wear at all. The protein-HA network plays a role in the wear process of implants, as recently indicated by DesJardins et al.¹⁰² who performed knee wear testing in a bovine serum + HA fluid. However, it remains uncertain to what extent HA interacts with the protein constituents in wear testing at clinically relevant levels of osmolality. It is uncertain whether adding HA to a protein rich medium affects the thermal stability and whether it is different from the thermal stability of SF. In any case, the thermal stability of SF has not been reported in the literature.

The involvement of phospholipids in the lubrication process has been suggested by *in vivo* and *in vitro* studies¹²⁴⁻¹²⁶. In particular, L- α -dipalmitoyl phosphatidcholine, referred to as surface active phospholipids (SAPLs), is a pulmonary surfactant and may add to the boundary lubrication process, despite its low concentration (Table 2.1). These SAPLs consist of a hydrophilic head group and a hydrophobic tail and may organise themselves into a bilayer structure^{127,128}. The measured organic phosphate (organic P) fluid concentration indicates the total phospholipid concentration while the measured free phosphate (inorganic P) may indicate vitamin D imbalance and kidney disease and may affect the protein structure. It still remains uncertain if phospholipids play a role in the lubrication process in the presence of several protein constituents and HA in knee simulator wear testing of PE. In recent years, a glycoprotein called lubricin has been identified as having a role in boundary lubrication at the cartilage-cartilage interface¹²⁹⁻¹³⁴, but its tribological implications at the CoCr-PE interface remain uncertain.

2.3.2 Lubrication of the Natural and Artificial Joint

The lubrication of the cartilage-cartilage interface has received tremendous attention in the past 50 years^{124,127,128,135-143}. Krishnan et al.^{142,144} suggested that a superficial zone of proteins was present at the articular cartilage surfaces but such proteins were deemed not to play a role tribologically. The study by Graindorge et al.¹²⁸ suggested the presence of a biphasic lipid layer at the cartilage-cartilage interface. Such a layer was suggested¹²⁸ to consist of two bimolecular sheets of phospholipids with their hydrophobic end pointing inwards of the layer. Graindorge et al.¹²⁷ reported that the μ_k obtained from cartilage-on-cartilage friction tests was still low even if the lipid layer was removed from the articulating surfaces. Such a finding suggested that the lipid layer was replenished from inside the cartilage. Recently, Basalo et al.¹⁴⁵ suggested that chondroitin sulphate, a major constituent of articular cartilage, reduced the μ_k . However, these friction tests were performed on a cartilage-on-glass interface which may not be clinically relevant.

The lubrication conditions in TKRs remain uncertain. Wang et al.¹⁴⁶ so stated that “*one of the areas in artificial joint tribology that is still the least understood is the mechanism of lubrication*”. Fluid film lubrication⁵³ and mixed lubrication^{147,148} have been proposed for total hip replacements (THRs). Design concepts such as the use of compliant layers that may facilitate fluid film lubrication in TKR have been proposed¹⁴⁹⁻¹⁵¹ but have not reached or come close to clinical application. In the author’s opinion, the higher conformity in THR may allow some fluid-film action to occur while the lower conformity in contemporary TKR may only permit boundary lubrication to occur. Wear mechanisms and the effect of lubricant composition on the PE wear in artificial joints is frequently discussed^{30,34-36,53,76,78,102,125,147,152-158}. Using human SF as the lubricant for wear testing would be the most clinically relevant but it is not available in large enough quantities with a maximum of only 0.5 - 10 ml per synovial joint⁷⁷. A volume of 40 - 400 ml per wear station is usually needed for a test interval of 0.5 million cycles (Mc). McKellop et al.¹⁵² suggested that protein rich media, such as calf serum, be used rather than distilled water (DW)

for the wear testing of the CoCr-PE interface. The presence of proteins in the test lubricant was deemed essential to mimic SF and to reproduce damage features seen on retrieved PE acetabular components. As mentioned in Section 2.2.3, using a protein rich lubricant inhibited a PE transfer layer onto the CoCr surface⁶³. Serro et al.¹⁵⁹ used atomic force microscopy to obtain direct evidence of protein adsorption onto the CoCr and PE bearing surfaces. This was surprising since the PE surface is considered hydrophobic. Proteins are known to adsorb onto hydrophobic surfaces but this is a thermodynamically driven process¹⁶⁰⁻¹⁶⁴. During surface adsorption, the protein structure may become damaged and become denatured. Such denaturation is often also referred to as degradation of the native protein structure. The extent of protein denaturing upon adsorption depends on the thermal stability of the protein solution, i.e. the higher the thermal stability, the lower the denaturation upon adsorption¹⁶⁴. Heuberger et al.⁷⁶ suggested this in their friction tests in which artificially denatured albumin proteins were adsorbed on the PE surface rather than native ones. This suggested that a compacted denatured protein layer adsorbed onto the hydrophobic PE surface. Increasing the concentration of denatured proteins correlated with increased μ_k ⁷⁶. Such an increase in μ_k was suggested to be associated with an enrichment of the protein boundary layer by denatured proteins. However, an increased μ_k does not necessarily coincide with a higher wear rate. For example, PE was reported to have a higher μ_k than poly-tetra-fluor-ethylene (PTFE) but also had a lower wear rate^{108,165}. Thus, it was deemed possible that higher μ_k coincided with lower wear, since wear depends on local energy release rates rather than overall dissipation and a strongly adsorbed denatured-layer might help reducing local peaks while still increasing overall dissipation¹⁶⁶. It remains to be investigated whether the concentration of denatured proteins impact the PE wear behaviour. The wear process may damage the proteins and that alters the native, folded protein structure. Such damage may initiate to protein unfolding, protein precipitation, and protein shear (Fig. 2.7). Protein unfolding may be promoted by load and motion during the wear test that generates heat at the CoCr-PE interface.

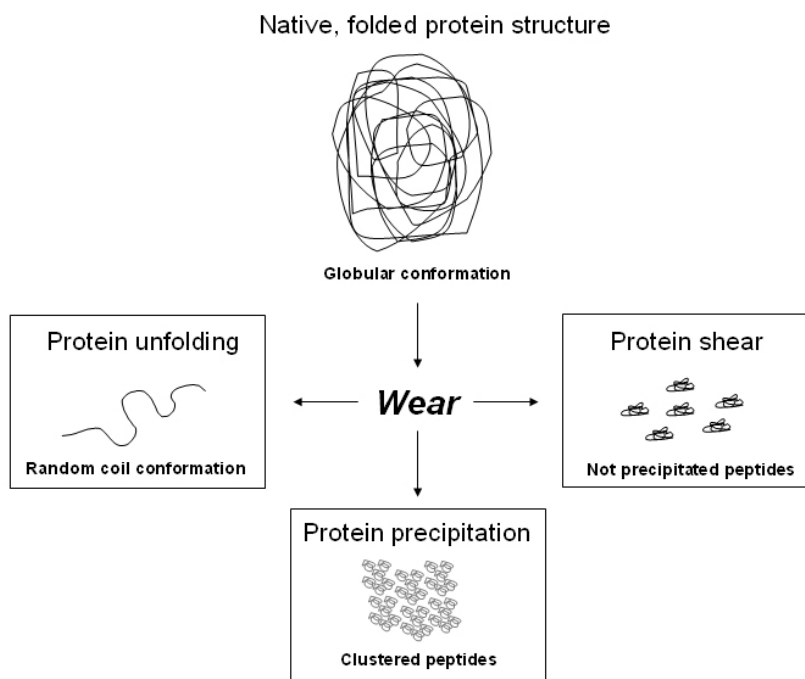


Figure 2.7: Schematic showing how the wear process may affect the native, folded protein structure. Wear may lead to protein damage and cause protein unfolding, protein precipitation and protein shear.

Liao et al.¹⁵⁴ conducted a hip simulator wear test and associated increased PE wear with increased lubricant temperature and increased protein precipitation. Exposing proteins to increased temperature (~ 60 °C) can lead to denaturation in form of protein unfolding¹⁶⁷⁻¹⁶⁹ that results in protein degradation and protein precipitation. The amount of total protein degradation can be determined by measuring the amount of amino acid molecules in the lubricant before and after the wear test using bicinchoninic acid (BCA) assay¹⁷⁰⁻¹⁷³. The reagents comprising the BCA assay are added to the diluted calf serum lubricant and react with the amino acid molecules. Such a reaction causes the diluted calf serum lubricant to alter its color. The extent of colorization indicates the protein concentration which can be measured using a spectrophotometer. Although the BCA assay is used to determine the total protein concentration it does not supply information about the protein

constituents. The calf serum lubricant is comprised of proteins constituents such as albumin, α -1-globulin, α -2-globulin, β -globulin, and γ -globulin which differ mainly in their structure and molecular weight. The protein constituent fractions can be determined by using electrophoresis. Liao et al.³⁵ suggested that the protein constituents played a role in the wear process and that the protein constituents were affected by the wear process. Such profiling separated the proteins constituents by their molecular weight. In any case, the PE wear rate was shown to increase with reduced total protein concentration (native + degraded + precipitated) in both hip and knee simulator wear tests^{45,174}. Wang et al.¹⁵⁶ suggested that the PE wear rate increased with decreasing total albumin to total globulin ratio (A/G). Other constituents such as HA and phospholipids were also suggested to affect the PE wear rate^{30,102,126,175} and these other constituents were included in an attempt to create a more clinically relevant lubricant for implant wear testing.

However, Mazzucco et al.³⁴ concluded from their pin-on-disc friction apparatus that neither proteins (albumin and globulins), phospholipids, or HA played a role in the lubrication process of artificial joints. As mentioned earlier in this Section, friction studies may not be useful to gain insight into the actual wear process. Thus, it remains uncertain whether the protein constituents such as albumin, α -1-globulin, α -2-globulin, β -globulin, and γ -globulin in presence of HA affect the thermal stability^{76,176} of the lubricant and thus the boundary lubrication which ultimately may affect the wear rate in knee simulator wear tests.

2.3.3 Joint Simulator Wear Testing

In the early days of implant wear testing, a simple test configuration such as a unidirectional pin-on-disc test was assumed to be sufficient to predict the clinical wear behavior of bearing materials^{152,177}. However, this approach was lacking clinically relevant geometry and motion. Knee simulators have

been developed to perform wear testing under conditions that closely mimic the clinical environment ^{157,178-181}. Simple tests may still be important to gain fundamental information of the tribosystem and may be used as screening tests prior to simulator wear testing but they must, as a minimum condition, impose reciprocating crossing-path motion at clinically realistic contact stress levels.

Knee wear simulators are believed to be more realistic but they are very expensive to both purchase and maintain. Also, there is no general consensus on conditions that must be imposed by the simulator. For example, force-controlled (FC) and displacement-controlled (DC) simulators were developed ^{178,182,183}. In both types of simulator, the flexion/extension (FE) motion was applied by a displacement actuator and vertical loading was applied by a load actuator. The anterior-posterior (AP) and internal-external (IE) displacements in FC simulators were a consequence of an applied AP load and an applied IE torque rather than imposed by displacement actuators as in DC simulators. The extent of these FC simulator displacements was directly influenced by the implant design and attenuating springs that represent some soft-tissue constraints and both took an increasing share of the force and torque as displacements increased. The most recent AMTI (Advanced Mechanical Technology Inc., Waltham, MA) knee simulator applies a “software” spring so that the force and torque drop as if a spring were there. The spring stiffness values in FC simulators were chosen based on various knee laxity studies ¹⁸⁴⁻¹⁸⁶ and this was further investigated by DesJardins et al. ^{180,181}. As previously mentioned, these springs were meant to simulate the soft tissue load attenuation (constraints) that would occur *in vivo* and thus allow realistic load components to act on the tibial insert. If the soft tissue constraints were well represented, the FC simulator had the advantage of allowing the wear to develop cycle by cycle in response to realistic tangential force components whereas the DC simulator would have the tangential load dropping off as wear progressed.

Although FC simulators allow the wear testing of any type of implant design, they may be particularly useful for more constrained implant designs such as those with PS fixed bearing inserts or those with fixed bearing, high

conformity inserts. Problems may arise with the FC simulator when low conformity or mobile bearings are tested which requires very careful spring adjustment to obtain a clinically relevant wear scar. Conversely, DC simulators apply a defined AP displacement and IE displacement, independent of the conformity or constraint of the implant. Consequently, testing high conformity inserts with the DC simulator may result in non-clinically relevant forces on the insert. Thus, DC simulators may be best suited for testing CR type inserts and mobile bearings. However, attempts were made to test high conformity CR insets in DC simulators. McNulty et al.¹⁸⁷ suggested to limit the AP displacement based on the actual tibiofemoral contact that was mediated by the implant conformity. Haider et al.¹⁸⁸ tested one type of implant under similar conditions in both FC and DC simulators and found no difference in wear rate, but showed some differences between AP motion and IE motion. Using the DC simulators requires knowledge about the *in vivo* kinematics of the specific implant. This is not necessary when FC simulators with quick acting feedback control systems are used with accurate representation of the soft tissue constraints and would favour such simulators particularly for the wear evaluation of new designs that have not been implanted.

The test condition such as loading, displacements and lubricant composition for FC simulator and DC simulators are specified in standard protocols (ISO-14243-1 and ISO-14243-3, respectively)^{40,41}. The recommended lubricant is calf serum, diluted with deionized water to a total protein concentration of 17 g/l. A microbial inhibitor such as sodium azide (SA) is recommended. Specifications on the protein constituent fractions or level of osmolality are not given. HA and phospholipids are not considered as constituents of the test lubricant. Kaddick and Wimmer³⁶ noted that different types of calf sera may lead to different wear rates in THR simulator testing. The types of calf sera used for implant wear testing vary between independent research laboratories and implant manufacturers³⁷. Wang et al.¹⁵⁶ suggested that the test lubricant should be classified based on physiological A/G ratio. They also added 0.34 g/l HA to the lubricant with SA as the microbial inhibitor

and did not observe an effect on the PE wear rate in their hip simulator study. DesJardins et al.¹⁰² added 1.5 g/l HA with a molecular weight of 2.3 MDa to bovine calf serum, used SA as the microbial inhibitor, and observed a 6.8-times increase in PE wear rate. Antimicrobial inhibitors, such as SA, are still widely used in simulator wear tests despite their ineffectiveness in inhibiting bacterial growth in pin-on-plate tests³⁰. Recently, Wimmer et al.¹⁸⁹ reported a 6.5-times higher PE wear rate in pin-on-disc test when microbial growth was observed in the lubricant. Clinically, bacterial contamination of SF is only a concern in the case of septic arthritis¹⁹⁰. Thus, various antibiotics have been used in knee wear testing to inhibit microbial contamination¹⁵⁷. Using antibiotics, however, may cause the microbes to develop resistance which may result in hazardous contaminants¹⁵⁷ that may be only controlled by *living antibiotics*¹⁹¹⁻¹⁹³. It remains uncertain to what extent bacterial contamination in knee simulator wear testing may affect PE wear and what the underlying reasons may be. In addition, the author was not aware of a study that investigated the effect of protein constituents, osmolality or HA in a sterile wear testing environment. Using API[®]-films¹⁹⁴ to identify the bacterium and Kirby-Bauer¹⁹⁵ method to determine the susceptibility of the contaminant towards certain antibiotics may be beneficial to develop a sterile environment for implant wear testing.

Circulation of the lubricant in the wear station may be another factor to affect the PE wear rate. Wang et al.¹⁵⁶ suggested to circulate the lubricant at a turnover rate of 2 ml/hour to mimic the clinical turnover rate of SF in the hip joint. Simulators such as the Endolab[®] knee simulator¹⁵⁷ and the Orbital hip simulator^{35,53,154} do not circulate the lubricant while both the AMTI knee simulator and AMTI hip simulator circulate the lubricant. During wear testing proteins become degraded and eventually precipitate out. Such protein precipitates have led to boundary lubricant films that reduced the PE wear rates in hip simulator tests without lubricant circulation^{35,196}. Wang et al.^{156,197} suggested to increase the lubricant volume from 100 ml to 500 ml to overcome both lubricant circulation and protein precipitation. Such an increased lubricant

volume was accompanied by 4-times lower PE wear rate and a lower protein precipitation. Thus, it remained unclear whether the increased lubricant volume or the reduced protein precipitation lowered the PE wear rate. Some research groups attempted to overcome the lubricant circulation and protein precipitation by replacing the lubricant as often as every 0.1 Mc^{156,198} or every 0.25 Mc^{35,157}. The ISO standard for knee simulator wear testing recommends replacing the test lubricant every 0.5 Mc without giving recommendations on the lubricant volume⁴¹. Recently, McNulty et al.⁴⁵ reported a 4.7-fold increase in PE wear rate when the total protein concentration was reduced from ~ 62 g/l to ~ 17 g/l. These tests were facilitated in an AMTI knee simulator that circulated the lubricant volume of 500 ml through each wear station and an externally located lubricant container adjacent to each wear station. The lubricant was replaced every 0.5 Mc. Such an arrangement may promote sedimentation of the protein precipitates in the external lubricant container which may inhibit the protein precipitates from reducing the PE wear rate. However, this hypothesis remains to be proven.

Wear of the PE component may either be evaluated by gravimetric assessment using a precision balance or by geometric assessment using a coordinate measurement machine (CMM), as described in ISO 14243-2⁴². The CMM is a mechanical system designed to move a measuring probe over the geometry of the PE inserts to determine its dimensions. Consequently, measuring the geometry of PE inserts at different wear test intervals allows a volumetric PE wear rate to be calculated. Using the CMM to determine the PE wear rate may be merited when the majority of geometric change is due to creep and not wear as it is the case for wear resistant XPE. Gravimetric wear assessment is not sensitive to geometric changes. However, PE is prone to absorb fluid, despite its hydrophobic properties, which may significantly affect the gravimetric wear assessment. In respect to wear testing, the amount of fluid absorption can be so high that it may outweigh the amount of PE wear. Fluid uptake is generally more pronounced at the beginning of the wear testing and stabilizes with advanced testing. Specimens of clinically relevant geometries

were *pre-soaked* in DW at room-temperature (RT) for 3 weeks or more to ensure that the fluid uptake of the PE inserts reached equilibrium. Although the procedures *during* wear testing are clearly stated, there is no clear guideline on how to pre-soak PE inserts prior to wear testing. Standardized methods of wear measurements⁴² suggest the PE inserts to be exposed to “a lubricant” and to “repeatedly remove” them for weight assessment until reaching a steady level. Several other researchers^{73,157,199-204} conducted fluid absorption studies to gain valuable insight on the fluid absorption behaviour. However, there is no clear definition on the intervals of repeated weight assessment, the lubricant or the temperature. It remains uncertain whether the pre-soaking period, repeated weight assessment, the weight assessment protocol itself (consecutive *cleaning, desiccation, weighing*), the type of lubricant and temperature would affect the weight gain of conventional, non-cross linked PE of geometries intended for implantation.

2.4 Bearing Surface

2.4.1 Manufacturing Process

PE is composed of long polymeric chains of ethylene which consists of two carbon atoms and four hydrogen atoms. A fine granular PE powder is produced by polymerization of ethylene. Such chemical reaction is a catalytic process that is driven by metal compounds which are referred to Ziegler-Natta catalysts²⁰⁵. The PE powder may then be further processed by three methods to manufacture orthopaedic devices. The first method is ram-extrusion of the powder into cylindrical bar stock (50, 62.5 and 75 mm diameter; 1.5 - 3 m in length) with the powder compacted and heated between $T = 180 - 200\text{ }^{\circ}\text{C}$ for consolidation²⁰⁶⁻²⁰⁸. In the second method, sheets (usually 120 cm x 320 cm) are produced after placing the PE powder into a mould. At first, the powder is cold pressed at a pressure of 5 - 10 MPa to remove excessive air and then completely fused under a temperature of 200 °C. The moulds are then cooled at a pressure of 7 - 10 MPa producing a sheet of thickness up to 75 mm. In the

third method, orthopaedic components can also be made by direct compression moulding where the powder is directly converted into the final product. Compared with the ram-extrusion and moulded sheet processes, the compression moulding requires no additional machining to produce the final component and a smooth surface finish can be achieved.

2.4.2 Properties

PE is called ultra-high molecular weight (or UHMWPE) when its molecular weight exceeds 1×10^6 g/mol²⁰⁶⁻²⁰⁸. In conventional PE, secondary forces hold the molecular chains together that result in crystalline lamellae (Fig. 2.8). Therefore this group of polymers can be re-melted and welded which is a characteristic of thermoplastics. As mentioned earlier in Section 2.2.3, thermoplastics may also be called partial-crystalline polymers due to their crystalline and amorphous structure. With increasing molecular weight of the thermoplastic, the melt temperature increases proportionally. Generally, when the temperature in these polymers is increased, firstly the amorphous area softens followed by the crystalline area due to the higher binding energy between individual polymer chains. Currently the PE used in the medical industry has a molecular weight of $3 - 6 \times 10^6$ g/mol, a melting point of 125 - 145 °C, and a density ranging from 0.930 to 0.940 mg/mm³. The main grades of powders used in orthopaedic devices are shown in the Table 2.2^{208,209}. The degree of polymerization is proportional to the molecular weight of the polymer while the crystallinity varies in the different types of resins and decreases with increasing molecular weight. This property has an influence on the fracture and fatigue characteristics of the polymer. With increasing crystallinity the resistance to propagation of fatigue cracks was found to improve, provided oxidation did not occur^{208,209}. The oxidation of the PE surface can cause embrittlement and increases the possibility of crack initiation and hence, results in more severe wear.

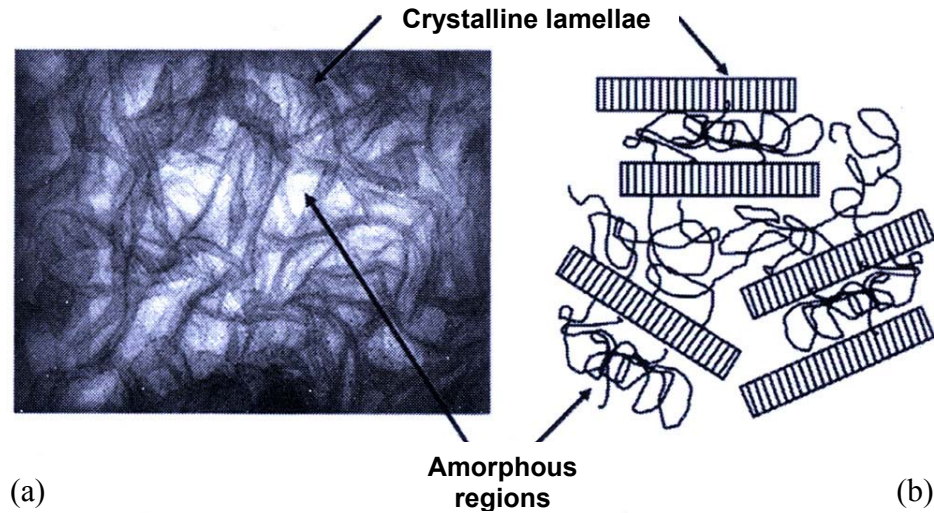


Figure 2.8: Microstructure of PE: transmission electron microscopy (a) and schematic (b) (from Kurtz et al. ²¹⁰).

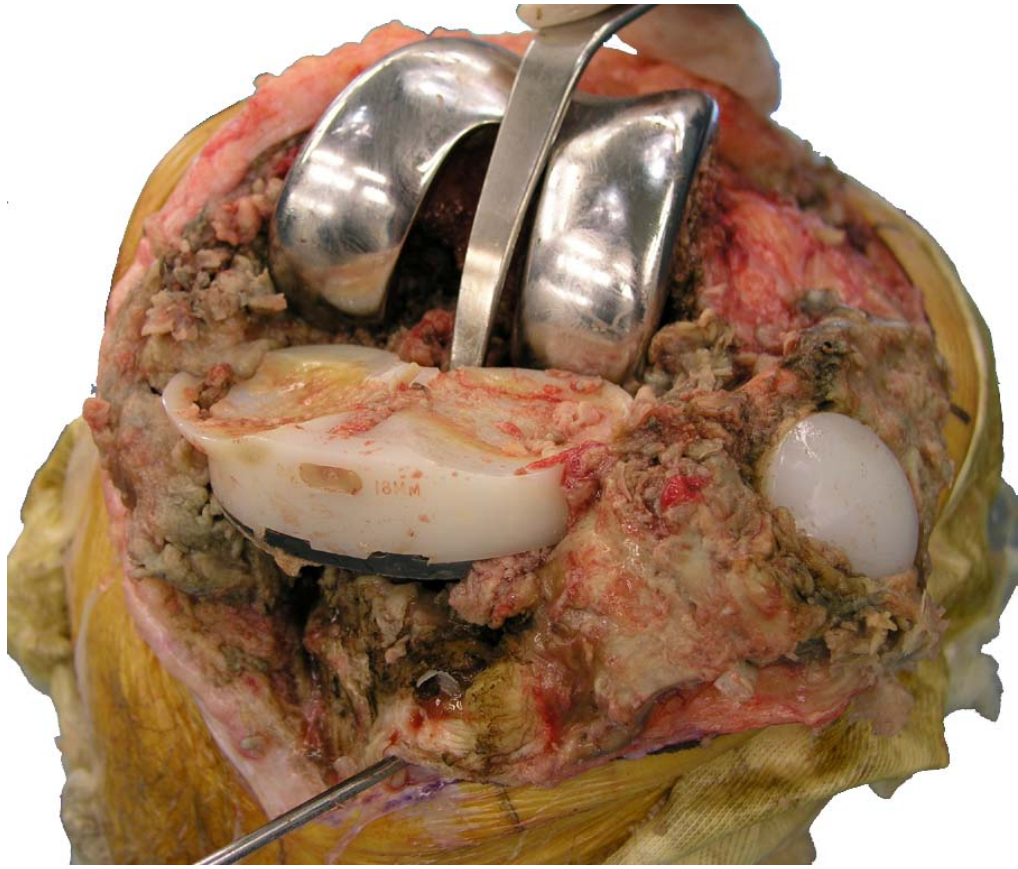
Table 2.2: Properties of three main grades of PE resin used for orthopaedic devices (data adapted from ^{208,210}). For the GUR resins, the first digit “1” stands for polyethylene, the second digit for the presence (“1”) or absence (“0”) of calcium stearate that was used for corrosion resistance, as a whitening agent and as a lubricant to facilitate the extrusion process. The third digit indicates the average molecular weight (“2” for 3.5×10^6 g/mol; “5” for $5.5\text{--}6 \times 10^6$ g/mol). The GUR stands for Granular UHMWPE Ruhrchemie (where Ruhrchemie AG (changed to Hoechst AG and is now known as Celanese AG) was a company in Oberhausen, Germany).

Resin name	Former resin designation	Ave. MW [10^6 g/mol] ^d	Tensile modulus [MPa]	Yield stress [MPa]	Impact strength [kJ/m ²]	Particle size [μ m]	Calcium stearate
GUR 1150 ^a	GUR 4150	5.5-6	680	≥ 17	≥ 130	140	Yes
GUR 1050 ^a	GUR 4050	5.5-6	680	≥ 17	130	140	No
GUR 1120 ^{a,c}	GUR 4120	3.5	720	≥ 17	210	140	Yes
GUR 1020 ^{a,c}	GUR 4020	3.5	720	≥ 17	210	140	No
1900 ^b	-	4.4-4.9	750	≥ 19	65	300	No
1900H ^b	-	>4.95	750	≥ 19	65	300	No

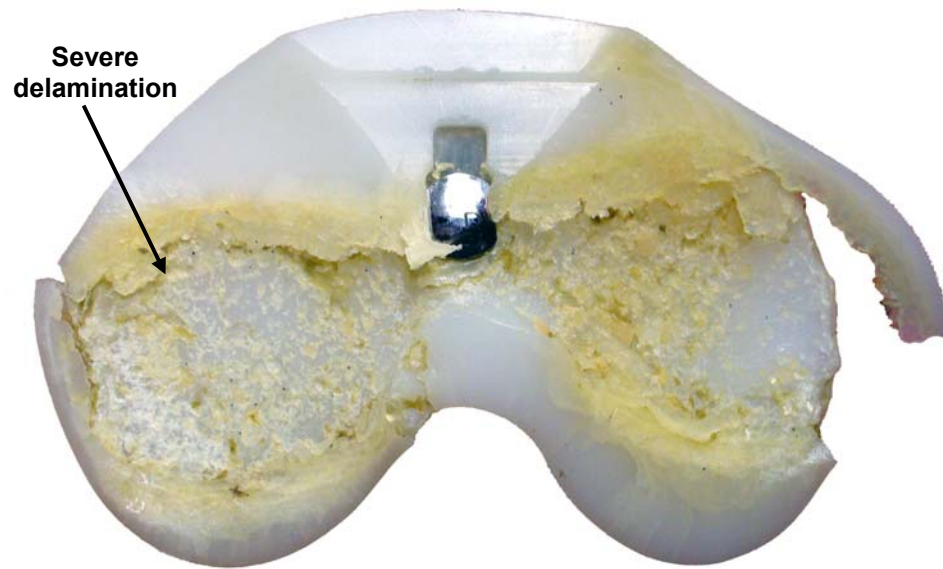
^a Ticona (Summit, NJ); ^b Montel (former Himont; Wilmington, DE); ^c also known as CHIRULENTM

2.4.3 Sterilization Techniques and Oxidative Degradation

All implant components must be sterilized before they are distributed to the surgeon for implantation^{207,209,211}. Until the early 1990's, gamma-in-air sterilization (GA) was widely used by orthopaedic companies with a dosage of 2 - 3.5 MRad. Besides the actual sterilization of the components, the gamma-irradiation disrupts the covalent PE bonds of the tibial insert, causing free radicals to occur which changes the mechanical properties of the PE^{206,212-216}. These changes in the mechanical properties occur because the free radicals can combine with ambient oxygen during the GA process, the shelf storage time²¹⁴ or even *in vivo*²¹⁷. Oxidative reaction of PE results in chain shortening, reduction of the molecular weight, reduced toughness, increased density as well as in a reduction in fracture strength and elongation to fracture. It also causes excessive wear *in vivo*. Delamination wear is a characteristic damage feature of oxidized PE inserts and has been reported to occur on the top side of the PE insert²¹⁸, on the post²¹⁹ of PS type inserts, but not on the distal (backside) surface²²⁰ (Fig. 2.9). The peak level of oxidation can be typically observed from 0.5 - 2 mm below the surface and can be observed as so called "white bands" after sectioning inserts. Although GA has been abandoned as a sterilization method, gamma-irradiation in inert atmosphere is still being used. Recently, Brandt et al.²²¹ reported severe delamination wear on two gamma-in-nitrogen sterilized PE inserts retrieved after 76 months (shelf storage prior to implantation = 13.6 months) and 170 months of implantation (shelf storage prior to implantation = 4.8 months), possibly indicating that *in vivo* oxidation had occurred as had been found by Kurtz et al.^{217,222} and Currier et al.²²³. Another sterilization technique is gamma-in-vacuum foil²²⁴. The process is similar to gamma-in-nitrogen, only that the tibia insert is irradiated in a barrier bag that contained a vacuum environment. Thus, the oxidation is suppressed pre-operatively, but can start again once the tibia insert is implanted because the synovial fluid carries oxygen that is able to react with the free radicals of PE. In any case, oxidation of the PE inserts may also be facilitated by the use of oxygen permeable packaging for irradiated inserts²²⁵.



(a)



(b)

5 mm

Figure 2.9: A failed AMK[®] (DePuy Orthopaedics Inc., Warsaw, IN) in a) intraoperative view during revision surgery and b) the retrieved PE insert. The PE insert was GA sterilized prior to implantation and showed severe delamination wear after its retrieval.

Other sterilization techniques without irradiation, such as gas-plasma (GP) and ethylene oxide (ETO) have been used. Non-gamma-in-air (NGA) sterilized PE, such as those exposed to ETO²²⁶, did not show any oxidation degradation in the form of white bands or delamination after prolonged implantation. GP is a surface sterilization method using plasma (ionized gas; peracetic acid, hydrogen peroxide) to oxidize biological organisms. A GP sterilization interval can take up to 4 h at low temperature (< 50 °C) and at low-pressure in a dry environment. ETO sterilization is performed by diffusing ETO into the near-surface regions. The process involves an 18 h preconditioning period at a temperature of 46 °C with a relative humidity of 65 %, accompanied by a 5 h exposure of 100 % ETO gas at a temperature of 46 °C and a pressure of 0.04 MPa. To guarantee the diffusion out of the polymer, an 18 h forced aeration period at the same temperature is required. So far, these sterilization techniques have not been associated with PE oxidation (on the shelf or *in vivo*) or with severe delamination wear on retrieved components²²⁷.

2.4.4 Microstructural Effects

Different PE resins have been shown to have also different mechanical properties and therefore affect the clinical wear behaviour of these implants. Incomplete fusion (weakness of bonding at the intergranular boundaries) during the manufacturing process of PE was shown to produce defects in the components that led to an increase in the occurrence of severe damage features such as cracking and delamination *in vivo*^{207-209,228,229}. Fusion effects can leave cavities behind that can serve as an onset for crack initiation during fatigue. Calcium stearate, a non-toxic stabilizer and lubricant, was originally added to facilitate PE processing and to enhance the white color of the PE but, unfortunately, lead to incomplete fusion and promoted long-term oxidation. The presence of fusion defects combined with calcium stearate has been associated with a decrease in ultimate tensile strength, elongation to fracture, fracture toughness, and fatigue resistance. Himont 1900 resins in both ram-

extrusion and direct compression moulding process have been shown to have superior resistance towards oxidation, delamination²³⁰ and excellent long-term results²³¹. White bands were observed on GUR 1150 (GUR 4150) while they did not occur on inserts made of Himont 1900 resin. Oxidation in Himont 1900 resin was significantly lower compared with the GUR resin after GA sterilization and implantation²³⁰. It was suggested that compression moulded PE inserts from Himont 1900 resin were less susceptible to chain scission caused by GA sterilization. Another reason for improved *in vivo* performance of Himont 1900 resin may be associated with its larger virgin particle size (~ 300 µm) compared with the GUR types (~ 140 µm). Increased particle size created fewer boundaries after consolidation. In addition, Himont 1900 resin was calcium stearate free and therefore, with the fewer boundaries, less prone to oxidation than the GUR 4150 resin. Berzins et al.²³² suggested in their retrieval study that GA sterilized inserts made of compression moulded resins may be more wear resistant than the GA sterilized machined components. They found that the severity of delamination increased with implantation period. Delamination was only observed on the compression moulded inserts after 60 months while it was already observed after as early as 10 months in the ram-extruded group²³³. In any case, GA sterilization should have been avoided.

2.4.5 Alternative Tibial Bearing Materials

Although only conventional PE was investigated in the present study, it was felt necessary to give a brief summary of bearing material alternatives to conventional PE. In the past thirty years, four major alternative bearing materials have been introduced into the orthopaedic field, as comprehensively summarized by Kurtz et al.²⁰⁶. In the 1970's, carbon fiber reinforced polyethylene (Poly IITM, Zimmer inc, Warsaw, IN) was introduced to the market with the goal to reduce wear. Adding short carbon fibers to the PE increased the compressive strength and ultimate tensile strength. It was hoped that this would increase extent the implant durability. Poly IITM failed after short

implantation periods, with patients showing severe osteolysis and catastrophic, mechanical failure of the insert. Fracture mechanical analysis revealed that the Poly II™ inserts had an 8-fold faster crack propagation compared with PE, suggesting that the carbon fiber-polyethylene interface may have enabled crack initiation. Clearly, this alternative bearing material was not adequately tested in knee wear simulators.

In the early 1990's, DePuy DuPont introduced a hot isostatically pressed PE for the hip replacements (Hylamer™) and as an alternative bearing material to PE on the knee side Hylamer-M™. Hylamer-M™ had a higher crystallinity and a higher modulus of elasticity than PE; yet lower than the Hylamer™ acetabular inserts. The increase in crystallinity made Hylamer more susceptible to oxidation after GA sterilization compared with GA sterilized PE and resulted in higher wear rate. Hylamer-M™ utilized in the in TKR was associated with severe delamination wear facilitated by GA sterilization^{234,235}. Thus, product lines of Hylamer™ and Hylamer-M™ were both discontinued. Recently, Brandt et al.²³⁶ showed that the surface damage on Hylamer-M inserts was dependent on the sterilization technique. GA sterilized Hylamer-M™ showed delamination wear while GP sterilized Hylamer-M™ did not show such damage feature. The revision rate for Hylamer-M™ (10 %) was comparable to the revision rate for conventional PE in primary total knees. Once again, this alternative bearing material was not adequately tested in knee wear simulators.

As mentioned earlier, GA sterilization of PE was replaced with non-gamma-in-air sterilization techniques (NGA) such as GP sterilization, ETO sterilization, gamma sterilization in inert atmospheres and gamma sterilization in vacuum to counteract the problems of oxidation. In the study performed by McKellop et al.²²⁹, the *in vitro* wear rate of ETO sterilized PE was higher than that of PE that was sterilized in gamma-inert or gamma-vacuum environment, suggesting that the gamma irradiation could sometimes be beneficial to the wear process. This was attributed to the cross-linking of the polymeric chains that was produced by the GA process. Such findings were also supported by *in vivo*

findings²¹⁶. Reduced wear resistance of highly gamma-irradiated PE was first suggested by Oonishi in 1971²⁰⁶. An irradiation dosage of 100 MRads was used to sterilize acetabular PE liners in air. Although the link between oxidative degradation and GA sterilization was not yet established as a precursor of white bands and delamination wear, the wear of the irradiated PE was lower than the non-irradiated PE. In any case, the increased wear resistance of gamma-irradiated PE and the oxidative stability of NGA inserts initiated the development of XPE. Cross-linking can either be achieved by irradiation, electron beam, peroxide chemistry or silane chemistry²⁰⁶. Most frequently, XPE is produced in inert atmospheres under irradiation followed by annealing or remelting to permit all the free radicals to bond and produce cross-links. This process has produced an alternative bearing material to conventional PE that resists oxidative degradation and wear^{72,206,237-239}.

Although cross-linking may clearly improve the wear resistance and oxidative stability of XPE in simulator studies, a drawback may be the reduction in fatigue properties and fracture toughness^{240,241}. So far, these possible limitations of XPE could not be confirmed in knee simulator studies, even under more aggressive wear testing using higher loading²⁴². However, Muratoglu et al.²⁴² used SA as the microbial inhibitor and did not add HA to the calf serum lubricant in their wear tests which may affect the wear behaviour of XPE. Recently, Medel et al.²⁴³ suggested an annealing process be used rather than a re-melting process for XPE since it preserves the fatigue and fracture resistance. In the application of XPE to hip implants, Bradford et al.²⁴⁴ assessed the surface damage on retrieved XPE acetabular inserts after a mean of 10 months of implantation showing some deformation and cracking on the surface that had not been seen after simulator wear testing. Although none of the acetabular XPE inserts were revised for implant failure, the use of XPE was cautioned²⁴⁵. Fisher et al.²⁴⁵ reported that the wear process produced a larger volume of wear particles with higher biological potential compared with PE and may increase the incidence of osteolysis and thus implant failure after long implantation periods. This view was corrected recently by Galvin et al.²⁴⁶, suggesting that

XPE produced both a lower volume and lower number of biologically active wear particles in hip simulations. However, the lubricant used contained SA and did not contain HA as a clinically relevant additive ²⁴⁶. Despite these concerns, highly XPE (irradiated with up to 10 MRads) is frequently used in THR. For TKR, XPE (irradiated with 2 - 5 MRads) is offered as an alternative to NGA sterilized PE but many surgeons are still hesitating to use it. The irradiation dosage is reduced for XPE intended for TKR because contact stress is higher and thus surface fatigue more likely ²⁴⁷.

The current decision to use PE or XPE depends on the type of insert used. In the case of CR type insert, XPE may be considered an attractive alternative; in the case of PS type insert, NGA sterilized PE remains the insert of choice due to concerns of possible post fracture due to reduced fracture toughness of XPE. It may therefore solely depend on the surgeon's preference for a specific insert type on whether a patient receives XPE or PE in their TKR ^{248,249}. The more conservative surgeon appears to be inclined to use NGA sterilized PE over any type of XPE based on the inferior performance of historically used alternative tibial bearing materials. The properties of currently available XPE were further described by Lewis ²⁵⁰ and Collier et al. ²⁵¹.

Last but not least, ceramic-on-ceramic bearings have been successfully utilized in the hip ²⁵² and consequently have also found some attention for TKR. A fully ceramic, mobile bearing was proposed by Heimke et al. ²⁵³ and has successfully been tested in a knee simulator ²⁵⁴. To the author's knowledge, the fully ceramic TKR is still in its infancy and more research appears to be necessary. It needs to be ensured that the ceramic meniscal components of this mobile design are not subject to dislocation ²⁵⁵ or component fracture ^{256,257}.

2.5 Clinical Wear and Osteolysis

2.5.1 The Source of Biologically Active Wear Particles

Wear particles are produced in all PE articulations involved in the wear process, i.e. top side, post, backside surface, and the patella. The characteristics (shape and size) of these wear particles are likely to be different and may depend on the motion in the individual articulations and on whether a mobile or a fixed TKR system is used. The mobile TKR may allow the PE insert to slide and rotate on the tibial tray while also articulating with the femoral component whereas the fixed TKR does not allow any gross motion between the PE and the tibia. Nowadays, fixed TKR represent the largest fraction of systems implanted and are classified into either modular (PE locked onto a metal tibial tray with a clamping mechanism that can be released) or non-modular (mono-block, components or PE components with a permanent mechanical interlock to a metal tibial tray) systems^{3,258}. Only the fixed, modular TKR were considered in the present thesis.

TKR systems evolved mainly during the 1970's and led to several favorable designs that were used clinically²⁵⁹. One of the most popular and successful TKR system was the mono-block, non-modular design with a posterior cruciate ligament substituting (PS) PE insert which was introduced by Insall et al.²⁶⁰ (Insall-Burstein[®], Zimmer Inc., Warsaw, IN). This particular system was implanted by cemented fixation and had excellent long-term results (> 20 years) and osteolysis apparently did not occur in the older, inactive patient cohort^{14,261-263}. In addition, osteolysis had not been found for other cemented non-modular PE inserts that were directly compression moulded using Himont 1900 resin²⁶⁴⁻²⁶⁸. A failure mechanism of early non-modular, mono-block inserts was associated with the collapse of the medial tibial plateau and was found problematic for patients with RA due to the reduction in bone quality. However, some patients with medial bone collapse actually started to heal again and did not require revision surgery²⁶⁹. Bartel et al.²⁷⁰ suggested that the PE insert should be metal-backed to allow the load to be more evenly distributed over the tibial bone and thus, many mono-block PE inserts were consequently

transformed into metal-backed PE inserts. Nowadays, TKR systems using non-modular, mono-block PE tibial components have comparable functional outcome to those using matched non-modular, metal-backed tibial components^{271,272}. Such indifference stimulated the orthopaedic companies to no longer offer the more expensive metal-backed non-modular TKR for implantation. Today, mono-block PE TKRs are preferred for use in older patients (> 70 years) with good bone stock and OA as their primary diagnose. Furthermore, Ranawat et al.²⁷³ reported on a follow-up of 430 TKR systems with mono-block PE that were implanted in younger (≤ 60 years of age), more active patients. None of the patients showed any indication of osteolysis on radiographs after a mean implantation of 5 years (range, 2 to 11 years) suggesting the benefits of mono-block PE inserts. However, the long-term performance of the mono-block PE inserts in younger, more active patients remains uncertain.

Modular TKR systems were introduced with the aim to offer the surgeon a larger intraoperative versatility of PE inserts. Such versatility was intended so that surgeon may select PE inserts of different thicknesses during the surgery to manage the flexion-extension gap most appropriately. It consequently reduced inventory costs and allowed an isolated exchange of the PE insert without revising the entire tibial component. The latter has only rarely been practically applied when GA sterilized PE was used which made the revision of the entire prosthesis necessary²⁷⁴⁻²⁷⁷. These modular components could either be implanted by cemented fixation or cementless fixation. Some surgeons^{278,279} were advocates of the cementless fixation, suggesting that it would reduce the shear stress at the interface between the tibia and the implant. However, tibial osteolysis was reported for cementless modular TKA^{13,218,280-282}. Such cementless fixation permitted PE to protrude into the screw holes (Fig. 2.10). Such protrusions in combination with cyclic loading and relative motion of the PE insert due to the slack in tibial tray locking mechanism (that can occur with advanced implantation period) caused osteolysis. Surrace et al.²⁸² reports a linear relationship between PE protrusion height and depth of tibial osteolysis.

Conditt et al.²⁸³ estimated a backside *wear* volume of up to 138 mm³/year for a modular TKR system with screw holes (AMK[®], DePuy Orthopaedics Inc., Warsaw, IN). In any case, cementless fixation and the use of trays with screw holes had been widely abandoned^{15,258,263,284-288} with the goal to create a barrier between the modular PE insert and the tibia to inhibit osteolysis.

The backside volumetric wear from PE inserts from contemporary modular TKR without screw holes and implanted by cemented fixation has been estimated in *in vitro* tests at a substantial 30 % of the total wear^{6,46}. The damage features at this highly conforming interface somewhat similar to the head-cup articulation in total hip implants²²⁰ in that the wear particles generated from the backside surface may be smaller than the wear particles from the top side surface^{220,289}. They are also more concentrated at the implant-bone interface than the particles produced at the tibiofemoral articulation²⁹⁰⁻²⁹². Unfortunately, such implants can still have an associated osteolysis²⁹³⁻²⁹⁶, particularly if the patient is young and overweight²⁹⁷. Currently, the Orthopaedic companies offer tibial trays made of either CoCr alloy or Ti alloy with a variety of tibial locking mechanisms and tray surface finishing.

Backside damage has been investigated in a number of studies of retrieved tibial inserts and various relationships of backside *damage* to backside *wear* have been suggested^{220,283,289,292,298-303}. The limited availability of retrieved knee implants has caused these studies to consider a variety of implant models and features with large differences in patient histories and still attempted to identify statistically significant influential factors for the backside damage. While such efforts are commendable and should be attempted, it is unfortunate that their findings have been uncertain enough to prevent clear confirmation of the effectiveness of many design features such as the tibial tray locking mechanism, the tibial tray surface finish, and the role of sterilization technique^{304,305}.

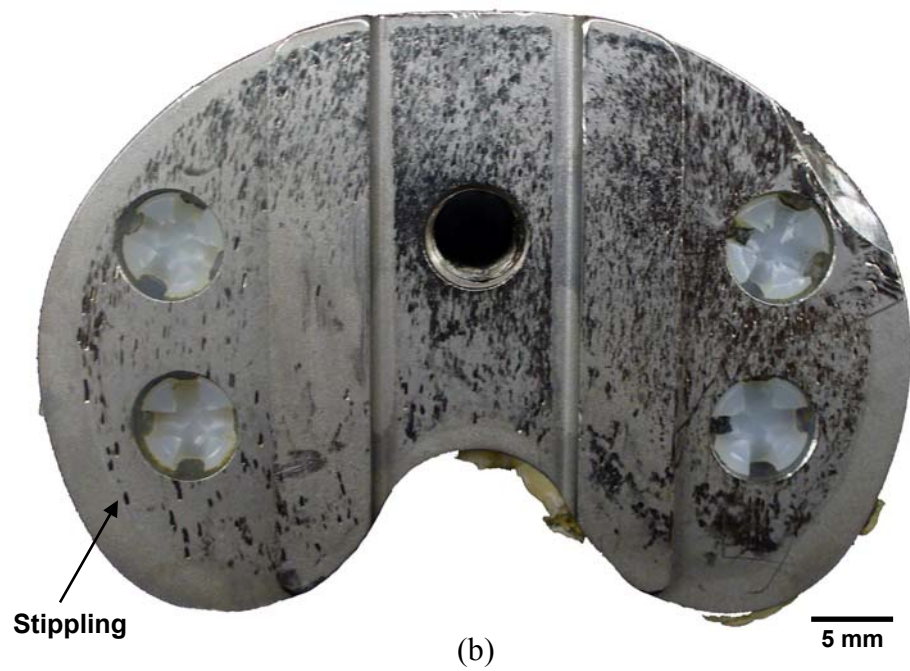
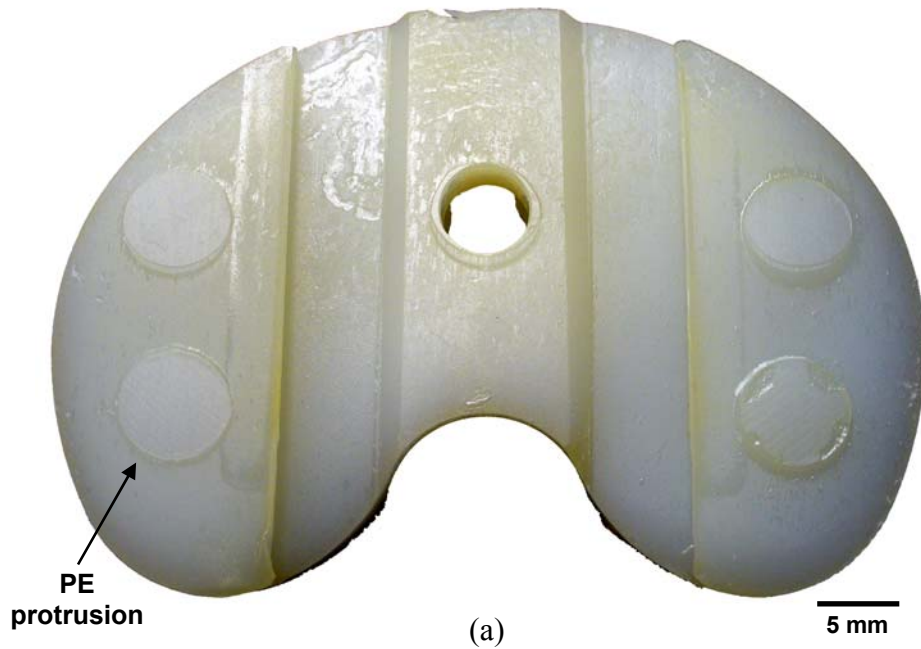


Figure 2.10: Image showing (a) the distal (backside) surface of the PE insert and (b) the proximal surface of the Ti alloy tibial tray of a retrieved TKR system (AMK[®], DePuy Orthopaedics Inc., Warsaw, IN). Note the wear pattern on the PE insert as well as on the tibial tray possibly caused by insert micromotion and presence of third-body wear particles. Such damage feature was referred to as stippling by Engh et al.²⁹⁹ and associated with osteolysis.

Metal-backed PE used for patella replacements were also deemed as a precursor of osteolysis^{13,306}. If the patella is resurfaced, which is still controversial³⁰⁷ and not frequently performed³, it may be best to cement an all-PE patella button to avoid any possible problem with patella backside wear³⁰⁸. Dorr¹⁵ suggested that wear and osteolysis are not issues for implants with mono-block PE tibial and patellar components along with CoCr femoral components all of which are implanted using cemented fixation.

2.5.2 Mechanisms of Bone Loss

The loss of bone can lead to implant instability and implant failure that makes revision surgery necessary. This can be initiated by both stress (and strain) shielding and periprosthetic osteolysis which have different mechanisms. Stress shielding causes bone loss in the absence of bone loading or more correctly in the absence of bone strain. This occurs when the implant carries the majority of the load as a result of its high modulus of elasticity³⁰⁹ and can occur in the distal aspect of the cementless implanted femoral components³¹⁰. Periprosthetic osteolysis is defined as bone resorption that is mediated by both wear particles and fluid-pressure^{10,12,311-314} and is considered most relevant to the present thesis.

In 1977, Willert¹⁰ was perhaps the first to suggest an adverse reaction of macrophages to wear particles and implicated this reaction as a precursor of implant loosening. This finding did not receive much attention for another decade; it was not until 1987 when osteolysis was only considered as *cement disease*³¹⁵. Jones and Hungerford³¹⁵ suggested that wear particles produced at the implant-bone cement interface initiated an inflammatory response that generated giant cells and activated bone resorption. Shortly after, PE wear particles were suggested to cause osteolysis particularly when a Ti alloy femoral head was articulated against a PE acetabular cup^{316,317}. Osteolysis became also apparent in TKR when cementless modular tibial components were used^{13,281}.

In periprosthetic osteolysis, the generated wear particles are suspended in body fluid that surrounds the implant-bone interface and are taken up by the adjacent tissue where they elicit a foreign body reaction. Concurrently, some wear particles are phagocytosed and carried away by the lymphatic system. If the level of wear particle generation exceeds the ability of the body to carry them away, the wear particles become more concentrated at the implant-bone interface. Micromotion between the implant-bone interfaces may result in pistoning and increase the local fluid pressure^{12,314}. Both the increased wear particle concentration and the increased localized fluid pressure may stimulate periprosthetic macrophages and various cytokines such that osteolysis is induced directly or indirectly (Fig. 2.11). *Direct osteolysis* is caused by the action of macrophages that are induced by foreign bodies. These macrophages can adopt osteoclast-like behaviour and initiate bone resorption. *Indirect osteolysis* is caused by the stimulation of macrophages which leads to enhanced production of proinflammatory mediators or cytokines. The cytokines that are released by these stimulated macrophages can be interleukin-1 β (IL-1 β), interleukin-6 (IL-6), tumor necrosis factor- α (TNF- α) and prostaglandin (PGE₂) and these cytokines act as osteoclast stimulants. The osteolytic response depends on the particle size and volume as well as on the patient immune system particularly with regard to their cytokine production^{318,319}. TNF- α was deemed to be the key cytokine involved in osteoclast stimulation³²⁰. In recent years, several *in vitro* studies³²¹⁻³²⁵ were undertaken to investigate the inhibition/blockage of cytokines on osteoclastogenesis. The results have been encouraging in animal studies and may suggest that inhibitors/blockers may be useful as therapeutic agents for the treatment of prosthetic loosening in humans and may be soon facilitated in clinical trials.

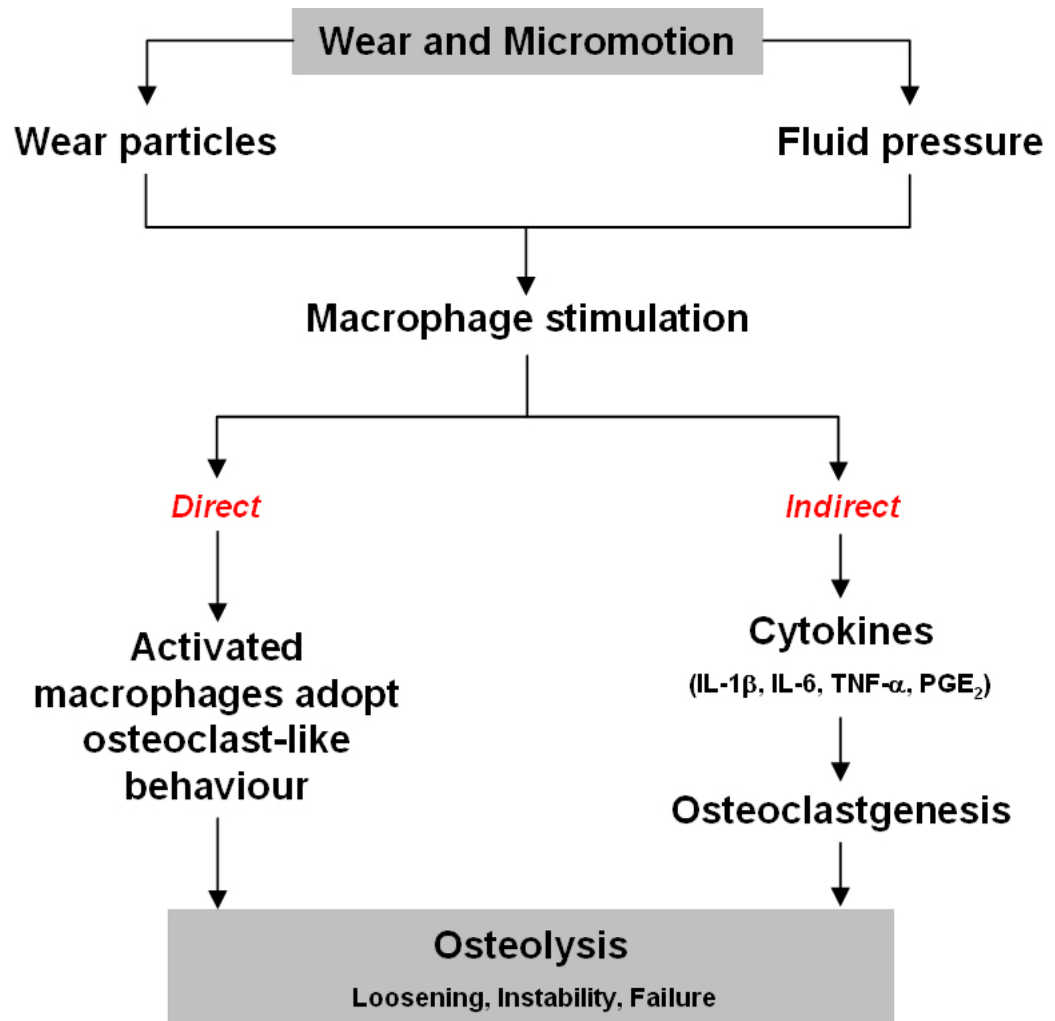


Figure 2.11: Display of the pathway of direct and indirect osteolysis mediated by wear particles and fluid pressure.

Wear particles can be characterized by their size and shape and were distinctively different in THR compared with modular TKR^{290,291,326}. The particles that caused with the highest cytokine production in macrophages and thus had the highest biological activity were of 0.1 - 1.0 μm in size at a volume of 10 - 100 mm^3/year ³²⁷. Large flake-like shaped particles having in-plane diameters of several micrometers were commonly observed in TKR but not in THR. In general, particles obtained from modular TKR were found to be much larger (up to 20 μm) compared with those from THR (mostly < 1 μm or “submicron”). The particle size dissimilarities between THR and modular TKR

may be related to the effect on wear of their different contact stress distributions and motions. The ball-in-socket geometry in THR results in a more uniform stress distribution and more multi-directional motion. Thus, the difference in particle morphology and size may be due to difference in the wear mechanisms acting in THRs and modular TKRs. However, the numbers of submicron wear particles and their volumetric concentrations in TKA were still substantial and have caused wear particle-induced osteolysis²⁸¹.

A large variety of particle sizes, shapes and textures have been found after modular TKA but “submicron” particles were less prevalent than in modular THR. The reduced number of submicron particles in TKR may explain the lower incidence of osteolysis in TKR because the submicron particles are the most active in the periprosthetic osteolysis process¹⁵. Recently, Tipper et al.³²⁸ conducted an *in vitro* wear test on THR and modular TKR with matched bearing materials (GUR 1020, gamma-vacuum-foil sterilized PE) and reported no significant difference between wear rates. Although nanometre-sized wear particles were isolated from both joint replacements, THR was shown to produce a larger number of small wear particles compared with TKR and thus, the particles from THR were found to have a higher osteolytic potential compared with particles found in modular TKR.

As a final comment, wear particles produced from any type of bearing surface such as metal-on-metal, ceramic-on-ceramic, ceramic-on-PE/XPE may be associated with osteolysis but the onset is delayed if the volumetric wear is low and thus, fewer wear particles are produced³²⁹⁻³³¹. In addition, the differences between the biological activity of various PMMA products^{332,333} suggested that the surgeon must/should also carefully select the type of bone cement for cemented fixation. Although the use of XPE is associated with lower volumetric wear it also produces a larger number of smaller wear particles with a higher biological potential^{245,334,335}. So far, XPE has not been associated with osteolysis, however, this may occur with more advanced implantation periods and increased application of XPE in younger, more active patients. Many studies were conducted on the shape of wear particle

characteristics in modular knees^{290,291,336,337}, however there is no study to date that directly compared the particle shape, size and population from non-modular TKR systems to modular TKR systems.

2.5.3 Clinical Wear Assessment

The current standard of the *in vivo* wear assessment of TKR systems is by visually evaluation of radiographs. The surgeon observes the gap between the metal femoral component and the metal tibial tray and attempts to estimate the severity of the wear. Unless the wear is very high, this technique fails to detect wear accurately³³⁸. Recently, radiostereometric analysis (RSA) has been introduced in an attempt to measure the linear depth penetration of the femoral component into the PE insert more accurately in TKR³³⁹. A short explanation on the basic principle of the RSA technique will be briefly given³⁴⁰. Tantalum beads, approximately 1 mm in diameter, are placed in the PE insert and in the adjacent bone of the tibial and femoral implant components during implantation. Radiographs are taken in the medial-lateral (ML) direction and in the anterior-posterior (AP) direction that show the location of the implanted beads and the implant components. These radiographs are then digitized to permit the computerized analysis via the RSA software program. This software program facilitates algorithms that calculate the distance between the beads and also enables the calculation of the change in distance between two radiographs taken from one patient after different implantation periods. This method gives some estimate on how much the flexion-extension gap was reduced due to wear or creep and is represented by the measured linear penetration. For a particular non-modular, metal-backed TKR system (AGC[®], Biomet Inc., Warsaw, IN), RSA was performed on 4 patients that received 6 TKRs³³⁹. A mean linear penetration of 0.075 mm/yr was estimated³³⁹. In addition, Gill et al.³³⁹ recorded the linear penetration at different flexion angles. A computer aided design (CAD) model of a femoral component and of a PE insert in contact was created and combined with the linear penetrations. This resulted in the

interpenetration of the femoral CAD model and the PE insert model which was calculated at different flexion angles to calculate the wear volume of approximately 100 mm³ per year. Simulator wear tests have shown that approximately 30% of the total wear volume in modular TKR is caused by the backside surface^{6,46} and thus, a total wear may be as high as 143 mm³/year. The use of RSA for *in vivo* wear evaluation in TKR is still being developed and requires expensive computer/instrumentation facilities (so-called RSA suite).

To gain insight into the *in vivo* wear process, the damage on retrieved implant components is routinely assessed. The damage analysis of retrieved implant components attempts to give some quantitative information on implant performance and can be compared with implants tested in knee wear simulators to estimate the fidelity of the simulation. Generally, measurements of mass and geometry are not used to determine wear of retrieved tibial inserts because the exact starting values are usually not known and the influence of fluid uptake would be difficult to determine. To quantify wear in an approximate manner, grading systems can be applied to produce damage scores under the assumption that surface damage correlates with wear^{26,302,341}. The damage score is usually based on both the extent of the damage area and the damage severity compared with the unworn surface. A number of different damage features can be observed on the retrieved insert and are subsequently assessed and graded. The sum of all scores is then reported as the total damage score. The most frequently used grading method was introduced by Hood in 1983²⁶. In this method, a damage score of 0, 1, 2 and 3 corresponds with 0 %, 0-10 %, 10-50 %, and 50 - 100 % surface damage.

Wasielowski et al.³⁴¹ slightly altered the Hood-method by measuring the damage area and damage severity for the proximal insert surface. They used generated digitized wear maps of the worn area of individual damage features and assigned the Hood-score based on the damage area. The damage severity was separately assessed with a subjective score of 1 (mild damage; just visible), 2 (moderate damage) or 4 (severe damage). For example, a moderately damaged implant with 70 % burnished area would receive a score of 3

following the Hood-method and a severity score of 2 which results damage score of $3 \times 2 = 6$. Reporting this type of damage score was believed to be more objective. This technique was used by others in its original and/or somewhat modified form for the proximal and the distal PE insert surface^{289,301,342}. Protrusions of the PE into the tibial tray screw holes (located underneath the tibiofemoral contact area and optionally used for temporary fixation when cementless fixation is employed) were assessed by measuring the protrusion height^{218,282} or assigning a severity score depending on the protrusion height³⁴². Cornwall et al.³⁴³ introduced a method that used digitized wear maps to quantify proximal PE bearing surface damage and represented the surface damage by the measured surface area over which it occurred. They suggested that the Hood-method was unsuitable for the damage assessment of severely worn (largely cracked and delaminated) PE inserts because it would underestimate surface damage. Although the method of Cornwall et al.³⁴³ was more reproducible³⁴⁴ it could only differentiate between either “no damage” or “complete damage” on the insert surface and thus, did not incorporate damage severity.

The examination of retrieved implants has been widely used by other investigators and has been described as a useful method for gaining insight into the *in vivo* wear process, particularly for the backside wear^{13,218,289,302,303,341,342}. There are differences between the wear scar generation on the insert in the tibiofemoral, post (if it is a PS insert) and backside articulations. The damage on the backside surface of modular TKR systems is deemed to develop more gradual compared with that of the tibiofemoral surface or post surfaces of the PE insert. Thus, a sensitive assessment method that permits the detection of such gradually surface damage may be necessary. Recently, in a backside wear study, Conditt et al.³⁰² modified the Hood-method (referred to as the Modified-method) by using equally spaced score intervals (severity score of 1 = 10 %, 2 = 20 %, ... 10 = 100 %). This particular method has been used on PE inserts from tibial trays with and without screw-holes, but not solely on PE inserts from trays without screw holes. In addition to the surface damage other clinical parameters

such as patient demographics, implant characteristics (shelf storage, resin type, insert type, sterilization technique, etc.), and treatment history (x-rays, medical treatment) were also collected ³⁰². Both the damage scores and clinical parameter were implemented in a statistical multiple linear regression model to determine possible design features that reduce backside damage. It remains uncertain if the backside damage scores of retrieved PE inserts from cemented tibial trays without screw holes are different for the Hood-method compared with the Modified-method.

2.6 Factors Influencing the Clinical Wear Performance

2.6.1 Implant Design

As mentioned previously, TKR systems can be classified as fixed bearings or mobile bearings. All mobile and some fixed bearing systems have a metal (Ti alloy or CoCr alloy) tibial tray. In fixed bearings, either modular (PE locked onto a metal tibial tray with a clamping mechanism that can be released) or non-modular (mono-block PE components or PE components with a permanent mechanical interlock to a metal tibial tray) systems are rigidly fixed onto the tibia by either cemented or cementless (only when a metal tibial tray is used) fixation. Fixed bearing designs have the following inherent design conflict. Higher tibiofemoral conformity, as seen, for example, in the classic condylar knee design ²⁶⁰, is accompanied with high stress transfer to the component-bone interface. However, lower tibiofemoral conformity, as seen, for example, in a round-on-flat knee design ³⁴⁵, is accompanied by reduced interface shear stresses but higher contact stresses and thus higher PE wear. Despite this design conflict, both the high and low conforming designs have shown excellent long-term clinical performance ^{14,231}.

Another design factor influencing *in vivo* performance of fixed bearings depends on whether the insert is of CR or PS type. Generally, CR inserts allow more of the natural kinematics, including femoral rollback, to occur while the PS type inserts constrain the motion more and thus add to the

stability. A PS type insert is also used in patients with insufficient posterior cruciate ligament stability. In some cases, CR type inserts may be associated with slightly higher stiffness (resistance towards joint motions) because of pain³⁴⁶. Rand et al.²⁵⁸ reported a survivorship of 91 % of patients with CR insert type and 76 % of patients with PS insert type at 10 years. The differences in survivorship between the CR type inserts and PS type inserts might have been reflected the use of modular tibial PE inserts components rather than the non-modular designs employed by Colizza et al.³⁴⁷, reporting a 98 % survivorship at 10 years follow up for PS type inserts. Impingement between the side walls of the intercondylar housing of the femoral component and the PS peg may transmit increased forces to the interface between the tibial PE insert and the metal tibial tray, resulting in wear and loosening²⁹⁵. Recently, Lee et al.³⁴⁸ showed that PS type inserts were affected by condylar lift-off at various flexion angles. Such condylar lift-off may promote eccentric loading and accelerate PE wear³⁴⁹. In addition, using a PS type insert introduces an additional bearing surface^{219,350} that produced more wear particles compared with the CR type inserts³⁵¹ and may facilitate osteolysis in the long-term. Using a CR type insert or PS type insert is largely dependent on the patient joint stability^{352,353} and according to Tanzer et al.³⁵⁴ may yield similar outcomes as long as the flexion-extension gap is balanced properly.

In mobile bearings, the PE insert is far less constrained than the PE insert in fixed bearings, allowing it to move somewhat freely over the tibial tray that can be implanted using cemented or cementless fixation. The PE insert may be allowed to “rotate” or to “rotate and translate” on the tibial tray. Here, the cruciate ligament is not sacrificed and only CR type inserts are available. The mobile bearing knee was developed to reduce contact stresses, thus decreasing fatigue wear of the PE insert, and to allow more normal kinematics to occur^{355,356}. The articulating surfaces are usually highly conforming and have shown to be associated with lower PE wear compared with fixed bearings, as long as the PE insert is allowed to rotate only⁶ and translational movement is inhibited³⁵⁷. It was suggested that the rotating platform mobile bearing knee designs

permit less multi-directional shear at the interface, allowing the PE chains to orient themselves in the direction of the linear-tracking motion^{39,67}. Such implants are deemed to be beneficial for younger, more active patients that require durability from their implant. However, insert dislocation in the miniscal mobile bearings is considered a limiting factor among surgeons. The superiority of mobile bearings over fixed bearing still remains to be proven^{255,356,358} and they only account for a small fraction of the TKR implanted on an annual basis³. It is deemed possible that mobile bearings will gain more popularity in the coming years with a higher population of young patients requiring TKA. In any of the implant designs described above, insert thickness and insert conformity are features of the PE insert that may affect the clinical performance^{270,359-361}. A minimum insert thickness of 6 mm for metal-backed fixed bearings was recommended for both modular and non-modular PE inserts³⁶⁰.

2.6.2 Femoral Component

Increased surface roughness of a hard surface facilitates abrasive wear when it is articulating against a softer bearing material such as PE³⁶². The femoral components can be scratched during implantation due to the presence of third wear particles and increase the wear of the PE insert^{363,364}. Ti alloy femoral components articulating against PE were associated with black discoloration of the synovium (metallosis) and increased PE wear that caused implant failure³¹⁷ (Fig. 2.12). CoCr alloys can be used because they have a higher surface hardness than Ti alloys and they are nowadays the most frequently used femoral components. However, the surface roughness of CoCr alloy femoral components was reported to still increase due to abrasive wear³⁶³ and tribochemical reaction¹⁰² *in vivo* which may accelerate PE wear. Also, Raab et al.³⁶⁵ showed that the CoCr femoral component can be scratched by surgical instruments during arthroscopy of TKR.

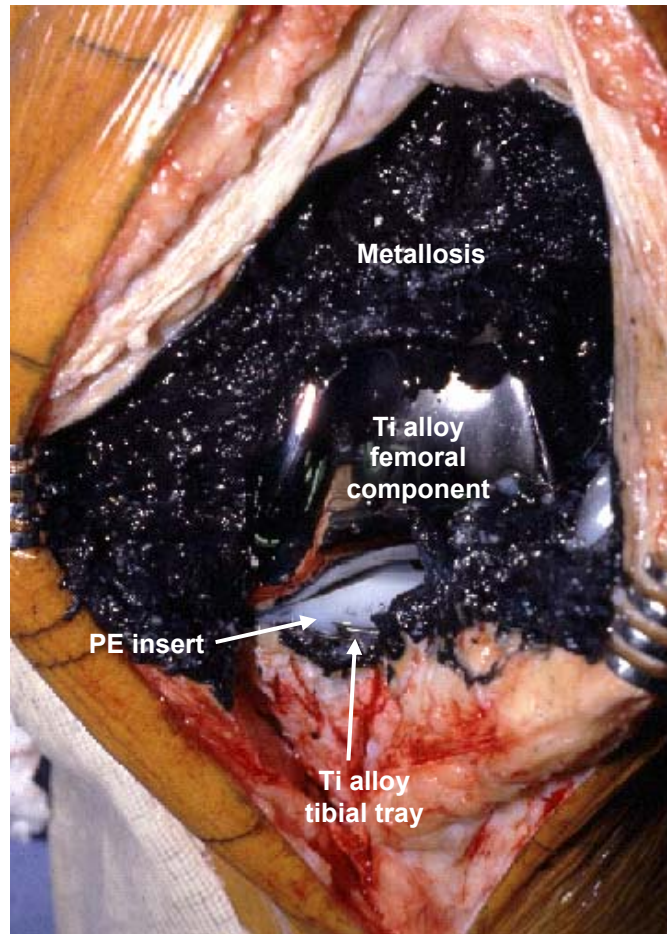


Figure 2.12: Intraoperative view of the discoloured synovium due to excessive wear of the Ti alloy femoral component against PE.

Replacing the CoCr alloy with a harder, oxidized zirconium femoral component significantly reduced the PE wear in simulator tests^{52,366,367}. It was suggested that the smoother and harder oxidized zirconium components had increased wettability (hydrophilicity) than the rougher CoCr alloy component which reduced adhesive wear and abrasive wear. In addition, Hallab et al.³⁶⁸ estimated that nearly 10 - 15 % of Americans are sensitive to Ni. CoCr alloy usually contains approximately 1 % Ni whereas it is not traceable in oxidized zirconium. Thus, an oxidized zirconium femoral component may be suitable for patients with Ni allergy³⁶⁹ in addition to its wear reducing characteristics. Alumina ceramic femoral components articulating against PE inserts have also

been used to offer a more wear resistant femoral component^{370,371}. The tibial tray can either be made of metal or even ceramic. Apparently, ceramic femoral components have been successfully used in Japan without any indication of component fracture³⁷¹. Nevertheless, the recent case report by Mochida et al.³⁷² illustrated osteolysis in four patients that received a cementless full-alumina TKR with an ETO sterilized PE insert.

2.6.3 Patient Characteristics

Patients conduct a variety of activities during their daily living³⁷³⁻³⁷⁶ and increased patient activity has been associated with higher PE wear, particularly in the heavier male patient³⁷⁷. Weiss et al.³⁷⁸ showed that despite increasing age, many patients with TKR participate in a wide range of recreational activities. Activities such as stretching, kneeling and gardening were most prevalent and important to the patients; they were also the most difficult to perform after TKA. Low impact/demand activities such as golf and swimming can be performed³⁷⁹, however, patients frequently ignore these suggestions and get involved in high demand activities such as marathon running which has resulted in catastrophic implant failure³⁸⁰. Patients that decided to expose their implant to activities such as cross-country or alpine skiing were more prone to osteolysis and implant failure³⁸¹. In addition, it also needs to be considered that the type of daily activities vary between cultures around the globe³⁸². Patients from non-western societies perform more a squatting, kneeling, or sitting cross-legged and many implants that are designed to accommodate such activities. The average number of walking steps taken by each leg has been estimated to be 2 Mc per year³⁸³.

2.6.4 Surgical Factor

The variability in surgical technique is another factor affecting the performance of implants and consequently the outcome for patients. Some indicators of patient outcome included the assessment of the post-operative behaviour such as pain and functional scores as well as the revision rate. Furthermore, some knee registries^{2,3} report the number of surgeries performed and the type of implant used. However, there is usually no comment on the surgeon specific outcome. Clearly, there are better outcomes and morbidities for patients receiving their joint replacements at high volume centres compared with low volume centres³⁸⁴⁻³⁸⁹. This suggests that a surgeon performing at a high volume centre may have developed a superior surgical technique compared with a surgeon operating at a low volume centre. However, there may also be superior care before and after surgery from the various support staff such as nurses and physiotherapists. It has been suggested that it would be in the best interest of the patient to receive the joint replacement by a surgeon operating at a high volume centre (> 200 procedures/year)³⁸⁷. In recent years, computer-assisted TKA has been introduced to aid surgery and has shown to produce encouraging results³⁹⁰. Although it remains uncertain whether computer-assisted TKA produces an improved outcome compared with conventional TKA, computer-assisted TKA may serve as a “teaching or control tool” for clinicians at low volume centres. Computer-assisted TKA may also aid in complex cases where patient factors can affect the visualization of implant placement, such as for severely morbidly obese patient.

2.7 Concluding Remarks

The present thesis attempts to address both the clinical and the *in vitro* testing aspects of the wear behaviour of TKR systems. The most frequently implanted contemporary TKR systems are of fixed, modular design and fixed by cement. Micromotion between the tibial PE insert and the cemented tibial tray is regarded as the *predominant* source of inflammatory wear debris in modular total knee replacements^{13,281,299} because, apparently, non-modular tibial components have not been associated with implant failure due to osteolysis^{14,264}. It remains uncertain to what extent the tibial clamping mechanism, surface finish, and other design features contribute to the amount of backside wear. Direct evidence for such influential factors on backside wear may be obtained by assessing the extent of surface damage on retrieved tibial components. Specifically, grading methods coupled with some statistical analysis are frequently used to assess the amount of damage on retrieved implants with the goal to gain some insight into the *in vivo* wear process. Such grading systems have been successfully used for the assessment of backside damage on retrieved tibial inserts from cementless and cemented tibial trays^{283,300,302}. The most frequently used grading systems are the Hood-method and the Modified-method. They both permit the simultaneous assessment of both the damage severity and damage area representing them both in one damage score. It is not clear which of these methods is the best for damage assessment of retrievals.

To gain further insight into the possible *in vivo* wear process, knee simulator wear testing under clinically relevant conditions is necessary. The lubrication in TKR systems may be mediated by boundary layers as indicated by some knee simulator wear tests and friction tests^{45,63,76-78}. The review of boundary lubrication and joint simulator wear testing indicates that proteins, which are amino acid polymers, are likely to adsorb to the bearing surfaces and interact when the surfaces approach each other under loading. Such interaction may result in shear of interacting protein chains and the extent to which this occurs may be inferred from biochemical tests to determine the quantity of

damaged proteins. It may also be possible that proteins become damaged by the circulation system of the knee simulator and not only in the CoCr-PE contact zone. The International Standards Organization (ISO) recommends the use of calf serum without giving recommendations on the protein constituent fractions, level of osmolality, consideration of HA as a relevant constituent, or recommends a clinically relevant level of thermal stability of SF that may be necessary for adequate boundary lubrication process. The thermal stability of the lubricant may be directly related to the amount of PE wear.

In addition, a variety of microbial growth inhibitors are tolerated by the ISO standards, such as SA and various antibiotics, without knowing much about the microbial contaminants. Furthermore, it remains uncertain to what extent such microbial inhibitors are effective in creating a necessary sterile environment for implant wear testing. Overall the literature review suggests conducting both clinical and laboratory studies of the wear in modular TKR systems. In particular, the review suggests that the fidelity of wear simulator testing could be improved from a biochemical, boundary lubrication perspective. Also, knowledge of clinical wear rates is deficient and so more studies of clinical wear are needed. The recent RSA analysis approaches to measuring wear *in vivo* are very promising but clinical wear assessment via grading methods are still most frequently used.

Chapter 3: Materials and Methods

3.1 Introductory Remarks

The present chapter gives the details of the materials and methods involved in the clinical investigations and *in vitro* investigations of the present thesis. The chapter is organized into seven sections. The methods and materials involved in an extensive retrieval study are presented in Section 3.2 involving 52 modular total knee replacements giving details of the implant and patient characteristics, damage features and damage assessment protocols. Four types of bovine calf serum solutions with various additives were used as lubricants in the knee wear simulator studies that were part of the present thesis. In addition, SF (the natural lubricant) from twenty human subjects was characterized and compared with the calf sera used in the simulator. All of these lubricants are described in Section 3.3. Next, a detailed description of the knee simulator wear apparatus and testing procedures are provided in Section 3.4. Biochemical and microbiological analyses were performed on the lubricants as described in Sections 3.5 and 3.6. Volumetric wear was determined from weight loss of the PE inserts. Surface analysis techniques such as SEM, X-ray analysis, and contact profilometry were used to investigate the wear mechanisms. All of these wear assessment procedures are described in Section 3.7. Finally, statistical tests were used extensively in both clinical investigations and *in vitro* investigations as described in Section 3.8. The approach taken in the present thesis was almost purely experimental and this accounted for the large number of different sections.

3.2 Implant Retrieval Analysis

3.2.1 Implant Characteristics

The retrieved tibial components, used in the present thesis, were selected from a larger collection of retrievals that had been collected, stored and catalogued at the LHSC. Upon retrieval from the patient, each component had been submersed in a 10 % buffered formalin solution, then cleaned in a non-abrasive fashion and stored in air at room temperature (RT). None of the retrieved implant components were subjected to ultra-sonic cleaning. For the present study, a total of 52 implants were selected and investigated including 12 model A implants (AMK[®], DePuy Orthopaedics Inc., Warsaw, IN), 16 model B implants (Genesis I[®], Smith & Nephew, Memphis, TN) and 24 model C implants (Genesis II[®], Smith & Nephew, Memphis, TN). Each model (A, B, or C) had a specific tray locking mechanism, surface finish and alloy (Table 3.1, Fig. 3.1). The surgeries were for both primary (42) and revision (10) cases. This further distinction was denoted as implant “type” because the primary implants (P) had shorter stems and less bulk than the revision implants (R).

Table 3.1: Implant design characteristics and the resultant classification.

Implant Name (Manufacturer)	Model	No. Retrieved	FEATURES locking mechanism, tray surface finish, tray alloy, implant type, insert type, sterilization
AMK [®] Anatomical Modular Knee (DePuy Orthopaedics, Warsaw, IN)	A	12	central dove-tail, polished CoCr alloy (ASTM F1537 or F75), all P, CR or PS, GA (2.5 - 4.0 MRad) or GP
Genesis I [®] (Smith & Nephew, Memphis, TN)	B	16	partial-peripheral, grit-blasted, Ti alloy (ASTM F136 or F1472), P or R CR or PS, GA (~3 MRad) or ETO
Genesis II [®] (Smith & Nephew, Memphis, TN)	C	24	partial-peripheral, polished, Ti alloy (ASTM F1472), P or R CR or PS, ETO

P = Primary, R = Revision, CR = Cruciate retaining, PS = Posterior stabilized, GA = Gamma-in-air; GP = Gas Plasma, ETO = Ethylene oxide, ASTM = American Society for Testing and Materials.

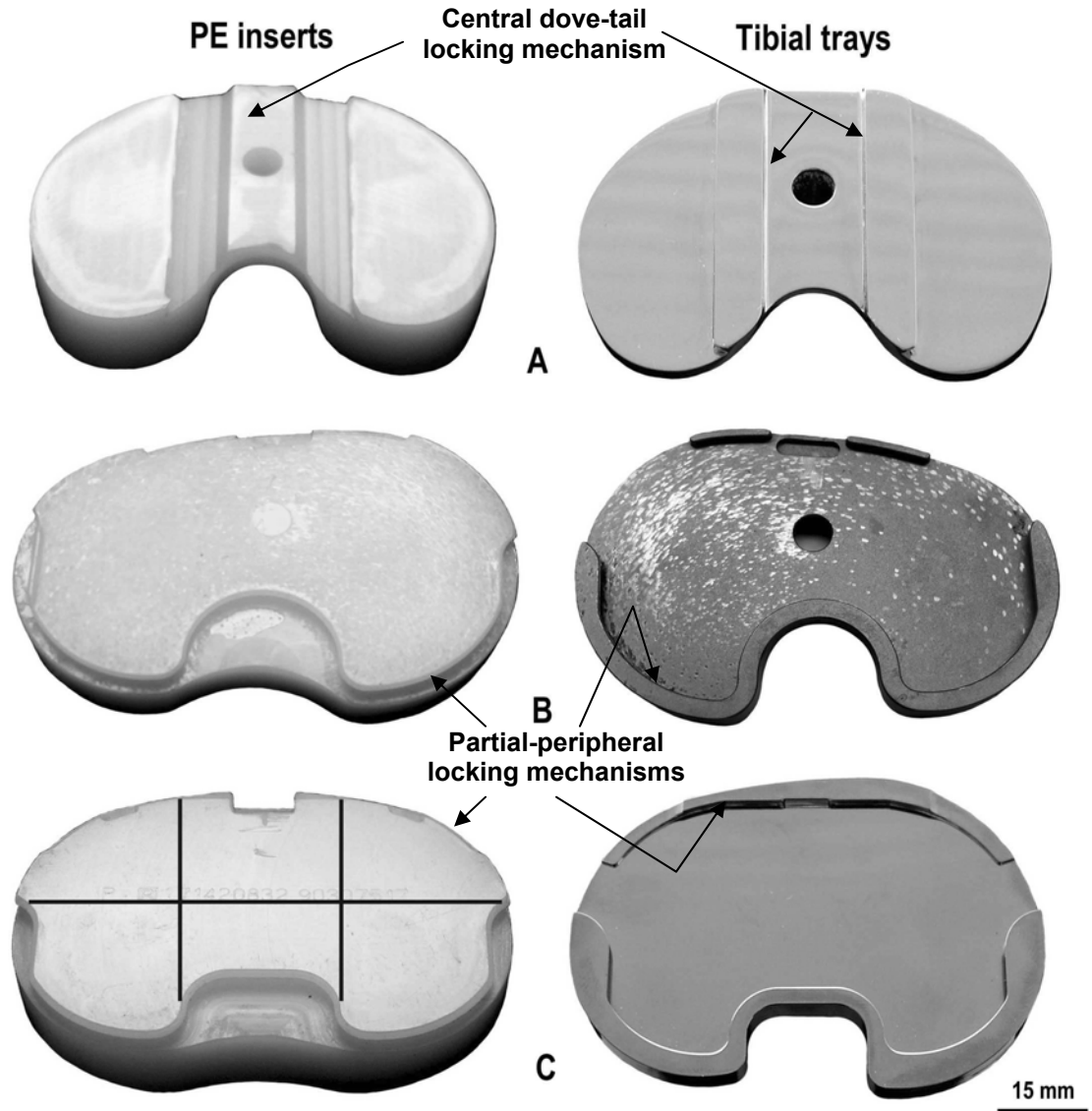


Figure 3.1: Typical backside surfaces of retrieved polyethylene (PE) inserts and their corresponding tibial trays for cases 12, 13 and 51 (see Table 3.1 for specific details). Model A is the AMK[®], model B is Genesis I and model C is Genesis II[®]. The six regions for damage analysis are shown on the PE insert of the model C implant.

The selected trays had all been fixed with cement and thus lacked screw holes that were typically used for the initial fixation associated with the application of bone in-growth surfaces. However, model B implants did have a central instrumentation hole to facilitate tray positioning. In the present study,

tables were developed that contained the detailed data values for each of the retrievals. The purpose of this level of detail and rigor was to permit the addition of new data and subsequent, or perhaps alternative, statistical analyses. Besides the implant model (A, B, or C) which essentially denoted a specific geometry and the femoral component alloy, each individual case had a number of specific implant features (Table 3.2).

Table 3.2: Implant characteristics for individual cases (Implant type: P = primary, R = revision; Insert type: CR = posterior cruciate retaining, PS = posterior cruciate substituting).

Case No.	Implant model	Insert type	Sterilization	Implant type	Shelf storage [months]	Insert thickness [mm]
1	A	PS	NGA	P	38.2	10
2	A	CR	GA	P	2.73	16
3	A	PS	GA	P	38.7	24
4	A	CR	NGA	P	13.8	16
5	A	PS	NGA	P	21.6	16
6	A	CR	GA	P	9.63	14
7	A	PS	GA	P	2.93	12
8	A	PS	NGA	P	35.8	18
9	A	CR	NGA	P	20.3	14
10	A	CR	GA	P	2.73	14
11	A	CR	NGA	P	56.1	12
12	A	CR	NGA	P	26.1	14
13	B	PS	GA	P	11.5	20
14	B	PS	GA	P	69.8	20
15	B	CR	NGA	P	3.29	12
16	B	PS	GA	P	56.8	10
17	B	PS	NGA	P	7.82	10
18	B	CR	NGA	P	25.1	12
19	B	PS	NGA	P	16.3	10
20	B	PS	GA	R	2.14	25
21	B	PS	GA	R	3.58	12
22	B	PS	GA	R	17.9	20
23	B	PS	GA	R	24.0	12
24	B	CR	GA	R	17.7	12

Table 3.2 (continued): Implant characteristics for individual cases (Implant type: P = primary, R = revision; Insert type: CR = posterior cruciate retaining, PS = posterior cruciate substituting).

Case No.	Implant model	Insert type	Sterilization	Implant type	Shelf storage [months]	Insert thickness [mm]
25	B	PS	GA	P	32.2	20
26	B	CR	GA	P	6.61	10
27	B	CR	GA	P	12.6	8
28	B	PS	GA	P	18.8	15
29	C	PS	NGA	R	1.58	15
30	C	PS	NGA	P	5.49	11
31	C	PS	NGA	P	5.29	18
32	C	PS	NGA	P	14.6	11
33	C	PS	NGA	R	56.4	21
34	C	PS	NGA	P	9.47	11
35	C	PS	NGA	P	5.00	13
36	C	PS	NGA	P	2.73	11
37	C	PS	NGA	P	19.9	13
38	C	PS	NGA	P	26.5	13
39	C	PS	NGA	P	5.16	11
40	C	PS	NGA	P	7.89	15
41	C	PS	NGA	P	6.67	13
42	C	PS	NGA	P	18.8	11
43	C	PS	NGA	R	29.5	21
44	C	PS	NGA	R	59.8	21
45	C	PS	NGA	P	4.77	11
46	C	PS	NGA	P	37.6	15
47	C	PS	NGA	P	11.5	15
48	C	PS	NGA	P	19.2	13
49	C	CR	NGA	P	16.5	13
50	C	PS	NGA	P	38.2	18
51	C	PS	NGA	P	6.35	11
52	C	PS	NGA	R	19.6	18

There were 13 CR and 39 PS inserts. All tibial inserts were machined from ram-extruded PE bar stock (GUR 1050, Ticona[®] Inc., Summit, NJ) with 17 sterilized by GA irradiation and 35 sterilized by NGA methods of either GP

or ETO. None of these PE inserts had been subjected to any additional cross-linking treatment for the specific purpose of reducing the wear. The mean tibial insert thickness was 14 mm (range, 8 mm - 25 mm) and for each of the B and C implant models an identification number was engraved into the backside surface of the PE insert by the manufacturer. Shelf storage time prior to implantation for the GA inserts was 19.4 months (range, 2.14 - 69.8 months) and for the NGA inserts 19.8 months (range, 1.58 - 58.2 months).

3.2.2 Patient Characteristics

Prospectively collected surgical data and clinical demographics were compiled for each patient from his/her individual data registered in the International Orthopaedic On-line Database³⁹¹ (Table 3.3). These data included the implantation period (IP), gender, mass, height, age, and the stated reason for the surgery itself. Model A implants were retrieved after a mean IP of 45 months (range, 1 - 86 months), model B implants after a mean IP of 64 months (range, 9 - 139 months), and model C implants after a much lower mean IP of 12 months (range, 0.5 - 34 months). The mean patient mass was 91.61 kg (range, 55 - 156 kg), the mean height was 1.66 m (range, 1.47 - 1.88 m) and the mean age was 68 years (range, 42 - 88 years). The original primary joint replacement surgeries were performed because of OA except for case 26 which was RA. The implants were retrieved from 24 male and 28 female patients. Some of the patients had been subjected to a second revision surgery and thus revision type implants were available for examination in the present study.

The stated reasons for revision surgery (both first and second) included infection (27), instability (10), and osteolysis (5). The remaining reasons for surgery included stiffness (3), for idiopathic (origin of unknown) pain (2), delamination at the tibiofemoral articulation (2), periprosthetic fracture (1), recurrent effusion (1), and patellar dislocation (1). The mean IP to revision surgery was 18 months for infection (range, 0.5 - 83 months), 49 months for

instability (range, 5 - 101 months), 84 months for osteolysis (range, 40 - 139 months) and 46 months due to all the remaining reasons (range, 3 - 97 months).

Table 3.3: Patient features for individual cases (M = male, F = female, IP = implantation period).

Case No.	IP [months]	Gender	Mass [kg]	Height [m]	Age [yrs]	Reason for Surgery
1	37.2	M	93.0	1.70	62	Idiopathic pain
2	76.6	M	93.0	1.75	74	Femoral osteolysis
3	49.1	F	79.0	1.58	80	Instability
4	35.2	M	72.0	1.62	48	Instability
5	38.0	F	82.0	1.60	84	Infection
6	66.5	F	95.3	1.70	77	Instability
7	70.3	M	88.0	1.70	74	Instability
8	16.6	F	83.0	1.70	42	Instability
9	1.18	M	89.0	1.83	78	Infection
10	86.4	F	82.0	1.62	79	Periprosthetic fracture
11	16.1	M	156.0	1.80	68	Infection
12	47.1	M	95.0	1.68	83	Instability
13	83.6	M	92.0	1.80	78	Recurrent effusion
14	34.9	M	96.6	1.73	70	Delamination
15	25.6	F	72.0	1.60	64	Infection
16	9.57	M	88.0	1.75	70	Infection
17	30.3	F	79.4	1.56	81	Infection
18	10.1	F	89.0	1.65	82	Stiffness
19	24.9	F	60.5	1.47	80	Infection
20	89.6	F	73.0	1.58	88	Instability
21	97.9	F	127.0	1.68	61	Delamination
22	96.2	M	77.7	1.73	74	Femoral osteolysis
23	87.4	M	121.0	1.81	75	Idiopathic pain
24	70.1	M	113.0	1.70	66	Femoral osteolysis
25	40.8	F	89.0	1.56	62	Tibial osteolysis
26	140.	F	55.0	1.62	59	Tibial osteolysis

Table 3.3 (*continued*): Patient features for individual cases (M = male, F = female, IP = implantation period).

Case No.	IP [months]	Gender	Mass [kg]	Height [m]	Age [yrs]	Reason for Surgery
27	101.0	M	101.0	1.71	64	Instability
28	82.8	F	58.0	1.65	77	Infection
29	2.27	M	95.7	1.70	54	Infection
30	16.3	F	117.0	1.52	50	Stiffness
31	9.80	F	93.4	1.56	71	Infection
32	0.53	F	73.0	1.61	74	Infection
33	3.39	F	86.0	1.57	61	Infection
34	3.42	F	117.0	1.52	60	Stiffness
35	23.3	M	78.0	1.53	49	Infection
36	17.3	F	92.0	1.53	66	Infection
37	12.3	M	82.0	1.72	74	Infection
38	13.2	F	105.0	1.72	50	Infection
39	17.0	F	97.0	1.52	49	Instability
40	25.3	F	69.0	1.68	80	Infection
41	5.26	F	65.0	1.59	78	Instability
42	15.2	M	114.0	1.88	72	Infection
43	6.87	M	132.0	1.70	63	Infection
44	1.78	F	90.0	1.57	61	Infection
45	4.31	F	92.0	1.52	51	Patellar dislocation
46	12.9	M	83.9	1.80	74	Infection
47	22.8	F	111.0	1.60	55	Infection
48	3.81	M	125.0	1.87	73	Infection
49	11.8	M	98.8	1.80	75	Infection
50	26.7	F	68.0	1.50	75	Infection
51	34.0	M	91.4	1.75	77	Infection
52	1.94	M	90.0	1.73	83	Infection

3.2.3 Damage Features

Generally, surface damage was indicated when the appearance was different from the original machining marks. At low IP, creep^{392,393} might have crushed the machining marks to some extent and thus the backside damage score (BDS) would be related to creep not wear. However, this distortion of the BDS by creep was deemed to be small. Retrieved tibial inserts were graded under 10X - 40X magnification using a stereo-light microscope (SZ-40, Olympus, Tokyo, Japan). Various damage features (burnishing, grooving, indentations, deformation, pitting, and stippling) were identified. An image of a worn backside area on a retrieved PE insert is shown in Figure 3.2. Burnishing was represented by a very smooth, highly polished and reflective area. Grooving was identified by detection of relatively long scratches having clear directional orientation. Elongated craters were also characterized as grooving (Fig. 3.3) and might have been caused by third-body abrasion. However, when the craters were round-shaped in the plane of the surface, they were classified as “pits” (Fig. 3.4). Indentations were characterized by randomly organized short scratches. Deformation was denoted by a depressed PE surface without major material removal which still permits the machining marks to be visible. Stippling was identified as a circumferential wear pattern on both the PE insert and the tibial tray. It was described explicitly by Engh et al.²⁹⁹ and such damage was shown in earlier in Figure 2.10.

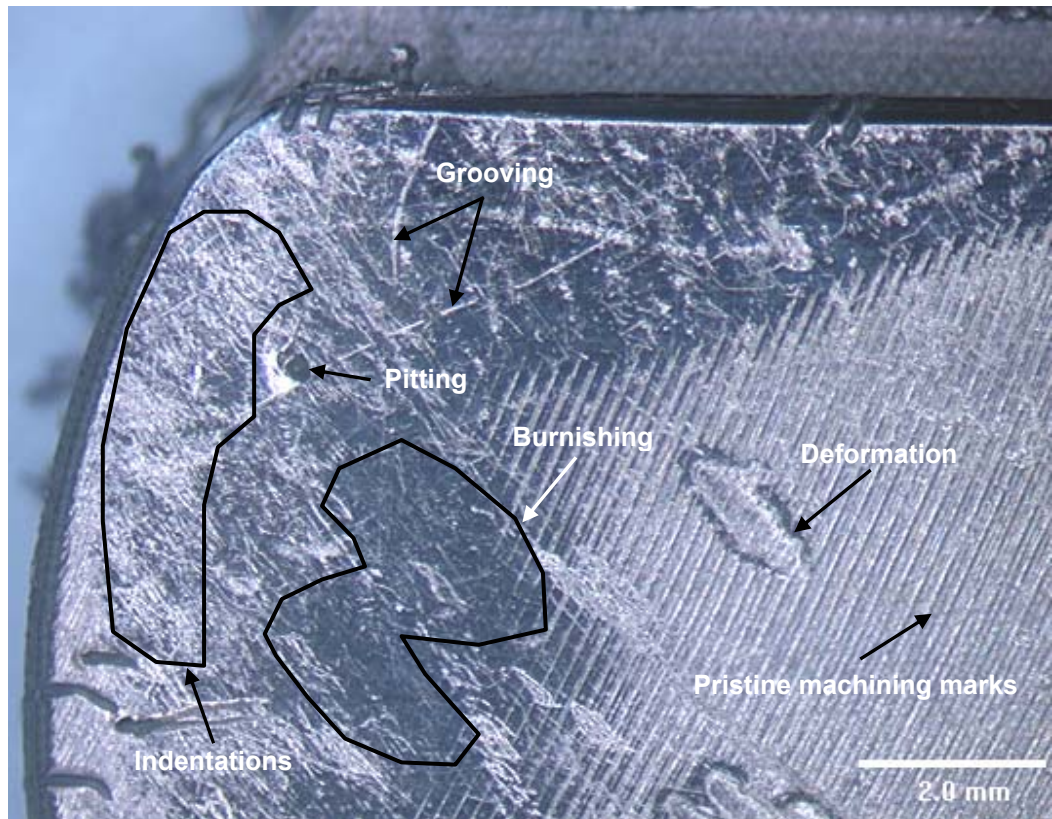


Figure 3.2: Macrograph of a worn PE backside surface showing damage features such as burnishing, grooving, indentations, deformation, and pitting relative to the unworn, pristine machining marks.

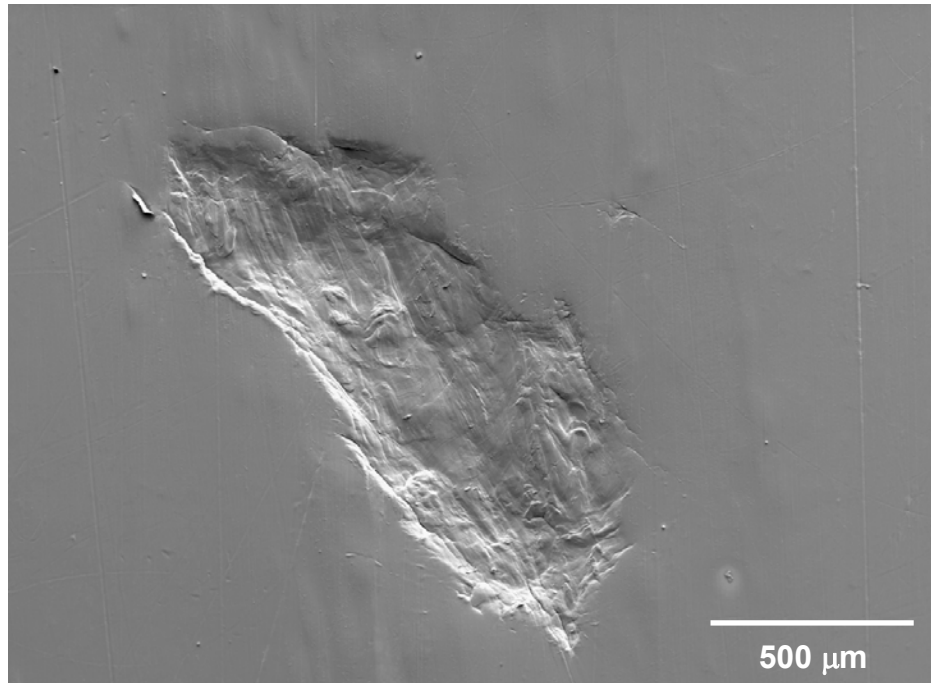


Figure 3.3: SEM image of an *elongated* surface crater possibly due to third-body abrasion. Such elongated craters were characterized as “grooving”.

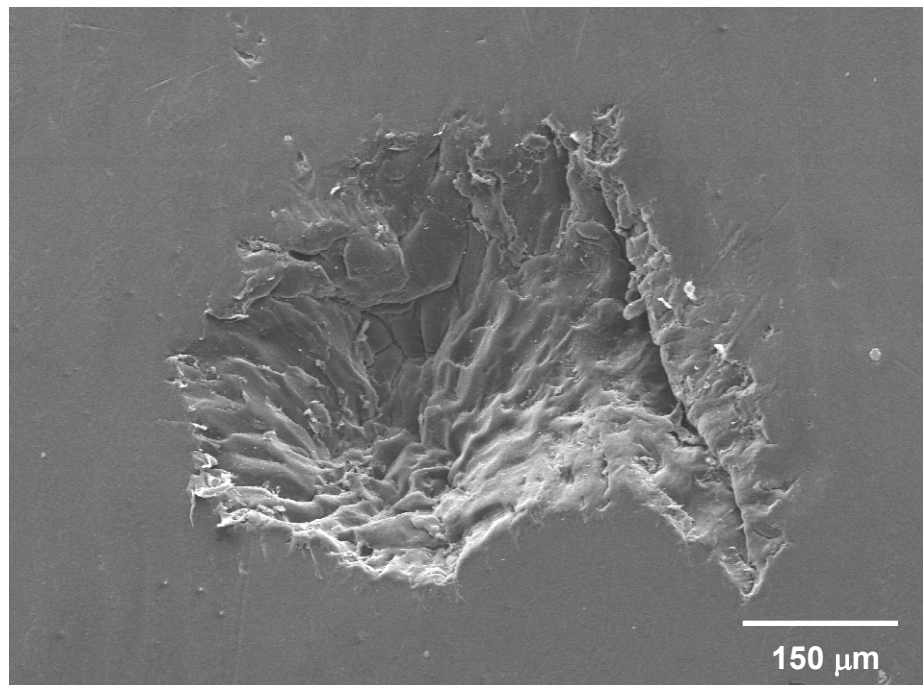


Figure 3.4: SEM image of a *round* surface crater possibly due to surface fatigue. Such craters were characterized as “pitting”.

3.2.4 Damage Assessment Protocol

The backside surfaces of the tibial inserts were divided into six regions^{44,300} as shown in Fig. 3.1 (Model C insert) to facilitate the estimation of areas exhibiting the various damage features. In each of the six regions, two semi-quantitative grading methods were applied to identify damage features based on severity and the proportion of the regions' surface area that was affected. The first method is referred to as the Hood-method²⁶ (see Section 2.5.3). Several studies^{220,282,300} have applied the Hood-method to identify backside damage in which the surface damage was assessed in severity increments of 0 %, 0 - 10 %, 10 - 50 % and 50 - 100 % were assigned scores of 0, 1, 2 and 3, respectively. The worst possible BDS for this method would be 108 (maximum score of 3 in each of the 6 sections for each of the 6 damage features) but it would be very difficult to distinguish the 6 damage features and judge their severity when they all applied over the total area available. The second method, referred to as the Modified-method, assessed the surface damage severity in regular decimal steps from 0 %, $0 \% \leq 10 \%$, $> 10 \leq 20 \%$ up to $> 90 \leq 100 \%$, assigning a score of 0, 1, 2 up to 10. The principle of the second Modified-method was developed independently by the author of the present thesis⁴⁴, but it had been used first by another research group³⁰². The worst possible BDS for this method would be 360 (maximum score of 10 in each of the 6 sections for each of the 6 damage features).

To illustrate the complexity of the Hood-method and the Modified-method of damage assessment, a conceptual example of surface damage is shown that has only one damage feature, two damage areas of varying amounts and damage intensities of varying extents (Fig. 3.5). Twelve different cases of surface damage are devised to illustrate how the two damage assessment methods function. In the conceptual example, the outer circle (of radius r_o) represents the total area that can be affected by surface damage. The inner circle (of radius r_i) represents an region (area B) with a certain severity of the damage feature. The difference between the total area and area B is labeled area A. The different gray scales are used to indicate the damage severity. For

example, a white area represents the unworn surface. To include the severity in the assessment, damage severity factors (DSF) were assigned as follows: no damage (DSF = 0), just visible damage (DSF = 0.33), clearly visible damage (DSF = 0.66), and complete damage (DSF = 1) to the approximated damage area. Implementing such damage severity factors was shown to permit a more objective assessment of surface damage.

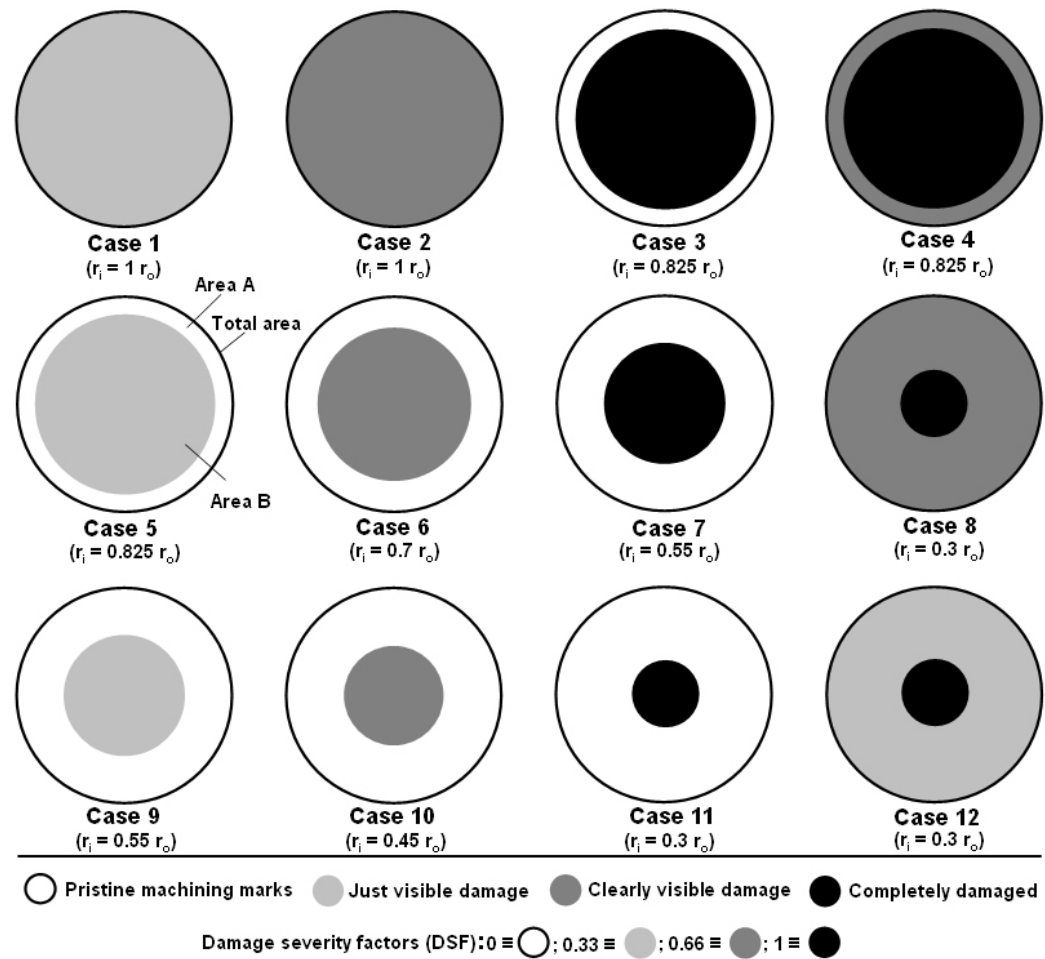


Figure 3.5: Schematic showing the illustration of 12 cases with 2 different areas of surface damage caused by one damage feature for the backside PE surface. Each of the large circles represents the total surface area. The increased darkness of the grey scales represented increasing damage and thus damage severity factors (DSF). The areas of damage and their severity were included in determining the total BDS for each case (Tables 3.4 and 3.5) ($r_i \equiv$ radius of the inner circle; $r_o \equiv$ radius of the outer circle).

Combining both area and severity in the aforementioned manner had been performed earlier by Wasielewski et al.³⁴¹ in combination with the Hood-method. Increasing the resolution of the DSF, i.e. using a scale from 1 to 10 rather than from 0 to 4 as used in the present study, was not conducted because it was difficult to differentiate between subtle changes in damage severity. The backside damage scores (BDS) were determined for the twelve cases, following both the Hood-method and the Modified-method as explained in Tables 3.4 and 3.5.

For example, the surface damage in case 4 is given as follows: area A was approximately 30 % of the total area, area B accounted for approximately 70 % of the total area. Area A was determined to have experienced surface damage but some machining marks remained and thus a DSF of 0.66 was assigned. Area B was complexly damaged with no machining marks remaining and thus a DSF of 1 was assigned. Depending on the grading method, the score for each area was multiplied with their corresponding DSF and then summed to give the total damage score. The total damage score for case 4 was 4.32 following the Hood-method and 8.98 following the Modified-method.

The actual assessments of the 6 damage features in the 6 regions of the inserts on each of the 52 inserts giving a total of 1836 values of BDS were not performed with the precision of the illustrative example. After looking at the insert with a low power optical microscope, the percentage of the total area that had a particular damage feature was estimated by eye rather than measured and the severity was estimated rather than quantified in some manner. Obviously some judgment was involved in both of the estimates and even if the areas had been determined more precisely, their boundaries would still be a judgment and so would the severity. These shortcuts did introduce a certain lack of precision but the overall accuracy was not considered to be compromised. Thus, the illustrative example was only intended to indicate the guiding principles of the damage assessment methods.

The total damage scores for all twelve cases were determined with both the Hood-method and the Modified-method (Figure 3.6). The total damage

scores were about the same for both methods when small amounts of surface area (10 - 30 %) were damaged (cases 9 - 11) but were varying amounts higher for the Modified-method when the damaged surface area was greater than 30% and the DSF was greater than zero (cases 1 - 8 and 12). These observations suggested that the modified method might provide better differentiation of the more damaged surfaces and this might be advantageous when correlating damage with certain features of the inserts. However, in severely damaged or worn surfaces damage features may overlap, making their identification and assessment more difficult.

Anterior BDS and posterior BDS values were assigned for comparison purposes by grouping the three anterior and the three posterior regions, respectively. Similarly, medial and lateral BDS were assigned by grouping the two medial and the two lateral regions, respectively. All specimens were randomized prior to the examination and the reported scores were the mean of the values found by two designated “observers”, the present author and a trained undergraduate student, Christopher M. Haydon, HBSoc. The BDS obtained by the author and the student using both the Hood-method and the Modified-method on the 52 retrieved PE inserts are shown in the Appendices A and B.

Table 3.4: Scoring procedure used with the Hood-method (see Fig. 3.5).

Case	Approx. Damage Area [%]		Damage Severity Factor (DSF)		BDS (0% ≡ 0; 0 ≤ 10% ≡ 1; >10 ≤ 50% ≡ 2; >50 ≤ 100% ≡ 3) x DSF		Total BDS
	A	B	A	B	A	B	
1	100	-	0.33	-	3 x 0.33	-	0.99
2	100	-	0.66	-	3 x 0.66	-	1.98
3	0	70	0	1	0	3 x 1	3
4	30	70	0.66	1	2 x 0.66	3 x 1	4.32
5	30	70	0	0.33	0	3 x 0.33	0.99
6	50	50	0	0.66	0	3 x 0.66	1.98
7	70	30	0	1	0	2 x 1	2
8	90	10	0.66	1	3 x 0.66	1 x 1	2.98
9	70	30	0	0.33	0	2 x 0.33	0.66
10	80	20	0	0.66	0	2 x 0.66	1.32
11	90	10	0	1	0	1 x 1	1
12	90	10	0.33	1	3 x 0.33	1 x 1	1.99

Table 3.5: Scoring procedure used with the Modified-method (see Fig. 3.5).

Case	Approx. Damage Area [%]		Damage Severity Factor (DSF)		BDS (0% ≡ 0; 0 ≤ 10% ≡ 1; >10 ≤ 20% ≡ 2; ...; > 90 - 100% ≡ 10) x DSF		Total BDS
	A	B	A	B	A	B	
1	100	-	0.33	-	10 x 0.33	-	3.3
2	100	-	0.66	-	10 x 0.66	-	6.6
3	0	70	0	1	0	7 x 1	7
4	30	70	0.66	1	3 x 0.66	7 x 1	8.98
5	30	70	0	0.33	0	7 x 0.33	2.31
6	50	50	0	0.66	0	5 x 0.66	3.3
7	70	30	0	1	0	3 x 1	3
8	90	10	0.66	1	9 x 0.66	1 x 1	6.94
9	70	30	0	0.33	0	3 x 0.33	0.99
10	80	20	0	0.66	0	2 x 0.66	1.32
11	90	10	0	1	0	1 x 1	1
12	90	10	0.33	1	9 x 0.33	1 x 1	3.97

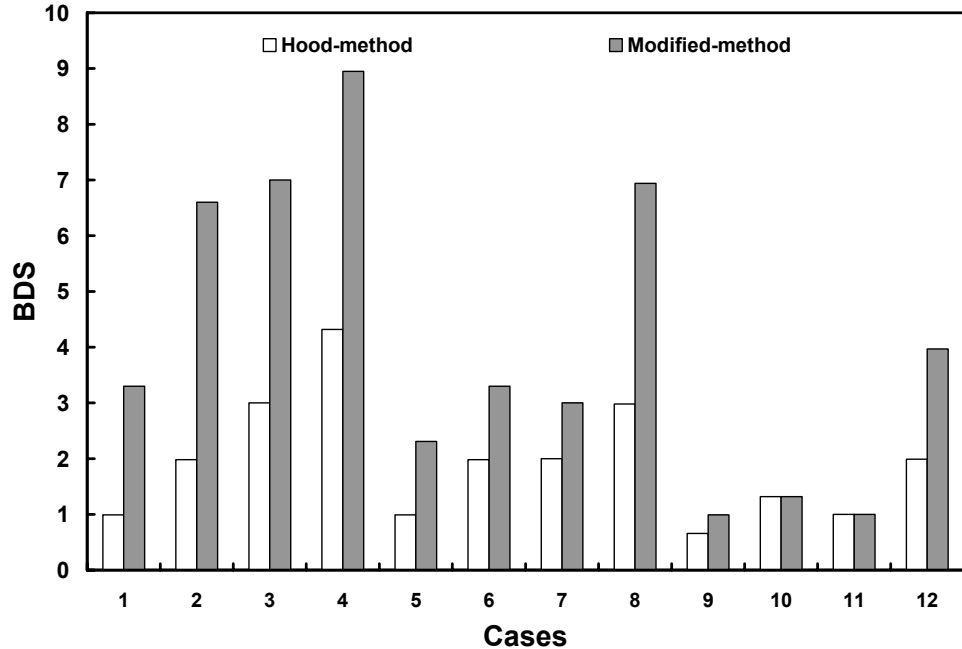


Figure 3.6: The damage score for the cases 1 - 12 obtained with the Hood-method and the Modified-method. Note the similarities between the damage score obtained with either method for mode 9 - 11 (small surface damage) and higher damage score for Modified-method.

3.2.5 Melt Annealing

A “melt-annealing” treatment, developed by Muratoglu et al.⁷⁴, was used to take advantage of the shape memory effect of PE and thus reverse some of the PE deformation. Retrieved PE inserts were placed in a nitrogen-flushed, low pressure oven and subsequently heated at rate of ~ 2 °C per min to an annealing temperature of ~ 120 °C. The samples were kept at the annealing temperature for 20 min and then cooled down to RT. If all the deformation were caused by creep, the original machining marks were expected to return because of this treatment. Afterwards, the surfaces were re-examined using a contact profilometer (Tencor[®] P-10, KLA-Tencor, Milpitas, CA) to evaluate the surface change whether the original machining marks had returned or not. However, this method ran into problems for PE inserts that had been sterilized in a way that caused polymeric chains to be severed and free radicals at the chain ends to combine with oxygen, such as for GA inserts. The oxidized PE

lost its internal structure and thus could be subject to creep and the machining marks would not recover.

3.3 Lubricants

3.3.1 Collection of Synovial Fluid

Prior to the initiation of the SF study, an application was submitted to the Ethics Committee at the University of Western Ontario for permission to obtain a sample of the SF from the knee of a patient just prior to surgical replacement of the knee with a primary TKR. Upon approval of the ethics application (Ethical Board Review Number 12536E), patients were recruited with the assistance of the research nurse Julie Marr. Each patient was provided with a consent form that had been approved by the Ethics Committee. Signatures were obtained prior to surgery. Patients who had previously received any knee injections for pain relief (i.e. Cortisone (a steroid hormone) or Synvisc[®] HYLAN G-F 20 (Genzyme, Cambridge, MA)), or patients with rheumatoid arthritis (RA) or other inflammatory arthritis, were eliminated from the study. Also, patients were excluded who were undergoing revision surgery or who had received a high tibial osteotomy.

Twenty patients were selected to participate in the present study (Table 3.6): ten male and ten female patients, with a mean age of 64.7 years (range, 60 - 70 years), undergoing surgery for primary TKA. Ten were right knee surgeries and ten were left knee surgeries. Based on the pre-admission notes, the patient-specific body-mass-index (BMI) measured on average 31 (range, 26 - 41 BMI). SF was drawn just prior to the first incision of the primary knee arthroplasty procedure, by four independent physicians (Drs. Robert B. Bourne, Steven J. MacDonald, Richard W. McCalden, and Douglas D. Naudie). Sterile techniques, as per hospital protocol, were maintained to protect the patient. The obtained SF quantity varied with a mean of 4 ml (range, 1 - 8 ml).

Table 3.6: Nomenclature and patient characteristics of SF samples.

SF identification	BMI	Gender	Knee	Age
SF1	41	F	Left	61
SF2	33	F	Left	64
SF3	31	M	Left	62
SF4	31	F	Right	68
SF5	24	F	Right	63
SF6	40	F	Left	69
SF7	26	M	Left	65
SF8	30	M	Left	70
SF9	27	F	Right	66
SF10	29	M	Right	70
SF11	32	F	Right	64
SF12	38	F	Left	62
SF13	31	F	Right	65
SF14	26	M	Left	63
SF15	38	F	Right	61
SF16	27	M	Right	60
SF17	26	M	Left	64
SF18	31	M	Left	60
SF19	30	M	Right	66
SF20	36	M	Right	70

3.3.2 Calf Sera

A number of calf sera were obtained from Hyclone (Logan, UT) and used in the wear simulator studies of the present thesis. They were bovine calf serum (BCS), newborn calf serum (NCS), alpha-calf serum (ACS) and iron-supplemented alpha-calf serum (ACS-I) with compositions as listed in Table 3.7. ACS and ACS-I had a low in γ -globulin fraction. All calf sera were delivered frozen in 500 ml containers and they were stored at -20 °C. Individual certificates of analysis were obtained for each batch of serum used to provide data on the individual protein and inorganic component concentrations. The total protein concentration and individual protein constituents fractions, varied to some extent for the different sera. The albumin fraction of ACS was

consistently found to be highest and very similar to that of ACS-I. The iron (Fe) concentration in ACS-I was at least 6.5-times higher than that for the other three sera. ACS-I was used consistently in actual wear testing experiments due to unavailability of ACS from the manufacturer.

Table 3.7: Characteristics of four calf sera. Note the difference in constituents.

Specifications	BCS	NCS	ACS	ACS-I
Lot #	AQC23290	APE21200	APL22372	AQE23894
Albumin [%]	51.7	40	71.7	66.3
α -1-globulin [%]	3	11.2	3.8	4.5
α -2-globulin [%]	12.7	22.8	8.4	8.2
β -globulin [%]	20.4	14.2	15.8	19.2
γ -globulin [%]	12.2	11.8	0.3	1.1
Total protein [g/l]	69	52	42	41
Fe [mmol/L]	0.0065	0.0157	0.0085	0.0877
Ca [mmol/L]	2.78	2.70	<0.5	<0.5
Inorganic P [mmol/L]	3.16	2.82	<0.2	<0.2
Mg [mmol/L]	1.02	1.06	0.06	0.08
pH	7.29	7.49	7.65	7.71
Osmolality [mmol/kg]	301	290	291	283

3.3.3 Lubricant Mixtures

Prior to commencing the wear tests, the calf sera were allowed to thaw overnight at RT. All sera were diluted to a total protein concentration of approximately 17 g/l as recommended by ISO 14243-3⁴¹ using either distilled water (DW), obtained from the internal hospital supply system, or phosphate-buffered, blood-bank saline solution (PBS; Cat. # 72060-034, VWR, Mississauga, ON). The PBS had a pH equivalent to that of human blood and was free of preservative. The PBS was recommended for serological testing as well as for general laboratory use and had been used by other research groups for implant wear testing³⁵. The osmolality of PBS was 286 ± 0.57 mmol/kg and this was about 6 times higher than that of DW having an osmolality of $46 \pm$

2.08 mmol/kg. The serum composition, dilution and additives were selected to match the conditions of tests conducted by DePuy Orthopaedics using the same implant model (Warsaw, IN) and thus allow comparisons of the wear data. Sodium hydroxide pellets were dissolved to raise pH level to a target value of 7.63 ± 0.1 which corresponded to that of the human body. Ethylene-diamine-tetraacetic acid (EDTA), a chelator with the ability to bind dissolved calcium and metal ions³⁹⁴, was added to a final concentration of 20 mmol/l to inhibit precipitates in the articulation that could affect the PE wear rate³⁵, as suggested by McKellop et al.¹⁵² and the wear studies at DePuy Orthopaedics by McNulty et al.⁴⁵⁻⁴⁷.

Two types of anti-microbial agents were added to the lubricants to inhibit microbial growth. SA was used as a microbial inhibitor based on the recommendations of McNulty et al.⁴⁵⁻⁴⁷. SA was added to lubricants to achieve a final concentration of 0.2 % per volume lubricant³⁰. Alternatively, an antibiotic-antimycotic (AA) mixture (Cat. # 15240-062, Invitrogen, Mississauga, ON) was added to the lubricant to inhibit microbial growth. The AA was expected to target a broad spectrum of bacteria, fungi, and yeasts. The AA contained 10,000 units of penicillin, 10,000 μg streptomycin, 25 μg amphotericin B/ml, and streptomycin sulfate as the antibiotic. The antimycotic constituent of AA was amphotericin B (Fungizone[®]) which was diluted by the manufacturer with a 0.85 % saline solution.

The AA was added to the lubricant at a concentration of 5 ml AA to 500 ml of the diluted serum lubricant that included all the previous additions at the beginning of the wear test for each station. Additional 5 ml of AA was periodically added (about every 0.16 Mc) to each wear station to maintain antimicrobial efficacy. In some of the lubricants, HA (Lifecore Biomedical, Inc.; MW = 1.78 MDa) was added to a final concentration of 1.5 g/l and dissolved by stirring for 12 h at 37 °C¹⁰². Considering the various solutions, a total of six different lubricants were used in the studies of the present thesis (Table 3.8).

Table 3.8: Lubricants used in the simulator wear tests.

Lubricant identification	Calf serum	Dilutive media	Antimicrobial agent	HA
BCS lubricant (BCS + DW + SA)	BCS	DW	SA	No
NCS lubricant (NCS + DW + SA)	NCS	DW	SA	No
ACS lubricant (ACS + DW + SA)	ACS	DW	SA	No
DW lubricant ACS-I + DW + AA)	ACS-I	DW	AA	No
PBS lubricant (ACS-I + PBS + AA)	ACS-I	PBS	AA	No
HA lubricant (ACS-I + PBS + AA + HA)	ACS-I	PBS	AA	Yes

3.4 Knee Simulator Wear Testing

3.4.1 Test Apparatus

A six station AMTI knee simulator (KS3-6-1000, Serial # 120219, AMTI, Waltham, MA) was acquired. This simulator was obtained to specifically test TKRs under physiological load and motions. After considerable delay, the knee simulator was installed in a large laboratory, located at the basement of the University Hospital at the LHSC. The simulator consisted of a left (L) bank and a right (R) bank with separate load and motion actuators. Each bank had three dynamic wear stations and two load-soak (LS) stations (Fig. 3.7 and 3.8). The wear stations were subject to vertical loading, flexion-extension (FE) motion, anterior-posterior (AP) motion and internal-external (IE) rotation. The AP and IE motions caused additional loading on the implant depending on the geometric constraints and this was recorded by multi-component load cells at each dynamic wear station. A pneumatically driven, medial-lateral loading actuator was installed (and could have been re-oriented to apply AP loading) but it was not used in the studies of the present thesis because the ISO recommendations for displacement controlled testing were followed⁴¹.

The LS stations only experienced vertical loading but had the same lubricant as the dynamic wear stations. The LS stations were used to provide control values for the change in fluid content of the PE inserts. It was assumed that any change in fluid content of the LS inserts would also have occurred for

the wear station inserts. Thus, the fluid content change could be used to correct the weight loss measurements of the wear station inserts that were then used to determine the volumetric wear. This approach to implant wear testing of PE components was well established¹⁵² and had been used in the wear tests performed by DePuy Orthopaedics by McNulty et al.^{45,47}.

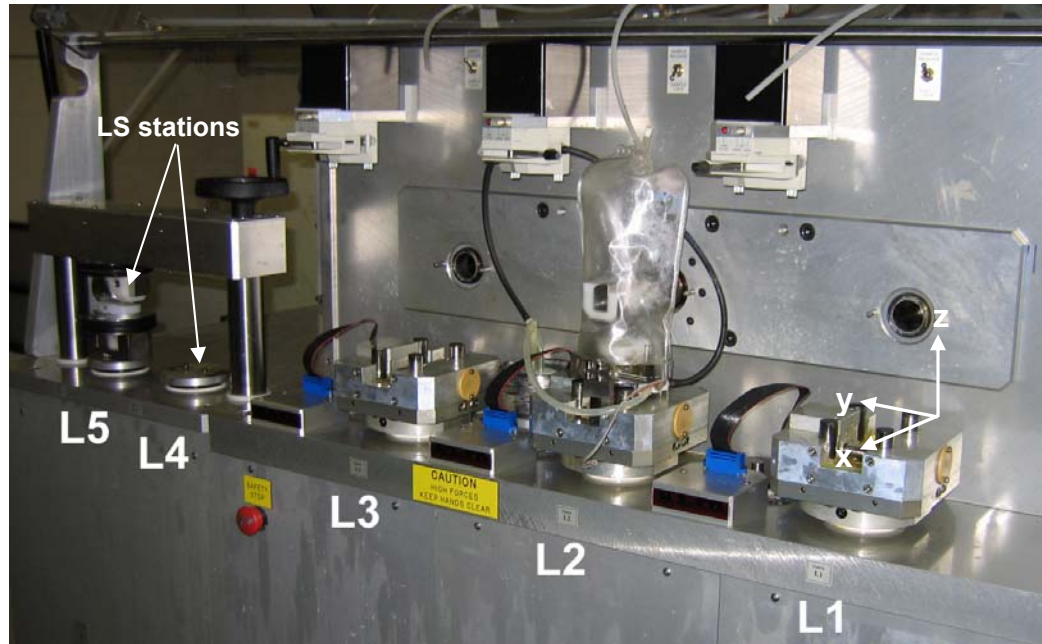


Figure 3.7: The left (L) bank of the AMTI knee simulator (AMTI, Waltham, MA). The stations L1, L2, and L3 are the wear stations (dynamic) while L4 and L5 are the load-soak (LS) stations (only vertical loading, no motion).

The knee simulator was controlled and operated by an external PC that used the AMTI (Waltham, MA) software packages (SIMMAC for wear testing and SIMCAL for calibration procedures). The software ran on a Windows XP operating system. The simulator had a L bank control and a R bank control, allowing the separate actuators (mentioned previously) on each bank to operate independently. In terms of computer hardware, each bank had separate control cards for each individual motion and for the vertical loading. Each control card had multiple potentiometers that could be adjusted during the calibration process. These adjustments made the actuators move in accordance with the

specified loading or displacement. For the linear and angular displacements and the vertical load, the control was closed loop and feedback control was present in the cycle-by-cycle operation of the wear simulator. The calibration settings were checked about every 1 Mc and a full scale calibration was performed about every 3 Mc[^]. The vertical displacement was measured by a position sensor located in each station that uses a pair of magnets to measure the movement. As mentioned previously, each wear station had an embedded multi-component force sensor that allowed the recording of F_x , F_y , F_z and M_x , M_y , M_z . This allowed the loads that resulted from the motions to be monitored.

The latest version of the AMTI knee wear simulator allows lateral loads to be controlled by a “software spring” that is meant to represent the soft tissue constraints acting on a knee implant *in vivo*. However, the extent of soft tissue constraint is difficult to estimate and varies considerably depending on the patient and soft tissue balancing performed during the surgery. In any case, the studies of the present thesis were conducted under conditions of motion control that was imposed in a closed loop fashion during a calibration procedure. The vertical load was imposed with some precision and continuously monitored and was considered a dominant factor in implant wear.

Each wear station had its own lubricant recirculation unit with a 500 ml reservoir, both externally located relative to each wear station. An externally located heater/chiller unit was set at 37.5 °C to ensure that each serum container was heated to a temperature of 37 ± 2 °C. A custom-built pneumatic intravenous (IV) bag inflation system was built to ensure that the IV bags covering the wear stations were permanently inflated during the wear tests. Inflating the bags ensured that no lubricant leakage occurred. Otherwise the bag collapsed, got pinched and eventually was punctured thus causing lubricant leakage that stopped the wear test. The LS stations did not have a recirculation unit and thus remained at RT. All wear tests were performed at a frequency of 1 Hz. The data from the force sensor and the displacement sensor were recorded at a rate of 200 data points/second at either every 0.01 Mc or every 0.1 Mc.

[^] AMTI recommends calibrating the simulator once a year (~ 12 Mc).

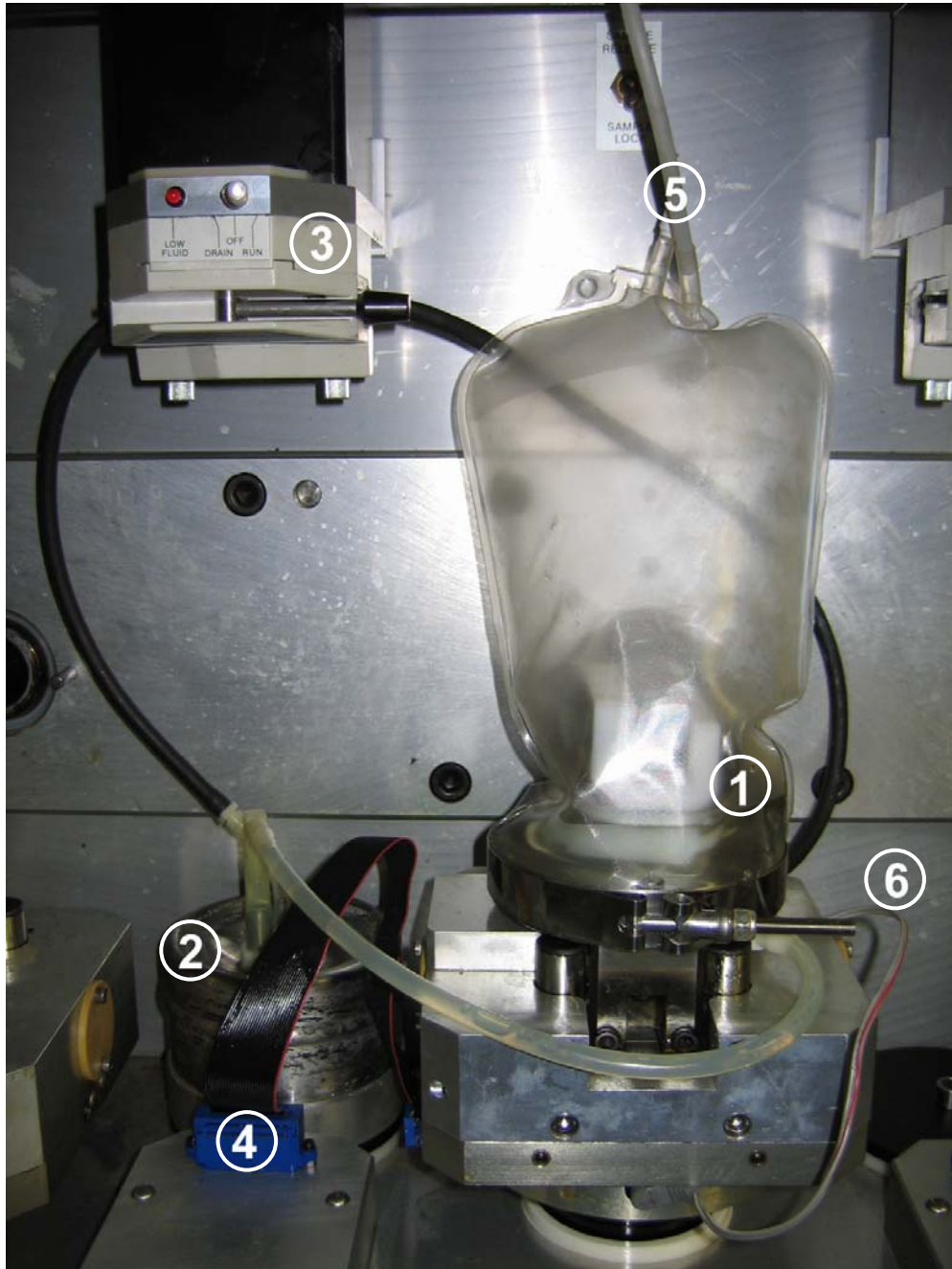


Figure 3.8: Image showing station L2 of the AMTI knee simulator (AMTI, Waltham, MA) with the following components: (1) an intravenous (IV) bag that contains the lubricant; (2) an externally located and heated fluid container; (3) a peristaltic recirculation pump; (4) a data transfer ribbon cable; (5) a PE hose that is connected to the IV bag and used to supply pressurized air to inflate the bag; (6) a thermo couple connected to the wear station to measure the lubricant temperature.

3.4.2 Calibration

Prior to the calibration, the knee simulator was run for 0.005 Mc following ISO 14243-3 without implant components to ensure the appropriate warming up of the hydraulic fluid and, subsequently, the simulator. The calibration of each wear station was performed after the author obtained specific training from AMTI (Waltham, MA) which involved using the supplied knee simulator manual and calibration kit. The calibration was performed by two individuals (the author and the laboratory technologist, Kory Charron) and required about 3 - 4 h. Calibrations were performed in four consecutive steps. These calibration steps involved the static displacements (i.e. FE motion, IE rotation, and AP translation), vertical load actuator, static force sensor, and dynamic performance. The calibrations were performed in accordance with the “user manual” supplied by AMTI (Waltham, MA) ³⁹⁵.

Essentially, the calibration procedures involved using a screwdriver to adjust potentiometers that were located on the control boards of the simulator. These potentiometers were identified in the user manual as the loop gain (affecting the speed on which the actuator was driven to meet a certain command), the feedback gain (affecting the span of the feedback), and the offset gain (affecting the offset of the feedback). The actual linear and angular displacements were measured with gauging tools. These included a digital vernier for the AP motion, a digital protractor for the FE motion, and an analog protractor for the IE rotation. The analog protractor was calibrated and measured with the digital protractor. The actual load calibration was done with the use of an S-beam load cell connected to the simulator to provide instant feedback to computer control unit. The vertical load actuator was set such that an applied 100 lbs resulted in the feedback of 1 V.

The control function implemented in the present knee simulator is briefly explained for the vertical load and a schematic is shown in Fig 3.9. A voltage command enters the load circuit board and passes the loop gain, loop offset, and feedback potentiometer. The command voltage is fixed by the machine setup values. The pump pressure is set for 800 psi and the area of the

actuator is 3.14 square inches. The static calibrations adjustments ensure that the actual applied load agrees with command voltage. Thus, the present knee simulator controls the load by measuring the manifold pressure which is applied to all stations on each bank.

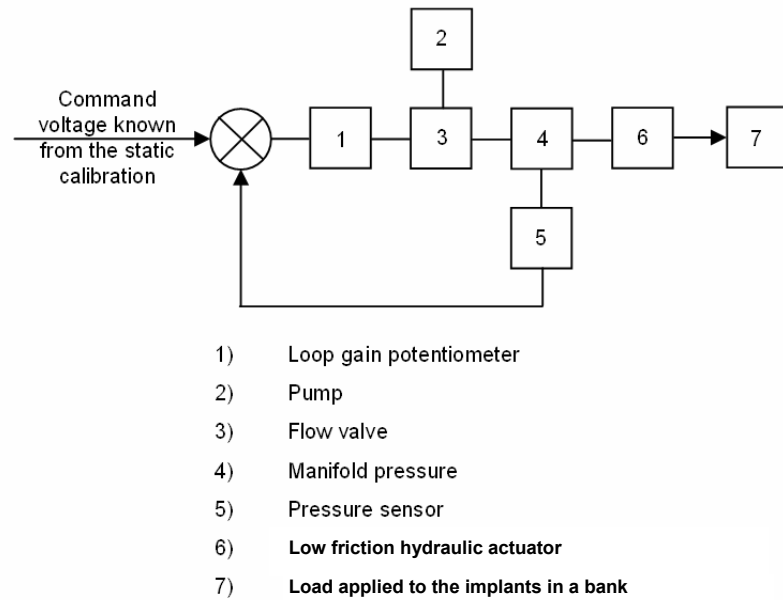


Figure 3.9: Schematic of the control function for the vertical load implemented in the knee simulator.

Such static calibration was followed by dynamic calibration where square waveforms were run for all motions and the vertical load. This was used to compare the commanded waveform with the feedback waveform. If necessary, the loop gain of each motion and load actuator was adjusted so the feedback waveform closely followed the applied square wave from. It is important to note that the dynamic calibration of the vertical load actuator was performed with all implants in place on the bank.

Prior to the calibration of the vertical load actuator, the units for the vertical load were switched from SI-units (N) to pounds (lbs). Thus, the load range of 0 - 4500 N became a range of 0 - 1012 lbs. After the calibration, the units of the vertical load were again switched back into N. If this was not

performed, the simulator would apply the load values in N as if they were lbs which would severely alter the wear test.

3.4.3 Imposed Loads and Displacements

Vertical loading and both linear and angular displacements were applied according to ISO 14242-3⁴¹ (Fig. 3.10 - 3.12). The ISO standard had taken values from various previous publications. For example, the vertical loading in the ISO standard had originated from Morrison et al.³⁹⁶. Text-files for the ISO load and displacement values were created and imported into the SIMMAC software to create a wear test program as illustrated in the AMTI manual³⁹⁵. In all wear tests of the present thesis, the ISO motion for DC simulator wear testing was applied to the low-conforming PE inserts of the AMK[®] implants. McNulty et al.⁴⁵ did the same in their wear testing of AMK[®] implants.

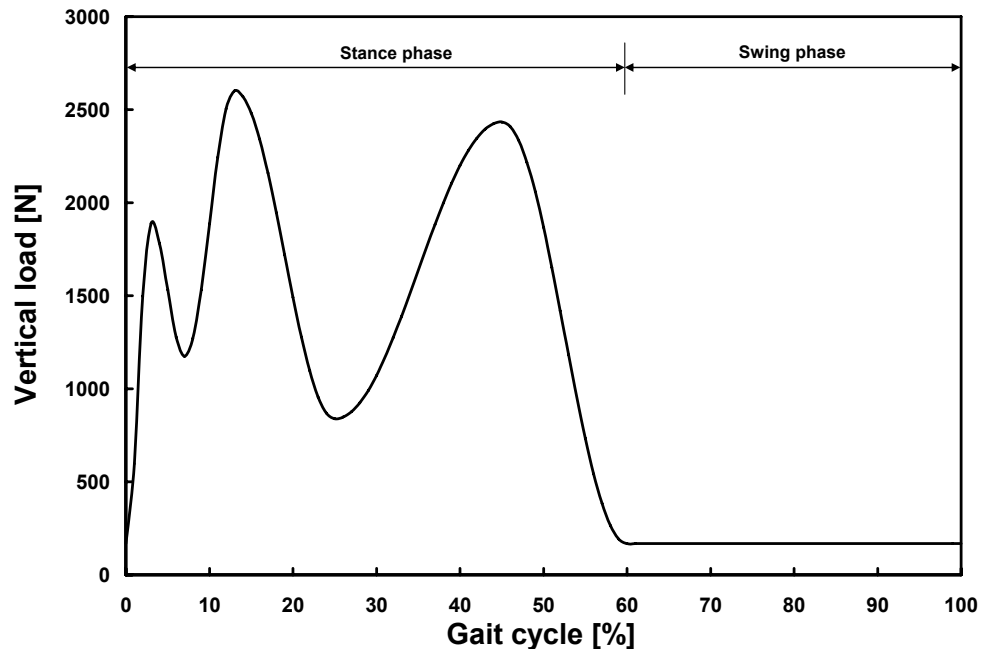


Figure 3.10: Vertical loading for level walking according to ISO 14243-3. Note the loading pattern during the stance phase and the constant low loading during the swing phase.

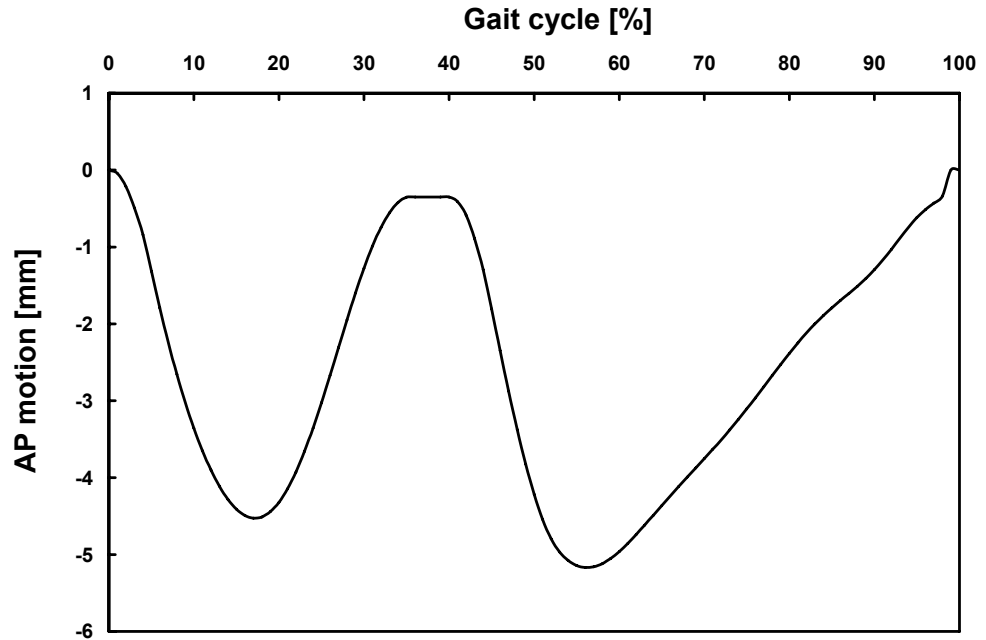


Figure 3.11: The anterior/posterior (AP) linear displacement according to ISO 14243-3.

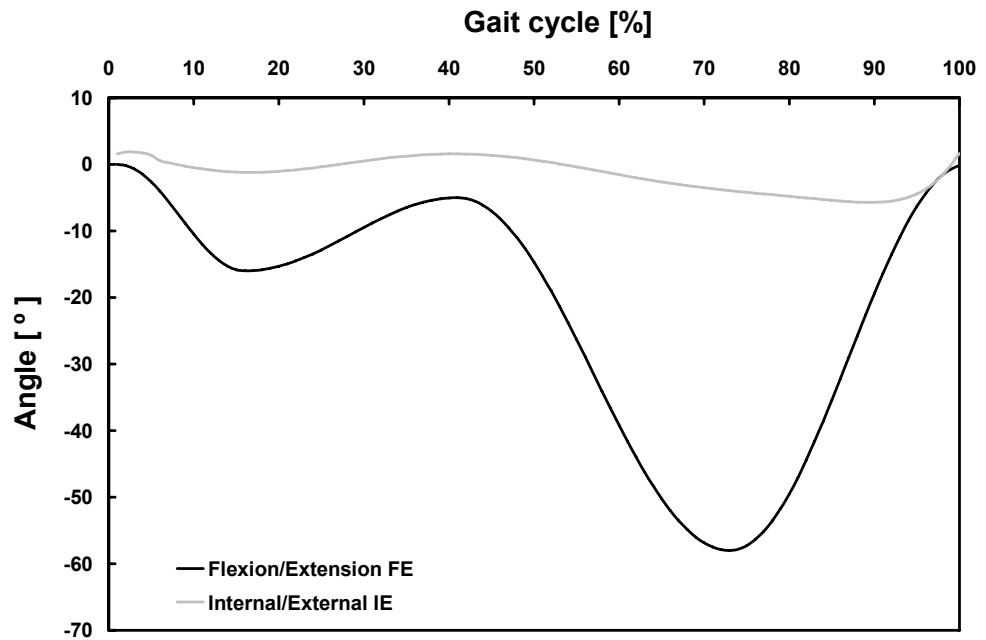


Figure 3.12: The flexion/extension (FE) and internal/external (IE) angular displacements according to ISO 14243-3.

To place the AMK[®] femoral components in clinically realistic position, they had to be offset by 11.4 mm in the posterior direction from the simulator zero position. Thus, the “user settings” were altered under the “system settings” dialog box in SIMMAC, where the “user zero” for the AP output channel was placed at 11.4 mm. The medial-to-lateral load distribution was 60-to-40 % and this distribution was achieved by off-setting the tibial tray fixture in the medial direction by approximately 0.07 times the width of the tibial tray ⁴¹.

3.4.4 Implants

The implant model that was chosen for the wear tests was a cruciate retaining design (AMK[®], DePuy Orthopaedics Inc., Warsaw, IN) (Fig. 3.13). All implants tested were size three and intended for the right knee. The PE inserts were machined from ram-extruded GUR 1050 (Ticona[®], NJ) to a thickness of 10 mm and were GP sterilized. This implant model had a history of clinical application and had been subjected to several design modifications. In particular, the tibial tray was originally manufactured of a cast Ti alloy with screw holes and the PE was GA sterilized. These features were blamed for severe osteolysis and catastrophic implant failure ²⁸¹. Recent design modifications included a highly polished cast CoCr alloy tibial tray and the use of inert sterilization techniques ³⁹⁷. The articulation was considered to be a low-conforming, ellipsoidal contact with relatively high contact stresses compared with other more conforming designs ³⁶⁰. However, the AMK[®] did allow the retained natural tissues to guide knee motion and had relatively low transmitted lateral forces.

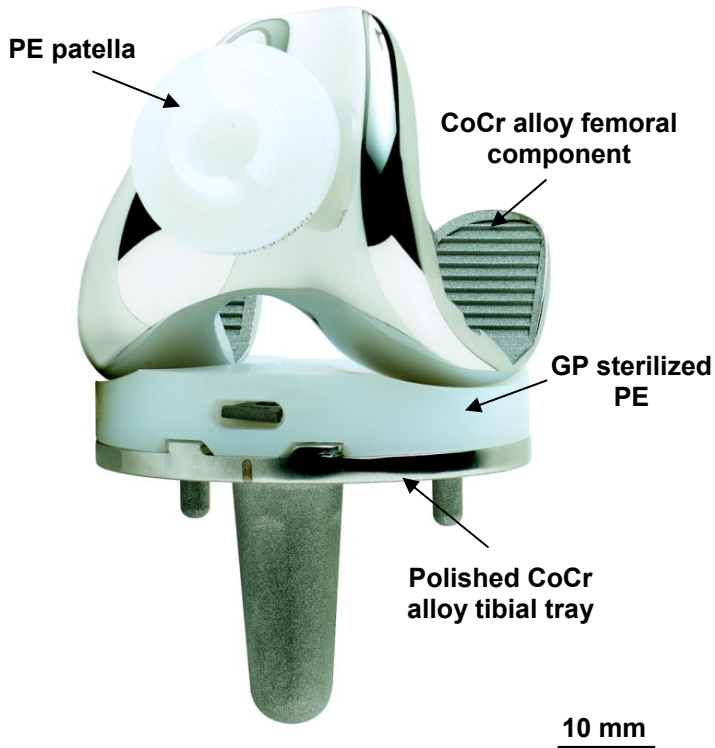


Figure 3.13: The AMK[®] total knee system (DePuy Orthopaedics Inc., Warsaw, IN). The patella was not used in the wear tests.

3.4.5 Implant Mounting

The femoral and tibial components were cemented onto their customized simulator fixtures⁴⁷ using antibiotic-free bone cement (SmartSet[™] Endurance Bone Cement, DePuy Orthopaedics, Warsaw, IN). For each station a volume of approximately 80 g (two packages) was mixed under a fume hood. Approximately 60 g was used to cement the tibial tray into the customized tibial fixture and approximately 20 g was used to cement the femoral component. The bone cement was of medium viscosity and was allowed to cure for almost 5 min. The cemented implant components were then loaded in a vice for their final positioning. Careful attention was paid to ensure that no implant surfaces were scuffed or scratched during the mounting procedure. Any excessive bone cement that squeezed out between the implant components and their fixtures was then carefully removed with a non-abrasive nylon stick.

Prior to the fixation of the tibial trays, a custom-made tibial tray template was fastened onto each tibial fixture to ensure the accuracy and precision of the tibial tray mounting for each wear station within a tolerance of ± 0.5 mm. A tapered style friction locking mechanism was located at the end of the femoral fixture shaft intended for the fine adjustment of the locking mechanism into the knee simulator. The inserts of each femoral shaft were tightened with a torque of 35 ft-lbs, as recommended by AMTI. The effective femoral shaft length was eventually defined by the depth penetration of the spigot into the shaft. A custom-made fixture was utilized to enable accurate adjustment of the shaft length (101.6 ± 0.2 mm). The torque and effective shaft length was checked every 2 Mc. All fixture components were ultrasonically cleaned prior to their assembly.

3.5 Biochemical Analyses

3.5.1 Protein Concentration and Degradation

The lubricants used in the wear simulations were damaged during the wear process. Such damage led to protein degradation that had to be characterized to be able to explain the overall acting wear mechanism. At the beginning of the wear tests the fresh lubricant used as the “starting material (SM)” was often translucent and yellow. As the wear test progressed, the lubricants lost their translucent feature and became opaque. Such altered visual appearance suggested that some protein constituents were damaged and had precipitated out of solution (Fig. 3.14). To separate the damaged proteins from the unworn proteins the lubricant samples had to be centrifuged. The lubricant samples were then placed in a centrifuge apparatus (Model 5417 R, Eppendorf AG, Hamburg, Germany) and subjected to a centrifugal acceleration of 20,000 G (where $G = 9.80665 \text{ m/s}^2$) for 40 min at 17 °C. This caused the suspended proteins to become compacted on the bottom of the tubes which resulted in a pellet. The fluid on top of the pellet was called the supernatant (SUP) and was free of any precipitates.

The pellets were stored at -20 °C and defrosted in some particular cases, to determine the precipitated protein concentration. The pellet was subsequently resuspended by adding 500 µl of a SDS-DTT solution, consisting of 10 % sodium-dodecyl-(lauryl)-sulfate (SDS) in PBS, containing 5 mmol/l dithiothreitol (DTT). The samples were then mixed for 1 min each and placed at 55 °C for 25 min, being mixed in 5 min intervals. Such a procedure had to be performed as it was not possible to determine the protein concentration directly on the compacted pellet.

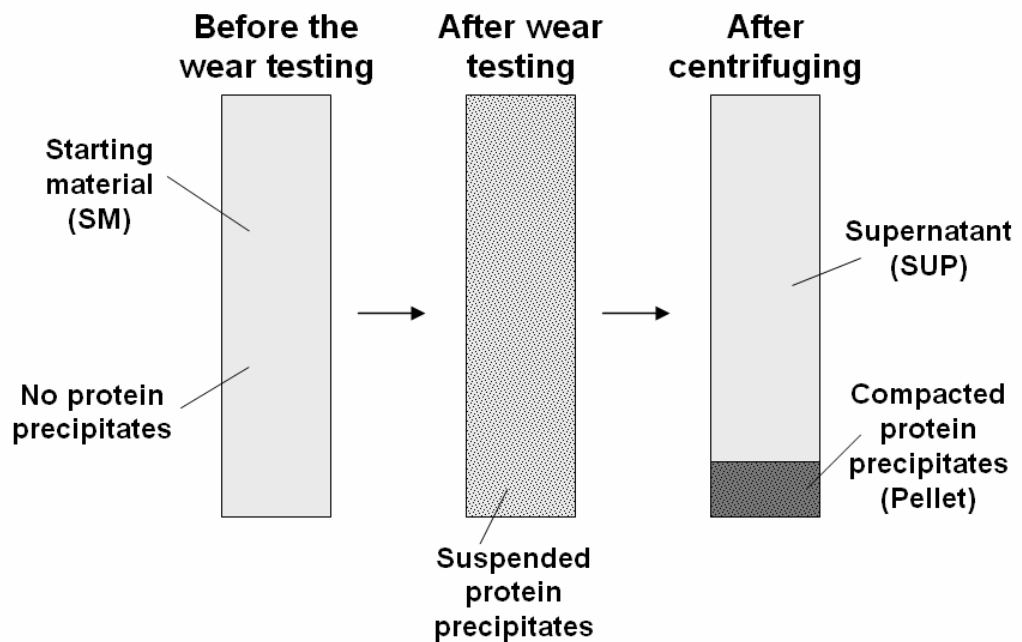


Figure 3.14: Schematic of lubricant protein precipitation and centrifuging. The fresh unworn lubricant is referred to as the starting material (SM). After the wear test the worn lubricant contains suspended protein precipitates. Centrifuging the worn lubricant separates the protein precipitates from the remaining lubricant (supernatant; SUP) in from of a compacted pellet.

The percent of protein degradation [%] caused by wear testing in the knee simulator was calculated from the measured protein concentration of the SM lubricant samples before testing and from the measured protein

concentration of the SUP samples of the lubricant that had been collected after the wear test. The protein concentrations in g/l of the SF samples from patients described in 3.3.1 and lubricants used in wear testing were determined using a bicinchonic acid protein assay kit (BCATM protein assay kit, Cat. # P123227, Pierce Chemicals, Rockford, IL). The key to this process was the biuret reaction that is well known in the field of biochemistry. In this reaction, the biuret reagent (copper sulfate in a strong base) builds a coloured complex between the peptide bonds of a protein and the Cu atoms. This is accompanied by reduction of Cu²⁺ to Cu⁺ by the protein in such an alkaline environment. A brief description on the current protein assay protocol is given subsequently and described in more detail in the BCA assay manual. The lubricant samples were diluted 100-times with PBS (10 µl lubricant sample + 990 µl PBS) and placed in 1 ml tubes (Eppendorf AG, Hamburg, Germany). Twelve measurements per lubricant sample were obtained and pipetted onto a microplate at volume of 25 µl each (Microtiter 96-well UV microplate; VWR Cat. # 14227-680) (Fig. 3.15). A volume of 200 µl of the BCA working reagent was added to each 25 µl in the wells. The microplate was then incubated at 37 °C for 30 ± 2 min. The absorbance of the incubated 225 µl fluid in each well was then measured using a spectrophotometer (Multiskan Spectrum, Thermo Labsystems, Thermo Electron Corporation, Milford, MA) at wave length of 562 nm.

The measured absorbance values needed to be transformed into protein concentration in g/l. Bovine serum albumin (BSA standard, BCATM protein assay kit, Cat. # P123227, Pierce Chemicals, Rockford, IL) with a protein concentration of 2 g/l was diluted with PBS to 0.0625, 0.125, 0.250, 0.375, 0.5, 0.750, and 1 g/l concentration to create a standard curve of the absorbance versus protein concentration. The BCA assay was used as in the aforementioned manner to obtain an absorbance for every BSA dilution. The equation of the standard curve was then used to convert the absorbance to a protein concentration for the lubricant. This allowed the absorbance measurements of the fluids to be converted into total protein concentration on g/l. The mean and SD for those measurements were then determined.

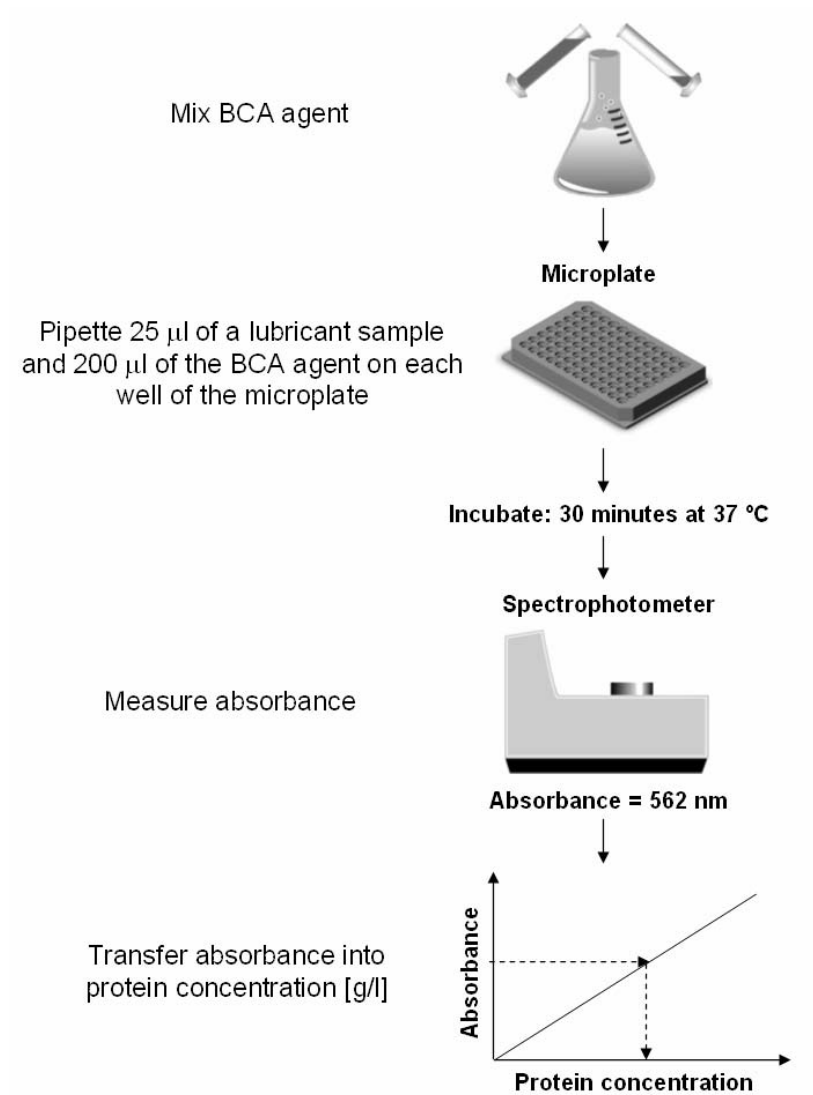


Figure 3.15: Procedure summary of running a BCA protein assay.

3.5.2 Electrophoresis

As mentioned in Section 3.3.2, the lubricants consisted of different types of proteins. Although the BCA assay can be used to determine the total protein concentration it is unable to measure the fractions of different types of proteins. Electrophoresis is a useful tool to determine the relative concentration of protein fractions in such lubricants that are comprised of different types of proteins³⁹⁸. Here, the protein is charged by an electric source and travels

though a porous membrane, which is referred to as the electrophoretic gel. The velocity of proteins travelling through a porous gel depends on several factors such as the applied electric strength, protein net charge, the viscosity of the protein mixture, and on the protein size (Fig. 3.16). Thus, the proteins with a small radius migrate deeper and faster into the gel, whereas proteins with a larger radius stay on top of the gel near the point of application of the fluid.

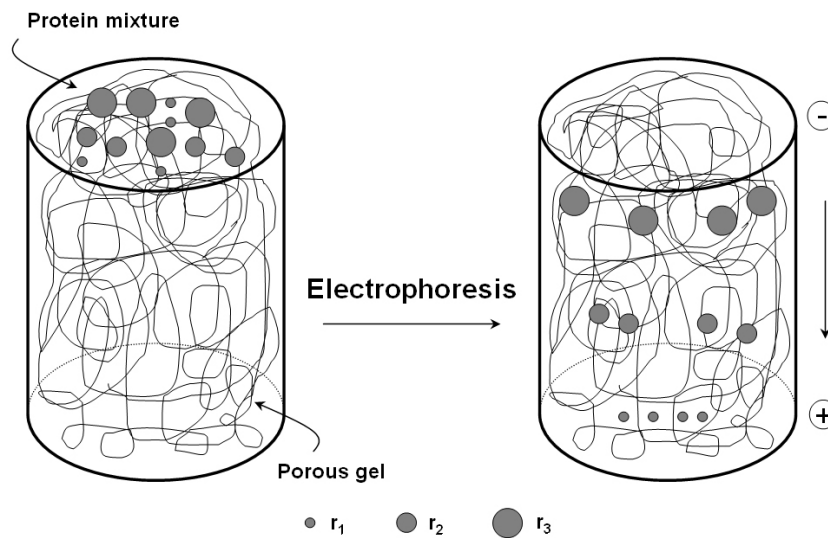


Figure 3.16: Sieving of proteins by a porous polyacrylamide gel (reproduced from ³⁹⁸).

Electrophoresis was applied to the SF samples and all lubricants used in the wear tests. Samples were brought to the Department of Immunology located at the University Hospital of the LHSC for electrophoretic analysis that were performed by the laboratory technician Janice Restorick. The apparatus used for the electrophoresis (Sebia Hydrasys[®], Sebia, Norcross, GA) permitted the running of 30 individual samples on one alkaline buffered (pH = 8.5) agar-based gel (Hydragel 30 β 1- β 2, Sebia, Norcross, GA). The apparatus was calibrated on a daily basis and was mainly used to evaluate the protein constituent fractions in patients. This gel separated five major protein fractions: albumin, α -1 globulin, α -2 globulin, β -globulin, and γ -globulin (Fig. 3.17). The gel was stained with Coomassie blue to allow the visualization of bands

indicating the protein content of the gel. The gels were scanned using an Epson scanner (Expansion 1600, Epson, Long Beach, CA). A software program (Sebia, Phoresis Release 4.9.0, Norcross, GA) was used to measure the relative intensities of each protein band. This apparatus has a calibrated densitometer that determines the intensity of individual protein bands which produces a sample specific density curve. The area under each peak represents the fraction [%] of each protein constituent. The loading volume per gel was 10 μ l.

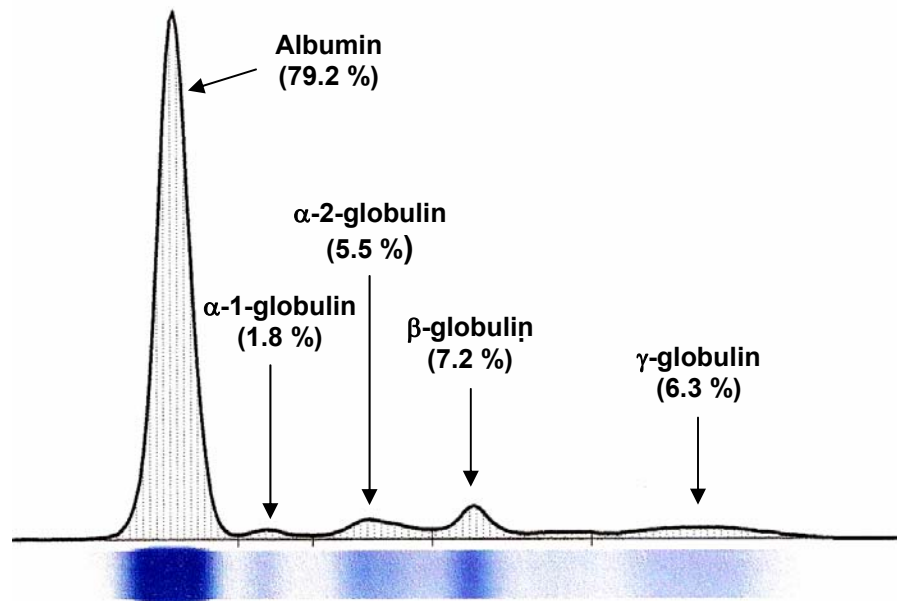


Figure 3.17: Image showing the characteristic migration pattern of a SF sample for the Hydragel 30- β 1- β 2 gel ³⁹⁹.

The SF had to be treated with hyaluronidase to reduce the viscosity of the lubricant. Hyaluronidase is an enzyme that catalyzes HA and increases the permeability of the protein constituents into the gel. Hyaluronidase powder (Hyalurono-glucosaminidase, H 3506, Sigma-Aldrich, St.Louis, MO) was diluted with PBS to a 71 g/l solution and was then added to 100 μ l of synovial fluid in a ratio of 1:20. Hyaluronidase samples were run by themselves as control specimens.

3.5.3 Peptide Concentration

As described in Section 2.2.4, proteins, colloids, and other polymers in solution may adsorb to bearing surfaces and affect the boundary lubrication process. Such adsorbed substances may become entangled under applied load and motion which may lead to damage at such entanglements. Mechanical shear⁴⁰⁰ or enzymatic digestion (proteolysis)⁴⁰¹ may cause the polypeptide chains in proteins to break into short amino acid chunks (peptides) (Fig. 3.18). The latter causes the digestion of covalent peptide bonds between amino acids and is considered an irreversible process. Thus, it was of interest to investigate how much the proteins became damaged by the wear process that led to such peptides that remained suspended in the lubricant sample after centrifuging.

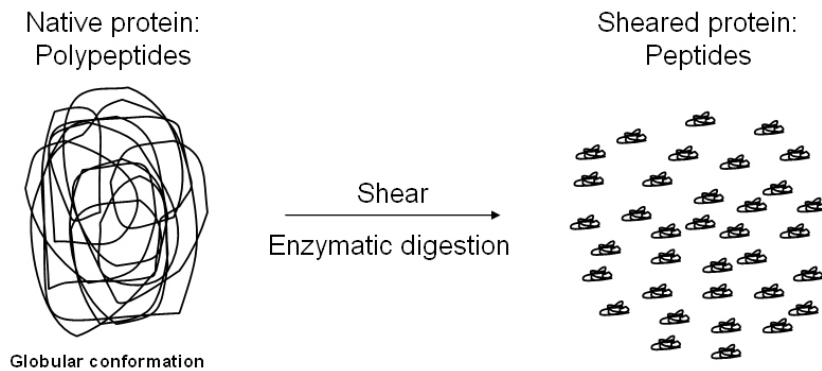


Figure 3.18: The effect of shear and enzymatic digestion on the protein structure. The native proteins (polypeptides) change from a globular conformation into small protein chunks, referred to as peptides.

Lubricant samples (SF, SM, SUP) were filtered through an ultrafine membrane (VIVASPIN 2, Vivascience Ltd., Stonehouse, UK) with a 2,000 Da molecular weight cut-off (MWCO). The VIVASPIN tubes were loaded with the lubricant (1 ml) and were spun at a fixed angle of 25 ° for 10 min at 10,500 G (Sorvall[®] RC-5B Refrigerated Superspeed Centrifuge). The peptide concentration was directly determined without any dilution using the aforementioned BCA assay. Ten measurements per lubricant sample were conducted and the mean and SD was reported.

According to the manufacturer of the ultrafine membrane, the concentrate recovery at a loading volume of 2 ml is 95% for the 2,000 Da MWCO. No standard fluid with a certain peptide concentration is supplied by the manufacturer to evaluate the accuracy and precision of the VIVASPIN tubes. Therefore it was decided to repeatedly measure BCS + DW + SA that was obtained from the knee simulator after a test interval of 0.5 Mc. The accuracy of the VIVASPIN tubes was regarded as the mean value of the five repeatedly measured peptide concentrations, and was within $\pm 1.65 \%$ of the mean from all measurements ($0.146 \pm 0.024 \text{ g/l}$) (Fig. 3.19).

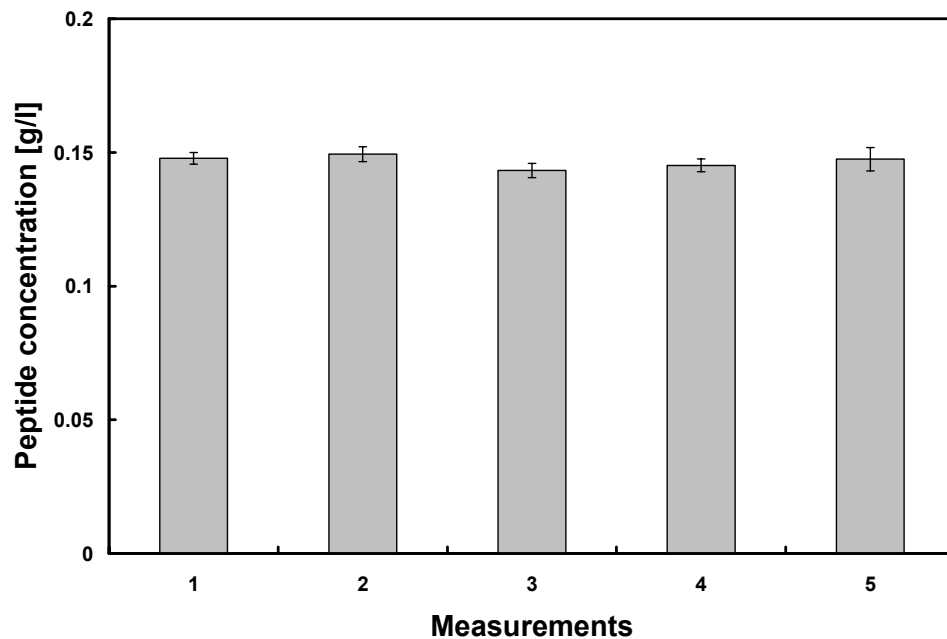


Figure 3.19: Peptide concentration of worn BCS determined in five separate VIVASPIN tubes to determine the accuracy and precision of the measurements (MWCO = 2,000 Da).

The precision of the repeated measurements can be interpreted as the standard deviation of all measurements ($\pm 0.036 \text{ g/l}$ or $\pm 2.45 \%$). Thus, such results suggested that one VIVAPSIN tube per test would be sufficient to determine an accurate and precise peptide concentration.

3.5.4 Osmolality

As described in Section 2.3.1, the osmolality is a direct measure of the ionic strength of a solution and is regarded as a systemic, patient specific value¹⁰⁶. The calf sera were either diluted with DW or PBS which had different levels of osmolality (see Section 3.3.3). Osmolality has been shown to affect the thermal stability of proteins in solution¹⁰⁴ and thus may affect the protein degradation and the PE wear rate in simulator wear testing. In the present study, an osmometer (Osmometer 5520, Wescor, Logan, UT) was used to determine the osmolality of the SF, different lubricants and their dilutive media. The osmometer determined the osmolality following the freezing-point depression test strategy at atmospheric pressure. This strategy permits the determination of the difference between freezing points of a pure solvent and a solution mixed with a solute. The difference between freezing points is directly proportional to the molar concentration of the solution. Prior to testing, the instrument was calibrated using a reference sample that had 290 mmol/kg (Calibration OPTI-Mole™, Wescor, Logan, UT). Triplicate measurements were obtained for each of the lubricant samples.

3.5.5 Differential Scanning Calorimetry

The stability of the folded protein conformation can be compromised by environmental changes such as temperature, pH, osmolality, and the presence of chemical denaturants (Fig. 3.20). Asperity interactions between articulating surfaces may cause an increase in localized temperature (flash-temperature)⁵⁶ and affect the interfacial behaviour of proteins, protein adsorption¹⁶⁴, and thus may promote adhesion/abrasion and PE wear. Differential Scanning Calorimetry (DSC) is a frequently used technique to study the stability of proteins. This technique permits one to obtain data on the calorimetric heat or enthalpic changes (ΔH) and entropic changes (ΔS) that occur as the protein is denatured. This technique appeared more appropriate for the lubricants consisting of multiple protein types than the circular-dichroism

technique that has been utilized to investigate the unfolding of pure albumin solutions^{76,78}. Since this is a thermodynamically driven process, the values are given in Kelvin [K] rather than in degrees Celsius [°C].

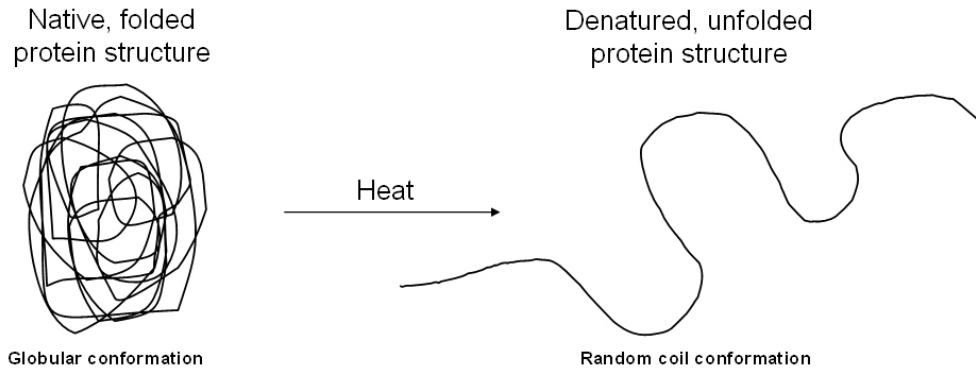


Figure 3.20: Schematic showing the principle of an irreversible unfolding process of a globular protein. Exposure to a heat source causes the protein to unfold from and to take on a random coil like structure.

The protein stability of a dilute protein solution depends on the partial molar heat capacity, c_p , at constant pressure. The change in c_p reflects the ability of the protein solution to absorb heat and cope with a defined increase in temperature. A protein in a dilute solution is in equilibrium between the native (folded) conformation and its denatured (unfolded) conformation. The stability of the native state is based on the magnitude of the Gibbs free energy (ΔG) of the system and the thermodynamic relationships between enthalpy (ΔH) and entropy (ΔS) changes:

$$\Delta G = \Delta H - T\Delta S \quad (3.1)$$

A positive ΔG indicates the native state is more stable than the denatured state; the more positive the ΔG , the greater the stability. In order to allow a protein to become unfolded, stabilizing forces need to be broken. Protein unfolding occurs when the entropic changes are significantly increased

to overcome stabilizing enthalpic interactions between protein hydrogen bonds, hydrophobic interactions and electrostatic interactions, resulting in an endothermic peak at a certain melting temperature T_m (Fig. 3.21). The T_m directly indicates the thermal stability of the protein. The higher the T_m the more stable is the protein at lower temperatures. ΔH is primarily due to changes in hydration of side chains that are buried in the native state and become exposed in the denatured state. The shift in baseline before and after the transition represents the change in c_p (Δc_p) of the protein in association with the solvent caused by unfolding.

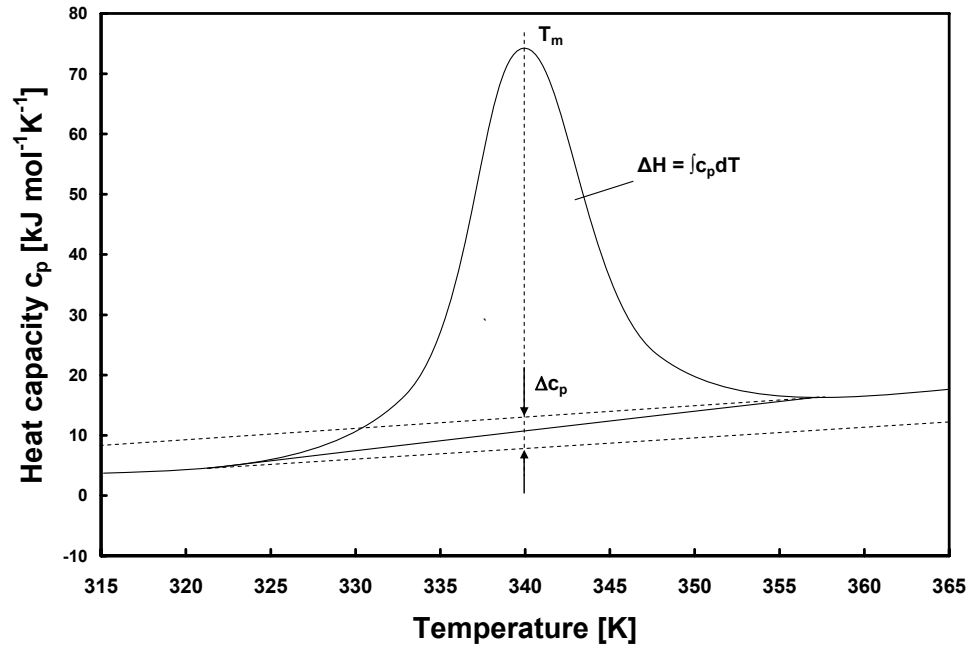


Figure 3.21: Schematic representation of a thermogram.

The sharpness of the transition peak is an index of the cooperative nature of the transition from native formation to denatured formation. The unfolding process becomes a multi-stage process when more than one peak is observed which means it is less cooperative. At temperature below T_m the concentration of native proteins is higher than of denatured proteins. The T_m at maximal c_p (T_m (cp-max)) is referred to as the transition point where half the

proteins are folded and half are unfolded. At this point $\Delta G = 0$ and the conformational entropy $\Delta S = \Delta H/T_m$ (c_p -max) can be directly calculated. During unfolding, a protein transforms from a single folded conformation to many random unfolded conformations. ΔS is the measure of disorder/randomness in a system and an increase in ΔS indicates the amount energy dissipated to transform proteins from native, folded conformation to random, unfolded conformation. Higher ΔS indicates higher conformational protein stability. Conformational entropy overcomes the stabilizing forces allowing the protein to unfold at temperatures where entropy becomes dominant.

A MicroCal VP-DSC calorimeter (MicroCal, Northhampton, MA) was used in the present study to obtain the thermogram for several lubricant mixtures. In particular, this was used to investigate the effects of osmolality and HA on the thermal stability of calf serum. Firstly, a baseline for the thermogram was established by scanning a buffer solution which consists of the medium used to dilute the calf serum. Secondly, each lubricant was diluted with a buffer solution to a total protein concentration of 6 g/l and were subsequently scanned. A scan rate of 60 K/hour was applied from 283 K to 368 K. The concentration molality was uniformly set at 0.05 mmol/L. A precise molar concentration of the sample calf serum was not available since the exact concentration of each of the individual protein constituents was unknown. Thus, only relative comparison between T_m , ΔH , and ΔS can be made. The contribution of the proteins to the calorimetrically measured c_p was determined by subtracting a scan of a buffer solution from the data prior to lubricant analysis. Such a procedure ensured that any effects of the solvent on the proteins were eliminated and the thermal signal is entirely due to the serum constituents. A software program (Origin 5.0, MicroCal, Northhampton, MA) was used to analyze the data. T_m , ΔH , and ΔS of the transition are calculated by fitting the data to a non-two-state transition model using non-linear least squares regression analysis (Levenberg-Marquardt non-linear least-square method)⁴⁰². The unfolding of the protein constituents of the calf serum based lubricants was considered an irreversible process¹⁶⁹.

3.5.6 Trace Elements

The concentrations of some trace elements such as calcium (Ca), magnesium (Mg), inorganic phosphorus (P) and iron (Fe) were determined for the SF samples and compared with the concentrations found in the various calf serum mixtures that were used in the wear testing with the knee simulator. A chemical analyzer (Synchron LX 20[®] Pro, Beckman Coulter, Fullerton, CA) was utilized to measure these concentrations. Depending on the element, different methodologies were used in the analyzer that is described elsewhere in more detail⁴⁰³⁻⁴⁰⁶. These measurements were performed by Janice Restorick at the Immunology laboratory at the LHSC. Triplicate measurements were obtained for each of the lubricant samples.

3.5.7 pH

Assessing the pH of the lubricant was recommended by ISO 14243-3 for displacement controlled wear testing. The pH of the lubricant indicates the level of acidity (pH < 7.00) or alkalinity (pH > 7.00) which is directly related to the activity of hydrogen ions in the solution. A pH-meter (SevenEasy, Mettler-Toledo, Columbus, OH) was utilized to conduct the pH measurements. The apparatus was calibrated prior to every measurement using four reference solutions with a pH of 4.01, 7.00, 9.21, and 10.01. The electrode tip was rinsed with DW after every measurement and remained suspended in DW until the next measurement. Three measurements per lubricant were performed and then reported as the mean with the according SD.

3.6 Microbiological Analysis

Some basic microbiological tests were performed with the goal to create a sterile environment for implant wear testing. Bell et al.³⁰ suggested that SA was ineffective in eliminating bacterial growth from wear tests. The subsequent techniques were used to identify the microbial contaminant and to investigate its biological behaviour during the wear tests.

3.6.1 Microbial Identification

A characteristic culture sample of the microbial contamination found in the knee simulator test lubricant was grown on LB agar on a petri dish¹⁹⁵. A colony was carefully picked from that petri dish without disturbing the LB Agar surface. The microbes were investigated using Gram stains. The Gram classification system is empirical, and largely based on differences in cell wall structure. Gram-negative microbes appear pink while Gram-positive microbes appear purple. To further identify the microbial contamination it was decided to use API[®] 20E system (Analytical Profile Index, Biomerieux, Inc., Hazelwood, MO). Such a system provided an easy way to identify members of the family *Enterobacteriaceae* and consisted of twenty microtubes and cupules, partly filled with dehydrated substrates^{194,195}. Each microtube indicates a certain compound in the microbial suspensions. Bacterial suspensions are then added to the microtubes, rehydrate the medium and cause a biochemical reaction, leading to color changes during their incubation or after specific reagents are added. Color changes indicate the presence or absence of a chemical action and thus, a positive or negative result.

3.6.2 Microbial Growth

Gaining insight into the growth behaviour of a microbe is performed by placing the present bacterium into a nutrient over a certain time frame and is considered a routine procedure in Microbiology¹⁹⁵. Microbial growth can be described as the process in which two daughter cells are produced by the cell division of one organism. Such a process is accompanied by local doubling of the bacterial population. If both daughter cells survive the microbial growth usually progresses in an exponential manner (Fig. 3.22). However, the microbial growth curve can be categorized into four major phases: *Lag Phase*: Immediately after inoculation of the cells into fresh medium, the population remains temporarily unchanged. Although there is no apparent cell division occurring, the cells may be growing in volume or mass, synthesizing enzymes, proteins, and increasing in metabolic activity. The microbes adapt themselves to growth conditions in the present environment. The length of the lag phase is apparently dependent on a wide variety of factors including the size of the inoculums; time necessary to recover from physical damage or shock in the transfer; time required for synthesis of essential coenzymes or division factors; and time required for synthesis of new (inducible) enzymes that are necessary to metabolize the substrates present in the medium; *Exponential Phase*: The exponential phase of growth is a pattern of balanced growth wherein all the cells are dividing regularly by binary fission, and are growing by geometric progression. The cells divide at a constant rate depending upon the composition of the growth medium and the conditions of incubation. The rate of exponential growth of a bacterial culture is expressed as generation time or doubling time of the bacterial population; *Stationary Phase*: Exponential growth cannot be continued forever in a batch culture (e.g. a closed system such as a test tube or flask). Population growth is limited by one of three factors: (1) exhaustion of available nutrients; (2) accumulation of inhibitory metabolites or end products; (3) exhaustion of space, in this case called a lack of “biological space”. During the stationary phase, if viable cells are being counted, it cannot be determined whether some cells are dying and an equal number of cells are dividing, or the

population of cells has simply stopped growing and dividing; *Death Phase*: If incubation continues after the population reaches stationary phase, a death phase follows, in which the viable cell population declines. During the death phase, the number of viable cells decreases exponentially, essentially the reverse of growth during the log phase. The bacteria run out of nutrients and die in an altered environment.

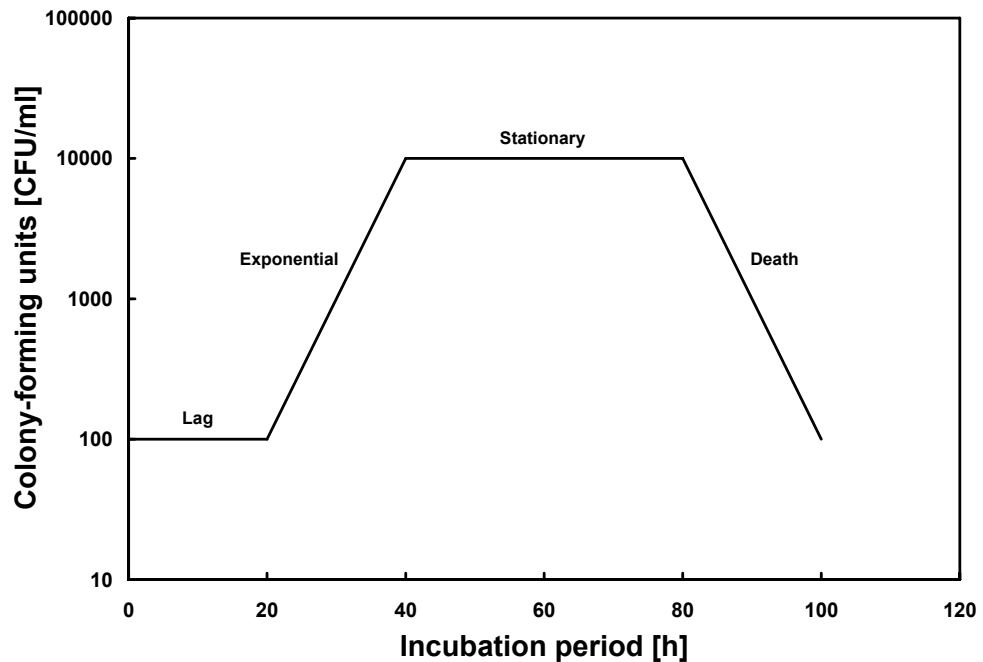


Figure 3.22: The microbial growth behaviour versus incubation period shown for an example bacterium. Note the four characteristic phases of bacterial growth: lag, exponential, stationary and death.

In the present study, lysogeny broth, also known as Luria-Bertani (LB) Agar (Cat. # 22700025, Invitrogen Canada Inc., Burlington, ON) served as a nutrient rich environment for bacterial growth and was obtained in powder form. This method has been widely utilized for investigations on bacterial growth^{407,408}. A mass of 15 g of LB Agar was diluted with 400 ml of double-deionized water and placed in a 1000 ml bottle. The mixture was then placed in a microwave oven and heated for 4 min. The bottle was then placed in an

autoclave for 15 min at approximately 20 °C. Parafilm (American National Can, Menasha, WI) was wrapped around the bottle neck to seal the lid. The bottle was left at RT for 24 h, causing the LB Agar to solidify. When needed, the LB agar bottle was placed in a microwave to be heated and liquefied. The liquid LB-agar was then poured on Petri dishes (100 mm diameter, Cat # CA73370-010, VWR, Mississauga, ON) around an open propane flame to inhibit contamination (aseptic environment). The prepared dishes were then placed at approximately 4 °C until further use.

Serum samples were taken from the wear stations by disconnecting the tubing from the external serum container to the peristaltic pump and switching the pump position to drain, thus removing fluid from the actual wear station. Prior to this, the surrounding environment was sprayed with alcohol to inhibit further possible contamination. Serum samples were drawn from all simulator stations (wear and load-soak) and diluted with LB medium to achieve countable colony-forming units (CFU/ml) on the LB Agar plates. The CFU/ml is determined by counting the number of cultures observed on the petri dish in consideration of the dilution factor. A total volume of 100 ml per sample was spread on each LB Agar Petri dish, with triplicates of each sample. The dishes were incubated for 18 ± 2 h at 37 °C. The grown colonies were then counted and the CFU/ml was then determined. Afterwards, the samples were placed in bio-hazardous container and sent for incineration.

3.6.3 Antimicrobial Susceptibility Test

Many substances used to treat infections are synthetically produced and referred to as antibiotics^{105,195}. No antibiotic inhibits all organisms and some microbes are naturally resistant to certain antibiotics. To evaluate the efficacy of certain antimicrobial agents, a disk diffusion test (or Kirby-Bauer Method) was applied. Five antibiotics were selected which are known to be effective against a number of Gram-negative and Gram positive microbes (Table 3.9). Penicillin and Carbenicillin are called *β -lactam* antibiotic because of their

chemical structure which is lethal to the microbial cell wall. Streptomycin and Tetracycline are *aminoglycosides* and are effective by binding to the microbial subunits and inhibit the microbe to synthesize proteins vital to its growth. Chloramphenicol is a *bacteriostatic* antibiotic which inhibits the growth or reproduction of microbes without killing them.

Table 3.9: Properties of the antibiotic discs.

Antimicrobial agent	Antibiotic Type
Penicillin	β -lactam
Carbenicillin	β -lactam
Streptomycin	Aminoglycoside
Tetracycline	Aminoglycoside
Chloramphenicol	Bacteriostatic

The observed microbial contaminant was plated onto petri dishes (Müller-Hinton agar, 4 mm agar thickness) and inoculated to form a microbial lawn. Antibiotic-doped paper discs were placed onto the inoculated petri dish. The inoculated petri dishes were then incubated for 16 - 18 h at 37 °C to allow microbial growth and time for the agents to diffuse from the paper disks into the agar on triplicate samples. The agent progressively diffuses into the agar and established a concentration gradient around the disk if the organism is susceptible to the agent, a clear concentric zone will form around the disk; this zone is called zone of inhibition (ZOI) and is antibiotic specific (Fig. 3.23). The diameter of the zone consequently depends upon the sensitivity of the bacteria to the specific antimicrobial agent and the radius at which the agent's minimum inhibitory concentration is reached.

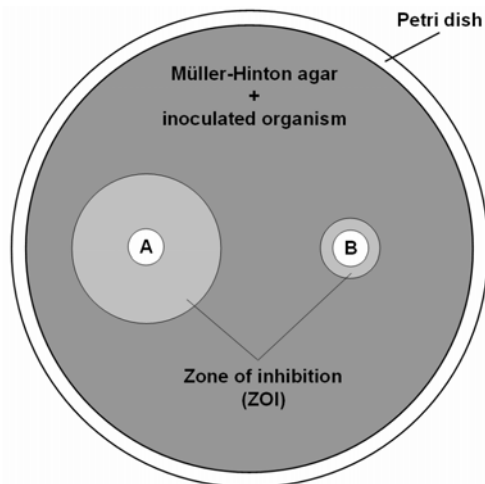


Figure 3.23: Schematic diagram showing the antimicrobial susceptibility test. Disk A and disk B represent antimicrobial disks; the zone of inhibition (ZOI) is larger for A than for B; agent in disk A more effective than B in inhibiting bacterial growth.

3.6.4 β -lactamase Test

This test was used to rapidly identify whether an isolated bacterium was resistant towards β -lactam antibiotics¹⁹⁵. The β -lactam ring is part of the chemical structure of many antibiotics and is known to have a lethal effect on bacteria by interfering with the cell wall synthesis. However, many bacteria have developed resistance towards these antibiotics by producing enzymes called β -lactamase. Such a production by bacterium hydrolyzes the β -lactam ring in the antibiotics and causes them to be ineffective. Partial chemical structure of an β -lactam antibiotic (penicillin) and the site of action for β -lactamase are illustrated in Figure 3.24. To test the bacterium's ability to produce β -lactamase, a paper disc containing nitrocefin (Cefinase[®] disks, Becton Dickinson, Franklin lakes, NJ) is smeared with the test organism on triplicate petri dishes. Nitrocefin is a cephalosporin and susceptible to most β -lactamases. If the organism produces β -lactamase at RT it will hydrolyze nitrocefin and show a pink/red spot on the disk (positive results). If no β -lactamase was produced by the bacteria the disk maintained its initial color or turned light yellow (negative result).

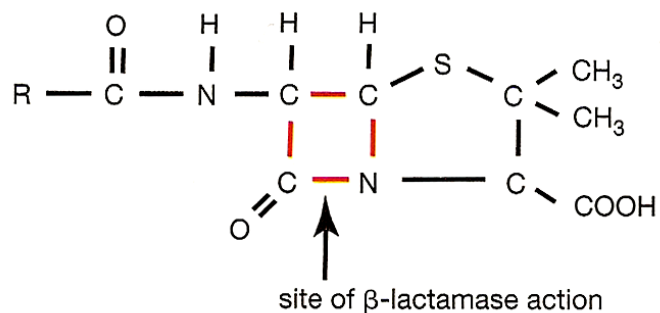


Figure 3.24: Image showing the β -lactam antibiotic structure for penicillin. The arrow indicates the site where the antibiotic can be neutralized by β -lactamase, generated by the microbe (from ¹⁹⁵).

3.7 Analytical Techniques and Methods

3.7.1 Cleaning and Desiccation

The implant components were carefully retrieved from each of the knee simulator stations after every test interval of 0.5 Mc so the gravimetric change (change in weight) of the PE inserts could be assessed. This was performed under consideration of ISO 14243-2 ⁴¹ and recommendations by DePuy Orthopaedics Inc., Warsaw, IN. The PE inserts were detached from the tibial tray and immediately placed in a 1000 ml beaker filled with DW at RT. This was followed by gently cleaning the PE inserts under hand-warm water with a non-abrasive nylon brush and water-diluted liquid soap (1:100; LiquiNox[®], Alconox, White Plains, NY) to remove serum residuals. The femoral components and cemented tibial trays were cleaned in the same manner, sprayed with ethyl-alcohol and left to dry at RT.

The PE inserts were then further processed: (1) placing the PE inserts in beaker with DW, (2) placing beaker in ultrasonic cleaner for 5 min, (3) rinsing with DW, (4) placing the PE inserts in beaker filled with water-diluted liquid soap, (5) placing the beaker with the PE inserts in the ultrasonic cleaner for 10 min, (6) rinsing the inserts with DW, (7) placing the PE inserts in beaker with DW, (8) placing beaker with the PE inserts in ultrasonic cleaner for 10 min, (9) rinsing the PE inserts with ethyl alcohol, (10) placing PE inserts in

ethyl alcohol for 5 min, (11) drying PE inserts with compressed nitrogen gas, (12) placing PE inserts in a desiccator for 30 min at 16 inHg. After the last process, the implants were left in the desiccator at atmospheric pressure, ready for their weight assessment. Desiccation of the PE inserts was found to be a necessary part of the protocol because non-desiccated PE inserts did not achieve a stable weight reading during weight measurements.

3.7.2 Weighing and Precision

The PE inserts were gravimetrically assessed during test intervals using a balance (AX 205, Mettler-Toledo, Columbus, OH) under some considerations of ISO 14243-2⁴¹ and recommendations by DePuy Orthopaedics Inc., Warsaw, IN. Prior to every weight assessment session, the balance was internally calibrated, following the instructions shown in the operating manual. A polonium bar serving as an anti-static tool was placed in the inner chamber of the balance to compensate for charging effects of the PE inserts that may interfere with the weight measurements. Prior to the weight assessment the precision of the balance had to be established. To do this, two reference weights were purchased (20 g, 100 g; ASTM Class 1; Troemner, Thorofare, NJ). The precision of the balance was estimated over five consecutive days, where each day the reference weights were measured five times during the time of 15 min (Table 3.10). The temperature and room humidity was also recorded. Although the precision of the balance was established, it was decided to both (a) internally calibrate the balance and to (b) measure the reference weight of 20 g and 100 g before and after every measurement session of each individual PE insert. Every PE insert was measured three times and then the mean and SD was reported.

Table 3.10: Repeated measurements of the 20 g and 100 g reference weights to establish the precision of the balance.

Day	Measurement	Reference Weight [mg]		Temperature [°C]	Relative Humidity [% r. H.]
		“20 g”	“100 g”		
1	1	20000.07	100000.07	20	59
	2	20000.04	100000.05	20	59
	3	20000.04	100000.03	21	59
	4	20000.03	100000.02	21	59
	5	20000.02	100000.01	21	59
2	1	20000.02	100000.05	20	58
	2	20000.03	100000.01	20	58
	3	20000.01	99999.98	20	58
	4	19999.96	99999.94	20	58
	5	19999.96	99999.96	20	58
3	1	19999.99	100000.04	20	61
	2	20000.01	100000.02	20	61
	3	20000.00	100000.02	20	61
	4	19999.98	100000.01	20	61
	5	19999.99	100000.01	20	61
4	1	20000.04	100000.04	20	59
	2	20000.06	100000.08	20	59
	3	20000.01	100000.00	20	59
	4	20000.00	100000.00	20	59
	5	19999.99	99999.99	20	59
5	1	20000.03	100000.01	21	58
	2	20000.02	100000.02	21	58
	3	19999.99	100000.00	21	58
	4	20000.01	99999.99	21	58
	5	20000.01	99999.99	21	58
Mean		20000.0124	100000.0136	20.32	59
SD		0.0272	0.0316	0.476	1.118
Min.		19999.96	99999.94	20	58
Max.		20000.07	100000.08	21	61
Rel. range		0.11	0.14	1	3

3.7.3 Interval Wear Volume and Wear Rate

The measured weight of the PE inserts was recorded and divided into two groups for both the L bank and the R bank into three wear stations and two LS stations. The total weight loss of each PE insert was determined after every 0.5 Mc by adding the mean mass gain of the PE inserts from the LS stations to the mean weight loss of the PE inserts from the wear stations. The total wear rate was then determined by first converting the gravimetric wear data into volumetric data using the PE density of 0.935 mg/mm³. Secondly, the cumulative volumetric wear was plotted versus the number of Mc. Linear regression analysis was performed on the volumetric wear of each implant over Mc and the slope of the trend line represented the wear rate. A mean gravimetric wear rate [mm³/Mc] and SD were calculated for three implants per bank.

3.7.4 Surface Characterization

The backside surfaces of the PE inserts and tibial tray were examined in more detail than was needed to determine BDS. In characterizing primary surface features, a scanning electron microscope (SEM) with field-emission (S-4500, Hitachi Electronics Ltd., Naka, Japan) was used under an accelerating voltage of 5, 15 and 20 keV. Images were taken using the secondary electron (SE) or backscattered-secondary electron (BSE) modes. The elemental compositions of some selected areas were investigated using energy dispersive X-ray analysis (EDX) with a special hardware attachment (EDAX[®] Phoenix Model, Mahwah, NJ). PE specimens were sputter coated with gold to eliminate charging effects on the surface. A contact profilometer (Tencor[®] P-10, KLA-Tencor, Milpitas, CA) with a stylus tip radius of 2 µm was used to obtain the R_a (centre-line average) surface roughness at various locations on the tray surface and with various cut-off lengths following DIN 4768⁴⁰⁹ and to produce surface maps of specific damage features. The referenced DIN standard suggests basing the cut-off length on the R_a value. Consequently, surface waviness may

have been reduced in a more equivalent manner. Ten measurements per sample were taken and their means and standard deviations were reported.

Surface roughness measurements and surface profiles were obtained from retrieved femoral components and from femoral components from knee simulator wear tests using a non-contact profilometer (Wyko[®] NT1100, Veeco Instruments Inc., Woodbury, NY). This was necessary because the contact profilometer was unable to conduct roughness measurements on the curved surface of the femoral condyles. A software program (Wyko[®] Vision32[™], Veeco Instruments Inc., Woodbury, NY) was used to flatten the raw surface profile data using the tilt function. In addition to R_a , the root-mean-square roughness, R_q , of the femoral component was also recorded. The R_q parameter weights the square of the asperity peak heights and is more sensitive than R_a , that averages the peak heights⁵¹. This was deemed important to characterize the wear on the femoral component.

3.8 Statistical Analysis

The retrieval data and the wear test data were analyzed using a statistic software program (SPSS Version 14, SPSS Inc., Chicago, IL). The manual under the help-menu for this software contained detailed description of the statistical tests. The following Sections the SPSS manual of the statistical tests in the present thesis were summarized and the rationale for their application is briefly noted (see Appendix C for details). Statistical Services (Erin P. Harvey) at the Department of Statistics and Actuarial Science, University of Waterloo, was consulted for guidance thought the statistical analysis.

3.8.1 Univariate Analysis

Data exploration was performed using bar-graphs, correlation analysis, descriptive statistical tests and univariate methods. Bar-graphs were plotted showing the mean and the standard deviation (SD) with a 95% confidence interval. Pearson correlation was applied to identify linear, parametric

correlations and the Spearman correlation was applied for non-parametric correlations. Logarithmic regression analysis (R^2_{\log}) was applied for the BDS of either assessment methods and IP. Linear regression analysis was applied to obtain a BDS-gradient between the BDS and IP for either grading method. Based on the Kolmogorov-Smirnov test for normality and histograms the Paired-samples t-test (parametric data) or the Wilcoxon-Rank test (non-parametric data) was applied to test for significant differences in BDS between observers and to compare matched groups of continuous variables. For multiple pair-wise comparisons between groups with the same dependent variable the Bonferroni-correction term ⁴¹⁰ was applied to establish the level of significance for each comparison ($p = 0.05/(\text{number of comparisons per group})$).

Student's t-tests (parametric data) or Mann-Whitney-U tests (non-parametric data) was applied to compare groups of independent samples. Analysis of variance coupled with the Fisher's protected least-square-different test as the post-hoc method (ANOVA and Fisher's) was used to compare groups of more than two categorical variables with non-harmonic sample sizes. Analysis of variance coupled with Tamhane as the post-hoc method (ANOVA and Tamhane) was used to compare groups of more than two categorical variables with harmonic sample sizes and unequal variances. A general linear model coupled with the Fisher's protected least-square-different test as the post-hoc method (GLM and Fisher's) was used to repeatedly measured groups of more than two categorical variables with non-harmonic sample sizes. A general linear model coupled with the Fisher's protected least-square-different test as the post-hoc method (GLM and Tamhane) was used to repeatedly measure groups of more than two categorical variables with harmonic sample sizes.

Normal distribution was assumed for the PE wear data obtained in the *in vitro* investigations. The use of statistical methods to the *in vitro* investigations may have been compromised by the relatively small number of wear results per wear test. Applying parametric statistical analysis to assess the differences between wear tests was used by other academic groups that also

work in the field of TKR wear ^{157,179} and thus such assumption was adapted when PE wear rates were compared.

3.8.2 Multiple Linear Regression Analysis

In many cases, retrieval studies are associated with some sort of statistical analyses but, unfortunately, there is no uniform statistical methodology ^{13,26,27,219,282,301,302,341,342,411,412}. This apparent failure to apply engineering methods to statistical analysis is perhaps a consequence of the many different types of data collected and the variety of proposed hypotheses. The application of multiple linear regression analysis (MLRA) has only occasionally been applied in retrieval studies ^{282,302,411,412}. Even here, the methodology does not appear uniform and interaction terms between independent variables have not been considered. After some initial data exploration, the present study applied MLRA using the enter-method followed by a backwards-stepwise procedure and included a consideration of some interaction terms ⁴¹³. At first, a linear regression analysis between BDS and IP was performed for specific categorical variables to determine the slope (BDS gradient) and intercept with the BDS-axis. Independent categorical variables were transferred into dummy-variables. First-order interactions ($X*Z$) between the independent continuous variables (X) and independent categorical variables (Z) were considered in some cases:

$$Y = \beta_0 + \beta_1 X + \beta_2 Z + \beta_3 X*Z + e \quad (3.2)$$

The regression coefficients are represented by β_n ; e is the error term. This type of analysis was followed by utilization of MLRA to test if significant differences between specific BDS gradients of various categorical variables existed ⁴¹³. To reduce multicollinearity problems, IP was centered by subtracting the respective mean (i.e. IP *minus* mean IP) before creating their interaction terms. Incrementally testing sum of squares was performed for categorical variables that had three or more degrees of freedom, resulting in

reduced regression models. An absolute minimum of five observations per variable for each categorical variable was the criterion to be included in the MLRA.

In Section 4.3, the total BDS for each insert along with the BDS values for individual damage features on an insert were the dependent continuous variables that were separately analyzed. Due to the unequal distribution of some independent categorical variables in Section 4.3, it was not appropriate to employ implant model, insert type and sterilization technique simultaneously in the MLRA. Their populations were unequally spread and therefore these variables were inter-related. For example, the model C implants had only one CR insert and only inserts of NGA sterilization. So, these independent categorical variables (implant model, insert type and sterilization method) were *individually* analyzed while accounting for other significant independent variables. The insert thickness was considered separate from implant model and was generally selected by surgeons based on their idea of appropriate soft tissue tensions, balancing for the individual patient and the intraoperative gap apparent between the femur and tibia.

Standardized residuals of the each MLRA for each grading method were plotted versus IP to assess for remaining patterns that could not be expressed in the regression model. An adjusted R^2 -value was reported to describe the regression analysis for each group since it accounted for changes by incorporating significant factors for small data sets⁴¹³. To determine the power (κ) of each regression model, an additional software program was applied (SamplePower™ 2.0, SPSS Inc., Chicago, IL) based on the total number of observations involved per model and the corresponding cumulative adjusted- R^2 -value obtained from the MLRA. In the MLRA analysis, the level of significance was set at $p = 0.05$ for all tests. The p -value times 100 is the percent chance that some characteristics of 2 or more samples indicate that they all come from the same population. In other words, if $p < 0.05$, there is a less than 5 % chance that the samples come from the same population. Such a finding is often used to indicate a “statistically significant difference”.

Chapter 4: Clinical Investigations: Results, Analysis and Discussion

4.1 Introductory Remarks

The present chapter has three Sections reporting on clinical investigations. In Section 4.2, the application of the Modified-method for damage assessment was investigated and comparisons were made with a similar damage assessment evaluation technique known as the Hood-method. Both of these methods require an observer to study the worn surface under a low power optical light microscope to determine values of backside damage score (BDS), as described in the previous chapter (Section 3.2).

In Section 4.3, the data values obtained from Modified-method were further analyzed; using advanced statistical methods (univariate analysis, MLRA). In addition, surface analysis (surface profilometry, SEM, EDX) was performed to gain more specific insight into dominant damage features of the *in vivo* backside wear. Based on both the statistical and surface analyses, wear mechanisms acting on the backside surface were proposed and implant design recommendations were given.

In Section 4.4, results were presented for the analysis of SF samples that were obtained from patients. Their protein composition, osmolality and trace elements (Ca, Mg, inorganic P and Fe) were then compared with four bovine serum mixtures that had been used in knee simulator wear testing in the present thesis (as described in Section 3.3). This investigation was conducted to link the retrieval and wear simulator studies of the present thesis with clinical reality and to support the focus on the influence of boundary lubrication on the wear of TKR implants.

4.2 Retrieval Analysis: Part 1, A Comparison Between Grading Methods

4.2.1 Introductory Remarks

It was hypothesized that the link between surface damage and clinical wear would depend on the ability of the grading method to find more surface damage for implants with features that were known to cause high clinical wear. For example, GA sterilized implants were known to sustain more volumetric wear than NGA sterilized implants when all other factors are equivalent. Thus, grading methods should detect more surface damage for GA sterilized implants when compared with NGA sterilized implants. Unfortunately, there were few other well-established features of clinical wear that could be used to evaluate and perhaps “calibrate” a grading method. In fact, grading methods were used *because* techniques had not been established to quantify clinical wear, although some recent efforts in this regard were beginning to show promise³³⁹. In the present section, the backside damage of 52 retrieved implants were assessed with two semi-quantitative grading methods (Section 3.2.4), referred to as the well-established Hood-method²⁶ and the Modified-method⁴¹⁴ that was recently developed by the present author. Both methods require the observer to combine both the severity and area of damage into one BDS. Individual damage features were given a BDS and the total BDS was determined by summing them. The total BDS values for each grading method were compared along with the BDS values for individual damage features. Also, multiple linear regression analysis (MLRA) was performed on the total BDS values from each grading method to investigate statistically whether the BDS and the BDS-gradient (slope of the curve fitted line for total BDS versus IP) were significantly different. Additional MLRA was performed on the BDS for individual damage features from the Hood-method and the Modified-method. In each MLRA model, the interaction (denoted by the * symbol) between sterilization technique (GA or NGA) and gender (M or F) were chosen as the independent *interaction* variables (GA*F, GA*M, NGA*M, NGA*F) along with implant type (A, B or C) as an independent *categorical* variable, and both insert thickness (IT) and

implantation period (IP) as independent *continuous* variables. The sole dependent variable was BDS. Such advanced statistical analysis was deemed necessary to illustrate the relative ability of the two grading methods to represent the surface damage.

4.2.2 Preliminary Data Exploration

Both the Hood-method and the Modified-method were used to detect surface damage on the distal (backside) surface of retrieved polyethylene inserts. The total BDS and individual damage feature scores obtained with the Modified-method showed no significant differences between observers. The total BDS and individual damage feature scores obtained with the Hood-method also showed no significant difference between observers except for the BDS for burnishing ($p = 0.004$, Paired-samples t-test) (Table 4.1).

Table 4.1: Comparison of the backside damage score (BDS) values obtained by the two observers.

BDS	p-value	
	Hood-method	Modified-method ¹
Total	0.653	0.758
Total burnishing	0.004	0.096
Total grooving	0.337	0.385
Total indentations	0.338	0.776
Total deformation	0.366 ¹	0.198
Total pitting	0.114 ¹	0.908
Total stippling	0.518 ¹	0.231

Paired-samples t-test; ¹Wilcoxon-Rank; level of significance = $0.05/6 = 0.0083$ following the Bonferroni-correction for multiple pair wise comparisons.

Since the Modified-method had 11 grading choices and awarded integer scores from 0 to 10, the mean BDS (36.47 ± 29.71) was significantly higher ($p = 0.003$, Wilcoxon-Rank) than the mean BDS (25.49 ± 12.93) of the Hood-method that had only 5 grading choices and awarded integer scores from 0 to 4. Also because of the larger number of grading choices, the SD of the

Modified-method was also higher than that of the Hood-method. More importantly, the correlation between the BDS and IP for the Modified-method and IP was stronger ($R = 0.716$, $p < 0.001$, Spearman correlation) compared with the correlation between BDS and IP for the Hood-method ($R = 0.487$, $p < 0.001$, Spearman correlation) (Fig. 4.1). Neither of these correlations intercepted with the origin. The BDS-gradient (the slope of the straight line fitted to the BDS versus IP data shown in Fig. 4.1) for the Modified-method was of 0.623 BDS/month while for the Hood-method it was 0.197 BDS/month. Furthermore, the BDS of both assessment methods revealed some indication of a logarithmic relationship of BDS versus IP with a rapid increase of BDS at low IP and a levelling off of the BDS at the higher values of IP ($R^2_{\log\text{-Hood}} = 0.261$, $p < 0.001$; $R^2_{\log\text{-Modified}} = 0.422$, $p < 0.001$).

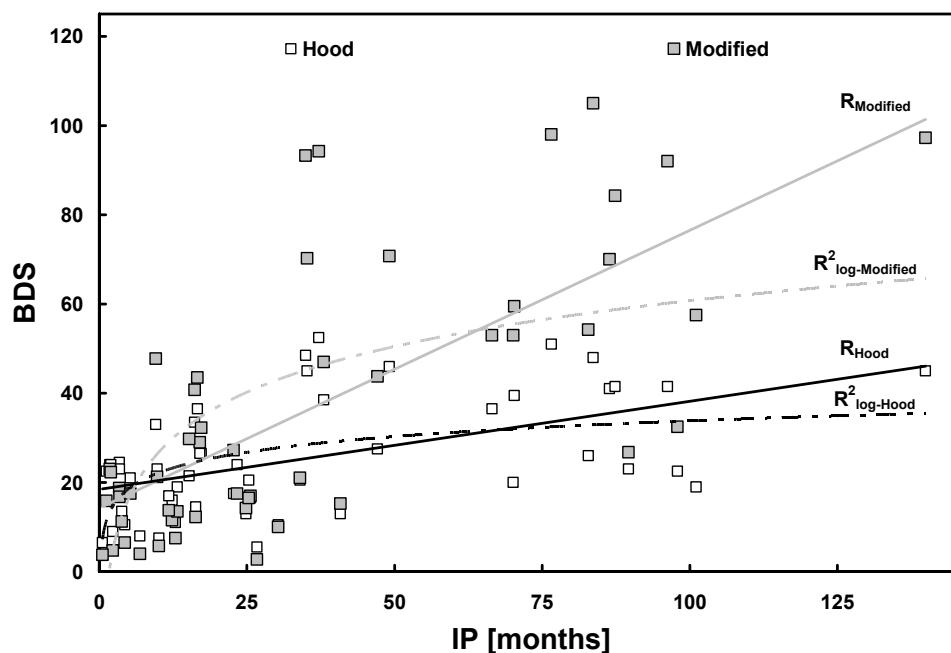


Figure 4.1: Backside damage score (BDS) obtained from the Hood-method and the Modified-method correlated with the implantation period (IP).

When the Modified-method was applied, the mean BDS values were significantly higher for both the model A implants ($p = 0.001$, Paired-samples t-

test) and the model B implants ($p = 0.001$, Paired-samples t-test) (Fig. 4.2). However, there was no statistically significant difference between the BDS values from the two grading methods for the model C implants ($p = 0.054$, Paired-samples t-test) perhaps because the mean IP values were significantly higher for model A implants and model B implants compared with the model C implants ($p \leq 0.001$, ANOVA and Fisher's). There was no statistically significant difference between the mean IP values for model A and B implants ($p = 0.058$, ANOVA and Fisher's).

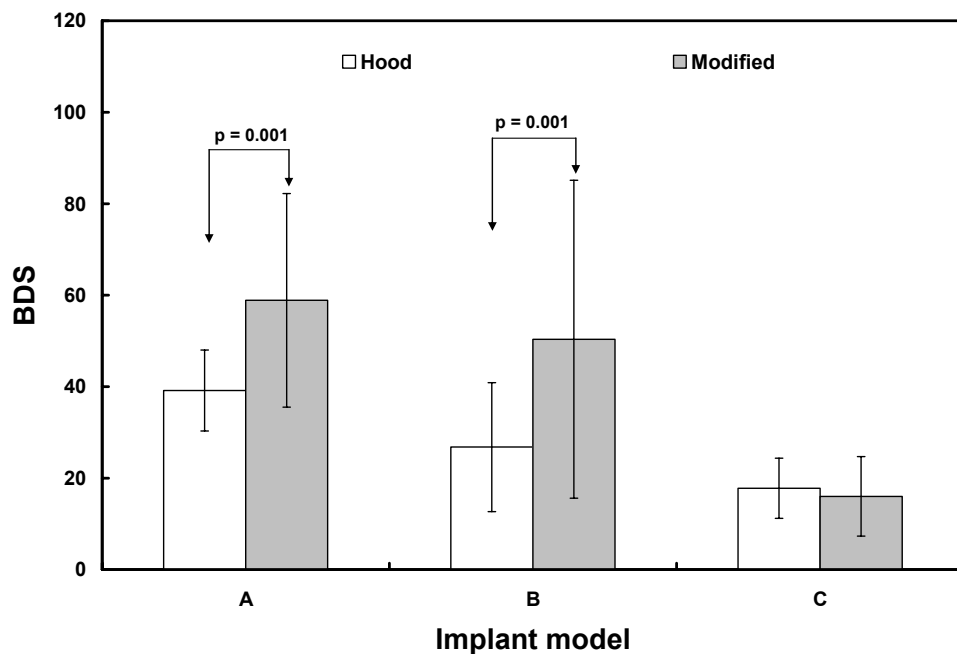


Figure 4.2: Backside damage score (BDS) for the three implant models analyzed with both damage assessment methods. Level of significance for each interaction term $p = 0.05/3 = 0.016$ following the Bonferroni-correction for multiple pair wise comparisons

A closer look was taken at the differences between the grading methods and the interactions between sterilization techniques and gender (sterilization*gender) (Fig. 4.3). The BDS for the Modified-method was significantly higher than the BDS for the Hood-method for both male and female patients that received GA inserts (GA*M versus GA*F; $p \leq 0.009$, Paired-samples t-test). Such differences were not observed for the male and

female patients that received NGA inserts ($p \geq 0.262$, Paired-samples t-test). The BDS for GA*M was not different than the BDS for GA*F when the Hood-method was used ($p = 0.245$, ANOVA and Fisher's). Interestingly, the BDS for GA*M was significantly higher than the BDS for GA*F when the Modified-method was used ($p = 0.021$, ANOVA and Fisher's).

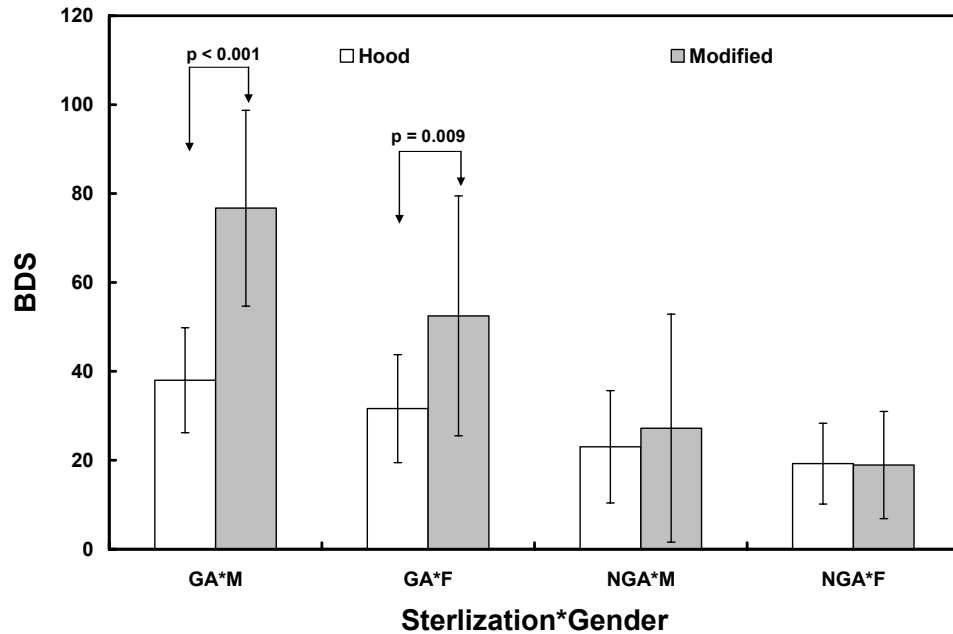


Figure 4.3: Backside damage score (BDS) for the interaction between sterilization and gender (Sterilization*Gender) which resulted in four interaction terms such as GA*M, GA*F, NGA*M, and NGA*F. Level of significance for each interaction term $p = 0.05/4 = 0.012$ (Bonferroni-correction).

To clarify where the significant differences may originate, the BDS values of each damage feature on each implant model (A, B and C) were individually assessed (Table 4.2). The main features of the data were considered as follows. For the model A implants, the mean burnishing BDS was higher ($p < 0.001$, Paired-samples t-test) when the Modified-method was used. Interestingly, the BDS for deformation for the model A implants was uncharacteristically higher when using the Hood-method compared with the Modified-method ($p = 0.002$, Paired-samples t-test). Stippling damage features

were not observed on retrieved model A implants. For model B implants, the mean indentation BDS was higher ($p < 0.001$, Paired-samples t-test) for the Modified-method. The mean indentation BDS was higher for the Modified-method ($p < 0.001$, Paired-samples t-test). The deformation damage feature was not a detected damage feature on the retrieved model B implants. For model C implants, the mean BDS for grooving and pitting ($p < 0.001$, Paired-samples t-test) and deformation ($p = 0.002$, Wilcoxon-Rank) showed higher mean BDS when the Hood-method was used. Stippling damage features were not observed on retrieved model C implants.

Table 4.2: The BDS values (mean and the SD) for individual damage features found on the surfaces of model A, B and C implants.

Implant Model	Damage Feature	BDS [Mean \pm SD]			
		Hood-method	Modified-method	Comparison	
				Modified (Hood)	p-value
A	Burnishing	14.04 \pm 3.76	29.83 \pm 12.31	higher	<0.001
	Grooving	8.41 \pm 2.48	10.79 \pm 6.31	not diff.	0.060
	Indentations	8.00 \pm 3.12	10.06 \pm 6.13	not diff.	0.052
	Deformation	2.16 \pm 1.88	1.72 \pm 1.69	lower	0.002
	Pitting	6.54 \pm 2.14	6.50 \pm 4.91	not diff.	0.209 ¹
	Stippling	-	-	N/A	N/A
B	Burnishing	3.18 \pm 3.41	3.07 \pm 3.77	not diff.	0.752
	Grooving	1.68 \pm 2.16	1.14 \pm 1.71	not diff.	0.095
	Indentations	13.78 \pm 4.27	28.98 \pm 16.07	higher	<0.001
	Deformation	-	-	N/A	N/A
	Pitting	1.62 \pm 2.23	1.53 \pm 3.01	not diff.	0.738
	Stippling	6.50 \pm 8.11	15.62 \pm 21.78	not diff.	0.035 ¹
C	Burnishing	6.29 \pm 1.98	5.51 \pm 3.77	not diff.	0.100
	Grooving	3.70 \pm 2.32	2.79 \pm 1.94	lower	<0.001
	Indentations	5.54 \pm 3.22	6.20 \pm 5.77	not diff.	0.372
	Deformation	0.83 \pm 1.06	0.55 \pm 0.83	lower	0.002 ¹
	Pitting	1.41 \pm 1.48	0.94 \pm 1.08	lower	<0.001
	Stippling	-	-	N/A	N/A

N/A = not applicable; SD = standard deviation; () = compared with; level of significance for each implant model $p = 0.05/6 = 0.0083$ (Bonferroni-correction); Paired-samples t-test or ¹Wilcoxon-Rank.

4.2.3 Multiple Linear Regression Analysis

Using MLRA, the BDS for the Modified-Method was significantly higher than for the Hood-method ($p \leq 0.001$) (Table 4.3). This was not surprising since the preliminary data analysis showed a higher BDS for the Modified-method for model A and model B implant but not model C implant. The Modified*IP interaction term was different from the Hood*IP interaction term ($p = 0.001$). When the meaning of the interaction terms was considered, this finding confirmed that the BDS-gradient (slope of the straight line fitted to the BDS versus IP data shown in Fig. 4.1) for the Modified-method was significantly higher than the BDS gradient for the Hood-method.

MLRA confirmed that males with GA inserts had significantly higher BDS than females with GA inserts using both the Hood-method ($p = 0.030$) and the Modified-method ($p < 0.001$) (Table 4.4 and 4.5). However, the Modified-method enabled the detection of significant differences between the BDS of males with NGA inserts and males with GA inserts ($p = 0.005$) as well as between the BDS of females with NGA inserts and males with GA inserts ($p = 0.005$) whereas the Hood-method ($p \geq 0.081$) did not show these differences. The type of surgery (primary or revision), insert thickness and IP were also significant in both the regression models obtained for Hood-method and the Modified-method (Table 4.4 and 4.5). An adjusted R^2 of 0.655 was found when applying MLRA to the data from the Modified-method whereas a much lower adjusted R^2 of 0.372 was found when applying MLRA to the data from the Hood-method (Table 4.4 and 4.5).

The power for both regression models was greater than 95% ($\kappa > 0.95$). Insert type, and patient mass, height and age were not significant in either regression model ($p > 0.05$). Standardized residuals showed that no unexplainable pattern remained after both regression models were applied (Fig. 4.4).

Table 4.3: MLRA of the BDS from the Hood-method and from the Modified-method.

Regression model	Grading methods		
Independent Variables	β_n	Dependent variable	p-value
Grading method		BDS	
Modified (Hood)	10.983	higher	<0.001
Modified*IP (Hood*IP)	0.425	different	0.001
IP	0.410	correlates pos.	<0.001
Adjusted R ² -value		0.488	

() = compared with; * indicates an interaction variable; IP = implanation period; level of significance = 0.05

Table 4.4: MLRA of the BDS from the Hood-method.

Regression model	Hood -method		
Independent Variables	β_n	Dependent variable	p-value
Sterilization*gender		BDS	
GA*F (GA*M)	-11.765	lower	0.030
NGA*M (GA*M)	-6.136	not different	0.309
NGA*F (GA*M)	-10.578	not different	0.081
Implant type			
P (R)	10.221	higher	0.016
Insert thickness	1.037	correlates pos.	0.019
IP	0.184	correlates pos.	0.022
Adjusted R ² -value		0.372	

GA = gamma-in-air; NGA = Non-gamma-in-air; M = male; F = female; IP = implantation period; () = compared with; * indicates an interaction variable; β_n = regression coefficients; level of significance = 0.05.

Table 4.5: MLRA of the BDS from the Modified-method.

Regression model	Modified-method		
Independent Variables	β_n	Dependent variable	p-value
Sterilization*gender		BDS	
GA*F (GA*M)	-36.428	lower	<0.001
NGA*M (GA*M)	-30.084	lower	0.044
NGA*F (GA*M)	-20.993	lower	0.005
Implant type			
P (R)	18.926	higher	0.009
Insert thickness	1.703	correlates pos.	0.023
IP	0.574	correlates pos.	<0.001
Adjusted R ² -value	0.655		

GA = gamma-in-air; NGA = Non-gamma-in-air; M = male; F = female; IP = implantation period; () = compared with; *indicates an interaction variable; β_n = regression coefficients; level of significance = 0.05.

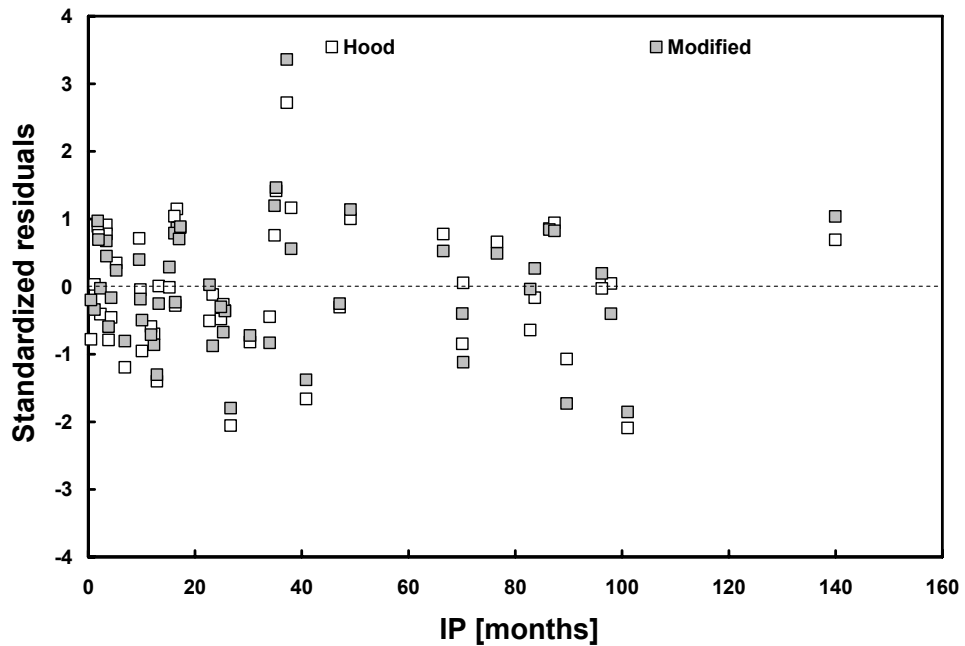


Figure 4.4: Standardised residuals obtained for the MLRA using the BDS from the Hood-method and from the Modified-method.

4.2.4 Discussion

The BDS assessment was directly influenced by the utilized damage assessment method. The BDS assessment by the two observers showed significant differences for the burnishing damage feature for the Hood-method, but not for the Modified-method. The IP appeared to affect the BDS for both methods. However, the stronger correlation between the BDS from the Modified-method versus the IP suggested that the Modified-method was more appropriate to try to relate to clinical wear that was known to be highly time-dependent.

Correlations between the topside damage scores and the IP (with a positive damage score offset) were reported when tibiofemoral PE damage²⁶ and tibial PE post damage²¹⁹ were analyzed. The suggested logarithmic behaviour between the BDS and IP that was observed for both grading methods might represent a general feature of semi-quantitative damage assessment methods. The high of BDS in both methods at low IP suggested that damage was quickly established. It was likely that deformation and creep were prevalent during this phase and thus the damage did not cause a higher run-in wear. Also, some initial surface damage on the PE insert prior to implantation may have occurred due to manufacturing and handling processes⁴¹⁵, which might have increased the BDS at low IP. The logarithmic regression at the high IP values suggested a leveling off of BDS for both the methods (Fig. 4.1). At this stage, further BDS might not be possible because the entire surface would be damaged. The backside surface might continue to experience PE damage (and wear) but it cannot be distinguished by any grading method. This might be a general limitation of these grading methods. However, it is considered likely that the BDS gradient at low to intermediate IP correlates with the wear rate.

The mean and the SD of the BDS obtained with the Modified-method were higher for implants retrieved after advanced IP (model A and B implant) and for damage features with high BDS (Table 4.2). At both high surface damage and advanced implantation periods that the Hood-method may have

underestimated surface damage as it assigns a score of 3 to a surface damage of $\geq 50\%$ to $\leq 10\%$. In contrast, the Modified-method assigned a score of 5 to a surface damage $\geq 50\%$ and would have assigned a maximal score of 10 to a surface damage $\leq 100\%$. Thus, using the Modified-method to assess surface damage may have produced a BDS with a higher resolution compared with the Hood-method. However, the retrieved model C implants (that had a low mean IP) and damage features with low mean BDS showed a significantly higher Hood-BDS. A $\sim 30\%$ damaged surface would receive a score of 2 from the maximal score of 3 according to the Hood-method. In contrast, the Modified-method would assign a score of 3 from a maximal score of 10 to such surface damage. Thus, the assigned score relative to the maximal score possible was much higher for the Hood-method when small amounts of surface damage were assessed. This may explain why the BDS the Hood-method under-estimated surface damage at the higher IP but over-estimated it at the lower IP.

Normalizing damage scores by IP (i.e. BDS/IP), as suggested by Puloski et al.²¹⁹, was inappropriate for the present data set because such a procedure required a linear BDS versus IP relationship that had an intercept at the origin. Using MLRA was more appropriate for this set of retrieval data since the intercept was based on the data supplied and did not have to be at the origin. The MLRA revealed that the mean BDS and the BDS-gradient were significantly higher for the Modified-method (Table 4.3). In addition, the BDS from the Modified-method combined with the MLRA enabled the detection of more significant factors that may describe the clinical backside wear behaviour. It was of particular concern that the Hood-method failed to detect a significant difference between the BDS of NGA inserts compared with males with GA inserts. GA sterilization as well as extended shelf storage time had been associated with premature and catastrophic PE insert failure due to severe cracking and delamination on the proximal surface due to alteration and reduction of mechanical properties^{213,214}. It was plausible that such effects allowed an increase in insert micromotion and were responsible for the increase

in BDS. Thus, it was reassuring to observe that the Modified-method detected such plausible effects caused by difference in sterilization technique.

4.2.5 Concluding Remarks

The Modified-method has shown to be a useful and superior tool to assess backside damage on retrieved tibial PE inserts from cemented tibial trays without screw holes. The Hood-method was found to be less appropriate for the assessment of backside damage in the present cohort of retrievals. In addition, the Modified-method accounted for more data variation and identified the type of sterilization technique as an influential factor on backside damage. The Hood-method did not detect such an influential factor. Hence, it was suggested to further use the Modified-method in retrieval analysis as it permitted the detection and confirmation of beneficial implant design features.

4.3 Retrieval Analysis: Part 2, Factors Influencing BDS

4.3.1 Introductory Remarks

The former Section established the superiority of the Modified-method compared with the Hood-method. The BDS obtained with the Modified-method was further analyzed in detail with univariate analysis and MLRA. This was conducted to gain some more insight on the possible clinical performance of the retrievals with the goal to give the physician and implant manufacturer recommendations on beneficial implant design improvements to reduce the incidence of severe backside damage and thus osteolysis. Based on these findings, some specific implants from the retrieval cohort were selected and characteristic damage features were assessed using surface analysis techniques. Such an analysis was deemed essential to illustrate the possible acting wear mechanisms in the boundary lubrication processes. An attempt was also made to answer the question whether the backside damage was caused by wear or dominantly deformation using a melt-annealing technique. A detailed statistical analysis coupled with detailed surface analysis was considered beneficial to support the possible suggestions for design modifications and raise awareness for the physician on the possible *in vivo* performance of such contemporary fixed bearings.

4.3.2 Preliminary Data Exploration

Correlation analysis suggested that IP was the only significant independent continuous variable overall that influenced BDS ($R = 0.688$, $p < 0.001$, Spearman correlation). Descriptive statistics suggested that IP had a significant influence on BDS for model A implants ($R = 0.614$, $p = 0.034$, Pearson correlation) and for model B implants ($R = 0.595$, $p = 0.015$, Pearson correlation) but not for model C implants ($R = 0.251$, $p = 0.238$, Pearson correlation) (Fig. 4.5). However, model C implants with IP greater than 15

months had significantly higher BDS than those implanted less than or equal to 15 months ($p = 0.028$, Student's t-test).

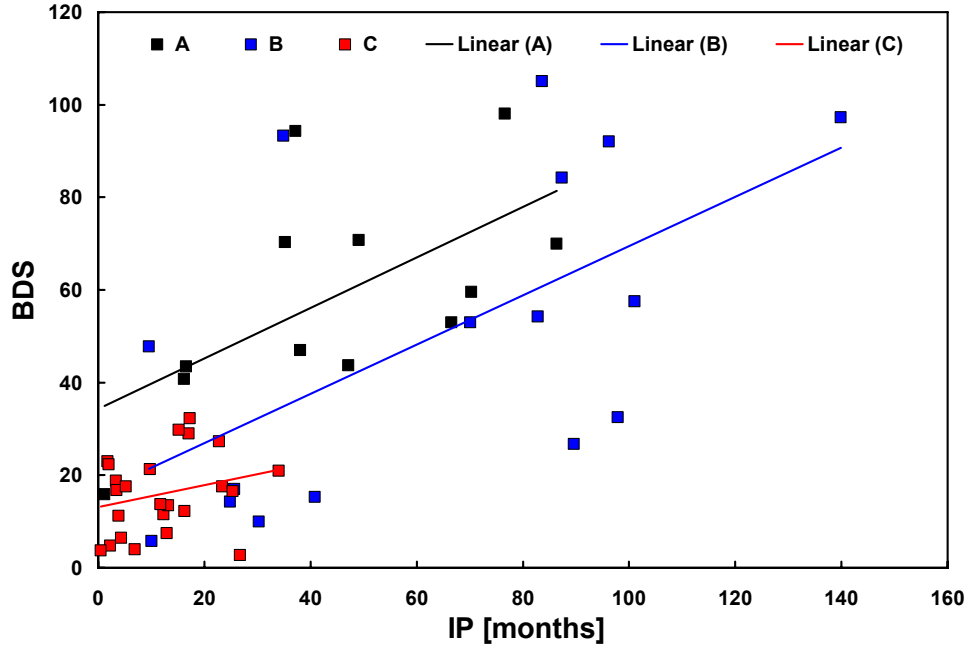


Figure 4.5: Linear correlations of BDS versus IP for implant models A, B, and C.

There appeared to be a gender related effect on BDS, particularly for the model B implant (Fig. 4.6). The BDS was higher for males than for females with model B implants ($p < 0.001$, ANOVA and Fisher's) but not for model A or model C implants ($p \geq 0.722$, ANOVA and Fisher's). GA inserts had both a higher mean BDS ($p < 0.001$, Student's t-test) and an obvious gender influence compared with NGA inserts (Fig. 4.7). The BDS was higher for GA inserts from males compared with GA inserts from females ($p = 0.021$, ANOVA and Fisher's), but there was no difference between gender in the NGA group ($p = 0.252$, ANOVA and Fisher's). When only the GA sterilized inserts were considered, shelf storage had a strong negative correlation with IP ($R = -0.546$, $p = 0.023$, Spearman correlation) and an even stronger correlation when only regarding GA inserts of group B ($R = -0.762$, $p = 0.004$, Spearman correlation).

A correlation between the shelf storage and IP was not observed for the NGA inserts ($R = -0.072$, $p = 0.680$, Pearson correlation).

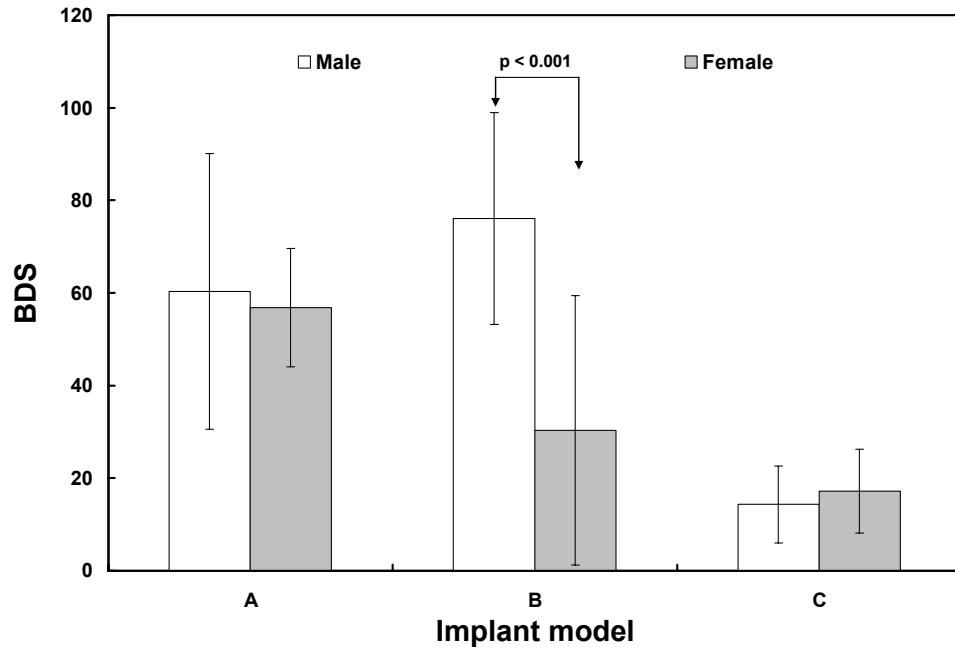


Figure 4.6: BDS grouped by implant model and gender.

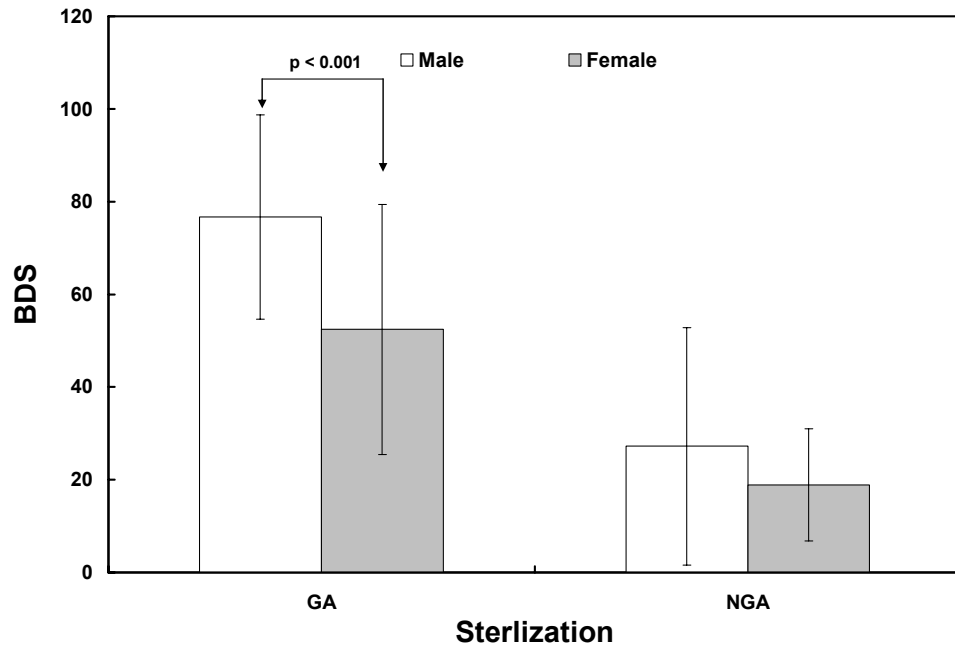


Figure 4.7: BDS grouped by sterilization techniques and gender.

CR inserts had significantly lower insert thickness values than PS inserts ($p = 0.027$, Student's t-test). Lower BDS was found for cases revised for infection compared with those revised for osteolysis ($p < 0.001$, ANOVA and Fisher's) but BDS did not differ for cases revised for osteolysis, instability or other reasons ($p > 0.079$, ANOVA and Fisher's). Only five cases were reported to be revised for osteolysis but these had the highest average IP ($p \leq 0.023$, ANOVA and Fisher's). Primary implants had a lower insert thickness than the revision components ($p = 0.003$, Student's t-test). Male patients had higher mass ($p = 0.013$, Student's t-test) and height ($p < 0.001$, Student's t-test) compared with female patients. The anterior BDS values were not different from the posterior BDS values ($p = 0.289$, Wilcoxon-Rank). The medial BDS values were not significantly higher than the lateral BDS values ($p = 0.083$, Wilcoxon-Rank), but a trend could be observed. The BDS gradients and intercepts with the BDS-axis for various categorical variables are shown in Table 4.6.

Table 4.6: Estimation of the BDS-gradient (and intercept) by linear regressions between BDS and IP for various independent categorical variables (BDS (IP) = BDS gradient (IP) + Intercept).

Independent categorical variables	BDS-gradient	Intercept
Reason for surgery		
IF	0.420	12.96
IS	0.190	37.714
O	0.776	5.334
OT	0.632	22.885
Sterilization		
GA	0.245	46.84
NGA	0.880	8.047
Gender		
M	0.779	16.834
F	0.488	11.662

BDS = Backside Damage Score; IP = Implantation Period; M = Male, F = Female; GA = Gamma-in-Air, NGA = Non-Gamma-in-Air; IF = Infection, IS = Instability, O = Osteolysis, OT = Others.

4.3.3 Multiple Linear Regression Analysis

The correlations and descriptive statistics used in the previous section were not as reliable as multiple linear regression analysis (MLRA) that determined the actual contribution of specific independent variables to the data variance and also allowed the study of the “interaction” terms between variables. Thus, the interactions between implant model and gender accounting for the variation in IP were considered using MLRA in analysis M1 (Table 4.7). After adjusting for the IP, several observations that were suggested by the data exploration could be confirmed by MLRA analysis. As shown in analysis M1, males with model B implants (B*M) were not different to either males of model A (A*M) or females of model A (A*F) implants ($p = 0.806$, $p = 0.235$ respectively or combined as $p \geq 0.235$). The findings of analysis M1 in Table 4.7 could be stated in somewhat more compact fashion. For example, females with model B implants were not different from either males or females with model C implants ($p \geq 0.191$). However, the males with model B implants plus both males and females with model A implants did have significantly higher BDS than females with model B implants plus both males and females with model C implants ($p < 0.001$). This last finding was suggested by Fig. 4.6 but confirmed here by MLRA.

Analysis M2 examined the interaction between sterilization techniques and gender on BDS and confirmed the findings illustrated in Fig. 4.7. There was a gender related effect on BDS for GA inserts with males having higher BDS ($p < 0.001$) while such an effect was not observed on NGA inserts ($p = 0.137$). Also, males with GA inserts had higher BDS than males with NGA inserts ($p = 0.044$), but such effect was not observed for females ($p = 0.137$). Additional factors emerged as significant in this analysis: patients with primary implant types had higher BDS than the patients with revisions implant types ($p = 0.009$); continuous variables such as insert thickness and IP correlated positively with BDS ($p \leq 0.023$). Furthermore, analysis M3 revealed that BDS was a function of gender, IP and shelf storage when only GA sterilized inserts of model B implants were selected. The exploration of insert type on BDS in

analysis M4 showed no difference in BDS between both CR and PS inserts ($p = 0.830$) after adjusting for other variables such as gender, insert thickness and implant type.

A higher adjusted- R^2 -value was obtained in analysis M4 and this permitted an investigation on the influence of reason for surgery, sterilization technique, gender, insert thickness and IP on BDS and to test differences between BDS-gradients. Interestingly, the independent variables corresponding to the reason for surgery showed the lowest total BDS for cases with osteolysis ($p \leq 0.004$) (Table 4.7). It was not surprising to observe higher BDS for GA inserts ($p = 0.012$) and male patients ($p = 0.001$). The interaction terms between dummy-variables and IP (IF*IP, IS*IP, O*IP, OT*IP; GA*IP, NGA*IP; M*IP, F*IP) were included in M6 to test for differences between BDS-gradients. The interaction term for osteolysis (O*IP) was different to infection (IF*IP), instability (IS*IP), and others (OT*IP) ($p \leq 0.001$); NGA*IP was different to GA*IP ($p = 0.002$); F*IP was different to M*IP ($p = 0.007$). This confirmed that the BDS-gradients, initially obtained with linear regression analysis, were highest for cases with osteolysis, NGA inserts, and male patients (Table 4.6).

MLRA was applied to individual damage features in analysis M6 and M7 and showed that the extent of burnishing was reduced for a partial-peripheral compared with a central dove-tail locking mechanism. This finding was indicated by Fig. 4.8 but confirmed by MLRA as follows. Model C implants with a polished tray surface and a partial-peripheral locking mechanism had a lower burnishing score than model B with a grit-blasted tray surface and a partial-peripheral locking mechanism ($p = 0.003$), thus suggesting that grit-blasted surfaces did cause less burnishing. However, model A with a polished tray and a central dove-tail had a much higher burnishing score than model C, thus suggesting that the partial-peripheral locking mechanism reduced burnishing. Indentation score was the highest for model B implants with the grit-blasted tray surface. The power in the preceding applications of MLRA was always calculated to be greater than 95% ($\kappa > 0.95$).

Table 4.7: Multiple linear regression analysis (MLRA); see the legend at the bottom of the table for an explanation of the various terms.

Analysis (Adj. R ²)	Independent variables	β_n	Dependent variable	p-value ¹
M1 (0.743)	Model*Gender		BDS	
	A*M (B*M)	-2.079	not diff.	0.806
	A*F (B*M)	-10.764	not diff.	0.235
	B*F (B*M)	-41.558	lower	<0.001
	C*M (B*M)	-34.579	lower	<0.001
	C*F (B*M)	-31.445	lower	0.001
	A*M (B*F)	39.479	higher	<0.001
	A*F (B*F)	30.794	higher	0.001
	B*M (B*F)	41.558	higher	0.001
	C*M (B*F)	6.979	not diff.	0.388
	C*F (B*F)	10.113	not diff.	0.191
IP	0.481	pos. corr.	<0.001	
M2 (0.655)	Sterilization*gender		BDS	
	GA*M (GA*F)	36.428	higher	<0.001
	NGA*M (GA*F)	15.435	not diff.	0.204
	NGA*F (GA*F)	6.344	not diff.	0.596
	GA*M (NGA*M)	20.993	higher	0.044
	NGA*F (NGA*M)	-9.091	not diff.	0.137
	Implant type		BDS	
	P (R)	18.926	higher	0.009
	Insert thickness	1.703	pos. corr.	0.023
	IP	0.574	pos. corr.	<0.001
M3 ² (0.643)	Gender		BDS	
	M (F)	30.636	higher	0.032
	IP	1.059	pos. corr.	0.006
	Shelf storage	1.312	pos. corr.	0.030
M4 (0.603)	Type		BDS	
	CR (PS)	-1.444	not diff.	0.830
	Gender		BDS	
	M (F)	18.656	higher	0.001
	Implant type		BDS	
	P (R)	18.188	higher	0.019
	Insert thickness	1.563	pos. corr.	0.040
	IP	0.643	pos. corr.	<0.001

Table 4.7 (continued): Multiple linear regression analysis (MLRA); see the legend at the bottom of the table for an explanation of the various terms.

Analysis (Adj. R ²)	Independent variables	β_n	Dependent variable	p-value ¹
M5 (0.766)	Reason for surgery		BDS	
	IF (O)	47.311	higher	0.004
	IS (O)	56.353	higher	0.001
	OT (O)	61.169	higher	<0.001
	IF*IP (O*IP)	-1.125	different	0.001
	IS*IP (O*IP)	-1.566	different	<0.001
	OT*IP (O*IP)	-1.064	different	<0.001
	Sterilization		BDS	
	GA (NGA)	23.653	higher	0.012
	GA*IP (NGA*IP)	-0.925	different	0.002
	Gender		BDS	
	M (F)	16.142	higher	0.001
	M*IP (F*IP)	0.381	different	0.007
	Insert thickness	1.154	pos. corr.	0.045
IP	1.831	pos. corr.	<0.001	
M6 (0.766)	Model		Burnishing Score	
	A (C)	20.562	higher	<0.001
	B (C)	-8.337	lower	0.003
	IP	0.114	pos. corr.	<0.002
M7 (0.655)	Model		Indentation Score	
	A (B)	14.543	lower	<0.001
	C (B)	3.746	lower	0.004
	IP	0.231	pos. corr.	<0.002

*indicates an interaction variable; () \equiv compared with; pos. = positive, neg. = negative, corr. = correlation; BDS = Backside Damage Score; IP = Implantation Period; M = Male, F = Female; GA = Gamma-in-Air, NGA = Non-Gamma-in-Air; CR = Cruciate Retaining, PS = Posterior Stabilized; IF = Infection, IS = Instability, O = Osteolysis, OT = Others; P = Primary, R = Revision; β_n = Regression coefficients; ¹Level of significance is $p \leq 0.05$; ²BDS of GA for model B implants only.

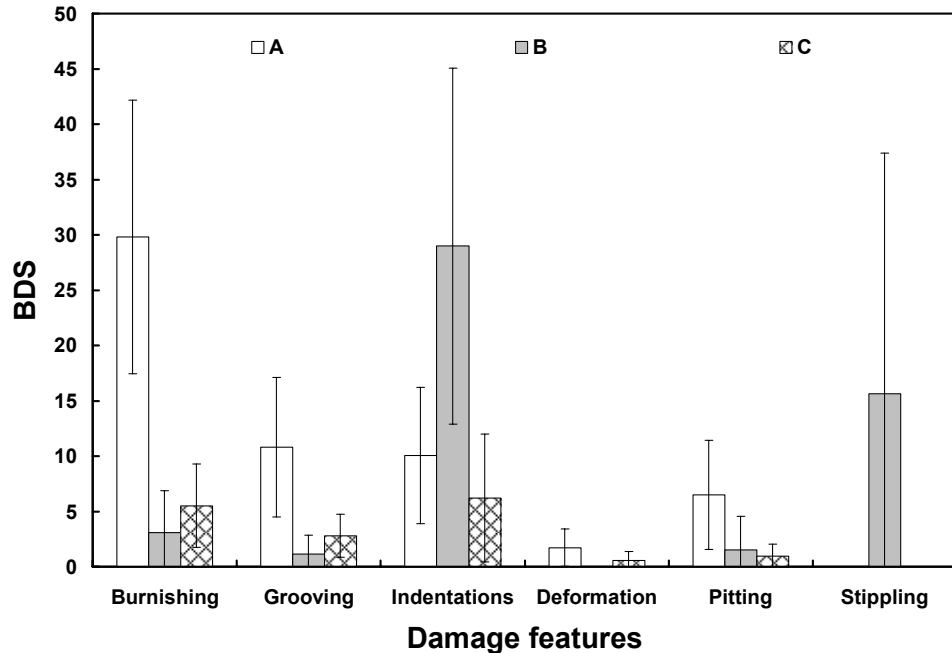


Figure 4.8: The backside damage scores of individual damage features grouped by implant model A, B and C.

4.3.4 Univariate Analysis

Further descriptive statistical analysis was performed to provide some preliminary data exploration that was not followed up with MLRA. Thus, the findings here were rather tentative. Grooving, deformation and pitting damage showed no relationship with IP or any other variable and were further investigated on the univariate level. Grooving was highest for model A implants ($p < 0.001$, ANOVA and Fisher's) with model B and C implants showing no significant differences ($p = 0.141$, ANOVA and Fisher's). Deformation was only observed in model A and C implants and was higher for the model A implants ($p = 0.015$, Mann-Whitney-U). Pitting was highest in model A implants ($p < 0.001$, ANOVA and Fisher's) with model B and C implants showing no significant differences.

Stippling was observed on some of the GA inserts of model B implants (cases 13, 14, 16, 21 - 24, 26, and 28; see Section 3.2 and for specific details) with a mean IP of 78.1 months (range, 9.57 - 139.9 months) and on most of the

PS type implants. Patient mass, height and age were not significantly different between model A, B and C implant ($p = 0.084$, ANOVA and Fisher's).

4.3.5 Surface Characterization

A typical surface of an insert that opposed a polished tibial tray (case 2; see Section 3.2 and for specific details) was examined in the SEM. Some micro damage was evident including ripples (aligned rows of nodules) and dispersed smeared nodules (Fig. 4.9). Submicron pulled-out fibrils were also present. Such an appearance was characteristic of the burnishing damage feature and low magnification.

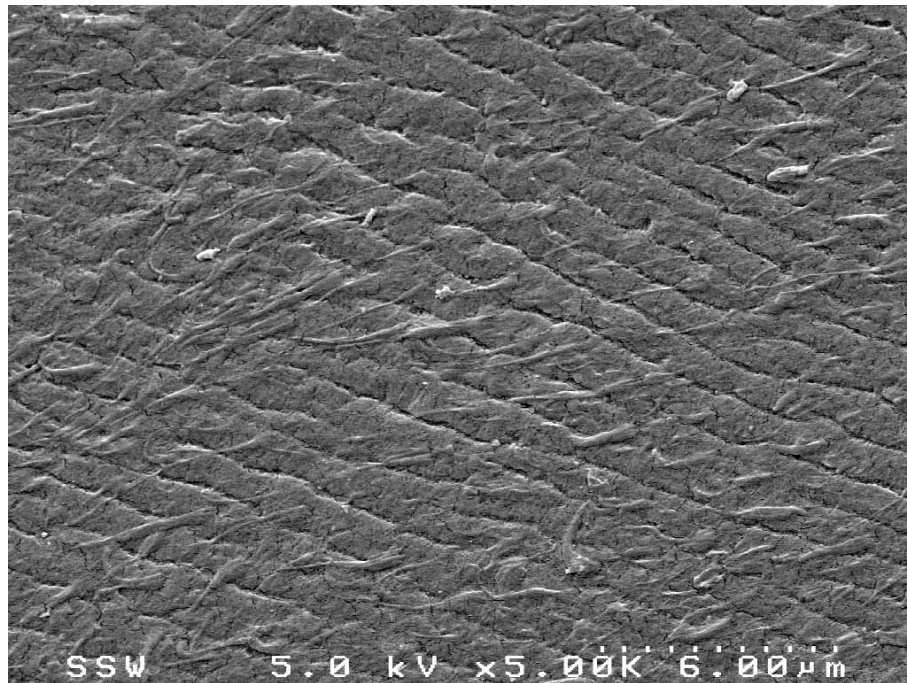
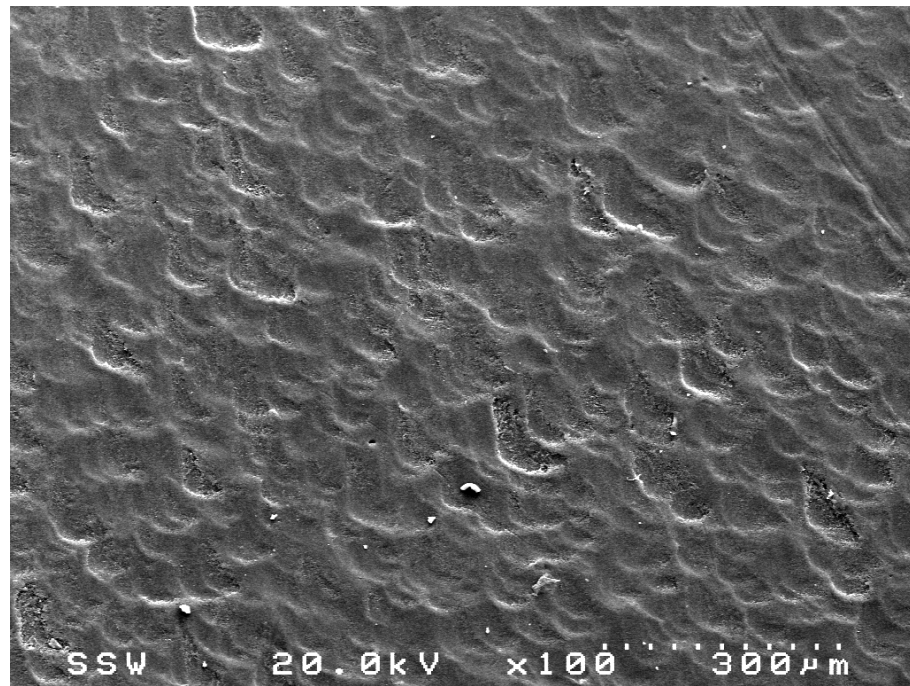


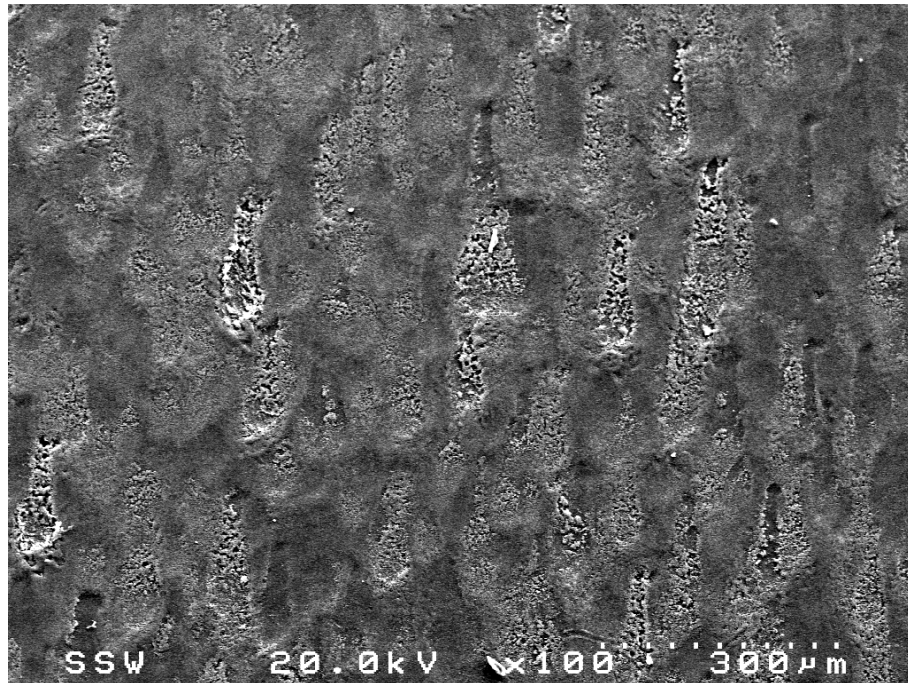
Figure 4.9: SEM image in SE mode of the backside of a PE insert from a model A implant (case 2; see Section 3.2 and for specific details) that had a polished tibial tray. Note the presence of ripples (aligned rows of nodules), dispersed smeared nodules and submicron pulled-out fibrils. This appearance was characteristic for the burnishing damage feature, most abundant on PE inserts from polished tibial trays.

A typical surface of an insert that opposed a grit-blasted tibial tray of model B implant (case 24) was also examined. For this insert, indentations had been observed during the BDS assessment and were now seen under higher magnification in the SEM (Fig. 4.10). The indentations at the circumference of the backside PE insert surface (Fig. 4.10.a) appeared to result from direct contact with the surface asperities of the rough tray surface. However, the surface directly under the centre of the tibiofemoral bearing surface revealed short grooves oriented in the anterior-posterior direction (Fig. 4.10.b). Some of the inserts from the model A implants (cases 5, 7, 8, and 12) and model C implants (cases 42, 47 and 51) also showed localized damage (mostly burnishing) directly under the centre of the tibiofemoral bearing surface.



(a)

Figure 4.10: SEM image in SE mode of the backside of a PE insert from a model B implant (case 27): (a) at the circumference (anterior direction \equiv top of page).



(b)

Figure 4.10 (continued): SEM image in SE mode of the backside of a PE insert from a model B implant (case 27): (b) directly underneath the tibiofemoral bearing surface (anterior direction \equiv top of page).

Nine retrieved grit-blasted model B tibial trays were available from inserts where indentations and stippling were observed (cases 13, 14, 16, 21-28). All of them showed some evidence of wear despite articulating with relatively soft PE. Only indentations were found in cases 13, 14, 16, 21 and 25. However, six trays from cases 22 - 24, 26 - 28 showed stippling (Fig. 4.11) and they had a mean IP of 96.24 months (range, 70.09 - 139.9 months). SEM of these areas for case 27 revealed localized wear with small grooves (width of approximately 3 μm) being present. There were no indications that abrasive particles were dragged into the area of stippling from the periphery, despite recent suggestions³⁰⁰.

Deposits on the retrieved grit-blasted trays were mainly of carbon composition, which might indicate that they were PE or acrylic (Fig. 4.12.a, 4.13.a). Embedded and fractured particles were observed on three new, never implanted tibial trays on the superior surface (Fig. 4.12.b, 4.13.b). Localized EDX analysis and EDX mapping revealed that these particles were rich in silicon and oxygen (presumably SiO_2) (Fig. 4.13 and Fig. 4.14). Six retrieved trays showed no embedded particles and three trays (cases 22, 25, and 27) revealed about two particles for every ten EDX measurements of suspicious areas that were rich in aluminum and oxygen (presumably Al_2O_3) (Fig. 4.13.c). For reference, an EDX spectrum of the tibial tray substrate of a model B implant was also taken (Fig. 4.13.d). According to the manufacturer, the final grit-blasting process for the tibial trays of the model B implants stayed the same for the duration of the production.

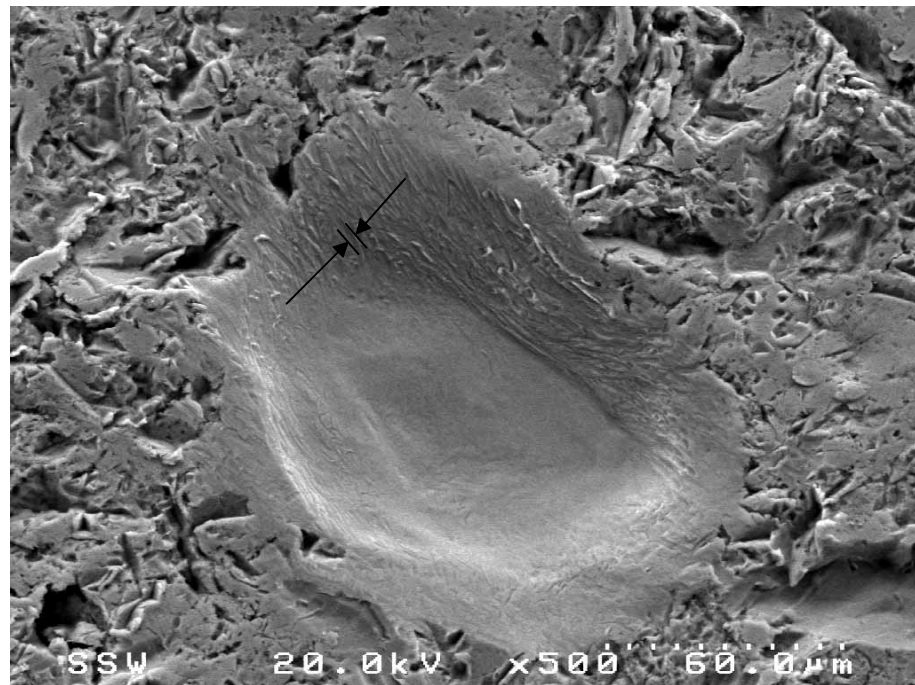
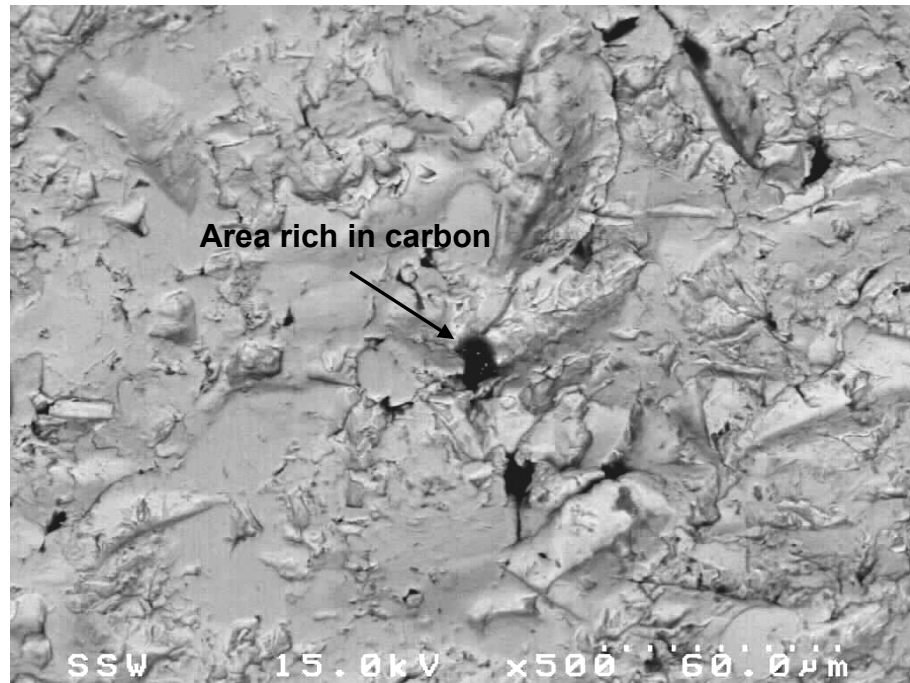
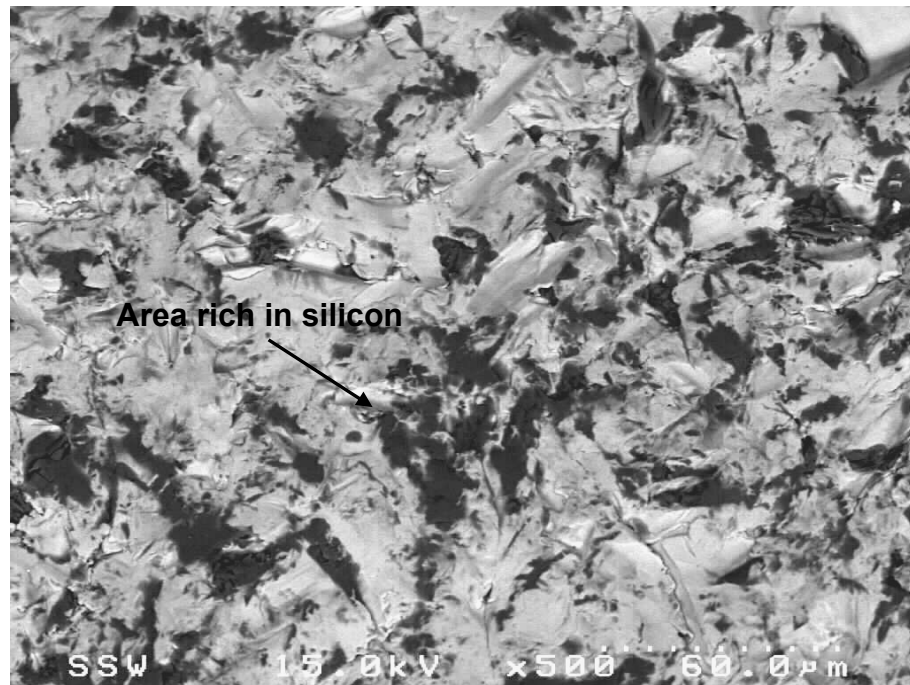


Figure 4.11: SEM image in SE mode of an individual stippling mark on the tray surface of a model B implant (case 27).

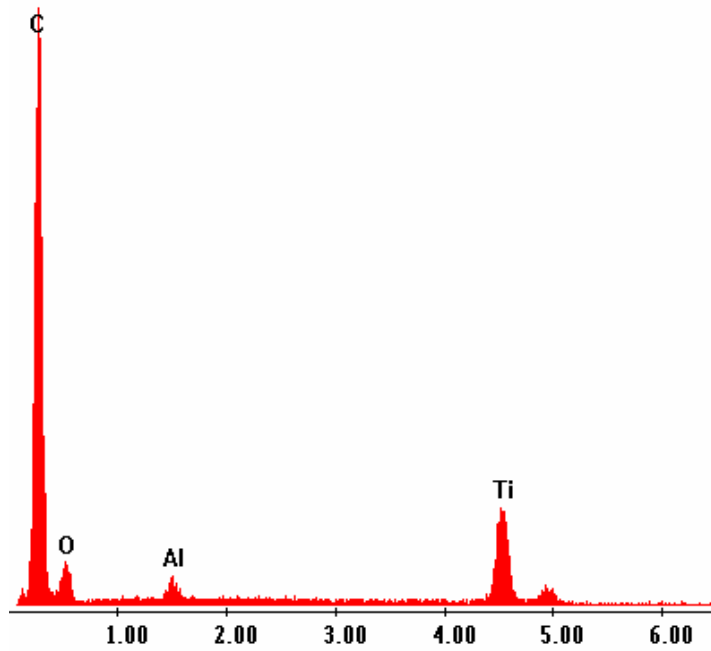


(a)

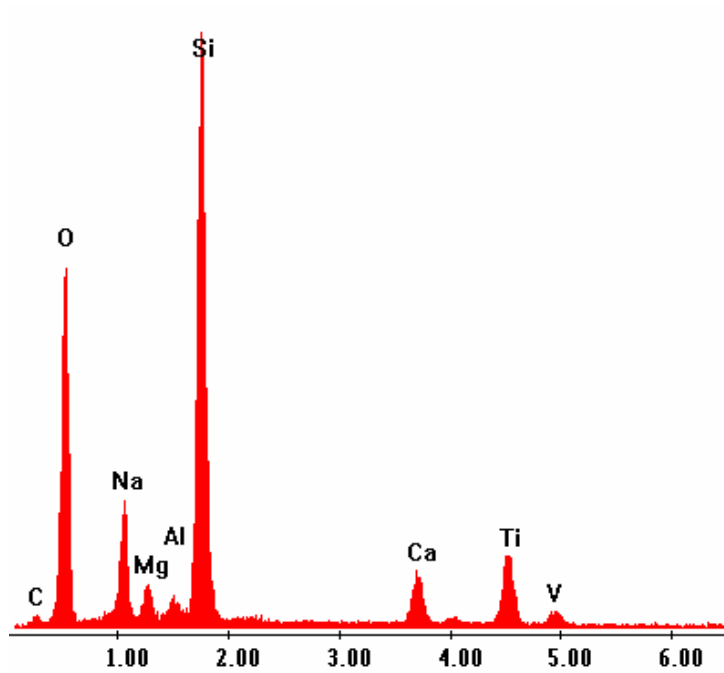


(b)

Figure 4.12: SEM image: (a) a retrieved model B tray (case 26) with the dark area rich in carbon and (b) a model B new, never implanted tibial tray (done in the BSE mode) with the dark area rich in silicon and oxygen (anterior direction \equiv top of page).

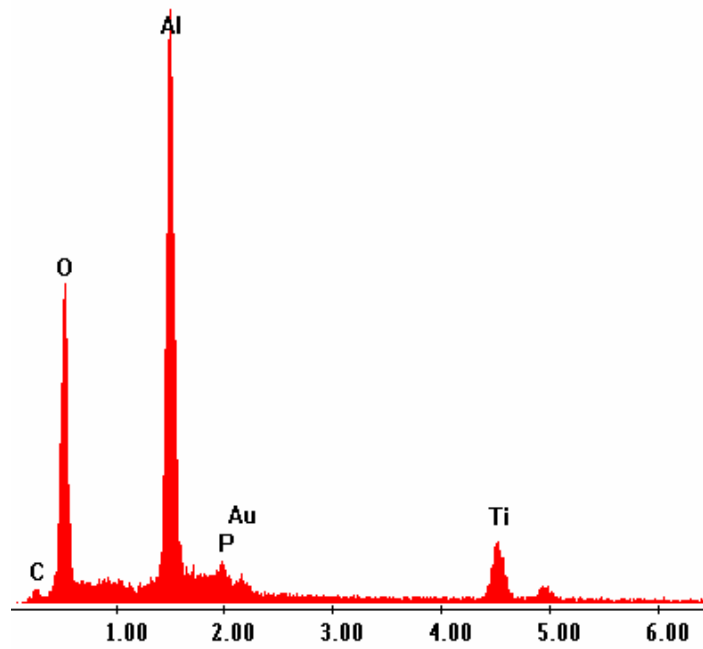


(a)

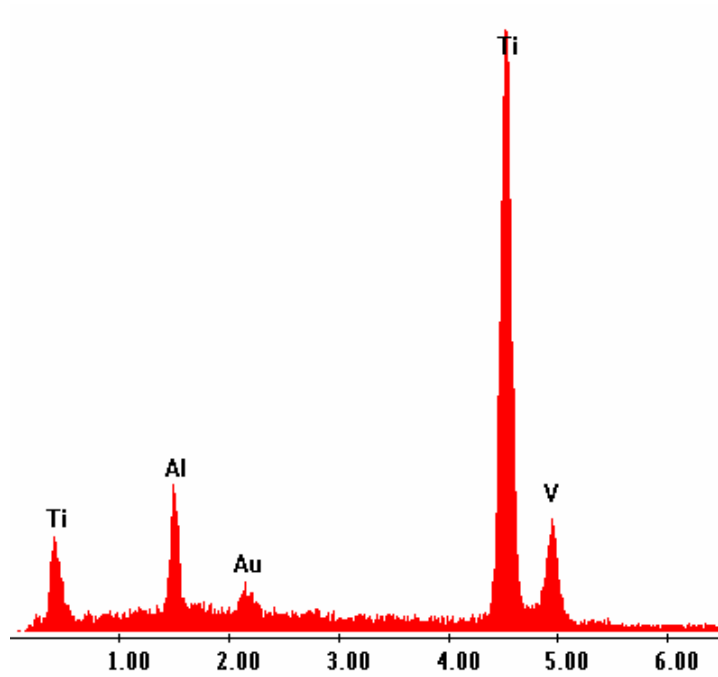


(b)

Figure 4.13: EDX spectra at 15 keV of (a) the carbon rich area on a retrieved model B tray (case 26), (b) the silicon and oxygen rich area on an as-manufactured model B tibial tray.

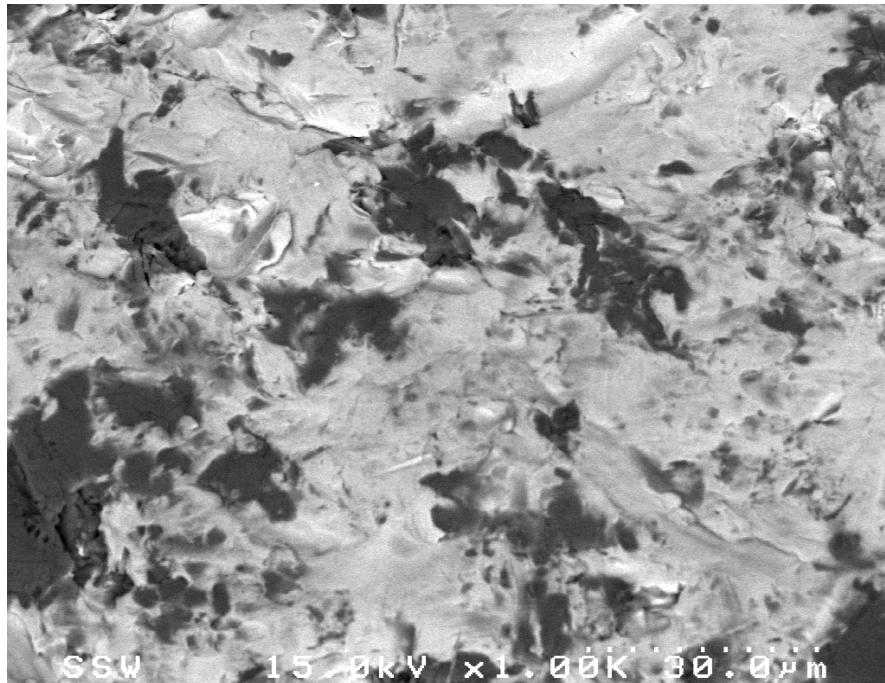


(c)

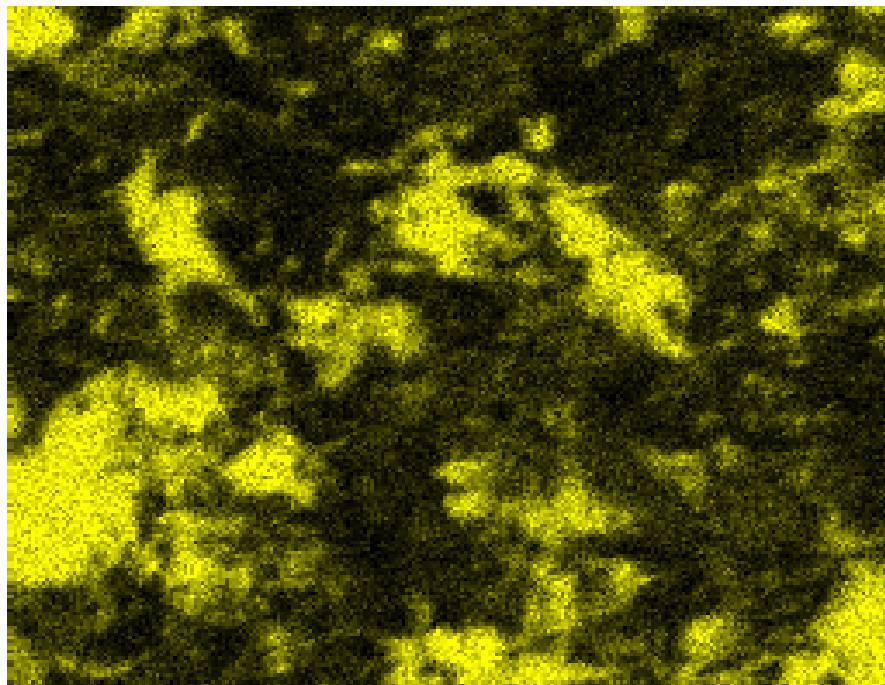


(d)

Figure 4.13 (continued): EDX spectra at 15 keV of (c) the aluminum and oxygen rich areas on a retrieved model B tibial tray (case 27), and (d) the tibial tray substrate of a model B implant.

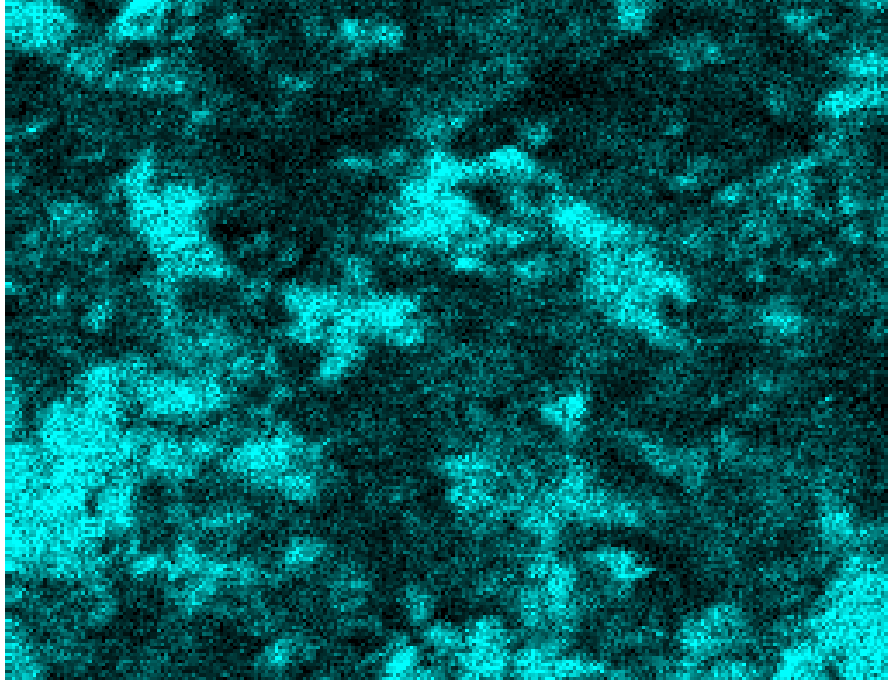


(a) BSE image

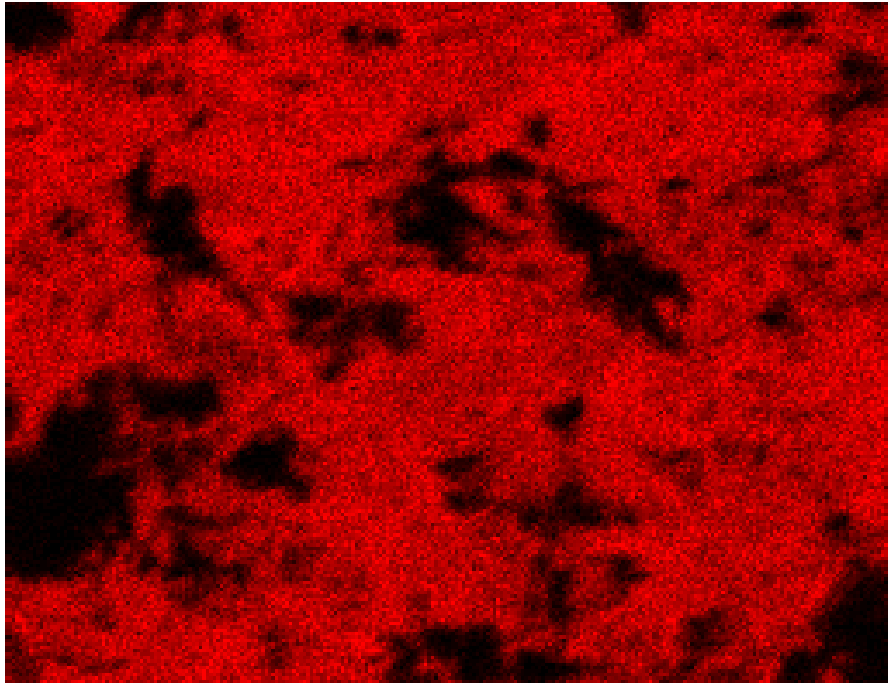


(b) Silicon (yellow)

Figure 4.14: EDX mapping on a specific area conducted on the as-manufactured tibial tray: (a) the surface image taken in the BSE mode and specifically running the EDX mapping for (b) silicon.



(c) Oxygen (turquoise)



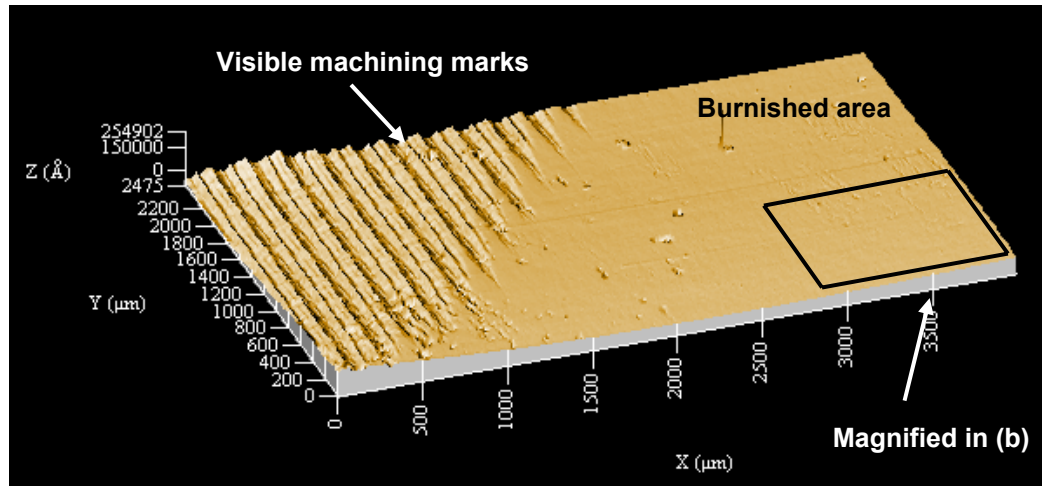
(d) Titanium (red)

Figure 4.14 (continued): EDX mapping on a specific area conducted on the as-manufactured tibial tray: specifically running the EDX mapping for (c) oxygen and for (d) titanium.

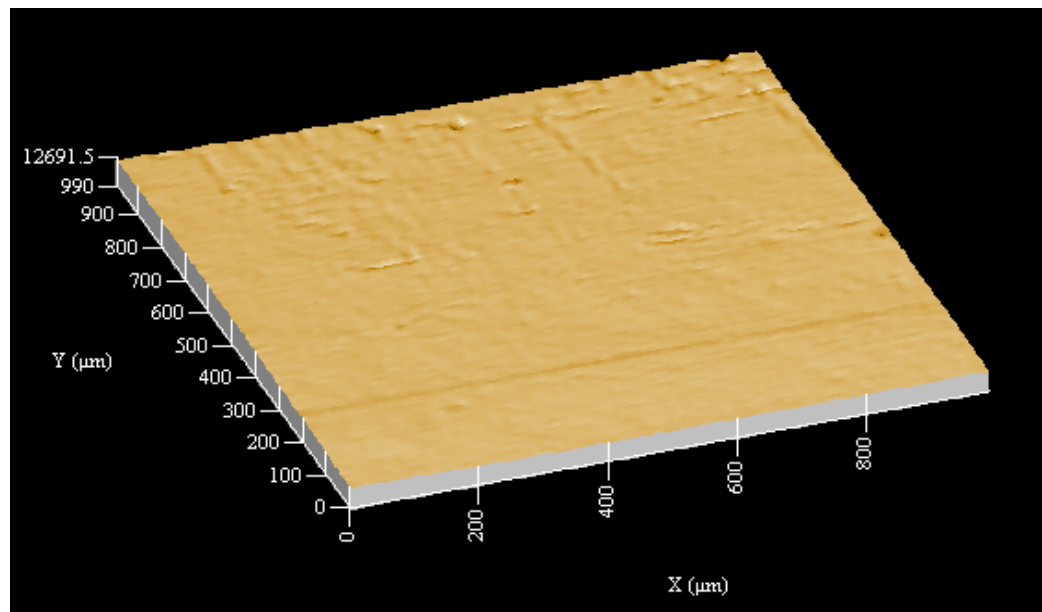
The indentations that were found on the PE of model C implants were predominantly in the peripheral region of the backside surface of the PE insert. Visual observation of the matching area on the polished tibial tray revealed that machining marks were still somewhat apparent. Measurements taken on three new, never implanted tibial trays (one from each implant model) revealed that the grit-blasted trays of model B implants had the highest roughness ($R_a = 935.9 \pm 172.2$ nm) compared with trays of model A and C implants ($p < 0.001$, ANOVA and Tamhane). Also, the roughness of the model A implant ($R_a = 16.0 \pm 5.6$ nm) was significantly lower than that of the model C implant ($R_a = 32.9 \pm 5.4$ nm) ($p < 0.001$, ANOVA and Tamhane).

4.3.6 Melt-Annealing

Burnishing was the most abundant damage feature on PE inserts retrieved from polished tibial trays. It was uncertain if burnishing was mainly due to deformation or due to wear. Load and motion may not necessarily cause PE wear but may result in creep of PE asperities⁷⁴. Such surface creep was shown to recover after the retrieved PE was melt-annealed. Thus, a PE insert from the retrieved model A implants was selected to elucidate on whether backside damage is caused by wear or by creep. The sections of the retrieved PE insert (case 4; GP sterilized PE insert) revealed a transition from original machining marks to a relatively smooth burnished zone (Fig. 4.15). After melt-annealing, the burnished surface was roughened with nearly no recovery of the machining marks (Fig. 4.16). R_a roughness measurements were taken before and after the melt-annealing well within the burnished area and in the area with visible machining marks. Such measurements revealed an increase in roughness from $R_a = 33.5 \pm 5.5$ nm to $R_a = 783.5 \pm 124.1$ nm ($\Delta R_a = 750.2$ nm) in the burnished area. Interestingly, the surface roughness in the area with the visible machining marks increased only by $\Delta R_a = 131.2$ nm from $R_a = 1315.9 \pm 130.4$ nm to $R_a = 1430.8 \pm 134.2$ nm.

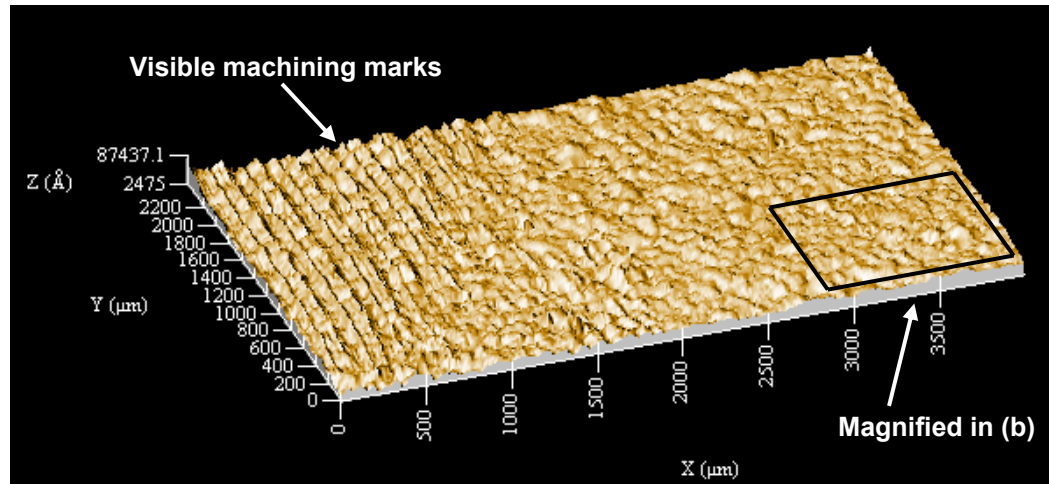


(a)

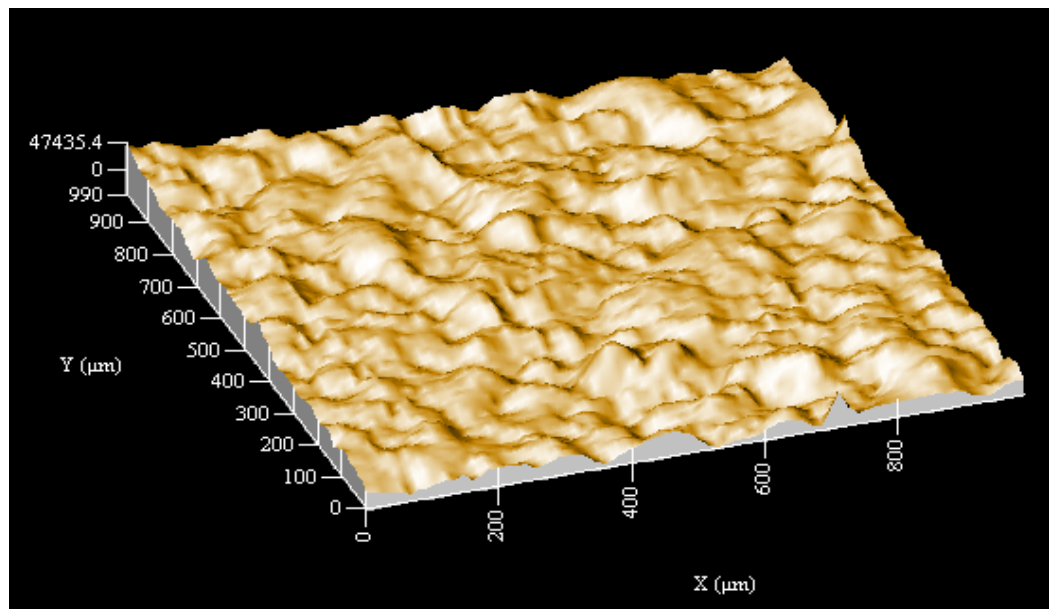


(b)

Figure 4.15: Surface profile of the retrieved model A implant PE inserts before melt-annealing: (a) retrieved and (b) the magnified area.



(a)



(b)

Figure 4.16: Surface profile of the retrieved model A implant PE inserts after melt-annealing: (a) retrieved and (b) the magnified area.

A static compression test was performed on a new, never implanted model A insert of 12 mm thickness (GP sterilized PE insert) in PBS at 37 °C for 336 h under a static axial load of $F_n = 4000$ N. The PE insert was submersed in the PBS at 37 °C for 72 h prior to the compression test to pre-soak the PE and again for 48 h after the compression test to “relax” the PE. The pre-soaking was performed to permit the surface asperities to gain fluid prior to the loading period. The post-conditioning was performed to allow the PE insert surface asperities to relax in the testing fluid so that equilibrium was achieved.

The R_a was measured at (i) after the 72 h of pre-conditioning (prior to loading), (ii) after the compression tests followed by 48 hours of relaxing (post to loading), and (iii) after the melt-annealing procedure (melt-annealed) (Table 4.8). The R_a was measured both directly under tibiofemoral bearing surface (loaded area) and at the centre of the PE insert near the locking pin (see Fig. 3.1 for details) (unloaded area). The surface roughness was reduced for the loaded area but increased for the unloaded area (possibly due to fluid sorption) during the compression test. After melt annealing, the loaded area as well as the unloaded area recovered to almost the same amount. Linear surface scans were taken from the loaded area at the different stages of the static compression test (Fig. 4.17). It appeared that the asperity height was reduced after the implant was subject to the static vertical load. The melt-annealing clearly increased the surface asperity height beyond the asperity height at test initiation.

Table 4.8: R_a roughness measured on a new, never implanted model A type PE inserts during the compression test.

Measurements	R_a Roughness [nm]	
	Loaded Area	Unloaded Area
i. Prior to loading	998.4 ± 65.9	1026.4 ± 96.1
ii. Post loading	704.1 ± 54.9	1252.7 ± 59.1
iii. Melt-annealed	1241.9 ± 160.5	1733.9 ± 83.6
iii minus ii	537.7 ± 189.9	481.2 ± 95.4

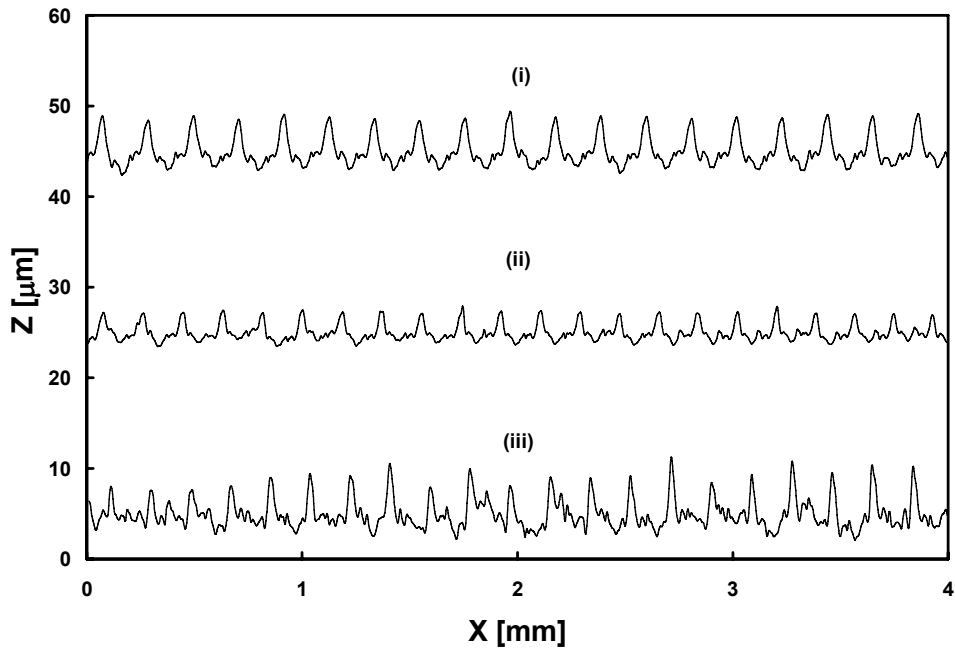


Figure 4.17: Linear surface scans taken on the backside surface of a new, never implanted model A insert: (i) before the compression tests (72 h pre-conditioned in PBS at 37 °C), (ii) after the compression test (48 h “relaxed” in PBS at 37 °C), and (iii) after melt annealing. During the compression test, a static vertical load of $F_n = 4000$ N was applied to the PE insert for 336 h.

4.3.7 Discussion on Retrieval Analysis

The present results have to be interpreted with caution since the findings were taken from implants that had failed clinically and thus they might not represent the cohort of well-functioning implants. Also, factors such as implant alignment, implant position, soft-tissue balance, patient activity and individual synovial fluid composition were not investigated. Nevertheless, the examination of retrieved implants had been widely used by other investigators and had been described as a useful method for gaining insight into the *in vivo* backside wear process^{13,218,289,302,303,341,342}. Unfortunately, direct measurements of mass and geometry could not be used to determine backside wear of retrieved tibial inserts because the exact starting values of both mass and geometry, the extent of creep and the amount of topside wear were not known. To quantify wear in an approximate manner, grading systems could be applied to produce damage scores.

The grading system approach was supported by the expectation that wear increases with IP and the positive correlations between the total BDS and IP reported by other investigators^{220,300,301}. Additional support was provided in the recent study by Hirakawa et al.²⁸⁹, reporting that the number of wear particles released into the soft tissue increased with IP for modular total knee replacements. However, a direct comparison between particles generated at the tibiofemoral articulation and at the backside surface regarding their osteolytic potential remained to be investigated. Unfortunately, a quantitative relationship between surface damage and volumetric wear has not yet been established accurately.

4.3.8 Discussion on Implant Design Issues

A number of key issues were clarified in the present study for the implant designer with evidence from a fairly large number of retrievals. Perhaps the most interesting aspect of the present study was the relative performance of the three implant models (Fig. 3.1). The Pearson correlation

also showed that IP did not significantly influence the BDS scores for model C implants and this finding was contrary to the overall positive correlation between BDS and IP. The MLRA showed that male patients had the lowest BDS values for model C compared with models A and B that were not different from each other (Fig. 4.6). For female patients, the MLRA showed that models B and C were not different from each other and had lower BDS than model A. The certainty of these findings was reduced by the low IP of the recently designed model C implants and the fact that most were removed for infection that might have limited patient mobility and thus BDS. In addition, the BDS was significantly higher for model C implants that were retrieved after an IP of greater 15 months ($p = 0.028$, Student's t-test), suggesting some degradation of the tibial locking mechanism might have occurred after about 15 months.

Specific information regarding implant design was ascertained from the comparisons of BDS values for the different implant models. The BDS values for the model C implants were lower for both males and females compared with model A. The main difference between these two implant models was the locking mechanism for the PE insert. Thus, it was considered likely that the lower BDS values for the model C implants occurred because their locking mechanism held the PE insert more tightly and reduced micromotion, and thus wear. This likely superiority of the partial-peripheral locking mechanism was the first major finding of the present study regarding implant design.

It was further supported when individual damage features were examined. The model C implants had less burnishing damage compared with the model A implants, thus supporting the idea that less micromotion occurred. In support, the retrieval study of Akisue et al.³⁰¹ also suggested lower BDS for inserts from trays with partial-peripheral locking mechanism compared with those from trays with central locking mechanism, but they did not apply MLRA to their data set. To the contrary, the retrieval study of Conditt et al.³⁰² recently suggested that backside damage was independent of tray locking mechanism design. Although they applied a stepwise linear regression analysis, the method

might have failed to separate out the relationship because of the many other differences. For example, their retrieval cohort contained 124 PE inserts of 12 different designs and included trays with and without screw holes.

More information regarding implant design was apparent when considering the BDS values for both model B and C implants. For the male patients, who often had higher mass and perhaps on average more intense physical activities than female patients^{377,416}, the BDS scores were higher. However, for female patients, the BDS values for the model B implants were lower compared with those of the male patients with the model B implants but the BDS values were not different for all patients with implant model C. This finding suggested that only under mild conditions did the grit-blasted surface of the tibial trays of model B implants hold the insert thus reducing backside motion and wear. This idea was also suggested by Silva et al.⁴¹⁷ but without the same authority because the average IP of their retrieved tibial components was much lower (average of 22 months; range 2 days to 42 months) compared with the present study. So, in the present study, male patients were likely to cause insert micro motion and subsequent damage from the rough grit-blasted surface despite the partial-peripheral locking mechanism. However, if a smooth tibial tray was employed, as in model C implant, the BDS values were reduced. Thus, the present retrieval study suggested that implant models with smooth surfaced tibial trays might be needed to reduce backside damage and thus wear for the heavier, more active patient even when a partial-peripheral locking mechanism was employed. The likely utility of a smooth surfaced tibial tray was the second major finding of the present study regarding implant design.

Both of the major findings of the present study regarding implant design were supported in a recent simulator wear study on model A implants by McNulty et al.⁴⁶. They compared the wear effect of tray surface finish and insert modularity (modular versus non-modular) on wear. A polished cobalt alloy tray was compared with a grit-blasted titanium alloy tray and the wear was reduced by 38 % ($5.56 \pm 0.42 \text{ mm}^3/\text{Mc}$ and $8.98 \pm 1.71 \text{ mm}^3/\text{Mc}$, respectively). Furthermore, there was no significant difference in wear for model A implants

of non-modular design compared with inserts that were clamped to tibial trays of both polished cobalt alloy and grit-blasted titanium thus representing a highly constrained locking mechanism. Thus, McNulty et al.⁴⁶ suggested that a highly constraining locking mechanism could reduce the need for tibial trays with smooth surfaces. It was also mentioned that additional simulator tests under more severe conditions should be conducted to confirm whether wear was indeed independent of surface finish for a highly constraining locking mechanism.

Further support for the findings of the present study was provided in the recent retrieval study by Collier et al.³⁹⁷ involving a 5 - 10 year follow-up of 300 patients with 365 CR knee replacements of model A implants. Based on their performed Cox-regression analysis, the incidence of osteolysis was significantly reduced for polished tibial trays and NGA sterilization. The benefit of NGA compared with GA sterilization was not a surprise and was supported by the findings of the present study. Effects of gender and extended shelf storage time were also identified as significant promoters of osteolysis. However, the role of locking mechanism apparently could not be ascertained from their data set.

Surprisingly, the BDS increased with increasing insert thickness in several of the regression models (M2, M4, and M5) in the present study. This result was contrary to recommendations for insert thickness based on other studies^{301,341,418} of implants with tibial trays having screw holes under the tibiofemoral contact area for cementless fixation. However, for the implants in the present study, the thinner inserts might have sustained more creep that allowed the partial-peripheral locking mechanism to better grip the insert and thus be more effective in preventing micromotion and wear. In the case of a large flexion-extension gap that requires the use of a thicker PE insert it may be best advised to use *augments* with the femoral component and below the tibial tray. Using *augments* reduces the flexion-extension gap and allows the implantation of a thinner PE insert in such a case.

As mentioned previously when discussing the recent study of Collier et al.³⁹⁷, retrieved inserts in the present study that were GA sterilized, had overall higher BDS and the BDS also increased with shelf storage for GA inserts of model B implants. GA sterilization with extended shelf storage was a well-known precursor^{213,214} of high wear and it was reassuring to find that the present grading system detected this effect. Recently, Rasquinha et al.²⁹⁶ hypothesized that GA sterilized PE insert possibly allowed more backside wear to occur. The lower BDS gradient for GA compared with NGA (M5) might have been caused by the GA inserts having enough damage to reach a BDS “saturation” level. In any case, the use of GA sterilization was condemned by the results of the present study.

The two insert types (CR or PS) did not show statistically different BDS values. The PS inserts had been expected to show more backside damage than the CR inserts because moments and tangential forces might be generated by the cam-post⁴¹⁹, resulting in a less effective locking mechanisms, more micro motion, and in higher BDS. However, this did not occur significantly and so BDS was found to be insensitive to whether a PS or CR implant was used.

The “reasons for surgery” in the present study reflected current trends to some extent⁸. To date, only three studies²⁹³⁻²⁹⁵ reported severe tibial osteolysis in cemented modular total knee replacements. The five cases of osteolysis in the present study, with their higher BDS-gradient, but low BDS values, should cause some immediate concern. It was considered plausible that once osteolysis was initiated, because of a higher backside wear rate, it developed rapidly enough that the implants were replaced before they could achieve higher BDS values. On the other hand, the BDS of inserts revised for infection (dominantly of model C implant) might have been somewhat over-estimated since some surface damage might have occurred during insert manufacturing and packing⁴¹⁵. Of further interest was the higher BDS for inserts from primary implant types over inserts from revision implant types. Jones et al.⁴²⁰ recently reported an increased metabolic activity for patients having primary implant types compared with patients having revision implant

types which may have led to increased BDS due to higher activity levels for patients with primary implant types.

4.3.9 Discussion on Surface Characterization

In addition to studying backside damage with a stereo microscope, the modified-method for BDS and statistical analysis, it was considered valuable to perform detailed surface characterization to obtain a better fundamental understanding of the damage features. The micro damage of burnishing observed on PE inserts retrieved from polished tibial trays was similar to micro damage seen on the main articulation of acetabular cups that were retrieved for osteolysis⁴²¹. It had been suggested that grit-blasted tibial trays had higher friction forces and thus less micro motion of the insert⁴¹⁷. However, micro-damage for the inserts opposing the grit-blasted tibial trays of the model B implants showed short grooves, suggesting that micromotion and damage still occurred.

The presence of the stippling damage feature mostly on PS inserts retrieved from grit-blasted trays suggested the frictional transmission of tibiofemoral rotational stresses and the presence of third-body wear particles²⁹⁵. The observed embedded and fractured particles in the new, never implanted grit-blasted trays were probably caused by repeated impacting of blunt particles from the slurry jet during the grit-blasting procedure, combined with the low fracture toughness of the abrasive particles (Al_2O_3 and SiO_2) and the low hardness of the titanium alloy⁴²²⁻⁴²⁴. Embedded particles were rarely found on retrieved grit-blasted tibial trays, suggesting that these particles were eventually released into the body. However, before being released, they probably contributed, with their high hardness and blunt shape, to third-body abrasive wear that appeared as stippling on the PE insert and metal tray. Although these observations and speculations amounted to circumstantial evidence, it might be beneficial for the proximal surface of titanium alloy tibial trays to be thoroughly cleaned or to avoid grit-blasting altogether.

4.3.10 Discussion on Melt-Annealing

The observed surface contour and profile changes after melt-annealing suggested some recovery of both the retrieved PE insert and the PE insert from the compression test. For the PE retrieval, the burnished area as well as the area with clearly visible machining marks recovered after melt-annealing which suggested some recovery of plastic deformation. The additional compression tests on one model A insert supplied more information. The amount of recovery for the PE insert in the loaded area and unloaded area test was similar. This suggested that residual stresses due to the manufacturing process may also be involved in the recovery process. Considering the recovery of both the retrieved insert and the insert from the compression test one may conclude that the removal of machining marks was due mostly to wear rather than deformation. Such recovery was suggested to diminish with increased level of oxidation in the PE ⁴²⁵. However, the analyzed inserts were GP sterilized which was documented as being stable regarding oxidation ²⁰⁶. This behaviour is likely to be different for highly XPE ⁷⁴. In any case, it was recognized that only one retrieved sample and only one as manufactured sample were utilized and may limit the conclusion of this smaller study.

4.3.11 Concluding Remarks

The selection of relatively large numbers of inserts of only three implant models combined with a modified grading system and a sophisticated statistical analysis allowed the identification of major influential factors in the multi-factorial process of backside wear. Evidence was obtained to support the use of the partial-peripheral locking mechanism and polished tibial tray surfaces. These features might be particularly beneficial for active male patients with high body weight. Insert thickness should be considered part of locking mechanism design. Some evidence was found for a high BDS gradient indicating that osteolysis, once initiated, developed rapidly in some patients. As expected, the use of GA sterilization with extended shelf-storage led to

increased BDS. Surface characterization suggested that a grit-blasted tibial tray still had PE insert micromotion and thus backside damage. Some contamination by the grit-blasting particles was found on new, never implanted tibial trays that might have caused third-body abrasive wear on the backside of the insert. The burnishing damage feature dominantly observed on inserts retrieved from polished tibial trays was suggested to be associated with an adhesive/abrasive wear mechanism. As a final comment, for all of the implant models, some backside damage was considered inevitable since deformation of the PE insert under cyclic loading had to allow some micromotion and slip to occur at the backside interface. Thus, either much better clamping mechanisms⁴⁶ or non-modular tibial components should perhaps be considered^{15,233,258,262,264,426-428}.

4.4 Lubricant Composition

4.4.1 Introductory Remarks

To gain more insight on the boundary lubrication process of PE, SF were sampled from twenty patients and analyzed for their biochemical properties (see Section 3.3.1 for details on SF). Total protein concentration, electrophoretic profiles, osmolality, and trace elements (Ca, Mg, inorganic P, and Fe) were measured and compared with the composition of calf sera that are frequently used for *in vitro* wear testing. This investigation was deemed necessary to set the precedence for the subsequently performed *in vitro* wear tests with the focus on the effects of SF constituents on PE wear.

4.4.2 Protein Concentration

The protein concentration of each SF sample was determined using the BCA assay immediately after sample collection from the patient. Visually, the SF samples varied in color from light yellow, to dark yellow up to light red. The light red color may have been due to some blood contamination caused

during sampling that could not be eliminated even by centrifuging the samples. The total protein concentration was measured from quadruplicate samples for each patient. The mean total protein concentration was 34.18 ± 4.77 g/l (Fig. 4.18). The distribution was Gaussian based on the histograms and was confirmed with the test for normality ($p = 0.932$, Kolmogorov-Smirnov test).

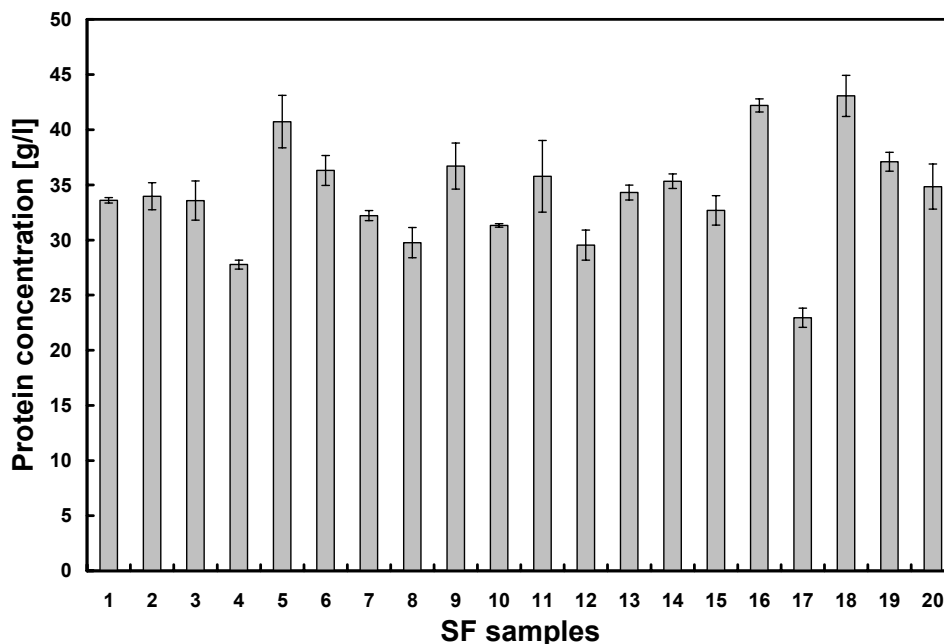


Figure 4.18: Protein concentration of the SF samples collected from patients 1 - 20.

4.4.3 Electrophoresis

As mentioned in Section 3.3, the SF samples were treated with hyaluronidase to break down the HA compound to facilitate electrophoresis. It remained uncertain whether hyaluronidase interfered with the electrophoresis. It was decided to conduct electrophoretic measurements in sextuplicate on a SF sample hyaluronidase treated from one patient (SF 20) and sextuplicate of hyaluronidase diluted with PBS to a concentration 10 g/l (Fig. 4.19). It can be clearly seen from the gel that hyaluronidase migrated towards the intensity of albumin. Comparing the intensity of both groups showed that the hyaluronidase

accounted for 9.66 ± 1.66 % of the albumin intensity. This suggested that a correction term for each SF sample has to be implemented to calculate the *real* protein constituent fractions. The corrected initial protein constituent fraction, ic_c , was then calculated for the remaining four protein fractions, α -1-globulin, α -2-globulin, β -globulin, and γ -globulin based on their initial measured fraction, ic_m :

$$ic_c = \frac{ic_{m-albumin} * 0.0966}{4} + ic_m \quad (4.1)$$

After conducting this correction, the albumin fraction was slightly reduced, while the individual fractions of the remaining protein constituents were consequently increased (Fig. 4.20). The distributions of all corrected constituents were Gaussian on histograms which were confirmed with the test for normality ($p \geq 0.154$, Kolmogorov-Smirnov test).

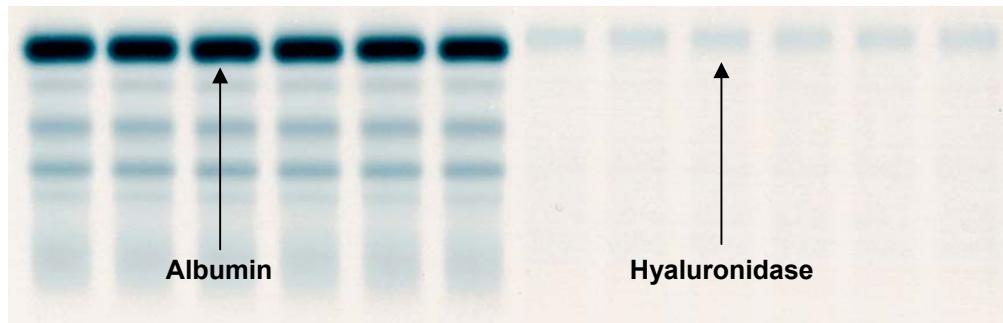


Figure 4.19: Electrophoretic profiles of six SF samples (patient SF 20) and six hyaluronidase samples. Note the migration of hyaluronidase towards albumin in the gel.

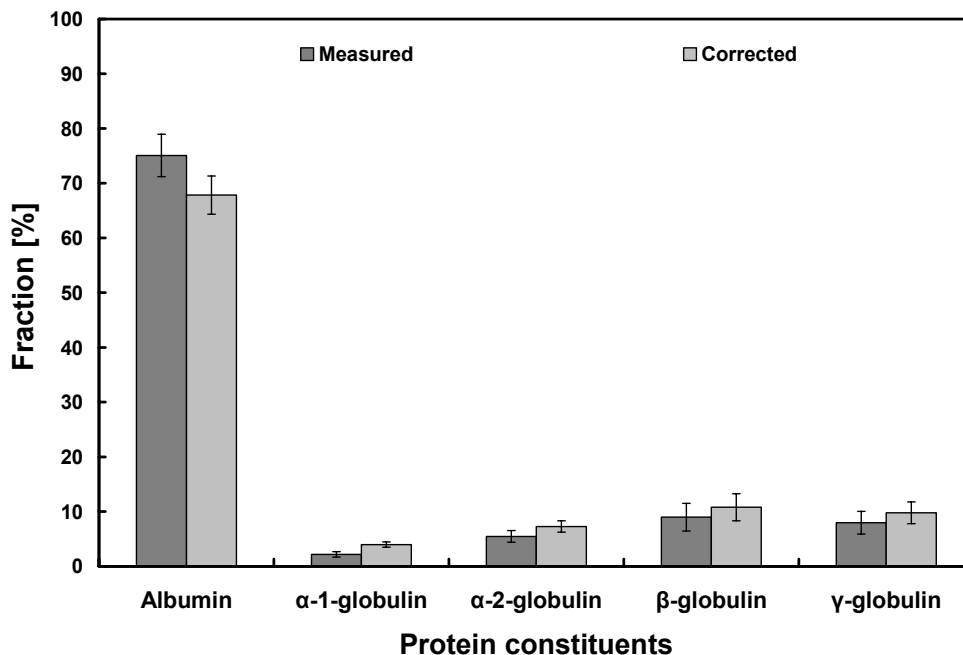


Figure 4.20: The *measured* fractions and the *corrected* fractions of albumin, α -1-globulin, α -2-globulin, β -globulin, and γ -globulin.

The distribution of all constituents for both male and female patient groups was Gaussian on histograms and was confirmed with the test for normality ($p \geq 0.200$ and $p \geq 0.277$, Kolmogorov-Smirnov test, respectively) (Fig. 4.21). There was no difference between male and female patients in the individual fractions of albumin, α -1-globulin, β -globulin, and γ -globulin ($p \geq 0.409$, Student's t-test). The α -2-globulin fraction was significantly higher for the female patients ($p = 0.010$, Student's t-test).

The calculated protein constituent fractions of the SF samples were graphed with the protein constituent fractions supplied from the manufacturer for BCS, NCS, ACS, and ACS-I (Fig. 4.22). It can clearly be seen that the albumin, α -1-globulin, α -2-globulin fractions of SF were closest to ACS and ACS-I. The β -globulin fraction of the SF samples was fairly similar to NCS and ACS. The γ -globulin fraction of the SF samples was closely matched by BCS and NCS.

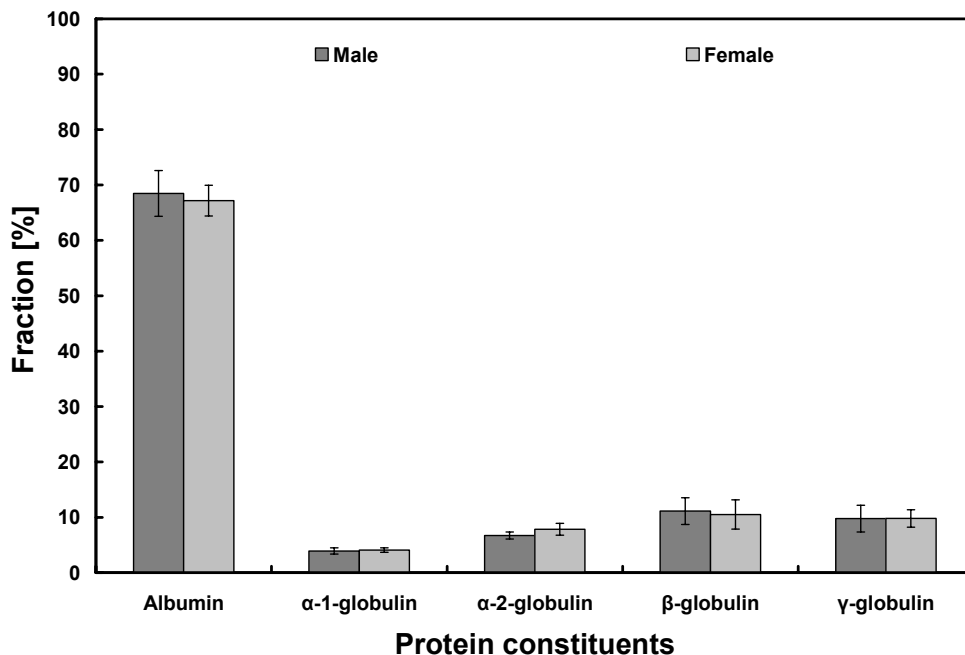


Figure 4.21: The corrected fraction of albumin, α -1-globulin, α -2-globulin, β -globulin, and γ -globulin for the male patients (n = 10) and the female patients (n = 10).

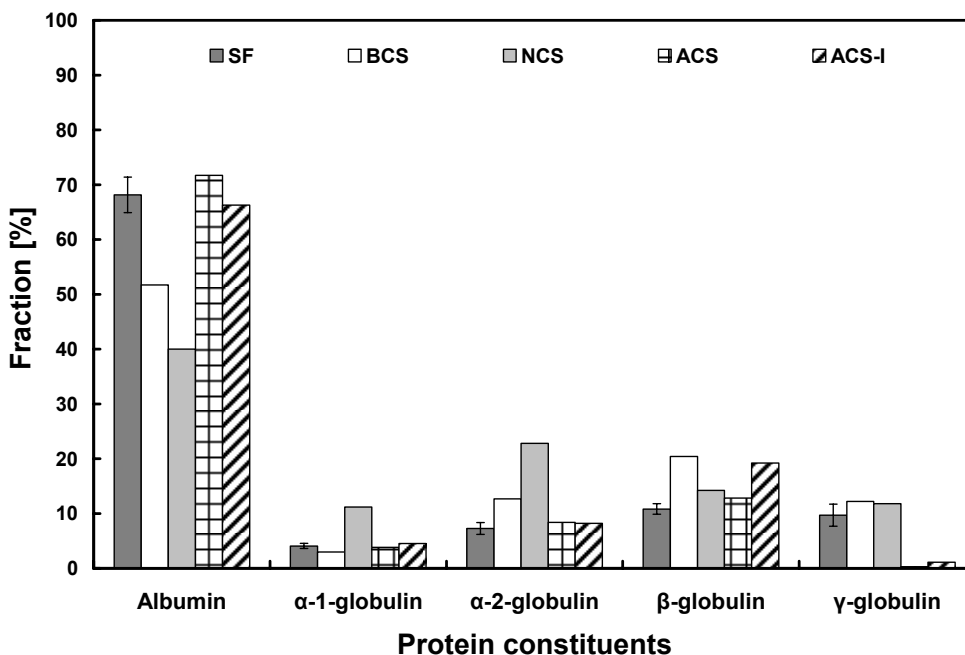


Figure 4.22: The fraction of albumin, α -1-globulin, α -2-globulin, β -globulin, and γ -globulin for the corrected SF (n = 20) and the calf sera such as BCS, NCS, ACS, and ACS-I according to the manufacturer (HyClone, Logan, UT).

4.4.4 Osmolality

The osmolality was determined for all SF samples and measured 310.20 ± 11.84 mmol/kg and was normally distributed ($p = 0.995$, Kolmogorov-Smirnov test) (Fig. 4.23). The mean osmolality value for all SF samples was compared with the values obtained for the calf sera such as BCS, NCS, ACS, and ACS-I that were either diluted with DW or PBS to a target protein concentration of 17 g/l according to ISO 14243-3⁴¹ (Table 4.9). It can be seen that the measured osmolality of SF, 100 % BCS, 100 % NCS, 100 % ACS, and 100 % ACS-I was equivalent to the osmolality for the sera diluted with PBS (Fig. 4.24). Strikingly, the serum dilution with DW resulted in approximately only half of the osmolality compared with SF samples.

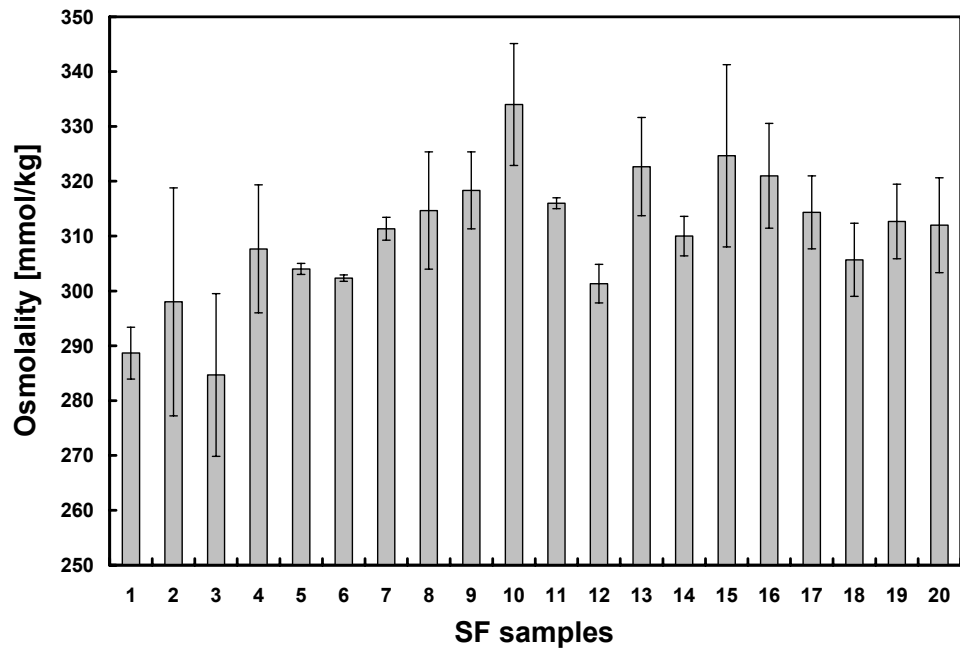


Figure 4.23: Osmolality of the SF samples collected from patient 1 - 20.

Table 4.9: Calf sera diluted with either DW or PBS to different amounts to obtain a protein concentration of 17 g/l according to ISO-14243-3⁴¹.

Diluted calf sera	Dilutive Media	Dilution [%]
BCS + DW	DW	25
NCS + DW	DW	33
ACS + DW	DW	40
ACS-I + DW	DW	41.5
BCS + PBS	PBS	25
NCS + PBS	PBS	33
ACS + PBS	PBS	40
ACS-I + PBS	PBS	41.5

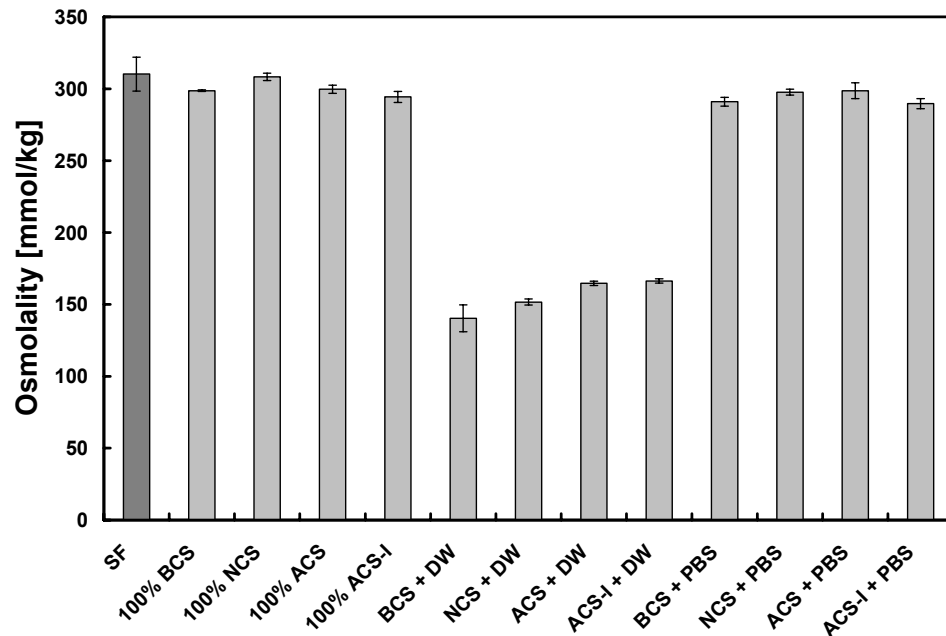


Figure 4.24: The osmolality for all SF samples, the undiluted calf sera (100 % BCS, 100 % NCS, 100 % ACS, 100 % ACS-I), and calf sera diluted with DW (BCS + DW, NCS + DW, ACS + DW, ACS-I + DW) and PBS (BCS + PBS, NCS + PBS, ACS + PBS, ACS-I + PBS) to a protein concentration of 17 g/l.

4.4.5 Trace Elements

The concentrations of Ca, Mg, inorganic P, and Fe were determined in all SF samples, 100 % BCS, 100 % NCS, 100 % ACS, and 100 % ACS-I (Fig. 4.25). The distribution of all trace elements were shown to be Gaussian on histograms and confirmed with the test for normality ($p \geq 0.616$, Kolmogorov-Smirnov test). The Ca and inorganic P concentration were highest in SF samples followed by Mg and Fe. A similar pattern can be observed for BCS, NCS and ACS, but not for ACS-I with a Fe concentration (0.087 mmol/l) close to its Mg concentration (0.080 mmol/l). However, none of the calf sera trace element concentrations were close to the concentrations of human SF samples.

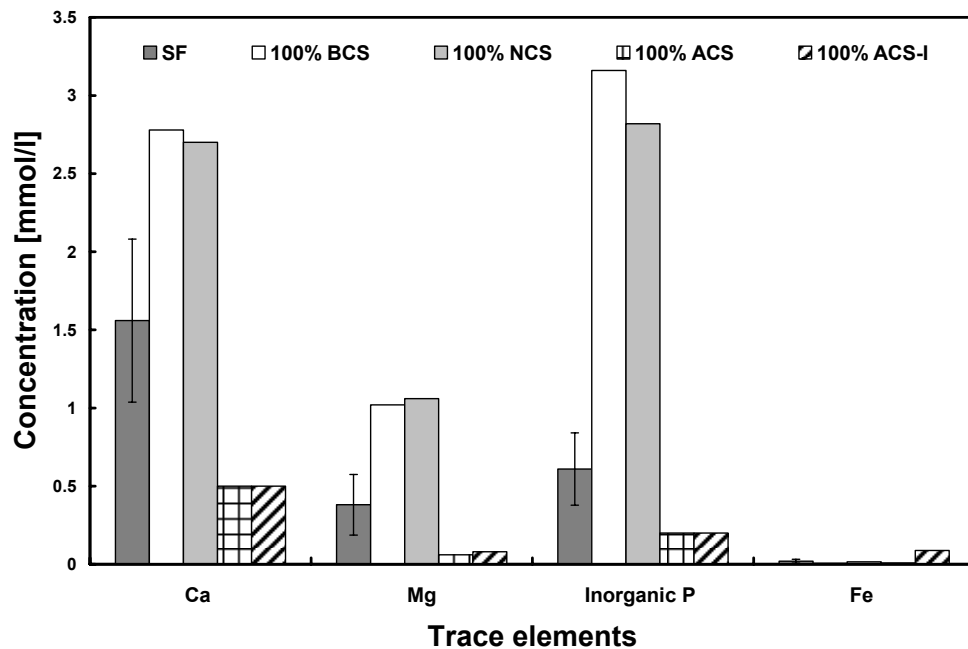


Figure 4.25: The trace element concentration of Ca, Mg, inorganic P, and Fe for SF, 100 % BCS, 100 % NCS, 100 % ACS, and 100 % ACS-I.

4.4.6 Discussion

Apart from water, proteins count for the largest fraction of constituents in SF. From the tribological perspective, proteins have been considered to play a role in the boundary lubrication process in natural human joints and therefore may also be of importance to artificial joints^{76,429}. In the present study, the average total protein concentration reached 34.19 ± 4.78 g/l and was comparable to historical values reported for OA hip (31.8 ± 1.9 g/l; $n = 21$)¹¹⁶ and to OA knees (27 ± 10 g/l; $n = 43$)³³. In any case, the total protein concentration was severely lower compared with any of the calf sera (BCS = 69 g/l; NCS = 52 g/l; ACS = 42 g/l; ACS-I = 41 g/l) in the undiluted form. In total knee wear testing, increased protein concentration resulted in reduced wear rates when an AMTI knee simulator was used⁴⁵. The use of calf serum with different protein constituent fractions may affect the PE wear rate but such an effect has not been established in knee wear testing.

The BCA assay has been shown to be a consistent and reliable method for testing human fluids⁴³⁰. The individual protein structure, the number peptides and the presence of four amino acids (cysteine, cystine, tryptophan and tyrosine) were known to be responsible for the colorimetric response in this biuret reaction¹⁷³. Although the phospholipid concentration (here the amount of organic P) was not evaluated in the present study, phospholipids are a constituent of SF but only at small concentrations of ~ 0.52 g/l³³. Thus, such small amounts of phospholipids in the SF may have somewhat affected the measurements obtained with the BCA¹⁷¹.

The electrophoresis measurements of the SF sample and of the calf sera allowed the comparison of the main protein constituents quantitatively. Implementing the correction term to calculate the *real* protein constituent fraction was necessary as hyaluronidase migrated towards albumin. Such correction, although only marginal, affected the fraction of the other protein constituents. Although there were ought to be differences between human and calf protein compounds, it was interesting to observe that albumin was most abundant in SF as well as in the calf sera. The fractions of the remaining

protein constituents were quite different from the human SF samples. Small et al. ¹⁰⁷ reported the composition of SF samples taken from 13 patients with rheumatoid arthritis, infectious arthritis (Reiter's syndrome) and chronic effusions. They reported concentrations of 48 % albumin, 5 % α -1-globulin, 9 % α -2-globulin, 12 % β -globulin and 25 % γ -globulin which were greatly different from the present. Yao et al. ^{108,431} determined the fractions of five human SF samples and compared their fractions to fresh BCS and bovine SF and found noticeable differences between both fluids which confirms some of the trends observed in the present study. Although further differences in viscosity and protein degradation were noted ^{108,431}, no comment on the effect of the different sera on the PE wear was made and remained under scrutiny.

Even though the osmolality of normal, healthy SF from human knees has been reported ¹⁰⁶, it has not been addressed in patients with OA. The osmolality of SF samples from healthy patients ¹⁰⁶ appeared not to be different to the OA samples or human serum samples in the present study. The osmolality of human SF samples from the present study was similar to the osmolality of the four undiluted calf sera (Fig. 4.24). Nevertheless, the dilution of any calf serum with DW to a target protein concentration of 17g/l ⁴¹, as recommended by ISO, was shown to result in non-clinically relevant osmolality levels. Others ^{35,157,175,432} used PBS or saline solution to dilute their serum for wear testing but without support to clinical relevance and whether osmolality may affect the PE wear rate. The present data recommend the use of PBS as the dilutive medium for the calf sera used in wear simulations, but the effects of osmolality on PE wear still remained uncertain. It may be possible that the increased ionic presence in the serum may improve the protein stability ¹⁰⁴, affect protein degradation and thus PE wear. Yet, this hypothesis remains to be proven. The measured trace elements such as Ca, Mg, inorganic P and Fe were somewhat different in concentration to the SF. While such elements are known to bind or add to proteins and other substances in the SF and calf sera ³⁹⁸, their effect on PE wear remained also unknown.

The four calf sera analyzed represent the main groups of calf sera that are currently used in the orthopaedic community to evaluate the wear performance of total joint replacements. HA, another main constituent of SF, was not measured in the SF samples in the present study, but their concentration in OA patients was recently reported elsewhere³¹. As a final comment, a recent improvement in the protein detection technique allows the identification of twenty highly abundant proteins in human plasma⁴³³. This may also be of benefit for the analysis of human SF samples but such analysis went beyond the scope of this thesis.

4.4.7 Concluding Remarks

The analysis of the SF samples revealed that the total protein concentration was 2-fold greater than the total protein concentration recommended by ISO-14243-3⁴¹ for simulator wear testing of TKRs. The protein constituent fractions of the calf sera were different from these in SF. ACS and ACS-I were closest in their protein constituent fractions to SF.

Diluting the calf sera with DW to a target protein concentration of 17 g/l, as recommended by ISO-14243-3⁴¹, resulted in non-clinically relevant levels of osmolality for the serum mixture. Using PBS as the dilutive media appeared more appropriate and produced osmolality levels similar to the levels measured in SF. In addition, the trace elements were also vastly different between SF and the calf sera. This investigation illustrated major differences of SF compared with the calf sera used for implant wear testing. It remains uncertain whether these differences affect the *in vitro* wear process and requires further attention.

Chapter 5: *In vitro* Investigations: Results, Analysis and Discussion

5.1 Introductory Remarks

As shown in Chapter 4, the surface damage appeared to occur in the boundary lubrication regime. The SF composition appeared to be vastly different to the calf serum composition in many aspects and may therefore impact the PE wear in knee simulator wear testing. The effect of test fluid composition, fluid-uptake and boundary lubrication on PE wear *in vitro* test environment was explored in this chapter.

Chapter 5 is divided into three major Sections. In Section 5.2, the effects of pre-soak media composition and design features on the fluid-uptake are explored. This was performed on GUR 1050 AMK[®] inserts that were sterilized in different environments (GA or GP) and varied in thickness. These inserts were subjected to pre-soak media at different temperatures and their weight gain assessed following several different protocols. In addition, a newly acquired displacement controlled knee simulator was commissioned for 3 Mc under consideration of a specifically designed commissioning protocol (CP) in combination with test parameters courteously supplied by DePuy Orthopaedics Inc. (Warsaw, IN). Such a wear test was necessary to characterize the station variation and other associated factors such as protein degradation and the amount of protein shear (characterized by the peptide concentration). In Section 5.3, the wear test from Section 5.2 was continued until a test maximum of 6 Mc on the same implant components. In particular, the effects of protein constituents of BCS, NCS, and ACS on PE wear were assessed and the extent of protein degradation, bacterial growth, and peptide concentration identified, which were then compared with the clinical findings illustrated in Section 4.4. In Section 5.4, the calf serum closest to human SF was then used to further explore the effects of serum osmolality and HA on PE wear using an alternative, but yet more effective bio-control agent to inhibit bacterial growth. Additional information was obtained by characterizing the protein degradation and peptide

concentration of different serum compositions and by applying surface characterization techniques. Such developments led to a possibly more clinically relevant lubricant for the evaluation of total knee joints.

5.2 Simulator Commissioning Tests

5.2.1 Introductory Remarks

The simulator commissioning tests were performed to gain insight into PE fluid uptake during soak testing (or, in other words, the PE mass gain behaviour when immersed in fluid), to perform initial wear tests with the knee simulator and to examine the biochemistry of the lubricating fluid during these initial wear tests. The AMK[®] knee implant made with GUR 1050 PE inserts was used in all wear testing in the present thesis. The PE fluid uptake was important because wear was assessed by measuring the overall mass loss and any fluid uptake that occurred during a wear test had to be added to the overall mass loss to determine the true wear. For the soak testing, 11 tests with 3 AMK[®] inserts in each (for a total of 33 inserts) were conducted to investigate the effect of measurement frequency, temperature, insert thickness, sterilization technique, soak period and fluid composition. The initial wear testing was conducted for a total of 3 Mc and identified variations in wear for individual stations and banks of stations in the knee simulator. The wear rates were compared with those obtained from previous testing conducted by DePuy Orthopaedics (Warsaw, IN) for the same AMK[®] implants in the same type of knee simulator under the same kinematics input and lubricating fluid composition. Finally, the biochemistry of the lubricating fluid was examined before and during the wear testing. This activity involved determining the amount of protein degradation, protein precipitation, and sedimentation. The peptide concentration was measured before and after the wear test to determine whether the proteins were damaged during the wear process. In addition, standard tests were performed to assess possible microbial contamination. All of the above commissioning tests were deemed important to identify possible

factors that could affect the PE wear behaviour and to establish a baseline for the planning of subsequent wear tests.

5.2.2 Soak Testing

Eleven soak tests were performed with each test involving three inserts (Table 5.1). Tests 1 - 5 were conducted first and used DW as the soaking fluid. Test 1 and 2 were performed to assess the effect of soaking period on fluid uptake (mass gain), with inserts left undisturbed in DW for either 46 days or 92 days. Tests 2 and 3 examined the influence of the mass measurement frequency on the mass gain with the inserts in Test 3 being repeatedly “disturbed” (removed from DW, cleaned, desiccated and weighing) during the test interval of 46 days. Tests 3 and 4 were conducted to assess the effects of insert thickness (10 mm versus 14 mm). Tests 4 and 5 were conducted to examine the influence of sterilization technique (GP versus GA). Tests 6 - 11 were conducted after Tests 1 - 5 and lasted for 46 days using only 14 mm thick inserts that had been GP sterilized.

Table 5.1: Illustration of 11 soak tests performed on three AMK[®] inserts each (n = 3)*.

Soak test	PE insert [Sterilization, thickness]	Measurement frequency	Temp.	Soak period [days]	Fluid composition
1	GP, 10 mm	Undisturbed	RT	92	DW
2	GP, 10 mm	Undisturbed	RT	46	DW
3	GP, 10 mm	Disturbed	RT	46	DW
4	GP, 14 mm	Disturbed	RT	46	DW
5	GA, 14 mm	Disturbed	RT	46	DW
6	GP, 14 mm	Undisturbed	RT	46	DW
7	GP, 14 mm	Undisturbed	RT	46	BCS + DW + SA
8	GP, 14 mm	Undisturbed	37 °C	46	DW
9	GP, 14 mm	Undisturbed	37 °C	46	BCS + DW + SA
10	GP, 14 mm	Disturbed	37 °C	46	DW
11	GP, 14 mm	Disturbed	37 °C	46	BCS + DW + SA

*see Table 3.8 in Chapter 3 for details of this lubricating fluid.

The issues of measurement frequency (undisturbed versus disturbed), temperature (RT versus 37 °C) and fluid (DW versus BCS + DW + SA) were examined (see Section 3.2.3 for details on the lubricant composition). There was no significant difference in fluid uptake between Tests 1 and 2 ($p = 0.064$, Student's t-test) (Fig. 5.1). Interestingly, repeatedly disturbing the inserts in Test 3 increased the mass gain by 116 % compared with Test 2 ($p \leq 0.001$, Student's t-test) over the same soak period.

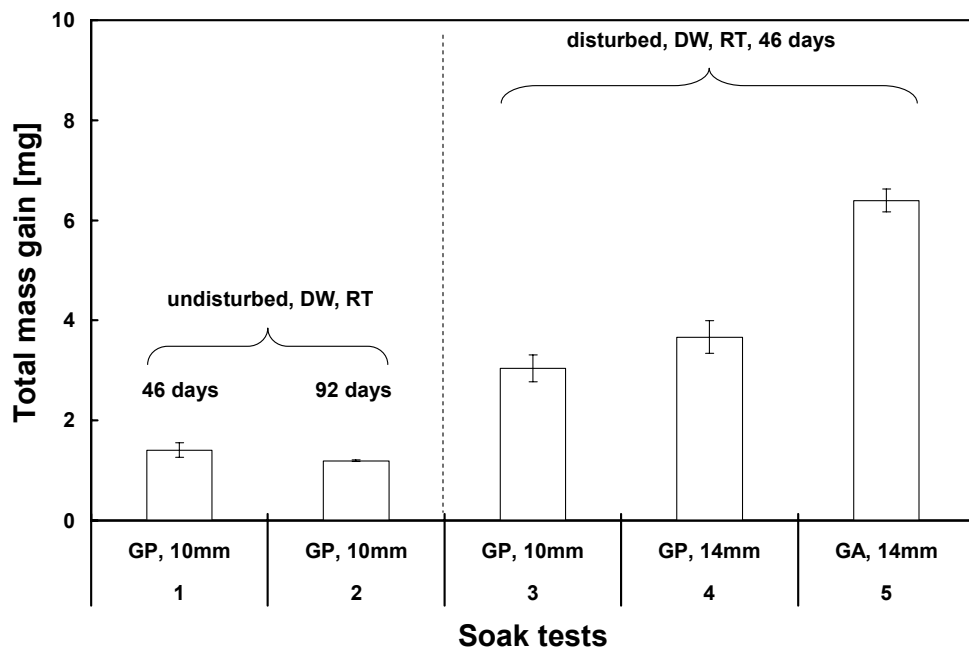


Figure 5.1: The fluid uptake of PE inserts soaking in DW at RT. Note the increased fluid uptake for the disturbed inserts over the undisturbed inserts and GA inserts over GP inserts.

Increasing the insert thickness from 10 mm to 14 mm (Test 3 versus Test 4) resulted in a slightly higher mass gain for the thicker insert but this was not significant ($p = 0.063$, Student's t-test). GA sterilized PE inserts gained significantly more mass than GP sterilized inserts, as shown in Test 4 and Test 5 ($p \leq 0.001$, Student's t-test). Also, the mass gain for the GP inserts appeared to approach steady-state after 46 days while the mass gain for the GA inserts

continued (Fig. 5.2). When considering the fluid uptake versus time behaviour of the inserts of Test 3 - 5, it was observed that the fluid uptake increased uniformly except for 3 distinct intervals in which fluid uptake decreased. According to the records, these intervals corresponded to a drop in RT from 25 °C to 21 °C caused by an electrical power surge disturbing the temperature control of the laboratory. This finding suggested that the fluid uptake of the PE inserts was sensitive to changes in temperature.

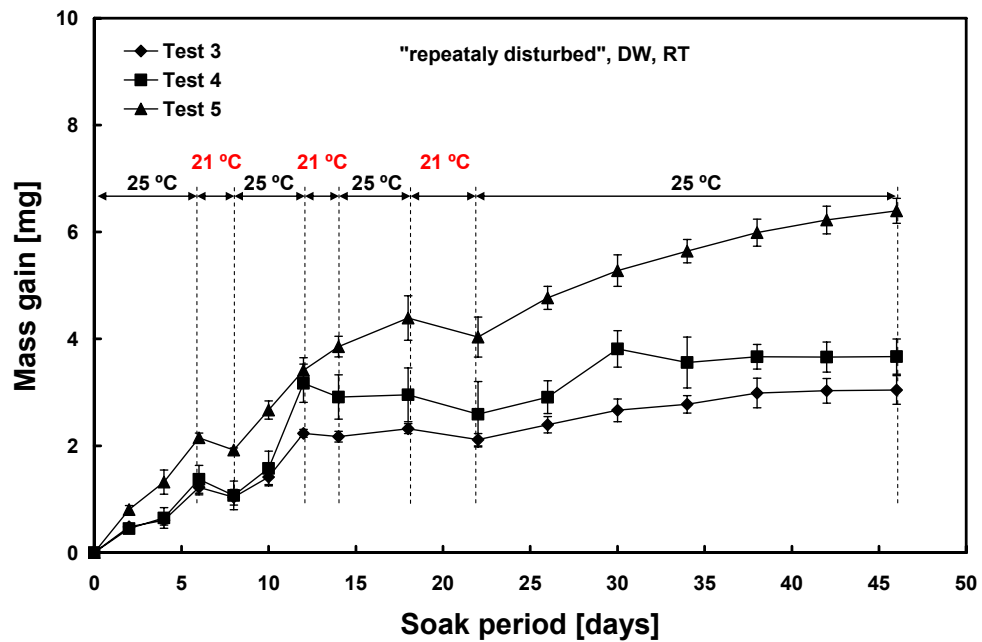


Figure 5.2: The mass gain of PE inserts submersed in DW at RT. The RT dropped from 25 °C to 21 °C three times during the 46 days and this drop was associated with some temporary mass loss. The changes in RT occurred during power surges in the laboratory.

Tests 6 - 11 involved immersing 14 mm thick, GP sterilized inserts for 46 days in either in DW or BCS lubricant (Table 3.8, Chapter 3) at either RT or 37 °C and performing frequent (disturbed) or infrequent (undisturbed) mass loss measurements (Table 5.1). The inserts showed various changes in their fluid uptake (Fig. 5.3). The reason for the change in fluid uptake for the BCS

lubricant fluid might be related to the addition of proteins and solved ions that are expressed in the osmolality. There was a statistically significant difference between the infrequently measured (undisturbed) fluid uptake for Test 6 using DW and Test 7 using the BCS lubricant at RT ($p = 0.044$, Student's t-test). Increasing the soak temperature from RT to 37 °C showed a significant increase for Test 9 using the BCS lubricant compared with Test 8 using DW ($p = 0.036$, Student's t-test). Similar behaviour was observed when the measurement frequency was increased (disturbed) in Test 11 and Test 10 ($p = 0.005$, Student's t-test). In all cases, the mass gain was significantly higher for inserts that were repeatedly disturbed during the soak period of 46 days, independent of the soak medium ($p \leq 0.001$, ANOVA and Fisher's).

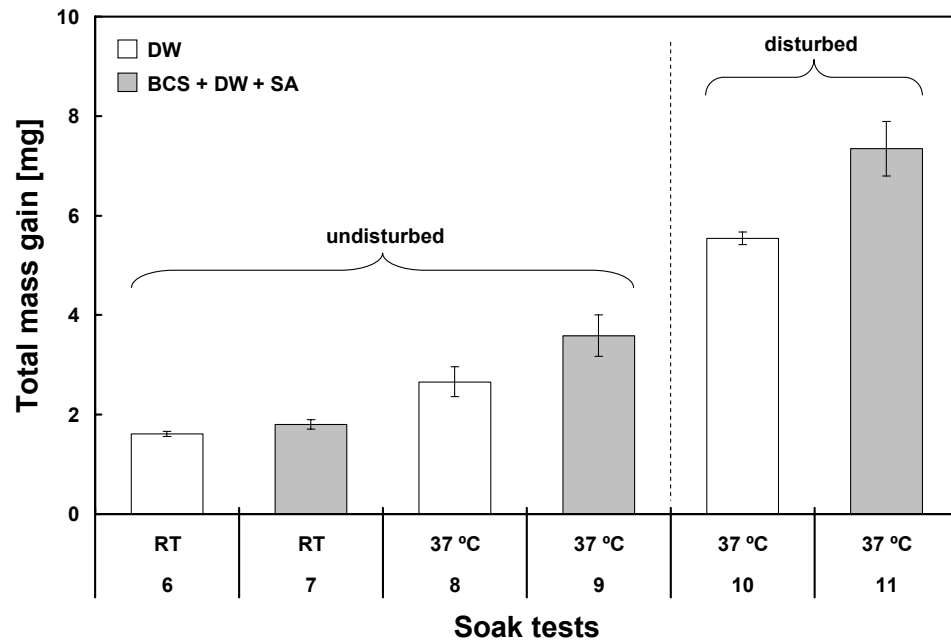


Figure 5.3: The mass gain of PE inserts submersed in DW and in the BCS lubricant at RT and 37 ± 2 °C of GP, 14 mm insert. The inserts were either left undisturbed or were repeatedly disturbed for 46 days. Note the increased mass gain for PE inserts subjected to the BCS lubricant, increased temperature and repeated disturbances.

5.2.3 Discussion of Soak Testing

All PE inserts gained mass during their specific soaking period. Increasing the soak period for the undisturbed inserts (Test 1 versus Test 2) from 46 days to 92 days did not affect the total mass gained. The insert possibly gained fluid more rapidly during the first 46 days and approached a soak-equilibrium after 92 days. Increasing the insert thickness from 10 mm to 14 mm (Test 3 and 4) increased the surface area, resulting in a higher mass gain (not significant). Thus, increasing the sample size per Test or using PE inserts with a thickness greater than 14 mm may have revealed a higher mass gain compared with the 10 mm thick inserts. However, increased mass gain for GA sterilized inserts over GP inserts was observed. Klapperich et al.²⁰¹ reported a higher mass gain for GA inserts over inert sterilized inserts which is in agreement with the present study. In addition, Nusbaum and Rose¹⁹⁹ reported a higher mass gain for irradiated PE samples than non-irradiated PE samples used for tensile strength tests. They suggested that the free radicals created during irradiation lead to an increase in carbonyl groups which may have made the PE more hydrophilic. Small temperature fluctuations affected the fluid uptake of the inserts during Tests 3, 4, and 5. Blanchet et al.⁷³ reported a 2-fold increase in mass for PE discs when the temperature of the medium was increased from RT to 37 °C and this was about the same as found in the present study. It was decided to pre-soak inserts at 37 °C since they would be exposed to this temperature when implanted and during wear testing.

Repeatedly disturbed PE inserts gained 2.2 times more mass than undisturbed inserts (Test 2 versus Test 3), despite the similar soak period. This suggests that repeated exposure of the inserts to the desiccation in the mass measuring protocol might have removed air inclusions in the insert surface layer and thus increased the porosity of the PE insert. This might be damaging and might influence the wear. Unfortunately, no universal consensus was reported in the literature regarding how frequently the PE inserts should be removed from the fluid during the pre-test soaking period. Schwenke et al.¹⁵⁷ repeatedly measured the mass gain of inserts until steady-state mass gain was reached. In

contrast, Yao et al.²⁰³ argued that pre-test soaking of the PE pins should not be performed since it significantly increased the wear in a pin-on-flat wear test and was not clinically realistic. Based on the present study, it was decided to subject the inserts to similar repeated disturbances during the pre-test soaking period as would occur during actual wear tests. Thus, fluid uptake would be measured about every 138 h (\equiv 0.5 Mc of a wear test interval) for at least 46 days until steady-state mass gain was achieved.

It still remained unclear why inserts submersed in DW (Test 6, Test 8, and Test 10) gained significantly less mass than inserts submersed in the BCS lubricant (Test 7, Test 9 and Test 11). Replacing DW with the BCS lubricant clearly increased the osmolality from 46.3 ± 2.08 mmol/kg for DW to 120.66 ± 1.15 mmol/kg for the BCS lubricant. The increase in osmolality was associated with an increase in ions and an introduction of proteins. Thus, it was uncertain if either the increase in ions or the presence of proteins was responsible for the increased mass gain. To explore this issue, an additional soak test on two groups of three GA inserts each was performed (LCS rotating platform PE inserts, GA sterilized; DePuy Orthopaedics, Warsaw, IN). Ideally, AMK[®] inserts should have been used but such inserts were no longer available since the model was discontinued in 2005. The inserts were submersed at 37 °C for 46 days in DW with an osmolality of 46 ± 2.08 mmol/kg and in PBS (no proteins) with an osmolality of 286 ± 0.57 mmol/kg (Fig. 5.4), which was similar to the test conditions of Test 8 and Test 9. There was no difference between the total mass increase of implants soaked in DW or PBS ($p = 0.302$, Student's t-test). Hence, the proteins may have been the driving force for increased mass gain and not the increased presence of ions. Such mass gain might be related to protein adsorption onto solid surfaces which in turn depended on the hydrophilic/hydrophobic surface characteristics, protein-protein interactions, protein-surface interactions, protein-solvent interactions, pH, ionic strength and consequently the conformational stability of the proteins^{160,162,163,434}. This finding was contrary to the pioneering study by Clarke et al.²⁰⁰ in which a higher mass gain was reported for inserts submersed in DW.

However, they used acetabular inserts manufactured from compression moulded PE, carbon-fibre reinforced PE and machined PE with calf serum diluted to only 50 % without EDTA and only 0.1 % SA. Clinically, the inserts are exposed to protein-rich body-fluids without weight bearing for some time after implantation which may allow some protein adsorption onto the surface. Thus, the inserts should be pre-soaked in the same fluid that would be used in the wear test. Nevertheless, it remained unknown if the pre-test soaking fluid would affect the PE wear behaviour during wear testing.

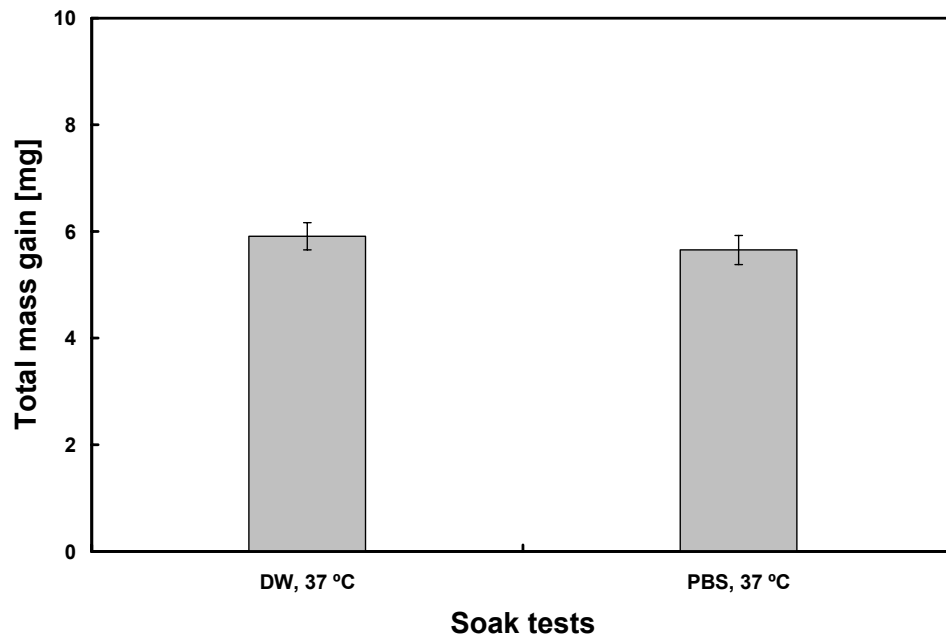


Figure 5.4: The total mass gain (fluid uptake) of GA inserts soaked in DW or PBS at 37 °C undisturbed for 46 days. There was no significantly different between groups despite the higher osmolality of PBS (286 ± 0.57 mmol/kg) compared with DW (46 ± 2.08 mmol/kg).

5.2.4 Concluding Remarks for Soak Testing

The soak tests showed that weight gain of the PE inserts was significantly influenced by the measurement frequency, temperature, sterilization technique and fluid composition. Thus, in wear testing, it was considered important that the soak controls have all these factors maintained the

same. In the measurement frequency influenced the fluid uptake. This suggested that the surface of the insert was physically altered by the act of measuring its mass and this might affect wear rates. The vacuum drying of the insert or desiccation was considered to be the likely cause of this change. While it might have been useful to explore a mass measurement protocol that involved less desiccation time and less powerful vacuum strengths, such explorations were beyond the scope of the present thesis. However, to ensure that the inserts were at steady-state saturation, pre-test soaking was done for at least 46 days with mass loss measurement every 138 h (\equiv 5 Mc) for all wear tests of the present thesis except the following commissioning wear tests.

5.2.5 Wear Testing

A total of 10 inserts (of 10 mm thickness) were soaked in DW and left undisturbed at RT for 92 days prior to wear testing to match the recommendations by DePuy. These inserts were used for a commissioning wear test that was conducted for 3 Mc. A complex commissioning protocol (CP) was developed (Table 5.2). All implants had their mass measured every 0.5 Mc. The implants for wear tests were named based on their initial placement at 0 Mc in the left bank of the knee wear simulator as L1, L2 and L3. Similarly, implants in the right bank were named R1, R2 and R3. The implants for load-soak tests were named L4 and L5 for the left bank and R4 and R5 for the right bank. All of the implants remained in their initial placement for the first test interval (0 - 1 Mc). After 1 Mc, the implants L1, L2, L3, L4, and L5 of the L bank were symmetrically “exchanged” with implants R1, R2, R3, R4, and R5 of the R bank for a second test interval (1 - 2 Mc). This second test interval was performed to assess possible differences in wear between banks. After 2 Mc, all the implants were returned to their initial positions. Then, the left bank implants were “rotated”, in that L1 was moved into station 2, L2 was moved into station 3, and L3 was moved into station 1 while L4 and L5 were simply exchanged. The right bank implants were also “rotated” in a similar manner.

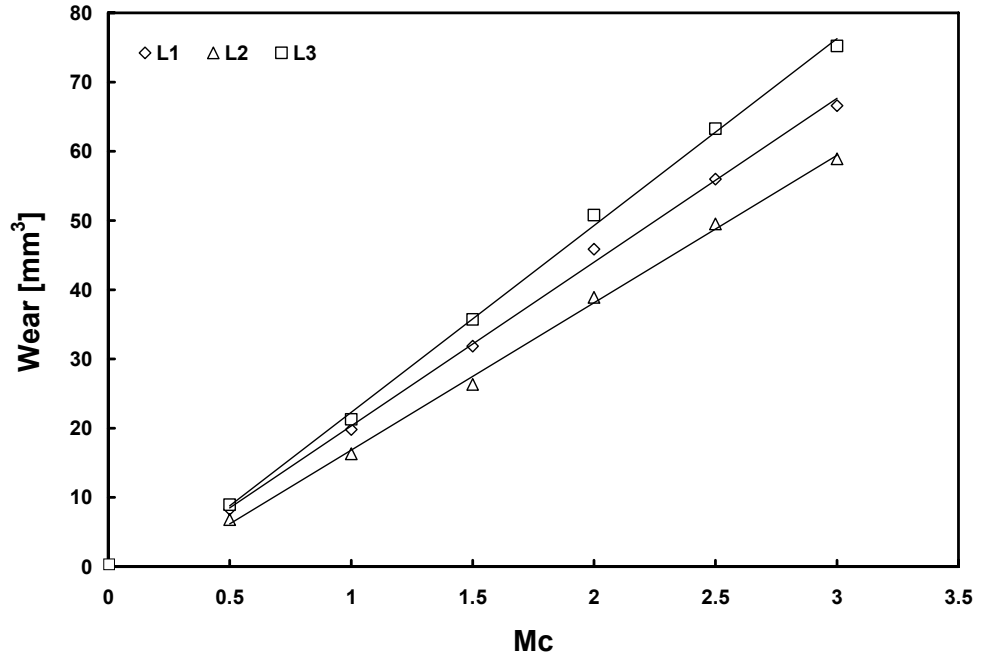
This third test interval (2 - 3 Mc) was performed to assess possible differences in wear between stations within a bank.

Table 5.2: Illustration of the commissioning protocol (CP) used in the knee wear simulator testing from 0 - 3 Mc.

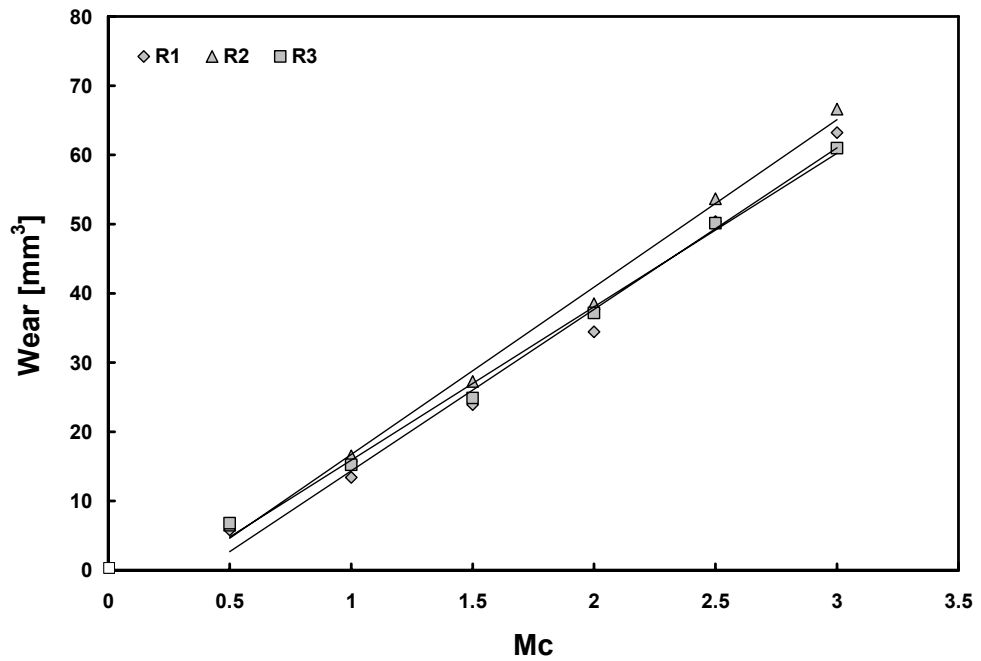
Test interval number	Test interval [Mc]	Knee Simulator									
		L bank					R bank				
		Wear stations			LS stations		Wear stations			LS stations	
		1	2	3	4	5	6	7	8	9	10
1	0 – 0.5	L1	L2	L3	L4	L5	R1	R2	R3	R4	R5
	0.5 – 1	L1	L2	L3	L4	L5	R1	R2	R3	R4	R5
2	1 – 1.5	R1	R2	R3	R4	R5	L1	L2	L3	L4	L5
	1.5 – 2	R1	R2	R3	R4	R5	L1	L2	L3	L4	L5
3	2 – 2.5	L3	L1	L2	L5	L4	R3	R1	R2	R5	R4
	2.5 – 3	L3	L1	L2	L5	L4	R3	R1	R2	R5	R4

There was no significant difference between the wear rates (slopes of the linear least squares curve fits of each implant) for the L implants ($23.98 \pm 2.85 \text{ mm}^3/\text{Mc}$) and R implants ($23.22 \pm 1.01 \text{ mm}^3/\text{Mc}$) from 0.5 - 3 Mc ($p = 0.686$, Student’s t-test). The total mean wear rate from 0.5 - 3 Mc for the L implants and R implants combined was $23.60 \pm 1.96 \text{ mm}^3/\text{Mc}$ (Fig. 5.5).

Symmetrical exchange of the L implants with the R implants between the L bank and the R bank at 1 Mc did not show a significantly different interval wear for the L implants or for the R implants ($p \geq 0.082$, ANOVA and Fisher’s) (Fig. 5.6). In contrast, the return of the L implants and R implants at 2 Mc to their original positions, combined with “rotation” among wear stations, did significantly affected the interval wear ($p \leq 0.036$, ANOVA and Fisher’s). The fluid uptake values for the load-soak L and R implants were only marginal affected by the alteration of the implant location and only had a small effect on the wear calculations in any case (Fig. 5.7).



(a) L implants



(b) R implants

Figure 5.5: The wear of (a) the L implants (L1, L2, and L3) and b) the R implants (R1, R2, and R3) during the commissioning protocol (CP) wear tests. The least squares linear-regression lines were fit through the wear data from 0.5 - 3 Mc. The interval from 0 - 0.5 Mc was regarded as the “run-in” phase.

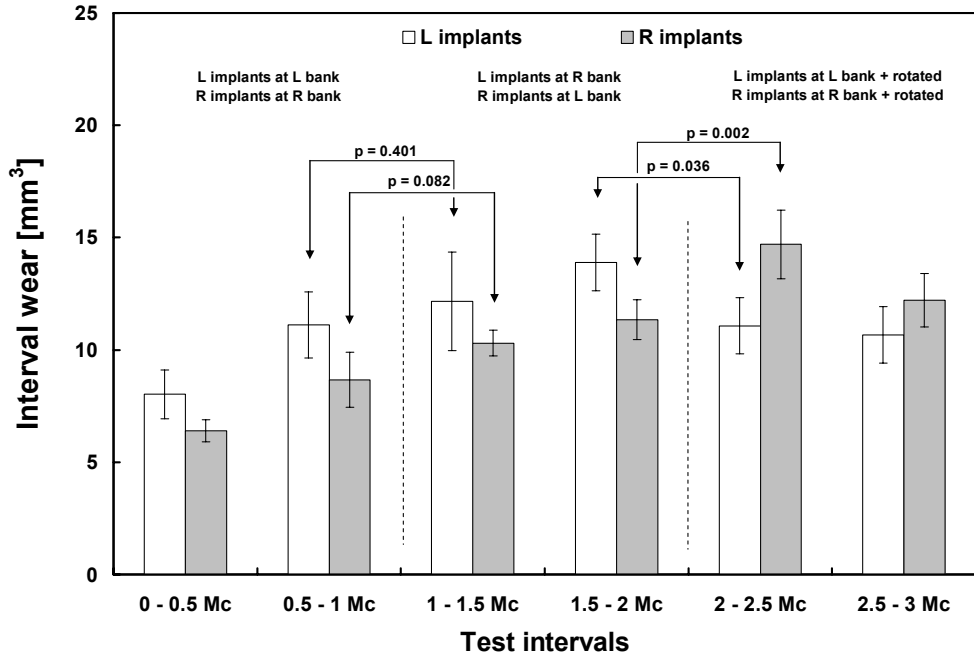


Figure 5.6: Interval wear volume of the L implants and the R implants during the 6 test intervals from 0 - 3 Mc. Note that the interval wear volumes of the L implants and R implants were significantly different between 1.5 - 2 Mc and 2 - 3 Mc ($p \leq 0.036$, ANOVA and Fisher's).

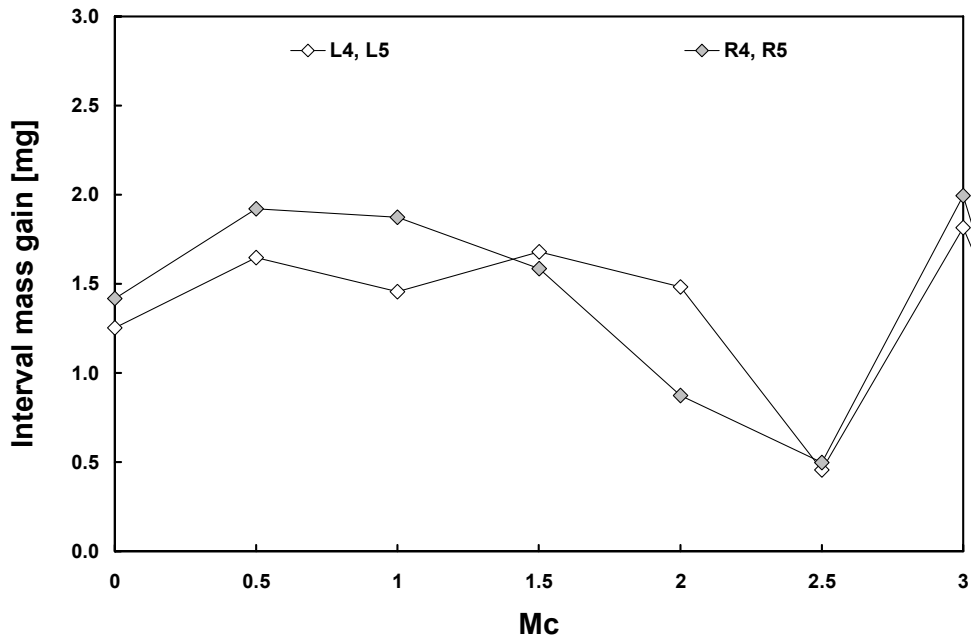


Figure 5.7: The average fluid uptake behaviour of the L4 and L5 implants and the R4 and R5 implants located in the LS stations (4 and 5; 9 and 10) from 0 - 3 Mc.

5.2.6 Discussion of Wear Testing

In the present commissioning wear tests, the implants were symmetrically exchanged between banks without a statistically significant difference in the interval but with $p = 0.082$ for the R implants there might actually be a difference that would emerge with more implant testing. However, when the implants were “rotated” between stations within a bank, the L implants had a statistically significant drop and the R implants had a statistically significant increase in interval wear. It would appear likely that there was a small difference from bank-to-bank and a somewhat larger difference from station-to-station with sometimes higher and sometimes lower wear. It was not clear whether implants should be kept in the same stations throughout a wear test or periodically shifted to be the most clinically realistic. However, the wear versus Mc data values of Fig. 5.5 did not show any drastic effects of changing banks or stations, it might be concluded that either changing or not changing stations would be acceptable.

To provide a check on the protocols of the wear testing of the present study, a comparison was made with similar wear testing performed by DePuy Orthopaedics Inc., Warsaw, IN. The DePuy wear rate⁴⁵ was determined using 3 implants in one bank of an AMTI knee wear simulator in a test interval from 3 - 5 Mc. The loads and motions imposed in the DePuy testing were essentially the same as those imposed in the present study. The DePuy implants had been first tested with 90 % BCS + DW + SA (~ 61 g/l total protein concentration) from 0 - 3 Mc and then tested with 25 % BCS + DW + SA (~ 17 g/l total protein concentration) from 3 - 5 Mc. Since wear is considered a cascading process, the 0 - 3 Mc history of the DePuy implants might have influenced the wear from 3 - 5 Mc and compromised the comparison with the results of the present study. Their implants were “rotated” among the stations within the bank every 0.5 Mc such that each implant moved to a higher number station except the implant in station 3 that moved back to station 1. Two load-soak implants were also run and every 0.5 Mc they were switched in position. At 3 Mc, each of DePuy’s 3 wear test implants had run in each station for a total of 1 Mc. In this manner,

DePuy avoided having to consider any station-to-station variation because each implant had been subjected to wear in each station. However, they had slightly changing wear patterns of their implants each time they changed the station in a manner that might, or might not, be a good representation of clinical wear patterns. A single patient would impose fairly specific load and motion conditions on an implant but they would be much more varied than those found in the wear simulator testing of both DePuy and the present study that followed ISO standards.

To compare the present wear rates with those of DePuy⁴⁵ presented a difficult problem. Since bank-to-bank variations were small, it was decided to calculate individual wear rates for the L implants and for the R implants from 0.5 - 2 Mc and from 2 - 3 Mc (Fig. 5.8) and to compare these rates to the wear rate of $30.80 \pm 1.97 \text{ mm}^3/\text{Mc}$ found by DePuy.

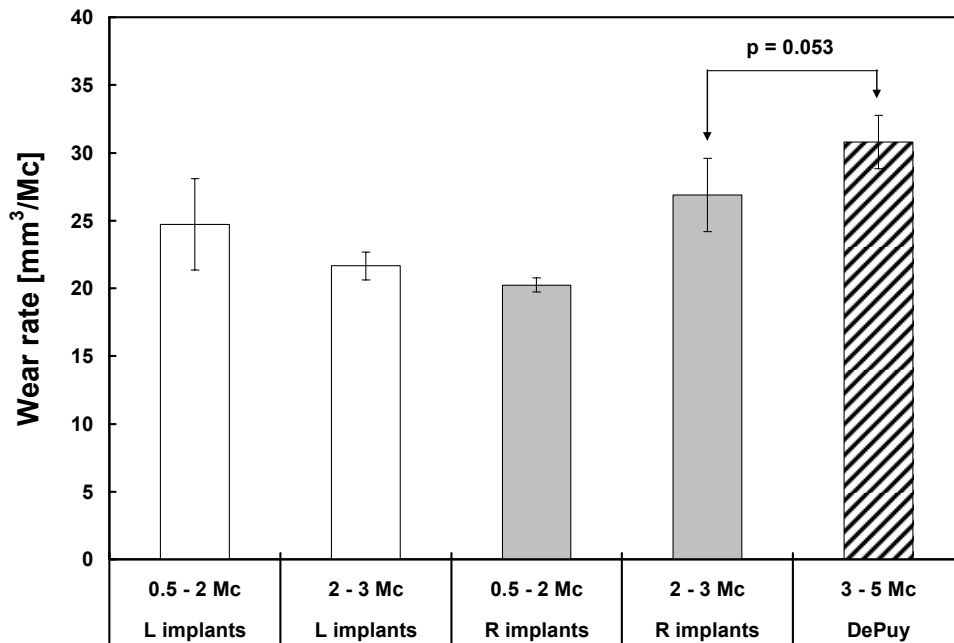
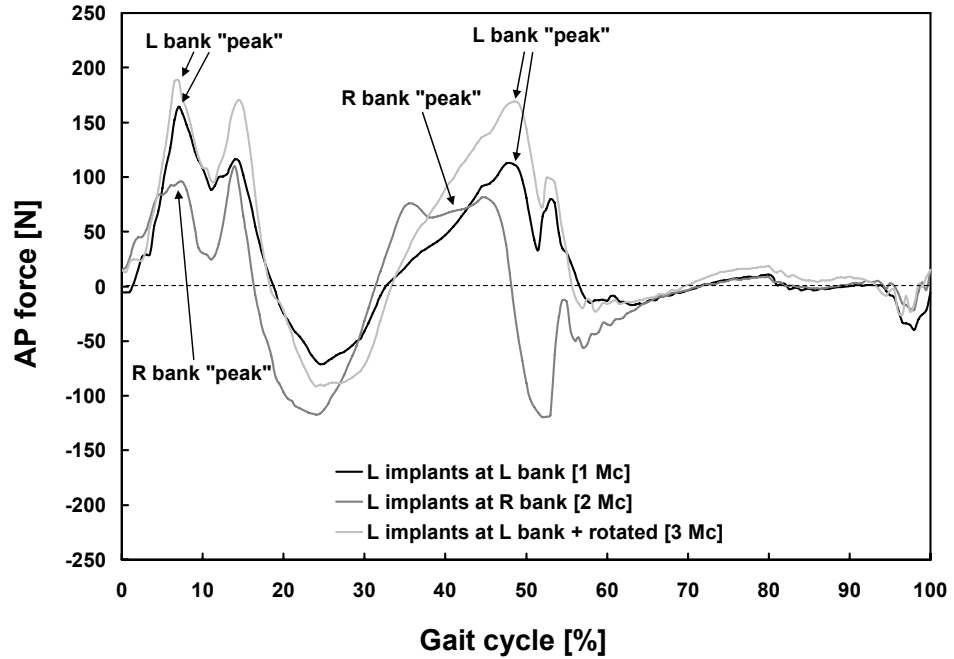


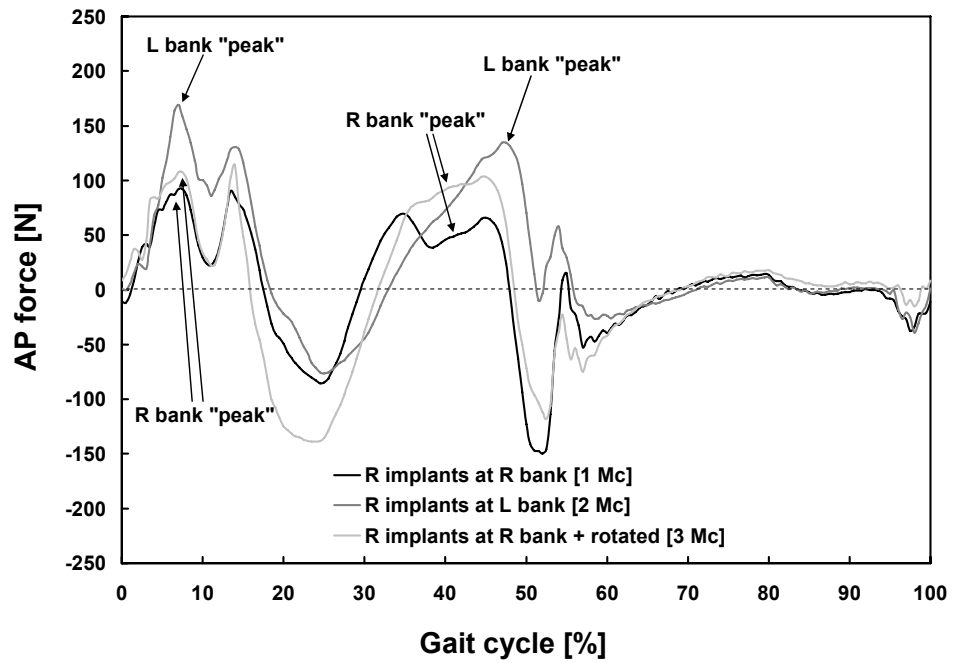
Figure 5.8: Illustration of wear rates obtained with the commissioning protocol (CP) and the wear rate found by DePuy in a 3 - 5 Mc interval for AMK[®] implants (GP, 10mm, GUR 1050). There was no significant difference between the wear rate of the R implants from 2 - 3 Mc and the DePuy wear rate ($p = 0.053$, ANOVA and Fisher's).

In the present study, the mean wear rate for the L implants *decreased* significantly from $24.72 \pm 3.36 \text{ mm}^3/\text{Mc}$ to $21.64 \pm 0.53 \text{ mm}^3/\text{Mc}$ when going from the interval of 0.5 - 2 Mc to the interval of 2 - 3 Mc ($p = 0.115$, ANOVA and Fisher's). Conversely, the wear rate for the R implants *increased* significantly from $20.25 \pm 1.03 \text{ mm}^3/\text{Mc}$ to $26.88 \pm 2.70 \text{ mm}^3/\text{Mc}$ when going from the interval of 0.5 - 2 Mc to the interval of 2 - 3 Mc ($p = 0.004$, ANOVA and Fisher's). The wear rates for the L implants in the interval of 0.5 - 2 Mc, the L implants in the interval of 2 - 3 Mc and the R implants in the interval of 0.5 - 2 Mc were significantly lower than the DePuy wear rate ($p \leq 0.007$, ANOVA and Fisher's). However, the wear rate of the R implants from 2 - 3 Mc was not statistically significantly different from the DePuy wear rate ($p = 0.053$, ANOVA and Fisher's).

To explore the differences between the stations, the loads and motions in the AP direction were recorded. The tangential force in the AP direction (AP force) of the L and R implants was compared at 1, 2 and 3 Mc (Fig. 5.9). The "peaks" of the AP force were higher in the L bank than in the R bank at similar points in the gait cycle and this behaviour was not influenced by exchanging the implants between banks. This suggested that the L bank and the R bank expose the implants to slightly different kinematics which could affect the wear rate. Such suggestions were confirmed when the vertical load FB of the L bank and the R bank were assessed (Fig. 5.10).



(a) L implants



(b) R implants

Figure 5.9: The AP force for (a) the L implants and (b) the R implants at test intervals of 1 Mc, 2 Mc, and 3 Mc.

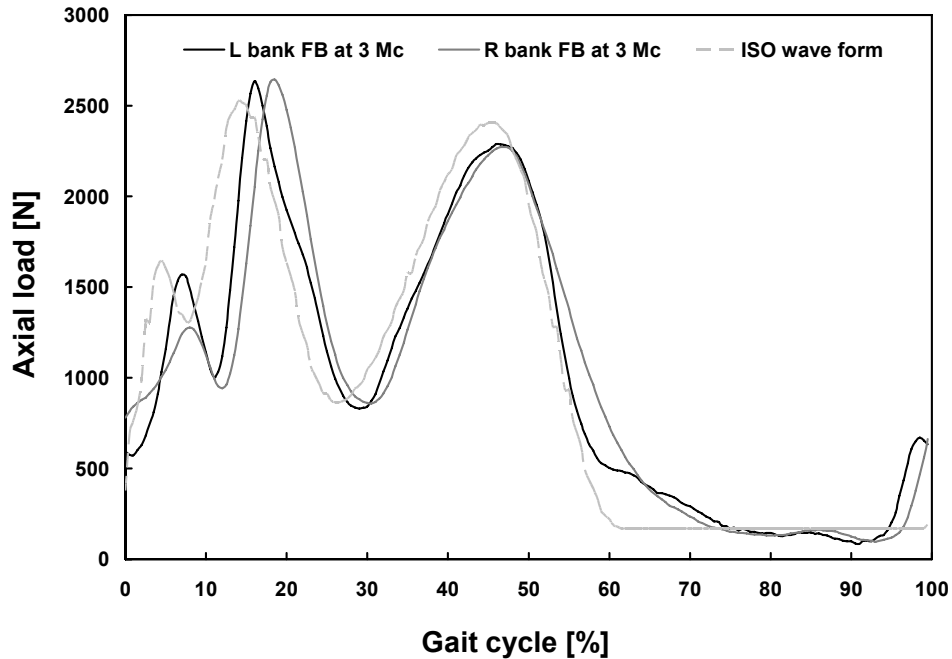


Figure 5.10: The vertical load FB of the L bank and the R bank at 3 Mc in reference to the vertical load waveform recommended by ISO. Note the distinct differences in vertical load between banks at approximately 8 % of the gait cycle.

5.2.7 Concluding Remarks on Wear Testing

Some overall concluding remarks on wear testing were formulated. The changes from bank-to-bank and station-to-station were essentially quite small. The total mean wear rate of the commissioning wear test was 22 % lower than those found by DePuy. Thus, it was considered likely that the present operation of the wear simulator and the mass measurements were equivalent to those of DePuy. One explanation for the lower wear rates of the present study was the reduced effect of a symmetric exchange of implants from bank-to-bank compared with station-to-station rotation. While the progressive changing of stations as performed by DePuy might, or might not, produce more clinically realistic wear rates, it was decided, in the present thesis, to keep implants at the same station throughout wear testing (thus avoiding changes in wear patterns caused by slight changes in loads and kinematics of the banks and stations) and to treat the L and R banks as essentially independent simulators

thus allowing the author to put sets of 3 implants with the same lubricant in each bank. In this manner, the wear behaviour for a number of different lubricating fluids could be explored in a fairly rigorous yet timely fashion and could be compared with each other.

5.2.8 Biochemical Testing of the Lubricating Fluid

The last test interval of the CP from 2.5 - 3 Mc was chosen to assess the damage behaviour of the BCS lubricant. Such an assessment included some biochemical analyses (see Section 3.4 for details) that were deemed important to identify some lubricant related factors that may play a role in the PE wear process. BCS lubricant samples were collected after the SM was prepared prior to wear testing and after the wear tests from each of the wear stations. The protein concentration of the SM of the BCS lubricant samples was 20.74 ± 0.82 g/l at the beginning of the test interval from 2.5 - 3 Mc and this value closely matched the ISO recommendations⁴¹. The BCS lubricant changed its appearance from being translucent at the start of the test (SM) to an opaque appearance after 0.5 Mc. This suggested that some proteins may have been precipitated during the wear tests. The serum samples collected from each wear station were centrifuged to obtain the precipitate-free SUP. The SUP and the SM were then used to calculate the protein degradation in each wear station. The protein degradation for the L implants was 31.21 ± 3.72 % and 29.85 ± 4.12 % for the R implants (Fig. 5.11). The total mean protein degradation for all implants was 30.53 ± 3.96 %.

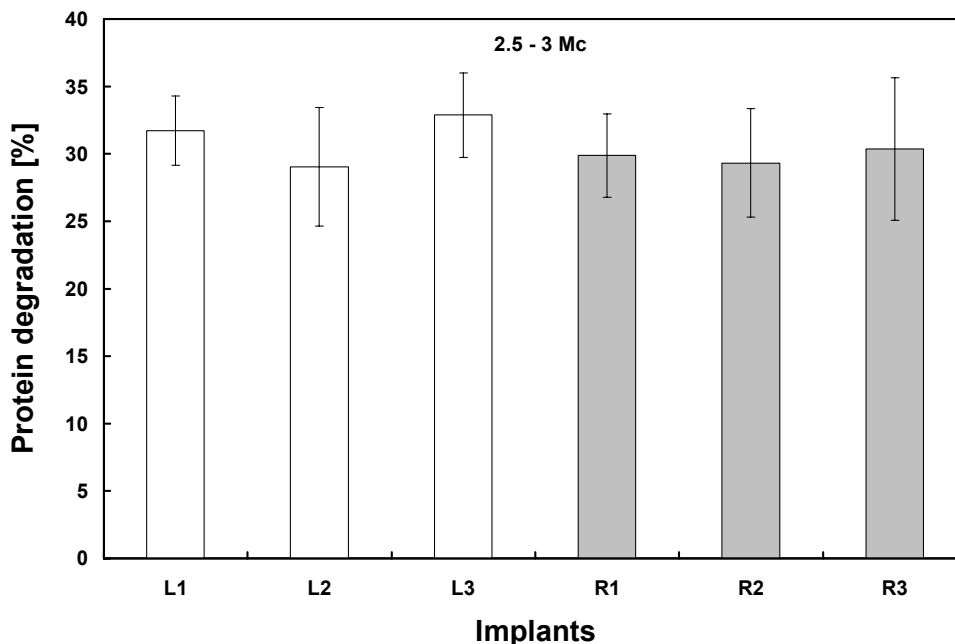


Figure 5.11: The protein degradation determined for each implant (L1, L2, L3, R1, R2, and R3) after the test interval of 2.5 - 3 Mc.

The SUP from each wear station was further used to investigate if sheared proteins that were not affected by precipitation remained suspended as peptides in the BCS lubricant. Peptides are fragments of proteins that can be measured using ultrafiltration methods, as described in Section 3.5.3. The SM and SUP for both the L implants and R implants were filtered through an ultra fine membrane (MWCO = 2,000 Da). Peptides that passed through the filter were further analyzed via BCA assay to determine their remaining concentration. Peptides were observed in all filtered BCS lubricant samples (Fig. 5.12). The mean peptide concentration in the SUP for the L implants was 0.138 ± 0.011 g/l and 0.124 ± 0.009 g/l for the R implants. The mean peptide concentration of the SUPs combined for the L and R implants was 0.131 ± 0.012 g/l, which was 3.3 times greater than the mean peptide concentration for the SM of 0.039 ± 0.004 g/l.

At disassembly of the implants from the simulator, it was generally recognized that some of the precipitates had settled that led to precipitate

deposits. A major precipitate deposit was found on the bottom of all six external fluid containers after each test interval of 0.5 Mc. Such deposits were approximately 5 - 10 mm in thickness. Precipitate deposits were only rarely observed in the wear station and when they were the location was usually on the circumference of the tibial tray fixture below the articulating tibial surface of the PE insert. A schematic of such precipitation occurring after each test interval is illustrated in Fig. 5.13. To compare the protein precipitate concentration in the wear station and the external fluid container, BCS lubricant samples were collected immediately at the end of the wear test of the 2.5 - 3 Mc test interval from both locations. At the end of the wear test interval, the peristaltic pump that circulated the lubricant was stopped. The external fluid container was disconnected from the circulating system and agitated to suspend the deposit. Lubricant samples were then obtained from both the wear station and the external fluid container. All samples were centrifuged to separate the precipitate from the BCS lubricant samples, which resulted in a compacted precipitate protein pellet and SUP for each wear station. The SUP was separated from the precipitate protein pellet so that the precipitate protein pellet could be further analyzed. The precipitate protein pellet was then re-suspended in a SDS-DTT solution (500 μ l). Samples were taken from this solution to determine the protein concentration with a BSA assay. The precipitate protein concentration in the external fluid container was found to be 2.6-times greater than the precipitate protein concentration that was circulated through the wear station for the L implants and the R implants (Fig. 5.14).

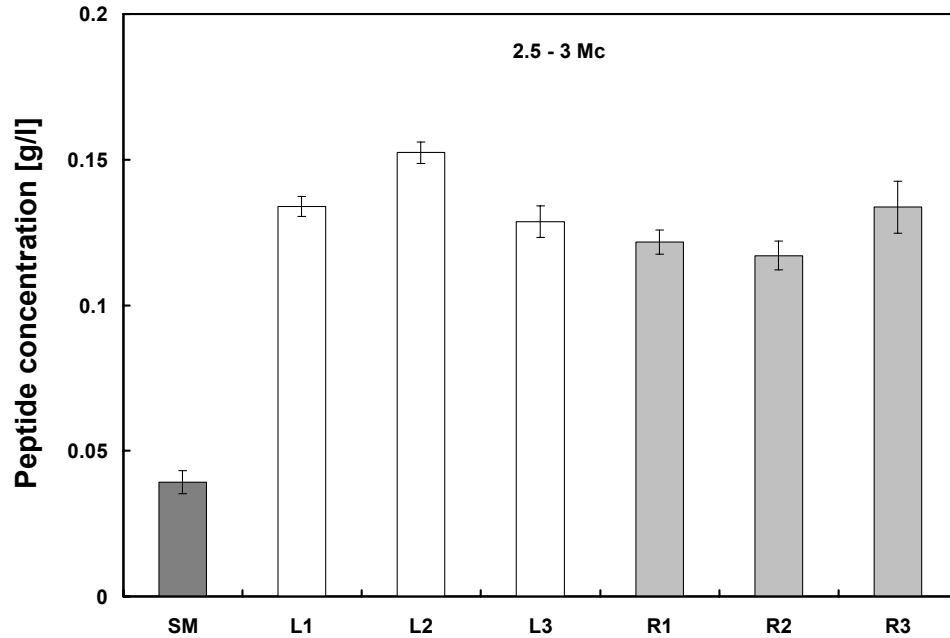


Figure 5.12: The peptide concentration of the starting material (SM) and implant-specific supernatant (SUP) for the BCS lubricant after a test interval of 2.5 - 3 Mc.

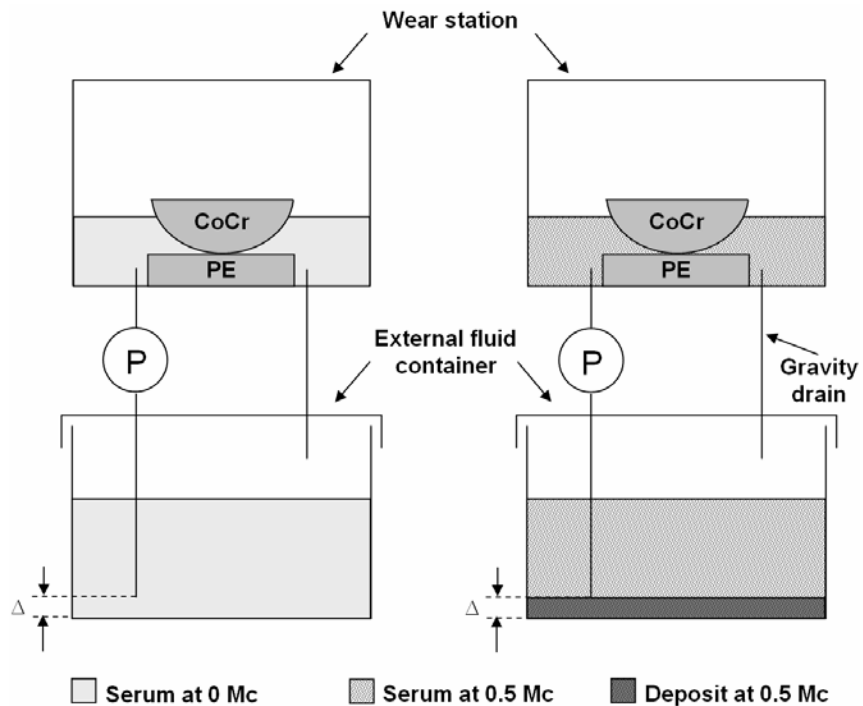


Figure 5.13: Schematic showing the settling out of protein precipitates in the BCS lubricant after 0.5 Mc compared with the BCS lubricant at 0 Mc. Such settling out of precipitated proteins led to obvious deposits in the each external fluid container after each test interval of 0.5 Mc. Note that the nozzle connected to the pump did not reach completely to the bottom of the fluid container.

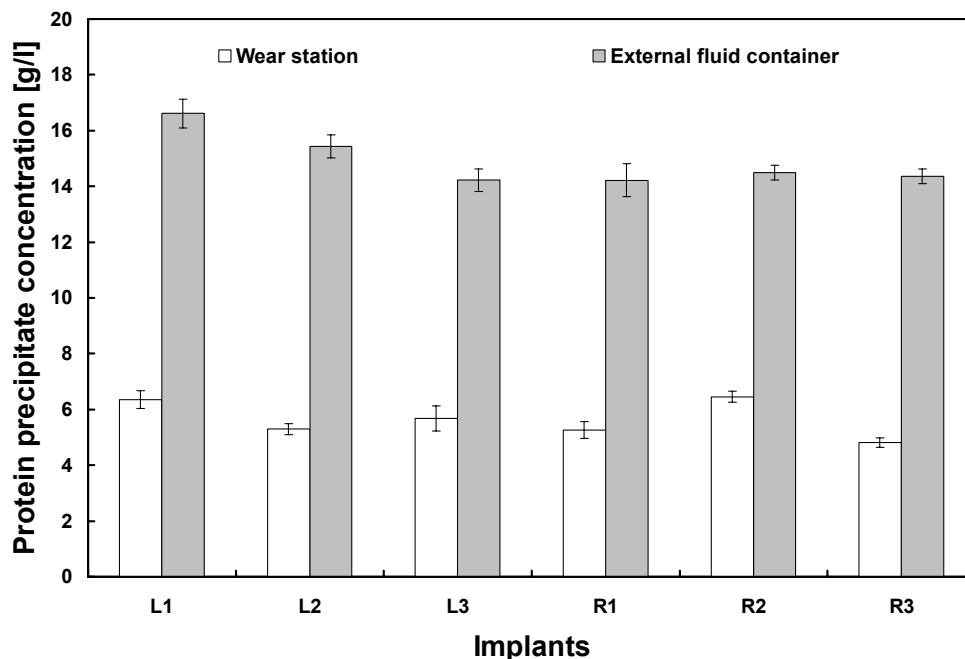


Figure 5.14: The protein precipitate concentration of the BCS lubricant samples obtained from the wear stations and the external fluid containers for the L implants and the R implants.

A distinct odor was recognized on the BCS lubricant samples after every the test interval of 0.5 Mc. Such an odor was not observed on any samples of the SM. This suggested that the air-inflated wear stations, in company with the protein degradation and 310 K test temperature may have enabled some bacterial growth. To confirm this suspicion, worn BCS lubricant samples were collected after 3 Mc, immediately placed onto LB agar and incubated for 18 h. Triplicate plates for each BCS lubricant indicated the same culture and thus one isolated organism was present. The specimen was then sent for identification to the Department of Microbiology at the University of Western Ontario, where an API[®]-film was used to identify the strain. The bacterium was highly motile and of a Gram-negative strain, identified as *Enterobacter* (genus) *Cloacae* (typos). The specific strain had to be named (JK-1; first initial of the author and of the colleague (K.K.E Mahmoud), since it was the only contaminant present in the test environment (Fig. 5.15).

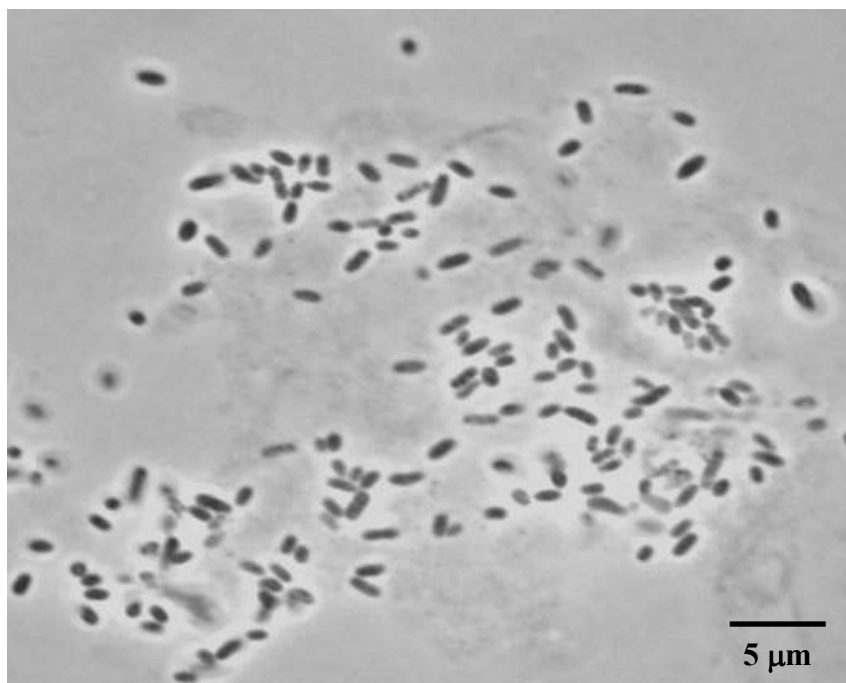


Figure 5.15: Micrograph showing the isolated bacterium *Enterobacter Cloacae* JK-1 (*E. cloacae* JK-1) present in the BCS lubricant after the test interval of 2.5 - 3 Mc.

5.2.9 Discussion of Biochemical Testing

The effect of protein concentration on wear has been considered in several hip simulator studies with either PE or PTFE as the bearing material^{35,37,155,156,165}. However, to the present author's knowledge, there were no studies that assess the effects of protein constituents using knee simulators. Liao et al.³⁵ investigated the effect of protein constituents on the wear of CoCr femoral heads and ceramic femoral heads articulating against acetabular PE inserts. They used a 12-station hip simulator with the implants in a non-anatomical position (cup-below-ball). The lubricating fluid chamber surrounding the implant was an open-system and filled with 40 ml of lubricant that was not circulated. The fluid loss due to evaporation was replenished with DW. They suggested that protein precipitates were trapped between the cup and the ball and acted as a solid lubricant thus reducing wear. A similar mechanism was suggested by Polineni et al.¹⁹⁶. There was concern in the

present study that some protein precipitates would have had a similar wear-reducing effect in total knee wear testing. As the wear in the test interval proceeds, it was considered likely that the sheared proteins cluster⁴³⁵, build aggregates and eventually precipitate which lead to deposits. Such phenomenon suggests that sheared proteins may behave similar to colloids. If sheared proteins behaved like colloids, their aggregation and sedimentation could be described with the diffusion-limited cluster aggregation model for colloids⁴³⁶. In this model, colloids traveled by diffusion and then clustered together to create aggregates that under the force of gravity fell down to produce a deposit. However, circulating the BCS lubricant through both the wear station and the external fluid container may have been beneficial by allowing protein precipitates to deposit preferably in the external fluid container. Such deposition of precipitated proteins may have prohibited the creation of a wear-reducing solid lubricant when a large lubricant volume of 500 ml was used. Although protein precipitation was considered clinically realistic, it was deemed unlikely that substantial protein precipitates deposits were formed at the CoCr-PE interface and affect the PE wear rate *in vivo* at relatively small volumes of SF. Interestingly, the total protein degradation for the BCS lubricant was close to the initial fractions of the β -globulins + γ -globulins protein fractions (32.6 %). It remained to be determined which specific protein constituents were precipitated and whether some protein constituents acted as a possible boundary lubricant.

Direct evidence was obtained that increased low-molecular-weight proteins after knee simulator wear testing remained suspended in the SUP after the wear process. The increased peptide concentration in the SUP of the BCS lubricant from all wear stations compared with that of the SM indicated that some specific proteins became denatured during the wear process and turned into peptides. The presence of peptides may suggest that certain protein constituents act as an active boundary lubricant, confirming studies conducted on a more fundamental tribological tests^{64,76}. If this is the case, the protein constituents and peptide concentration in the lubricant may be important to the

wear process because such peptides may adsorb to the bearing surfaces. In a series of seven additional tests, an attempt was made to find various factors (Table 5.3) besides the tribology of the implant contact responsible for increasing the peptide concentration in the BCS lubricant using ultrafiltration techniques (see Section 3.5.3 for details). All tests were conducted for 138 h to mimic a test interval of 0.5 Mc. All BCS lubricant samples were aseptically prepared. The BCS lubricant samples in Test 3, 5 and 6 were each mounted on the stations of the simulator. No bacterial growth was detected before and after those tests. The peptide concentration was the lowest for SM in Test 1 ($p \leq 0.001$, ANOVA and Tamhane) (Fig. 5.16). Circulating the BCS lubricant through the closed pipe circulation system of the knee simulator (Test 7) resulted in the highest peptide concentration for the tests ($p \leq 0.001$, ANOVA and Tamhane). This high peptide concentration was probably caused by the shear at the peristaltic pump-tube interface. Exposing the BCS lubricant to air at RT, in air at RT while shaking, in air at 37 °C, and shaking at 37 °C in a closed system and tube shear in a closed pump circuit all increased the peptide concentration (Tests 2 - 7). This behaviour might have been related to *proteolytic activity*⁴⁰¹ with the directed digestion of proteins by enzymes but further exploration was considered to be beyond the scope of the present thesis.

Table 5.3: Test protocol used in additional tests to find causes of peptide generation besides the tribology of the implant contact (BCS lubricant used in all tests).

Test	Protocol	Exposure to
1	- fresh BCS + DW + SA	- N/A
2	- RT - 138 h - open cap tubes	- air at RT
3	- RT - 138 h - open cap tubes - shaken under ISO I/E rotation	- air at RT while shaking
4	- 37 °C - 138 h - open cap tubes	- air at 37 °C
5	- 37 °C - 138 h - open-cap tubes - shaken under ISO I/E rotation	- air at 37 °C while shaking
6	- 37 °C - for 138 h - closed cap tubes - shaken under ISO I/E rotation	- shaking at 37 °C in a closed system
7	- RT - 138 h - closed-pipe system - circulated by the peristaltic pump	- tube shear in a closed pump circuit

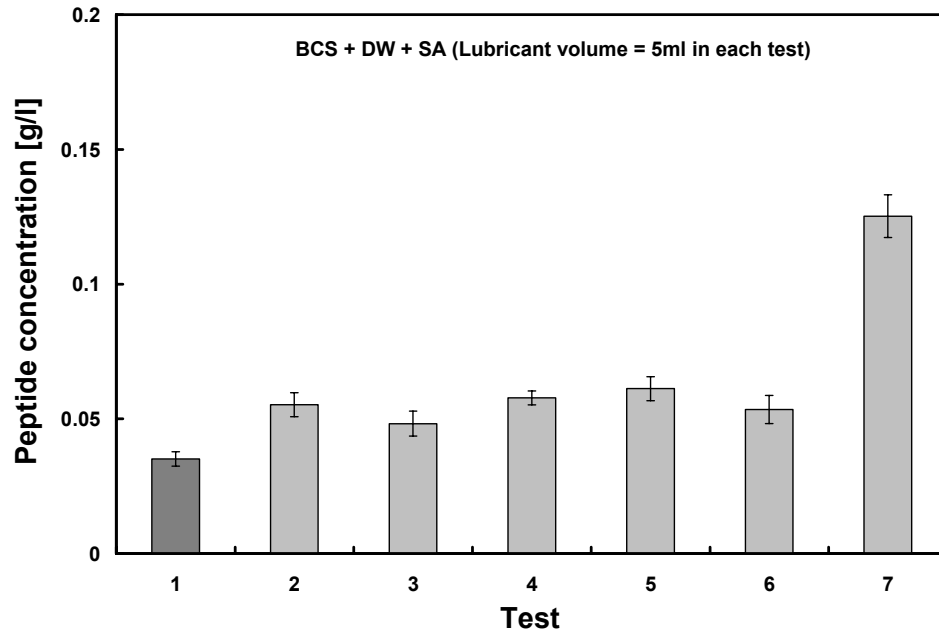


Figure 5.16: The peptide concentration of the BCS lubricant samples used in the additional tests described in Table 5.3. These tests were conducted to isolate sources that increased the peptide concentration besides the tribology of the implant contact.

The bacterial contamination despite the use of SA was a worrisome finding because such test conditions did not mimic the sterile environment found in the clinical application of TKRs. SA had been successfully used to inhibit a large number of microbes from growing on nutrient-rich Petri dishes, even after 48 h at 37 °C with a concentration of only 0.02 %^{437,438}. Therefore, it was surprising to observe bacterial growth in all of the wear stations after 3 Mc, despite the higher SA concentration of 0.2 %. It may have been possible that high concentrations of SA were ineffective after 48 h. It is suggested that some contamination was introduced by the air hoses used to inflate the IV bags in each station throughout each wear test interval. According to the manufacturer, the BCS is passed through a membrane with 0.45 µm porosity (United States Pharmacopeia XIII, Chapter 71). The filter was incubated for 14 days, continuously monitored and when no growth was found the BCS was declared negative for bacteria and fungi. Thus, serum contamination by the

manufacturer was deemed unlikely. Furthermore, incubating SM samples on LB agar did not show any bacterial growth even after 72 h. Some bacterial contamination might have remained on the customized fixtures (despite thorough cleaning) after they were exposed to metalworking fluids during the milling process than can contain *E. cloacae*⁴³⁹. Bell et al.³⁰ recognized bacterial growth in their pin-on-plate wear tests with SA, but did not isolate the type of bacterium. Therefore, using SA as a bio-control for implant wear testing was obviously inappropriate. Evaluating knee implants in presence of bacterial contamination was not considered clinically relevant and introduced the risk that the bacteria might influence the proteins which in turn might change the implant tribology. Alternative microbial inhibitors such as certain antibiotics were used in the past in knee wear simulators¹⁵⁷, but the possible effect on the PE wear rate had not been determined.

5.2.10 Concluding Remarks for Biochemical Testing

The protein degradation, precipitate protein concentration and peptide concentration should have been evaluated after every test interval of 0.5 Mc. In this manner, it might be possible to correlate wear with protein degradation and obtain information relevant to the boundary lubrication mechanisms acting in various knee simulator wear tests. Proteins seemed to play a role in the wear process by acting as boundary additives in the lubricating fluid. The total protein degradation may be considered as a function of both the precipitated protein concentration and the relative change in peptide concentration. The characteristics of the BCS + DW + SA changed during a test interval of 0.5 Mc as summarized in Fig. 5.17. Microbial contamination was not inhibited by SA and thus other means of bacterial control should be considered in subsequent wear testing.

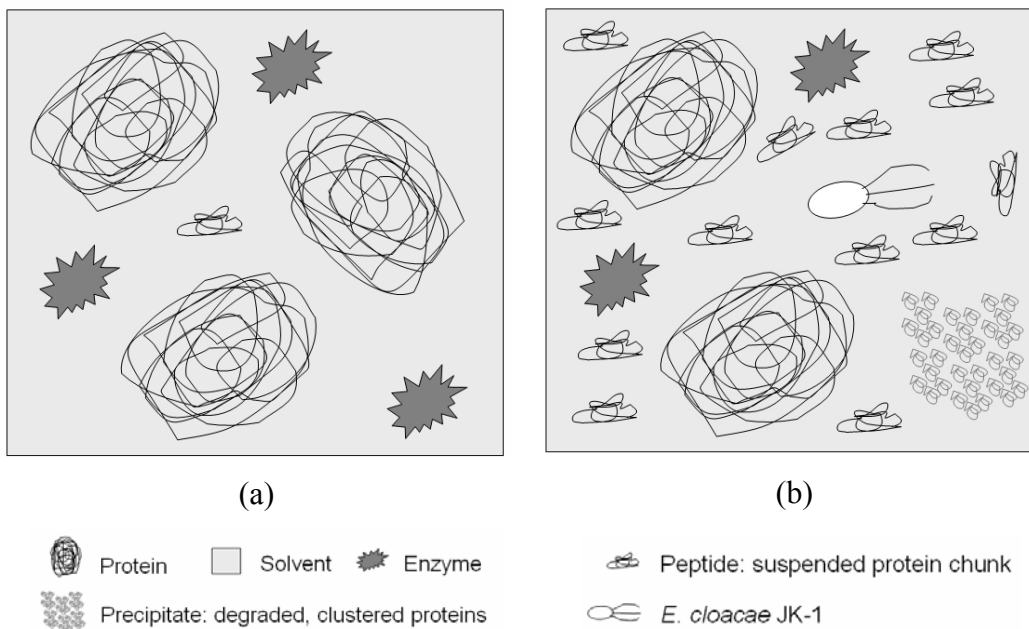


Figure 5.17: Schematic of the BCS lubricant at (a) 0 Mc and (b) after a test interval of 0.5 Mc. Note the presence of proteins, peptides and perhaps enzymes suspended in the fluid at 0 Mc. The characteristics of the BCS lubricant at 0.5 Mc were vastly different, showing precipitates (degraded, clustered proteins), more peptides (suspended protein chunks) and bacterial contamination (*E. cloacae* JK-1).

5.3 The Effects of Calf Sera on Wear, Protein Degradation, and Bacterial Growth

5.3.1 Introductory Remarks

After completing the clinical investigations and after successfully commissioning of the knee simulator, the effect of calf sera on PE wear was further explored. As shown in Table 3.7 of Section 3.3.2, the initial concentrations of the protein constituents were different for the various calf sera. In the present section, wear tests were performed on three calf sera that had been frequently used in wear simulations. These calf sera were diluted with DW and had SA added as the microbial inhibitor. Protein degradation, electrophoresis, peptide concentration, and bacterial growth were assessed during specific test intervals for the purpose of gaining insight into the possible boundary lubrication conditions.

In addition, a pilot study was conducted to examine the influence of AA compared with SA on protein degradation, peptide concentration and bacterial growth. The purpose of this pilot study was to gain insight into the wear process with and without microbial contamination to determine whether it was necessary to create a sterile environment in order to obtain clinically-relevant wear.

5.3.2 Wear

After the commissioning wear tests that were described in Section 5.2 had been conducted, the same implant components were tested for an additional 3 Mc, first in a new lubricant and then again in the original BCS lubricant, as indicated in Table 5.4. After the commissioning wear test, the implants were not switched between wear stations. The L implants were tested in the ACS lubricant for 1.5 Mc and then in the original BCS lubricant for another 1.5 Mc. Similarly, the R implants were tested in the NCS and then in the BCS lubricant. The volumetric wear of the individual L implants and individual R implants

from 0.5 - 6 Mc was determined (Fig. 5.18). Linear-regression analysis was performed to determine the wear rate for each implant.

Table 5.4: Test protocol from 0 - 6 Mc.

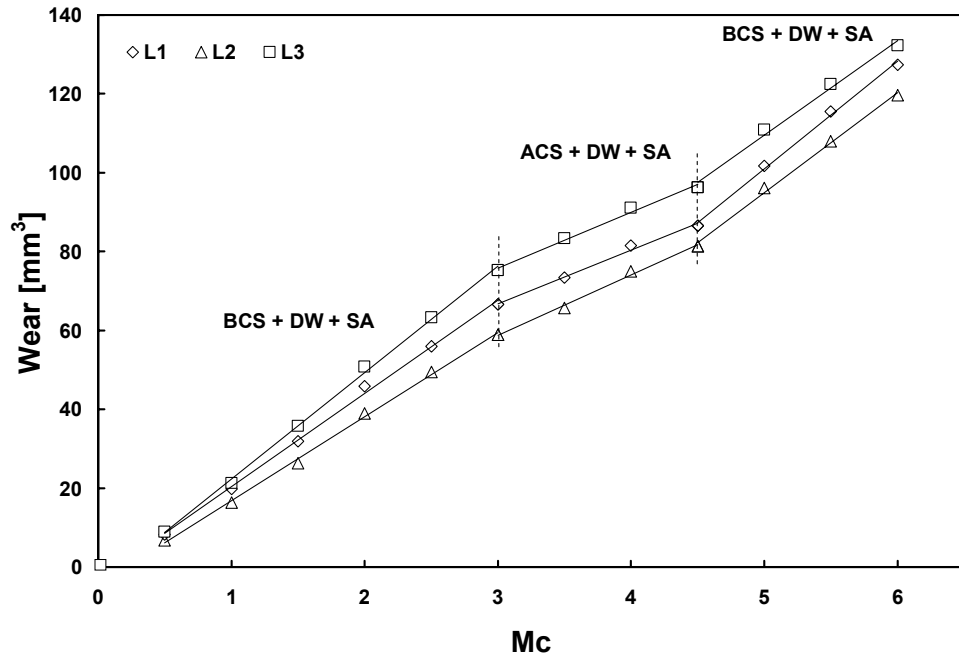
Mc	Lubricant	
	L implants	R implants
0 - 3	BCS + DW + SA	BCS + DW + SA
3 - 4.5	ACS + DW + SA	NCS + DW + SA
4.5 - 6	BCS + DW + SA	BCS + DW + SA

BCS = bovine calf serum; DW = distilled water; SA = sodium azide; ACS = alpha calf serum; NCS = newborn calf serum.

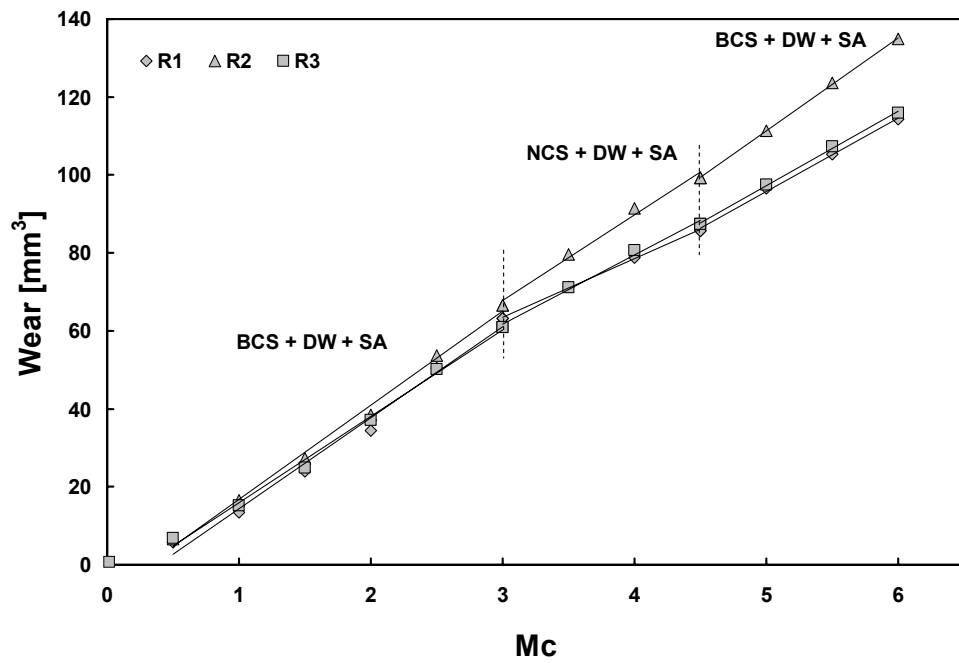
For the L implants (Fig. 19.a), the average wear rate of 23.98 ± 2.85 mm³/Mc for the BCS lubricant changed to a statistically significantly different lower average wear rate of 14.38 ± 0.85 mm³/Mc when the ACS lubricant was used ($p < 0.001$, GLM and Fisher's). When the lubricant was changed from the ACS back to the BCS, the average wear rate of 25.50 ± 1.66 mm³/Mc was not statistically significantly different from the average value that was found the first time using the BCS lubricant ($p = 0.377$, GLM and Fisher's).

For the R implants (Fig. 19.b), the average wear rate of 23.22 ± 1.01 mm³/Mc for the BCS lubricant changed to a statistically significantly different lower average wear rate of 18.23 ± 3.48 mm³/Mc for when the NCS lubricant was used ($p = 0.016$, GLM and Fisher's).

When the lubricant was changed from the NCS back to the BCS, the average wear rate of 20.59 ± 2.78 mm³/Mc was not statistically significantly different from the average value that was found the first time using the BCS lubricant ($p = 0.145$, GLM and Fisher's).

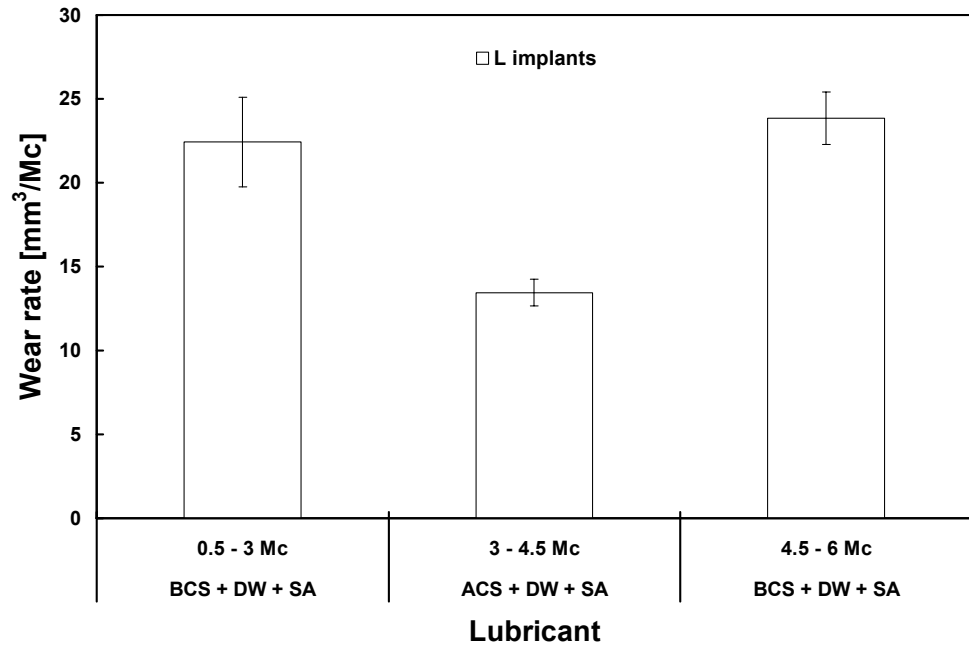


(a) L implants

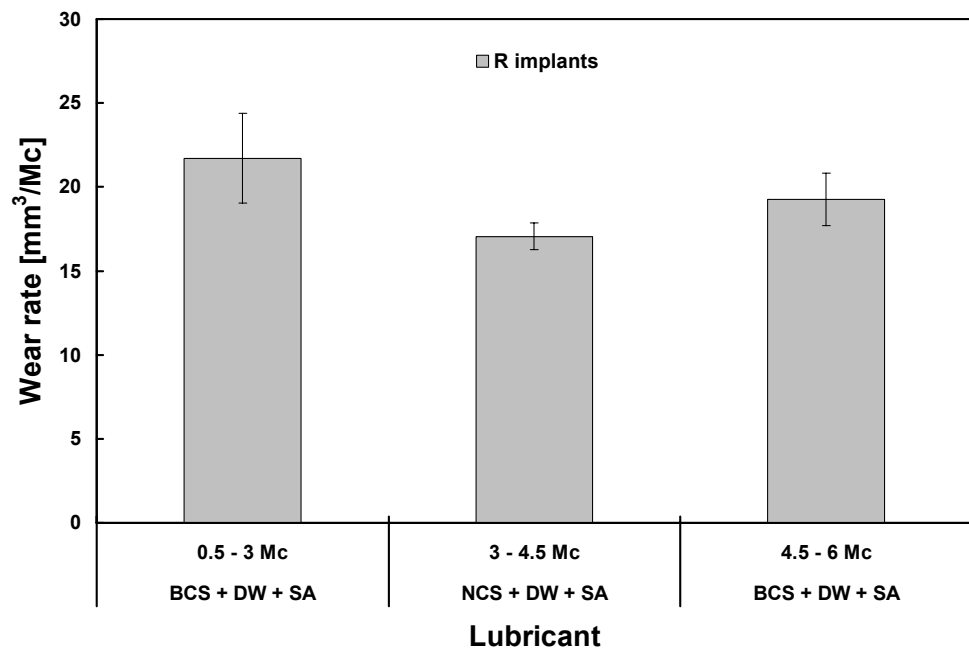


(b) R implants

Figure 5.18: The wear behaviour of the (a) L implants (L1, L2, L3) and (b) R implants (R1, R2, R3) during 0.5 - 6 Mc.



(a) L implants



(b) R implants

Figure 5.19: The wear rates of (a) the L implants and (b) the R implants obtained after the wear tests during 0.5 - 6 Mc.

Based on visual observations, the damage features on the top side surface of the PE inserts were burnishing, grooving, indentations and some striations. The backside PE surface showed large areas of burnishing accompanied by small amounts of grooving and indentations. Pitting and delamination were not seen at any stage of testing.

To determine whether the differences in the wear rates were related to individual or combinations of the initial serum components (Table 3.7, Section 3.3.2), a series of correlations were performed. The highest correlation coefficient ($R = 0.865$, $p < 0.001$, Spearman correlation) occurred when the wear rates were correlated with the combined albumin + α -globulin fraction (Fig. 5.20). This correlation suggested that a combination of these constituents may act as an effective boundary lubricant.

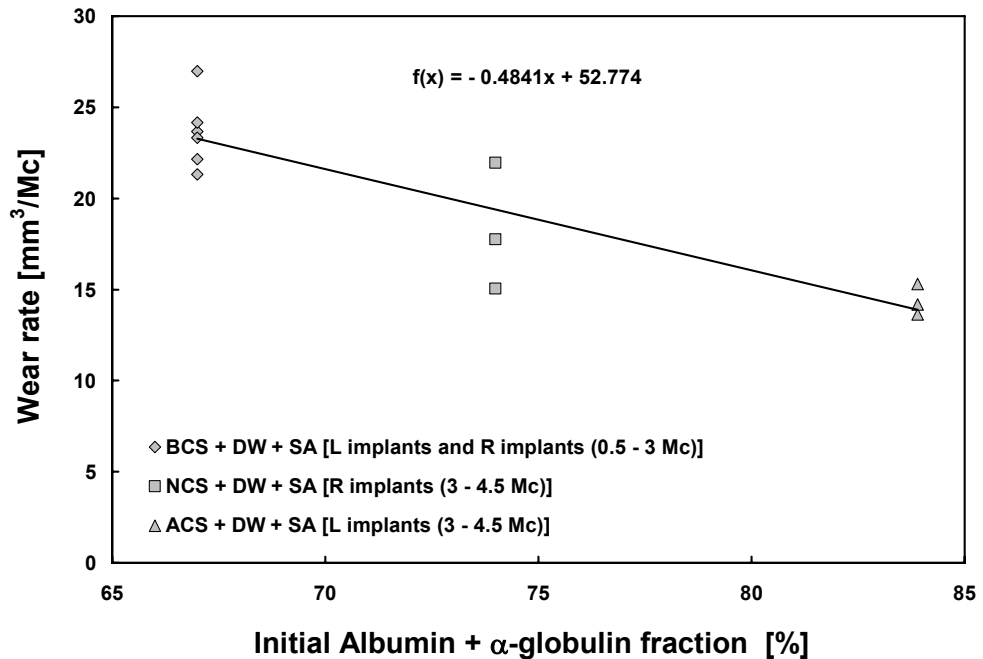


Figure 5.20: The correlation of wear rates with initial combined albumin + α -globulin fraction for the lubricants. Each data point represents the value obtained from a single wear test.

5.3.3 Protein Degradation

Section 5.2 indicated that the wear process led to significant protein degradation for the BCS lubricant. Hence, the protein degradation was evaluated for all three lubricants used in the present study. For the L implants (Fig. 5.21.a), the average protein degradation of 31.21 ± 3.72 % for the BCS lubricant changed to a statistically significantly lower average protein degradation of 7.77 ± 3.87 % when ACS lubricant was used ($p < 0.001$, GLM and Fisher's). When the lubricant was changed from the ACS lubricant back to the BCS lubricant, the average protein degradation of 32.22 ± 7.77 % was not statistically significantly different from the average value that was found the first time using the BCS lubricant ($p = 0.444$, GLM and Fisher's). For the R implants (Fig. 5.21.b), the average protein degradation of 29.85 ± 4.12 % for the BCS lubricant changed to a statistically significantly somewhat lower value of 25.14 ± 2.87 % when NCS lubricant was used ($p < 0.001$, GLM and Fisher's). When the lubricant was changed from the NCS lubricant back to the BCS lubricant, the average protein degradation of 29.53 ± 8.31 % was not statistically significantly different from the average value that was found the first time using the BCS lubricant ($p = 0.804$, GLM and Fisher's).

To determine whether the differences in the protein degradation were related to individual or combinations of the initial serum components (Table 3.7, Section 3.3.2), a series of correlations were performed. The highest correlation coefficient ($R = 0.836$, $p < 0.001$, Spearman) occurred when the protein degradation rates were correlated with the combined β -globulin + α -globulin fraction (Fig. 5.22). This correlation suggested that a combination of these protein constituents were the most susceptible to degradation.

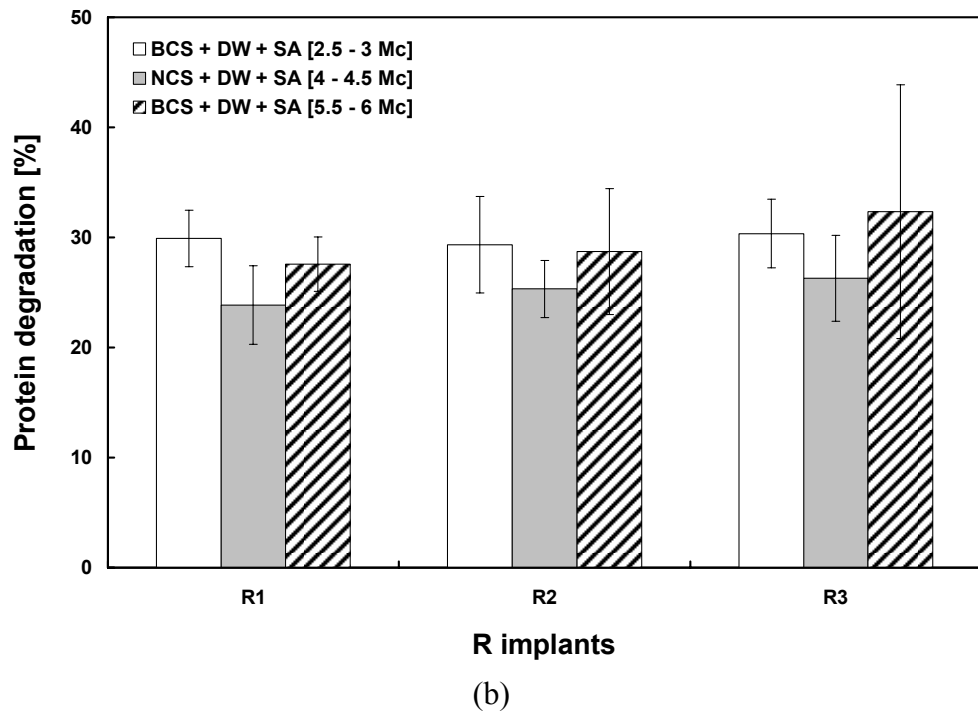
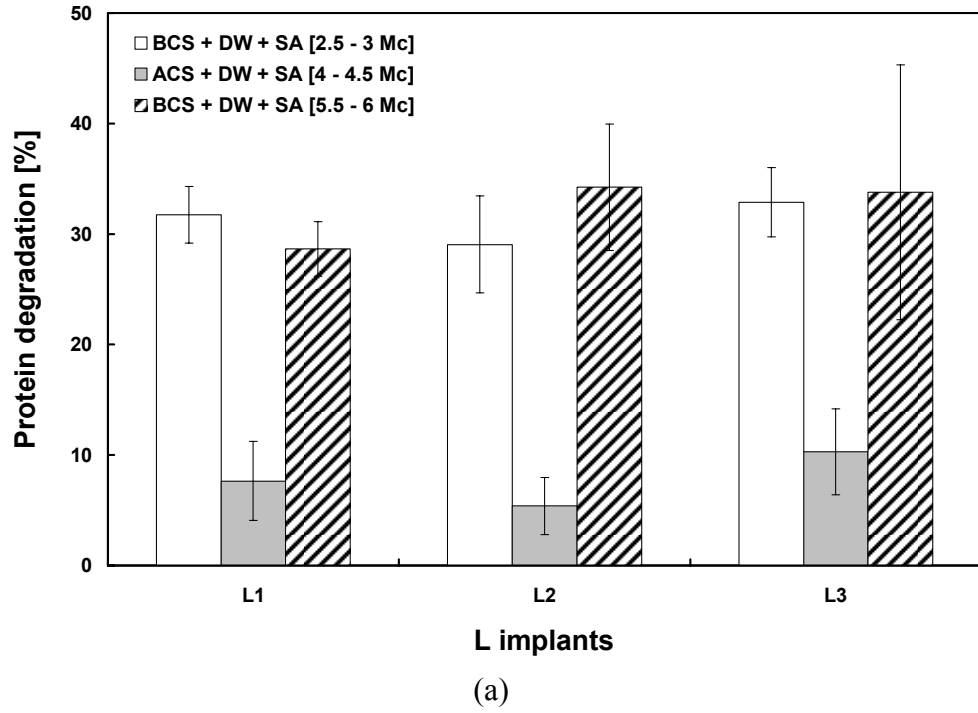


Figure 5.21: The protein degradation of (a) the L implants and (b) the R implants.

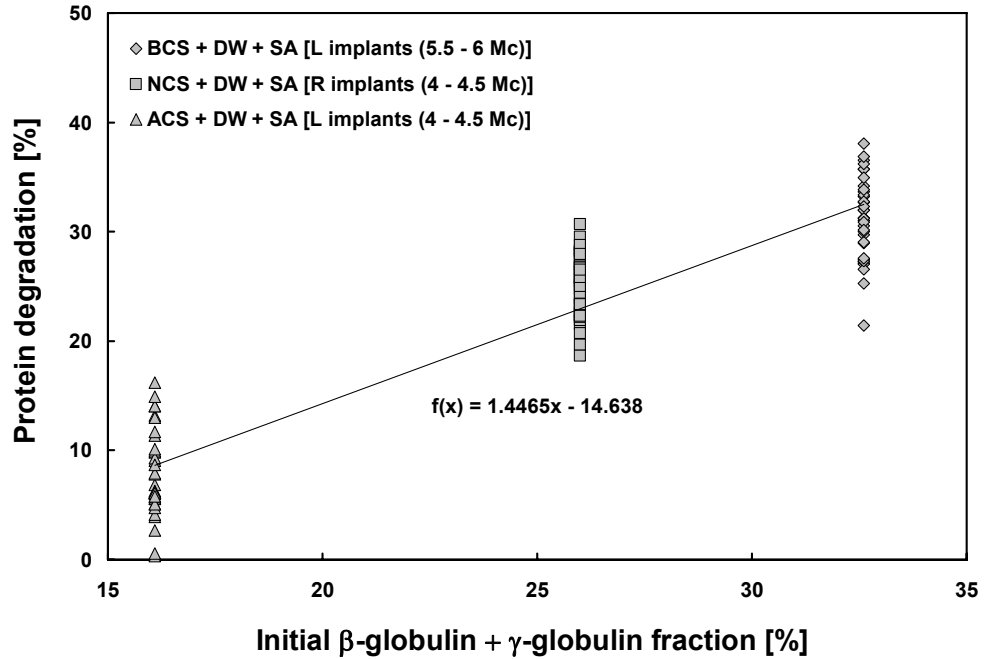
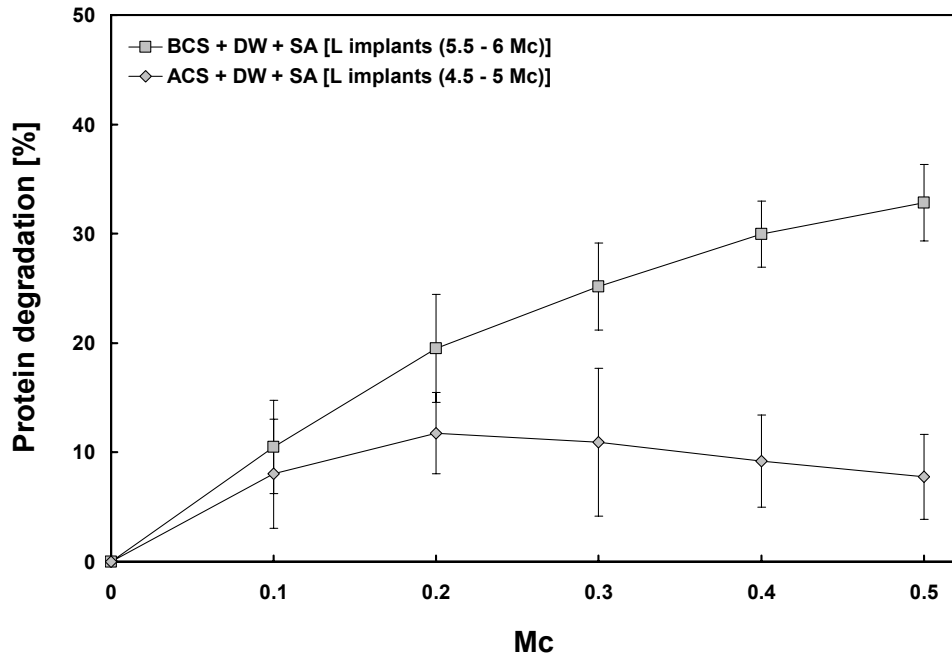


Figure 5.22: The correlation of protein degradation during the wear tests with initial combined β -globulin + γ -globulin fraction. Four protein degradation values were determined for each wear station and so each data value above represents a single value.

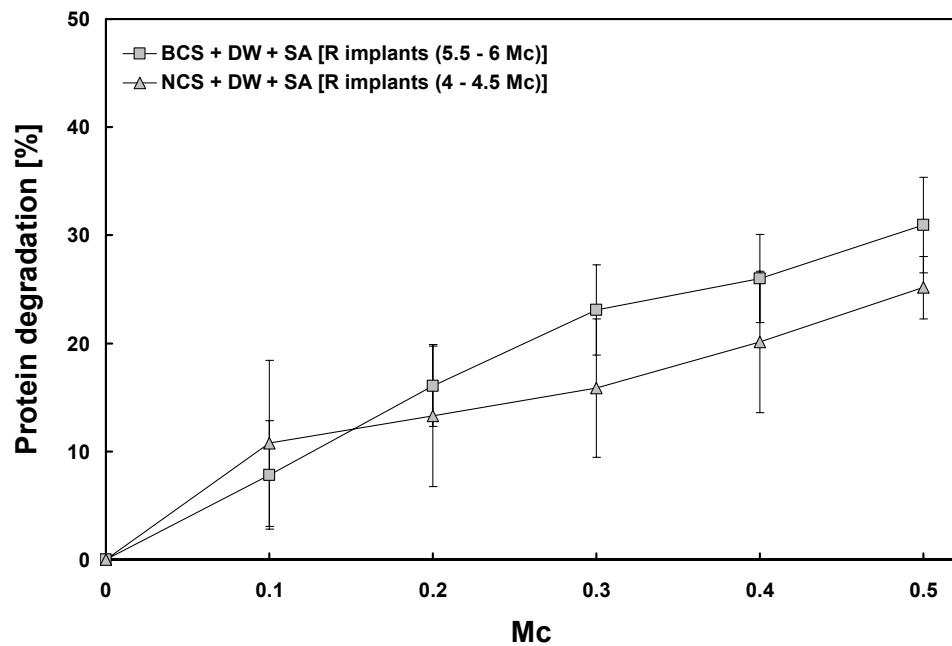
5.3.4 Protein Degradation versus Time

Visually, all sera in all the wear stations become more opaque after only 0.06 Mc indicating that some degradation had occurred. Protein degradation increased with time but perhaps not in the same manner for all lubricants. The protein degradation was evaluated for each of the three lubricants mentioned in Table 5.4 every 0.1 Mc of one test interval of 0.5 Mc.

These measurements were performed on the L implants (Fig. 5.23.a) when the ACS lubricant was used from 4 - 4.5 Mc and when the BCS lubricant was used from 5.5 - 6 Mc. Also, these measurements were performed on the R implants (Fig. 5.23.b) when the NCS lubricant was used from 4 - 4.5 Mc and the BCS lubricant was used from 5.5 - 6 Mc.



(a) L implants



(b) R implants

Figure 5.23: Protein degradation measured every 0.1 Mc during a test interval of 0.5 Mc for the BCS lubricant, NCS lubricant, and ACS lubricant. The data points represent the mean value accompanied with their standard deviation.

The protein degradation proceeded in an approximately the same linear fashion to reach about 30 % at 0.5 Mc for the BCS lubricant used with both L and R implants and for the NCS lubricant used with the R implants. However, the ACS lubricant used with the L implants reached a maximum of about 8 % at 0.1 Mc and then stayed at this value until 0.5 Mc and thus had less protein degradation than the other lubricants.

5.3.5 Electrophoresis

The findings in Section 5.2 and Section 5.3.2 indicated that certain protein constituents in the lubricants might have acted as effective boundary lubricants. Electrophoresis testing permitted the assessment of the protein constituent fractions of the lubricants before and after the wear tests. Such information was deemed important to identify which protein constituents were damaged during the wear process.

Triplicate samples were obtained from the SM at the beginning of a test interval (assuming the SM was the same for each station) and from the SUP of each station (1, 2, and 3) at the end of the test interval after 0.5 Mc. Specifically, the SUP samples of the BCS lubricant were obtained from the L implants after the 5.5 - 6 Mc test interval, the SUP samples of the NCS lubricant were obtained from the R implants after 4 - 4.5 Mc, and the SUP samples for the ACS lubricant were obtained from the L implants after 4 - 4.5 Mc. The samples were sent to the Department of Immunology at the LHSC for electrophoresis testing and, as expected, there were differences between the SM and SUP (Fig. 5.24). The SM of the BCS and NCS lubricants were rich in γ -globulin, which corresponded well with the data given by the certificate of analysis from the manufacturer.

The protein constituent fractions obtained from the electrophoresis of the SM and SUPs were then multiplied by the measured protein concentration that had been used to calculate the protein degradation in Section 5.3.3. The concentration of each protein constituent was determined (Fig. 5.25). Such

analysis gave detailed information on the degradation of each protein constituent in each lubricant and indicated that all protein constituents were affected by the wear process.

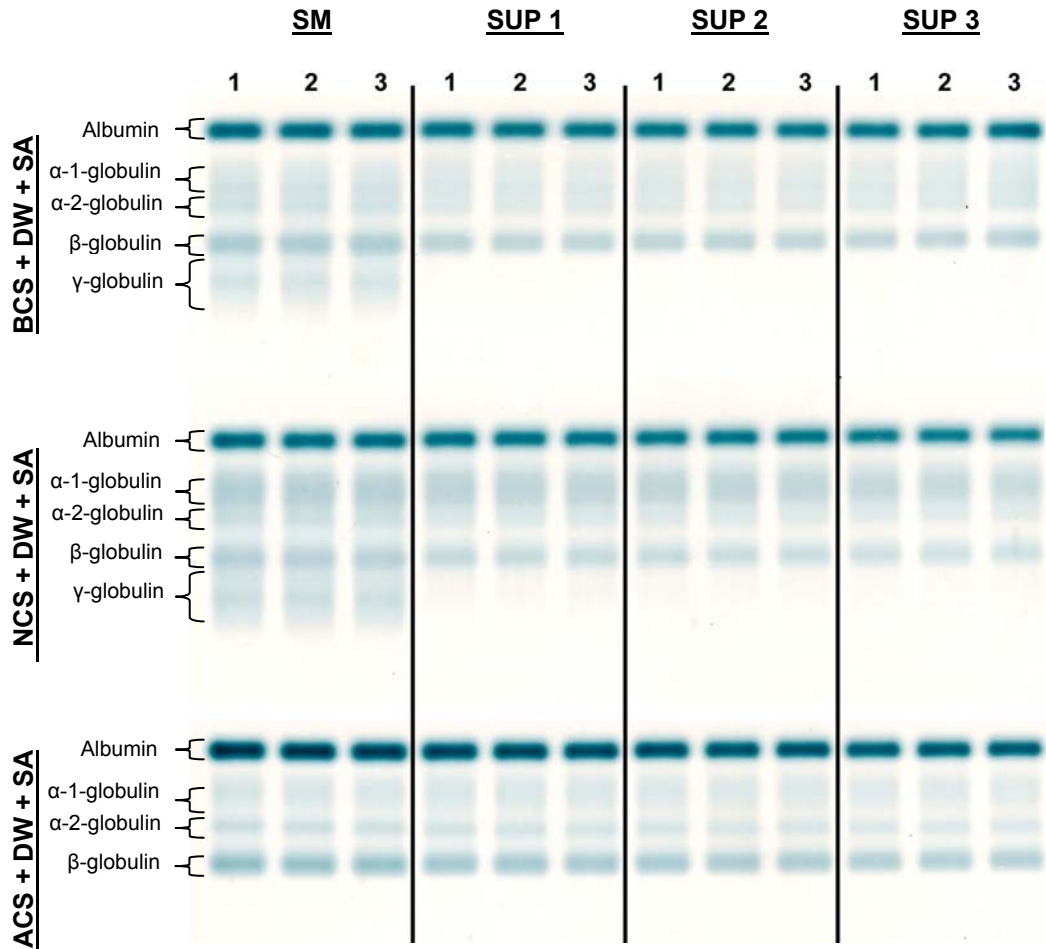
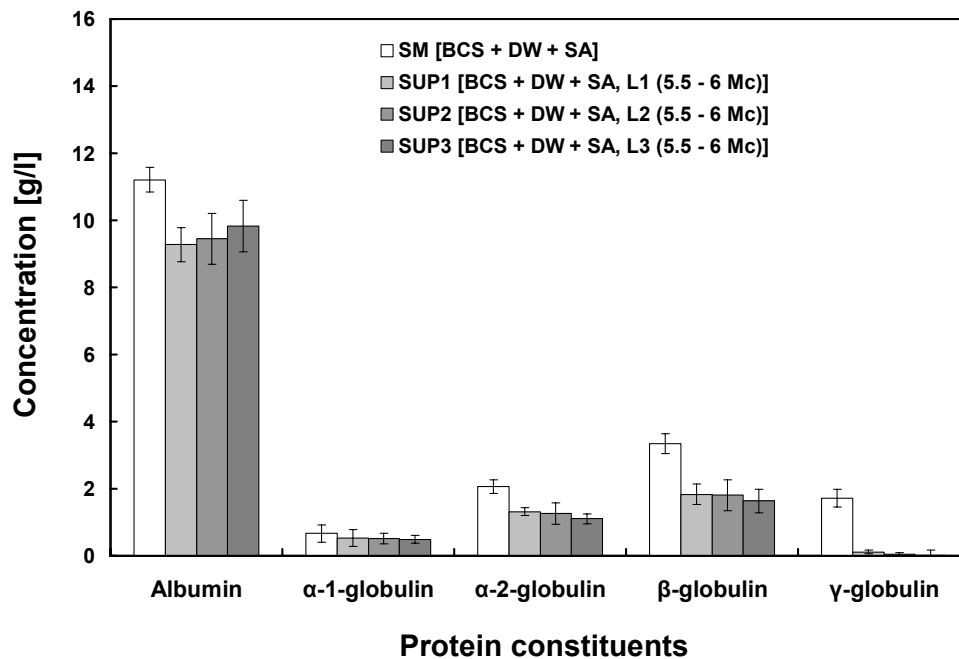
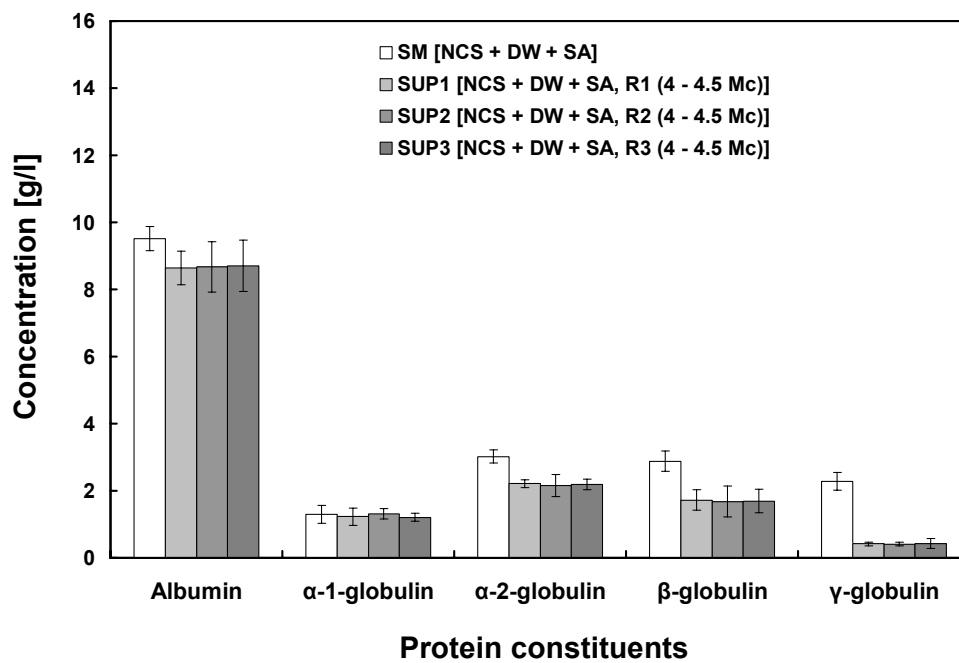


Figure 5.24: Electrophoresis results for the starting material (SM) at the beginning of the test interval (0 Mc) and for the supernatants (SUPs) at the end of a test interval (after 0.5 Mc) for the BCS lubricant, NCS lubricant, and ACS lubricant.

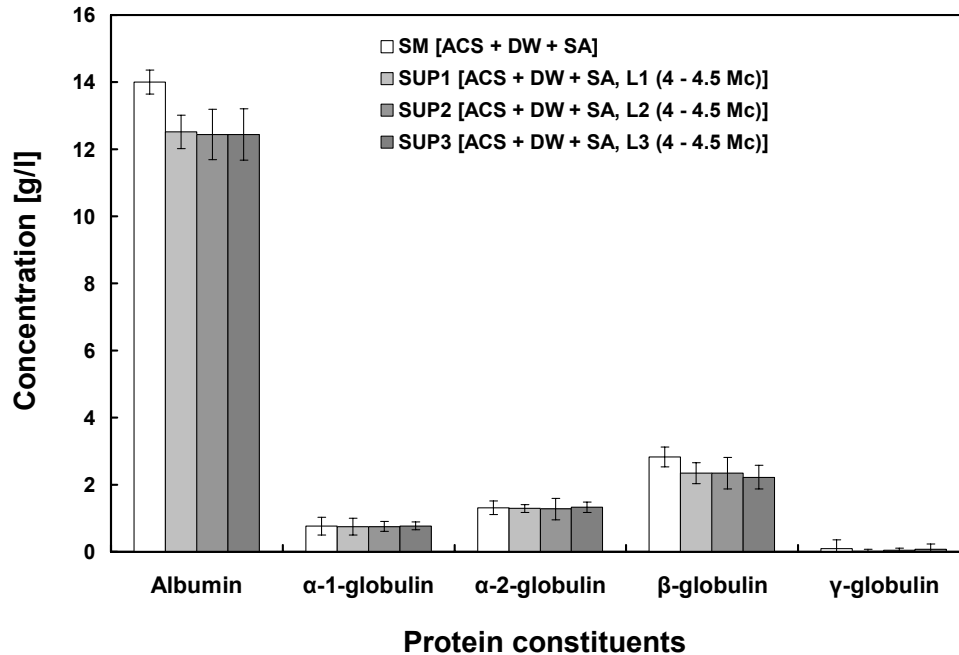


(a) BCS lubricant



(b) NCS lubricant

Figure 5.25: The protein constituent fractions for the starting material (SM) at 0 Mc and the supernatant (SUP) after 0.5 Mc for each implant: (a) the BCS lubricant and (b) the NCS lubricant.



(c) ACS lubricant

Figure 5.25 (continued): The protein constituent fractions for the starting material (SM) at 0 Mc and the supernatant (SUP) after 0.5 Mc for each implant: c) the ACS lubricant.

5.3.6 Peptide Concentration

Sections 5.2 had shown that the SUP for the BCS lubricant showed a higher peptide concentration after the wear test. The SUPs that were created for the electrophoresis tests were further analyzed using the VIVASPIN tubes and the BCA assay (Fig. 5.26). As expected, the peptide concentration in the SUP was higher than the peptide concentration in the SM for all lubricants after wear test interval of 0.5 Mc. The SM of the NCS lubricant had the highest peptide concentration ($p \leq 0.006$, ANOVA and Fisher's), followed by the SM of BCS + DW + SA ($p < 0.001$, ANOVA and Fisher's), while the SM of the ACS lubricant had the lowest peptide concentration ($p < 0.001$, ANOVA and Fisher's). Such a finding suggested that the ACS lubricant may have been more resistant towards protein damage compared with the BCS lubricant and NCS lubricant.

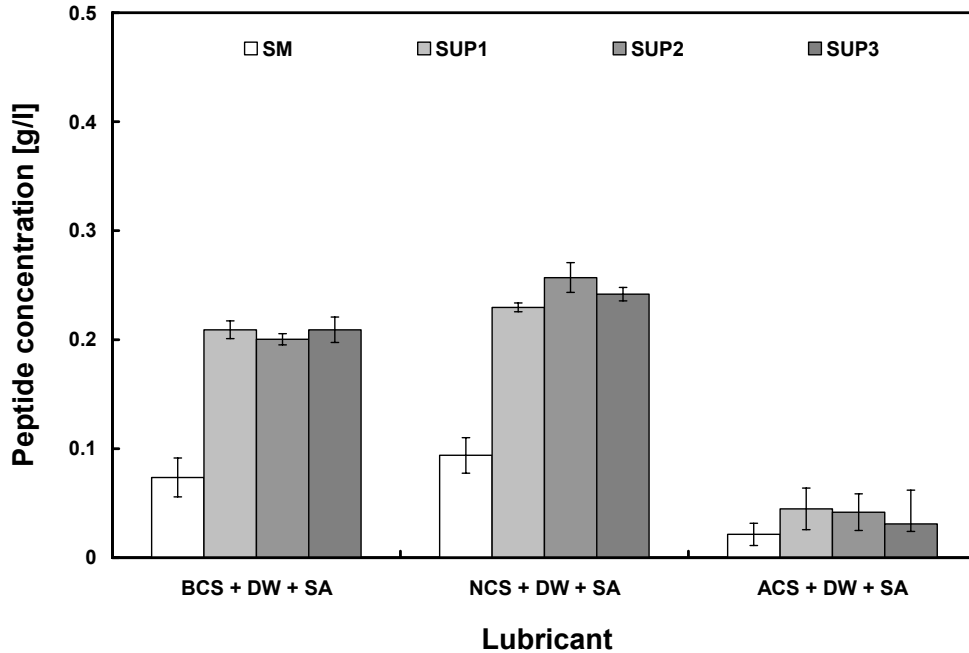


Figure 5.26: The peptide concentration of the starting material (SM) and implant specific SUP (SUP1, SUP2, and SUP3) for all serum lubricants.

5.3.7 pH

The pH was measured before and after the wear test interval 0.5 Mc to investigate to what extent the pH changed for the three lubricants, especially when SA was used as the microbial inhibitor that may allow bacterial growth (see Section 5.2). It was suspected that bacterial growth may have affected the pH. The wear rates were fairly constant for a given lubricant over a number of 0.5 Mc test intervals. Thus, changes in pH values were considered likely to be the same for any 0.5 Mc test interval. As shown in Fig. 5.27, the starting values for pH were all about the same but somewhat higher for the NCS lubricant. The pH changed over the 0.5 Mc in a statistically significantly manner only for the BCS and NCS lubricant ($p \leq 0.005$, ANOVA and Fisher's). The pH of the ACS lubricant appeared not to be affected during the wear interval.

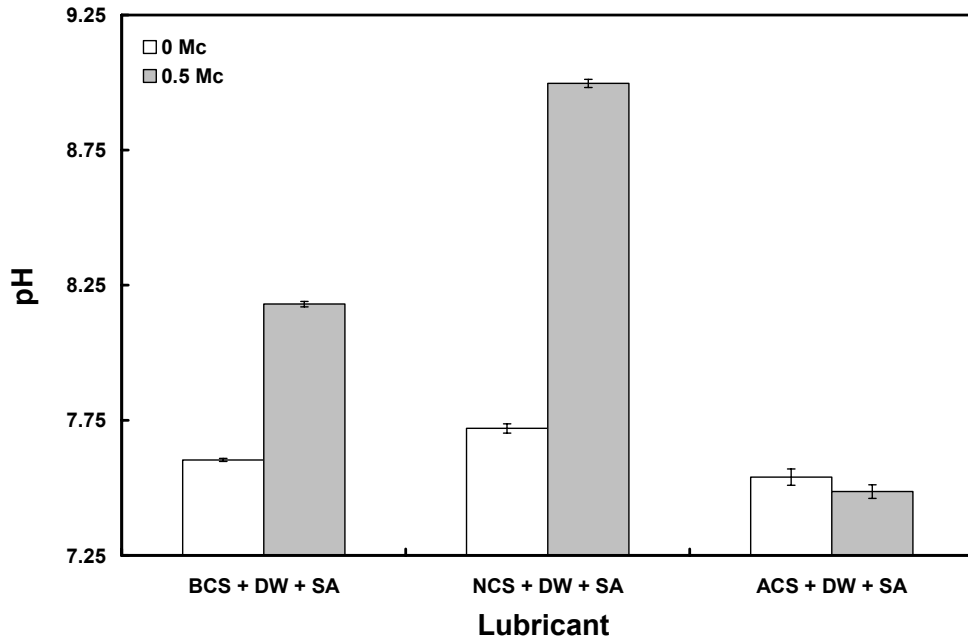
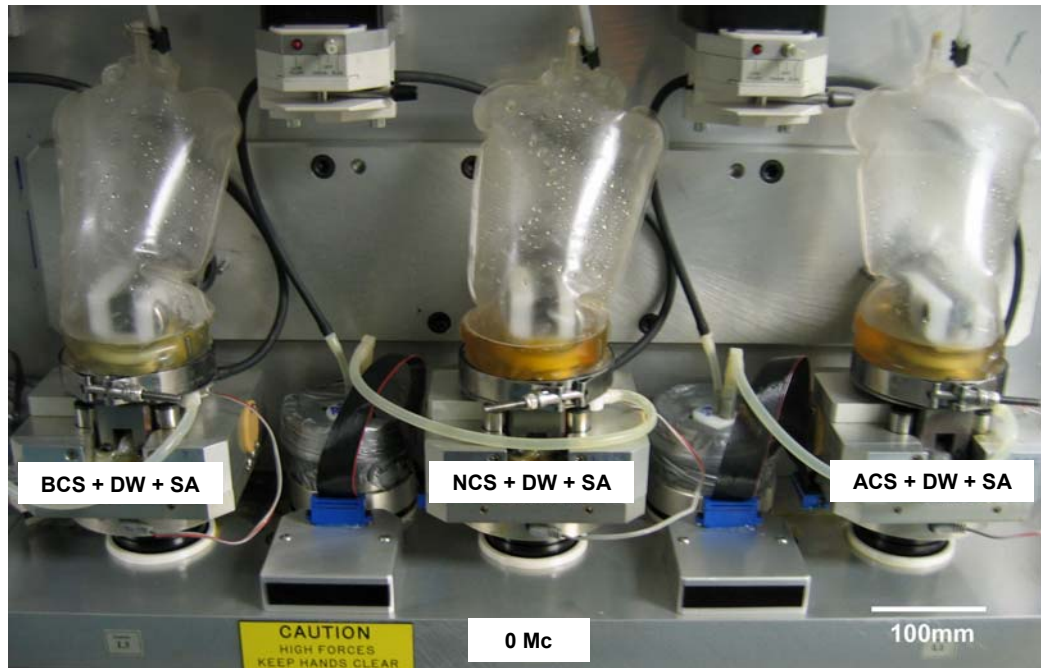


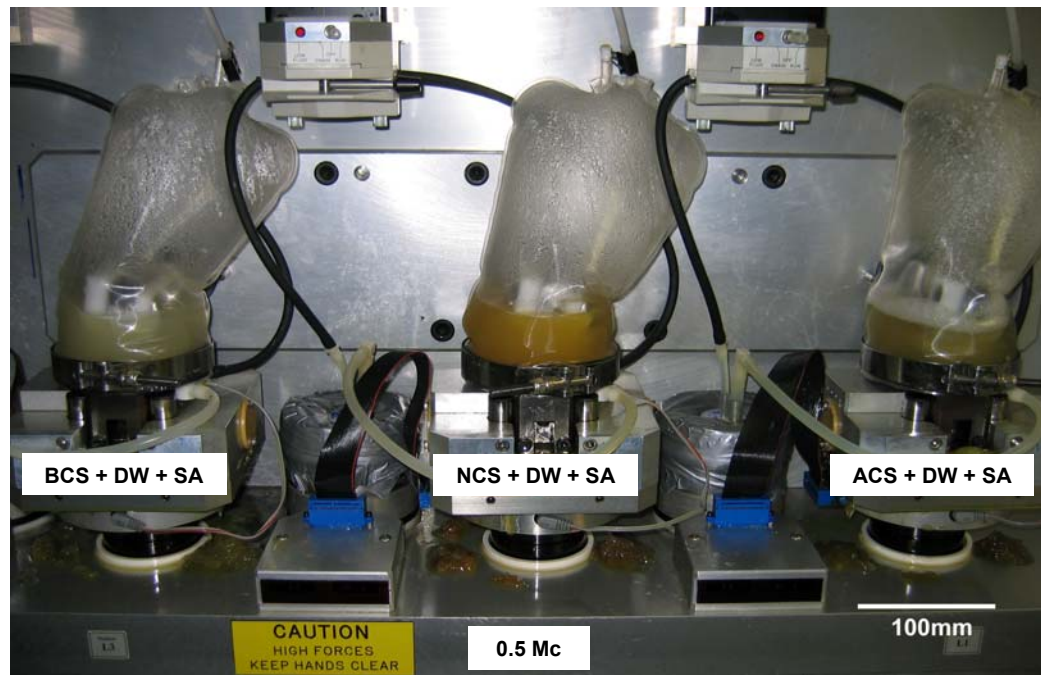
Figure 5.27: The pH for the serum lubricants at the start (0 Mc) and at the end of a test interval (0.5 Mc).

5.3.8 Bacterial Growth and Peptide Concentration

Section 5.2 indicated that bacterial growth occurred in the wear tests. Since *E. cloacae* JK-1 was found in the protein rich BCS lubricant and proteins influenced the simulator wear of implants, it was considered important to investigate the bacterial growth in all three lubricants. To determine the amount of bacteria in the lubricant, samples are plated on LB agar and incubated (see Section 3.6.2 for details on microbial growth). The colony-forming units (CFU/ml) are then counted and graphed. Thus, two additional wear tests were performed, each for 0.5 Mc, on the L implants. These tests were conducted with a more specific focus on the effects of the two antimicrobial inhibitors on bacterial growth (SA and AA). In the first 0.5 Mc wear test, each of the lubricants contained SA as the microbial inhibitor. In the second 0.5 Mc wear test SA was replaced with AA. An image of the L implants on the L bank was taken before and after the wear test (Fig. 5.28).



(a) Start of the test interval



(b) End of the test interval

Figure 5.28: Images showing the L implants located at the L bank of the knee simulator for the serum lubricants with SA.

It can be seen that all SMs were translucent, yet with a yellowish appearance at 0 Mc. Instead, the serum after 0.5 Mc appeared opaque, indicating that some degradation and precipitation had occurred. The wear stations were sampled at the start of the tests (0 Mc) and every 0.1 Mc onwards. No bacterial growth was detected on triplicate LB agar petri dishes in any of the wear stations at 0 Mc. Bacterial growth was observed after the first 0.1 Mc in all the wear stations with SA as the antimicrobial inhibitor (Fig. 5.29). Each point of bacterial growth in the graph was reported as the mean of the three measurements (the SD of the CFU/ml were small and were not visible on the graph due to the logarithmic scale of this axis). The NCS lubricant had a higher bacterial growth than the BCS lubricant until approximately 0.35 Mc. The bacterial growth was the least for the ACS lubricant. As an illustration of the extent of bacterial growth, photographs of the LB agar petri dishes incubated with the lubricant samples after 0.5 Mc were obtained (Fig. 5.30).

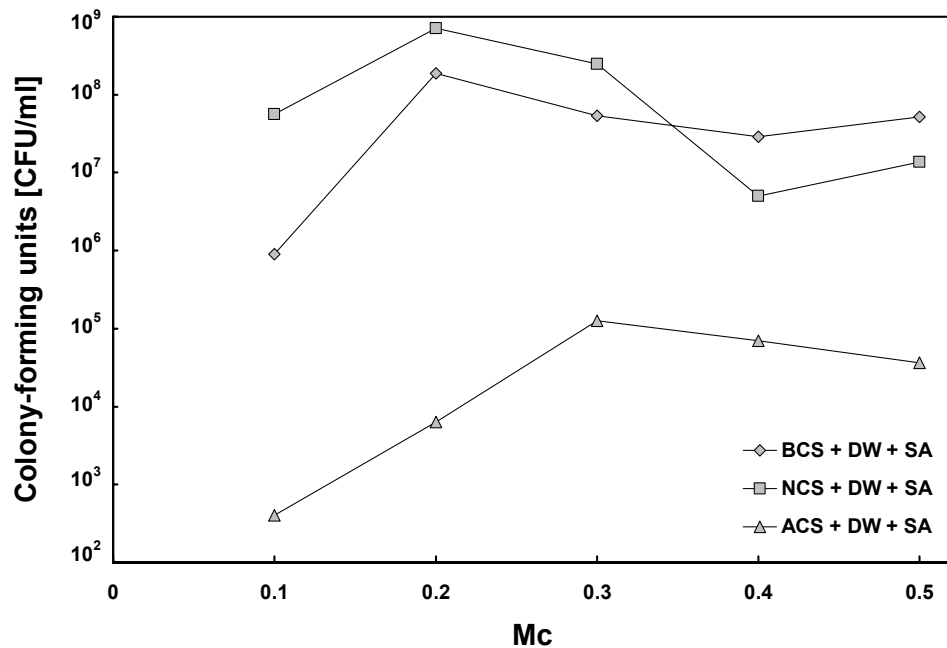


Figure 5.29: The colony-forming units per ml serum (CFU/ml) for the BCS, NCS and ACS lubricants through a test interval from 0 - 0.5 Mc. Note that there was no bacterial growth at test initiation test but this could not be plotted above because the vertical axis had a log scale.

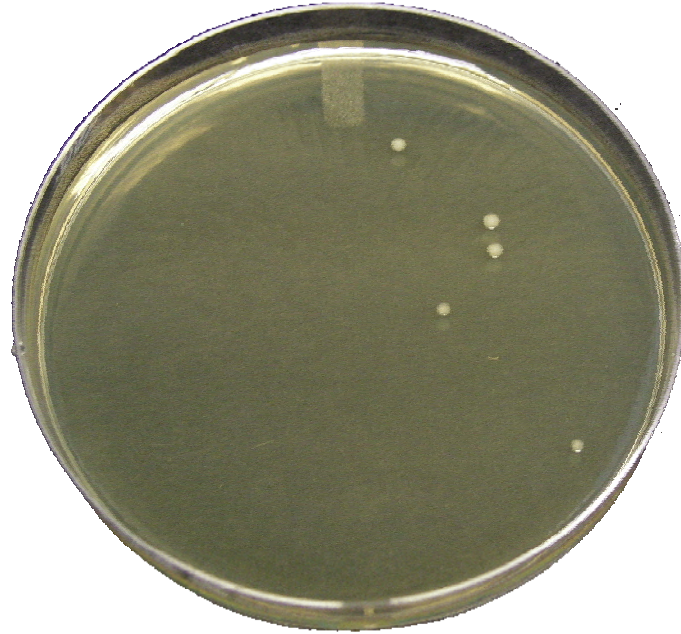


(a) BCS + DW + SA (100 μ l), 10^5 -times diluted



(b) NCS + DW + SA (100 μ l), 10^5 -times diluted

Figure 5.30: Images showing the incubated LB agar dishes after they were plated with serum sample from (a) the BCS lubricant and (b) the NCS lubricant obtained after 0.5 Mc. Serum samples were diluted with LB buffer to allow the count of colony forming units.



(c) ACS + DW + SA (100 μ l), 10^3 -times diluted

Figure 5.30 (continued): Image showing the incubated LB agar dishes after they were plated with serum samples from (c) the ACS lubricant obtained after 0.5 Mc. Serum samples were diluted with LB buffer to allow the count of colony forming units.

During the second wear test of 0.5 Mc, bacterial growth was *completely eradicated* when AA was used as the microbial inhibitor. The serum lubricants remained translucent throughout the test interval. Replacing SA with AA in all three lubricants (Fig. 5.31) did not cause a statistically significant change in the protein degradation ($p = 0.059$, GLM and Tamhane) but it did obviously increase the peptide concentration in all three serum lubricants (Fig. 5.32). This suggested that *E. cloacae* JK-1 possibly consumed the peptides.

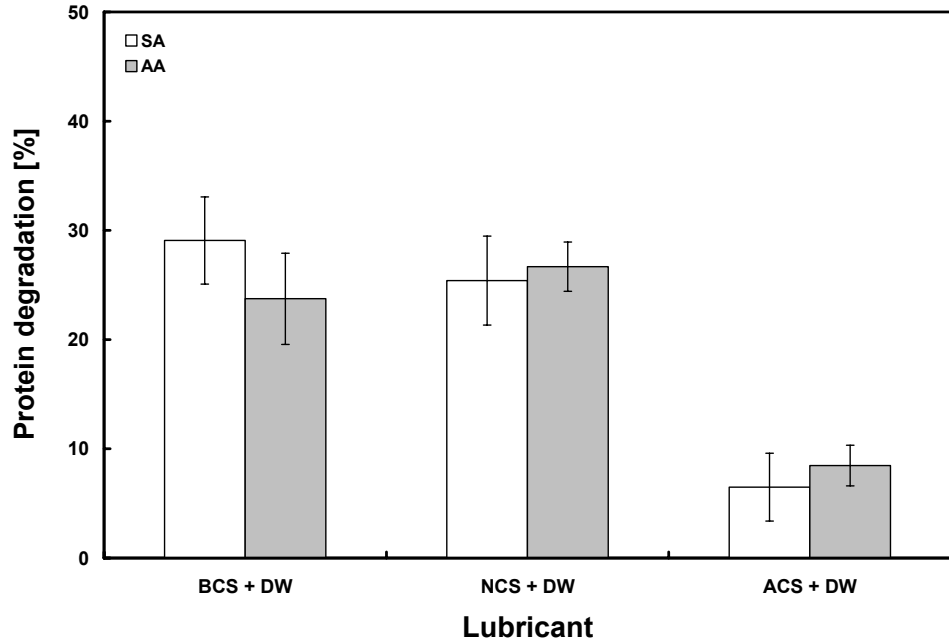


Figure 5.31: The protein degradation for BCS + DW, NCS + DW, and ACS + DW when either SA or AA was used as the microbial inhibitor. Note that the protein degradation was not different for NCS + DW and ACS + DW.

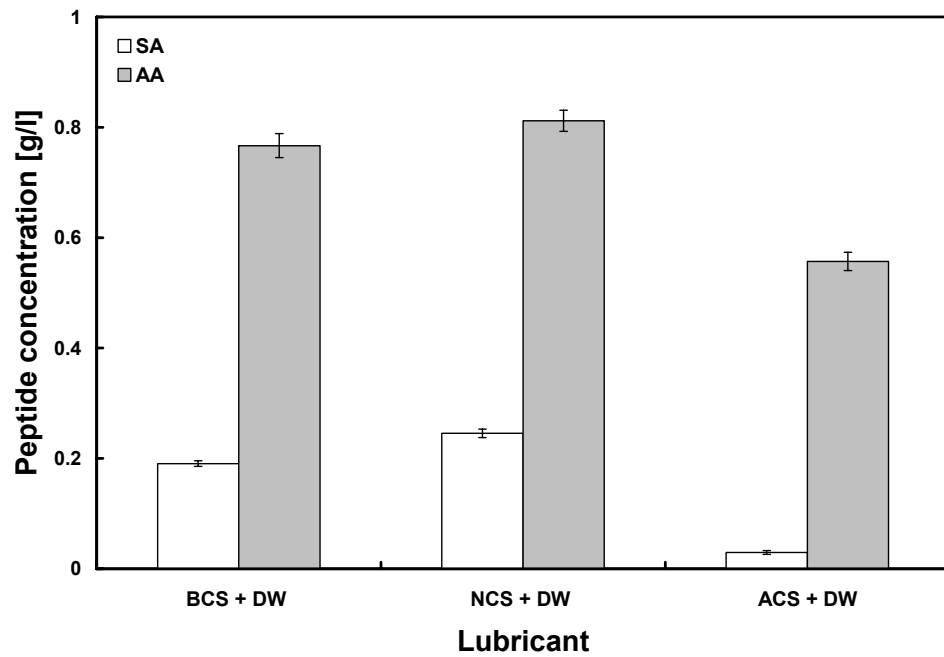


Figure 5.32: The peptide concentration of the serum lubricants after 0.5 Mc when SA was replaced with AA as the microbial inhibitor.

5.3.9 Discussion of Wear

One of the major goals during the wear evaluation of total knee joints was to expose the implants to clinically relevant test conditions. Such test conditions included physiological loading, displacements, implant mounting and lubrication. Choosing the appropriate lubricant for wear testing has been important to the wear process in the past ^{152,421}. Using a protein based serum instead of DW as the lubricant had been shown to reproduce similar surface damage features observed on retrieved total hip replacements ^{152,421}. Such findings suggested that proteins played an important role in the boundary lubrication process. The effect of proteins on wear has received considerable attention in the past ^{35-37,165,440}, but only in total hip wear simulations and without enough focus on individual protein constituents.

The International Standards Organization (ISO) developed a standard ⁴¹ that imposed some uniform procedures (such as testing in either load or motion control) for knee wear testing that permitted manufactures to sell implants that have performed adequately in one of the uniform test procedures. Such uniform test procedures were considered useful by the present author for comparison purposes between laboratories and for different implants. However, given the complexity of knee simulator testing and the many “worst-case” scenarios that could occur for various patients and implants, the present author suggests that the limited number of uniform test procedures proposed by the ISO left the patient subject to clinical disasters that could have been anticipated and prevented by performing a series of true simulator tests that explored different scenarios. In any case, the ISO uniform procedures could be changed as new laboratory investigations were performed and contributing to the changing of the ISO procedures was one of the goals of the present thesis.

As discussed in Section 2.3.3, the ISO standard stipulated testing in “calf serum” diluted with DW to a total protein concentration of 17 g/l. However, certain ranges of protein constituents were not given. Based on the present author’s observations of the serum market, a number of different types of calf sera were available and the protein constituents varied between serum

suppliers even when the trade name of the serum was identical. Thus, wear test laboratories were able to use a variety of calf sera to evaluate their implant components^{6,35,37,156,157} which would have affected the wear results and thus impaired judgments regarding the clinical performance of knee implants. It was also considered relevant to note that very few studies of clinical wear of knee implants had been performed³³⁹ because of the difficulties in measuring clinical wear and thus few clinical wear rates were available for comparison with simulator testing.

The analyses of human SF in Section 4.4 indicated that the ACS lubricant had protein constituents that were the closest to SF and quite different from the BCS and NCS lubricants. However, it remained unknown whether protein constituents affected the simulator wear rate for knee implants although the proteins affected the PE wear rate in hip simulators. This provided a strong argument for using the ACS lubricant in wear simulator testing. Furthermore, the simulator wear studies revealed the ACS lubricant produced different wear compared with the typically used BCS lubricant and the occasionally used NCS lubricant. This finding suggests that the different protein composition made a difference to the simulator wear and thus the type of serum lubricant was an issue that should not be ignored. Finally, the simulator wear could be directly correlated with the combined albumin + α -globulin fraction and the ACS lubricant had the highest level of this combined constituent. Overall, the findings in the present study suggested that the current ISO standard for knee implant wear testing should specifically specify the use of ACS lubricant.

Some minor errors and uncertainties affected the present simulator wear investigation. The BCA assay (Fig. 5.33) showed that the calf sera had a total protein concentration of 19 ± 2 g/l rather than being exactly equal to the target total protein concentration of 17g/l that was given in the ISO standard. The protein concentration was obtained by using the “certificate of analysis” to obtain the starting protein concentration and then diluting the solution accordingly with DW. The higher measured value might have been a bias error in the BCA assay or in the actual mixing procedure. In any case, it was deemed

unlikely that the relatively small fluctuations between the total initial protein concentrations of the three lubricants had a strong effect on the PE wear rate.

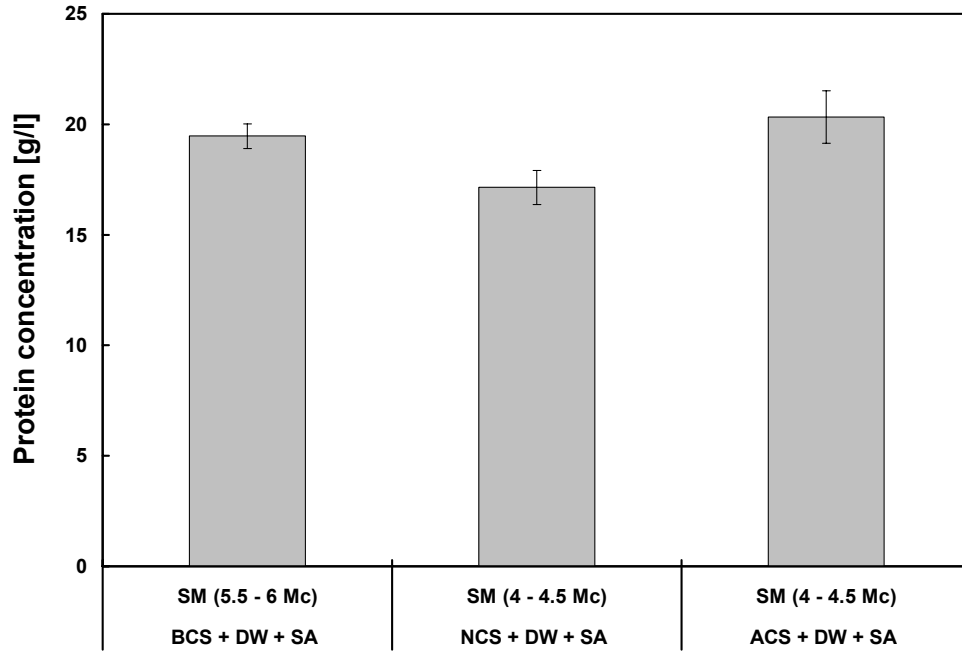


Figure 5.33: The protein concentrations of the starting material (SM) for the serum lubricants that were measured prior to the various test intervals.

On average, the LS specimens from both the L bank and the R bank had considerable fluctuations in their mass from 3 - 6 Mc (Fig. 5.34). The interval mass gain from 0 - 3 Mc was given in Figure 5.7 of Section 5.2 and had somewhat less drastic fluctuations. The change in serum lubricant might have caused the increased fluctuations since serum composition has been shown to influence the LS fluid uptake¹⁵⁷. The reasons for these fluctuations are not known and might have been an accurate representation of the fluid uptake of the implants being subjected to motion and thus wear. Fortunately, the wear was considerably larger in a given interval than the fluctuations in the LS implant

weights and thus the behaviour of the LS specimens did not significantly influence the wear or wear rates.

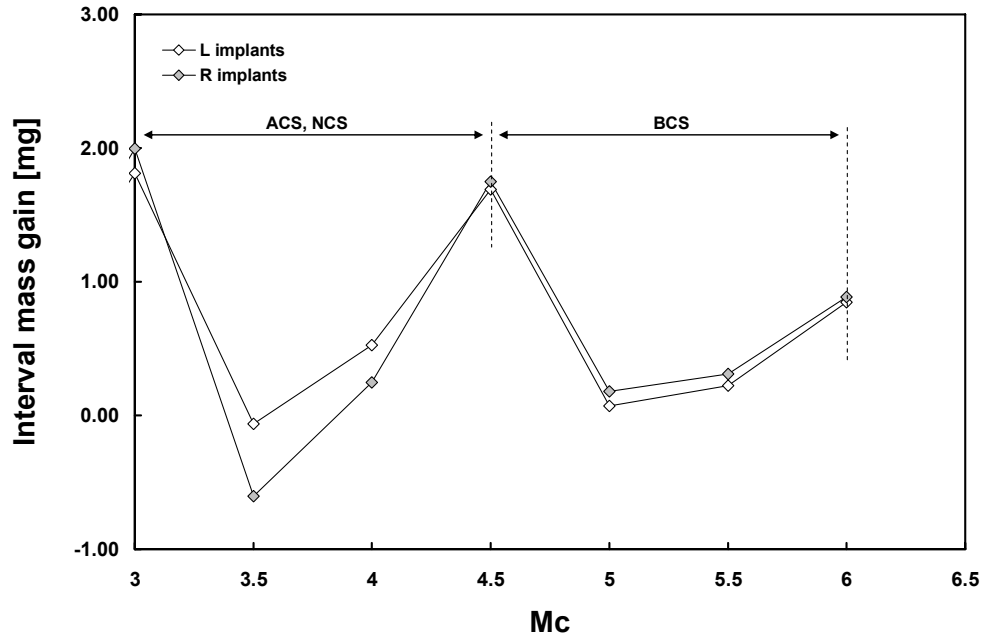


Figure 5.34: Graph showing the mass gain of the LS stations for the L implants (L4, L5) and the R implants (R4, R5). Note the mass loss during the interval from 3 - 3.5 Mc and from 4.5 - 5 Mc when the lubricant was changed between wear tests.

5.3.10 Discussion of Protein Degradation and Electrophoresis

A relationship between the protein degradation and the wear rate results could now be discussed. Increased protein degradation (Fig. 5.35) correlated with increased wear rates ($R = 0.775$, $p < 0.001$, Spearman correlation). The ACS lubricant had the highest albumin + α -globulin fractions, the lowest protein degradation and the lowest wear rate. As mentioned in the last section, it also had protein constituents that were closest to SF. Thus, it would seem that using the BCS and NCS lubricants were likely to result in protein degradation and wear rates that were not clinically relevant.

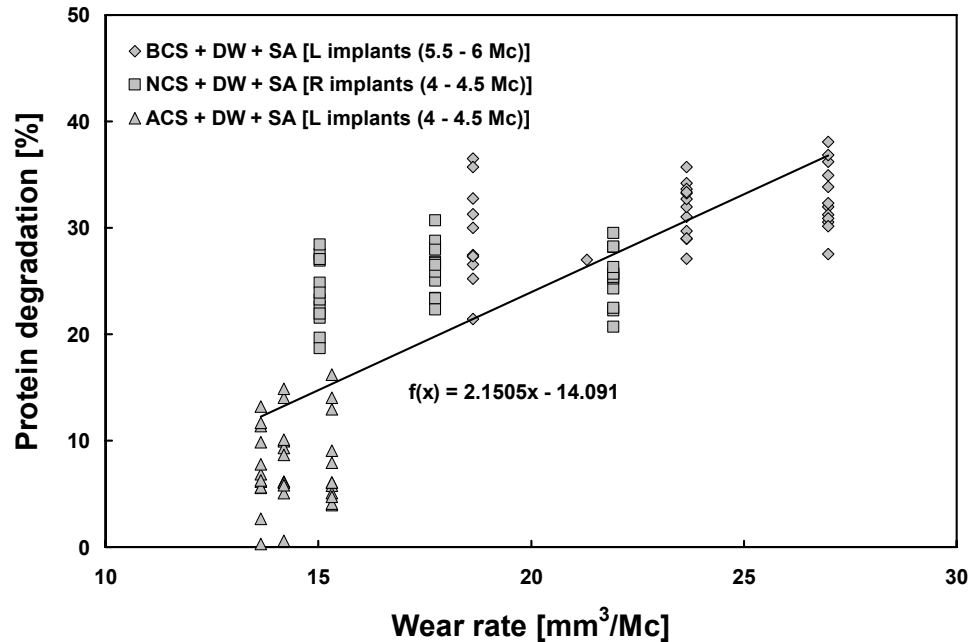


Figure 5.35: The correlation between the protein degradation and the wear rates. Each data point represented a single protein degradation measurement taken from one station.

The electrophoresis results could be further consolidated to show clearly that all protein constituents were affected by the wear process (Fig. 5.36). The ratio of albumin/globulin had been used to correlate with wear in several hip simulator studies^{37,156}, but the individual involvements of other protein constituents (i.e. albumin, α -1-globulin, α -2-globulin, β -globulin and γ -globulin) were not identified. The present study suggested that the wear rate correlated best with the albumin + α -globulin fraction of the total protein content rather than the A/G ratio.

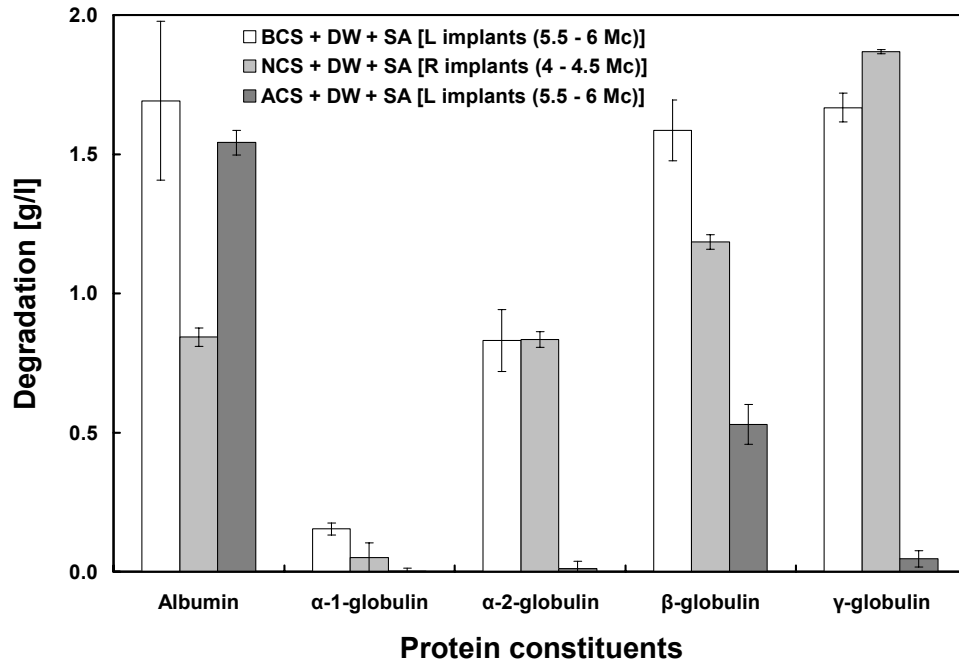


Figure 5.36: A summary of the protein constituent degradation for the serum lubricants.

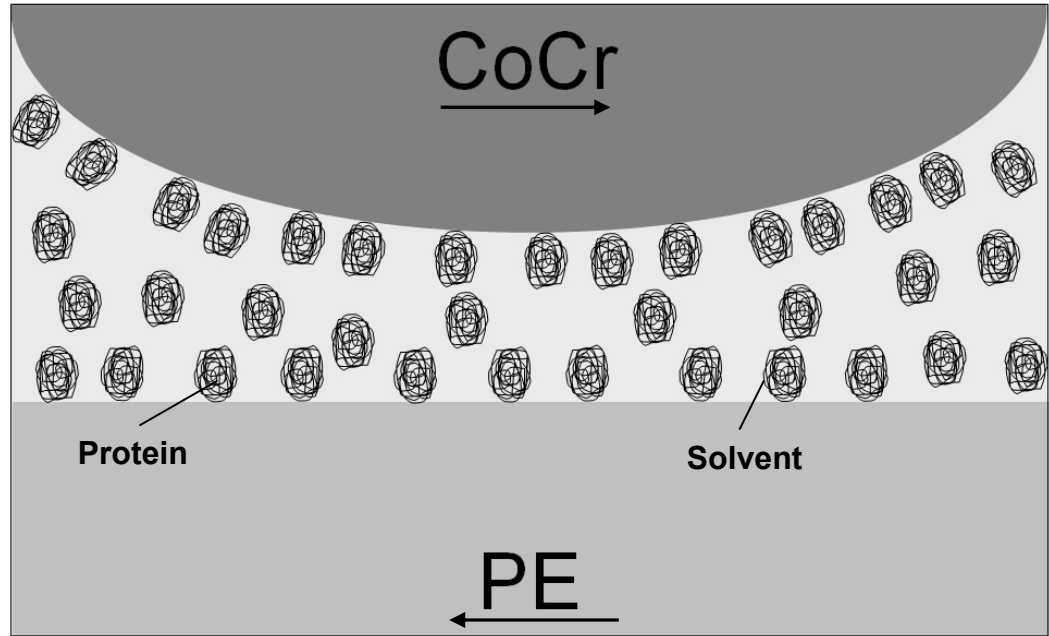
5.3.11 Discussion of Boundary Lubrication

Although some plausible lubrication mechanisms had been suggested for synovial joints^{127,128,145}, the lubrication mechanisms in knee implants remain uncertain. Recent studies^{64,76,441} indicated that the friction in joint replacements might depend on the surface chemistry of the bearing material and on the adsorption behaviour of proteins. However, the effects of proteins on PE wear remain uncertain. The present study suggested through correlations that protein constituents played a significant role in the wear process and thus acted as boundary lubricants. In the next paragraphs, a speculative explanation for the boundary lubrication is devised and explained. While such explanations cannot be proven with data from the present thesis, they were considered worth discussing as a possible foundation for future studies.

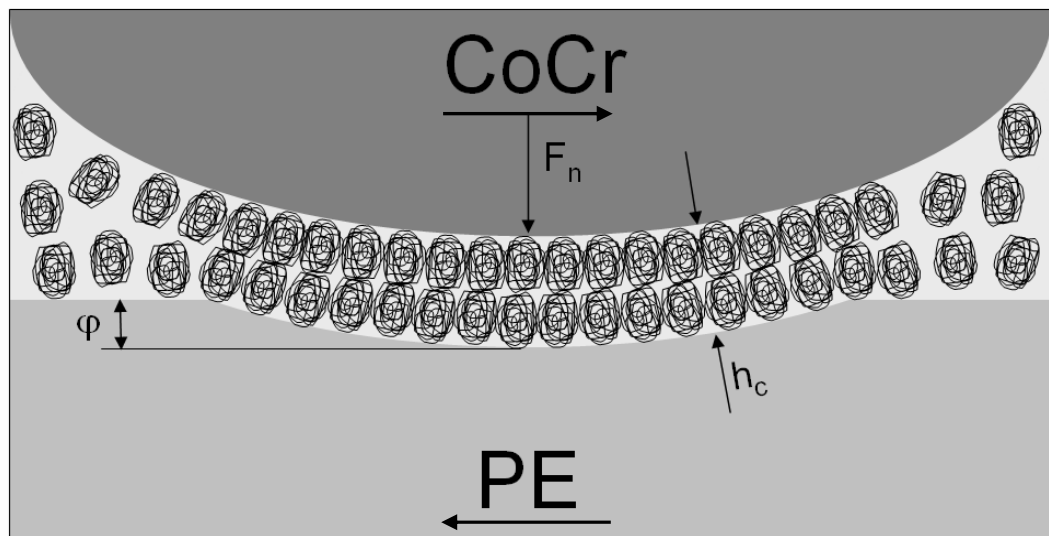
The protein-containing lubricants used in the present study could be regarded as a homogenous suspension that consisted of two phases⁴⁴². One phase could be comprised of dispersed proteins that were stabilized by steric

repulsion which could protect against protein–protein attraction. The other phase could be comprised of a continuous solvent. Such a description had been used by Graham⁴⁴³ and Ostwald⁴⁴⁴ for colloidal dispersions. Pauli¹¹²⁻¹¹⁴ was the first to propose a direct relationship between colloids and proteins. Thus, considering the protein-containing lubricants used in the present study as a colloidal dispersion might be an attractive approach to elucidate the possible lubricating effects of proteins in the present tribosystem. Georges et al.^{91,92,96} were the first to propose a boundary lubrication model for colloids adsorbed to the bearing surface and such an approach may be transferable to the CoCr-PE bearing. They suggested that some colloids ($\sim 100 \text{ \AA} = 10 \text{ nm}$) adsorbed to the interface and built a heterogeneous layer.

A schematic diagram of the speculated condition at the CoCr-PE interface is shown in Fig. 5.37 and magnified in Fig. 5.38. Increased normal loading (F_n) may reduce the surface separation (h_c) of the CoCr-PE bearing and may cause the solvent to be expelled from the contact zone and cause some deformation (ϕ) of the softer PE insert⁹¹. It is further speculated that the occurrence of such a “squeeze” phenomenon may lead to consolidation^{79,89,429} and result in a compacted solid protein layer with possible entanglements between protein chains. The applied load and motions as well as on the generated temperature at the interface may facilitate the degradation of certain protein constituents thus increasing the peptide concentration. In support of this theory, organic deposits have been found on the articulating surfaces of retrieved metal-on-metal hip implants^{53,153,158} that may have been generated as a result of tribochemical interactions between surface asperities in the presence of proteins. Such findings may support the present simulator wear studies and suggest that protein constituents are involved in the *in vivo* wear process.

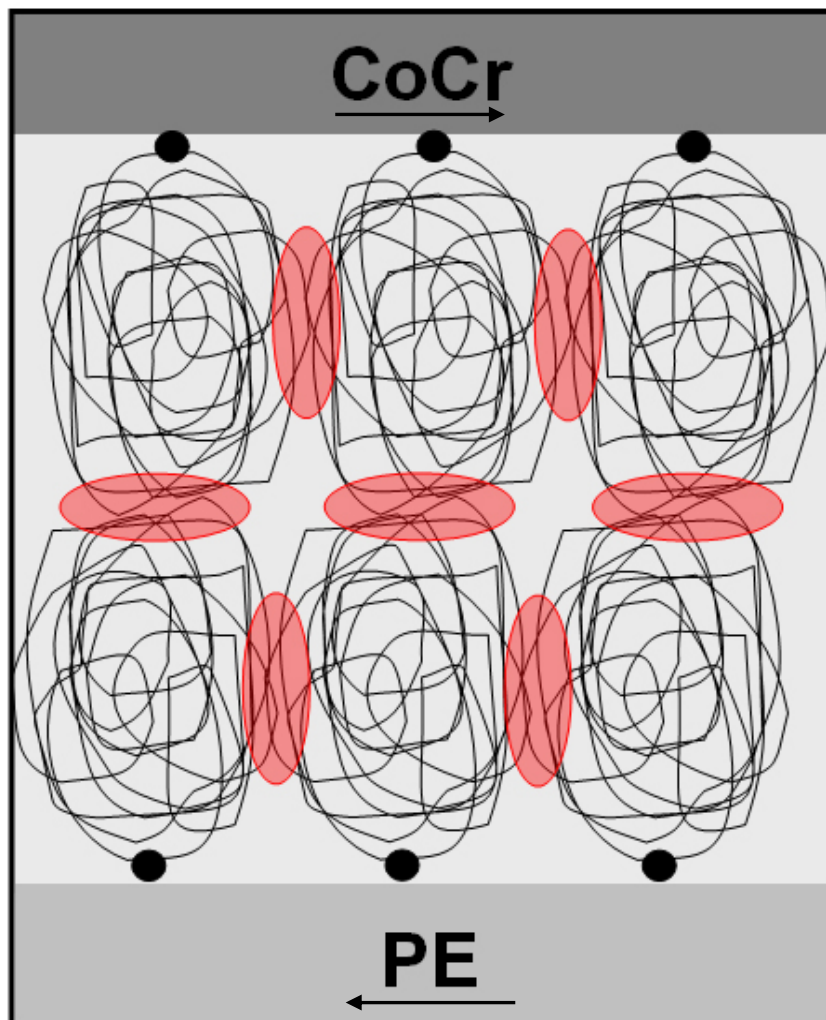


(a)



(b)

Figure 5.37: Schematic of the protein constituents at the CoCr-PE interface: a) heterogeneous distribution of proteins when the normal force (F_n) is zero and some protein constituents are absorbed on the CoCr and PE surface; b) the protein constituents are compacted when the surfaces approach each other when F_n increases. This speculative model was based on the model by Georges et al.⁹² for a thin colloid layer. The arrows indicate the direction of surface motion.






 Protein
  Protein-substrate bonds
  Entangled protein chains

Figure 5.38: Magnified view of the compacted protein layer proposed in Fig 5.37.b. Protein adsorption may have led to protein-substrate bonds. Increased F_n may have been associated with interpenetration of protein constituents which may have led to entangled protein chains. The arrows indicate the direction of surface motion.

The PE wear rate was reduced with increasing albumin + α -globulin concentration. This suggested that both the type of protein constituents and the number of protein constituents comprising the proposed protein layer played a role in the wear process. It is speculated that a decreased number of protein constituents may have reduced the mechanical properties of the protein layer and decreased h_c ⁹⁴. A decrease in h_c possibly causes more asperity contact and thus, promotes adhesive and abrasive wear. Such speculation may be supported by a recent study of McNulty et al.⁴⁵ who tested similar AMK[®] components (10 mm PE (GUR 1050) inserts, GP sterilized) in an AMTI knee simulator with a similar BCS lubricant. Reducing the total protein concentration from 61 g/l to 17 g/l was associated with a 5.4-times increased PE wear rate.

Shen et al.⁴⁴⁵ reported that the AP force was susceptible to the lubricant composition in the knee wear testing. They also associated a higher AP force with a higher PE wear rate, which may be supported by the present study. For the L implants, the magnitude of AP force was lower for the ACS lubricant compared with the BCS lubricant (Fig 5.39). For the R implants, the magnitude of AP shear force was similar between the NCS lubricant and the BCS lubricant. All of this suggested that the ACS lubricant allowed lower μ_k and this would be consistent with the higher albumin + α -globulin fractions causing a thick, compacted protein layer that acted as a boundary lubricant and helped reduce the wear rate compared with the other serum lubricants.

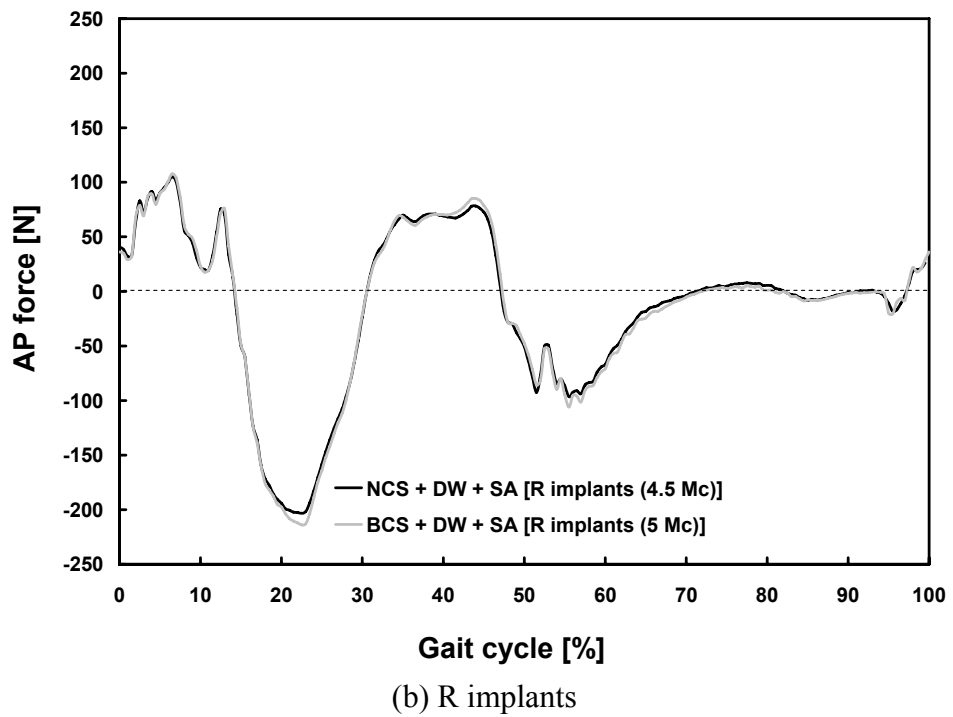
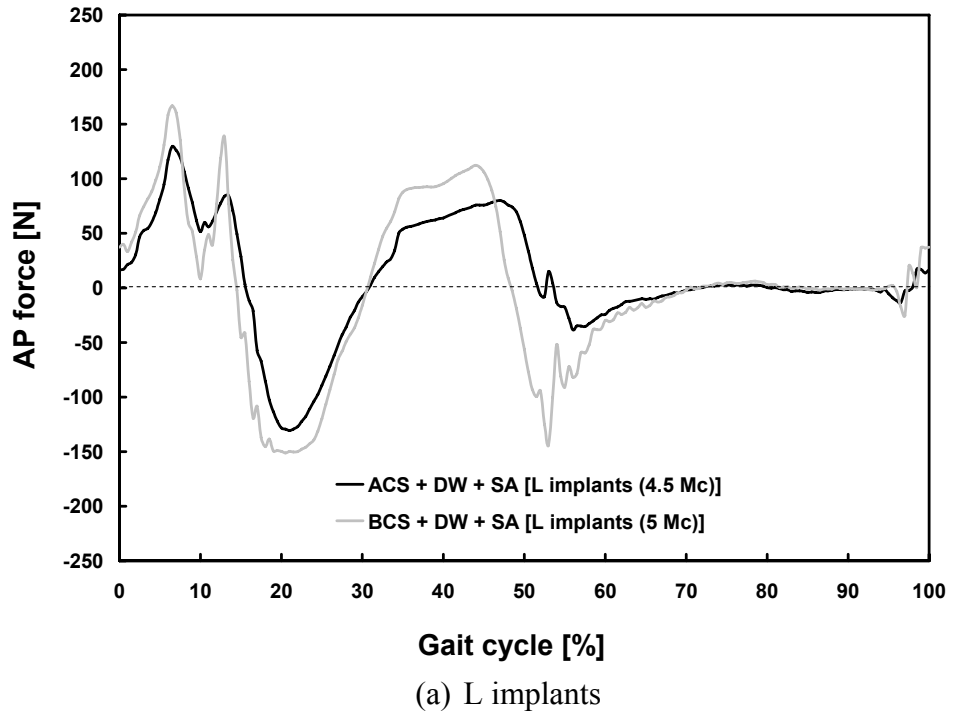


Figure 5.39: The AP force for the serum lubricants.

5.3.12 Discussion of Bacterial Growth and Inhibition

Bacterial contamination in the BCS lubricant was reported in Section 5.2 and the type of organism was identified. It was of further interest to investigate whether the amount of bacterial growth depended on the type of calf serum. The CFU of the calf sera after 0.5 Mc correlated with their initial β -globulin + γ -globulin fractions, suggesting that the bacterium was feeding on those specific constituents (Fig. 5.40). The CFU/ml for the NCS lubricant obtained after 28 h was comparable with the CFU/ml for NCS + DW + SA reported by Bell et al.³⁰. Clearly, SA should not be used in any of the three calf sera with the goal to inhibit bacterial growth but was chosen in the present study to be consistent with Section 5.2. Although the protein degradation was not effected by the type of antimicrobial inhibitor, the peptide concentration significantly increased when SA was replaced with AA. This suggested that *E. cloacae* JK-1 digested some denatured proteins which also caused an increase in pH. It was deemed possible that *E. cloacae* JK-1 secreted some alkaline substance which may have been responsible for such an increase in pH. This suggested that the bacterium and the proteins directly interact with each other and such a mechanism may be pharmacology related. Certain proteins, human serum albumin in particular, are well known for their drug delivery function. It can bind with certain chemical compounds of the antibiotic and deliver it to the place of need in the body. Antibiotics such as penicillin and streptomycin, which were the main constituents of AA, were frequently used in clinical applications and were suggested to bind onto the albumin protein¹⁰⁹⁻¹¹¹. Such binding of AA onto proteins constituents may have preserved some specific proteins from bacterial attack. It remains to be seen which constituents of the AA were actually effective in inhibiting bacterial growth, but such investigations went beyond the scope of this section of the present thesis.

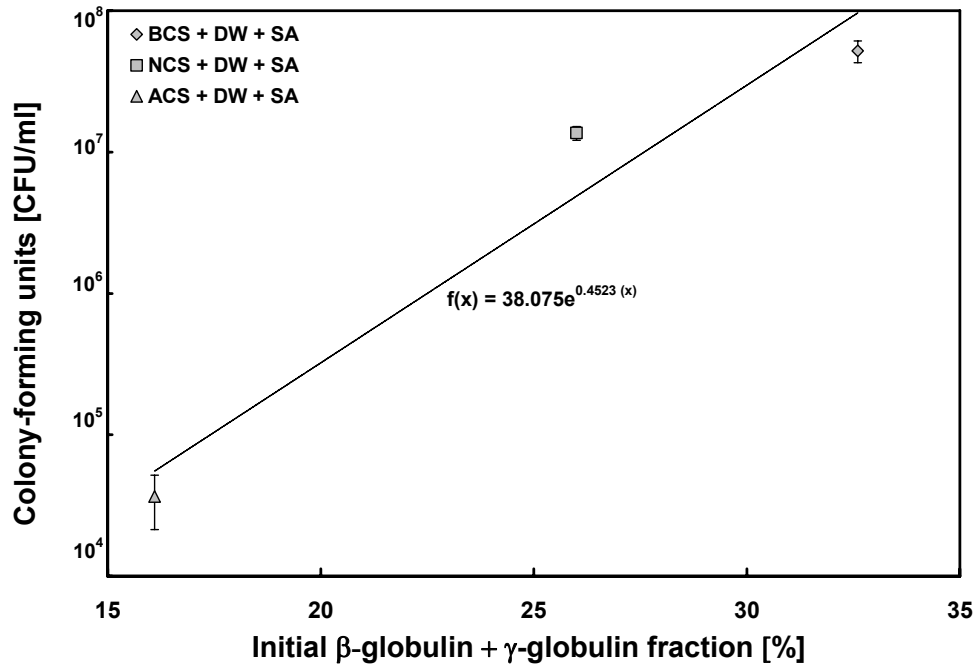


Figure 5.40: The relationship between the initial β - γ -globulin concentrations and the colony forming units (CFU/ml) for three types of calf sera.

It remains uncertain if peptide concentration and the type of microbial inhibitor play a role in boundary lubrication process. Wimmer et al.¹⁸⁹ reported a 6.5-times higher wear rate when microbial contamination was present in the calf serum but they did not investigate the effects of peptide concentration on PE wear.

As a final comment, the presence of *E. cloacae* JK-1 was of concern, particularly since the knee simulator was located in a hospital environment. Paterson et al.⁴⁴⁶ reported that hospital-bound Gram-negative bacteria may mutate and develop resistance to a wide range of antibiotics and may become a serious threat for patients with compromised immune response. Thus, monitoring the bacterial growth was suggested during further testing to enable immediate actions if the bacterium develops AA resistance.

5.3.13 Concluding Remarks

The type of serum and its individual constituents significantly affected the wear rate in displacement-controlled simulator wear testing. All protein constituents were affected by the wear process. BCS and NCS were condemned from knee simulator wear testing since their protein constituents were significantly different to SF and the difference in protein constituents affected the wear rate. ACS, with closest composition to SF, was recommended for further wear testing and for future versions of the ISO standard. It was also recommended to further examine the serum protein constituents based on their effectiveness in the boundary lubrication process. Using SA as a microbiological inhibitor was not a successful way to inhibit bacterial growth in any serum after 0.1 Mc of testing.

The present study suggested that the microbial contaminant *E. cloacae* JK-1 fed on the peptides that remained suspended in the calf sera. The use of AA effectively inhibited any bacterial growth that resulted in a high peptide concentration, which may or may not affect the boundary lubrication.

It was speculated that a compacted protein layer formed at the CoCr-PE interface which acted as a solid lubricant under high loads. The wear behaviour of total knee replacements was highly sensitive to changes in lubricant composition and requires further attention. Aspects such as serum osmolality and the addition of HA to serum lubricants need to be assessed regarding their effects on PE wear.

5.4 Effects of HA Additions and Osmolality Levels on PE Wear

5.4.1 Introductory Remarks

In this final Section of Chapter 5, the effects of HA and osmolality of the dilutive medium (DW versus PBS) on the PE wear rate were investigated. ACS-I was selected as the calf serum base for the wear tests (see Section 3.2.2 for details of its composition). As shown in Section 5.2 and 5.3, SA was not an effective microbial inhibitor and thus AA was used enable sterile wear testing. Protein degradation, electrophoresis and peptide concentration were assessed to gain insight into the wear behaviour of the lubricants used in the present chapter. Surface analysis methods such as SEM, roughness measurements, and surface profilometry were performed on the femoral CoCr components to assess the possible role of the metal bearing surface on the PE wear rate. In addition, the thermal stability of the lubricants was assessed and compared with SF. The efficacy of AA after prolonged testing periods was assessed and alternative microbial inhibitors were proposed. Such extensive analysis was deemed necessary to explain the possible wear mechanisms occurring in the boundary lubrication regime that was imposed on the implants and to guarantee a sterile environment for knee implant wear testing.

5.4.2 Wear

Ten GP sterilized inserts (10 mm, GUR 1050) were pre-soaked in DW at 37 °C, repeatedly disturbed, desiccated and weighed every 138 h ($\equiv 0.5$ Mc). The pre-soaking period was 70 days which exceed the recommended pre-soaking period of at least 46 days (see Section 5.2 for details). DW was chosen as the pre-soaking fluid over the test lubricant to investigate whether the type of pre-soaking fluid would affect the PE wear rate. As it turned out, it was inappropriate to presoak in DW as explained subsequently. The mass gain during the pre-soaking period for the L implants (2.68 ± 0.55 mg) and for the R implants (3.07 ± 0.40 mg) was not statistically significantly different ($p = 0.312$,

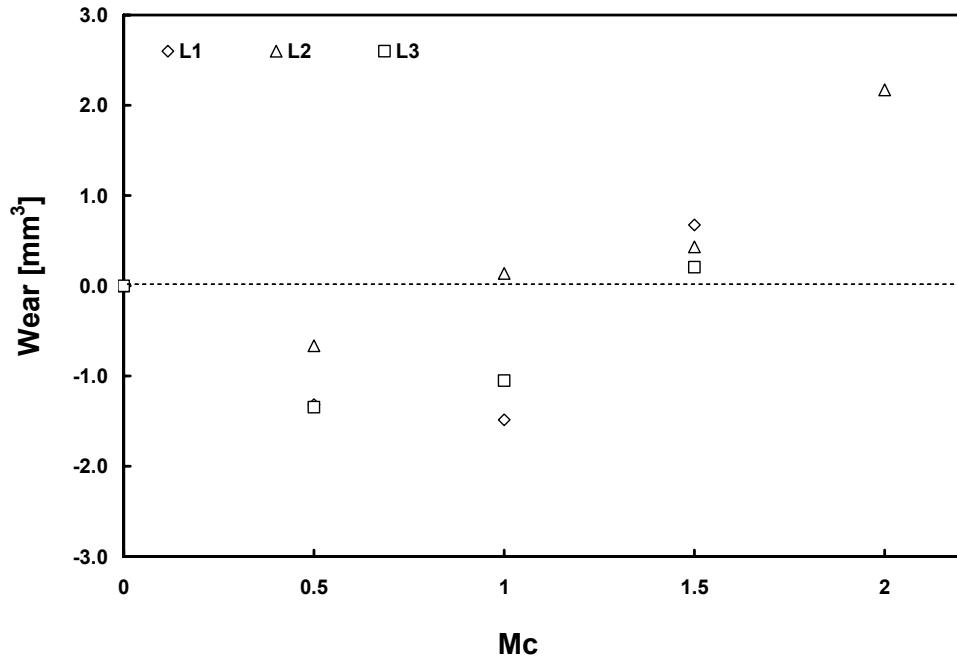
Paired-samples t- test). The wear was determined after 5.5 Mc of simulator testing as described in Table 5.5. The ACS-I + AA for the L implants was either diluted with PBS or PBS + HA. A slight increase in osmolality from 312 ± 1.00 mmol/kg to 321 ± 2.64 mmol/kg was observed when HA was added to ACS-I + PBS + AA, possibly due to the inherent HA osmolality of ~ 50 mmol/kg. The ACS-I + AA for the R implants was either diluted with PBS or DW. The implants remained in the same stations for the entire wear test.

Table 5.5: Test protocol showing the lubricant compositions and their corresponding osmolality levels.

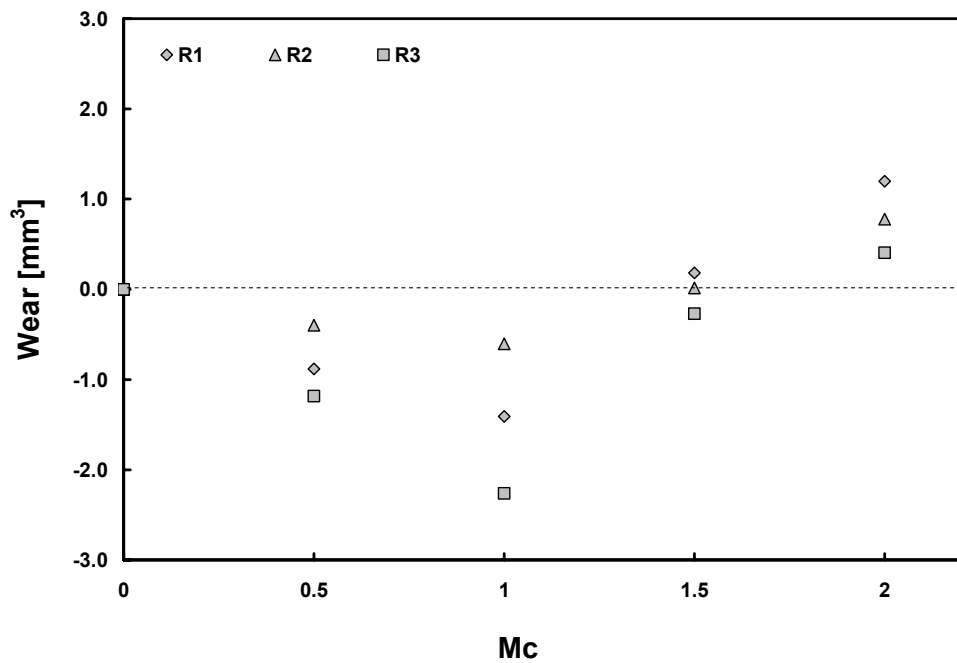
Test interval [Mc]	Lubricants (Osmolality [mmol/kg])	
	L implants (L1, L2, L3)	R implants (R1, R2, R3)
0 – 3.5	ACS-I + PBS + AA (312 ± 1.00)	ACS-I + PBS + AA (312 ± 1.00)
3.5 – 5.5	ACS-I + PBS + AA + HA (321 ± 2.64)	ACS-I + DW + AA (145 ± 2.00)

ACS-I + PBS + AA is referred to as the “PBS lubricant”; ACS-I + DW + AA is referred to as the “DW lubricant”, and ACS-I + PBS + AA + HA is referred to as the “HA lubricant”.

The L and R implants both experienced a distinct mass gain (negative wear volume) during the test period of 1 Mc (Fig. 5.41). The pre-soaking procedure in DW might have caused the implants to gain more mass once the soak media was replaced with the serum lubricants. This mass gain might not have been mimicked adequately in the LS specimens and thus the mass loss due to wear would be overwhelmed by an unaccounted fluid uptake. Thus, the wear results for the first 1 Mc were not considered and linear regression was only performed on the wear results from 1 - 3.5 Mc and from 3.5 - 5.5 Mc to determine the PE wear rates. The average PE wear rate for the L implants increased 2-times from 5.04 ± 0.56 mm³/Mc to 10.24 ± 2.04 mm³/Mc when HA was added to the lubricant (Fig. 5.42). Such a change was statistically significant ($p = 0.013$, Student’s t-test).

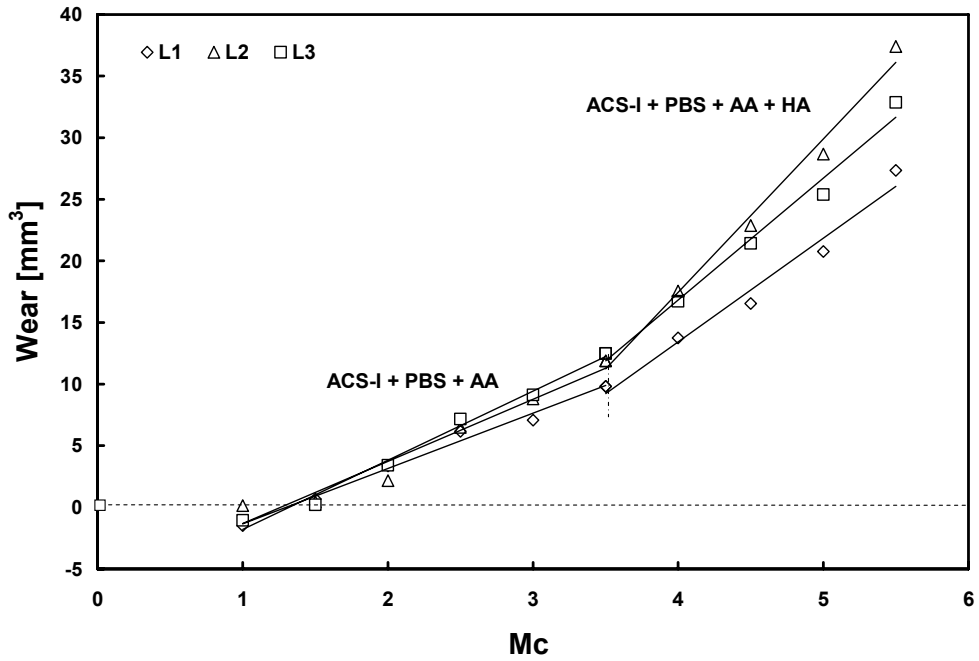


(a) L implants

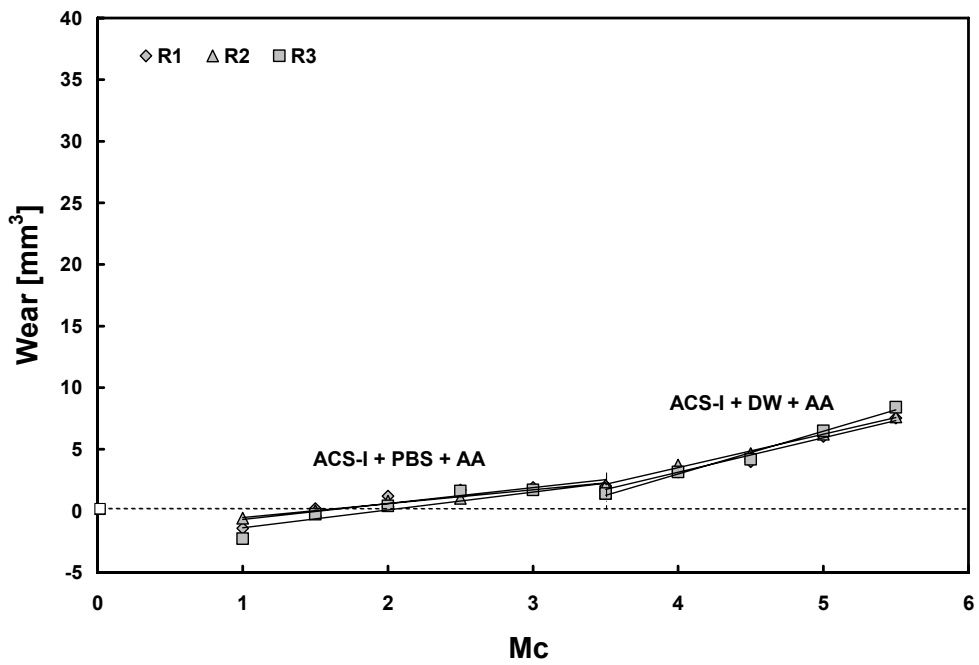


(b) R implants

Figure 5.41: The wear behaviour for (a) the L implants (L1, L2, and L3) and (b) R implants (R1, R2, and R3) from 0 - 2 Mc. Note the negative wear volume due to PE mass gain during the initial 1 Mc.



(a) L implants



(b) R implants

Figure 5.42: The wear behaviour of the (a) L implants (L1, L2, and L3) and (b) R implants (R1, R2, and R3) from 1 - 5.5 Mc.

The mean PE wear rate for the R implants increased 2.3-times from $1.29 \pm 0.17 \text{ mm}^3/\text{Mc}$ to $2.99 \pm 0.16 \text{ mm}^3/\text{Mc}$ when PBS was replaced with DW as the dilutive medium. This change was also statistically significant ($p = 0.003$, Student's t-test).

The differences between lubricant temperatures in the wear stations were small (Fig. 5.43). In addition, the wear rate of the L implants was significantly higher than the R implants when ACS-I + PBS + AA was used on both banks from 1 - 3.5 Mc ($p < 0.001$, Student's t-test).

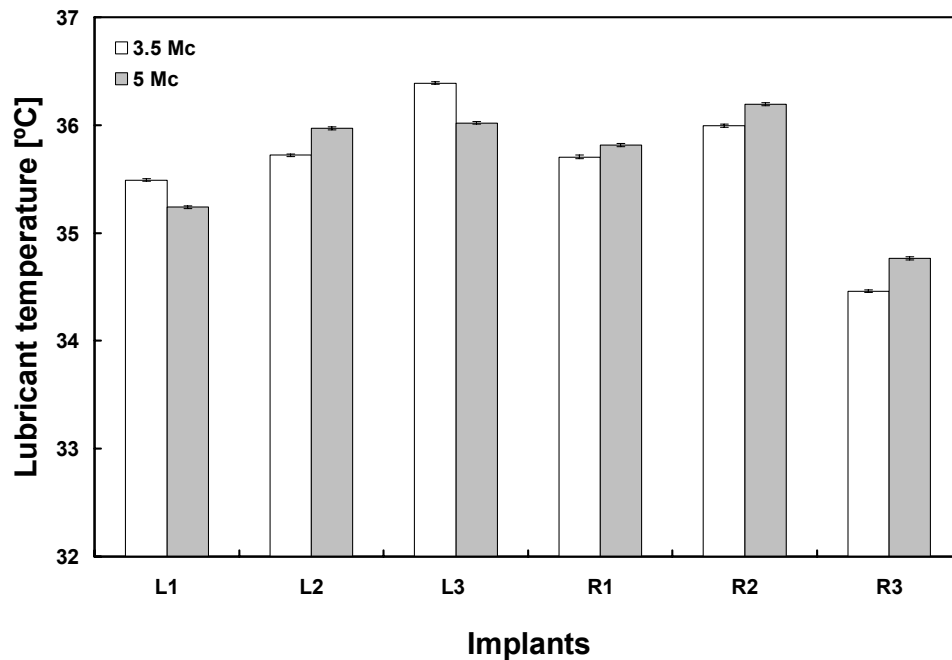


Figure 5.43: The lubricant temperature in the wear stations of the L implants (L1, L2, and L3) and R implants (R1, R2, and R3) at 3.5 Mc and at 5 Mc.

The AP force for the L implants was higher compared with AP force for the R implants at around 8 % of the gait cycle and again at around 45 % of the gait cycle (Fig. 5.44). The higher AP force might have been caused by some slight motion difference of the L bank that caused minor interference at the interface compared with the R bank. The higher wear rate of the L implants might have been caused by the higher AP force.

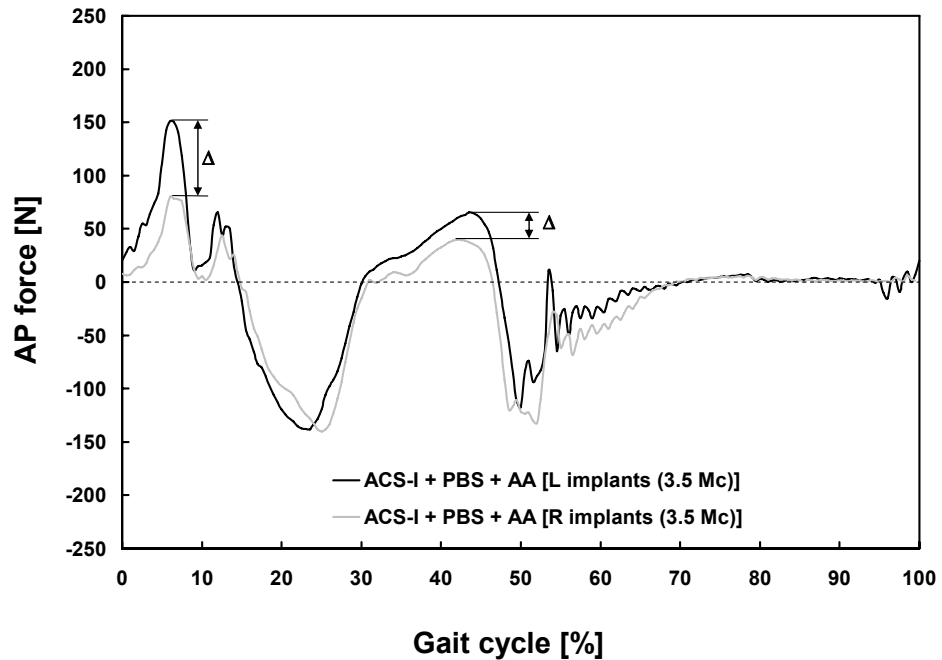


Figure 5.44: The AP force for the L implants and the R implants tested with the PBS lubricants after 3.5 Mc.

5.4.3 Protein Concentration and Electrophoresis

The protein concentration of the lubricants used to test L implants and R implants was measured on the SM at 0 Mc and on the SUPs after 3 - 3.5 Mc and after 5 - 5.5 Mc of wear testing. Electrophoresis measurements were also obtained to determine the amount of degradation of the individual protein constituents.

For the L implants (Fig. 5.45.a), the protein concentration of the SM for the L implants tested with PBS lubricant was not statistically significantly different from SUP1 or SUP2 ($p \leq 0.409$, ANOVA and Fisher's) but SUP3 was higher than the SM ($p = 0.002$, ANOVA and Fisher's). When HA was added to the lubricant, the protein concentration of the SM for the L implants was higher than the SUPs ($p \leq 0.001$, ANOVA and Fisher's).

For the R implants (Fig. 5.45.b), the protein concentration of the SM for the R implants tested with the PBS lubricant was not different to SUP1 or

SUP2 ($p \leq 0.171$, ANOVA and Fisher's) but SUP3 was higher than SM ($p = 0.003$, ANOVA and Fisher's).

The protein concentration of the SM for the L and R implants measured at 3 - 3.5 Mc was lower than the SUP 3 but the average value was lower than all the SUPs. Thus, the average protein degradation was not calculated because it would have resulted in negative values. Instead, it was decided to give the protein concentration of the SM and the SUP for each of the protein constituents from the electrophoresis measurements. The protein constituent fractions obtained by the electrophoresis were multiplied by the mean protein concentration determined with the BCA assay for each station to obtain the protein constituent fractions (Fig. 5.46 and 5.47). Interestingly, the total protein concentrations were higher for the SM after the 3 - 3.5 Mc test interval in contrast to the measurements using the BCA assay. This suggested that errors had occurred in the BCA measurements for the 3 - 3.5 Mc test interval.

The average protein concentration of the SUPs in Fig. 5.46 and 5.47 were subtracted from that of the SM to obtain the concentration of degraded proteins. All protein constituents were affected by the wear process in all four lubricants (Fig. 5.48). However, it can be seen that ACS-I + PBS + AA only marginally degraded for the L implants and the R implants. A greater change in protein degradation was observed for HA lubricant and for the DW lubricant.

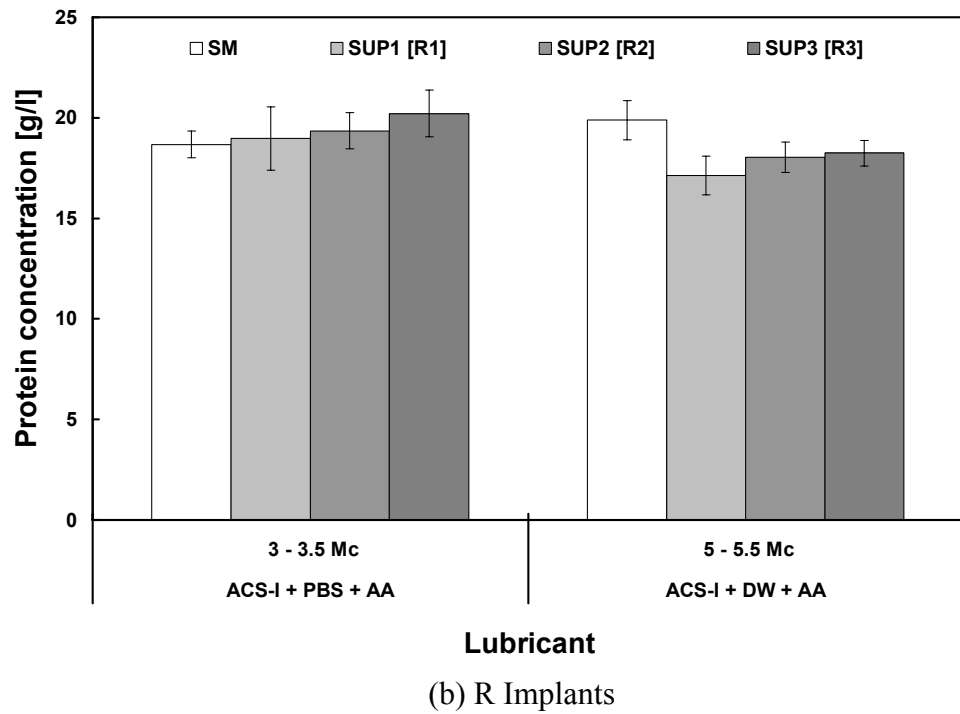
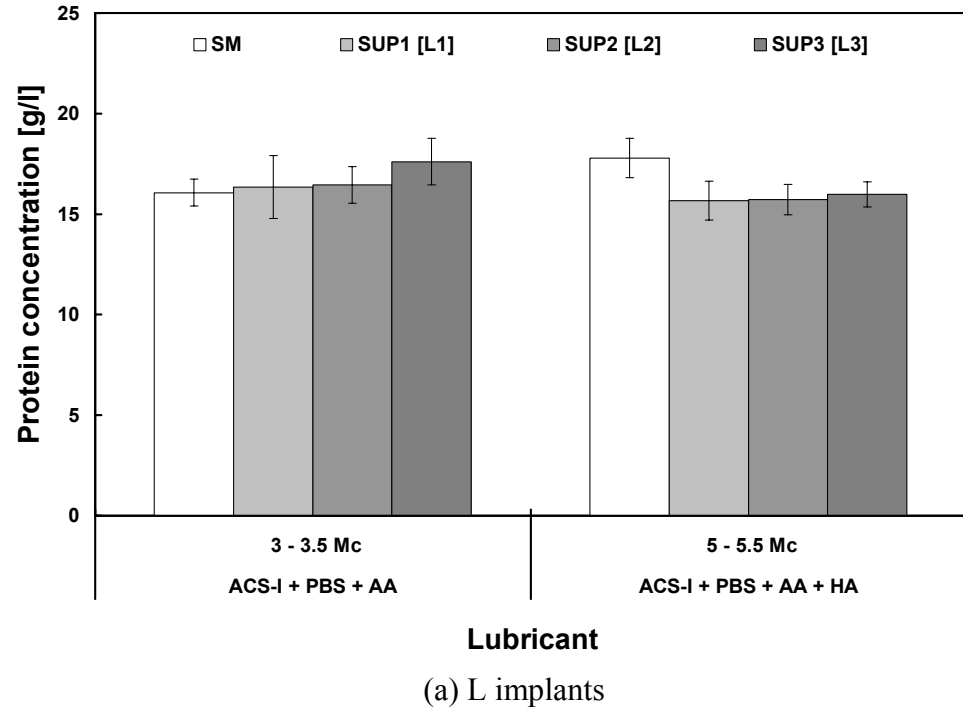
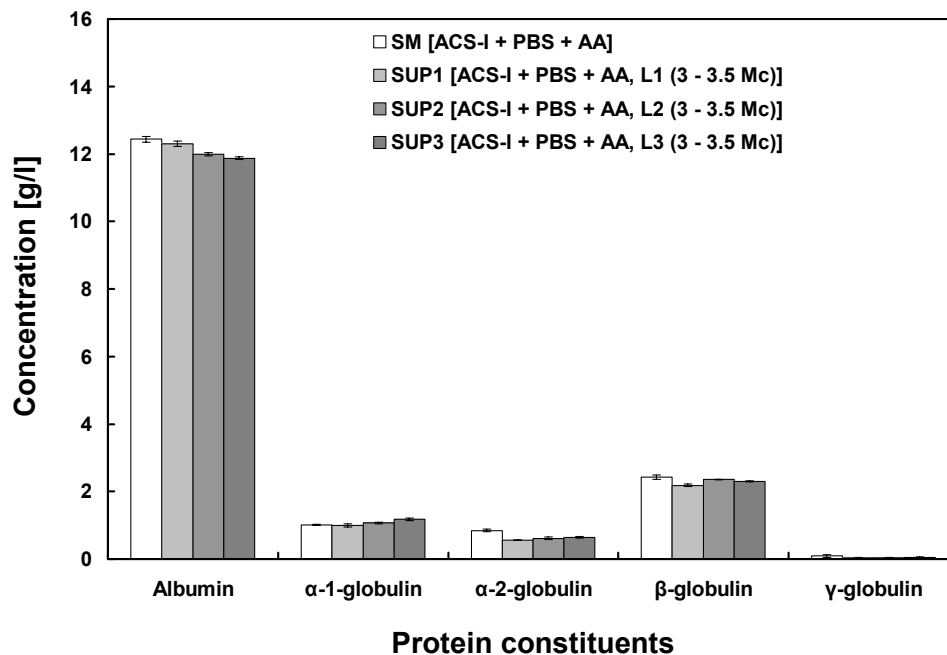
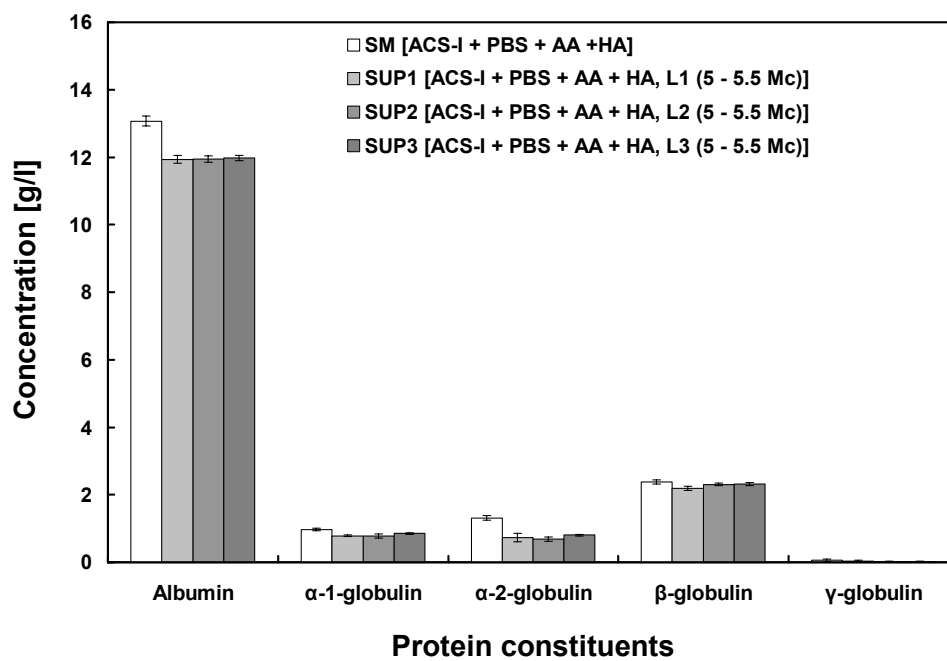


Figure 5.45: The protein concentrations for (a) the L implants and (b) the R implants.

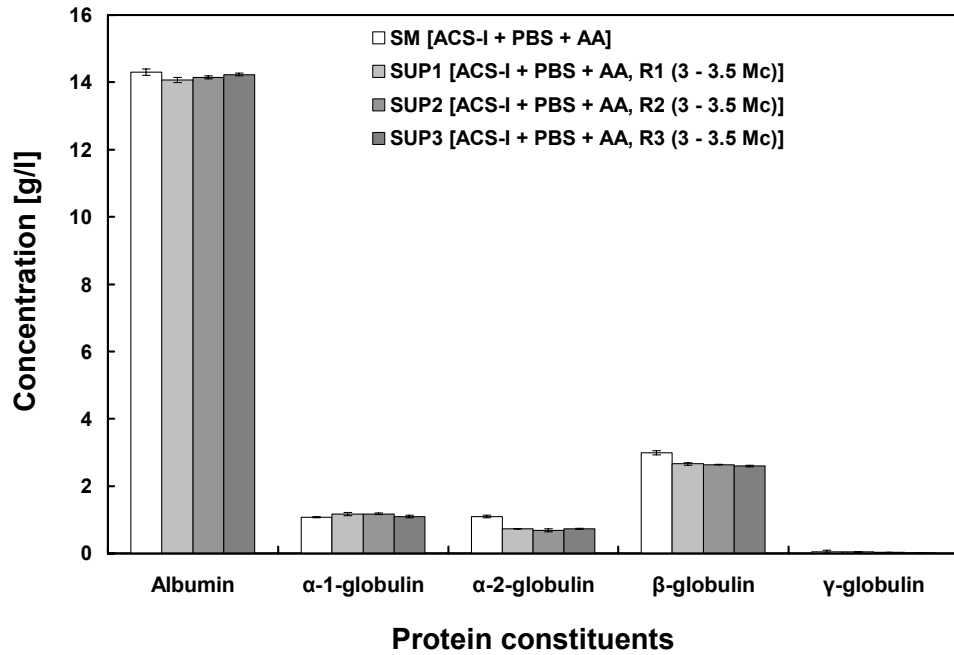


(a) ACS-I + PBS + AA (3 - 3.5 Mc)

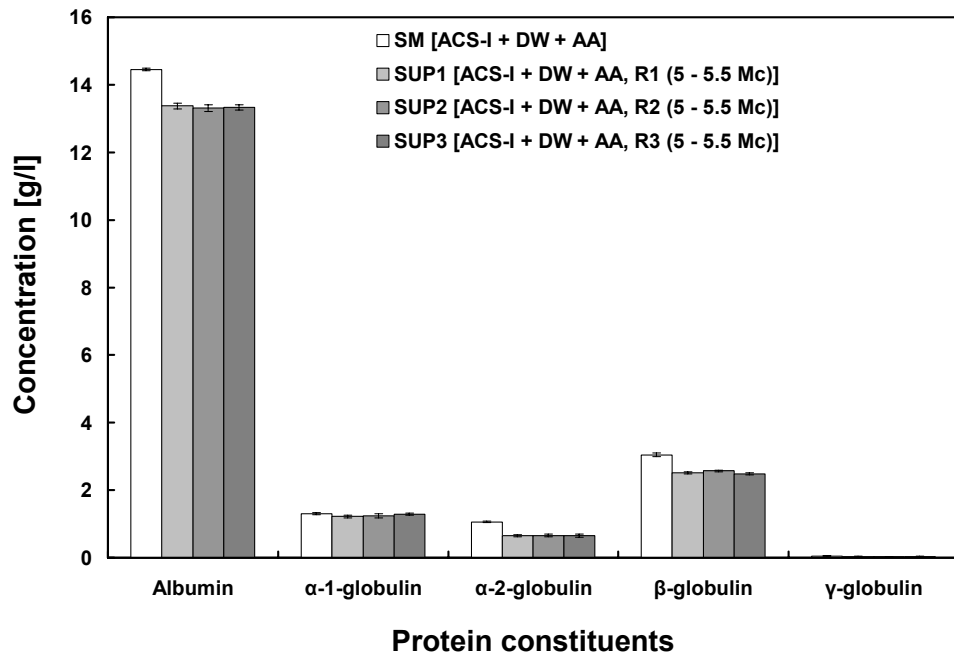


(b) ACS-I + PBS + AA + HA (5 - 5.5 Mc)

Figure 5.46: The protein constituent fractions for the L implants after a test interval of 0.5 Mc: (a) the PBS lubricant and (b) the HA lubricant.



(a) ACS-I + PBS + AA (3 - 3.5 Mc)



(b) ACS-I + DW + AA (5 - 5.5 Mc)

Figure 5.47: The protein constituent fractions for the R implants after a test interval of 0.5 Mc: (a) the PBS lubricant and (b) the DW lubricant.

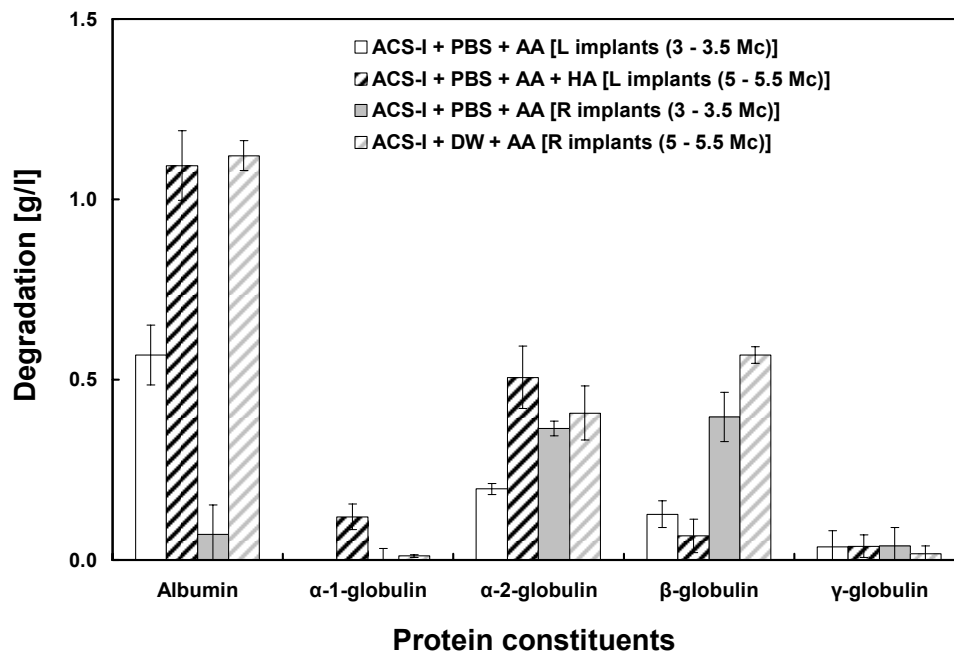
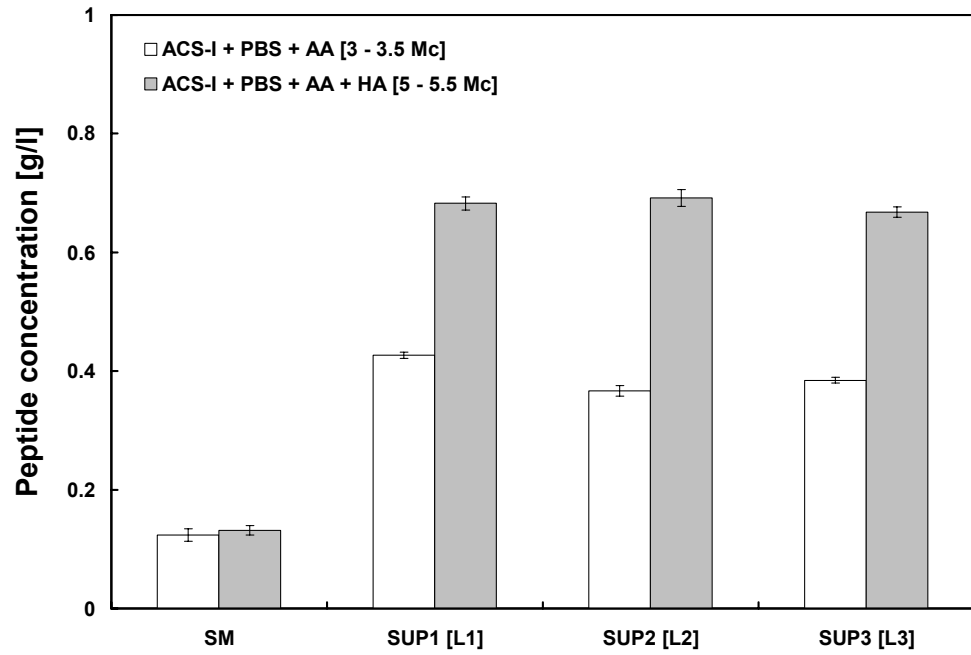


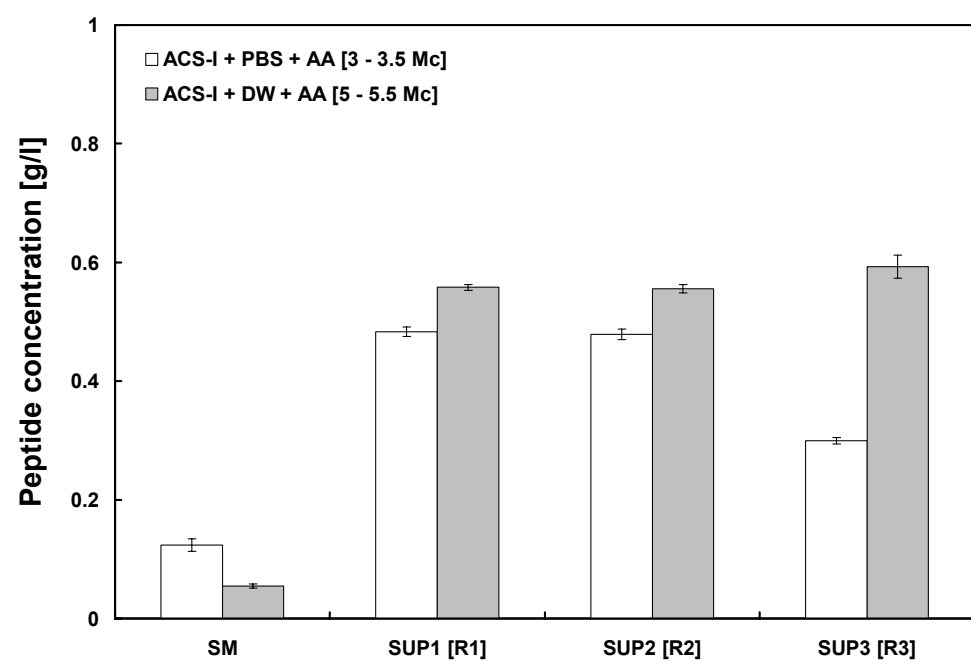
Figure 5.48: The protein constituent degradation for the serum lubricants.

5.4.4 Peptide Concentration

The peptide concentration increased in all lubricants (Fig. 5.49). For the L implants, the peptide concentration for the PBS lubricant increased 3.2-times in the SUP and 5.2-times for the HA lubricant compared with the SMs. For the R implants, the peptide concentration for the PBS lubricant increased 3.4-times in the SUP and 10.4-times for the DW lubricant. The peptide concentration was highest in the HA lubricant ($p \leq 0.001$, GLM with Tamhane), lower for the DW lubricant ($p \leq 0.001$, GLM with Tamhane), and lowest for the PBS lubricant ($p \leq 0.001$, GLM with Tamhane). There was no significant difference between the mean peptide concentration of the PBS lubricant used in both L and the R implants ($p = 0.438$, GLM with Tamhane). An increased relative change in peptide concentration (peptide concentration in the SUP *minus* the peptide concentration in the SM) coincided with increased wear rates when HA was added to the lubricant for the L implants and when PBS was replaced with DW as the dilutive medium (Fig. 5.50).



(a) L implants



(b) R implants

Figure 5.49: The peptide concentration of the SM and the SUPs.

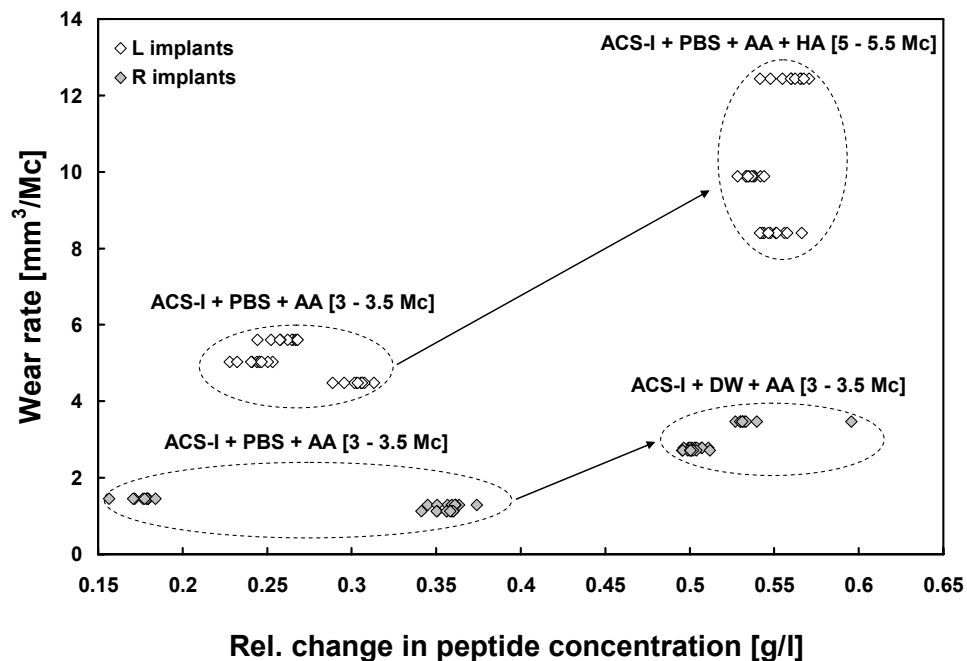
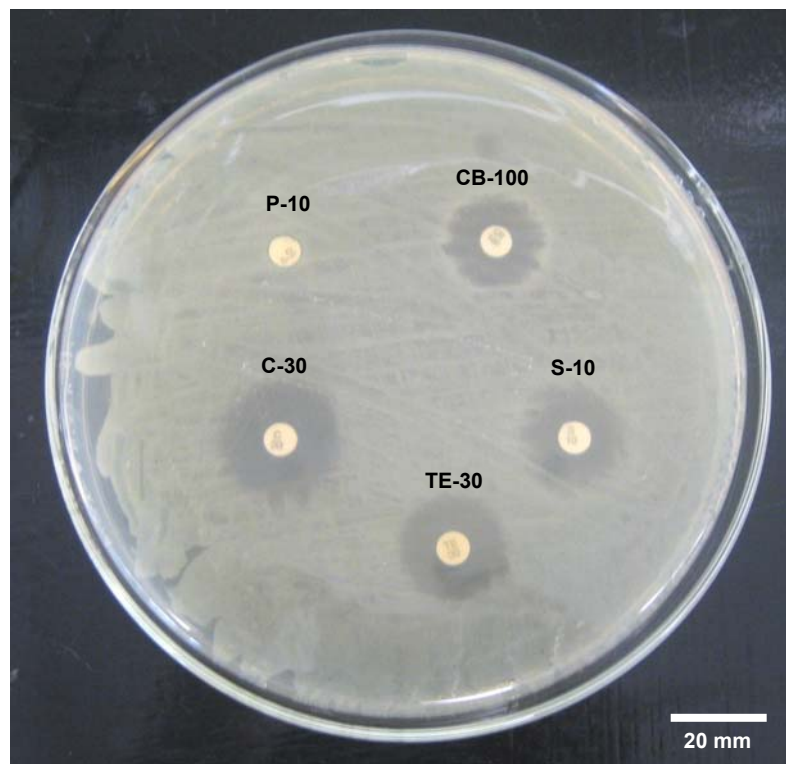


Figure 5.50: The wear rate plotted versus the relative change in peptide concentration (peptide conc. “SUP” minus peptide conc. “SM”).

5.4.5 Microbial Resistance

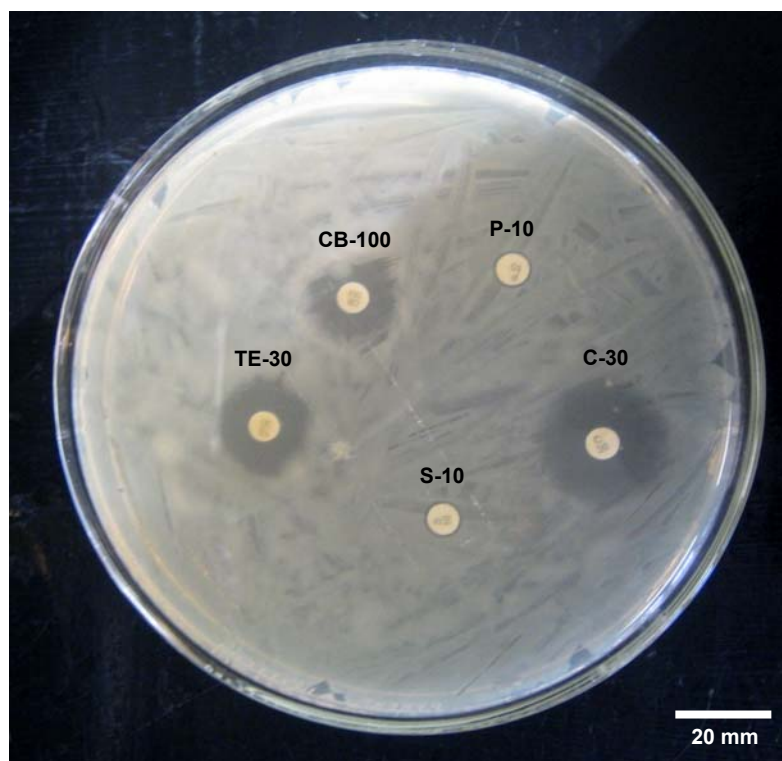
Microbial contamination was assessed after a total of 0.5 Mc and 5.5 Mc. Microbial contamination was not detected after 0.5 Mc but was detected after 5.5 Mc. The serum samples from the L implants and the R implants after 5.5 Mc showed that an isolated *E. cloacae* organism reoccurred. This indicated that *E. cloacae* JK-1 might have developed some resistance toward AA and possibly resulted in an altered organism. This organism was referred to as *E. cloacae* JK-2. Thus, it was deemed necessary to investigate to which AA constituents the *E. cloacae* JK-2 developed its resistance. To do this, the antimicrobial susceptibility test described in Section 3.5.3 was used. Antibiotic discs containing streptomycin and penicillin were placed on the Müller-Hinton agar petri dishes. The Müller-Hinton agar petri dishes were inoculated with either *E. cloacae* JK-1 or *E. cloacae* JK-2. In addition, three more antibiotic discs containing carbenicillin, tetracycline, and chloramphenicol were also

placed on the petri dishes to investigate if they would inhibit the growth of *E. cloacae* JK-1 and of *E. cloacae* JK-2 for future knee simulator testing. *E. cloacae* JK-1 was resistant towards penicillin and carbenicillin; intermediate resistant towards streptomycin and tetracycline; and highly susceptible to chloramphenicol (Fig. 5.51; Table 5.6). *E. cloacae* JK-2 was resistant towards penicillin, streptomycin and carbenicillin; intermediate resistant towards tetracycline; and highly susceptible to chloramphenicol.



(a)

Figure 5.51: The MH-plates incubated with a) *E. cloacae* JK-1 collected in Section 5.3 (no exposure to AA). Note that *E. cloacae* JK-1 was resistant towards penicillin (P-10) and carbenicillin (CB-100).



(b)

Figure 5.51 (continued): The MH-plates incubated with *E. cloacae* JK-2 collected in Section 5.4 after 5.5 Mc. Note how *E. cloacae* JK-2 developed further resistant towards streptomycin (S-10) in Section 5.4 after 5.5 Mc.

Table 5.6: The zone of inhibition (ZOI) for several antibiotic disks (penicillin (P-10); streptomycin (S-10); carbenicillin (CB-100); tetracycline (CB-30), chloramphenicol (C-30)) incubated on *E. cloacae* JK-1 collected in Section 5.3 (no exposure to AA) and *E. cloacae* JK-2 collected in Section 5.4 after being exposed to AA for 5.5 Mc.

Zone of inhibition for several antibiotics (Nomenclature, disk potency)	<i>E. cloacae</i>	
	JK-1 collected in Section 5.2; no exposure to AA	JK-2 collected in Section 5.4; exposure to AA
Penicillin (P-10; 10 U*)	0 mm (R)	0 mm (R)
Carbenicillin (CB-100; 100 µg)	14 ± 1 mm (R)	14 ± 1 mm (R)
Streptomycin (S-10; 10 µg)	14 ± 1 mm (I)	0 mm (R)
Tetracycline (TE-30; 30 µg)	15.33 ± 1 mm (I)	15 ± 2 mm (I)
Chloramphenicol (C-30; 30 µg)	26 ± 1 mm (S)	27 ± 1 mm (S)

R ≡ *E. cloacae* was resistant to AA; I ≡ *E. cloacae* JK has intermediate resistant to AA; S ≡ *E. cloacae* JK is susceptible to AA. Zone diameter interpretive standards: penicillin, R: ZOI ≤ 28 mm; streptomycin, I: ZOI = 12 - 14 mm; carbenicillin, R: ZOI ≤ 19 mm; tetracycline, I: ZOI = 15 - 18 mm; chloramphenicol, S: ZOI ≥ 18 mm¹⁹⁵ (*1U ≈ 1.660538782 x 10⁻²⁷ kg).

5.4.6 Differential Scanning Calorimetry

The thermal stability of the lubricants indicated how resistant the proteins were to shear damage under load and motion and thus degradation. There was also some merit in comparing the thermal stability of the serum lubricants with SF since an ideal serum lubricant would have similar thermal stability to SF. To gain some insight into the thermal stability of the lubricants triplicate samples of the DW lubricant, the PBS lubricant, the HA lubricant, and SF (SF 7, SF 8, and SF 18) were analyzed using Differential Scanning Calorimetry (DSC) methods. Such basic DSC measurements were outsourced and performed by Lee-Ann Brière at the Department of Biochemistry, UWO (see Section 3.5.5 for details on the methods for DSC measurements). The buffer solutions in the DSC tests were DW + AA, PBS + AA, PBS + AA + HA and PBS for the lubricants ACS-I + DW + AA, ACS-I + PBS + AA, ACS-I + PBS + AA + HA, and SF, respectively. DW lubricant and ACS-I + PBS + AA had a significantly lower change in enthalpy (ΔH) compared with ACS-I + PBS + AA + HA and SF ($p \leq 0.004$, ANOVA and Tamhane) (Fig. 5.52 - 5.54). Both the transition midpoint temperature (T_{m1}) and the maximal specific heat capacity at constant pressure (c_{p-max}) increased when ACS-I + AA was diluted with PBS instead with DW. Such change in dilutive medium increased the osmolality of the lubricant (Table 5.5). However, T_{m1} for PBS lubricant was lower compared with SF. The DW lubricant and PBS lubricant did not have a T_{m3} . As explained earlier in Section 3.5.5, the unfolding, of the HA lubricant was highly cooperative (only one very well defined c_p -peak during unfolding) and had a comparable T_{m1} to SF. The unfolding of SF samples was a multi-stage process showing three T_m , with T_{m1} having the highest c_p (Table 5.7). The unfolding of SF was consequently less cooperative (several c_p -peaks during the unfolding) than for the HA lubricant. ACS-I + DW + AA had a lower T_{m1} and $T_{m(c_p-max)}$ compared with SF. The thermograms of SF were similar between samples SF 7, SF 8, SF 18. The unfolding of SF was less cooperative than ACS-I + PBS + AA + HA but showed similar in $T_{m(c_p-max)}$, ΔH and ΔS (Fig.

5.55, 5.56). The ΔS for the lubricants was almost proportional to ΔH since the $T_{m(\text{cp-max})}$ was of the same order of magnitude between the lubricants.

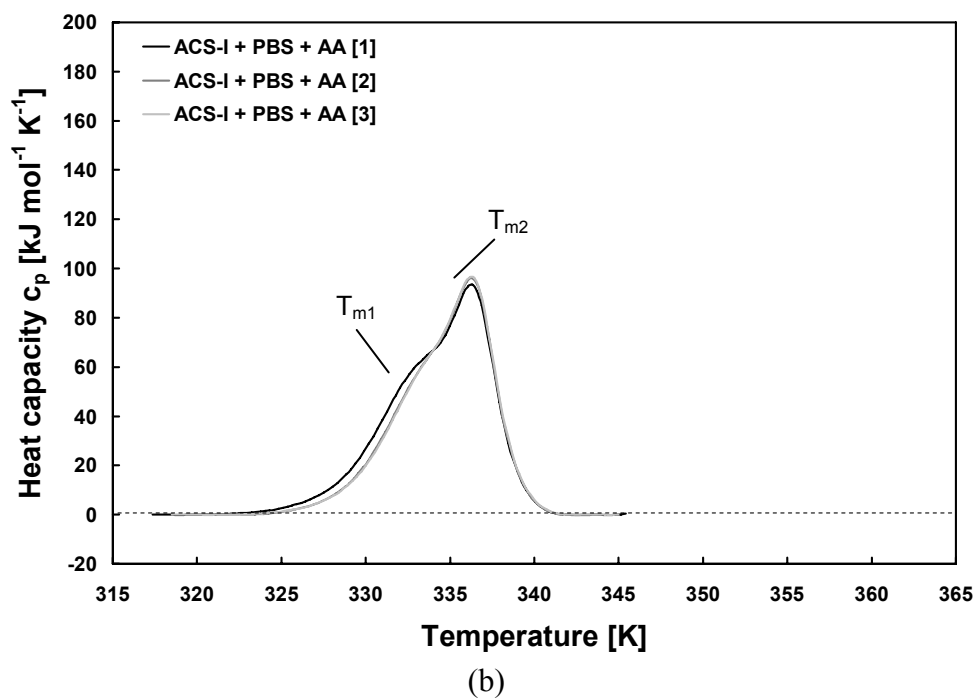
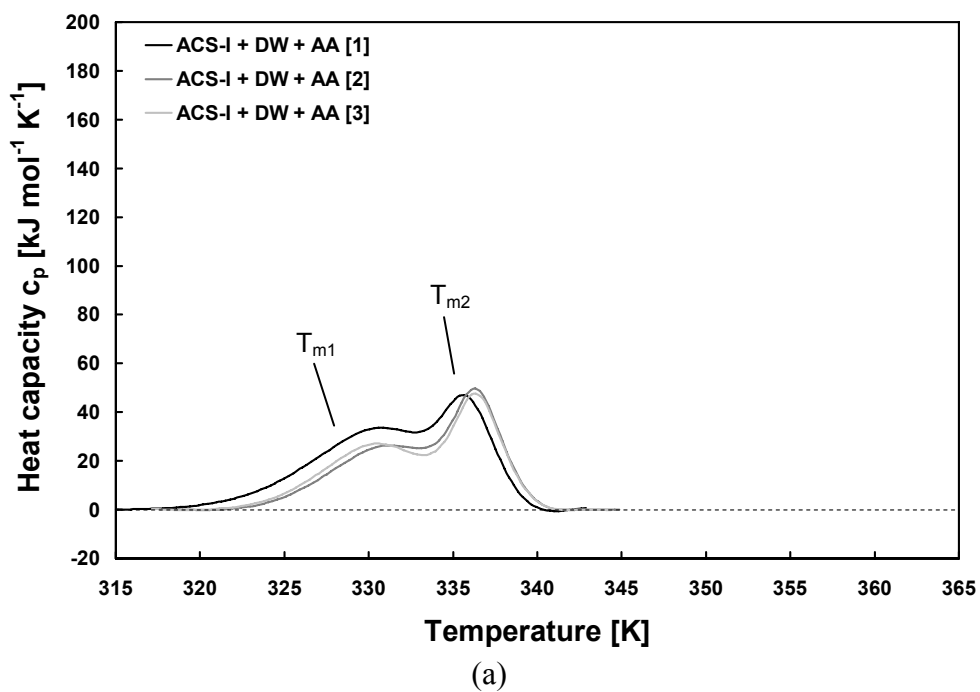
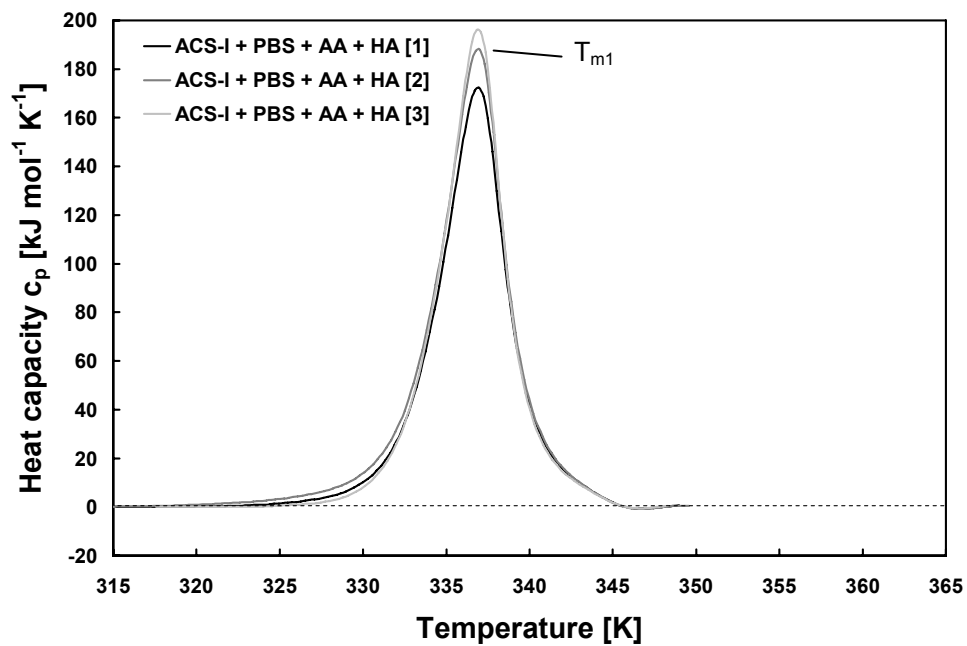
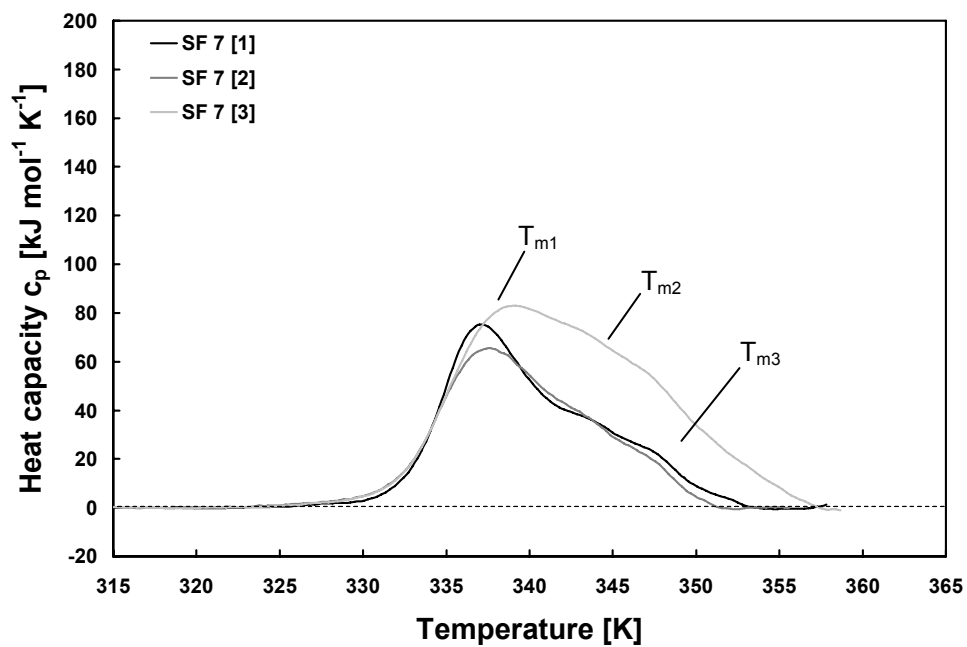


Figure 5.52: Thermogram of (a) the DW lubricant and (b) the PBS lubricant. Note the differences between the shapes of the curves of the DW lubricant and the PBS lubricant.

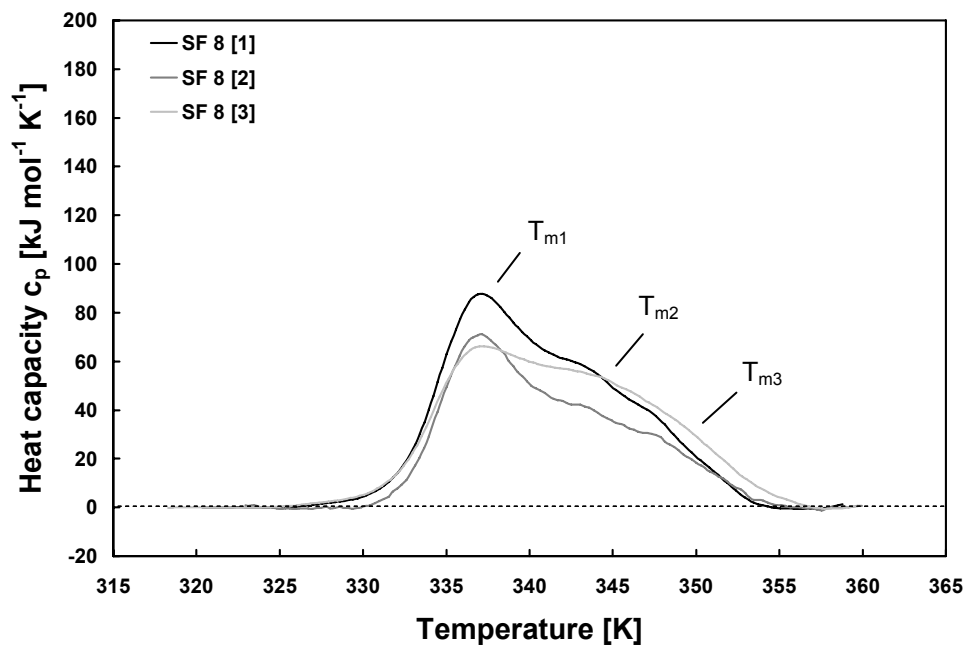


(a)

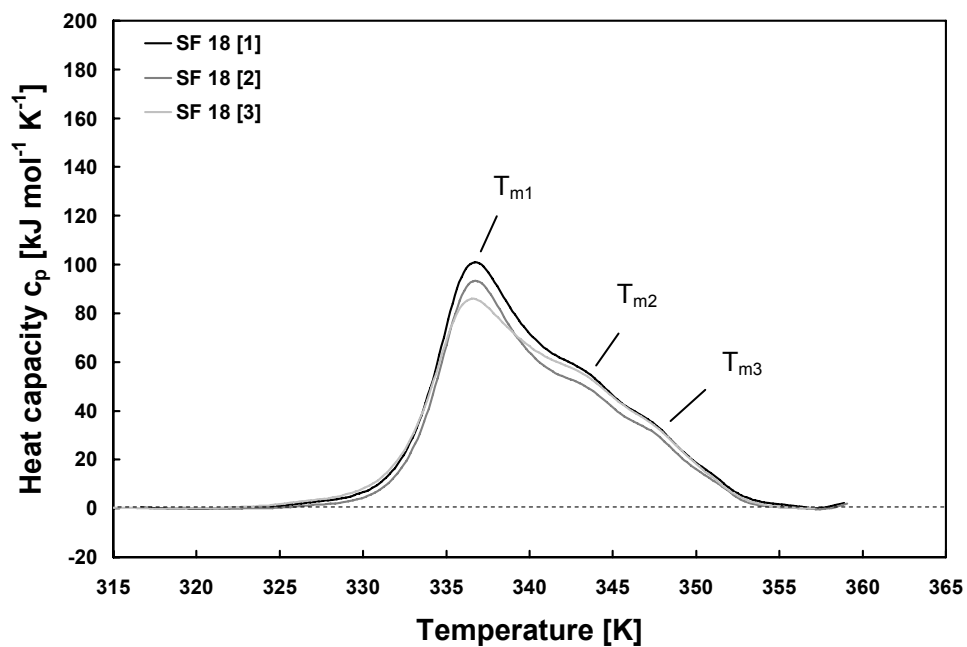


(b)

Figure 5.53: Thermogram of (a) the HA lubricant and (b) SF 7. Note the differences between the shapes of the curves of the HA lubricant and SF 7.



(a)



(b)

Figure 5.54: Thermogram of SF 8 and SF 18. Note the similarity between the shapes of the curves of SF 8 and SF 18.

Table 5.7: Transition midpoint temperatures, T_m , of the DW lubricant, PBS lubricant, HA lubricant, SF 7, SF 8, and SF 18 ($n = 3$).

Lubricant	Transition midpoint temperature T_m [K]		
	T_{m1}	T_{m2}	T_{m3}
ACS-I + DW + AA	330.71 ± 1.55	336.30 ± 1.22	N/A
ACS-I + PBS + AA	333.39 ± 1.05	336.46 ± 0.05	N/A
ACS-I + PBS + AA + HA	337.32 ± 0.58	N/A	N/A
SF 7	337.32 ± 1.83	342.87 ± 1.33	347.72 ± 3.87
SF 8	336.73 ± 0.52	342.63 ± 1.73	348.40 ± 2.22
SF 18	336.35 ± 2.13	341.26 ± 4.26	347.48 ± 2.01

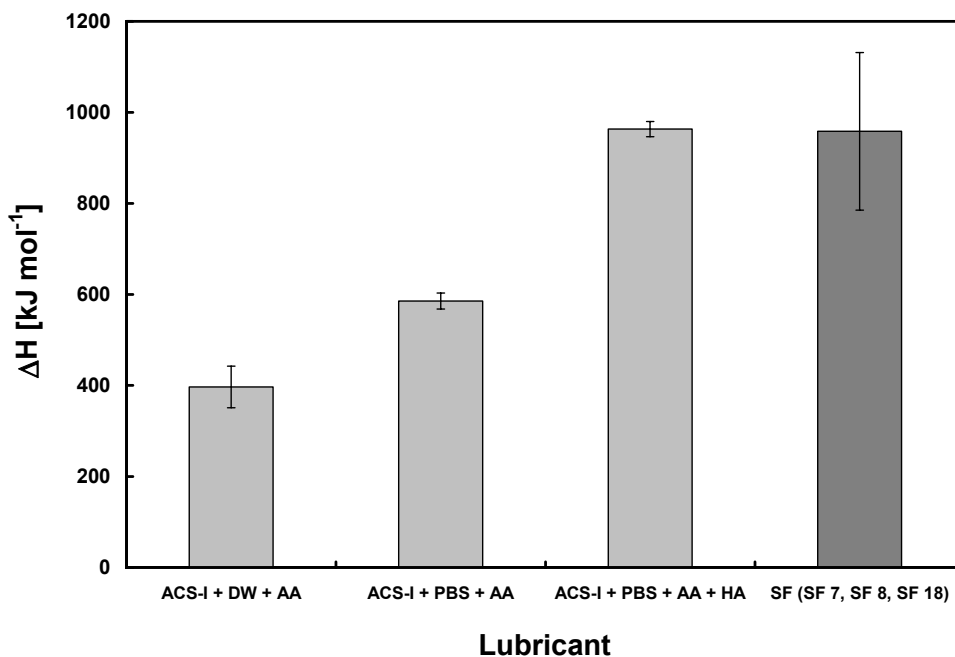


Figure 5.55: The change in enthalpy, ΔH , for the DW lubricant, the PBS lubricant, the HA lubricant and SF (SF 7, SF 8, SF 18). Note the similarity in magnitude between the HA lubricant and SF.

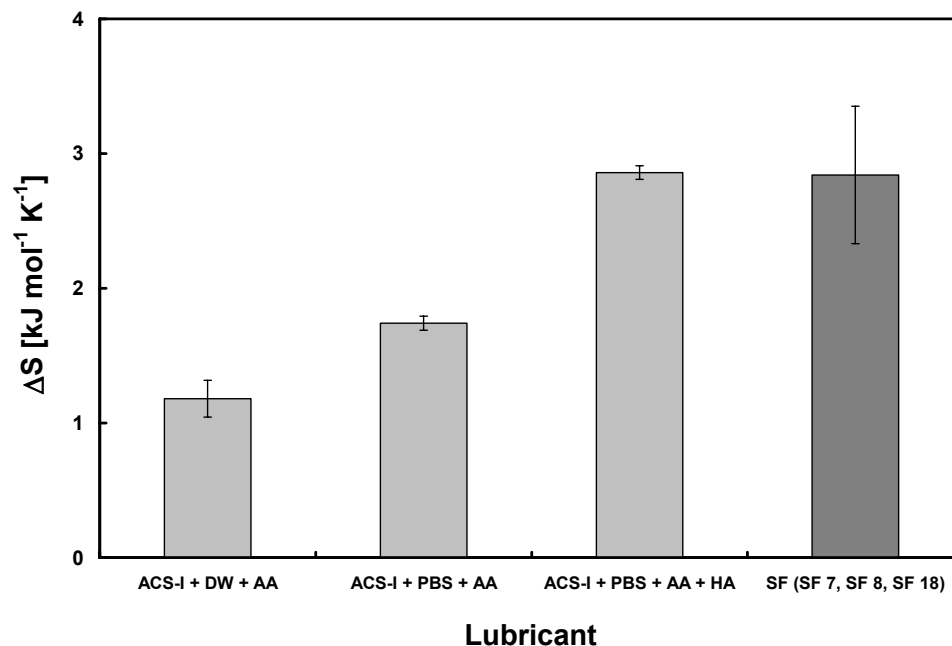
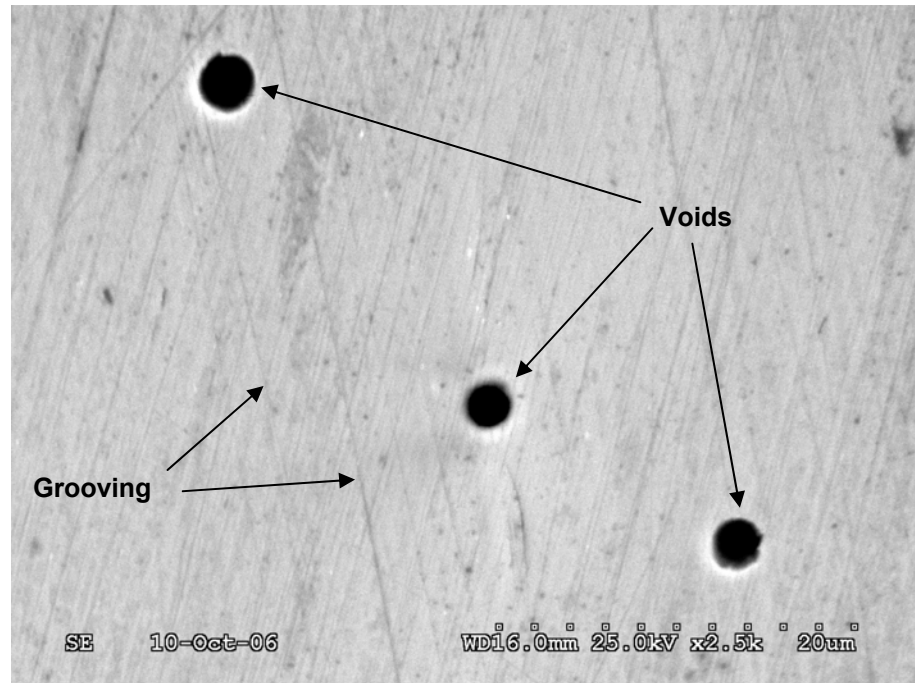


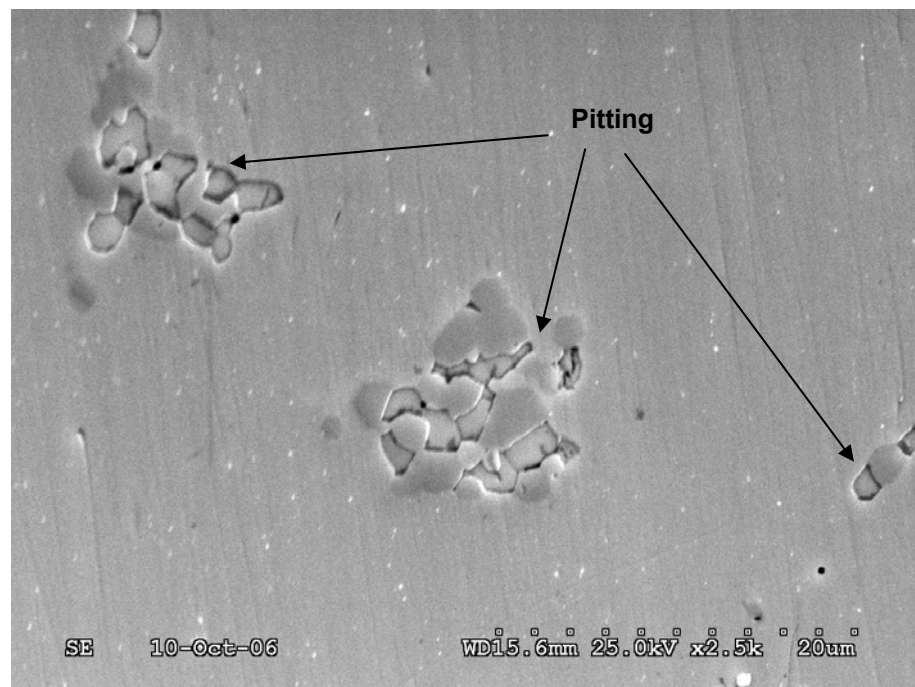
Figure 5.56: The change in entropy, ΔS , for the DW lubricant, the PBS lubricant, the HA lubricant, and SF (SF 7, SF 8, SF 18). Note the similarity between the HA lubricant and SF.

5.4.7 Scanning Electron Microscopy

Observing the bearing surface of an as-received (obtained directly from the manufacturer) femoral component under the SEM (Hitachi Electronics Ltd., Naka, Japan) revealed some voids (Fig. 5.57.a). Some grooves from the polishing process were also observed. Assessing the surface damage on femoral components, that had been retrieved from patients undergoing revision surgery, revealed a characteristic pitting feature (Fig. 5.57.b). Interestingly, such pitting features were also observed on the femoral component of the L implants worn with both ACS-I + PBS and ACS-I + PBS + HA and on the femoral components worn with both ACS-I + PBS and ACS-I + DW (Fig. 5.58). This indicated that the retrieved cast femoral components, the cast R implants, and the cast L implants might have sustained by some corrosion type of surface damage (tribochemical wear mechanism).

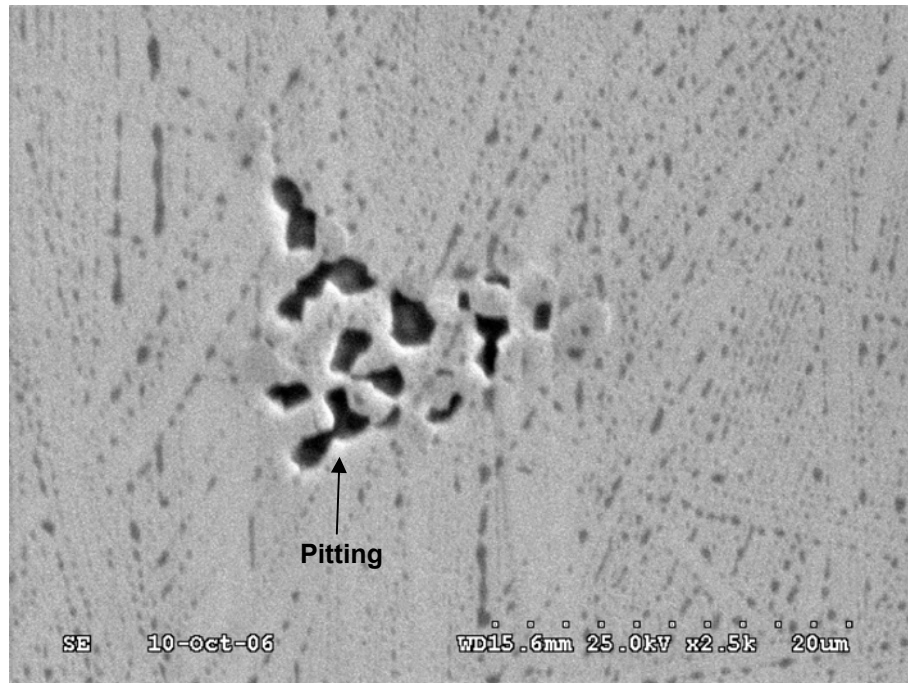


(a)

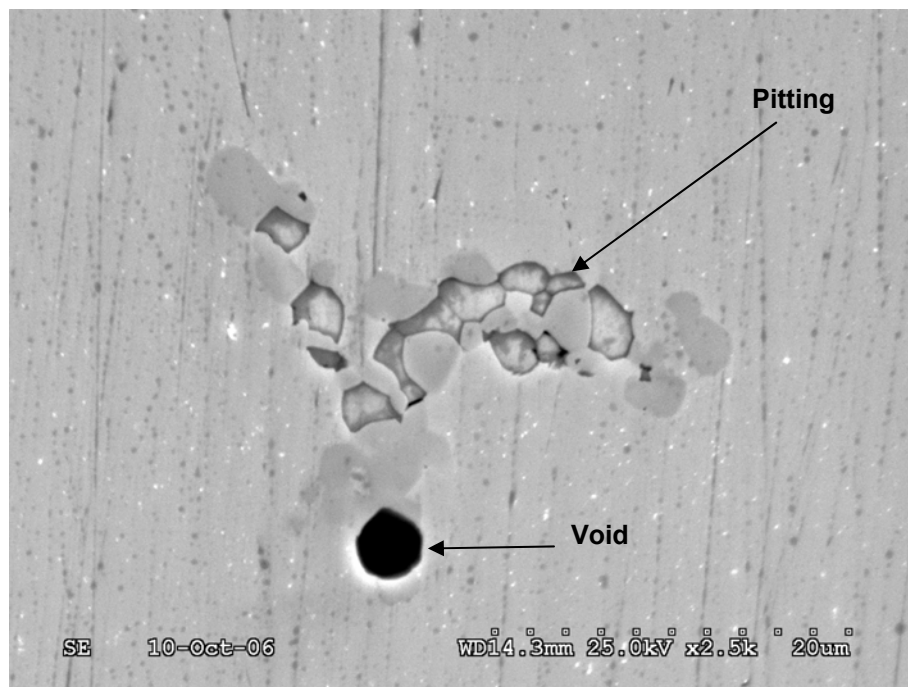


(b)

Figure 5.57: SEM micrographs showing typical surface features on a) an as-received cast femoral component and b) a retrieved cast femoral component (IP = 102.05 months). Note the voids on the as-received femoral components and the pits on the retrieved femoral component (anterior direction \equiv top of page).



(a)



(b)

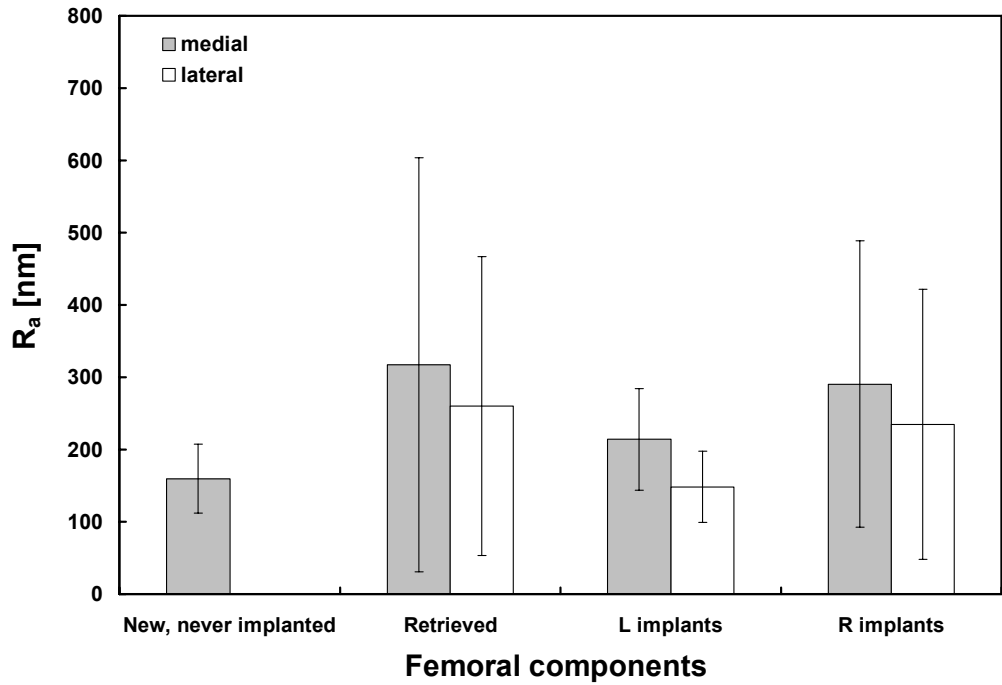
Figure 5.58: SEM micrographs showing typical surface features on (a) a cast femoral component of the L implants (L2; worn with ACS-I + PBS + AA and ACS-I + PBS + AA + HA) and (b) a cast femoral component of the R implants (R2; worn with ACS-I + PBS + AA and ACS-I + DW + AA) after 5.5 Mc. Note the pitting in both micrographs (anterior direction \equiv top of page).

5.4.8 Femoral Surface Roughness Measurements

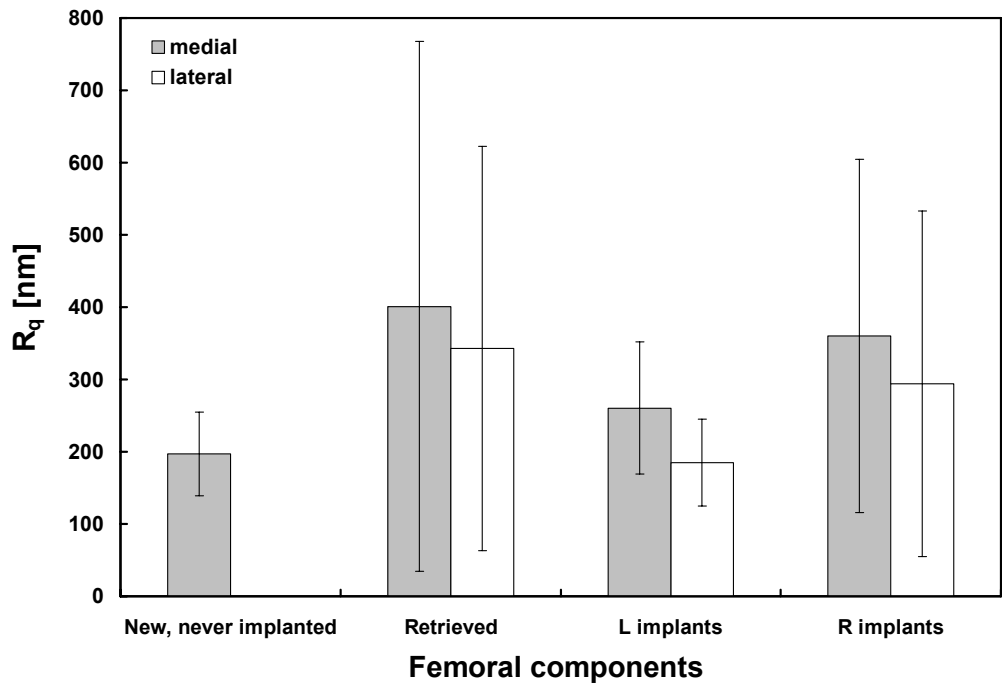
The centre line average (R_a) and root mean square (R_q) surface roughness values were measured using a non-contact profilometer (Wyko[®] NT1100, Veeco Instruments Inc., Woodbury, NY) on an as-received femoral component, on six retrieved AMK[®] femoral components (IP = 66.83 ± 39.05 months; range, 16.14 - 114.15 months), and on the femoral components from the L implants and the R implants after 5.5 Mc. The R_a and R_q for the as-received component had the lowest surface roughness ($p < 0.001$, ANOVA and Fisher's) (Table 5.8, Fig. 5.59). The R_a and R_q for the L implants were significantly lower than for the R implants ($p \leq 0.034$, Student's t-test). The medial sides of the femoral components of the L implants had a higher R_q ($p = 0.024$, Paired-samples t-test) and R_a ($p = 0.031$, Paired-samples t-test) compared with their lateral sides. Such findings were not observed on the R implants ($p \geq 0.470$, Paired-samples t-test). The R_a and R_q for the L implants was significantly lower than the R_a and R_q for the retrievals ($p = 0.004$, ANOVA and Tamhane). The R_a and R_q for the R implants did not have a statistically significant difference compared with the values for the retrievals ($p = 0.843$, ANOVA and Tamhane).

Table 5.8: Surface roughness measurements (R_a , R_q) for the AMK[®] femoral components.

Femoral components		Surface roughness [nm]	
		R_a [mean \pm SD]	R_q [mean \pm SD]
New, never implanted (n = 1)	Medial	159.69 \pm 47.90	196.98 \pm 57.77
Retrieved (n = 6)	Medial	401.11 \pm 366.64	317.53 \pm 286.56
	Lateral	342.86 \pm 279.39	260.03 \pm 206.94
L implants (n = 3)	Medial	213.93 \pm 70.56	260.29 \pm 91.42
	Lateral	184.85 \pm 59.78	185.95 \pm 59.78
R implants (n = 3)	Medial	290.46 \pm 197.91	360.14 \pm 244.46
	Lateral	234.90 \pm 183.79	293.82 \pm 239.15



(a) R_a

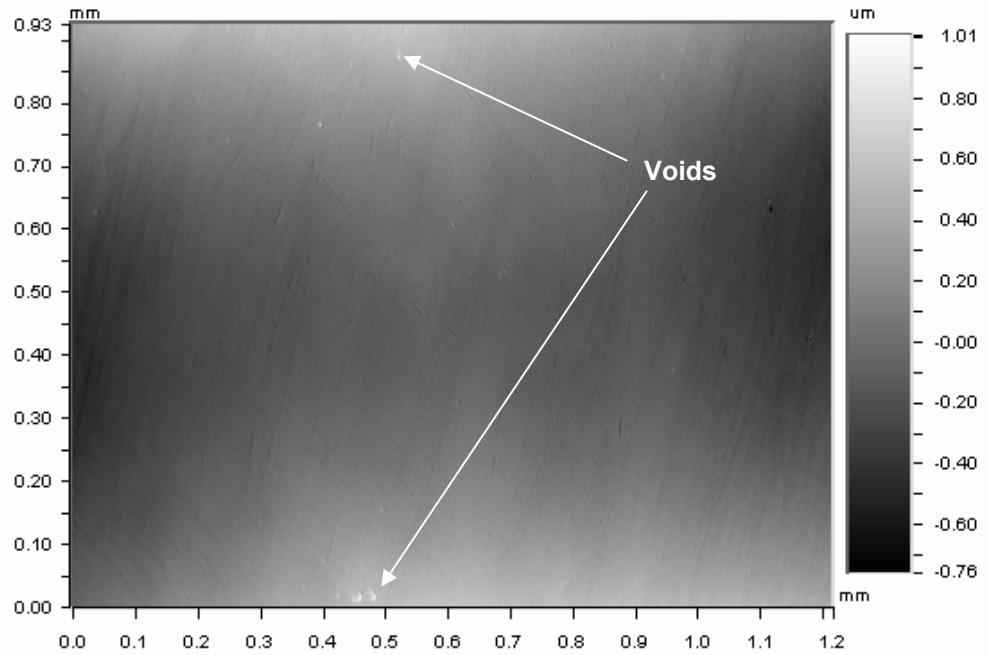


(b) R_q

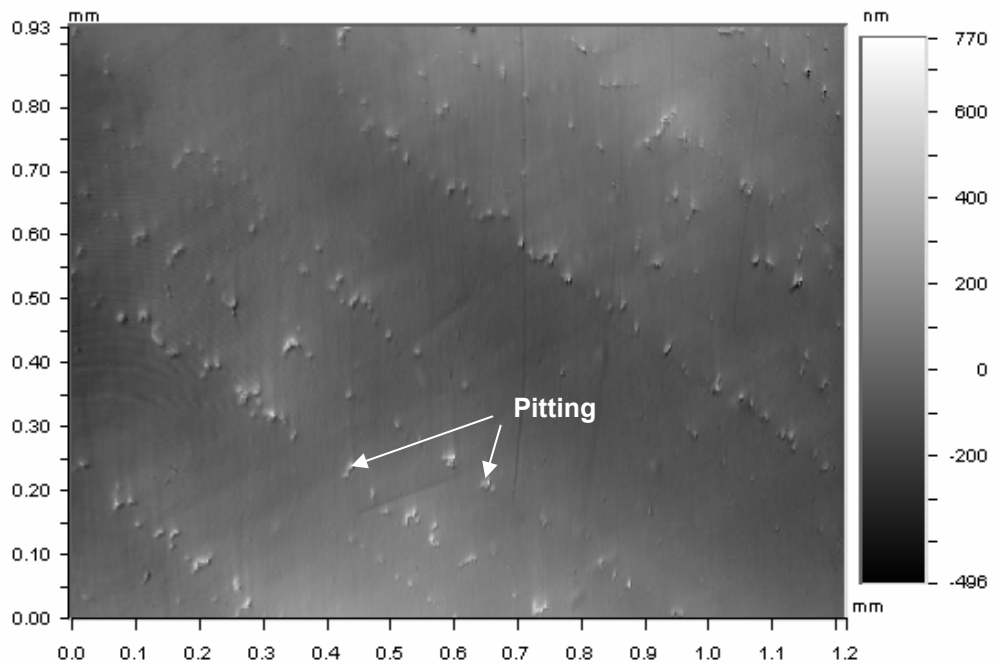
Figure 5.59: Surface roughness for several femoral components.

5.4.9 Surface Profiles

Surface profiles were obtained from the femoral components that had been studied in the SEM as described in Section 5.4.8. The as-received femoral component appeared to have few voids on the bearing surface (Fig. 5.60). The smooth surface profile (see gray scale bar on the right of the figures) confirmed the low surface roughness measured in Section 5.4.9. The retrieved femoral component revealed many imperfections, some of which were similar to the surface pitting features that were also observed in the SEM. The surface profile of the retrieved femoral component was similar in appearance and scale to the surface profile of the L implants (L2; worn with ACS-I + PBS + AA and ACS-I + PBS + AA + HA) after 5.5 Mc (Fig. 5.61). The surface profile of the R implants (R2; worn with ACS-I + PBS + AA and ACS-I + DW + AA) appeared rougher than surface profile for the retrieved femoral components and the L implants. The pitting damage feature was observed on the retrieved femoral components and all femoral components from the simulator wear tests (L implants and R implants).

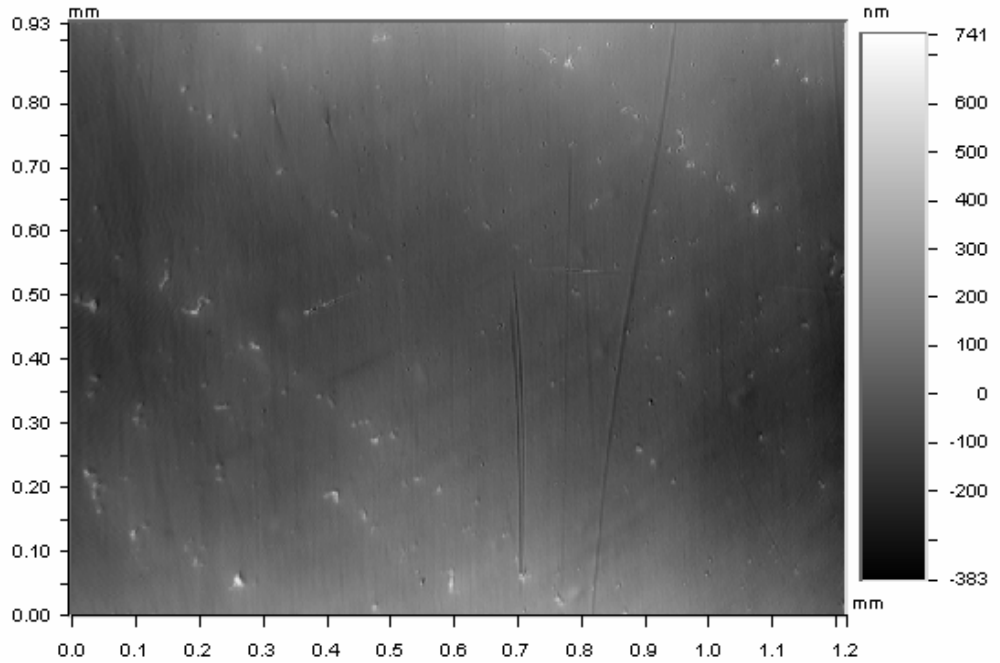


(a) New, never implanted femoral component

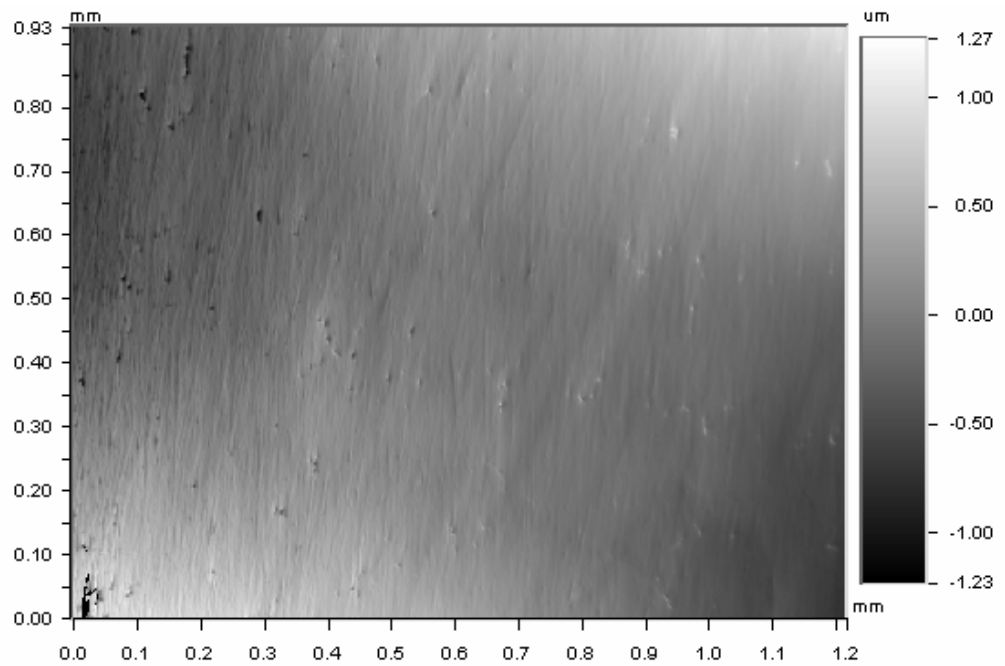


(b) Retrieved femoral component (IP = 102 months)

Figure 5.60: Surface profile obtained with the WYCO profilometer (anterior direction \equiv top of page).



(a) L implant femoral component (L2; tested in ACS-I + PBS + AA and ACS-I + PBS + AA + HA)



(b) R implant femoral component (R2; tested in ACS-I + PBS + AA and ACS-I + DW + AA)

Figure 5.61: Surface profiles obtained with the WYCO profilometer after 5.5 Mc. Note the scaling difference between the surface profiles of (a) and (b), confirming the rougher surface for the R implants (anterior direction \equiv top of page).

5.4.10 Discussion of the Mass Gain Period

Pre-soaking the PE inserts in DW and subsequently exposing the PE inserts to ACS-I + PBS + AA and wear testing resulted in a negative wear volume during the first Mc of testing. As mentioned in Section 5.2, increased osmolality caused by the presence of proteins might have increased the fluid sorption if it had been used during the pre-soaking period of PE inserts rather than DW. A sudden uptake of fluid was blamed for the measurements of negative wear that occurred in the wear testing of the present section. Thus, the PE inserts should be subjected to the similar soaking medium (and measuring protocol) during the pre-soaking period as used during the actual wear testing and such practices should be included in ISO 14243^{41,42}.

5.4.11 Discussion on the Effects of HA on PE Wear

HA has been recognized in the past as a constituent of SF^{116,447,448}. However, this constituent has only received minor attention in pin-on-plate friction tests³⁴ and a more substantial but limited attention in simulator wear testing of knee implants^{102,156}. Mazzucco et al.³⁴ used HA in their friction studies and reported that HA did not affect the boundary lubrication process under unidirectional sliding. Their HA had an average molecular weight (MW) of 1.8 MDa and an average concentration of 1.5 g/l based on measurements of SF from a 42 patients. Such values were adopted for the lubricant mixtures in the present thesis. Wang et al.¹⁵⁶ based their HA concentration of 0.34 g/l on a study by Saari et al.¹¹⁶ which was less than a quarter of the concentration suggested by Mazzucco³¹. Although Wang et al.¹⁵⁶ used ACS diluted to a protein concentration of 35 g/l, an effect of HA on PE wear was not reported in their hip simulator wear tests. DesJardins et al.¹⁰² conducted the simulator wear tests on knee implants using HA in the lubricant and using a force controlled simulator. They selected the HA concentration and its MW from earlier published work^{116,448,449} since the data by Mazzucco et al.³¹ was not available at that time. DesJardins et al.¹⁰² reported a higher PE wear rate when

HA was added to the lubricant. The investigations of the present thesis also found that the PE wear rate was higher. As shown in Table 5.9, there were many differences between the wear test conditions of DesJardins et al.¹⁰² and those of the present thesis such as differences in serum type, total protein concentration, microbial inhibition, dilutive media and the MW of the added HA. DesJardins et al.¹⁰² did not investigate the amount of protein degradation, change in peptide concentration or the effects of HA on the thermal stability of the lubricant.

Table 5.9: The lubricant composition used in the present study compared with the composition utilized by DesJardins et al.¹⁰².

Lubricant composition	Present Study	DesJardins et al. ¹⁰²
Serum type	ACS-I	BCS
Total protein concentration [g/l]	17	30
Type of microbial inhibitor	AA	SA
Dilutive media	PBS	DW
HA molecular weight [MDa]	1.78	2.3
HA concentration [g/l]	1.5	1.5

The amplifying effect of adding HA on the PE wear rate in the investigations of the present thesis was only 29 % of that value reported by Desjardins et al. (2-times rather than 6.88-times). They suggested that some tribo-corrosion occurred on the femoral components due to the presence of Cl ions in the HA compound which increased its surface roughness, and thus increased abrasive wear. Such tribo-corrosion might have included the repeated removal of a passive layer from the CoCr surface. The wear behaviour of such a passive layer under sliding conditions might depend on the friction forces, bearing material properties, surface topography, and the electrolytic conductivity and potential of the lubricant⁶⁰. In the present study, the as-received femoral components showed small round voids, so called *Kirkendall* holes, which were possibly introduced during the casting process. Such voids

might have affected the roughness measurements and might have promoted tribo-corrosion which could cause pitting surface damage^{102,363}. DesJardins et al.¹⁰² did not observe any tribo-corrosion on the femoral components worn in the lubricant without HA, which was contrary to the present study. The HA used in the present wear tests did not contain any Cl ions (Lifecore Biomedical, Chaska, MN). However, the L implants and the R implants were exposed to PBS that contained Cl ions and these ions might have promoted the tribo-corrosion. It was then expected that a higher R_a and R_q of the femoral components would have caused a higher PE wear rate when HA was added to the lubricant¹⁰². Surprisingly, the femoral components of the L implants worn with HA in the lubricant had lower R_a and R_q values than the femoral components of the R implants worn without HA. However, comparing the wear behaviour of the L implants and the R implants might have been compromised because the L implants had higher wear for all lubricants perhaps because the kinematics of the L bank differed somewhat for that of the R bank.

The biochemical analyses of the lubricants also gave some unanticipated findings. It was intuitively felt that a lower thermal stability would suggest that the proteins in a lubricant would degrade more easily and this would be accompanied by an increased peptide concentration and higher PE wear. Thus, it was expected that a lower thermal stability would occur for ACS-I + PBS + AA + HA compared with ACS-I + PBS + AA. Instead, DSC analysis showed that the thermal stability of ACS-I + PBS + AA was lower than that of both ACS-I + PBS + AA + HA and SF. The similar thermal stability of ACS-I + PBS + AA + HA and SF suggested that adding the selected HA was essential to mimic the thermal stability of SF. Thus, a closer look at the possible interactions between proteins and HA was taken.

In 2000, Xu et al.¹²² showed that HA created covalent bonds with native albumin proteins when $\text{pH} \leq 5$. Interestingly, at the physiological pH of 7.2, interactions between the long HA chains and the albumin were dominated by van der Waal's forces and thus binding via strong covalent bonds was unlikely to occur. In the present study, the pH-level uniformly dropped from

7.6 ± 0.1 at the start of the wear tests to approximately 6.8 ± 0.2 after a test interval. Such decrease in pH was possibly due to the repeatedly added AA with a pH = 5.2. Oates et al.¹²³ suggested that the proteins remained aggregated in a tenuous polymeric network and stayed entangled within the HA chains at such pH levels. In addition, proteins were reported to be more thermodynamically stable in less hydrated environments^{168,176}. Under such conditions, proteins were less vulnerable to rapid, reversible local disruption of their structure and therefore required higher ΔH to initiate unfolding. Since HA is known for its ability to retain H₂O¹²¹, it followed that adding HA to the lubricant possibly decreased the amount of *free* H₂O in the solvent and therefore increased the thermal stability of the proteins. Reduced hydration possibly enhanced the *hydrophobic effect* in proteins, suggesting that the hydrophobic residues in proteins became buried inside the core of the proteins. Such an effect may have contributed to protein aggregation in the protein-HA network¹²³. In the present study, the unfolding process of SF appeared to be less cooperative compared with ACS-I + PBS + AA + HA, despite the lubricants' similarities in ΔH and ΔS . Such findings suggested that the SF protein constituents required higher temperatures to complete their irreversible unfolding^{104,169}. Higher thermal stability of human serum albumins compared with bovine serum albumin has been recently reported and may explain such higher unfolding temperature for SF⁴⁵⁰. Last but not least, it was likely that the remaining globulin protein constituents affected the thermal behaviour of ACS-I. However, it went beyond the scope of this thesis to conduct a detailed thermal analysis of individual protein constituents in solution with HA to gain insight on their individual effects on T_m , ΔH and ΔS .

The protein constituent degradation and the relative change in peptide concentration were higher for ACS-I + PBS + AA + HA compared with ACS-I + PBS + AA and coincided with a 2-times increase in PE wear rate. In Section 5.3, the author showed that the simulator wear process at the CoCr-PE interface depended significantly on the type of protein constituents and their individual concentrations. It was speculated that the proteins were consolidated under load

and motion which possibly led to a solid-like protein layer that acted as a solid lubricant. Generally, the ability of a solid-like structure to carry large loads without failure depends on the ductility of the material that comprises such a structure. Highly ductile materials have a superior ability to dissipate applied stresses by plastic deformation compared with materials of low ductility.

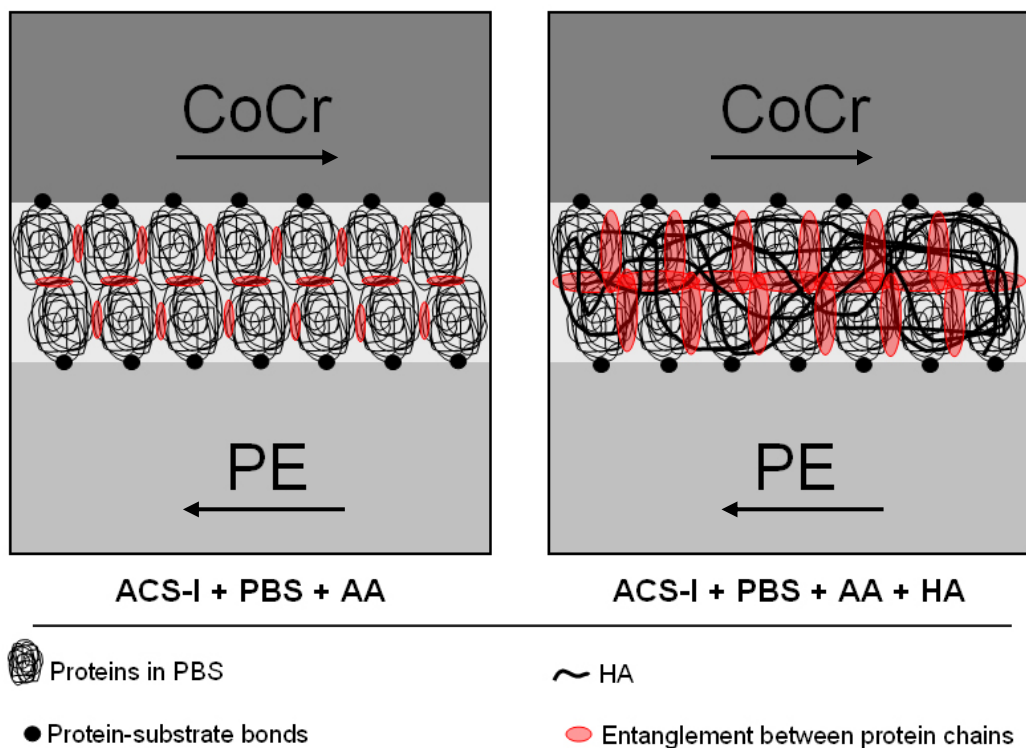


Figure 5.62: Schematic showing the possible protein interactions in the protein layer at the CoCr-PE interface for ACS-I + PBS + AA and ACS-I + PBE + AA + HA during the wear test. Adding HA to ACS-I + PBS + AA increased the thermal stability of the lubricant. It was speculated that ACS-I + PBS + AA + HA was less ductile under load and motion than ACS-I + PBS + AA due to the protein-HA network. The limited ability of ACS-I + PBS + AA + HA to dissipate plastic deformation possibly led to higher temperature and higher shear inside the protein layer and increased the protein degradation and the peptide concentration despite its higher thermal stability compared with ACS-I + PBS + AA. It was speculated that such a conditions were comparable to the *kneading effect*, which is known to occur in ductile metals under high shear forces⁴⁵¹ and in polymer processing equipment⁴⁵² and was deemed responsible for the higher PE wear rate for ACS-I + PBS + AA + HA compared with ACS-I + PBS + AA. The arrows indicate the direction of surface motion.

It is speculated that adding HA to the ACS-I + PBS + AA possibly reduced the ductility of the compacted protein layer under load and motion but also increased the thermal stability of the lubricant. Consequently, such a protein layer was impaired in its ability to dissipate large plastic deformation which may have led to a localized increase in temperature and shear inside the protein layer (Fig. 5.62). Similar behavior can be observed in both ductile metals under high shear forces⁴⁵¹ and polymer processing equipment⁴⁵² and is referred to as the *kneading effect*. Such an effect may have amplified both the unfolding of the protein constituents as well as the shearing of the entangled protein chains. Increased protein constituent degradation might then have promoted adhesive/abrasive wear and increased the PE wear rate. The AP force measured at the simulator was higher for ACS-I + PBS + AA + HA compared with ACS-I + PBS + AA which might support the present speculations (Fig. 5.63).

The protein constituents of ACS-I + PBS + AA + HA were affected by the wear process *in vitro*; but are SF protein constituents also affected by the wear process at the CoCr-PE interface? In an attempt to answer this question a 5,000 cycle (83 min) “SF wear test” with 10 ml of mixed SF was performed on implant L2. SF samples of 10 patients (SF 3, SF 4, SF 5, SF 6, SF 7, SF 8, SF 11, SF 13, SF 14, and SF 16) were mixed (SF_{mix}). The SF_{mix} had a protein concentration of 30.90 ± 1.24 g/l and a peptide concentration of 0.397 ± 0.004 g/l. All bearing surfaces were wetted with SF_{mix} prior to wear testing. The test was performed in an open system and the SF_{mix} was repeatedly pipetted (every 3 – 5 cycles) onto the anterior aspect of the femoral component which allowed the SF_{mix} to be dragged into the interface by the articulating surfaces. The protein concentration of the SUP measured 25.98 ± 1.31 g/l. The peptide concentration in SF_{mix} increased by 56 % to 0.618 ± 0.010 g/l. The electrophoretic profile of the SF_{mix} was different between the SM and the SUP (Fig. 5.64). This suggested that proteins in the SF were affected by the wear process at the CoCr-PE interface *in vitro* and it was deemed possible that such effects might also be observed *in vivo*.

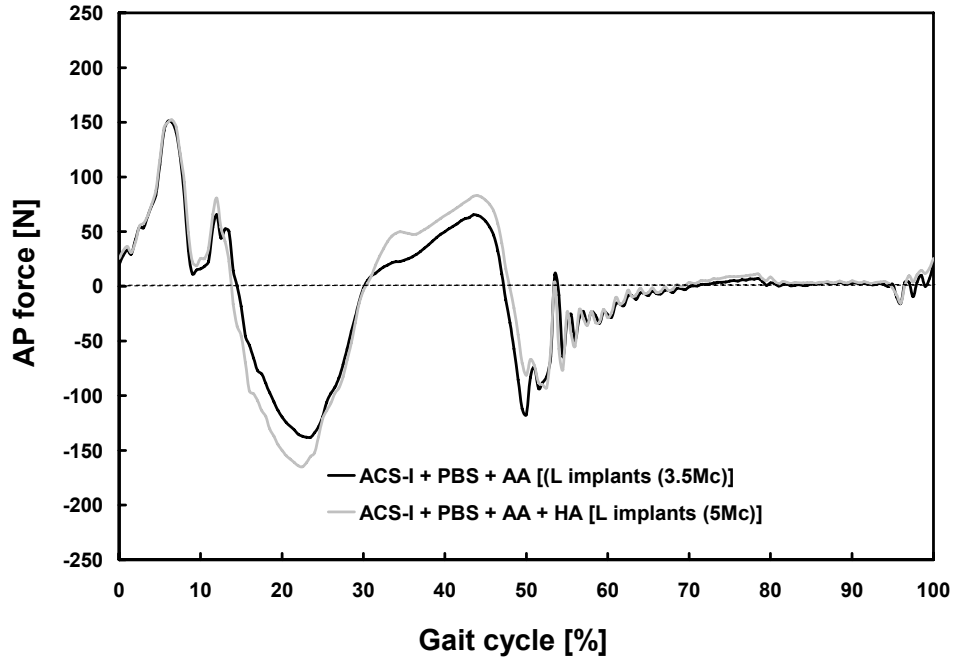


Figure 5.63: The AP force for the L implants tested with ACS-I + PBS + AA after 3.5 Mc and tested with ACS-I + PBS + AA + HA after 5 Mc. Note the higher AP force for the L implants at approximately 20 % gait cycle and 45 % gait cycle which may have been responsible for the higher wear rate for the L implants.

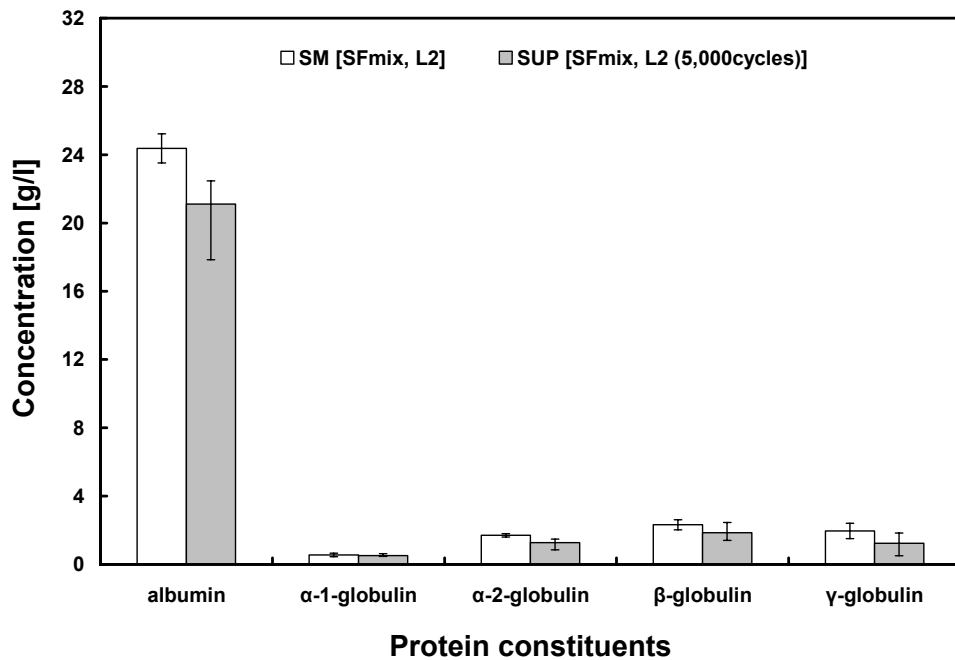


Figure 5.64: The protein constituent fractions for the SF_{mix} starting material (SM; protein concentration = 30.90 ± 1.24 g/l) and the SF_{mix} supernatant (SUP; 25.98 ± 1.31 g/l) after a test interval 5,000 cycles. Note that all protein sub-constituents wear affected by the wear process.

5.4.12 Discussion on the Effects of Osmolality on PE Wear

To the author's knowledge, this is the first study correlating PE wear with the osmolality and thermal stability of lubricants that is relevant to knee implants (and perhaps other joint replacements). Reduced osmolality was associated with reduced T_m , ΔH , and ΔS and was accompanied with increased PE wear rates. It was interesting to observe that non-clinically relevant levels of osmolality increased the PE wear and the ISO standard specifies using DW for serum dilution despite its low osmolality. Increased osmolality in ACS-I + PBS + AA over ACS-I + DW + AA was possibly due to increase in ions in PBS compared with DW. The osmolality was an indicator of the ionic strength of a solution; an increase in osmolality (as occurred when PBS was used instead of DW) caused a reduction in PE wear rate, affecting the peptide concentration as well as the unfolding characteristics of the proteins. The main difference between the dilutive media was that NaCl, the main constituent of PBS, was at a concentration of 150 mmol/l (pH = 7.2). Gionacola et al.¹⁰⁴ investigated the effects of NaCl concentration (pH = 7.0) on the thermal stability of bovine serum albumin (BSA) using similar DSC methods. A strong thermal stabilization effect of NaCl on BSA was observed with increased NaCl concentration, ranging from 0 - 1000 mmol/l. It was suggested that the stabilizing effect of NaCl was due to the reduced electrostatic repulsion between the net charges of the proteins, consequently reinforcing the native protein conformation. Diluting ACS-I + AA with low osmolality DW reduced the thermal stability (T_m , ΔH , ΔS) of the lubricant compared with ACS-I + PBS + AA. It was speculated that lower osmolality reduced the protein conformation and resulted in lower, non-native protein conformational stability. Non-native protein conformation may have increased entanglements between neighboring proteins chains and reduced the ductility of the consolidated protein layer under load and motion during wear testing. The lower T_m for ACS-I + DW + AA compared with ACS-I + PBS + AA may have initiated protein unfolding at a lower contact temperature, consequently increasing the protein constituent degradation and peptide concentration (Fig. 5.65). Such circumstances may

have promoted adhesive/abrasive wear and increased the PE wear rate for ACS-I + DW + AA compared with ACS-I + PBS + AA. The slightly higher AP force measured for ACS-I + DW + AA compared with ACS-I + PBS + AA may support this suggestion (Fig. 5.66).

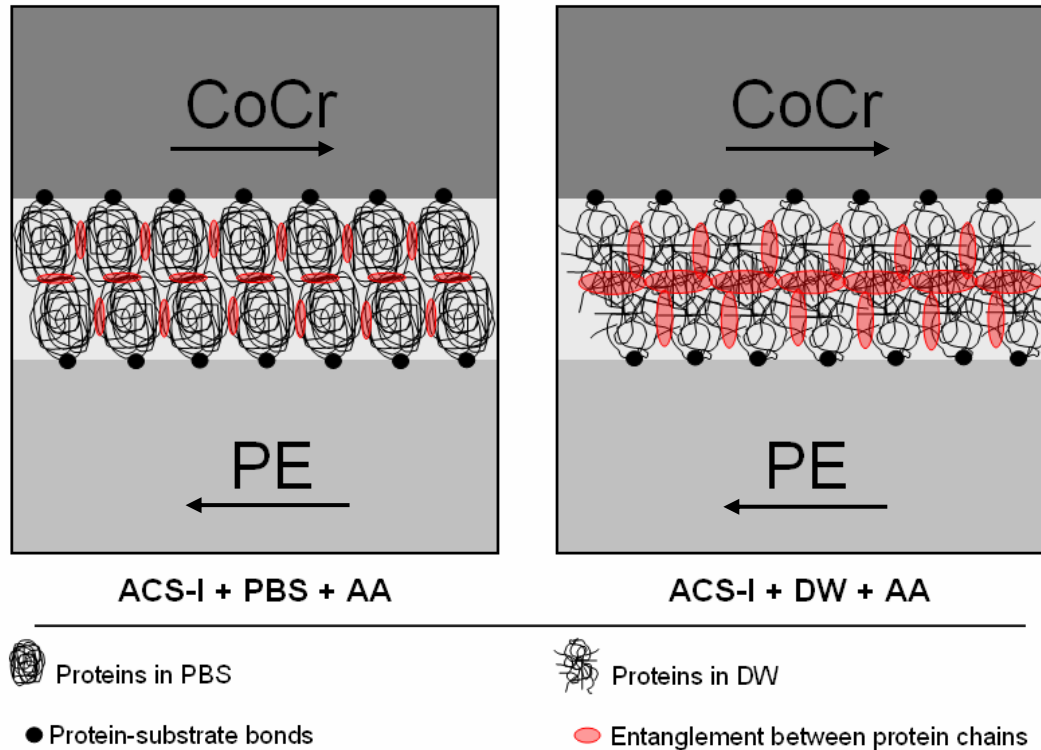


Figure 5.65: Schematic showing the possible protein interactions in the protein layer at the CoCr-PE interface for ACS-I + PBS + AA and ACS-I + DW + AA during the wear test. The higher protein constituent degradation and peptide concentration for the latter lubricant may have been initiated by diluting the ACS-I + AA with DW. The proteins in DW had a lower T_m , ΔH , and ΔS than the proteins in PBS and thus were deemed to have a lower conformational stability. Such lower conformational stability possibly caused more entanglements between protein chains which may explain the higher peptide concentration ACS-I + DW+ AA compared with ACS-I + PBS + AA after wear testing. Such circumstances may explain the higher PE wear rate obtained with ACS-I + DW + AA compared with ACS-I + PBS + AA used as the lubricant. The arrows indicate the direction of surface motion.

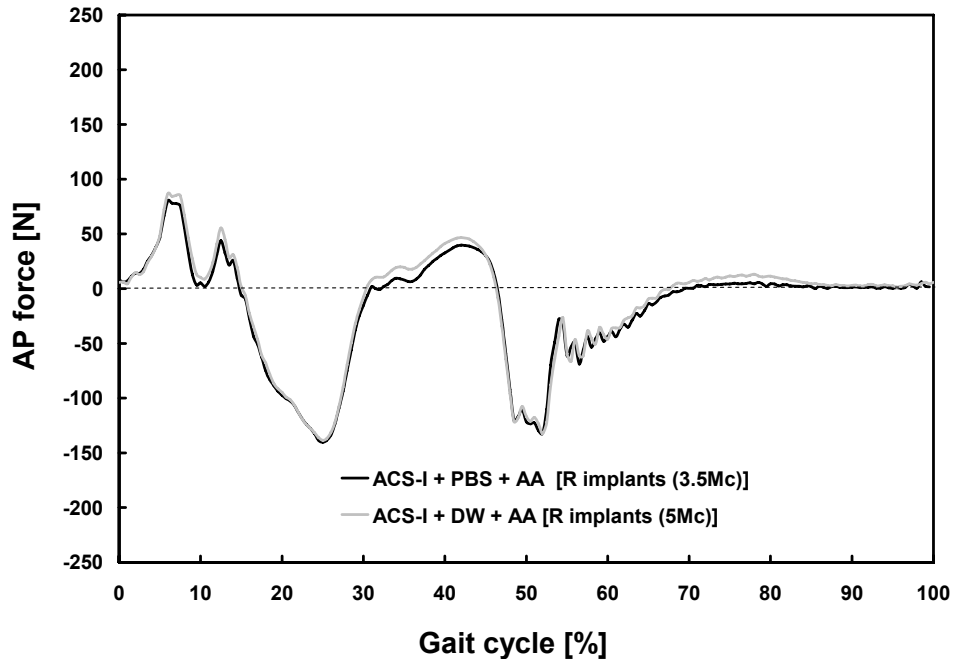


Figure 5.66: The AP force for the R implants tested with ACS-I + PBS + AA after 3.5 Mc and tested with ACS-I + DW + AA after 5 Mc. Note the higher AP force for the R implants at 30 % gait cycle to 45 % gait cycle.

5.4.13 Discussion on Clinical Relevance of the PE Wear Rates

The present study suggested that HA and clinically relevant levels of osmolality were important constituents in the lubricant to mimic the SF *in vitro*. However, it still remained uncertain how the *in vitro* wear tests related to the clinical wear performance of TKRs. Very recently, Gill et al.³³⁹ published a study that gave some insight into the *in vivo* volumetric wear of a total knee replacement. Linear penetration of the femoral component into the PE insert was estimated using RSA techniques and calculating the mean penetration at flexion angles such as 0, 15, 30, 45 and 60 ° under weight bearing. The study was conducted on four patients with six, non-modular AGC total knee systems (Biomet, Warsaw, IN) which had been implanted for 76 months (range, 70 - 85 months). The mean linear penetration was reported to be 0.075 mm/year which was approximately equivalent to a volumetric wear rate of 100 mm³/year³³⁹.

To compare the clinical findings by Gill et al.³³⁹ to the findings of the present thesis, it was only necessary to compare their values with the linear

penetration of the femoral component into the PE insert in the knee simulator wear tests, a quantity which was routinely measured in the wear testing. Of main interest were the recordings from 3.5 - 5 Mc (data from 5 - 5.5 Mc was lost) when the lubricant HA lubricant was used in the wear tests. The linear penetration for the L implants was calculated as the mean at 3.5 Mc and 5 Mc, subtracted from each other and divided by 1.5 Mc, which resulted in a mean linear penetration of 0.06 ± 0.02 mm/Mc (range, 0.002 - 0.128 mm/Mc) for the HA lubricant. Such linear depth penetration measured in simulator wear tests stood in quite good agreement with the clinical linear penetration reported by Gill et al.³³⁹. In comparison, wear tests with conventional BCS + DW + SA¹⁵² approached a mean penetration rate of 0.12 ± 0.04 mm/Mc, thus further questioning the clinically relevance of BCS + DW + SA. Nevertheless, the AGC total knee system is somewhat different from the AMK[®] knee system and thus, a comparison between penetration rates should be conducted with caution.

In addition, the level of activity simulated in the *in vitro* tests and found in the clinical environment might also be different which might affect the comparison between the values obtained for the linear penetration into the PE inserts. The *in vitro* test protocol recommended by ISO⁴¹ considered 1 Mc as the number of cycles performed by the patient under level walking on an annual basis. However, the number of cycles might reach up to 2 Mc/year for patients with joint replacements³⁸³ and might include a variety of different activities⁴⁵³. Recently, other activity activities such as stair climbing^{453,454} were added to the level walking activity simulations in knee implant wear testing which would increase the PE wear rate. If 2 Mc/year were adopted, the simulator penetration rate would be 0.12 ± 0.04 mm/year with the HA lubricant compared with 0.24 ± 0.08 mm/year for the conventional BCS + DW + SA. The penetration rate with the HA lubricant was much closer to the clinical rate estimated by Gill et al.³³⁹ than the penetration occurring when the conventional lubricant was used.

5.4.14 Discussion on Microbial Resistance and Countermeasures

It was deemed necessary to investigate to which antibiotic substances *E. cloacae* JK-1 became resistant. The β -lactamase Test described in Section 3.5.4 was used for this purpose. It was observed that *E. cloacae* JK-1 developed resistance towards antibiotics with a β -lactam ring in their chemical structure such as penicillin and carbenicillin. This suggested that the *E. cloacae* JK-2 produced β -lactamase, which was confirmed with the pink colour of the disk placed on the incubated *E. cloacae* JK-2 (Fig. 5.67). The somewhat limited efficacy of *aminoglycosides*, streptomycin in particular, might have caused *E. Cloacae* JK-1 to develop resistance. It was speculated that such resistance was mediated by the genetic mutation, particularly of the plasmid and chromosome constituents of *E. cloacae* JK-2 (Fig. 5.68)¹⁰⁵.



Figure 5.67: Image showing the positive response (pink color) of the Cefinase[®] disk placed on *E. cloacae* JK-2 grown on LB agar. Cefinase[®] disk was placed on incubated *E. coli* ML35 as a control and showed no discoloration of the Cefinase[®] disk (negative response; not shown).

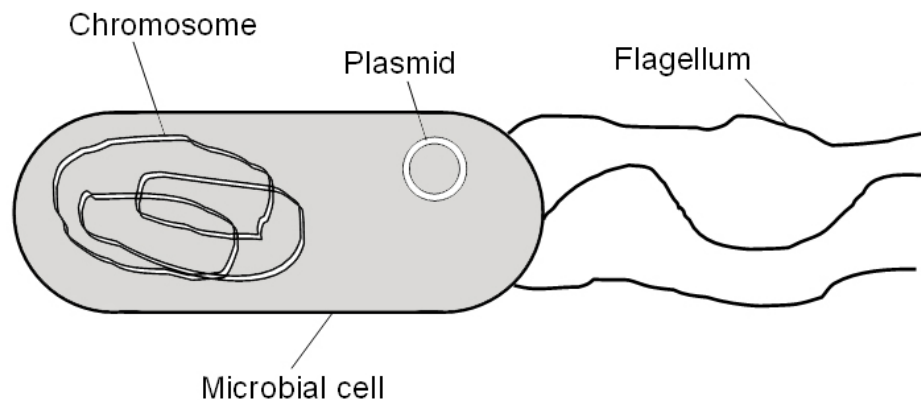


Figure 5.68: Schematic of a microbe showing the chromosome, plasmid and flagellum.

Plasmids are genetic deoxyribonucleic acid (DNA) elements of the bacteria that replicate independently of the host chromosome. A chromosome is a single large macromolecule of DNA in a microbial cell ¹⁰⁵. Every plasmid contains at least one DNA sequence that serves as an origin of replication, which enables the plasmid DNA to be duplicated independently from the chromosomal DNA. Plasmids often contain genes or gene cassettes that confer a selective advantage to the bacterium harboring them, such as the ability to make the bacterium antibiotic resistant ¹⁰⁵. Such streptomycin resistance may be due to a resistant plasmid-encoded enzyme that chemically alters the structure of the antimicrobial by processes such as *phosphorylation* or *adenylation*. Some clinical isolates of *E. Cloacae* have been reported to contain plasmids with antibiotic resistance genes ^{455,456} which may support such speculation. However, additional microbiological tests were deemed necessary but conducting such tests went beyond the scope of this thesis.

E. cloacae JK-2 showed intermediate susceptibility towards tetracycline and susceptibility for chloramphenicol. Although chloramphenicol appears to be the most effective antibiotic for further wear tests, it needs to be kept in mind that *E. cloacae* strains ⁴⁵⁷ and other Gram-negative bacteria can develop resistance towards this and other antibiotics ^{446,458}. Chloramphenicol resistance may develop due to a resistant plasmid-encoded enzyme that

chemically alters the structure of the antimicrobial agent by a process called *acetylation*. Exposing wear testing personnel to such a multi-resistant microbe may be hazardous to their health. In addition, with the simulator located in the basement of the hospital, such microbial contamination may significantly endanger the health of patients in the case the mutated and resistant microorganism spreads. This may require the use of more powerful antibiotics for wear testing and patients and could consequently lead to antibiotic overuse and highly hazardous organisms that can not be controlled. Although antibiotics should be used in wear tests to mimic the sterile *in vivo* environment, it is definitely not the intention to create a hazardous work environment. The opportunity of abandoning SA due to its unsuitability for microbial inhibition in wear testing was very much appreciated due to its highly toxic characteristics⁴⁵⁹. It is speculated by the author of the present thesis that microbial contamination may differ among wear test laboratories. Thus, recommending one specific antibiotic to eliminate microbial contamination in wear tests cannot be made. The cycling of antibiotics⁴⁶⁰, as performed in hospitals dealing with chronic infections (i.e. intensive care units), may be an attractive alternative treatment for extensive wear testing. In any case, a round robin test between implant wear testing laboratories may be beneficial with the goal to establish a database on microbial contaminants and show ways of more favorable treatments.

The microbial contamination found in the present test was a Gram-negative bacterium and its growth may be inhibited with the use of bacterial predator *Bdellovibrio bacteriovorus* strain 109J (referred to as *Bdellovibrio*; approximately 1 μm in length and 0.2 μm in width)^{191-193,461}. This predator bacterium, both Gram-negative and antibiotic resistant, has the fascinating ability to prey on other Gram-negative bacteria. It has shown potential usefulness as an active biological control of pathogenic and spoilage organisms in foods. Since *Bdellovibrio* is a prey dependent bacterium, i.e. it lives off the bacterium¹⁹¹; it is not able to grow in the nutrient rich media and loses viability once the contaminant is eliminated. The life cycle of *Bdellovibrio* can be

separated into two major phases: (a) free-swimming phase to search and attack the prey and (b) the growth phase spend inside the periplasm, the space between the plasma membrane and the outer membrane of the prey (Fig. 5.69)^{191-193,461}. During the free-swimming phase the *Bdellovibrio* collides with the prey cell and attaches itself irreversibly to the surface. *Bdellovibrio* penetrates the outer membrane of the prey and obliterates the prey by halting its respiration and growth. While residing in the periplasm the *Bdellovibrio* grows and divides by exploiting the cells' macromolecules for nutrients and essential building blocks. The *Bdellovibrio* grow inside the killed cell in a structure termed a bdelloplast. After all resources of the prey have been exhausted, the *Bdellovibrio* lyse the remains of the prey cell and swim away to target new hosts^{191-193,461}.

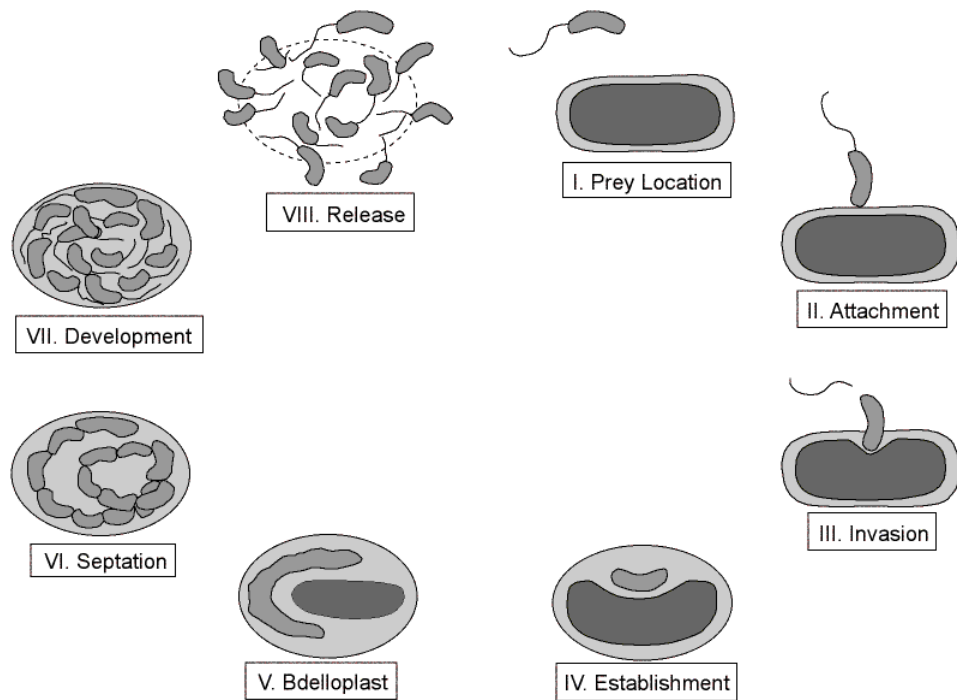


Figure 5.69: Schematic of the two-phase life cycle of *Bdellovibrio*, which consists of a free-swimming phase in a solvent and a growth phase inside its Gram-negative prey bacterium¹⁹³ (Max Planck Institute for Developmental Biology, Tübingen, Germany).

In a pilot study, *Bdellovibrio* was cultured on *E. cloacae* JK-2 in HM-buffer (3 mmol/l 4-(2-hydroxyethyl)-1-piperazineethanesulfonic acid (Sigma-Aldrich, St. Louis, MO), pH = 7.6, with 1 mmol/l CaCl₂ and 0.1 mmol/l MgCl₂) following recently published methods^{461,462}. The predation of *Bdellovibrio* on *E. cloacae* JK-2 was monitored every 3 h using a phase contrast light microscope. The turbidity (Klett units; 1 Klett unit \approx 5 x 10⁶ CFU/ml; Klett-Summerson photoelectric colormeter with a green filter) was measured on triplicate samples (30 °C, shaking at 175 rpm) to assess the predation of *Bdellovibrio* on *E. cloacae* JK-2 in sidarm flasks every 24 h up to 72 h. Reduced Klett units for *E. cloacae* JK-2 + *Bdellovibrio* indicated successful predation (Fig. 5.70).

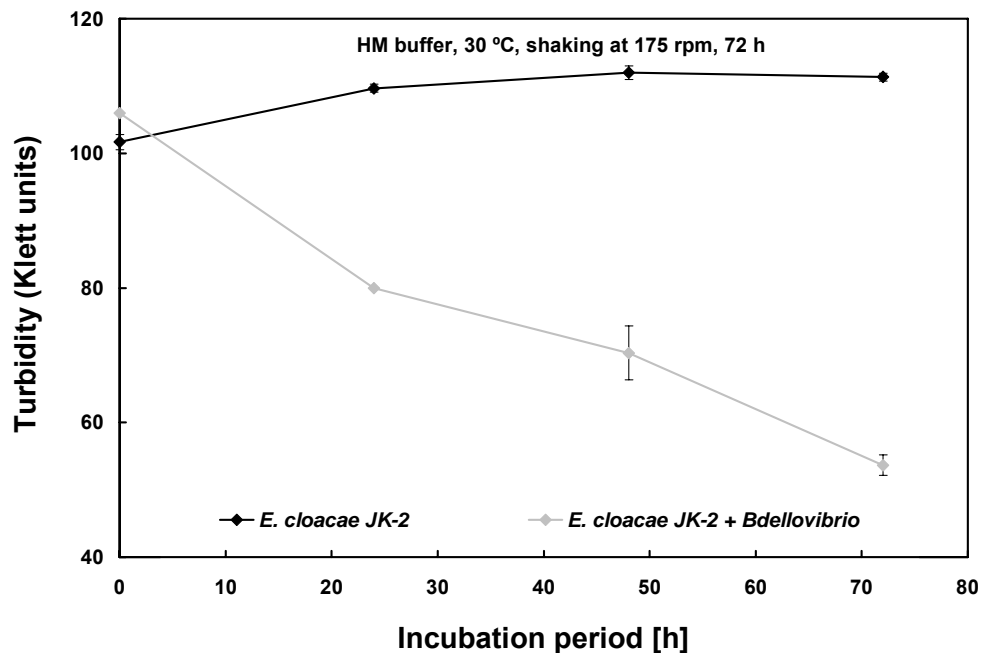


Figure 5.70: Turbidity measurements of HM-buffer with both *E. cloacae* JK-2 with AA and *E. cloacae* JK-2 + *Bdellovibrio*. The turbidity in Klett units is an indicator of the number *E. cloacae* JK-2 in the HM buffer. Note the decrease in turbidity for when *E. cloacae* JK-2 was doped with *Bdellovibrio* (1 Klett unit \approx 5 x 10⁶ CFU/ml). Such decrease in turbidity indicated that *Bdellovibrio* was able to prey on *E. cloacae* JK-2.

To authors knowledge this is the first approach towards developing a *biological agent* with the potential use in implant wear testing. Further investigations are needed to test the predation of *Bdellovibrio* on *E. cloacae* JK-2 in ACS-I + PBS + HA, to determine the appropriate dosage of *Bdellovibrio* cells to be applied for the wear test in the knee simulator, and how *Bdellovibrio* affects the lubricating properties. This went beyond the scope of this thesis.

5.4.15 Concluding Remarks

The PE wear rate was affected by both HA and the dilutive media added to ACS-I + AA. The lubricant composed of ACS-I + PBS + AA + HA had a higher wear rate compared with ACS-I + PBS + AA. This was associated with higher protein degradation and increased peptide concentration despite the higher thermal stability (T_m , ΔH , ΔS) of ACS-I + PBS + AA + HA which was similar to the thermal stability of SF. The higher thermal stability for ACS-I + PBS + AA + HA compared with ACS-I + PBS + AA might be due to the added HA, which has the ability to retain polar H₂O from the solvent and consequently stabilizing the proteins by enhancing their hydrophobic interactions. Furthermore, it was suggested that the lubricating protein layer of ACS-I + PBS + AA + HA was less ductile than ACS-I + PBS + AA under load and motion. Such lower ductility of ACS-I + PBS + AA + HA might have reduced the plastic deformation that could reduce surface friction and damage thus leading to high shear forces inside the protein layer and increased the temperature at the CoCr-PE interface. It was speculated that this effect was similar to *kneading effect*, commonly observed in ductile metals and highly viscous polymer solutions under high shear forces^{451,452} which increased both the protein degradation and peptide concentration compared with ACS-I + PBS + AA.

Diluting ACS-I + AA with DW instead with PBS reduced the osmolality of the lubricant to non-clinically relevant osmolality levels. Such a procedure showed to increase the PE wear rate, protein degradation and peptide concentration. The thermal stability was lower for both ACS-I + DW + AA and

ACS-I + PBS + AA compared with both ACS-I + PBS + AA + HA and SF. It was suggested that NaCl in PBS stabilized the protein structures by influencing their repulsive forces. The present study suggested that the temperature in the contact point exceeded $T_m = 58\text{ }^\circ\text{C}$ to initiate protein unfolding for ACS-I + DW + AA. The serum temperature in hip simulator studies was considered likely to cause protein degradation and wear rates with calf serum based lubricants^{154,463,464}. The temperature in CoCr-PE interface was suggested to reach up to $60\text{ }^\circ\text{C}$ and such surface temperatures probably occurred in the present study. In any case, the thermal stability of ACS-I + DW + AA and ACS-I + PBS + AA were lower than SF and thus not clinically relevant. This suggested that both HA and NaCl in PBS were essential additives to ACS-I + AA to mimic of SF.

Using AA as the microbial inhibitor was accompanied with reoccurrence of *E. cloacae* after 5.5 Mc. This indicated that the *E. cloacae* JK-1 possibly mutated and developed resistance towards the AA constituents such as penicillin and streptomycin. Such mutation resulted in a new organism, referred to as *E. cloacae* JK-2. It was suggested that *E. cloacae* JK-2 produced β -lactamase that disables the β -lactam ring. Such a β -lactam ring is a part of the chemical structure in both penicillin and streptomycin and kills the organism by interacting with the cell wall of the bacterium. *E. cloacae* JK-2 was also found to be resistant to carbenicillin (β -lactam antibiotic) and tetracycline, but was susceptible to chloramphenicol. Based on the literature, it was deemed possible that *E. cloacae* JK-2 could further develop resistance even against chloramphenicol. The use of the predator bacterium *Bdellovibrio* as a *biological antibiotic* was recommended so that it would prey on *E. cloacae* JK-2 in HM buffer. Further research on the use of *Bdellovibrio* use in ACS-I + PBS + HA is required.

Chapter 6: Conclusions and Future Work

6.1 Clinical Investigations

The type of grading method used to assess the surface backside surface damage of PE inserts significantly affected the outcome of the retrieval study. The strategy used in the Modified-method estimated the surface damage area in 10 % increments and assigned a damage severity that translated into a BDS of 1 - 10 and was found to be superior when compared with the Hood-method (see Chapter 3 and Section 4.2 for details). The analysis of BDS data from implant retrievals with MLRA, in addition to univariate methods, allowed the identification of a substantial number of factors that were relevant to knee implant design.

Further analysis of the BDS obtained with the Modified-method suggested that the backside damage process was influenced by patient factors and design features (Chapter 4.3). A polished tibial tray with a partial-peripheral locking mechanisms would significantly reduce the BDS for male patients. Increased shelf storage was directly related to the IP of patients with GA sterilized inserts. Thicker inserts caused higher BDS and a grit-blasted tibial tray was associated with damage features that were characteristic of abrasive wear. Embedded particles from the grit-blasting process were likely to be released after implantation and to contribute to the abrasive wear. The micro-damage of the burnishing was comparable to the micro-damage found on acetabular cups that were retrieved due to complications arising from osteolysis⁴²¹. Burnishing was significantly reduced with a partial-peripheral locking mechanism.

In Section 4.4, the protein concentration of SF from patients with OA was found to be 2-fold higher than the protein concentration recommended by the standard, ISO-14243-3⁴¹. The total protein concentration, protein constituent fraction, and trace element concentration of SF was quite different from BCS, NCS, ACS, and ACS-I lubricants used in knee simulator wear testing. However, ACS and ACS-I were closest to SF in their protein constituent

fractions. Using DW as the dilutive media resulted in non-clinically relevant levels of osmolality for BCS, NCS, ACS, and ACS-I. The high osmolality of PBS allowed the serum dilution to clinically relevant osmolality levels.

6.2 *In vitro* Investigations

The commissioning tests for the knee wear simulator were reported in Section 5.2 and gave useful information on the pre-soak behaviour of PE and the variation in PE wear between the individual simulator stations. The pre-soaking protocol affected the fluid uptake that caused mass gain of the PE inserts. The mass gain was higher for PE inserts soaking in protein-rich medium. The pre-soaking of PE inserts should be conducted under the same protocols as would occur during wear testing. These protocols included setting soak temperature, setting weighing frequency, cleaning, desiccating and weight measurement itself. The pre-soaking media affected the PE wear rate as shown in Section 5.4. The fluid used for pre-soaking and for the LS stations should be the same as the lubricant used for wear testing.

The wear rates obtained from the testing with the BCS lubricant, NCS lubricant, and ACS lubricant (Fig. 6.1) showed that protein constituent fraction had a significant influence. The wear rates behaved in the following manner: when the sera were diluted with: BCS lubricant > NCS lubricant > ACS lubricant. Increased albumin + α -1-globulin fraction reduced the PE wear rate. SA was ineffective as a microbial inhibitor in all three lubricants. The microbial contamination was identified as Gram-negative *E. cloacae*, strain JK-1. Increased β -globulin + γ -globulin fraction correlated with increased protein degradation and increased CFU/ml. Under consideration of literature on boundary lubrication and the similarities of protein-rich lubricants to colloidal suspensions, the findings suggested that the boundary lubrication process was possibly governed by a compacted protein layer under load and motion.

Adding HA to the lubricant increased the thermal stability of ACS-I + PBS + AA by dehydrating the solvent and the proteins compared with ACS-I + PBS + AA and increased the PE wear rate (Fig. 6.2). The thermal stability of

ACS-I + PBS + AA + HA was equivalent to the thermal stability of SF from osteoarthritic patients. It was proposed that adding HA to the lubricant reduced the ductility of the protein layer. Such a reduction might have decreased the ability of the protein layer to accommodate plastic deformation without delaminating which lead to increased protein degradation, peptide concentration and ultimately also increased the PE wear rate.

Using low-ion DW to dilute the ACS-I lubricant resulted in osmolality levels that were not clinically relevant and increased the PE wear rate. Using high-ion PBS to dilute the ACS-I lubricant reproduced clinically relevant osmolality levels, increased the thermal stability and lowered the wear rates (Fig. 6.3). It was suggested that the NaCl in solution (that caused the higher osmolality levels) stabilized the repulsive forces between the proteins in the lubricant and thus made the protein layer more resistant to the imposed loads and motions. This protein layer possibly protected the PE surface and reduced the wear rates.

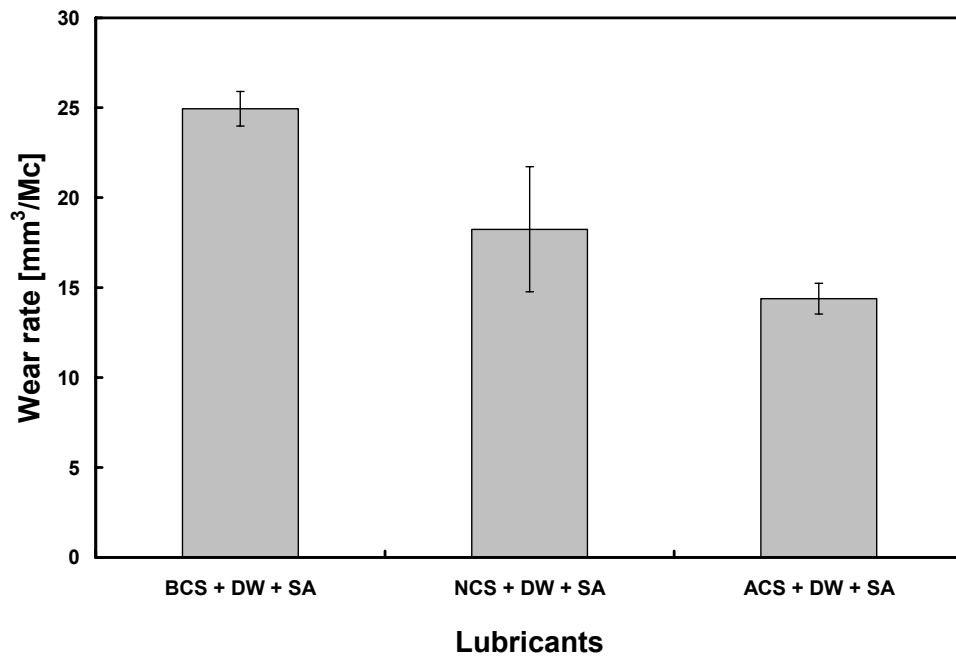


Figure 6.1: Wear rates for serum lubricants that did not have HA or PBS in them.

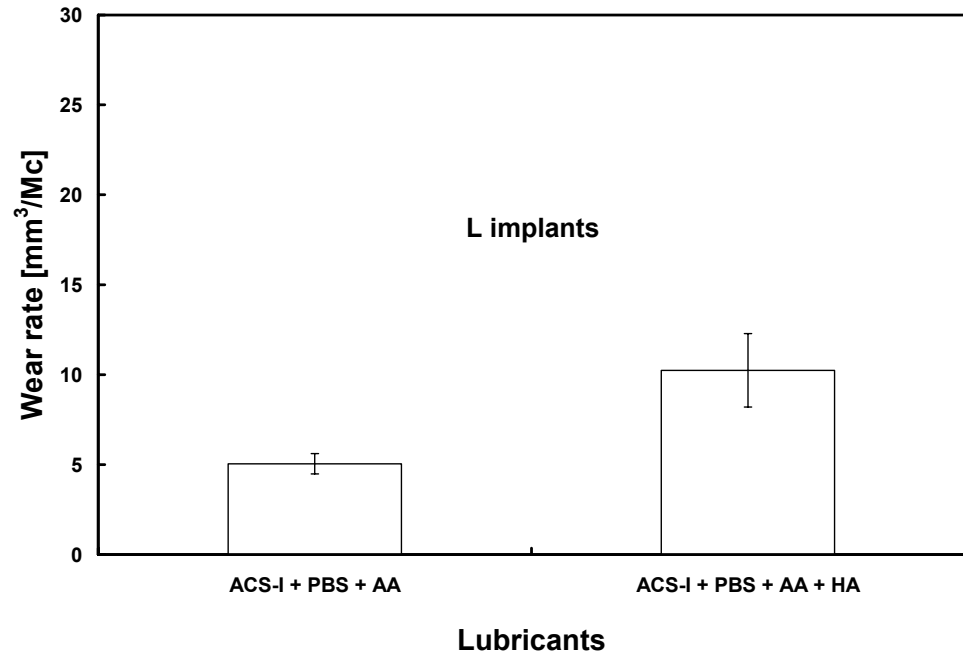


Figure 6.2: Wear rates for serum lubricants that included PBS with or without HA.

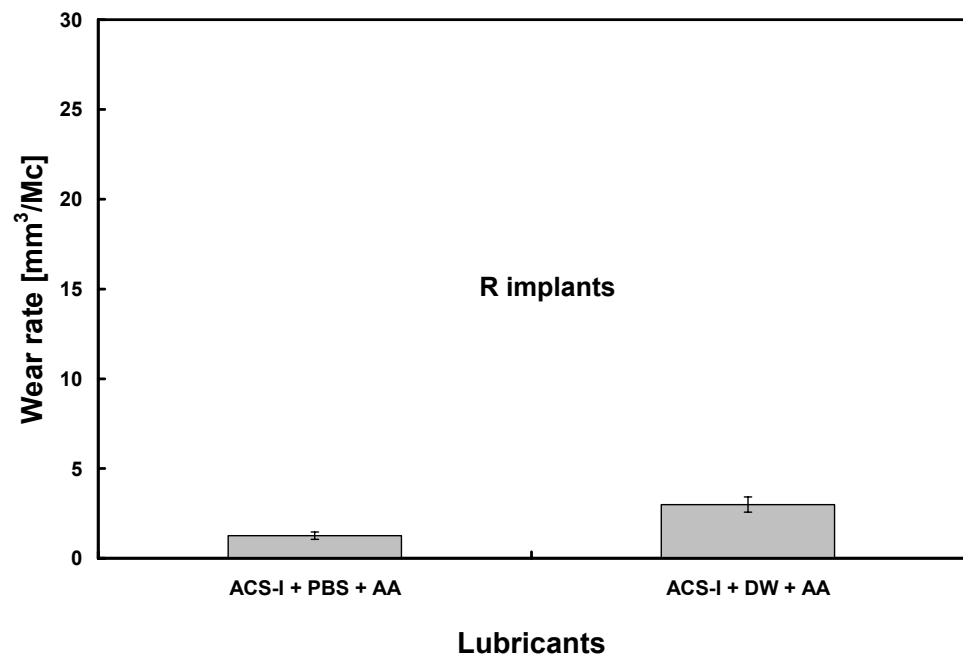


Figure 6.3: Wear rates for serum lubricants diluted with PBS or DW.

The wear rates of implants in the L and R banks were not significantly different when BCS + DW + SA was used as the lubricant. However, the wear rates were significantly different when ACS-I + PBS + AA was used (Fig. 6.2 and Fig. 6.3). Consequently, the simulator consisted of L and R banks that were essentially independent and could be considered as two separate simulators. The wear rates of the lubricants were higher when SA was used as the microbial inhibitor compared with AA (Fig. 6.1, 6.2, and 6.3). The findings in Section 5.3 suggested that SA did not inhibit microbial growth after only 28 h (or 0.1 Mc) of wear testing. Microbial growth in the lubricants was associated with reduced peptide concentration, suggesting that the *E. cloacae* JK-1 metabolized such peptides. Replacing SA with AA in the ACS-I lubricant increased the peptide concentration 11-times (Fig 6.4). The protein constituent fractions of ACS and ACS-I were similar. There was no statistically significant difference between the peptide concentrations when Fe-rich ACS-I was used in wear tests compared with ordinary ACS ($p = 0.170$, ANOVA and Tamhane). In any case, EDTA was added to all lubricants and which should have guaranteed the binding of free Fe. Thus, when the wear rates of ACS + DW + SA were compared with the wear rate of ACS-I + DW + AA; (replacing SA with AA) caused a 4-times decrease in wear rate (Fig. 6.5).

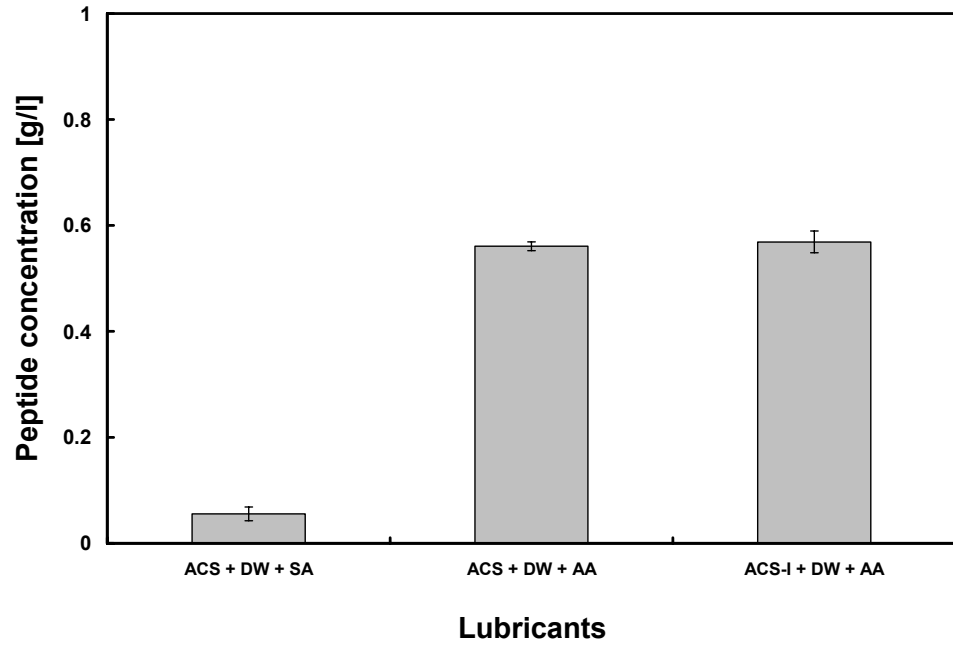


Figure 6.4: The peptide concentration for various ACS lubricants (MWCO = 2,000 Da).

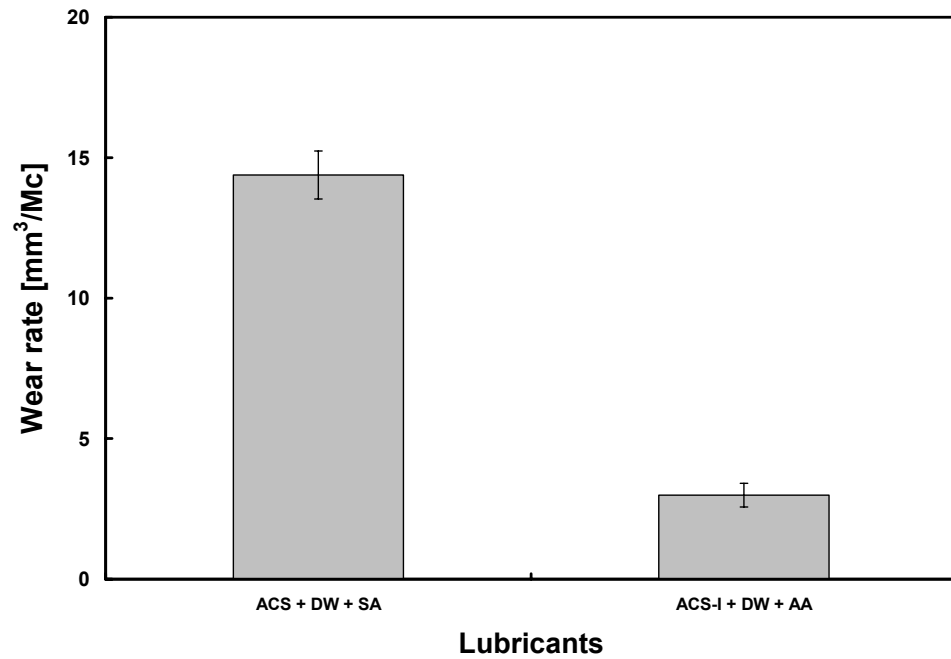
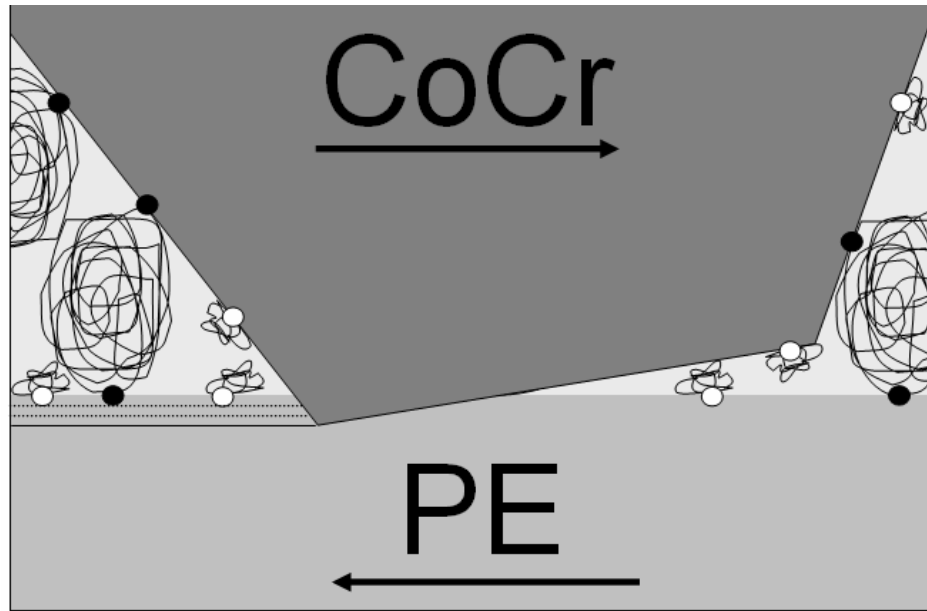


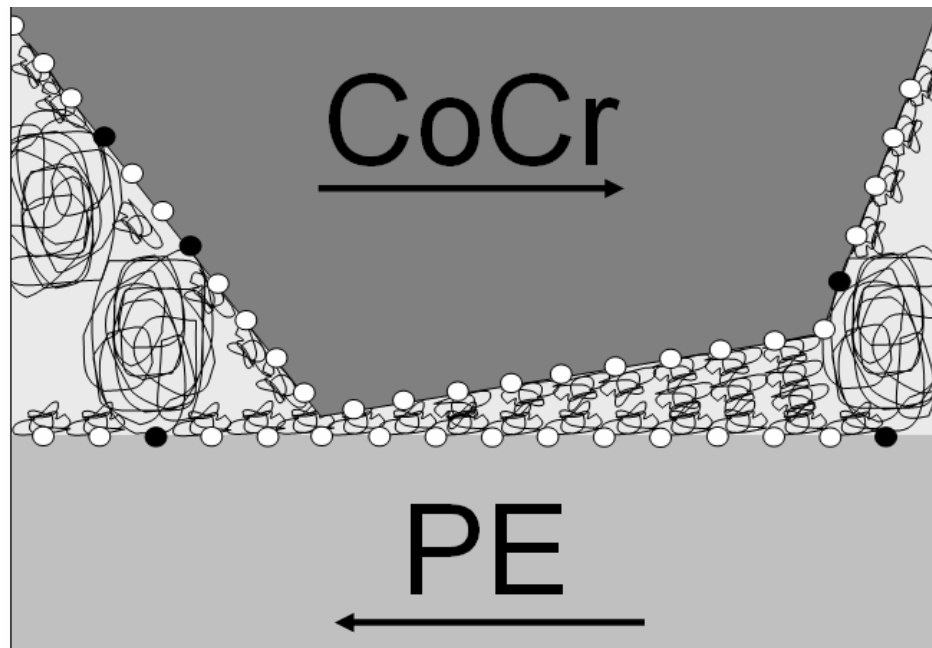
Figure 6.5: Wear rates for ACS with either SA or AA.

An attempt was made to explain this phenomenon by considering the adsorption behaviour of degraded proteins onto the hydrophobic PE surface during wear^{76,78,160,164}. Increased adsorption of degraded protein might form a boundary lubricant with the peptides adsorbed to the PE surface in form of a thin layer (or conditioning film), with an average molecular weight of 2,000 Da (Fig. 6.6). This protein layer might require considerable energy to be squeezed out of the contact zone to allow the onset of adhesive/abrasive wear^{97,98,465}. In any case, the suggested thin layer boundary lubrication should be further explored, in particular the suggested protein-mediated squeeze-out phenomenon. It appears that the possibly surface near peptide layer in addition to the protein layer has a tremendous affect on PE wear.

Future work might include the characterization of wear particles collected from implants worn with ACS-I + PBS + AA + HA. Such wear particle should be compared with those obtained from patients with TKRs. Future research might also include knee simulator wear testing with ACS-I + PBS + AA + HA at a total protein concentration at 34 g/l to match the mean protein concentration of SF obtained from patients with OA. Such wear tests should consider higher loads and increased motions to mimic other patient activities in addition to level walking. The present study could then be followed by the wear evaluation of new bearing materials such as XPE.



(a) SA as the microbial inhibitor (few peptides)



(b) AA as the microbial inhibitor (many peptides)

- | | |
|--|---|
|  Protein |  Protein-substrate bonds |
|  Peptide: suspended protein chunk |  Peptide-substrate bonds |

Figure 6.6: Schematic showing a CoCr-PE asperity in contact.

References

1. Philbin EF, Ries MD, Groff GD, Sheesley KA, French TS, Pearson TA. Osteoarthritis as a determinant of an adverse coronary heart disease risk profile. *J Cardiovasc Risk* 1996; 3 (6): 529 - 33.
2. Hip and Knee Replacements in Canada. Canadian Joint Replacement Registry 2006.
3. The Swedish Knee Arthroplasty Register. Dept. of Orthopedics, Lund University Hospital 2006; 2: 1 - 27.
4. Kurtz S, Ong K, Lau E, Mowat F, Halpern M. Projections of primary and revision hip and knee arthroplasty in the United States from 2005 to 2030. *J Bone Joint Surg Am* 2007; 89 (4): 780 - 5.
5. Kuster MS, Wood GA, Stachowiak GW, Gachter A. Joint load considerations in total knee replacement. *J Bone Joint Surg Br* 1997; 79 (1): 109 - 13.
6. McEwen HM, Barnett PI, Bell CJ, Farrar R, Auger DD, Stone MH, Fisher J. The influence of design, materials and kinematics on the in vitro wear of total knee replacements. *J Biomech* 2005; 38 (2): 357 - 65.
7. Clarke I, Scott, W. N., Insal, J. N., Pedersen, H.B., Math, K. R., Vigorita, V. J., Cushner, F.D. *Anatomy. Surgery of the Knee* (ed. Insall, Scott) 2001; 1(13-76).
8. Sharkey PF, Hozack WJ, Rothman RH, Shastri S, Jacoby SM. Insall Award paper. Why are total knee arthroplasties failing today? *Clin Orthop* 2002 (404): 7 - 13.
9. Rorabeck CH. The unstable total knee: causes and cures. *Knee* 2001; 8 (3): 179 - 86.
10. Willert HG. Reactions of the articular capsule to wear products of artificial joint prostheses. *J Biomed Mater Res* 1977; 11 (2): 157 - 64.
11. Ingham E, Fisher J. The role of macrophages in osteolysis of total joint replacement. *Biomaterials* 2005; 26 (11): 1271 - 86.

12. Aspenberg P, van der Vis H. Fluid pressure may cause periprosthetic osteolysis. Particles are not the only thing. *Acta Orthop Scand* 1998; 69 (1): 1 - 4.
13. Peters PC, Engh GA, Dwyer KA, Vinh TN. Osteolysis after total knee arthroplasty without cement. *J Bone Joint Surg Am* 1992; 74 (6): 864 - 76.
14. Rodriguez JA, Bhende H, Ranawat CS. Total condylar knee replacement: a 20-year follow-up study. *Clin Orthop Relat Res* 2001 (388): 10 - 7.
15. Dorr LD. Contrary view: wear is not an issue. *Clin Orthop* 2002 (404): 96 - 9.
16. Zum Gahr K-H. Microstructure and Wear of Materials. *Tribology Series* 1987; 10: 48 - 485.
17. NRC. A Strategy for Tribology in Canada. 1987.
18. Lavernia CJ, Drakeford MK, Tsao AK, Gittelsohn A, Krackow KA, Hungerford DS. Revision and primary hip and knee arthroplasty. A cost analysis. *Clin Orthop Relat Res* 1995 (311): 136 - 41.
19. Salomone MM, Durieux ME. Revision total knee arthroplasty does not increase PACU utilization. *Clin Orthop Relat Res* 2006; 446: 208 - 13.
20. Lavernia C, Lee DJ, Hernandez VH. The increasing financial burden of knee revision surgery in the United States. *Clin Orthop Relat Res* 2006; 446: 221 - 6.
21. Derrett S, Paul C, Morris JM. Waiting for elective surgery: effects on health-related quality of life. *Int J Qual Health Care* 1999; 11 (1): 47 - 57.
22. Kelly KD, Voaklander DC, Johnston WC, Suarez-Almazor ME. Equity in waiting times for major joint arthroplasty. *Can J Surg* 2002; 45 (4): 269 - 76.
23. Hirvonen J, Blom M, Tuominen U, Seitsalo S, Lehto M, Paavolainen P, Hietaniemi K, Rissanen P, Sintonen H. Health-related quality of life in patients waiting for major joint replacement. A comparison between patients and population controls. *Health Qual Life Outcomes* 2006;4:3.

24. Rosemann T, Gensichen J, Sauer N, Laux G, Szecsenyi J. The impact of concomitant depression on quality of life and health service utilisation in patients with osteoarthritis. *Rheumatol Int* 2007; 27 (9): 859 - 863.
25. Colditz GA. Economic costs of obesity and inactivity. *Med Sci Sports Exerc* 1999; 31 (11 Suppl): S 663 - 7.
26. Hood RW, Wright TM, Burstein AH. Retrieval analysis of total knee prostheses: a method and its application to 48 total condylar prostheses. *J Biomed Mater Res* 1983; 17 (5): 829 - 42.
27. Landy MM, Walker PS. Wear of ultra-high-molecular-weight polyethylene components of 90 retrieved knee prostheses. *J Arthroplasty* 1988; 3 Suppl: S 73 - 85.
28. Young SK, Keller TS, Greer KW, Gorhan MC. Wear Testing of UHMWPE Tibial Components: Influence of Oxidation. *Journal of Tribology* 2000; 122: 323 - 331.
29. Naudie DD, Ammeen DJ, Engh GA, Rorabeck CH. Wear and osteolysis around total knee arthroplasty. *J Am Acad Orthop Surg* 2007; 15 (1): 53 - 64.
30. Bell J, Besong, A. A., Tipper, J. L., Ingham, E., Wroblewski, B. M., Stone, M. H., Fisher, J. Influence of gelatin and bovine serum lubricants on ultra-high molecular weight polyethylene wear debris generated in in vitro simulations. *Proc Inst Mech Eng [H]* 2000; 214 (5): 513 - 8.
31. Mazzucco D. Variation in Joint Fluid Composition and its Effect on the Tribology of Replacement Joint Articulation. PhD Thesis 2003; MIT, 2003.
32. Mazzucco D, McKinley G, Scott RD, Spector M. Rheology of joint fluid in total knee arthroplasty patients. *J Orthop Res* 2002; 20 (6): 1157 - 63.
33. Mazzucco D, Scott R, Spector M. Composition of joint fluid in patients undergoing total knee replacement and revision arthroplasty: correlation with flow properties. *Biomaterials* 2004; 25 (18): 4433 - 45.

34. Mazzucco D, Spector M. The John Charnley Award Paper. The role of joint fluid in the tribology of total joint arthroplasty. *Clin Orthop Relat Res* 2004 (429): 17 - 32.
35. Liao YS, Benya PD, McKellop HA. Effect of protein lubrication on the wear properties of materials for prosthetic joints. *J Biomed Mater Res* 1999; 48 (4): 465 - 73.
36. Kaddick C, Wimmer MA. Hip simulator wear testing according to the newly introduced standard ISO 14242. *Proc Inst Mech Eng [H]* 2001; 215 (5): 429 - 42.
37. Clarke IC, Chan FW, Essner A, Good V, Kaddick C, Lappalainen R, Laurent M, McKellop H, McGarry W, Schroeder D. Multi-laboratory simulator studies on effects of serum proteins on PTFE cup wear. *Wear* 2001; 250 (1 - 12): 188 - 198.
38. Tanner SL, DesJardins, J., Pace, T.B., Weinbrenner, D. and LaBerge, M. Development of a Clinically Relevant TKR Simulation Test Lubricant. Proc of the 29th Annual Meeting of the Society for Biomaterials, Reno, NV, 2003.
39. Wang A, Stark, C., Dumbleton, J. H. Mechanistic and morphological origins of ultra-high molecular polyethylene wear debris in total joint replacement prostheses. *Proc Inst Mech Eng [H]* 1996; 210: 141 - 155.
40. ISO-14243-1. International Organization for Standardization, London: Implants for Surgery: Wear of Total Knee Joint Prostheses. Part 1: Loading and Displacement Parameters for Wear Testing Machines with Load Control and Corresponding Environmental Conditions for Test. 2002.
41. ISO-14243-3. International Organization for Standardization, London: Implants for Surgery: Wear of Total Knee Joint Prostheses. Part 3: Loading and Displacement Parameters for Wear Testing Machines with Displacement Control and Corresponding Environmental Conditions for Test. 2004.
42. ISO-14243-2. Implants for Surgery -Wear of total knee prostheses Part 2: methods of measurement. 2000.

43. Brandt JM, Haydon, C. M., Medley, J. B., McCalden, R.W., MacDonald, S. J., Rorabeck, C. H., and Bourne, R. B. Backside Wear of Polyethylene tibial Inserts: Is Creep Important? *Trans Ortho Res Soc* 2003; 49: 1419.
44. Brandt JM, Haydon CM, Medley JB, McCalden RW, MacDonald SJ, Rorabeck CH, Bourne RB. Modular Tibial Components in Total Knee Arthroplasty: Do They Have a Future? *Trans Ortho Res Soc* 2003; 49: 1401.
45. McNulty D, Swope S, DiSilvestro M. Influence of Tray Surface Finish on Modular Tibial Tray Micromotion and Wear. *Trans Ortho Res Soc* 2005; 51: 1677.
46. McNulty D, Swope SW. Wear of Non-Modular and Modular Total Knee Tibial Components. Proc. of the 31th Annual Meeting of the Society for Biomaterials, Memphis, TN, USA, 2005.
47. McNulty D, Swope SW. Influence of Polyethylene Processing, Tibial Surface Finish and Modular Locking Mechanism Design on In-vitro Wear for Total Knee Arthroplasty. *Trans Ortho Res Soc* 2005;51:840.
48. Dowson D. History of Tribology. Bookcraft (Bath) Ltd, 1998 1998;2nd Edition.
49. Bowden FP, Tabor D. The Friction and Lubrication of Solids. Oxford University Press 1964.
50. Jacobson B. The Stribeck memorial lecture. Tribology International NORDTRIB symposium on Tribology 2002 2003; 36 (11): 781 - 789.
51. Stachowiak GW, Batchelor, A.W. Engineering Tribology. 2001;2nd Edition: 483 - 592.
52. White SE, Whiteside LA, McCarthy DS, Anthony M, Poggie RA. Simulated knee wear with cobalt chromium and oxidized zirconium knee femoral components. *Clin Orthop* 1994 (309): 176 - 184.
53. Chan FW, Bobyn JD, Medley JB, Krygier JJ, Tanzer M. The Otto Aufranc Award. Wear and lubrication of metal-on-metal hip implants. *Clin Orthop Relat Res* 1999 (369): 10 - 24.

54. Stachowiak GB, Stachowiak GW, Brandt JM. Ball-cratering abrasion tests with large abrasive particles. *Tribology International* 2006; 39 (1): 1 - 11.
55. Trezona RI, Allsopp, D. N., Hutchings, I. M. Transitions between two-body and three-body abrasive wear: influence of test conditions in the microscale abrasive wear test. *Wear* 1999; 225 - 229 (Part 1): 205 - 214.
56. Kuhlmann-Wilsdorf D. Flash temperatures due to friction and Joule heat at asperity contacts. *Wear* 1985; 105 (3): 187 - 198.
57. Sullivan JL. Boundary lubrication and oxidational wear. *J. Phys. D: Appl. Phys.* 1986; 19: 1999 - 2011.
58. Quinn TFJ. A Review on Oxidational Wear. NASA Interdisciplinary Collaboration in Tribology 1983; Nasa Contractor Report 3686.
59. Stott FH. The role of oxidation in the wear of alloys. *Tribology International* 1998;31(1-3):61-71.
60. Landolt D. Electrochemical and materials aspects of tribocorrosion systems. *Journal of Physics D: Applied Physics* 2006;39:3121-3127.
61. Michaelis W. Einführung in die Kunststoffverarbeitung. Hanser Verlag 1992.
62. Briscoe BJ, Sinha SK. Wear of polymers. *Proc IMechE, Part J, J of Engng Tribology [J]* 2002; 216: 401 - 413.
63. Gispert MP, Serro AP, Colaco R, Saramago B. Friction and wear mechanisms in hip prosthesis: Comparison of joint materials behaviour in several lubricants. *Wear* 2006; 260 (1-2): 149 - 158.
64. Widmer MR, Heuberger, M., Voros, J., Spencer, N.D. Influence of polymer surface chemistry on frictional properties under protein-lubrication: implications for hip-implant design. *Tribology Letters* 2001; 10 (1-2): 111 - 115.
65. Senior JM, West GH. Interaction between lubricants and plastic bearing surfaces. *Wear* 1971; 18 (4): 311 - 323.

66. Wang A, Sun DC, Yau S-S, Edwards B, Sokol M, Essner A, Polineni VK, Stark C, Dumbleton JH. Orientation softening in the deformation and wear of ultra-high molecular weight polyethylene. *Wear* 1997; 203-204: 230 - 241.
67. Bragdon CR, O'Connor, D. O., Lowenstein, J. D., Jasty, M., Syniuta, W. D. The importance of multidirectional motion on the wear of polyethylene. *Proc Inst Mech Eng [H]* 1996; 210 (3): 157 - 165.
68. Saikko V. A multidirectional motion pin-on-disk wear test method for prosthetic joint materials. *J Biomed Mater Res* 1998; 41 (1): 58 - 64.
69. Wimmer MA, Andriacchi TP. Tractive forces during rolling motion of the knee: implications for wear in total knee replacement. *J Biomech* 1997; 30 (2): 131- 137.
70. Johnson TS, Laurent MP, Yao JQ, Gilbertson LN. The effect of displacement control input parameters on tibiofemoral prosthetic knee wear. *Wear 13th International Conference on Wear of Materials* 2001; 250 (1 - 12): 222 - 226.
71. Kawanabe K, Clarke IC, Tamura J, Akagi M, Good VD, Williams PA, Yamamoto K. Effects of A-P translation and rotation on the wear of UHMWPE in a total knee joint simulator. *J Biomed Mater Res* 2001; 54 (3): 400 - 406.
72. Muratoglu OK, Bragdon, C. R., O'Connor, D. O., Jasty, M., Harris, W. H. A novel method of cross-linking ultra-high-molecular-weight polyethylene to improve wear, reduce oxidation, and retain mechanical properties. Recipient of the 1999 HAP Paul Award. *J Arthroplasty* 2001; 16 (2): 149 - 160.
73. Blanchet TA, Peterson, S. L., Roseneberg, K.D. Serum Lubricant Absorption by UHMWPE Orthopaedic Bearing Implants. *Journal of Tribology* 2002; 124 (1).
74. Muratoglu OK, Ruberti J, Melotti S, Spiegelberg SH, Greenbaum ES, Harris WH. Optical analysis of surface changes on early retrievals of highly cross-linked and conventional polyethylene tibial inserts. *J Arthroplasty* 2003; 18 (7 Suppl 1): 42 - 47.
75. Myshkin NK, Petrokovets MI, Kovalev AV. Tribology of polymers: Adhesion, friction, wear, and mass-transfer. *Tribology International: A Celebration Issue* 2006; 38 (11 - 12): 910 - 921.

76. Heuberger MP, Widmer MR, Zobeley E, Glockshuber R, Spencer ND. Protein-mediated boundary lubrication in arthroplasty. *Biomaterials* 2005; 26 (10): 1165 - 1173.
77. Brown SS, Clarke IC. A Review of Lubrication Conditions for Wear Simulation in Artificial Hip Replacements. *Tribology Transactions* 2006; 49 (1): 72 - 78.
78. Fang HW, Shih ML, Zhao JH, Huang HT, Lin HY, Liu HL, Chang CH, Yang CB, Liu HC. Association of polyethylene friction and thermal unfolding of interfacial albumin molecules. *Applied Surface Science* 2007; 253 (16): 6896 - 6904.
79. Israelachvili JN, McGuiggan P, Gee M, Homola A, Robbins M, Thompson P. Liquid dynamics in molecularly thin films. *J. Phys.: Condens. Matter* 1990; 2: SA 89 - SA 98.
80. Israelachvili JN, Stephen JK, Fetters LJ. Measurements of dynamic interactions in thin films of polymer melts: The transition from simple to complex behavior. *Journal of Polymer Science Part B: Polymer Physics* 1989; 27 (3): 489 - 502.
81. Gee LM, McGuiggan PM, Israelachvili J. Liquid to solidlike transitions of molecularly thin films under shear. *J. Chem. Phys.* 1990; 93 (3).
82. Klein J, Kumacheva E, Perahia D, Mahalu D, Warburg S. Interfacial Sliding of Polymer-Bearing Surfaces. *Faraday Discussions* 1994.
83. Klein J, Kumacheva E, Mahalu D, Perahia D, Fetters LJ. Reduction of frictional forces between solid surfaces bearing polymer brushes. 1994; 370 (6491): 634 - 636.
84. Klein J, Kumacheva E, Perahia D, Fetters LJ. Shear forces between sliding surfaces coated with polymer brushes: The high friction regime. *Acta Polymerica* 1998; 49 (10 - 11): 617 - 625.
85. Eiser E, Klein J, Witten TA, Fetters LJ. Shear of Telechelic Brushes. *Physical Review Letters* 1999; 82 (25): 5076 LP - 5079.
86. Kong YC, Tidesley Dj, Alexandre J. The molecular dynamics simulation of boundary-layer lubrication. *Molecular Physics* 1997; 92 (1): 7 - 18.

87. Raviv U, Giasson S, Kampf N, Gohy JF, Jerome R, Klein J. Lubrication by charged polymers. *Nature* 2003; 425 (6954): 163 - 165.
88. Tsarkova LA, Protsenko PV, Klein J. Interactions between Langmuir-Blodgett Polymer Monolayers Studied with the Surface Force Apparatus. *Colloid Journal* 2004; 66 (1): 84 - 94.
89. Tsarkova L, Zhang X, Hadjichristidis N, Klein J. Friction and Relaxation Dynamics of Highly Extended Polymer Brush Melts under Compression and Shear. *Macromolecules* 2007; 40 (7): 2539 - 2547.
90. Klein J. Personal communication. 2007.
91. Georges J-M, Loubet J-L. Pressure effects on the shearing of a colloidal thin film. *J. Phys.: Condens. Matter* 1991; 3: 9545 - 9550.
92. Georges J-M, Mazuyer D, Tonck A, Loubet J-L. Lubrication with a thin colloid layer. *J. Phys.: Condens. Matter* 1990; 2: SA 399 - SA 403.
93. Georges JM, Millot S, Loubet JL, Tonck A, Mazuyer D. Surface roughness and squeezed films at molecular level. *Tribology Series* 1993; 25 (Thin Films in Tribology): 443 - 452.
94. Pelletier E, Montfort PP, Loubet J-L, Tonck A, Georges J-M. Dynamics of Compressed Polymer Layers Adsorbed on Solid Surfaces. *Macromolecules* 1995; 28 (6): 1990 - 1998.
95. Mazuyer D, Tonck A, Georges J-M, Loubet J-L. Microtribology, Squeeze, and Friction of the Colloidal Layer. *Lubrication Science* 1995; 7 (4): 309 - 317.
96. Georges J-M, Tonck A, Loubet J-L, Mazuyer D, Georges E, Sidoroff F. Rheology and Friction of Compressed Polymer Layers Adsorbed on Solid Surfaces. *J. Phys. II France* 1996; 6: 57 - 76.
97. Persson BNJ, Tosatti E. Layering transition in confined molecular thin films: Nucleation and growth. *Physical Review B* 1994; 50: 5590 - 5599.
98. Persson BNJ, Mugele F. Squeeze-out and wear: fundamental principles and applications. *Journal of Physics: Condensed Matter* 2004; 16 (10): R 295 - R 355.

99. Zheng X, Baker H, Hancock WS. Analysis of the low molecular weight serum peptidome using ultrafiltration and a hybrid ion trap-Fourier transform mass spectrometer. *Journal of Chromatography A* 29th International Symposium on High Performance Liquid Phase Separations and Related Techniques - Part II 2006; 1120 (1 - 2): 173 - 184.
100. Atkinson K, Reginato AM. The Synovium. *The Adult Knee* (ed. Callaghan, J.J., Rosenberg, A.G., Rubash, H.E., Simonian, P.T., Wickiewicz, T.L.), 2003: 203 - 212.
101. Revell PA. Synovial lining cells. *Rheumatology International* 1989 ; 9 (2): 49 - 51.
102. DesJardins I, Aurora A, Tanner SL, Pace TB, Acampora KB, Laberge M. Increased total knee arthroplasty ultra-high molecular weight polyethylene wear using a clinically relevant hyaluronic acid simulator lubricant. *Proc Inst Mech Eng [H]* 2006; 220 (5): 609 - 623.
103. Sugio S, Kashima A, Mochizuki S, Noda M, Kobayashi K. Crystal structure of human serum albumin at 2.5 Å resolution. *Protein Eng* 1999; 12 (6): 439 - 446.
104. Giancola C, De Sena C, Fessas D, Graziano G, Barone G. DSC studies on bovine serum albumin denaturation. Effects of ionic strength and SDS concentration. *Int J Biol Macromol* 1997; 20 (3): 193 - 204.
105. *Biology of Microorganisms* (Madigan, M. T.; Martinko, J.M.). 2006 (11th Edition): 274, 693.
106. Baumgarten M, Bloebaum RD, Ross SD, Campbell P, Sarmiento A. Normal human synovial fluid: osmolality and exercise-induced changes. *J Bone Joint Surg Am* 1985; 67 (9): 1336 - 1339.
107. Small DM, Cohen AS, Schmid K. Lipoproteins of Synovial Fluid as Studied by Analytical Ultracentrifugation. *J Clin Invest* 1964; 43: 2070 - 2079.
108. Yao JQ, Laurent MP, Johnson TS, Blanchard CR, Crownshield RD. The influences of lubricant and material on polymer/CoCr sliding friction. *Wear* 2003; 255 (1 - 6): 780 - 784.

109. Fischer JJ, Jardetzky O. Nuclear Magnetic Relaxation Study of Intermolecular Complexes. The Mechanism of Penicillin Binding to Serum Albumin. *J Am Chem Soc* 1965; 87: 3237 - 3244.
110. Scholtan W, Rosenkranz H, Scheer M. Binding of sisomicin and streptomycin to human albumin. *Infection* 1978; 6 (4): 162 - 165.
111. Rosenkranz H, Scheer M, Scholtan W. Binding of aminoglycoside antibiotics to human serum proteins. III. Effect of experimental conditions. *Infection* 1978; 6 (2): 57 - 64.
112. Pauli W. Beziehungen der Kolloidchemie zur Physiologie. *Journal Colloid & Polymer Science* 1906; 1 (4): 101 - 107.
113. Pauli W. Kolloidchemische Studien am Eiweiß. *Journal Colloid & Polymer Science* 1908; 3 (1): 2 - 13.
114. Pauli W. Über die Beziehungen der Proteine zu Kolloiden und Elektrolyten. *Naturwissenschaften* 1932; 20 (2): 28 - 37.
115. Laurent TC, Laurent UB, Fraser JR. The structure and function of hyaluronan: An overview. *Immunol Cell Biol* 1996; 74 (2): A1 - A7.
116. Saari H, Santavirta, S., Nordstrom, D., Paavolainen, P., Konttinen, Y. T. Hyaluronate in total hip replacement. *J Rheumatol* 1993; 20 (1): 87 - 90.
117. Holmes MW, Bayliss MT, Muir H. Hyaluronic acid in human articular cartilage. Age-related changes in content and size. *Biochem J* 1988; 250 (2): 435 - 441.
118. Ayral X. Injections in the treatment of osteoarthritis. *Best Practice & Research Clinical Rheumatology* 2001; 15 (4): 609 - 626.
119. Divine JG, Zazulak BT, Hewett TE. Viscosupplementation for knee osteoarthritis: a systematic review. *Clin Orthop Relat Res* 2007; 455: 113 - 122.
120. Waddell DD, Bricker DC. Total knee replacement delayed with Hylan G-F 20 use in patients with grade IV osteoarthritis. *J Manag Care Pharm* 2007; 13 (2): 113 - 121.

121. Tsunenaga M, Tominaga N, Nishiyama T, Yamashita T, Fukuyama M, Miyata T, Furuse M. Hyaluronic acid-containing aqueous solution or aqueous dispersion of collagen. U.S. patent 5,137,875, 1992.
122. Xu S, Yamanaka J, Sato S, Miyama I, Yonese M. Characteristics of complexes composed of sodium hyaluronate and bovine serum albumin. *Chem Pharm Bull (Tokyo)* 2000; 48 (6): 779 - 783.
123. Oates KM, Krause WE, Jones RL, Colby RH. Rheopexy of synovial fluid and protein aggregation. *J R Soc Interface* 2006; 3 (6): 167 - 74.
124. Hills BA. Boundary lubrication in vivo. *Proc Inst Mech Eng [H]* 2000; 214 (1): 83 - 94.
125. Bell J, Tipper JL, Ingham E, Stone MH, Fisher J. The influence of phospholipid concentration in protein-containing lubricants on the wear of ultra-high molecular weight polyethylene in artificial hip joints. *Proc Inst Mech Eng [H]* 2001; 215 (2): 259 - 263.
126. Saikko V, Ahlroos T. Phospholipids as boundary lubricants in wear tests of prosthetic joint materials. *Wear* 1997; 207 (1 - 2): 86 - 91.
127. Graindorge S, Ferrandez W, Ingham E, Jin Z, Twigg P, Fisher J. The role of the surface amorphous layer of articular cartilage in joint lubrication. *Proc Inst Mech Eng [H]* 2006; 220 (5): 597 - 607.
128. Graindorge S, Ferrandez W, Jin Z, Ingham E, Grant C, Twigg P, Fisher J. Biphasic surface amorphous layer lubrication of articular cartilage. *Med Eng Phys* 2005; 27 (10): 836 - 844.
129. Zappone B, Ruths M, Greene GW, Jay GD, Israelachvili JN. Adsorption, lubrication, and wear of lubricin on model surfaces: polymer brush-like behavior of a glycoprotein. *Biophys J* 2007; 92 (5): 1693 - 1708.
130. Gleghorn JP, Jones AR, Flannery CR, Bonassar LJ. Boundary mode frictional properties of engineered cartilaginous tissues. *Eur Cell Mater* 2007; 14: 20 - 28; discussion 28 - 29.
131. Jones AR, Flannery CR. Bioregulation of lubricin expression by growth factors and cytokines. *Eur Cell Mater* 2007; 13: 40 - 5; discussion 45.

132. Jones AR, Gleghorn JP, Hughes CE, Fitz LJ, Zollner R, Wainwright SD, Caterson B, Morris EA, Bonassar LJ, Flannery CR. Binding and localization of recombinant lubricin to articular cartilage surfaces. *J Orthop Res* 2007; 25 (3): 283 - 292.
133. Elsaid KA, Jay GD, Chichester CO. Reduced expression and proteolytic susceptibility of lubricin/superficial zone protein may explain early elevation in the coefficient of friction in the joints of rats with antigen-induced arthritis. *Arthritis Rheum* 2007; 56 (1): 108 - 116.
134. Jay GD, Torres JR, Warman ML, Laderer MC, Breuer KS. The role of lubricin in the mechanical behavior of synovial fluid. *Proceedings of the National Academy of Sciences* 2007; 104 (15): 6194 - 6199.
135. Blumberg BS. Joint lubrication. *Bull Rheum Dis* 1958; 9 (2): 169 - 170.
136. Dintenfuss L. Lubrication in Synovial Joints: A Theoretical Analysis. *J Bone Joint Surg Am* 1963; 45: 1241 - 1256.
137. Medley JB, Dowson D, Wright V. Transient elastohydrodynamic lubrication models for the human ankle joint. *Eng Med* 1984; 13 (3): 137 - 151.
138. Walker PS, Dowson D, Longfield MD, Wright V. "Boosted lubrication" in synovial joints by fluid entrapment and enrichment. *Ann Rheum Dis* 1968; 27 (6): 512 - 520.
139. Ateshian GA, Lai WM, Zhu WB, Mow VC. An asymptotic solution for the contact of two biphasic cartilage layers. *J Biomech* 1994; 27 (11): 1347 - 1360.
140. Soltz MA, Basalo IM, Ateshian GA. Hydrostatic pressurization and depletion of trapped lubricant pool during creep contact of a rippled indenter against a biphasic articular cartilage layer. *J Biomech Eng* 2003; 125 (5): 585 - 593.
141. Park S, Costa KD, Ateshian GA. Microscale frictional response of bovine articular cartilage from atomic force microscopy. *J Biomech* 2004; 37 (11): 1679 - 1687.

142. Krishnan R, Kopacz M, Ateshian GA. Experimental verification of the role of interstitial fluid pressurization in cartilage lubrication. *J Orthop Res* 2004; 22 (3): 565 - 570.
143. Crockett R, Grubelnik A, Roos S, Dora C, Born W, Troxler H. Biochemical composition of the superficial layer of articular cartilage. *J Biomed Mater Res A* 2007; 82 (4): 958 - 964.
144. Krishnan R, Caligaris M, Mauck RL, Hung CT, Costa KD, Ateshian GA. Removal of the superficial zone of bovine articular cartilage does not increase its frictional coefficient. *Osteoarthritis Cartilage* 2004; 12 (12): 947 - 955.
145. Basalo IM, Chahine NO, Kaplun M, Chen FH, Hung CT, Ateshian GA. Chondroitin sulfate reduces the friction coefficient of articular cartilage. *J Biomech* 2007; 40 (8): 1847 - 1854.
146. Wang A, Essner A, Polineni VK, Stark C, Dumbleton JH. Lubrication and wear of ultra-high molecular weight polyethylene in total joint replacements. *Tribology International* 1998; 31 (1 - 3): 17 - 33.
147. Jin ZM. Analysis of mixed lubrication mechanism in metal-on-metal hip joint replacements. *Proc Inst Mech Eng [H]* 2002; 216 (1): 85 - 89.
148. Auger DD, Dowson, D., Fisher, J., Jin, Z. M. Friction and lubrication in cushion form bearings for artificial hip joints. *Proc Inst Mech Eng J Eng Med* 1993; 207 (1): 25 - 33.
149. Auger DD, Dowson, D., Fisher, J. Cushion form bearings for total knee joint replacement. Part 2: Wear and durability. *Proc Inst Mech Eng J Eng Med* 1995; 209 (2): 83 - 91.
150. Auger DD, Dowson, D., Fisher, J. Cushion form bearings for total knee joint replacement. Part 1: Design, friction and lubrication. *Proc Inst Mech Eng [H]* 1995; 209 (2): 73 - 81.
151. Stewart T, Jin ZM, Fisher J. Friction of composite cushion bearings for total knee joint replacements under adverse lubrication conditions. *Proc Inst Mech Eng [H]* 1997; 211 (6): 451 - 465.

152. McKellop H, Clarke, I. C., Markolf, K. L., Amstutz, H. C. Wear characteristics of UHMW polyethylene: a method for accurately measuring extremely low wear rates. *J Biomed Mater Res* 1978; 12 (6): 895 - 927.
153. Wimmer MA, Loos J, Nassutt R, Heitkemper M, Fischer A. The acting wear mechanisms on metal-on-metal hip joint bearings: in vitro results. *Wear* 2001; 250 (1 - 12): 129 - 139.
154. Liao YS, McKellop H, Lu Z, Campbell P, Benya P. The effect of frictional heating and forced cooling on the serum lubricant and wear of UHMW polyethylene cups against cobalt-chromium and zirconia balls. *Biomaterials* 2003; 24 (18): 3047 - 3059.
155. Liao Y-S, McNulty D, Hanes M. Wear rate and surface morphology of UHMWPE cups are affected by the serum lubricant concentration in a hip simulation test. *Wear* 2003; 255 (7 - 12): 1051 - 1056.
156. Wang A, Essner A, Schmidig G. The effects of lubricant composition on in vitro wear testing of polymeric acetabular components. *J Biomed Mater Res* 2004; 68B (1): 45 - 52.
157. Schwenke T, Kaddick C, Schneider E, Wimmer MA. Fluid composition impacts standardized testing protocols in ultrahigh molecular weight polyethylene knee wear testing. *Proc Inst Mech Eng [H]* 2005; 219 (6): 457 - 64.
158. Wimmer MA, Sprecher C, Hauert R, Täger G, Fischer A. Tribochemical reaction on metal-on-metal hip joint bearings: A comparison between in-vitro and in-vivo results. *Wear* 2003; 255 (7 - 12): 1007 - 1014.
159. Serro AP, Gispert MP, Martins MC, Brogueira P, Colaco R, Saramago B. Adsorption of albumin on prosthetic materials: implication for tribological behavior. *J Biomed Mater Res A* 2006; 78 (3): 581 - 589.
160. Norde W, Lyklema J. Why proteins prefer interfaces. *J Biomater Sci Polym Ed* 1991; 2 (3): 183 - 202.
161. Norde W, Lyklema J. Protein Adsorption and Bacterial Adhesion to Solid Surfaces: A Colloid-Chemical Approach. *Colloids and Surfaces* 1989; 38: 1 - 13.

162. Hlady VV, Buijs J. Protein adsorption on solid surfaces. *Curr Opin Biotechnol* 1996; 7 (1): 72 - 77.
163. Malmsten M. Formation of Adsorbed Protein Layers. *Journal of Colloid and Interface Science* 1998; 207: 186 - 199.
164. Haynes CA, Norde W. Structures and Stabilities of Adsorbed Proteins. *Journal of Colloid and Interface Science* 1995; 169 (2): 313 - 328.
165. Good VD, Clarke IC, Gustafson GA, Downs B, Anissian L, Sorensen K. Wear of ultra-high molecular weight polyethylene and poly-tetra-fluor-ethylene in a hip simulator: a dose-response study of protein concentration. *Acta Orthop Scand* 2000; 71 (4): 365 - 369.
166. Heuberger MP. Personal communication. 2007.
167. Makhatadze GI, Privalov PL. On the entropy of protein folding. *Protein Sci* 1996; 5 (3): 507 - 510.
168. Makhatadze GI, Privalov PL. Hydration effects in protein unfolding. *Biophysical Chemistry* 1994; 51 (2 - 3): 291 - 309.
169. Pico GA. Thermodynamic features of the thermal unfolding of human serum albumin. *International Journal of Biological Macromolecules* 1997; 20 (1): 63 - 73.
170. Jenzano JW, Hogan SL, Noyes CM, Featherstone GL, Lundblad RL. Comparison of five techniques for the determination of protein content in mixed human saliva. *Anal Biochem* 1986; 159 (2): 370 - 376.
171. Kessler RJ, Fanestil DD. Interference by lipids in the determination of protein using bicinchoninic acid. *Anal Biochem* 1986; 159 (1): 138 - 142.
172. Smith PK, Krohn RI, Hermanson GT, Mallia AK, Gartner FH, Provenzano MD, Fujimoto EK, Goeke NM, Olson BJ, Klenk DC. Measurement of protein using bicinchoninic acid. *Analytical Biochemistry* 1985; 150 (1): 76 - 85.
173. Wiechelman KJ, Braun RD, Fitzpatrick JD. Investigation of the bicinchoninic acid protein assay: identification of the groups responsible for color formation. *Anal Biochem* 1988; 175 (1): 231 - 237.

174. Liao Y-S, McNulty D, Hanes M. Wear rate and surface morphology of UHMWPE cups are affected by the serum lubricant concentration in a hip simulation test. *Wear* 14th International Conference on Wear of Materials 2003; 255 (7 - 12): 1051 - 1056.
175. Kitano T, Ateshian, G. A., Mow, V. C., Kadoya, Y., Yamano, Y. Constituents and pH changes in protein rich hyaluronan solution affect the biotribological properties of artificial articular joints. *J Biomech* 2001; 34 (8): 1031 - 7103.
176. Privalov PL, Dragan AI. Microcalorimetry of biological macromolecules. *Biophys Chem* 2007; 126 (1 - 3): 16 - 24.
177. Cornwall GB, Bryant JT, Hansson CM. The effect of kinematic conditions on the wear of ultra-high molecular weight polyethylene (UHMWPE) in orthopaedic bearing applications. *Proc Inst Mech Eng [H]* 2001; 215 (1): 95 - 106.
178. Walker PS, Blunn GW, Broome DR, Perry J, Watkins A, Sathasivam S, Dewar ME, Paul JP. A knee simulating machine for performance evaluation of total knee replacements. *J Biomech* 1997; 30 (1): 83 - 89.
179. Barnett PI, McEwen HM, Auger DD, Stone MH, Ingham E, Fisher J. Investigation of wear of knee prostheses in a new displacement/force-controlled simulator. *Proc Inst Mech Eng [H]* 2002; 216 (1): 51 - 61.
180. DesJardins JD, Walker PS, Haider H, Perry J. The use of a force-controlled dynamic knee simulator to quantify the mechanical performance of total knee replacement designs during functional activity. *J Biomech* 2000; 33 (10): 1231 - 1242.
181. DesJardins JD, Walker, P.S., Haider, H, Perry J. The influence of soft tissue constraint on the mechanical performance of different TKR designs. Presented at the 9th Mtg Eur Orthop Res Soc, Brussels, Belgium, June 3 - 4, 1999.
182. Burgess IC, Kolar, M., Cunningham, J. L. and Unsworth, A. Development of a six station knee wear simulator and preliminary wear results. *Proc Inst Mech Eng J Eng Med* 1997; 211 (1): 37 - 47.
183. Walker PS, Blunn GW, Perry JP, Bell CJ, Sathasivam S, Andriacchi TP, Paul JP, Haider H, Campbell PA. Methodology for long-term wear testing of total knee replacements. *Clin Orthop* 2000 (372): 290 - 301.

184. Blankevoort L, Huiskes R, de Lange A. The envelope of passive knee joint motion. *J Biomech* 1988; 21 (9): 705 - 720.
185. Fukubayashi T, Torzilli PA, Sherman MF, Warren RF. An in vitro biomechanical evaluation of anterior-posterior motion of the knee. Tibial displacement, rotation, and torque. *J Bone Joint Surg Am* 1982; 64 (2): 258 - 264.
186. Markolf KL, Bargar WL, Shoemaker SC, Amstutz HC. The role of joint load in knee stability. *J Bone Joint Surg Am* 1981; 63 (4): 570 - 585.
187. McNulty DE, Swope, S.W. and Liao, Y.-S. Clinical implications of the proposed ISO Total Knee Simulation Displacement Inputs on Tibiofemoral Kinematics for Confirming Designs. Proc of the 29th Annual Meeting of the Society for Biomaterials, Reno, NV, 2003.
188. Haider H, Alberts LA, Laurent MP, Johnson TS, Yao JQ, Gilbertson LN, Walker PS, Neff JR, Garvin KL. Comparison between force-controlled and displacement-controlled in-vitro testing on a widely used TKR implant. Proc of the 48th Annual Meeting of the Orthopaedic Research Society, Dallas, Texas 2002.
189. Wimmer MA, Sah R, Madsen L, Viridi A. The effect of antibacterial and antifungal additives on the wear rate of ultra-high molecular weight polyethylene. Symposium on Wear of Articulating Surfaces: Understanding Joint Simulation, ASTM Meeting, Dallas, 2005.
190. Goldenberg DL. Septic arthritis. *Lancet* 1998;351(9097): 197 - 202.
191. Hespell RB, Thomashow MF, Rittenberg SC. Changes in cell composition and viability of *Bdellovibrio bacteriovorus* during starvation. *Arch Microbiol* 1974; 97 (4): 313 - 327.
192. Fratamico PM, Whiting RC. Ability of *Bdellovibrio bacteriovorus* 109J to Lyse Gram-Negative Food-Borne Pathogenic and Spoilage Bacteria. *Journal of Food Protection* 1995; 58 (2): 160 - 164.
193. Rendulic S, Jagtap P, Rosinus A, Eppinger M, Baar C, Lanz C, Keller H, Lambert C, Evans KJ, Goesmann A and others. A predator unmasked: life cycle of *Bdellovibrio bacteriovorus* from a genomic perspective. *Science* 2004; 303 (5658): 689 - 692.

194. Holmes B, Willcox WR, Lapage SP. Identification of Enterobacteriaceae by the API 20E system. *J Clin Pathol* 1978; 31 (1): 22 - 30.
195. Leboffe MJ, Pierce B. *Microbiology: Laboratory Theory and Application*. 2002: 220.
196. Polineni VK, Wang A, Essner A, Stark C, Dumbleton JH. Effect of Lubricant Protein Concentration on the Wear of UHMWPE Acetabular Cups against Cobalt-Chrome and Alumina Femoral Heads. 23rd Annual Meeting of the Society of Biomaterials 1997:154.
197. Wang A, Polineni, V. K., Essner, A., Stark, C., Dumbleton, J. Quantitative Analysis of Serum Degradation and its effect on the outcome of hip joint simulator wear testing of UHMWPE. *Trans Orthop Res Soc*; 45; 1999.
198. Benson LC, DesJardins, J. D. and LaBerge, M. Effects of in vitro wear of machined and molded UHMWPE tibial inserts on TKR kinematics. *J Biomed Mater Res* 2001; 58 (5): 496 - 504.
199. Nusbaum HJ, Rose RM. The effects of radiation sterilization on the properties of ultrahigh molecular weight polyethylene. *J Biomed Mater Res* 1979; 13 (4): 557 - 576.
200. Clarke IC, Starkebaum W, Hosseinian A, McGuire P, Okuda R, Salovey R, Young R. Fluid-sorption phenomena in sterilized polyethylene acetabular prostheses. *Biomaterials* 1985; 6 (3): 184 - 188.
201. Klapperich C, Niedzwiecki, S., Ries, M., Pruitt, L. Fluid sorption of orthopedic grade ultrahigh molecular weight polyethylene in a serum environment is affected by the surface area and sterilization method. *J Biomed Mater Res* 2000; 53 (1): 73 - 75.
202. Bragdon CR, O'Conner D, Weinberg EA, Skehan H, O.K. M, Lowenstein JD, W.H. H. The effects of load plus motion versus load alone on fluid imbibition into UHMWPE. *Trans Ortho Res Soc* 1999; 45 (824).
203. Yao JQ, Blanchet TA, Murphy DJ, Laurent MP. Effect of fluid absorption on the wear resistance of UHMWPE orthopedic bearing surfaces. *Wear* 2003; 255 (7 - 12): 1113 - 1120.

204. Scholes SC, Unsworth A. The wear properties of CFR-PEEK-OPTIMA articulating against ceramic assessed on a multidirectional pin-on-plate machine. *Proc Inst Mech Eng [H]* 2007; 221 (3): 281 - 289.
205. Corradini P, Guerra G, Cavallo L. Do New Century Catalysts Unravel the Mechanism of Stereocontrol of Old Ziegler-Natta Catalysts? *Acc. Chem. Res.* 2004; 37 (4): 231 - 241.
206. Kurtz SM, Muratoglu, O. K., Evans, M., Edidin, A. A. Advances in the processing, sterilization, and crosslinking of ultra-high molecular weight polyethylene for total joint arthroplasty. *Biomaterials* 1999; 20 (18): 1659 - 1688.
207. Lewis G. Polyethylene wear in total hip and knee arthroplasties. *J Biomed Mater Res* 1997; 38 (1): 55 - 75.
208. Silva M, Schmalzried, T.P. Polyethylene in Total Knee Arthroplasty. *The Adult Knee* (ed. Callaghan, J.J., Rosenberg, A.G., Rubash, H.E., Simonian, P.T., Wickiewicz, T.L.) 2003; 1: 279 - 288.
209. Li S, Burstein, A. H. Ultra-high molecular weight polyethylene. The material and its use in total joint implants. *J Bone Joint Surg Am* 1994; 76 (7): 1080 - 1090.
210. Muratoglu OK, Vitteteo DA, Rubash HE. Damage of Implant Surfaces in Total Knee Arthroplasty. *The Adult Knee* (ed. Callaghan, J.J., Rosenberg, A.G., Rubash, H.E., Simonian, P.T., Wickiewicz, T.L.) 2003; 1: 297 - 313.
211. McGloughlin TM, Kavanagh AG. Wear of ultra-high molecular weight polyethylene (UHMWPE) in total knee prostheses: a review of key influences. *Proc Inst Mech Eng [H]* 2000; 214 (4): 349 - 359.
212. Sutula LC, Collier JP, Saum KA, Currier BH, Currier JH, Sanford WM, Mayor MB, Wooding RE, Sperling DK, Williams IR and others. The Otto Aufranc Award. Impact of gamma sterilization on clinical performance of polyethylene in the hip. *Clin Orthop* 1995(319): 28 - 40.
213. Collier JP, Sperling DK, Currier JH, Sutula LC, Saum KA, Mayor MB. Impact of gamma sterilization on clinical performance of polyethylene in the knee. *J Arthroplasty* 1996; 11 (4): 377 - 389.

214. Currier BH, Currier JH, Collier JP, Mayor MB, Scott RD. Shelf life and in vivo duration. Impacts on performance of tibial bearings. *Clin Orthop* 1997 (342): 111 - 122.
215. Blunn G, Brach del Preva, E. M., Costa, L., Fisher, J., Freeman, M. A. Ultra high molecular-weight polyethylene (UHMWPE) in total knee replacement: fabrication, sterilization and wear. *J Bone Joint Surg Br* 2002; 84 (7): 946 - 949.
216. Bargmann LS, Bargmann, B. C., Collier, J. P., Currier, B. H., and Mayor, M. B. Current sterilization and packaging methods for polyethylene. *Clin Orthop* 1999 (369): 49 - 58.
217. Kurtz SM, Rinnac CM, Hozack WJ, Turner J, Marcolongo M, Goldberg VM, Kraay MJ, Edidin AA. In vivo degradation of polyethylene liners after gamma sterilization in air. *J Bone Joint Surg Am* 2005; 87-A (4): 815 - 823.
218. Engh GA, Dwyer KA, Hanes CK. Polyethylene wear of metal-backed tibial components in total and unicompartmental knee prostheses. *J Bone Joint Surg Br* 1992; 74 (1): 9 - 17.
219. Puloski SK, McCalden RW, MacDonald SJ, Rorabeck CH, Bourne RB. Tibial post wear in posterior stabilized total knee arthroplasty. An unrecognized source of polyethylene debris. *J Bone Joint Surg Am* 2001; 83-A (3): 390 - 397.
220. Gabriel SM, Dennis DA, Honey MJ, Scott RD. Polyethylene wear on the distal tibial insert surface in total knee arthroplasty. *The Knee* 1998; 5: 221 - 228.
221. Brandt JM, McCalden RW, Medley JB, MacDonald S, Bourne MH, Rorabeck CH. Delamination Wear on Retrieved Gamma-in-Nitrogen Sterilized Polyethylene Inserts. *Trans Ortho Res Soc* 2005:1867.
222. Kurtz SM, Purtill J, Sharkey P, Topper J, MacDonald D, Kraay MJ, Goldberg VM, Parvizi J, Rinnac CM. Clinical Significance of In Vivo Oxidation for Gamma Sterilized Tibial Inserts. *Trans Ortho Res Soc* 2006; 52: 552.
223. Currier BH, Currier JH, Mayor MB, Lyford KA, Van Citters DW, Collier JP. In vivo oxidation of gamma-barrier-sterilized ultra-high-molecular-weight polyethylene bearings. *J Arthroplasty* 2007; 22 (5): 721 - 731.

224. McNulty DE, Liao YS, Haas BD. The influence of sterilization method on wear performance of the low contact stress total knee system. *Orthopedics* 2002; 25 (2 Suppl): s243 - s246.
225. Costa L, Bracco P, Brach del Prever EM, Kurtz SM, Gallinaro P. Oxidation and oxidation potential in contemporary packaging for polyethylene total joint replacement components. *J Biomed Mater Res B Appl Biomater* 2006; 78 (1): 20 - 26.
226. Williams IR, Mayor, M. B., Collier, J. P. The impact of sterilization method on wear in knee arthroplasty. *Clin Orthop* 1998 (356): 170 - 180.
227. White SE, Paxson, R. D., Tanner, M. G., Whiteside, L. A. Effects of sterilization on wear in total knee arthroplasty. *Clin Orthop* 1996 (331): 164 - 171.
228. Muratoglu OK, Mark, A., Vittetoe, D. A., Harris, W. H., Rubash, H. E. Polyethylene damage in total knees and use of highly crosslinked polyethylene. *J Bone Joint Surg Am* 2003; 85-A Suppl 1: S7 - S13.
229. McKellop HA, Shen FW, Campbell P, Ota T. Effect of molecular weight, calcium stearate, and sterilization methods on the wear of ultra high molecular weight polyethylene acetabular cups in a hip joint simulator. *J Orthop Res* 1999;17(3):329-39.
230. Currier BH, Currier, J. H., Collier, J. P., Mayor, M. B. Effect of fabrication method and resin type on performance of tibial bearings. *J Biomed Mater Res* 2000; 53 (2): 143 - 151.
231. Ritter MA, Berend, M. E., Meding, J. B., Keating, E. M., Faris, P. M., Crites, B. M. Long-term follow-up of anatomic graduated components posterior cruciate-retaining total knee replacement. *Clin Orthop* 2001 (388): 51 - 57.
232. Berzins A, Jacobs, J. J., Berger, R., Ed, C., Natarajan, R., Andriacchi, T., Galante, J. O. Surface damage in machined ram-extruded and net-shape molded retrieved polyethylene tibial inserts of total knee replacements. *J Bone Joint Surg Am* 2002; 84-A (9): 1534 - 1540.
233. Keating EM, Meding, J. B., Faris, P. M., Ritter, M. A. Long-term follow-up of non-modular total knee replacements. *Clin Orthop* 2002 (404): 34 - 39.

234. Ahn NU, Nallamshetty L, Ahn UM, Buchowski JM, Rose PS, Lemma MA, Wenz JF. Early failure associated with the use of Hylamer-M spacers in three primary AMK total knee arthroplasties. *J Arthroplasty* 2001; 16 (1): 136 - 139.
235. Ries MD, Bellare A, Livingston BJ, Cohen RE, Spector M. Early delamination of a Hylamer-M tibial insert. *The Journal Of Arthroplasty* 1996; 11 (8): 974 - 976.
236. Brandt J-M, Young C, Naudie D, MacDonald SJ, Rorabeck CH. Performance of Hylamer-M in Revision Total Knee Arthroplasty. Society for Biomaterials Annual Meeting, Chicago, IL, April 18-21st, 2007.
237. McKellop H, Shen FW, Lu B, Campbell P, Salovey R. Development of an extremely wear-resistant ultra high molecular weight polyethylene for total hip replacements. *J Orthop Res* 1999; 17 (2): 157 - 167.
238. Muratoglu OK, Bragdon, C.R., O'Conner, D., Jasty, M., Harris, W.H. A Highly Crosslinked, Melted Ultra-High Molecular Weight Polyethylene: Expanded Potential for Joint Arthroplasty. *World Tribology Forum in Arthroplasty* (ed. C. Rieker/U. Wyss), 2001 (245).
239. Muratoglu OK, O'Connor DO, Bragdon CR, Delaney J, Jasty M, Harris WH, Merrill E, Venugopalan P. Gradient crosslinking of UHMWPE using irradiation in molten state for total joint arthroplasty. *Biomaterials* 2002; 23 (3): 717 - 724.
240. Baker DA, Hastings, R. S., Pruitt, L. Study of fatigue resistance of chemical and radiation crosslinked medical grade ultrahigh molecular weight polyethylene. *J Biomed Mater Res* 1999; 46 (4): 573 - 581.
241. Bradford L, Baker D, Ries MD, Pruitt LA. Fatigue crack propagation resistance of highly crosslinked polyethylene. *Clin Orthop Relat Res* 2004 (429): 68 - 72.
242. Muratoglu OK, Bragdon, C. R., O'Connor, D. O., Perinchief, R. S., Jasty, M., Harris, W. H. Aggressive wear testing of a cross-linked polyethylene in total knee arthroplasty. *Clin Orthop* 2002 (404): 89 - 95.

243. Medel FJ, Pena P, Cegonino J, Gomez-Barrena E, Puertolas JA. Comparative fatigue behavior and toughness of remelted and annealed highly crosslinked polyethylenes. *J Biomed Mater Res B Appl Biomater* 2007.
244. Bradford L, Baker DA, Graham J, Chawan A, Ries MD, Pruitt LA. Wear and surface cracking in early retrieved highly cross-linked polyethylene acetabular liners. *J Bone Joint Surg Am* 2004; 86-A (6): 1271 - 1282.
245. Fisher J, McEwen HM, Tipper JL, Galvin AL, Ingram J, Kamali A, Stone MH, Ingham E. Wear, debris, and biologic activity of cross-linked polyethylene in the knee: benefits and potential concerns. *Clin Orthop Relat Res* 2004 (428): 114 - 119.
246. Galvin AL, Tipper JL, Jennings LM, Stone MH, Jin ZM, Ingham E, Fisher I. Wear and biological activity of highly crosslinked polyethylene in the hip under low serum protein concentrations. *Proc Inst Mech Eng [H]* 2007; 221 (1): 1-10.
247. Asano T, Akagi M, Clarke IC, Masuda S, Ishii T, Nakamura T. Dose effects of cross-linking polyethylene for total knee arthroplasty on wear performance and mechanical properties. *J Biomed Mater Res B Appl Biomater* 2007.
248. Jasty M, Rubash HE, Muratoglu O. Highly cross-linked polyethylene: the debate is over--in the affirmative. *J Arthroplasty* 2005; 20 (4 Suppl 2): 55 - 58.
249. Ries MD. Highly cross-linked polyethylene: the debate is over--in opposition. *J Arthroplasty* 2005; 20 (4 Suppl 2): 59 - 62.
250. Lewis G, Carroll, M. Effect of crosslinking UHMWPE on its tensile and compressive creep performance. *Biomed Mater Eng* 2001; 11 (3): 167 - 183.
251. Collier JP, Currier, B. H., Kennedy, F. E., Currier, J. H., Timmins, G. S., Jackson, S. K., Brewer, R. L. Comparison of cross-linked polyethylene materials for orthopaedic applications. *Clin Orthop* 2003 (414): 289 - 304.

252. Colwell CW, Jr., Hozack WJ, Mesko JW, D'Antonio JA, Bierbaum BE, Capello WN, Jaffe WL, Mai KT. Ceramic-on-Ceramic Total Hip Arthroplasty Early Dislocation Rate. *Clin Orthop Relat Res* 2007; Publish Ahead of Print.
253. Heimke G, Leyen S, Willmann G. Knee arthroplasty: recently developed ceramics offer new solutions. *Biomaterials* 2002; 23 (7): 1539 - 1551.
254. Leyen S, Dietrich, M., Silberer, P. Investigation of the wear behaviour of a ceramic knee concept with floating meniscal bearing. 2003; *Compliant and Hard Bearing Surfaces for Artificial Joints, Alternative Solutions and Future Directions: Proceedings of the 4th International Biotribology Forum and 24th Biotribology Symposium, Fukuoka, Japan* (Jin, Z, Medley, J.B. (ed)).
255. Kim YH, Kook HK, Kim JS. Comparison of fixed-bearing and mobile-bearing total knee arthroplasties. *Clin Orthop* 2001 (392): 101 - 115.
256. Skinner HB. Ceramic bearing surfaces. *Clin Orthop* 1999 (369): 83 - 91.
257. Masonis JL, Bourne RB, Ries MD, McCalden RW, Salehi A, Kelman DC. Zirconia femoral head fractures: a clinical and retrieval analysis. *J Arthroplasty* 2004; 19 (7): 898 - 905.
258. Rand JA, Trousdale RT, Ilstrup DM, Harmsen WS. Factors affecting the durability of primary total knee prostheses. *J Bone Joint Surg Am* 2003; 85-A(2): 259 - 265.
259. Robinson RP. The early innovators of today's resurfacing condylar knees. *J Arthroplasty* 2005; 20(1 Suppl 1): 2 - 26.
260. Insall J, Ranawat CS, Scott WN, Walker P. Total condylar knee replacement: preliminary report. *Clin Orthop Relat Res* 1976 (120): 149 - 154.
261. Pavone V, Boettner F, Fickert S, Sculco TP. Total condylar knee arthroplasty: a long-term follow-up. *Clin Orthop Relat Res* 2001 (388): 18 - 25.

262. Rodriguez JA, Baez N, Rasquinha V, Ranawat CS. Metal-backed and all-polyethylene tibial components in total knee replacement. *Clin Orthop* 2001 (392): 174 - 183.
263. O'Rourke MR, Callaghan JJ, Goetz DD, Sullivan PM, Johnston RC. Osteolysis associated with a cemented modular posterior-cruciate-substituting total knee design: five to eight-year follow-up. *J Bone Joint Surg Am* 2002; 84-A (8): 1362 - 1371.
264. Berend ME, Ritter MA, Meding JB, Faris PM, Keating EM, Redelman R, Faris GW, Davis KE. Tibial component failure mechanisms in total knee arthroplasty. *Clin Orthop* 2004 (428): 26 - 34.
265. Thadani PJ, Vince KG, Ortaaslan SG, Blackburn DC, Cudiamat CV. Ten- to 12-year follow-up of the Insall-Burstein I total knee prosthesis. *Clin Orthop* 2000 (380): 17 - 29.
266. Weber AB, Worland, R. L., Keenan, J., Van Bowen, J. A study of polyethylene and modularity issues in >1000 posterior cruciate-retaining knees at 5 to 11 years. *J Arthroplasty* 2002; 17 (8): 987 - 991.
267. Faris PM, Ritter, M. A., Keating, E. M., Meding, J. B., Harty, L. D. The AGC all-polyethylene tibial component: a ten-year clinical evaluation. *J Bone Joint Surg Am* 2003; 85-A (3): 489 - 493.
268. Emerson RH, Jr., Higgins LL, Head WC. The AGC total knee prosthesis at average 11 years. *J Arthroplasty* 2000; 15 (4): 418 - 423.
269. Berend ME. Personal communication. 2004.
270. Bartel DL, Burstein AH, Santavicca EA, Insall JN. Performance of the tibial component in total knee replacement. *J Bone Joint Surg Am* 1982; 64 (7): 1026 - 1033.
271. Udomkiat P, Dorr LD, Long W. Matched-pair analysis of all-polyethylene versus metal-backed tibial components. *J Arthroplasty* 2001; 16 (6): 689 - 696.
272. Najibi S, Iorio R, Surdam JW, Whang W, Appleby D, Healy WL. All-polyethylene and metal-backed tibial components in total knee arthroplasty: a matched pair analysis of functional outcome. *J Arthroplasty* 2003; 18 (7 Suppl 1): 9 - 15.

273. Ranawat AS, Mohanty SS, Goldsmith SE, Rasquinha VJ, Rodriguez JA, Ranawat CS. Experience With an All-Polyethylene Total Knee Arthroplasty in Younger, Active Patients With Follow-up From 2 to 11 Years. *J Arthroplasty* 2005; 20 (6 Suppl 3): 7-11.
274. Bert JM, Reuben, J., Kelly, F., Gross, M., Elting, J. The incidence of modular tibial polyethylene insert exchange in total knee arthroplasty when polyethylene failure occurs. *J Arthroplasty* 1998; 13 (6): 609 - 614.
275. Engh GA, Koralewicz LM, Pereles TR. Clinical results of modular polyethylene insert exchange with retention of total knee arthroplasty components. *J Bone Joint Surg Am* 2000; 82(4): 516 - 523.
276. Babis GC, Trousdale RT, Pagnano MW, Morrey BF. Poor outcomes of isolated tibial insert exchange and arthrolysis for the management of stiffness following total knee arthroplasty. *J Bone Joint Surg Am* 2001; 83-A (10): 1534 - 1536.
277. Babis GC, Trousdale RT, Morrey BF. The effectiveness of isolated tibial insert exchange in revision total knee arthroplasty. *J Bone Joint Surg Am* 2002; 84-A(1): 64 - 68.
278. Whiteside LA. Clinical results of Whiteside Ortholoc total knee replacement. *Orthop Clin North Am* 1989; 20 (1):113 - 124.
279. Hofmann AA, Wyatt RW, Beck SW, Alpert J. Cementless total knee arthroplasty in patients over 65 years old. *Clin Orthop Relat Res* 1991 (271): 28 - 34.
280. Engh GA, Parks NL, Ammeen DJ. Tibial osteolysis in cementless total knee arthroplasty. A review of 25 cases treated with and without tibial component revision. *Clin Orthop* 1994(309):33-43.
281. Lewis PL, Rorabeck CH, Bourne RB. Screw osteolysis after cementless total knee replacement. *Clin Orthop* 1995(321):173-7.
282. Surace MF, Berzins A, Urban RM, Jacobs JJ, Berger RA, Natarajan RN, Andriacchi TP, Galante JO. Coventry Award paper. Back surface wear and deformation in polyethylene tibial inserts retrieved postmortem. *Clin Orthop* 2002 (404): 14 - 23.

283. Conditt MA, Ismaily SK, Alexander JW, Noble PC. Backside Wear of Modular Ultra-High Molecular Weight Polyethylene Tibial Inserts. *J Bone Joint Surg Am* 2004; 86 (5): 1031 -1037.
284. Ezzet KA, Garcia, R., Barrack, R. L. Effect of component fixation method on osteolysis in total knee arthroplasty. *Clin Orthop Relat Res* 1995 (321): 86 - 91.
285. Laskin RS, Maruyama Y, Villaneuva M, Bourne R. Deep-dish congruent tibial component use in total knee arthroplasty: a randomized prospective study. *Clin Orthop Relat Res* 2000 (380): 36 - 44.
286. Berger RA, Lyon, J. H., Jacobs, J. J., Barden, R. M., Berkson, E. M., Sheinkop, M. B., Rosenberg, A. G., and Galante, J. O. Problems with cementless total knee arthroplasty at 11 years follow-up. *Clin Orthop* 2001 (392): 196 - 207.
287. Brassard MF, Insall JN, Scuderi GR, Colizza W. Does modularity affect clinical success? A comparison with a minimum 10-year followup. *Clin Orthop Relat Res* 2001(388): 26 - 32.
288. Dixon MC, Brown RR, Parsch D, Scott RD. Modular fixed-bearing total knee arthroplasty with retention of the posterior cruciate ligament. A study of patients followed for a minimum of fifteen years. *J Bone Joint Surg Am* 2005; 87 (3): 598 - 603.
289. Hirakawa K, Bauer TW, Yamaguchi M, Stulberg BN, Wilde AH. Relationship between wear debris particles and polyethylene surface damage in primary total knee arthroplasty. *J Arthroplasty* 1999; 14 (2): 165 - 171.
290. Schmalzried TP, Campbell P, Schmitt AK, Brown IC, Amstutz HC. Shapes and dimensional characteristics of polyethylene wear particles generated in vivo by total knee replacements compared to total hip replacements. *J Biomed Mater Res* 1997; 38 (3): 203 - 210.
291. Shanbhag AS, Bailey HO, Hwang DS, Cha CW, Eror NG, Rubash HE. Quantitative analysis of ultrahigh molecular weight polyethylene (UHMWPE) wear debris associated with total knee replacements. *J Biomed Mater Res* 2000; 53(1): 100 - 110.

292. Li S, Scuderi G, Furman BD, Bhattacharyya S, Schmiegg JJ, Insall JN. Assessment of backside wear from the analysis of 55 retrieved tibial inserts. *Clin Orthop* 2002 (404): 75 - 82.
293. Ries MD, Guiney, W., Jr., and Lynch, F. Osteolysis associated with cemented total knee arthroplasty. A case report. *J Arthroplasty* 1994; 9 (5): 555 - 558.
294. Griffin FM, Scuderi GR, Gillis AM, Li S, Jimenez E, Smith T. Osteolysis associated with cemented total knee arthroplasty. *J Arthroplasty* 1998; 13 (5): 592 - 598.
295. Mikulak SA, Mahoney OM, dela Rosa MA, Schmalzried TP. Loosening and osteolysis with the press-fit condylar posterior-cruciate-substituting total knee replacement. *J Bone Joint Surg Am* 2001; 83-A (3): 398 - 403.
296. Rasquinha VJ, Ranawat CS, Cervieri CL, Rodriguez JA. The press-fit condylar modular total knee system with a posterior cruciate-substituting design. A concise follow-up of a previous report. *J Bone Joint Surg Am* 2006; 88 (5): 1006 - 1010.
297. Robinson EJ, Mulliken, B. D., Bourne, R. B., Rorabeck, C. H., Alvarez, C. Catastrophic osteolysis in total knee replacement. A report of 17 cases. *Clin Orthop* 1995(321):98-105.
298. Parks NL, Engh GA, Topoleski LD, Emperado J. The Coventry Award. Modular tibial insert micromotion. A concern with contemporary knee implants. *Clin Orthop* 1998 (356): 10 - 15.
299. Engh GA, Lounici S, Rao AR, Collier MB. In vivo deterioration of tibial baseplate locking mechanisms in contemporary modular total knee components. *J Bone Joint Surg Am* 2001; 83-A (11): 1660 - 1665.
300. Rao AR, Engh GA, Collier MB, Lounici S. Tibial interface wear in retrieved total knee components and correlations with modular insert motion. *J Bone Joint Surg Am* 2002; 84-A (10): 1849 - 1855.
301. Akisue T, Yamaguchi M, Bauer TW, Takikawa S, Schils JP, Yoshiya S, Kurosaka M. "Backside" polyethylene deformation in total knee arthroplasty. *J Arthroplasty* 2003;18(6): 784 - 791.

302. Conditt MA, Stein JA, Noble PC. Factors affecting the severity of backside wear of modular tibial inserts. *J Bone Joint Surg Am* 2004;86-A(2):305-11.
303. Conditt MA, Thompson MT, Usrey MM, Ismaily SK, Noble PC. Backside wear of polyethylene tibial inserts: mechanism and magnitude of material loss. *J Bone Joint Surg Am* 2005; 87-A (2): 326-331.
304. Engh GA. What is the Clinical Scope of Implant Wear in the Knee and How has it Changed Since 1995? In Wright T. M., Goodman S. B. (eds). *Implant Wear in Total Joint Replacement*. Rosemont, IL, American Academy of Orthopaedic Surgeons 2001: 8 - 12.
305. Wright TM. Diminishing Backside Wear. *Proceedings of The Knee Society and The American Association of Hip and Knee Surgeons 2004; Combined Specialty Day Meeting, San Francisco, CA.*
306. Kim YH, Oh JH, Oh SH. Osteolysis around cementless porous-coated anatomic knee prostheses. *J Bone Joint Surg Br* 1995; 77 (2): 236 - 241.
307. Burnett RS, Haydon CM, Rorabeck CH, Bourne RB. Patella resurfacing versus non-resurfacing in total knee arthroplasty: results of a randomized controlled clinical trial at a minimum of 10 years' followup. *Clin Orthop Relat Res* 2004 (428): 12 - 25.
308. Larson CM, McDowell CM, Lachiewicz PF. One-peg versus three-peg patella component fixation in total knee arthroplasty. *Clin Orthop Relat Res* 2001(392):94-100.
309. Sumner DR, Galante JO. Determinants of stress shielding: design versus materials versus interface. *Clin Orthop Relat Res* 1992 (274): 202 - 212.
310. Van Lenthe GH, de Waal Malefijt MC, Huiskes R. Stress shielding after total knee replacement may cause bone resorption in the distal femur. *J Bone Joint Surg Br* 1997; 79 (1): 117 - 122.
311. Willert HG, Bertram H, Buchhorn GH. Osteolysis in alloarthroplasty of the hip. The role of bone cement fragmentation. *Clin Orthop Relat Res* 1990 (258): 108 - 121.

312. Willert HG, Bertram H, Buchhorn GH. Osteolysis in alloarthroplasty of the hip. The role of ultra-high molecular weight polyethylene wear particles. *Clin Orthop Relat Res* 1990 (258): 95 - 107.
313. Harris WH. The problem is osteolysis. *Clin Orthop* 1995 (311): 46 - 53.
314. Aspenberg P. Wear and osteolysis in total joint replacements. *Acta Orthop Scand* 1998; 69 (4): 435 - 436.
315. Jones LC, Hungerford DS. Cement disease. *Clin Orthop Relat Res* 1987 (225): 192 - 206.
316. Lombardi AV, Jr., Mallory TH, Vaughn BK, Drouillard P. Aseptic loosening in total hip arthroplasty secondary to osteolysis induced by wear debris from titanium-alloy modular femoral heads. *J Bone Joint Surg Am* 1989; 71 (9): 1337 - 1342.
317. Nasser S, Campbell, P. A., Kilgus, D., Kossovsky, N., Amstutz, H. C. Cementless total joint arthroplasty prostheses with titanium-alloy articular surfaces. A human retrieval analysis. *Clin Orthop* 1990 (261): 171 - 185.
318. Green TR, Fisher J, Stone M, Wroblewski BM, Ingham E. Polyethylene particles of a 'critical size' are necessary for the induction of cytokines by macrophages in vitro. *Biomaterials* 1998; 19 (24): 2297 - 2302.
319. Matthews JB, Besong AA, Green TR, Stone MH, Wroblewski BM, Fisher J, Ingham E. Evaluation of the response of primary human peripheral blood mononuclear phagocytes to challenge with in vitro generated clinically relevant UHMWPE particles of known size and dose. *J Biomed Mater Res* 2000; 52 (2): 296 - 307.
320. Ingham E, Fisher, J. Biological reactions to wear debris in total joint replacement. *Proc Inst Mech Eng J Eng Med* 2000; 214 (1): 21 - 37.
321. Childs LM, Goater JJ, O'Keefe RJ, Schwarz EM. Efficacy of etanercept for wear debris-induced osteolysis. *J Bone Miner Res* 2001; 16 (2): 338 - 347.

322. Boyce BF, Li P, Yao Z, Zhang Q, Badell IR, Schwarz EM, O'Keefe RJ, Xing L. TNF-alpha and pathologic bone resorption. *Keio J Med* 2005; 54 (3): 127 - 131.
323. Schwarz EM, Lu AP, Goater JJ, Benz EB, Kollias G, Rosier RN, Puzas JE, O'Keefe RJ. Tumor necrosis factor-alpha/nuclear transcription factor-kappaB signaling in periprosthetic osteolysis. *J Orthop Res* 2000; 18 (3): 472 - 480.
324. Goater JJ, O'Keefe RJ, Rosier RN, Puzas JE, Schwarz EM. Efficacy of ex vivo OPG gene therapy in preventing wear debris induced osteolysis. *J Orthop Res* 2002; 20 (2): 169 - 173.
325. Ulrich-Vinther M, Carmody EE, Goater JJ, K Sb, O'Keefe RJ, Schwarz EM. Recombinant adeno-associated virus-mediated osteoprotegerin gene therapy inhibits wear debris-induced osteolysis. *J Bone Joint Surg Am* 2002 ;84-A (8): 1405 - 1412.
326. Schmalzried TP, Jasty M, Rosenberg A, Harris WH. Polyethylene wear debris and tissue reactions in knee as compared to hip replacement prostheses. *J Appl Biomater* 1994; 5 (3): 185 - 190.
327. Green TR, Fisher J, Matthews JB, Stone MH, Ingham E. Effect of size and dose on bone resorption activity of macrophages by in vitro clinically relevant ultra high molecular weight polyethylene particles. *J Biomed Mater Res* 2000; 53 (5): 490 - 497.
328. Tipper JL, Galvin AL, Williams S, McEwen HM, Stone MH, Ingham E, Fisher J. Isolation and characterization of UHMWPE wear particles down to ten nanometers in size from in vitro hip and knee joint simulators. *J Biomed Mater Res A* 2006; 78 (3): 473 - 480.
329. Firkins PJ, Tipper JL, Ingham E, Stone MH, Farrar R, Fisher J. A novel low wearing differential hardness, ceramic-on-metal hip joint prosthesis. *J Biomech* 2001; 34 (10): 1291 - 1298.
330. Campbell PA, Wang M, Amstutz HC, Goodman SB. Positive cytokine production in failed metal-on-metal total hip replacements. *Acta Orthop Scand* 2002; 73 (5): 506 - 512.
331. Brown C, Fisher J, Ingham E. Biological effects of clinically relevant wear particles from metal-on-metal hip prostheses. *Proc Inst Mech Eng [H]* 2006; 220 (2): 355 - 369.

332. Ingram JH, Kowalski R, Fisher J, Ingham E. The osteolytic response of macrophages to challenge with particles of Simplex P, Endurance, Palacos R, and Vertebroplastic bone cement particles in vitro. *J Biomed Mater Res B Appl Biomater* 2005; 75 (1): 210 - 220.
333. Skoglund B, Aspenberg P. PMMA particles and pressure--a study of the osteolytic properties of two agents proposed to cause prosthetic loosening. *J Orthop Res* 2003; 21(2): 196 - 201.
334. Endo MM, Barbour PS, Barton DC, Fisher J, Tipper JL, Ingham E, Stone MH. Comparative wear and wear debris under three different counterface conditions of crosslinked and non-crosslinked ultra high molecular weight polyethylene. *Biomed Mater Eng* 2001; 11 (1): 23 - 35.
335. Endo M, Tipper JL, Barton DC, Stone MH, Ingham E, Fisher J. Comparison of wear, wear debris and functional biological activity of moderately crosslinked and non-crosslinked polyethylenes in hip prostheses. *Proc Inst Mech Eng [H]* 2002; 216 (2): 111 - 122.
336. Beaulé PE, Campbell PA, Walker PS, Schmalzried TP, Dorey FJ, Blunn GW, Bell CJ, Yahia L, Amstutz HC. Polyethylene wear characteristics in vivo and in a knee stimulator. *J Biomed Mater Res* 2002; 60 (3): 411 - 419.
337. Howling GI, Barnett, P. I., Tipper, J. L., Stone, M. H., Fisher, J., Ingham, E. Quantitative characterization of polyethylene debris isolated from periprosthetic tissue in early failure knee implants and early and late failure Charnley hip implants. *J Biomed Mater Res* 2001; 58 (4): 415 - 420.
338. Sanzen L, Sahlstrom A, Gentz CF, Johnell IR. Radiographic wear assessment in a total knee prosthesis. 5- to 9-year follow-up study of 158 knees. *J Arthroplasty* 1996; 11 (6): 738 - 742.
339. Gill HS, Waite JC, Short A, Kellett CF, Price AJ, Murray DW. In vivo measurement of volumetric wear of a total knee replacement. *Knee* 2006; 13 (4): 312 - 317.
340. Valstar ER, Gill R, Ryd L, Flivik G, Borlin N, Karrholm J. Guidelines for standardization of radiostereometry (RSA) of implants. *Acta Orthop* 2005; 76 (4): 563 - 572.

341. Wasielewski RC, Galante JO, Leighty RM, Natarajan RN, Rosenberg AG. Wear patterns on retrieved polyethylene tibial inserts and their relationship to technical considerations during total knee arthroplasty. *Clin Orthop* 1994 (299): 31 - 43.
342. Wasielewski RC, Parks N, Williams I, Surprenant H, Collier JP, Engh G. Tibial insert undersurface as a contributing source of polyethylene wear debris. *Clin Orthop* 1997 (345): 53 - 59.
343. Cornwall GB, Bryant, J. T., Hansson, C. M., Rudan, J., Kennedy, L. A., Cooke, T. D. A quantitative technique for reporting surface degradation patterns of UHMWPE components of retrieved total knee replacements. *J Appl Biomater* 1995; 6 (1): 9 - 18.
344. Grochowsky JC, Alaways LW, Siskey R, Most E, Kurtz SM. Digital photogrammetry for quantitative wear analysis of retrieved TKA components. *J Biomed Mater Res B Appl Biomater* 2006; 79 (2): 263 - 267.
345. Feng EL, Stulberg SD, Wixson RL. Progressive subluxation and polyethylene wear in total knee replacements with flat articular surfaces. *Clin Orthop Relat Res* 1994 (299): 60 - 71.
346. Laskin RS, Beksac B. Stiffness after total knee arthroplasty. *J Arthroplasty* 2004; 19 (4 Suppl 1): 41 - 46.
347. Colizza WA, Insall JN, Scuderi GR. The posterior stabilized total knee prosthesis. Assessment of polyethylene damage and osteolysis after a ten-year-minimum follow-up. *J Bone Joint Surg Am* 1995; 77 (11): 1713 - 1720.
348. Lee SY, Matsui N, Kurosaka M, Komistek RD, Mahfouz M, Dennis DA, Yoshiya S. A posterior-stabilized total knee arthroplasty shows condylar lift-off during deep knee bends. *Clin Orthop Relat Res* 2005 (435): 181 - 184.
349. Dennis DA, Komistek RD, Walker SA, Cheal EJ, Stiehl JB. Femoral condylar lift-off in vivo in total knee arthroplasty. *J Bone Joint Surg Br* 2001; 83 (1): 33 - 39.
350. Komistek RD, Scott RD, Dennis DA, Yaszg D, Anderson DT, Hajner ME. In vivo comparison of femorotibial contact positions for press-fit posterior stabilized and posterior cruciate-retaining total knee arthroplasties. *J Arthroplasty* 2002; 17 (2): 209 - 216.

351. Minoda Y, Kobayashi A, Iwaki H, Miyaguchi M, Kadoya Y, Ohashi H, Yamano Y, Takaoka K. Polyethylene wear particles in synovial fluid after total knee arthroplasty. *Clin Orthop Relat Res* 2003 (410): 165 - 172.
352. Morgan H, Battista V, Leopold SS. Constraint in primary total knee arthroplasty. *J Am Acad Orthop Surg* 2005; 13 (8): 515 - 524.
353. Clark CR, Rorabeck CH, MacDonald S, MacDonald D, Swafford J, Cleland D. Posterior-stabilized and cruciate-retaining total knee replacement: a randomized study. *Clin Orthop Relat Res* 2001 (392): 208 - 212.
354. Tanzer M, Smith K, Burnett S. Posterior-stabilized versus cruciate-retaining total knee arthroplasty: balancing the gap. *J Arthroplasty* 2002; 17 (7): 813 - 819.
355. Kaper BP, Smith PN, Bourne RB, Rorabeck CH, Robertson D. Medium-term results of a mobile bearing total knee replacement. *Clin Orthop* 1999 (367): 201 - 209.
356. Callaghan JJ, Insall JN, Greenwald AS, Dennis DA, Komistek RD, Murray DW, Bourne RB, Rorabeck CH, Dorr LD. Mobile-bearing knee replacement: concepts and results. *Instr Course Lect* 2001; 50: 431 - 449.
357. Bourne RB, Masonis J, Anthony M. An analysis of rotating-platform total knee replacements. *Clin Orthop Relat Res* 2003 (410): 173 - 180.
358. Bourne RB, Masonis, J., Anthony, M. An analysis of rotating-platform total knee replacements. *Clin Orthop* 2003 (410): 173 - 180.
359. Bartel DL, Rawlinson, J. J., Burstein, A. H., R, C. S., Flynn, W. F., Jr. Stresses in polyethylene components of contemporary total knee replacements. *Clin Orthop* 1995 (317): 76 - 82.
360. Bartel DL, Bicknell VL, Wright TM. The effect of conformity, thickness, and material on stresses in ultra-high molecular weight components for total joint replacement. *J Bone Joint Surg Am* 1986; 68 (7): 1041 - 1051.

361. Bartel DL, Burstein AH, Toda MD, Edwards DL. The effect of conformity and plastic thickness on contact stresses in metal-backed plastic implants. *J Biomech Eng* 1985; 107 (3): 193 - 199.
362. Muratoglu OK, Burroughs BR, Bragdon CR, Christensen S, Lozynsky A, Harris WH. Knee simulator wear of polyethylene tibias articulating against explanted rough femoral components. *Clin Orthop Relat Res* 2004 (428): 108 -113.
363. Que L, Topoleski LD, Parks NL. Surface roughness of retrieved CoCrMo alloy femoral components from PCA artificial total knee joints. *J Biomed Mater Res* 2000; 53 (1): 111 - 118.
364. Caravia L, Dowson D, Fisher J, Jobbins B. The influence of bone and bone cement debris on counterface roughness in sliding wear tests of ultra-high molecular weight polyethylene on stainless steel. *Proc Inst Mech Eng [H]* 1990; 204 (1): 65 - 70.
365. Raab GE, Jobe CM, Williams PA, Dai QG. Damage to cobalt-chromium surfaces during arthroscopy of total knee replacements. *J Bone Joint Surg Am* 2001; 83-A (1): 46 - 52.
366. Ezzet KA, Hermida JC, Colwell CW, Jr., D'Lima DD. Oxidized zirconium femoral components reduce polyethylene wear in a knee wear simulator. *Clin Orthop Relat Res* 2004 (428): 120 - 124.
367. Spector BM, Ries, M. D., Bourne, R. B., Sauer, W. S., Long, M., Hunter, G. Wear performance of ultra-high molecular weight polyethylene on oxidized zirconium total knee femoral components. *J Bone Joint Surg Am* 2001; 83-A Suppl 2 Pt 2: 80 - 86.
368. Hallab N, Merritt K, Jacobs JJ. Metal sensitivity in patients with orthopaedic implants. *J Bone Joint Surg Am* 2001; 83-A (3): 428 - 436.
369. Laskin RS. An oxidized Zr ceramic surfaced femoral component for total knee arthroplasty. *Clin Orthop Relat Res* 2003 (416): 191 - 196.
370. Akagi M, Nakamura T, Matsusue Y, Ueo T, Nishijyo K, Ohnishi E. The Bisurface total knee replacement: a unique design for flexion. Four-to-nine-year follow-up study. *J Bone Joint Surg Am* 2000; 82-A (11): 1626 - 1633.

371. Koshino T, Okamoto, R. Takagi, T. Yamamoto, K. Saito, T. Cemented ceramic YMCK total knee arthroplasty in patients with severe rheumatoid arthritis. *J Arthroplasty* 2002; 17 (8): 1009 - 1015.
372. Mochida Y, Bauer TW, Koshino T, Hirakawa K, Saito T. Histologic and quantitative wear particle analyses of tissue around cementless ceramic total knee prostheses. *J Arthroplasty* 2002; 17 (1): 121 - 128.
373. Hewes GW. The anthropology of posture. *Scientific American* 1957; 196: 122 - 132.
374. McLeod PC, Kettelkamp DB, Srinivasan V, Henderson OL. Measurements of repetitive activities of the knee. *J Biomech* 1975; 8 (6): 369 - 373.
375. Seedhom BB, Wallbridge NC. Walking activities and wear of prostheses. *Ann Rheum Dis* 1985; 44 (12): 838 - 843.
376. Morlock M, Schneider E, Bluhm A, Vollmer M, Bergmann G, Muller V, Honl M. Duration and frequency of every day activities in total hip patients. *J Biomech* 2001; 34 (7): 873 - 881.
377. Schmalzried TP, Shepherd EF, Dorey FJ, Jackson WO, dela Rosa M, Fa'vae F, McKellop HA, McClung CD, Martell J, Moreland JR and others. The John Charnley Award. Wear is a function of use, not time. *Clin Orthop* 2000 (381): 36 - 46.
378. Weiss JM, Noble PC, Conditt MA, Kohl HW, Roberts S, Cook KF, Gordon MJ, Mathis KB. What functional activities are important to patients with knee replacements? *Clin Orthop* 2002 (404): 172 - 88.
379. Healy WL, Iorio R, Lemos MJ. Athletic activity after joint replacement. *Am J Sports Med* 2001; 29 (3): 377 - 388.
380. Kuster MS, Spalinger E, Blanksby BA, Gachter A. Endurance sports after total knee replacement: a biomechanical investigation. *Med Sci Sports Exerc* 2000; 32 (4): 721 - 724.
381. Gschwend N, Frei T, Morscher E, Nigg B, Loehr J. Alpine and cross-country skiing after total hip replacement: 2 cohorts of 50 patients each, one active, the other inactive in skiing, followed for 5-10 years. *Acta Orthop Scand* 2000; 71 (3): 243 - 249.

382. Mulholland SJ, Wyss UP. Activities of daily living in non-Western cultures: range of motion requirements for hip and knee joint implants. *Int J Rehabil Res* 2001; 24 (3): 191- 198.
383. Silva M, Shepherd, E. F., Jackson, W. O., Dorey, F. J., Schmalzried, T. P. Average patient walking activity approaches 2 million cycles per year: pedometers under-record walking activity. *J Arthroplasty* 2002; 17 (6): 693 - 697.
384. Cram P, Rosenthal GE, Vaughan-Sarrazin MS, Wolf B, Katz JN. A comparison of total hip and knee replacement in specialty and general hospitals. *J Bone Joint Surg Am* 2007; 89 (8): 1675 - 1684.
385. Katz JN, Mahomed NN, Baron JA, Barrett JA, Fossel AH, Creel AH, Wright J, Wright EA, Losina E. Association of hospital and surgeon procedure volume with patient-centered outcomes of total knee replacement in a population-based cohort of patients age 65 years and older. *Arthritis Rheum* 2007; 56 (2): 568 - 574.
386. Solomon DH, Chibnik LB, Losina E, Huang J, Fossel AH, Husni E, Katz JN. Development of a preliminary index that predicts adverse events after total knee replacement. *Arthritis Rheum* 2006; 54 (5): 1536 - 1542.
387. Katz JN, Barrett J, Mahomed NN, Baron JA, Wright RJ, Losina E. Association between hospital and surgeon procedure volume and the outcomes of total knee replacement. *J Bone Joint Surg Am* 2004; 86-A(9): 1909 - 1916.
388. Mitsuyasu S, Hagihara A, Horiguchi H, Nobutomo K. Relationship between total arthroplasty case volume and patient outcome in an acute care payment system in Japan. *J Arthroplasty* 2006; 21 (5): 656 - 663.
389. Lavernia CJ, Guzman JF. Relationship of surgical volume to short-term mortality, morbidity, and hospital charges in arthroplasty. *J Arthroplasty* 1995; 10 (2): 133 - 140.
390. Luring C, Bathis H, Tingart M, Perlick L, Grifka J. Computer assistance in total knee replacement - a critical assessment of current health care technology. *Comput Aided Surg* 2006; 11 (2): 77 -80.
391. International Orthopaedics On-line Database. www.ortech-dc.com, info@ortech-dc.com.

392. Sychterz CJ, Engh CA, Jr., Yang A, Engh CA. Analysis of temporal wear patterns of porous-coated acetabular components: distinguishing between true wear and so-called bedding-in. *J Bone Joint Surg Am* 1999; 81 (6): 821 - 830.
393. Isaac GH, Dowson D, Wroblewski BM. An investigation into the origins of time-dependent variation in penetration rates with Charnley acetabular cups--wear, creep or degradation? *Proc Inst Mech Eng J Eng Med* 1996; 210 (3): 209 -216.
394. Ernst E. Chelation Therapy for Peripheral Arterial Occlusive Disease : A Systematic Review. *Circulation* 1997; 96 (3): 1031 - 1033.
395. AMTI Six Station Knee Simulator Manual. AMTI (Waltham, MA) www.amtiweb.com.
396. Morrison JB. Function of the knee joint in various activities. *Biomed Eng* 1969; 4 (12): 573 - 580.
397. Collier MB, Engh CA, Jr., Mcauley JP, Ginn SD, Engh GA. Osteolysis After Total Knee Arthroplasty: Influence of Tibial Baseplate Surface Finish and Sterilization of Polyethylene Insert. Findings at Five to Ten Years Postoperatively. *J Bone Joint Surg Am* 2005; 87 (12): 2702 - 2708.
398. Streyer L. *Biochemistry*. 1995(Fourth Edition).
399. Sebia HYDRAGEL beta1-beta2.
400. Yuh-Fun Maa CCH. Effect of high shear on proteins. *Biotechnology and Bioengineering* 1996; 51 (4): 458 - 465.
401. Crawford AS, Schuchard MD, Megigh RJ, kappel WK, Scott GBI. Proteolytic Activity Quantification and protease Inhibition in Human Serum and Plasma Samples for Proteomic Analysis. *Proc Am Soc Biochem Mol Bio* 2005: D78.
402. More JJ. Levenberg--Marquardt algorithm: implementation and theory. 1977; United States. p Pages: 13.
403. Chemistry Information Sheet A18471, Beckman Coulter, Fullerton, CA, October 2005.

404. Chemistry Information Sheet A18491, Beckman Coulter, Fullerton, CA, September 2005.
405. Chemistry Information Sheet A18526, Beckman Coulter, Fullerton, CA, September 2005.
406. Chemistry Information Sheet A18545, Beckman Coulter, Fullerton, CA, August 2005.
407. Anderson EH. Growth Requirements of Virus-Resistant Mutants of Escherichia Coli Strain "B". Proc Natl Acad Sci U S A 1946;32(5):120-8.
408. Bertani G. Studies on lysogenesis. I. The mode of phage liberation by lysogenic Escherichia coli. J Bacteriol 1951; 62 (3): 293 - 300.
409. DIN-4768. Determination of values of surface roughness parameters R_a , R_z , R_{max} using electrical contact (stylus) instruments: concepts and measuring conditions. Beuth Verlag, Berlin, Germany 1990.
410. Bland JM, Altman DG. Multiple significance tests: the Bonferroni method. Bmj 1995; 310 (6973): 170.
411. Jasty M, Goetz DD, Bragdon CR, Lee KR, Hanson AE, Elder JR, Harris WH. Wear of polyethylene acetabular components in total hip arthroplasty. An analysis of one hundred and twenty-eight components retrieved at autopsy or revision operations. J Bone Joint Surg Am 1997; 79 (3): 349 - 358.
412. Sychterz CJ, Orishimo KF, Engh CA. Sterilization and polyethylene wear: clinical studies to support laboratory data. J Bone Joint Surg Am 2004; 86-A (5): 1017 - 1022.
413. Kleinbaum DG, Kupper, L.L., Muller, K.E., Nizam A. Applied Regression Analysis and Multivariable Methods. 1998(Duxbury Press, 3rd Edition): 111 - 279.
414. Brandt JM, Medley JB, Haydon CM, McCalden RW, MacDonald SJ, Bourne RB, Rorabeck CH. Retrieval Analysis in Total Joint Replacement: Does the Grading Method Matter? 5th Combined ORS Meeting, Banff, Alberta, Canada, 2004:243.

415. Cuckler JM, Lemons, J., Tamarapalli, J.R., Beck, P. Polyethylene Damage on the Nonarticular Surface of Modular Total Knee Prostheses. *Clin Orthop* 2003; 410: 248 - 253.
416. Schmalzried TP, Szuszczewicz ES, Northfield MR, Akizuki KH, Frankel RE, Belcher G, Amstutz HC. Quantitative assessment of walking activity after total hip or knee replacement. *J Bone Joint Surg Am* 1998; 80 (1): 54 - 59.
417. Silva M, Kabbash CA, Tiberi JV, 3rd, Park SH, Reilly DT, Mahoney OM, Schmalzried TP. Surface damage on open box posterior-stabilized polyethylene tibial inserts. *Clin Orthop* 2003 (416): 135 - 144.
418. Chang DC, Goh JC, Teoh SH, Bose K. Cold extrusion deformation of UHMWPE in total knee replacement prostheses. *Biomaterials* 1995;16 (3): 219 - 223.
419. Wasielewski RC. The causes of insert backside wear in total knee arthroplasty. *Clin Orthop* 2002(404):232 - 246.
420. Jones DL, Cauley JA, Kriska AM, Wisniewski SR, Irrgang JJ, Heck DA, Kwok CK, Crossett LS. Physical activity and risk of revision total knee arthroplasty in individuals with knee osteoarthritis: a matched case-control study. *J Rheumatol* 2004; 31 (7): 1384 - 1390.
421. McKellop HA, Campbell P, Park SH, Schmalzried TP, Grigoris P, Amstutz HC, Sarmiento A. The origin of submicron polyethylene wear debris in total hip arthroplasty. *Clin Orthop* 1995 (311): 3 - 20.
422. Lawn BR, Hockey BJ, Wiederhorn SM. Atomically sharp cracks in brittle solids: an electron microscopy study. *Journal of Materials Science* 1980;15: 1207 -1223.
423. Zu JB, Burstein GT, Hutchings IM. A comparative study of the slurry erosion and free-fall particle erosion of aluminium. *Wear* 1991; 149 (1 - 2): 73 - 84.
424. Ricci JL, Kummer FJ, Alexander H, Casar RS. Technical Note: Embedded Particulate Contaminants in Textured Metal Implant Surfaces. *Journal of Biomedical Materials Research* 1992; 3: 225 - 230.
425. Muratoglu OK. 2002: personal communication.

426. Victor J, Crites B, Ritter M. The tibial component should routinely be modular and metal-backed rather than all polyethylene: Pro and Con. In Laskin, R.S. (ed.): *Controversies in Total Knee Replacement*. Oxford University Press 2001: 21 - 39.
427. Berend ME, Ritter MA. The pros and cons of modularity in total knee replacements. *J Bone Joint Surg Am* 2002; 84 - A (8): 1480 - 1; author reply 1481.
428. Ranawat AS, Mohanty SS, Goldsmith S, Rasquinha SVJ, Rodriguez JA, Ranawat CS. Experience with an All-Polyethylene TKR in Younger, Active Patients with Follow-Up from Two to Eleven Years. *J Arthroplasty* 2005; 20 (2): 266.
429. Klein J. Molecular mechanisms of synovial joint lubrication. *Proc. IMechE Part J: J. Engineering Tribology* 2006; 220: 691 - 710.
430. Keller RP, Neville MC. Determination of total protein in human milk: comparison of methods. *Clin Chem* 1986; 32 (1 Pt 1): 120 - 123.
431. Yao JQ, Laurent MP, Gilbertson LN, Blanchard CR, Crownshied RD, Jacobs JJ. A Comparison of Biological Lubricants to Bovine Calf Serum for Total Joint Wear Testing. *Trans Ortho Res Soc* 2003; 1004.
432. Rieker C, Schoen R, Liebentritt G, Gnepf P, Roberts P, Griporis P. In-Vitro tribology of Large Metal-on-Metal Implants - Influence of Clearance. *Trans Ortho Res Soc* 2004; 50: 123.
433. Crawford AS, Schuchard MD, Melm CD, Chapman HA, Wildsmith J, Ray KB, Mehig R, Chen DE, Scott GBI. Novel ProteoPrep 20 Immunoaffinity Depletion Resin for Human Plasma. *Sigma-Aldrich.com* 2006: 10 - 15.
434. Lu DR, Lee SJ, Park K. Calculation of solvation interaction energies for protein adsorption on polymer surfaces. *J Biomater Sci Polym Ed* 1991; 3 (2): 127 - 147.
435. Stradner A, Sedgwick H, Cardinaux F, Poon WCK, Egelhaaf SU, Schurtenberger P. Equilibrium cluster formation in concentrated protein solutions and colloids. *Nature* 2004; 432 (25): 492 - 495.

436. Allain C, Cloitre M, Wafra M. Aggregation and Sedimentation in Colloidal Suspensions. *Physical Review Letters* 1995; 74 (8): 1478-1481.
437. Lichstein HC, Soule MH. Studies of the Effect of Sodium Azide on Microbic Growth and Respiration. *Journal of Bacteriology* 1944: 221-230.
438. Driehuis F, Wouters JT. Effect of growth rate and cell shape on the peptidoglycan composition in *Escherichia coli*. *J. Bacteriol.* 1987; 169 (1): 97-101.
439. Passman FJ. Microbial Problems in Metalworking Fluids. *Journal of the Society of Tribologists and Lubrication Engineers* 1988; 5: 431 - 433.
440. Wang A, Polineni, V. K., Essner, A., Stark, C., Dumbleton, J. The impact of lubricant concentration on the outcome of hip joint simulator testing. *Trans Orthop Res Soc* 1999; 24.
441. Karuppiah KKS, Sundararajan S, Xu ZH, Li X. The effect of protein adsorption on the friction behavior of ultra-high molecular weight polyethylene. *Tribology Letters* 2006; 22 (2): 181 - 188.
442. Granick S, Kumar SK, Amis EJ, Antonietti M, Balazs AC, Chakraborty AK, Grest GS, Hawker C, Janmey P, Kramer EJ and others. Macromolecules at surfaces: Research challenges and opportunities from tribology to biology. *Journal of Polymer Science Part B-Polymer Physics* 2003; 41: 2755 - 2793.
443. Graham T. On the Absorption and Dialytic Separation of Gases by Colloid Septa. *Philosophical transactions of the Royal Society of London* 1866;156 : 399 - 439.
444. Ostwald W. Einige Bemerkungen zur Systematik der Kolloide. *Colloid & Polymer Science* 1908; 3 (1): 28- 30.
445. Shen M, Norris J, Rieker C. Serum Effect on Wear of UHMWPE Tibial Insert in Knee Simulator Testing. *Trans Soc Biomat* 2003; 29: 41.

446. Paterson DL. Resistance in Gram-negative bacteria: Enterobacteriaceae. *Am J Infect Control* 2006; 34(5 Suppl 1): S20 - S28; discussion S64-73.
447. Swann DA, Radin EL, Nazimiec M, Weisser PA, Curran N, Lewinnek G. Role of hyaluronic acid in joint lubrication. *Ann Rheum Dis* 1974; 33 (4): 318 - 326.
448. Yamada H, Morita, M., Henmi, O., Miyauchi, S., Yoshida, Y., Kikuchi, T., Terada, N., Washimi, O., Washimi, Y., Seki, T. Hyaluronan in synovial fluid of patients with loose total hip prosthesis. Comparison with hyaluronan in patients with hip osteoarthritis and idiopathic osteonecrosis of femoral head. *Arch Orthop Trauma Surg* 2000; 120 (9): 521 - 524.
449. Delecrin J, Oka, M., Takahashi, S., Yamamuro, T., Nakamura, T. Changes in joint fluid after total arthroplasty. A quantitative study on the rabbit knee joint. *Clin Orthop* 1994 (307): 240 - 249.
450. Michnik A, Michalik K, Kluczewska A, Drzazga Z. Comparative DSC study of human and bovine serum albumin. *Journal of Thermal Analysis and Calorimetry* 2006; 84 (1).
451. Mannesmann M. Manufacture of Seamless Tubes. U.S. patent 361,954, 1887.
452. Gogos CC, Tadmor Z, Kim MH. Melting phenomena and mechanisms in polymer processing equipment. *Advances in Polymer Technology* 1998; 17 (4): 285 - 305.
453. McLeod PC, Kettelkamp, D. B., Srinivasan, V., Henderson, O. L. Measurements of repetitive activities of the knee. *J Biomech* 1975; 8 (6): 369 - 373.
454. Benson LC, DesJardins, J. D., Harman, M. K. and LaBerge, M. Effect of stair descent loading on ultra-high molecular weight polyethylene wear in a force-controlled knee simulator. *Proc Inst Mech Eng J Eng Med* 2002; 216 (6): 409 - 418.
455. Paauw A, Verhoef J, Fluit AC, Blok HE, Hopmans TE, Troelstra A, Leverstein-van Hall MA. Failure to control an outbreak of qnrA1-positive multidrug-resistant *Enterobacter cloacae* infection despite adequate implementation of recommended infection control measures. *J Clin Microbiol* 2007; 45 (5): 1420 - 1425.

456. Kim SH, Wei CI. Expression of AmpC beta-lactamase in *Enterobacter cloacae* isolated from retail ground beef, cattle farm and processing facilities. *J Appl Microbiol* 2007; 103 (2): 400 - 408.
457. Gallo S, Chevalier J, Mahamoud A, Eyraud A, Pages J-M, Barbe J. 4-alkoxy and 4-thioalkoxyquinoline derivatives as chemosensitizers for the chloramphenicol-resistant clinical *Enterobacter aerogenes* 27 strain. *International Journal of Antimicrobial Agents* 2003; 22 (3): 270 - 273.
458. George AM. Multidrug resistance in enteric and other Gram-negative bacteria. *FEMS Microbiol Lett* 1996; 139 (1): 1 - 10.
459. Chang S, Lamm SH. Human Health Effects of Sodium Azide Exposure: A Literature Review and Analysis. *International Journal of Toxicology* 2003; 22 (3): 175 - 186.
460. Brown EM, Nathwani D. Antibiotic cycling or rotation: a systematic review of the evidence of efficacy. *J Antimicrob Chemother* 2005; 55 (1): 6 - 9.
461. Flannagan RS, Valvano MA, Koval SF. Downregulation of the *motA* gene delays the escape of the obligate predator *Bdellovibrio bacteriovorus* 109J from bdelloplasts of bacterial prey cells. *Microbiology* 2004; 150 (Pt 3): 649 - 656.
462. Brandt J-M, Mahmoud KK, Charron KD, Zhao L, MacDonald SJ, Koval S, Medley JB. Bacterial Growth in Implant Wear Testing - Can a Predator Bacterium be used to Create a Sterile Environment? Proceedings of the 26th Annual Canadian Biomaterials Society Meeting, London, ON, May 25-27th, 2007.
463. Lu Z, McKellop, H. Frictional heating of bearing materials tested in a hip joint wear simulator. *Proc Inst Mech Eng [H]* 1997; 211 (1): 101 - 108.
464. Lu Z, McKellop, H., Liao, P., Benya, P. Potential thermal artifacts in hip joint wear simulators. *J Biomed Mater Res* 1999; 48 (4): 458 - 464.
465. Chen N, Maeda N, Tirrell M, Israelachvili J. Adhesion and Friction of Polymer Surfaces: The Effect of Chain Ends. *Macromolecules* 2005; 38 (8): 3491 - 3503.

Appendices

Appendix A: BDS following the Hood-method

The backside damage on the retrieved PE inserts was assessed by two observers. The author of this thesis was referred to as “Observer 1” who trained the student (Christopher M. Haydon, HBSc) “Observer 2” in the damage assessment methods.

Observer 1

Case No.	BDS					
	Burnishing	Grooving	Indentation	Deformation	Pitting	Stippling
1	18.0	8.0	10.0	5.0	9.0	N/A
2	11.0	14.0	14.0	1.0	8.0	N/A
3	16.0	10.0	11.0	0	8.0	N/A
4	17.0	10.0	6.0	6.0	6.0	N/A
5	10.0	9.0	11.0	3.0	6.0	N/A
6	18.0	7.0	7.0	0	4.0	N/A
7	15.0	11.0	10.0	4.0	6.0	N/A
8	14.0	5.0	7.0	4.0	7.0	N/A
9	7.0	7.0	7.0	2.0	4.0	N/A
10	17.0	9.0	7.0	1.0	7.0	N/A
11	13.0	8.0	7.0	0	6.0	N/A
12	16.0	5.0	2.0	1.0	3.0	N/A
13	6.0	6.0	18.0	N/A	0	18.00
14	7.0	6.0	17.0	N/A	3.0	17.00
15	3.0	1.0	10.0	N/A	3.0	1.00
16	2.0	0	13.0	N/A	6.0	12.00
17	0	0	9.0	N/A	1.0	.00
18	1.0	0	5.0	N/A	1.0	.00
19	0	1.0	11.0	N/A	0	.00
20	8.0	2.0	12.0	N/A	1.0	.00
21	1.00	3.0	14.0	N/A	4.0	1.00

Observer 1 (continued)

Case No.	Backside Damage Score					
	Burnishing	Grooving	Indentation	Deformation	Pitting	Stippling
22	2.0	0	13.0	N/A	6.0	17.0
23	0	0	9.0	N/A	1.0	18.0
24	1.0	0	5.0	N/A	1.0	4.0
25	.00	1.0	11.0	N/A	0	0
26	8.0	2.0	12.0	N/A	1.0	18.0
27	1.0	3.0	14.0	N/A	4.0	0
28	4.0	0	18.0	N/A	2.0	3.0
29	8.0	0	14.0	N/A	0	N/A
30	0	0	18.0	N/A	0	N/A
31	0	2.0	12.0	N/A	0	N/A
32	10.0	0	18.0	N/A	0	N/A
33	0	0	18.0	N/A	0	N/A
34	1.0	1.0	17.0	N/A	4.0	N/A
35	5.0	1.0	2.0	0	0	N/A
36	10.0	4.0	1.0	0	1.0	N/A
37	8.0	2.0	6.0	2.0	6.0	N/A
38	6.0	0	0	0	0	N/A
39	6.0	5.0	9.0	4.0	3.0	N/A
40	6.0	6.0	5.0	6.0	1.0	N/A
41	8.0	5.0	2.0	3.0	5.0	N/A
42	6.0	3.0	14.0	1.0	2.0	N/A
43	6.0	6.0	4.0	0	0	N/A
44	6.0	2.0	7.0	2.0	1.0	N/A
45	14.0	5.0	9.0	0	2.0	N/A
46	5.0	6.0	8.0	0	0	N/A
47	7.0	6.0	6.0	0	2.0	N/A
48	13.0	4.0	1.0	0	0	N/A
49	5.0	2.0	1.0	0	0	N/A
50	4.0	6.0	11.0	0	2.0	N/A
51	5.0	0	6.0	0	0	N/A
52	6.0	1.0	1.0	2.00	1.0	N/A

Observer 2

Case No.	Damage Score					
	Burnishing	Grooving	Indentation	Deformation	Pitting	Stippling
1	16.0	15.0	6.0	4.0	14.0	N/A
2	16.0	12.0	13.0	2.0	11.0	N/A
3	18.0	11.0	10.0	1.0	7.0	N/A
4	17.0	9.0	6.0	6.0	7.0	N/A
5	11.0	8.0	11.0	2.0	6.0	N/A
6	16.0	6.0	6.0	2.0	7.0	N/A
7	14.0	9.0	4.0	0	6.0	N/A
8	12.0	5.0	8.0	5.0	6.0	N/A
9	2.0	6.0	3.0	2.0	5.0	N/A
10	17.0	4.0	15.0	0	5.0	N/A
11	11.0	7.0	9.0	0	6.0	N/A
12	15.0	7.0	2.0	1.0	3.0	N/A
13	6.0	6.0	18.0	N/A	0	18.0
14	6.0	4.0	17.0	N/A	2.0	18.0
15	3.0	1.0	9.0	N/A	2.0	0
16	2.0	2.0	14.0	N/A	11.0	4.00
17	0	0	9.0	N/A	2.0	0
18	0	1.0	6.0	N/A	1.0	0
19	0	2.0	12.0	N/A	0	0
20	8.0	2.0	12.0	N/A	1.0	0
21	0	3.0	14.0	N/A	3.0	2.0
22	4.0	0	18.0	N/A	2.0	18.0
23	10.0	0	15.0	N/A	0	18.0
24	0	0	18.0	N/A	0	0
25	0	10.0	2.0	N/A	0	0
26	8.0	0	18.0	N/A	0	18.0

Observer 2 (continued)

Case No.	Damage Score					
	Burnishing	Grooving	Indentation	Deformation	Pitting	Stippling
27	2.0	0	18.0	N/A	0	0
28	2.0	1.0	17.0	N/A	3.0	3.0
29	6.0	0	3.0	1.0	0	N/A
30	4.0	4.0	4.0	1.0	0	N/A
31	7.0	4.0	8.0	2.0	1.0	N/A
32	6.0	1.0	0	.00	0	N/A
33	4.0	6.0	7.0	2.0	3.0	N/A
34	6.0	7.0	5.0	1.0	3.0	N/A
35	7.0	7.0	2.0	2.0	7.0	N/A
36	6.0	4.0	15.0	0	2.0	N/A
37	4.0	6.0	6.0	0	0	N/A
38	6.0	4.0	7.0	2.0	1.0	N/A
39	9.0	5.0	7.0	0	2.0	N/A
40	4.0	6.0	8.0	0	4.0	N/A
41	2.0	8.0	6.0	2.0	3.0	N/A
42	7.0	4.0	13.0	0	1.0	N/A
43	4.0	0	3.0	1.0	0	N/A
44	5.0	7.0	10.0	0	3.0	N/A
45	3.0	1.0	6.0	0	0	N/A
46	6.0	0	2.0	1.0	2.0	N/A
47	6.0	5.0	6.0	0	3.0	N/A
48	5.0	0	8.0	0	0	N/A
49	6.0	5.0	7.0	0	0	N/A
50	3.0	0	2.0	0	0	N/A
51	8.0	2.0	8.0	0	2.0	N/A
52	8.0	7.0	7.0	1.0	1.0	N/A

Appendix B: BDS following the Modified-method

Observer 1

Case No.	Damage Score					
	Burnishing	Grooving	Indentation	Deformation	Pitting	Stippling
1	49.0	9.5	11.0	4.5	8.0	N/A
2	37.0	23.0	21.0	1.5	15.5	N/A
3	27.0	13.0	16.0	0	7.5	N/A
4	38.0	15.5	5.5	5.0	5.5	N/A
5	16.0	12.0	14.5	3.0	6.0	N/A
6	44.0	5.5	7.0	0	2.0	N/A
7	30.0	19.0	15.5	4.0	6.0	N/A
8	25.0	3.5	8.0	3.5	6.0	N/A
9	6.5	5.0	5.5	1.0	2.5	N/A
10	38.0	10.5	7.5	0.5	6.0	N/A
11	21.0	10.0	6.5	0	5.0	N/A
12	34.0	4.5	1.5	0.5	2.0	N/A
13	6.0	6.0	36.0	N/A	0	51.0
14	8.0	5.0	43.0	N/A	1.5	36.0
15	2.0	1.0	13.5	N/A	2.0	0
16	1.5	0	22.0	N/A	3.0	21.0
17	0	0	7.5	N/A	0.5	0
18	0.5	0	3.0	N/A	0.5	0
19	0	0.5	10.0	N/A	0	0
20	5.0	1.0	19.5	N/A	0.5	0
21	1.0	1.5	26.0	N/A	2.5	1.0
22	2.0	0	41.0	N/A	2.0	37.0
23	10.5	0	24.0	N/A	0	35.0
24	0	0	49.0	N/A	0	2.0
25	0	1.0	16.5	N/A	0	0
26	12.5	0	35.0	N/A	0	48.0

Observer 1 (continued)

Case No.	Damage Score					
	Burnishing	Grooving	Indentation	Deformation	Pitting	Stippling
27	0	0	56.5	N/A	0	0
28	1.0	1.0	46.0	N/A	2.0	3.0
29	2.5	0.5	1.0	0	0	N/A
30	3.5	2.5	3.5	0.5	0	N/A
31	8.5	2.0	4.5	1.50	5.5	N/A
32	3.5	0.5	0	0	0	N/A
33	4.5	3.5	8.0	3.0	2.5	N/A
34	4.0	5.0	4.0	4.0	0.5	N/A
35	6.5	2.5	1.0	3.5	3.0	N/A
36	3.5	3.5	26.5	0	1.5	N/A
37	3.5	5.5	3.0	0	0	N/A
38	3.0	2.0	7.0	1.0	1.0	N/A
39	19.5	4.0	9.5	0	1.5	N/A
40	2.0	3.5	10.5	0	2.0	N/A
41	1.0	8.0	6.0	1.0	1.5	N/A
42	7.5	4.0	20.5	0	0.5	N/A
43	2.5	1.0	0.5	0	0	N/A
44	3.5	4.00	12.5	0	1.5	N/A
45	2.5	0.5	4.0	0	0	N/A
46	6.0	1.0	0.5	1.0	0.5	N/A
47	19.0	2.5	0.5	0	0	N/A
48	5.0	0	9.0	0	0	N/A
49	4.0	4.5	7.0	0	0	N/A
50	1.5	0.5	1.0	0	0	N/A
51	10.0	2.0	8.5	0	1.5	N/A
52	11.5	5.0	6.0	0.5	0.5	N/A

Observer 2

Case No.	Damage Score					
	Burnishing	Grooving	Indentation	Deformation	Pitting	Stippling
1	41.0	30.0	5.5	2.5	27.50	N/A
2	37.0	23.0	21.0	1.5	15.50	N/A
3	47.0	14.5	12.0	0.5	4.00	N/A
4	42.0	12.0	6.0	5.0	6.00	N/A
5	12.5	9.0	16.0	1.0	4.00	N/A
6	35.5	2.5	3.5	0.5	5.50	N/A
7	26.5	10.0	2.5	0	5.50	N/A
8	20.5	3.5	8.5	5.0	3.50	N/A
9	3.0	3.5	1.5	1.5	2.50	N/A
10	37.5	4.0	31.5	0	4.50	N/A
11	15.5	7.5	12.0	0	4.00	N/A
12	32.5	8.5	2.0	0.5	1.50	N/A
13	6.0	6.0	45.0	N/A	0	54.0
14	6.0	4.0	34.0	N/A	2.0	47.0
15	2.5	0.5	11.5	N/A	1.0	0
16	1.0	2.0	21.5	N/A	21.5	2.0
17	0	0	10.5	N/A	1.5	0
18	0	1.0	6.0	N/A	0.5	0
19	0	2.0	16.0	N/A	0	0
20	3.0	0	24.0	N/A	0.5	0
21	0	1.5	27.0	N/A	2.5	2.0
22	4.0	0	42.0	N/A	2.0	54.0
23	13.0	0	32.0	N/A	0	54.0
24	0	0	54.0	N/A	0	1.0
25	0	1.5	11.5	N/A	0	0
26	8.0	0	42.0	N/A	0	49.0

Observer 2 (continued)

Case No.	Damage Score					
	Burnishing	Grooving	Indentation	Deformation	Pitting	Stippling
27	2.0	0	56.5	N/A	0	0
28	3.0	1.0	45.5	N/A	3.0	3.0
29	3.5	0	1.5	0.5	0	N/A
30	11.5	2.0	1.0	0	0	N/A
31	6.5	3.0	8.5	1.5	1.0	N/A
32	3.0	0.5	0	0	0	N/A
33	2.0	4.0	6.5	2.0	1.5	N/A
34	3.5	8.0	2.5	0.5	1.5	N/A
35	6.0	4.5	1.0	2.0	5.0	N/A
36	4.5	2.0	21.0	0.5	1.5	N/A
37	2.5	4.5	4.0	0	0	N/A
38	3.5	2.0	6.0	0.5	1.0	N/A
39	13.0	3.0	6.0	0	1.5	N/A
40	3.0	4.0	7.5	0	0.5	N/A
41	5.5	4.5	6.0	0	1.5	N/A
42	6.5	2.0	18.5	0	0	N/A
43	2.	0	1.5	0.5	0	N/A
44	4.0	6.5	12.0	0	2.0	N/A
45	3.0	0	3.0	0	0	N/A
46	3.5	0	1.0	0.5	1.0	N/A
47	7.5	4.0	20.5	0	0.5	N/A
48	5.0	1.0	2.0	0.5	0	N/A
49	4.0	3.5	4.5	0	0	N/A
50	1.5	0	1.0	0	0	N/A
51	12.5	2.5	4.0	0.5	0.5	N/A
52	8.5	4.5	4.0	1.0	3.0	N/A

Appendix C: Statistical Analyses

Tests for Normality

The distribution of the data population can be assessed by evaluating histograms and by applying the Kolmogorov-Smirnov test. The latter test is used to decide if a sample comes from a population with a specific distribution and this is indicated by the obtained p-value.

Correlation Analysis

Correlation is a common measure of the relation between two variables. The Pearson correlation assumes that the data is normal distributed (parametric data). The Spearman correlation assesses how well an arbitrary monotonic function could describe the relationship between two variables, without making any assumptions about the frequency distribution of the variables (non-parametric data). When measured in a population the correlations are designated by the letter R. The correlation coefficient reflects the degree of linear relationship between two variables. It ranges from + 1 to - 1. A correlation of + 1 means that there is a perfect positive linear relationship between variables. A correlation of - 1 means that there is a perfect negative linear relationship between variables. A correlation of 0 means there is no linear relationship between the two variables. Correlations are rarely if ever 0, 1, or - 1.

Regression Analysis

Regression analysis can be used as a descriptive method of data analysis (such as linear or logarithmic curve fitting) without relying on any assumptions about underlying processes generating the data. The key relationship in a regression is the regression equation. A regression equation contains regression parameters whose values are estimated using the data. The estimated parameters measure the relationship between the dependent variable and each of the independent variables. When a regression model is used, the

dependent variable is modeled as a random variable because of either uncertainty as to its value or inherent variability. The data are assumed to be sample from a probability distribution, which is usually assumed to be a normal distribution.

Paired Samples Analysis

The paired samples t-test is used on parametric data to test the null hypothesis that the average of the differences between a series of paired observations is zero. Observations are paired when, for example, they are performed on the same samples or subjects. The Wilcoxon-Rank test is used on data in place of a paired-samples t-test when the populations being compared are non-parametric. Like the t-test, the Wilcoxon-Rank test involves comparisons of differences between measurements, so it requires that the data are measured at an interval level of measurement. However it does not require assumptions about the form of the distribution of the measurements. It should therefore be used whenever the distributional assumptions that underlie the t-test cannot be satisfied.

Independent Samples Analysis

Student's t-test requires that the samples are collected from two different populations of randomly selected individuals from the same populations at different times. Normal distribution of the data set is also required. The Mann-Whitney-U test is a non-parametric test for assessing whether two samples of observations come from the same distribution. It requires the two samples to be independent, and the observations to be ordinal or continuous measurements, i.e. one can at least say, of any two observations, which is the greater.

Analysis of Variance

The analysis of variance (ANOVA) is used to test differences among three or more independent groups of samples and assumes normal distribution. The general linear model (GLM) is used to test differences among three or more independent groups of samples that have been repeatedly measured. If either of the tests supply evidence that a significant difference exists it is necessary to investigate this by using a post-hoc (latin for: after the fact) test. Such tests have a numerical way of objectively deciding if a certain difference is actually significant or not. The post-hoc test actually compares the mean of each group comprising the data set and identifies in which group the significant differences are located. The Fisher's least squared post-hoc method and the Tamhane post-hoc method were selected in the present thesis.

Nomenclature

AA	Antibiotic-Antimycotic	
A_a	Apparent contact area	[mm ²]
A_r	Real asperity contact area	[mm ²]
ACS	Alpha calf serum (low γ -globulin)	
ACS-I	Alpha calf serum (low γ -globulin, Fe supplemented)	
ACS + DW + SA	ACS lubricant	
ACS-I + DW + AA	DW lubricant	
ACS-I + PBS + AA	PBS lubricant	
ACS-I + DW + AA + HA	HA lubricant	
A/G	Albumin/globulin ratio	
ANOVA	Analysis of variance	
AP	Anterior-posterior	
BCS	Bovine calf serum	
BCS + DW + SA	BCS lubricant	
BDS	Backside damage score	
CFU/ml	Colony forming units/ml	
c_p	Heat capacity	[kJ mol ⁻¹]
CP	Commissioning protocol	
CR	Cruciate ligament retaining	
DC	Displacement control	
DSC	Differential scanning calorimetry	
DSF	Damage severity factor	
DW	Distilled water	
ETO	Ethylene oxide sterilization	
F	Female patients	
F_f	Frictional force	[N]
F_n	Normal load	[N]
FC	Force control	
FE	Flexion-extension	
GA	Gamma-in-air sterilization	
GLM	General linear model	
GP	Gas-plasma sterilization	
h_c	Protein layer contact layer thickness	[nm]
ΔH	Change in enthalpy	[kJ mol ⁻¹]
HA	Hyaluronic acid	
IE	Internal-external	
IF	Cases revised for infection	
IP	Implantation period	[months]

IS	Cases revised for instability	
LB	Luria-Bertani	
M	Male patients	
Mc	Million cycles	
ML	Medial-lateral	
MLRA	Multiple linear regression analysis	
MW	Molecular weight	[MDa]
MWCO	Molecular weight cut off	[Da]
NCS	Newborn calf serum	
NCS + DW + SA	NCS lubricant	
NGA	Non-gamma-in-air sterilization	
OA	Osteoarthritis	
OS	Cases revised for osteolysis	
OT	Other reasons for revision	
P	Primary implant type	
p	Level of significance	
PBS	Phosphate-buffered saline solution	
PE	Polyethylene	
PS	Posterior ligament substituting	
PTFE	Poly-tetra-fluor-ethylene	
R	Revision implant type	
RA	Rheumatoid arthritis	
R _a	Centre-line surface roughness	
R _q	Root-mean square surface roughness	
RT	Room temperature	°C
SA	Sodium azide	
SD	Standard deviation	
ΔS	Change in entropy	[kJ mol ⁻¹ K ⁻¹]
SF	Synovial fluid	
SM	Lubricant starting material	
SUP	Lubricant supernatant	
THR	Total hip replacement	
TKA	Total knee arthroplasty (replacement surgery)	
TKR	Total knee replacement	
T _m	Transition midpoint temperature	[K]
XPE	Cross-linked polyethylene	
β _n	Regression coefficient	
φ	Deformation	[nm]
μ _s , μ _k	Friction coefficient (static, kinetic)	